?, 260 C1

Peri-Tethys Memoir 3

Stratigraphy and Evolution of Peri-Tethyan Platforms

Edited by
Sylvie CRASQUIN-SOLEAU
& Éric BARRIER

MÉMOIRES DU MUSÉUM NATIONAL D'HISTOIRE NATURELLE
TOME 177
1998

COM

Source : MNHN, Paris

MÉMOIRES DU MUSÉUM NATIONAL D'HISTOIRE NATURELLE

Rédacteur en chef *(Editor-in-Chief)* : Jean-Lou JUSTINE
Rédacteurs (*Editors*) : Jean-Marie BETSCH, Philippe BOUCHET, Christian ÉRARD & Jean-Lou JUSTINE
Assistantes de rédaction (*Copy editor*) : Bernadette GOTTINI-CHARLES & Laurence BÉNICHOU

Adresse (*Address*)
Mémoires du Muséum national d'Histoire naturelle
57, rue Cuvier
F-75005 Paris
Tél. : [33] 01 40 79 34 37
Fax. : [33] 01 40 79 38 08
e-mail : memoires@mnhn.fr

Les *Mémoires du Muséum national d'Histoire naturelle* publient des travaux originaux majeurs, tels que des monographies ou des volumes à auteurs multiples. Les auteurs sont invités, pour toutes les questions éditoriales, à prendre contact avec le directeur de la publication. Les manuscrits peuvent être en français ou en anglais.

The Mémoires du Muséum national d'Histoire naturelle *publishes major original contributions, such as monographs or multi-authored volumes. Prospective authors should contact the Editor-in-Chief. Manuscripts in French or English will be considered.*

Vente en France :

MUSÉUM NATIONAL D'HISTOIRE NATURELLE
SERVICE DES PUBLICATIONS SCIENTIFIQUES
Diffusion : Delphine HENRY
57, rue Cuvier
F-75005 Paris
Tél. : [33] 01 40 79 37 00
Fax : [33] 01 40 79 38 40
e-mail : dhenry@mnhn.fr

Sales Office:

UNIVERSAL BOOK SERVICES
Dr W. BACKHUYS
P.O. Box 321
NL-2300 AH Leiden
The Netherlands
Tel. : [31] (71) 517 02 08
Fax : [31] (71) 517 18 56
e-mail: backhuys@euronet.nl

Parution et prix irréguliers. Les ordres permanents d'achat et les commandes de volumes séparés sont reçus par le **Service des Publications Scientifiques, Diffusion** (pour la France et les DOM-TOM uniquement), ou par **Backhuys Publishers**. Catalogue sur demande. Une liste des derniers titres parus figure en page 3 de couverture.

Volumes are published at irregular intervals, and at irregular prices. Standing orders and orders for single volumes should be directed to the ***Service des Publications Scientifiques du Muséum****, (France and DOM-TOM only) or* ***Backhuys Publishers****. Price list and catalogues are available on request. Recently published memoirs are listed on page 3 of the cover.*

Printed on acid-free paper
Imprimé sur papier non acide

Source : MNHN, Paris

Bibliothèque Centrale Muséum
3 3001 00025345 9

Source : MNHN, Paris

Source : MNHN, Paris

Source : MNHN, Paris

Cover photograph / *Photographie de couverture:*

The Carnian Sidi Stout unconformity in the Dahar cliff (Saharan platform, southern Tunisia). The late Carnian Rehach dolomites rest unconformably over the whole Late Permian to middle Carnian sequence. This unconformity is related to middle-late Carnian dextral transcurrent movements along E-W trending faults (see BOUAZIZ *et al.*, this volume).

Discordance carnienne de Sidi Stout dans la falaise du Dahar (plate-forme saharienne, Tunisie méridionale). Les dolomies de Rehach (Carnien supérieur) reposent en discordance sur la série d'âge permien supérieur à carnien moyen. Cette discordance résulte du jeu de grands décrochements dextres orientés est-ouest au Carnien moyen-supérieur (BOUAZIZ et al., ce volume).

The Peri-Tethys Program, sponsored by international industries (AGIP, ARCO, BRGM, CHEVRON, CONOCO, EAP(ELF), EXXON, SHELL, SONATRACH, TOTAL), research centres (CNRS, IFP), and a university (UPMC), started in 1993. It examines the influence of Tethyan evolution on the bordering cratons since its birth (through the break-up of Pangea), its life (by the extension and formation of oceanic seaways) and finally its death (by collision between the main bordering plates which led to inversion within the epicratonic basins).

Volumes déjà parus/*Previously published volumes*:

Peri-Tethys Memoir 1 (1994): *Peri-Tethyan platforms. Proceedings of the IFP/Peri-Tethys Research Conference.* Technip, Paris: 1-275. ISBN: 2-7108-0679-7.

Peri-Tethys Memoir 2 (1996): Structure and Prospects of Alpine Basins and Forelands. *Mém. Mus. natn. Hist. nat.*, **170**: 1-550 (+ Atlas). ISBN: 2-85653-507-0.

Peri-Tethys Memoir 3 (1998): Stratigraphy and Evolution of Peri-Tethyan Platforms. *Mém. Mus. natn. Hist. nat.*, **177**: 1-262. ISBN: 2-85653-512-7.

Aussi/*Also*

Peri-Tethys: stratigraphic correlations 1 (1997). 330 pp. *Geodiversitas*, **19** (2): 169-499. ISSN: 1280-9659.

Source : MNHN, Paris

Peri-Tethys Memoir 3

Stratigraphy and Evolution of Peri-Tethyan Platforms

BIBL. DU MUSÉUM PARIS

Source : MNHN, Paris

ISBN : 2-85653-512-7
ISSN : 1243-4442
© Éditions du Muséum national d'Histoire naturelle, Paris, 1998

PHOTOCOPIES :

Les *Publications Scientifiques du Muséum* adhèrent au Centre Français d'Exploitation du Droit de Copie (CFC), 20, rue des Grands Augustins, 75006 Paris. Le CFC est membre de l'International Federation of Reproduction Rights Organisations (IFRRO). Aux États-Unis d'Amérique, contacter le Copyright Clearance Center, 27, Congress Street, Salem, Massachusetts 01970.

PHOTOCOPIES:

The Scientific Publications of the Muséum *adhere to the Centre Français d'Exploitation du Droit de Copie (CFC), 20, rue des Grands Augustins, 75006 Paris. The CFC is a member of International Federation of Reproduction Rights Organisations (IFRRO). In USA, contact the Copyright Clearance Center, 27, Congress Street, Salem, Massachusetts 01970.*

Source : MNHN, Paris

MÉMOIRES DU MUSÉUM NATIONAL D'HISTOIRE NATURELLE

TOME 177

Peri-Tethys Memoir 3

Stratigraphy and Evolution of Peri-Tethyan Platforms

edited by

Sylvie CRASQUIN-SOLEAU [1] & Éric BARRIER [2]

[1] Université Pierre et Marie Curie / CNRS
Département de Géologie Sédimentaire
T15-25, E.4, case 104
4, Place Jussieu
F-75252 Paris Cedex 05

[2] Université Pierre et Marie Curie / CNRS
Département de Géotectonique
T25-26, E.1, case 129
4, Place Jussieu
F-75252 Paris Cedex 05

ÉDITIONS
DU MUSÉUM
PARIS

1998

Source : MNHN, Paris

Source : MNHN, Paris

CONTENTS
SOMMAIRE

Pages

NORTHERN PLATFORM

1. **Stratigraphy and sequence stratigraphy of the Upper Carboniferous and Lower Permian in the Donets Basin** 9
Alain IZART, Céline BRIAND, Denis VASLET, Daniel VACHARD, Jean BROUTIN, Robert COQUEL, Alexander MASLO, Natalia MASLO & Raissa KOZITSKAYA

2. **Stratigraphic correlations of the Upper Permian and Triassic beds from the Volga-Ural and Cis-Caspian regions** 35
Edwar A. MOLOSTOVSKY, Ija I. MOLOSTOVSKAYA & Maxim G. MINIKH

3. **The Domanikoid facies of the Russian Platform and basin paleogeography** 45
Valentina S. VISHNEVSKAYA

4. **Paleomagnetism of Permian to Jurassic formations from the Turan Plate** 71
Marie M. LEMAIRE, Evgueni L. GUREVICH, Khodjamourad NAZAROV, Michel WESTPHAL, Hugues FEINBERG & Jean-Pierre POZZI

5. **Reconstruction of paleostress fields in Crimea and the North West Caucasus, relationship with major structures** 89
Aline SAINTOT, Jacques ANGELIER, Alexander ILYIN & Oleg GOUSHTCHENKO

6. **Neogene evolution of he Carpathian foothills: insights from the romanian diapir fold area** 113
Jean-Claude HIPPOLYTE & Mircea SANDULESCU

7. **The Moesian Platform as a key for understanding the geodynamical evolution of the Carpatho-Balkan alpine system** 127
Françoise BERGERAT, Pierre MARTIN & Dimo DIMOV

8. **Scythian Platform: chronostratigraphy and polyphase stages of tectonic history** 151
Anatoly M. NIKISHIN, Sierd CLOETINGH, Serguei N. BOLOTOV, Evgenij Yu. BARABOSCHKIN, Ludmila F. KOPEAVICH, Bronislav P. NAZAREVICH, Dmitri I. PANOV, Marie-Françoise BRUNET, Andrei V. ERSHOV, Vera V. ILINA, Svetlana S. KOSOVA & Randell A. STEPHENSON

9. **Scythian Platform, Caucasus and Black Sea region: Mesozoic-Cenozoic tectonic history and dynamics** 163
Anatoly M. NIKISHIN, Sierd CLOETINGH, Marie-Françoise BRUNET, Randell A. STEPHENSON, Serguei N. BOLOTOV & Andrei V. ERSHOV

Source : MNHN, Paris

SOUTHERN PLATFORM

10. **Triassic series on the Saharan Platform in Algeria; Peri-Tethyan onlaps and related structuration** 177
Hamid Aït SALEM, Sylvie BOURQUIN, Louis COUREL, Berrached FÉKIRINE, Cherfi HELLAL, Leïla MAMI & Mohamed TEFIANI

11. **New data on the Jurassic and Neogene to Quaternary sedimentation in the Danakil Horst and Northern Afar Depression, Eritrea** 193
Mario SAGRI, Ernesto ABBATE, Augusto AZZAROLI, Maria Laura BALESTRIERI, Marco BENVENUTI, Piero BRUNI, Milvio FAZZUOLI, Giovanni FICCARELLI, Marta MARCUCCI, Mauro PAPINI, Guilio PAVIA, Viviano REALE, Lorenzo ROOK & Tewelde Medhin TECLE

12. **Tectonic evolution of the Southern Tethyan margin in Southern Tunisia** 215
Samir BOUASSIZ, Éric BARRIER, Jacques ANGELIER, Pierre TRICART & Mohammed M. TURKI

13. **Structural inheritance and kinematics of folding and thrusting along the front of the Eastern Atlas Mountains (Algeria and Tunisia)** 237
Dominique FRIZON DE LAMOTTE, Éric MERCIER, Fatima OUTTANI, Belkacem ADDOUM, Hacène. GHANDRICHE, Jamel OUALI, Samir BOUAZIZ & Jean ANDRIEUX

INDEX 253

Source : MNHN, Paris

1

Stratigraphy and sequence stratigraphy of the Upper Carboniferous and Lower Permian in the Donets Basin

Alain IZART [1], *Céline* BRIAND [1][2], *Denis* VASLET [2], *Daniel* VACHARD [3], *Jean* BROUTIN [4], *Robert* COQUEL [3], *Alexander* MASLO [5], *Natalia* MASLO [5] & *Raissa* KOZITSKAYA [5]

[1] Laboratoire de Géologie des ensembles sédimentaires, Université de Nancy I
UMR CNRS 7566, B.P. 239, F-54506 Vandœuvre les Nancy, France

[2] BRGM - SGN/GEO, B.P. 6009, F-45060 Orléans Cedex 2, France

[3] Laboratoire de Paléontologie, Université Sciences et Technologies de Lille
URA CNRS 1365, F-59655 Villeneuve d'Ascq Cedex, France

[4] Laboratoire de Paléobotanique, Université P. et M. Curie, 12, rue Cuvier, F-75005 Paris, France

[5] National Academy of Sciences of Ukraine, Institute of geological Sciences
55b Chaklov street, Kiev 252601, Ukraine

ABSTRACT

The Artemovsk geological survey published numerous logs for the Moscovian, Kasimovian, Gzhelian and Lower Permian in a transitional area between continental and marine environments of the Donets Basin. New results concern the stratigraphy according to fusulinids, plants and palynomorphs and sequence stratigraphy. They have been developed by comparison of our observations on cross-sections near Artemovsk and the published coal mine logs. In the Donets Basin, the Kasimovian forms a second order sequence as in the Moscow Basin, that can be subdivided into three third order sequences, which can be further subdivided into fourth order sequences. The Kasimovian is equivalent to the lower Stephanian of the western European basins. The Gzhelian forms a second order sequence that can be subdivided into four third order sequences, which can be further subdivided into fourth order sequences. The Gzhelian is equivalent to the upper Stephanian and the lowermost Autunian of the western European basins. The Asselian is a second order sequence that shows a lowstand and a transgressive system tract during the early and middle Asselian, a highstand system tract during the late Asselian, that continues during the Sakmarian. In the Donets Basin, the fourth order sequences of the Carboniferous begin with an erosive base and show a succession of elementary sequences with fluvial sandstone, coal-bearing, limestone and deltaic facies. The fluvial sandstone represents a period of aggradation, the coal and the limestone a transgressive period and the deltaic facies a period of progradation. These fourth order sequences have a higher amplitude than the third order sequences and obscure these latter sequences. The second order sequence equivalent to the Kasimovian represents a lowstand system tract with fluvial sandstone and a transgressive system tract with limestone in the early Kasimovian, a highstand system tract with deltaic facies in the middle and late Kasimovian. The second order sequence equivalent to the Gzhelian presents a lowstand system tract with fluvial sandstone and a transgressive system tract with limestone during the early and middle Gzhelian, a highstand system tract with deltaic facies

IZART, A., BRIAND, C., VASLET, D., VACHARD, D., BROUTIN, J., COQUEL, R., MASLO, A., MASLO, N. & KOZITSKAYA, R., 1998.— Stratigraphy and sequence stratigraphy of the Upper Carboniferous and Lower Permian in the Donets Basin. *In*: S. CRASQUIN-SOLEAU & É. BARRIER (eds), Peri-Tethys Memoir 3: stratigraphy and evolution of Peri-Tethyan platforms. *Mém. Mus. natn. Hist. nat.*, **177** : 9-33. Paris ISBN : 2-85653-512-7.

Source : MNHN, Paris

during the late Gzhelian. The uppermost Gzhelian, equivalent to the lowermost Autunian, and the Asselian consist of red fluvial deposits with some Autunian plants and lagoonal limestones. The sequences are controlled by regional tectonic subsidence in the graben and the uplift of the horsts and / or by eustasy with either a plate-tectonic or a glacial origin. However, other investigations, especially radiometric dating, will be useful for solving this problem. Each third order sequence corresponds to a biozone of fusulinids. Lithological and biological sequences are identical. The thicknesses and tectonic subsidence decrease gradually from the Moscovian to the Sakmarian. Hiatuses exist between the Sakmarian and Tatarian and between Tatarian and Lower Triassic, corresponding to an uplift or a tectonic inversion period. The drift of the Pangea into equatorial latitude during Carboniferous and tropical latitude near the Carboniferous / Permian boundary explains the differences in lithology (coal / evaporites, red beds), plants (hygrophylous / xerophylous) between Carboniferous and Permian.

RÉSUMÉ

Stratigraphie et stratigraphie séquentielle du Carbonifère supérieur et du Permien inférieur dans le bassin du Donetz.

Le service géologique d'Artemovsk a publié de nombreux logs pour le Moscovien, le Kasimovien, le Gzhélien et le Permien inférieur dans une zone de transition entre le domaine continental et marin du bassin du Donetz. Les nouveaux résultats concernent la stratigraphie d'après les fusulines, la flore et la microflore, et la stratigraphie séquentielle. Ils ont été obtenus en comparant nos observations sur les coupes situées près d'Artemovsk et les logs miniers. Dans le bassin du Donetz, les dépôts du Kasimovien forment une séquence du deuxième ordre comme dans le bassin de Moscou, qui peut être subdivisée en trois séquences du troisième ordre, elles-mêmes subdivisées en séquences du quatrième ordre. Le Kasimovien est équivalent au Stéphanien inférieur des bassins de l'Europe de l'Ouest. Les dépôts du Gzhélien forment une séquence du deuxième ordre qui peut être subdivisée en quatre séquences du troisième ordre, elles-mêmes subdivisées en séquences du quatrième ordre. Le Gzhélien est l'équivalent du Stéphanien supérieur et de la partie inférieure de l'Autunien des bassins de l'Europe de l'Ouest. Les dépôts de l'Assélien et du Sakmarien forment une séquence du deuxième ordre qui présente le cortège de bas niveau et le cortège transgressif pendant l'Assélien inférieur et moyen et le cortège de haut niveau pendant l'Assélien supérieur et le Sakmarien. Dans le bassin du Donetz, les séquences du quatrième ordre du Carbonifère commencent avec une base érosive et montrent une succession de séquences élémentaires avec grès fluviatile, charbon, calcaire et faciès deltaïque. Le grès fluviatile représente une période d'agradation, le charbon et le calcaire une période transgressive et le faciès deltaïque une période de progradation. Les séquences du quatrième ordre ont une amplitude plus grande que les séquences du troisième ordre et les masquent. La séquence du deuxième ordre du Kasimovien présente un cortège de bas niveau avec grès fluviatile et un cortège transgressif avec calcaire pendant le Kasimovien inférieur, et un cortège de haut niveau pendant le Kasimovien moyen et supérieur. La séquence du deuxième ordre du Gzhélien présente un cortège de bas niveau avec grès fluviatile et un cortège transgressif avec calcaire pendant le Gzhélien inférieur et moyen, et un cortège de haut niveau avec des faciès deltaïques pendant le Gzhélien supérieur. La partie supérieure du Gzhélien, encore appelée Orenburgien, équivalente de la partie inférieure de l'Autunien, et l'Assélien consistent en des dépôts fluviatiles et lagunaires rouges à plantes d'âge Autunien. Les séquences sont contrôlées par la subsidence tectonique régionale dans le graben du Donetz et le soulèvement des horsts qui l'entourent et / ou par l'eustatisme soit avec une origine glaciaire soit liée à la tectonique des plaques. Cependant, d'autres investigations, en particulier géochronologiques seraient utiles pour résoudre ce problème. Chaque séquence du troisième ordre correspond à une biozone de fusulines. Les séquences lithologiques et biologiques sont identiques. Les épaisseurs et la subsidence tectonique décroissent graduellement du Moscovien au Sakmarien. Des hiatus existent entre le Sakmarien et le Tatarien et entre le Tatarien et le Trias inférieur, correspondant à un soulèvement ou à une période d'inversion tectonique. La dérive de la Pangée au travers des zones équatoriale pendant le Carbonifère et tropicale pendant le Permien expliquent les différences dans la lithologie (charbon/évaporites, couches rouges), plantes (hygrophiles/xérophiles) entre le Carbonifère et le Permien.

INTRODUCTION

The Donets Basin, an Ukrainian coal-bearing zone, forms a part of the Pripyat-Dnieper-Donets rift (Fig. 1a) that extends from the Baltic to the Caspian Sea across Belarus, Ukraine and Russia (AISENVERG *et al.*, 1975; CHEKUNOV *et al.*, 1993). This zone is situated between two basement horsts that provide sediments: the Voronezh crystalline massif in the north and the Ukrainian crystalline massif in the south. STEPHENSON *et al.* (1993), STOVBA *et al.* (1995) discussed the rift development of the Dnieper-Donets basin: pre- and syn-rift stages during the Devonian and Early Carboniferous, post-rift stage with extensional rejuvenations during the Late Carboniferous, post-rift stage between the Permian and Tertiary with an uplift in the Permian and a tectonic inversion in the Early Tertiary. During the Carboniferous, the Donets basin was a paralic coal zone forming a transitional domain between the paralic and limnic western European coal basins (e.g.: the North France paralic coal Basin and the Saint-Etienne limnic coal Basin) and the sea on the Russian platform (IZART & VACHARD, 1994). Therefore, the Donets basin is a key area for solving the problems of correlations between the continental and marine deposits during the Carboniferous.

After our synthesis (IZART & VACHARD, 1994), this publication provides new data on the sedimentology and stratigraphy in the Donets Basin which could be useful for improving global

Source : MNHN, Paris

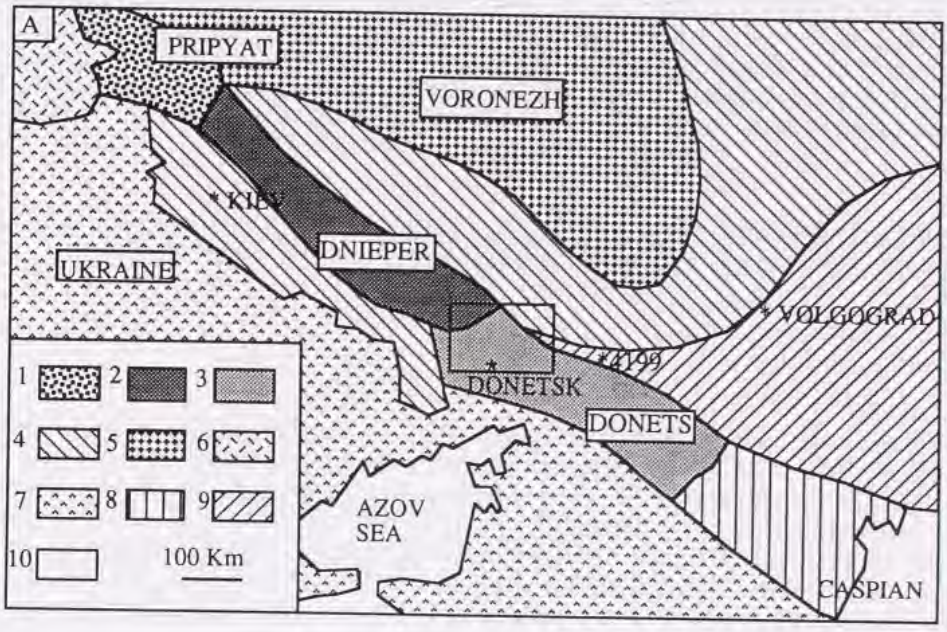

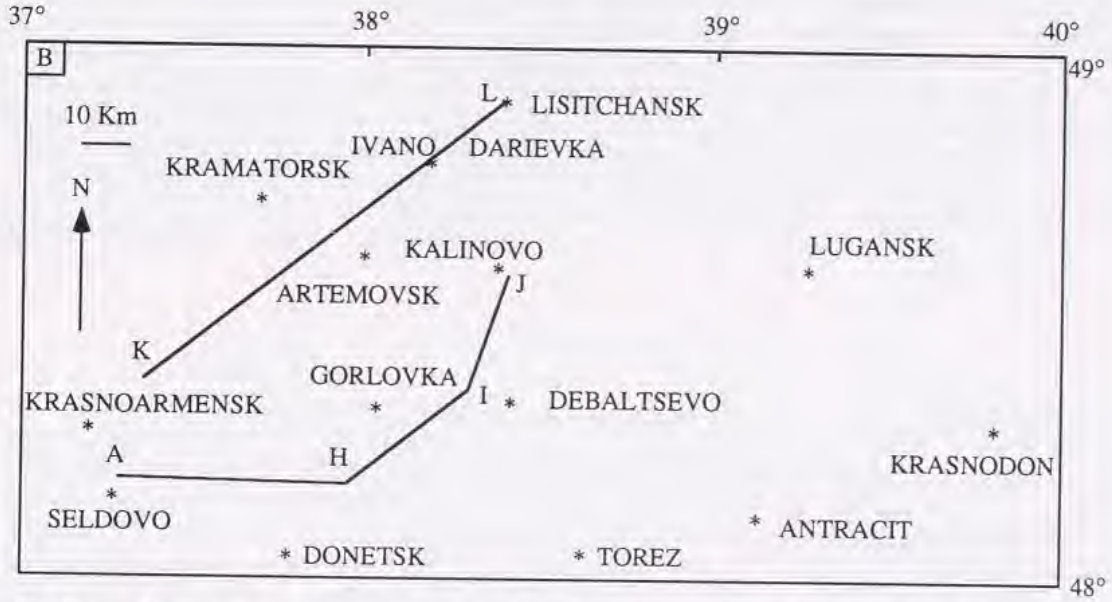

FIG. 1.— The Pripyat-Dnieper-Donets Basin. **A**: Sketch of the Prypiat-Dnieper-Donets Basin. 1, Pripyatsky graben; 2, Dnieper graben; 3, Donets graben; 4, Borders of the basin; 5, Voronezh crystalline massif; 6, Pripyatskaia anticline; 7, Ukrainian crystalline massif; 8, Karpinsky arch; 9, North Caspian syncline; 10, Sea. The rectangle represents the map B. **B**: Location of the cross-sections in the Donets Basin. AHI: Mine logs from Artemovsk geological survey (MAKAROV, 1985). J: Kalinovo cross-section studied by our team. KL: Kalmuys-Bakhmutskaya cross-section (MOVSKOVICH & REDICHKIN, 1980).

*FIG. 1.— Le bassin Pripyat-Dnieper-Donetz. **A** : Carte géologique schématique du bassin Pripyat-Dnieper-Donetz. 1, graben du Pripyat; 2, graben du Dnieper; 3, graben du Donetz; 4, bordures du bassin; 5, massif cristallin du Voronezh; 6, anticlinal de Pripyat; 7, massif cristallin d'Ukraine; 8, arche de Karpinsky; 9, synclinal Nord caspien; 10, Mer. Le rectangle représente la carte B. **B** : Carte de situation des coupes du bassin du Donetz. AHI : logs miniers du service géologique d'Artemovsk (MAKAROV, 1985). J : coupe de Kalinovo étudiée par notre équipe. KL : coupe Kalmuys-Bakhmutskaya (MOVSKOVICH & REDICHKIN, 1980).*

Source : MNHN, Paris

correlations. In 1994, some logs of the Moscow platform have been surveyed with Russian stratigraphers (BRIAND *et al.*, in press) and of the Donets Basin with Ukrainian stratigraphers of the Kiev Institute of Geological Sciences in a cross-section in Kalinovo (J, Fig.1b) for the Moscovian (IZART *et al.*, 1996), Kasimovian, Gzhelian and Lower Permian. Sedimentological and biostratigraphical studies of the foraminifera, conodonts, plants and spores are now in progress. This publication deals with the sequence stratigraphy and biostratigraphy of the Kasimovian, Gzhelian and Lower Permian of the Donets Basin in a transitional zone between continental and marine areas and the geological controls in this basin.

STRATIGRAPHY AND SEQUENCE STRATIGRAPHY OF THE KASIMOVIAN, GZHELIAN AND LOWER PERMIAN OF THE DONETS BASIN

STRATIGRAPHIC OUTLINE

Ukrainian stratigraphers have published many contributions on the geology and stratigraphy of this basin. ZHEMCHUZHNIKOV *et al.* (1959-1960) presented a cyclostratigraphy of the Moscovian of the Donets Basin. AISENVERG *et al.* (1960, 1975) published on the stratigraphy of the Carboniferous of the Donets. STSCHEGOLEV (1960, 1965, 1975) and BOYARINA (1994) published on Carboniferous and Early Permian floras. MAKAROV (1985) presented many logs in the transitional area between continental and marine deposits along the cross-section AHIJ for the Kasimovian-Gzhelian (Fig. 1b). KOZITSKAYA *et al.* (1978) published a biostratigraphic scale for conodonts of the Donets Basin. SOLOVIEVA (1985) and SOLOVIEVA *et al.* (1985 a, b) proposed new stratigraphic correlations for the Donets Basin. DAVYDOV (1990) published on Kasimovian and Gzhelian foraminifera. KAGARMANOV & DONAKOVA (1990) proposed correlations between Moscow platform, Ural and Donets basins. MOVSKOVICH & REDICHKIN (1980) presented a cross-section of the Lower Permian, while AISENVERG *et al.* (1975) and LAPTCHIK (1970) published many logs of the Lower Permian in the Artemovsk area and Dnieper Basin. AISENVERG *et al.* (1960, 1975) described lithostratigraphic units named suites (Table 1) in the Donets Basin and these subdivisions have been chosen for the description. But, KAGARMANOV & DONAKOVA (1990) named these suites horizons (Table 1) and change their boundaries. The horizons in the russian terminology are identical with the Formations in the standard terminology (SALVADOR, 1994).

The table 1 shows the lithostratigraphy, the biostratigraphy and the chronostratigraphy of the Donets Basin. Chronostratigraphic equivalences are proposed between the Ukraine, the eastern Europe (Russia) and the western Europe.

METHODOLOGY

Facies data and paleoenvironments interpretations are based on the logs (e.g.: Fig. 2). For further information refer to MAKAROV (1985) along the cross-section AHIJ (Fig. 1). The authors checked some data in the field (J, Fig. 1) and further data will be presented by BRIAND (Thesis in progress).

AISENVERG *et al.* (1975) and MAKAROV (1985) distinguish in the Moscovian, Kasimovian and Gzhelian of the Donets Basin: a- marine deposits (M) with marine limestones and claystones and marine deltaic siltstones and claystones, b- transitional deposits with lagoonal or lacustrine claystones and lagoonal or lacustrine deltaic siltstones or sandstones, c- swampy deposits with coal seams, d- continental deposits (F) with fluvial sandstones. Marine bands are indicated by capital letters (e.g.: N, Fig. 2) and coal seams with small letters (e.g.: n). Deltaic deposits exhibit coarsening upward sequences from shale to sandstone and fluvial deposits fining upward sequences from sandstone to shale. Channels and cross-beddings occur in the fluvial sandstones.

A sequence stratigraphy has been established on the basis of lithological and paleoenvironmental data and new field data. The environments were sorted out between two trends, one marine at the left (M) and the other continental (F) at the right to exhibit the retrogradation and the transgression towards the west and the progradation and the regression towards the east according to the location of the sea on the Moscow platform.

Source : MNHN, Paris

TABLE 1.— Stratigraphy of the Kasimovian, Gzhelian and Lower Permian in the Donets Basin. (1) AISENVERG *et al.* (1960, 1975), (2) KAGARMANOV & DONAKOVA (1990), (3) VACHARD & MASLO (this note), (4) Donets local megafloral zones according to STSCHEGOLEV & KOZITSKAYA (1984) and BOYARINA (submitted), (5) this note.
PRL: *Pecopteris arcuata, Raminervia mariopteroides, Lodevia nicklesii*
ASA: *Asterotheca daubreii, Sphenopteris germanica, Alethopteris subelegans*
ASE: *Alethopteris subelegans, Sphenopteris germanica, Ernestiodendron filiciformis*

TABLEAU 1.— Stratigraphie du Kasimovien, Gzhélien et Permien inférieur du bassin du Donetz. (1) AISENVERG et al. *(1960, 1975), (2) KAGARMANOV & DONAKOVA (1990), (3) VACHARD & MASLO (cette note), (4) zones locales florales du Donetz d'après STSCHEGOLEV & KOZITSKAYA (1984) et BOYARINA (soumis), (5) cette note.*

LITHOSTRATIGRAPHY			BIOSTRATIGRAPHY		CHRONOSTRATIGRAPHY	
Marine Bands (1)	Suites (1)	Horizons (2)	Fusulinids (3)	Plants (4)	Western Europe Continental "Stages" (5)	Eastern Europe Marine Stages (5)
T_7	P_1-krm (T)	Kramatorsky	*"Sakmarella" moelleri*			Sakmarian
T_1						
	P_1-sl (S)	Slavjansky	*Sphaero-schwagerina sphaerica*			As 3
S_1						
R_4	P_1-nk (R)	Nikitovsky	*Sphaero-schwagerina moelleri*		Autunian	As 2
R_1				*Autunia conferta Lebachia angustifolia*		
Q_{11}	P_1-krt (Q)	Kartamyshky	*Sphaero-schwagerina fusiformis*			As 1
Q_8						
Q_6				ASE		
Q_4			*Ultradaixina bosbytauensis*			
Q_1				ASA		C_3F
P_6	C_3^3 (P)	Mironovsky	*Daixina robusta*			
P_5				PRL		
			Daixina sokensis			C_3E
P_3						
P_2		Kalinovsky	*Jigulites jigulensis*	*Asterotheca densifolia*	Upper Stephanian	C_3D
P_1						
O_8	C_3^2 (O)		*Triticites rossicus Triticites stuckenbergi*	*Odontopteris osmundaeformis*		C_3C
O_5						
O_4^6						
O_4^5		Torezky	*Triticites acutus Triticites quasiarcticus*			C_3B
O_4						
O_3			*Montiparus montiparus*	*Asterotheca lamuriana*	Lower Stephanian	C_3A_2
O_1^1						
O_1	C_3^1 (N)		*Protriticites pseudo-montiparus Obsoletes obsoletus*	*Neuropteris ovata*		C_3A_1
N_5^1						
N_5			*Praeobsoletes burkemensis*			
N_4						
N_3		Sanjarovsky	*Fusulina cylindrica*	*Neuropteris ovata*	Westphalian D	Moscovian
N_1						

Source : MNHN, Paris

The authors use sequence stratigraphy (VAN WAGONER *et al.*, 1988) in a transitional area between a more continental area westwards in the Dnieper Basin and a more marine area eastwards, because the erosion surfaces are well exposed and the maximal flooding surfaces are well recognizable and placed at the acme of the fusulinids biozone. In figures 2 and next, high-frequency sequences (about 40 Ka-100 Ka), fourth order (about 400 Ka), third order (about 1 Ma) and second order sequences are described. In the sequence stratigraphy, a parasequence is defined between two flooding surfaces. But, the first particular problem that was perceived by SHANLEY & MC CABE (1994) for the application of sequence stratigraphic concepts to continental strata was: "What, if anything, is the continental equivalent to a parasequence?". In this type of paralic coal basin, the authors prefer to use the term elementary sequence defined between two more continental trends, the base and the top of the sequence. An elementary sequence is a high-frequency sequence, probably a fouth order sequence (about 100 Ka) or a fifth order sequence (about 40 Ka). Each sequence presents either three facies / paleoenvironments: a- more continental at the sequence base, b- more marine at the maximal flooding surface and c- more continental at the sequence base of the upper sequence. Four facies types may also occur: a- plus b- plus c- plus a coal transgressive facies. Locally, below the fluvial channel, an additionnal facies at the top of the delta shows the degree of erosion and the names of eroded beds are added between brackets. Various cases can exist for the more continental trend: base of fluvial sandstone, seat earth at the base of coal seam and for the more marine trend: limestone top or marine, lagoonal or lacustrine claystone.

The sequence continuity has been checked all along the cross-section by comparing the logs (Fig. 2). This continuity is very reliable, because bore holes and underground mine exposures are numerous. These were already synthesized by MAKAROV (1985). Especially marine bands are reliable stratigraphic markers all across the Dnieper-Donets Basin. For the sake of simplicity, a stratigraphic correlation will not be proposed for the elementary sequences. The marine bands can be followed all over the cross-sections with a lateral passage between marine and lagoonal facies, except when there are eroded upstream. Correlations are proposed for the fourth order sequences by junction-dash by using the high degree of erosion at the base of channel for locating the base of the sequence. The order of each sequence and the distinction between fourth, third and second order sequences are discussed in the text according to the average duration of each sequence (CARTER *et al.*, 1991, Table 2). From the detailed figures 2 and next, it is difficult to observe third order and second order sequences, because a suite does not correspond to a third order sequence. All the bore holes described by MAKAROV (1985) are used here and figure 3 shows a simplified presentation of these sequences.

STRATIGRAPHY AND SEQUENCE STRATIGRAPHY OF THE $C^{1}_{3(N)}$ SUITE

LITHOSTRATIGRAPHY

Data have been recovered in the AHIJ area (Fig. 1b, Fig. 2) near Artemovsk (MAKAROV, 1985). Three bore holes have been selected: 3924 in A, 4180 in H, 7045-7046 in I and the Kalinovo cross-section in J. A cross-section in Kalinovo in J has been surveyed for checking the lithology and environments. MAKAROV (1985) presented a cross-section composed of fifteen boreholes in AHIJ area. This suite was defined between N_1 and O_1 (Table 1). The boundary between the Moscovian and Kasimovian has been placed either in N_2 (AISENVERG *et al.*, 1960, 1975) or in N_4 (KAGARMANOV & DONAKOVA, 1990 and SOLOVIEVA *et al.*, 1985a).

BIOSTRATIGRAPHY AND CHRONOSTRATIGRAPHY

FUSULINIDS.— This suite comprises two fusulinid biozones characterizing the upper Moscovian and lower Kasimovian (Table 1). VILLA *et al.* (1993) reported the occurence of *Protriticites* in N^{1}_{2}. They defined the *Protriticites ovatus*, *Quasifusulinoides quasifusulinoides*, *Praeobsoletes tethydis* biozone between N^{1}_{2} and N^{1}_{5} which is an indeterminate interval attributable to the Moscovian or the Kasimovian. The Moscovian *Praeobsoletes burkemensis* biozone defined by REMIZOVA (1995) could be represented by the interval N_4 and N^{1}_{5} in the Donets Basin. VILLA *et al.* (1993) reported the occurence of *Obsoletes* in N^{1}_{5}. The *Protriticites pseudomontiparus* and *Obsoletes obsoletus* biozone C_3A_1 dated as Kasimovian is correlatable with the interval between N^{1}_{5} and O^{1}_{1}. Between N_2 and O_1 appears to evolve progressively with a gradual transition from the Moscovian to the Kasimovian: the appearance of *Quasifusulinoides* in

Source : MNHN, Paris

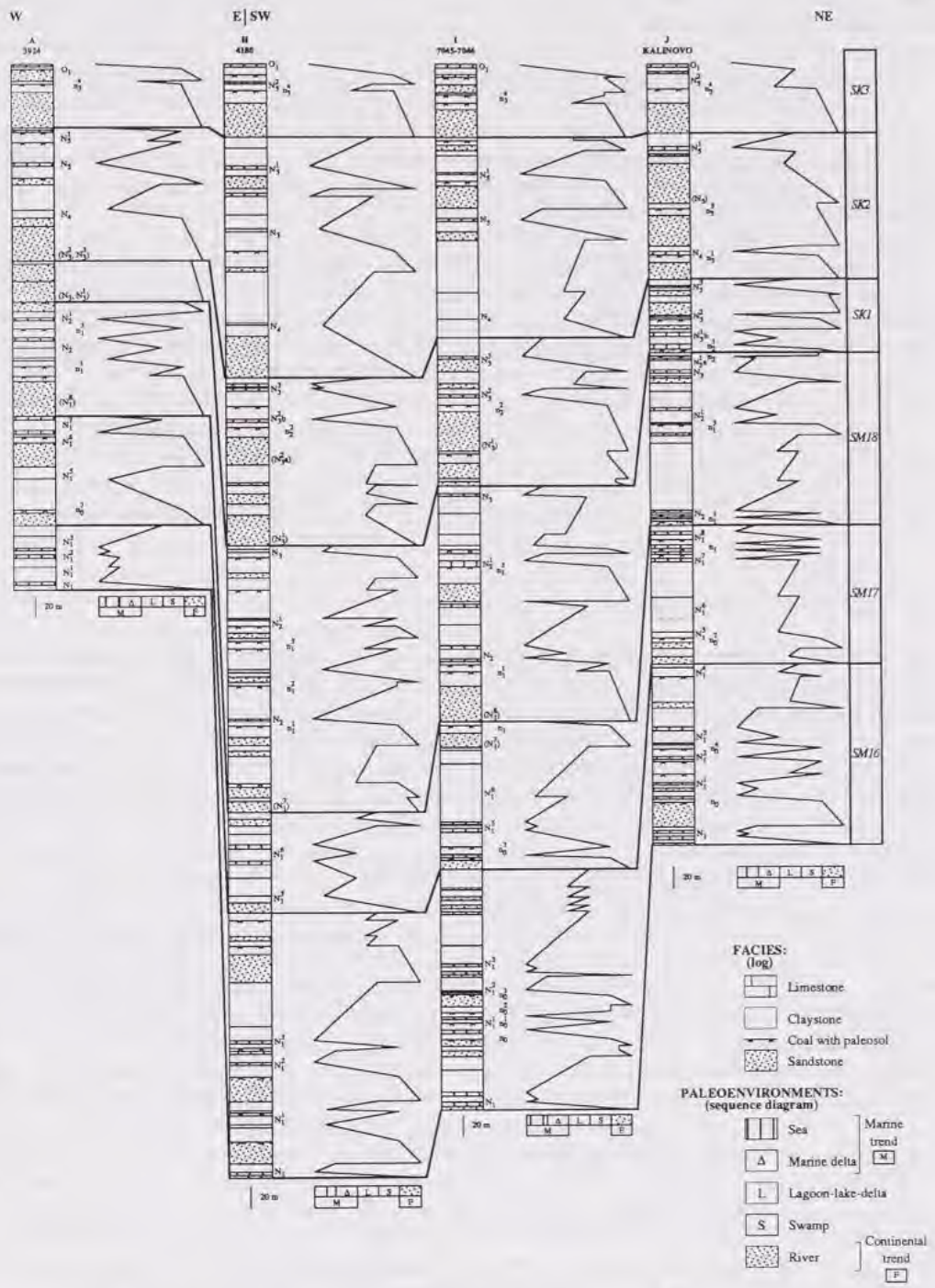

FIG. 2.— Lithostratigraphy and sequence stratigraphy of the C_3^1 (N) Suite in the southern transitional area AHI and in the northern transitional area J in Kalinovo. The notations in capital letter represent the marine bands (e.g.: N_1), in small letter the coal seams (e.g.: n_0) and in brackets the name of eroded beds.

FIG. 2 — Lithostratigraphie et stratigraphie séquentielle de la Suite $C_3^{1(N)}$ dans les zones de transition AHI et J à Kalinovo. Les notations en lettres majuscules représentent les niveaux marins (par exemple : N_1), en lettres minuscules les veines de charbon (par exemple : n_0) et entre crochets le nom des couches érodées.

Source : MNHN, Paris

N_2, the disappearance of *Fusulinella bocki* and appearance of *Fusulina cylindrica* in N_3, the appearance of *Protriticites* and *Praeobsoletes* in N_4, an acme of *Protriticites* in N_5, the appearance of *Tubiphytes*, *Archaelithophyllum lamellosum* and *Obsoletes* in N_5^1 and an acme of *Obsoletes* in O_1. The fusulinids occuring between N_5^1 and O_1 are the same as those in the *Protriticites pseudomontiparus-Obsoletes obsoletus* C_3A_1 biozone which is dated as early Kasimovian, i.e. the Krevyakinian of the Moscow Basin. KOZITSKAYA *et al.* (1978) found a similar gradual transition in the conodonts and they defined the base of the Kasimovian in N_5^1. As it is difficult to attribute the interval N_2^1 - N_5^1 to the Moscovian or the Kasimovian, a sedimentological criterion, the highest erosion at the base of the sandstone between N_3 an N_4 (see after the sequence stratigraphy), has been preferred to determine the limit between the Moscovian and the Kasimovian.

PLANTS.— In Kartanash, STSCHEGOLEV *in* AISENVERG *et al.* (1975, p. 232) and STSCHEGOLEV & KOZITSKAYA (1984) found hygrophilous plants with *"Asterotheca" lamuriana* in n_3^3 below the sandstone. And at the top of the sandstone, he collected xero- and mesophilous plants with *Walchia (*al. *Lebachia) piniformis*, *Culmitzschia (*al. *Lebachia) parvifolia*, *Cordaites* sp. Silicified logs of *Dadoxylon* sp. was found in the sandstones between O_2 and O_4. If the Donets Basin is compared with the Saint-Etienne Basin, only *"Asterotheca lamuriana"* is considered as early Stephanian. Most of other plants are rather long-ranging and not restricted to the Stephanian. As the plants are absent between N_3 and N_4, the same sedimentological criterion as for the Moscovian has been used to determine the limit between the Westphalian and the lower Stephanian. The lower Stephanian extends thus from the base of the sandstone between N_3 and N_4 to O_5 and is equivalent to the Kasimovian according to these new identifications.

SEQUENCE STRATIGRAPHY (Figs 2, 3)

HIGH-FREQUENCY AND FOURTH ORDER SEQUENCES.— Six sequences are proposed for this suite (Figs 2, 3): three attributed to the upper part of the Myachkovian (SM16 to SM18) and three to the lower Kasimovian (SK1 to SK3). The duration of the Kasimovian was about five million years, the duration of these individual sequences is less than one million years and they are therefore fourth order sequences.

The sequences SM6 to SM18 present elementary sequences with four facies / paleoenvironments: a- sandstone (fluvial) - b- coal (swampy) - c- limestone (marine) - d- coal (swampy) during the aggradation and the retrogradation, or three: a- coal (swampy) - b- claystone (lagoonal) - c- coal (swampy) during the progradation. The sequences SK1 to SK3 show elementary sequences with four facies / paleoenvironments: a- sandstone (fluvial) - b- coal (swampy) - c- limestone (marine) - d- sandstone (fluvial) during the aggradation, the retrogradation and the progradation. So, these elementary sequences gather in a stacking pattern with erosion at the base, an aggradation for the fluvial sandstones in a lowstand system tract. The erosion is low at the base of SM16 and SM17, strong at the base of SM18 (Fig. 3), where N_1^7 and N_1^8 are eroded in the bore holes 3924, 4180, 7045. The erosion is strong at the base of SK1 as N_3^1 is eroded in the bore holes 3924, 4180, 7045, strong at the base of SK2 as N_3^2, N_3^3 are partly eroded in 3924, strong at the base of SK3, as N_5^1 is partly eroded in 3924 and the top of the deltaic deposits in the other bore holes. A retrogradation in a transgressive system tract is observed between the flooding surface and the maximal flooding surface, and a progradation in a highstand system tract between the maximal flooding surface and the base of the next sequence. The flooding surface is positioned at the first coal seam of the sequence in n_0 for SM16, in n_0^7 for SM17, in n_1^1 for SM18, in n_2^1 for SK1, in n_3^1 below N_4 or SK2 and in n_3^4 for SK3. The maximal flooding surface is placed at the top of the more transgressive limestone of the sequence with some uncertainty in comparing the logs, in N_1^1 to N_1^3 for SM16, in N_1^5 for SM17, in N_2 for SM18, in N_3^1 b for SK1, in N_4 for SK2, in O_1 for SK3. The more transgressive limestone is the limestone that presents the highest spatial amplitude in the basin (see figure 3). For each sequence, these three system tracts thus form a fourth order sequence.

The thickness of these sequences increases towards the east and decreases towards the north, the thickness of sandstone increases westwards and the marine deposits increase eastwards. An evolution of the degree of erosion can be observed at the base of the Kasimovian: middle below N_2, high below N_3^1 b and N_4. In conclusion, the limit would be between N_3 and N_4.

THIRD ORDER SEQUENCE.— The fourth order sequences in the upper part of this suite form a third order sequence. A fluvial lowstand system tract is positioned between the erosive surface on N_3 and the coal seam n_3^1. A transgressive system tract is placed between the flooding surface n_3^1 and the maximal

Source : MNHN, Paris

flooding surface O_1. A highstand system tract is positioned between O_1 and the base of the next sequence. O_1 was chosen according to the appearance of the first typical Kasimovian foraminifera in this marine band. This sequence is dated as early Kasimovian or Krevyakinian in Moscow Basin.

STRATIGRAPHY AND SEQUENCE STRATIGRAPHY OF THE $C^2_{3(O)}$ SUITE

LITHOSTRATIGRAPHY

Data are recorded from the AHIJ area (Fig. 1b, Fig. 4) near Artemovsk (MAKAROV, 1985). Three bore holes have been selected: 3881 in A, A441 in H, 7048 in I and the Kalinovo cross-section in J. A cross-section in Kalinovo in J has been surveyed for checking the lithology and environments. MAKAROV (1985) presented a cross-section composed of fifteen boreholes in the AHIJ area. This suite was defined between O_1 and P_1 by Ukrainian stratigraphers. And the boundary between the Kasimovian and Gzhelian has been placed variously in P_1 (AISENVERG *et al.*, 1960, 1975) or in O_6 (KAGARMANOV & DONAKOVA, 1990 and SOLOVIEVA *et al.*, 1985a).

BIOSTRATIGRAPHY AND CHRONOSTRATIGRAPHY

FUSULINIDS.— This suite corresponds to three Fusulinid biozones characterizing middle Kasimovian, upper Kasimovian and lower Gzhelian (Table 1). VILLA *et al.* (1993) reported the appearance of *Montiparus* in O^1_1 , a limestone under O_2. They defined the *Montiparus montiparus* biozone C_3A_2 between O^1_1 and O_4. *Montiparus* and *Quasifusulina longissima* occur in O_2; there is an acme of *Montiparus* in O_3. These fusulinids correspond to the biozone C_3A_2 and indicate a middle Kasimovian age, the Khamovnichian in the Moscow Basin.

DAVYDOV (1990) and VILLA *et al.* (1993) observed *Triticites quasiarcticus* in O_4, O^1_4 and SEMINA (1984) found *Triticites acutus* in O^6_4. The first *Triticites* without specific identification occur in O^1_4 and O^3_4. These fusulinids correspond to the *Triticites acutus-Triticites quasiarcticus* biozone B and indicate a late Kasimovian age, the Dorogomilovian and Yausian in the Moscow Basin.

DAVYDOV (1990) reported the occurence of *Nodosaria* cf. *ronda* and *Triticites rossicus* in O_5 and O_6. Our identifications confirm these data. These foraminifera correspond to the *Triticites rossicus-Triticites stuckenbergi* biozone C_3C and indicate a early Gzhelian age, the Rechitskian and Amerevian in the Moscow Basin. DAVYDOV (1990) reported here also the first *Jigulites* and *Daixina* corresponding to the *Jigulites altus* subzone. A sedimentological criterion, the highest erosion at the base of the sandstone between O^5_4 and O^6_4 (see after the sequences stratigraphy) has been preferred to determine the limit between the Kasimovian and the Gzhelian.

PLANTS.— This suite corresponds to two plant biozones characterizing lower Stephanian and upper Stephanian. STSCHEGOLEV *in* AISENVERG *et al.* (1975) and STSCHEGOLEV & KOZITSKAYA (1984) found *"Asterotheca" lamuriana* and *Neuropteris ovata* up to O_5. *Neuropteris ovata* ranges from the Westphalian D to early Stephanian in the North France Basin (LAVEINE, 1986) and in the Saint-Etienne Basin (DOUBINGER *et al.*, 1995, table 8). In the Donets Basin, the lower Stephanian continues thus to O_5 and is equivalent to the Kasimovian according to our new identifications.

STSCHEGOLEV, *in* AISENVERG *et al.*, 1975) found between O_5 and O_7 hygrophilous plants with *Asterotheca densifolia*. This taxon is known in the upper Stephanian of the Saint-Etienne Basin (DOUBINGER *et al.*, 1995). The same sedimentological criterion as for the Gzhelian has been used to determine the base of the upper Stephanian placed at the base of the sandstone between O^5_4 and O^6_4 . The upper Stephanian extends thus from this sandstone to p_4 and is equivalent to the Gzhelian *pro parte*.

SEQUENCE STRATIGRAPHY

HIGH-FREQUENCY AND FOURTH ORDER SEQUENCES.— Seven sequences are proposed here for this suite (Fig. 4, Fig. 3) with one attributed to the middle Kasimovian (SK4), three to the upper Kasimovian (SK5 to SK7) and three to the lower Gzhelian (SG1 to SG3). The duration of the Kasimovian was about five million years, and of the Gzhelian, about five million years, the duration of these individual sequences is less than one million years, they are therefore fourth order sequences.

Source : MNHN, Paris

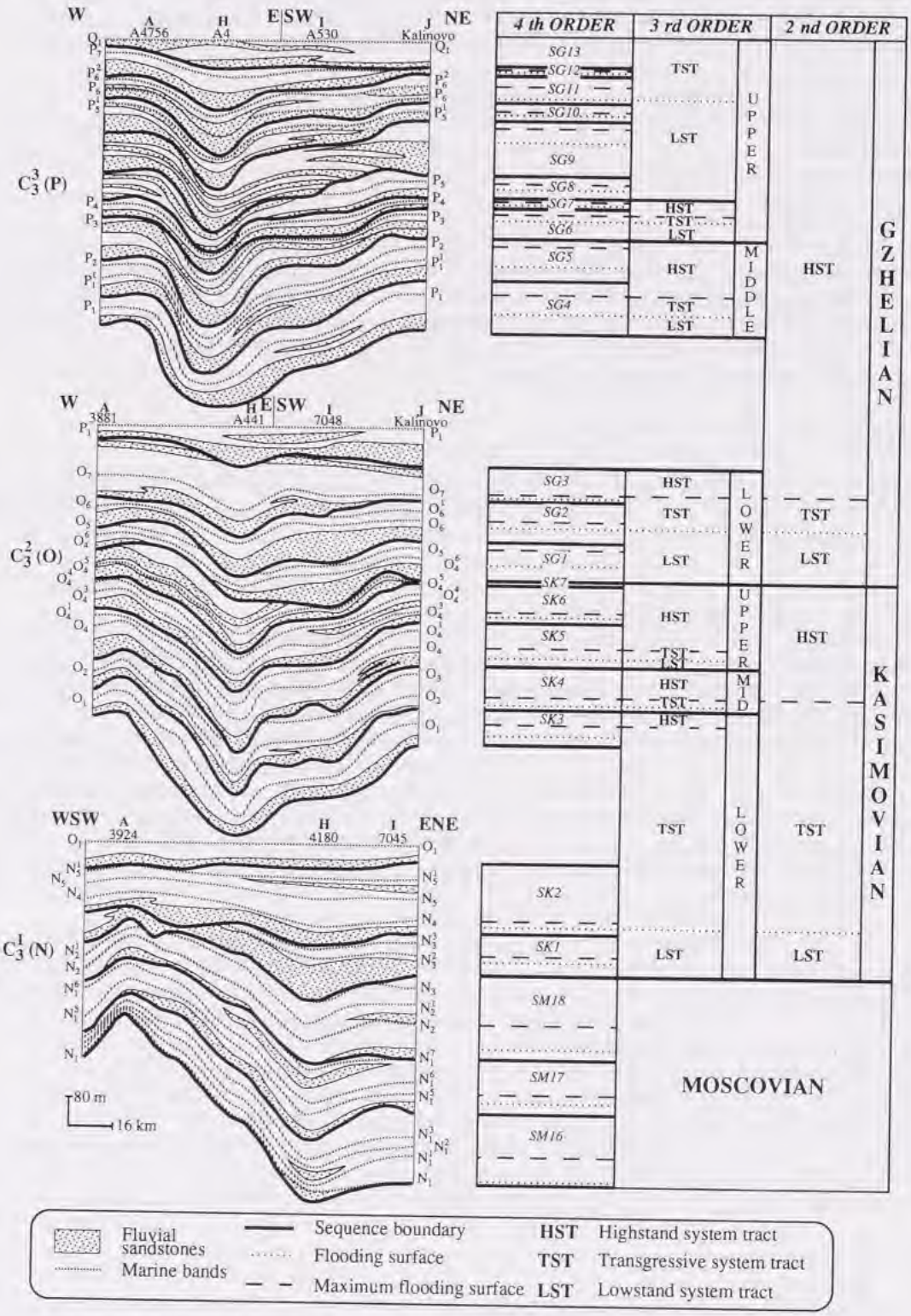

FIG. 3.— Sequence stratigraphy of the Kasimovian and Gzhelian in the Donets Basin.
FIG. 3.— Stratigraphie séquentielle du Kasimovien et du Gzhélien du bassin du Donetz.

Source : MNHN, Paris

The sequences SK4, SK7, SG1 and SG2 present elementary sequences with four facies / paleoenvironments: a- sandstone (fluvial)- b- coal (swampy) - c- limestone (marine) - d- coal (swampy) during the aggradation, the retrogradation and the progradation. The sequences SK5, SK6 and SG1 present elementary sequences with four facies / paleoenvironments: a- sandstone (fluvial) - b- coal (swampy) - c- limestone (marine) - d- coal (swampy) during the aggradation and the retrogradation or three: a- coal (swampy) - b- claystone (lagoonal) - c- coal (swampy) during the progradation. So, these elementary sequences gather in a stacking pattern with erosion at the base, an aggradation for the fluvial sandstones in a lowstand system tract. The erosion is low at the base of the sequences SK4, SK5, SK7, strong at the base of the sequence SK6, as O_4^2 is eroded in bore holes 3881 and A441. The erosion is strong at the base of the sequence SG1, SG2 as O_2^4 and O_5 are eroded in the bore hole A441, and in SG3 as O_6^1 is eroded in bore holes A441 and 3881. A retrogradation in a transgressive system tract is observed between the flooding surface and the maximal flooding surface; a progradation in a highstand system tract between the maximal flooding surface and the base of the next sequence. The flooding surface is placed at the top of the sandstone in the sequences SK7 and SG1 and of the first coal seam of the sequence in o_1 for SK4, in o_1^2 for SK5, in o_2^1 for SK6, in o_2^5 for SG2 and o_3^1 for SG3. The maximal flooding surface is positioned at the top of the more transgressive limestone of the sequence with some uncertainty in comparing the logs, in O_2 for SK4, in O_4 for SK5, in O_4^3 for SK6, in O_4^5 for SK7, in O_4^6 for SG1, in O_6 for SG2, O_7 for SG3. For each sequence, these three system tracts thus form a fourth order sequence.

The thickness of these sequences increases towards the east and decreases towards the north. The thickness of sandstone increases westwards and northwards and the marine deposits increase eastwards. A strong erosion can be observed at the base of the Gzhelian (SG1 to SG3). In conclusion, the Gzhelian limit would be below O_5.

THIRD ORDER SEQUENCES.— The fourth order sequences in this suite form three third order sequences (Fig. 3). The first begins below O_2 and consists of one fourth order sequence dated as middle Kasimovian by foraminifera. Other fourth order sequences have been eroded by the erosive surface below O_4. A fluvial lowstand system tract is placed between the erosive surface on O_1 and the coal seam o_1. A transgressive system tract is positioned between the flooding surface o_1 and the maximal flooding surface O_2. A highstand system tract is placed between the maximal flooding surface O_2 and the base of the next sequence below O_4.

The second third order sequence begins below O_4 and consists of three fourth order sequences dated as late Kasimovian by foraminifera. The lowstand system tract is placed between the erosive surface below O_4 and the top of the sandstone, the transgressive system tract between the top of the sandstone and the maximal flooding surface O_4, the highstand system tract between O_4 and the base of the next sequence below O_4^6.

The third third order sequence consists of three fourth order sequences dated as early Gzhelian. A fluvial lowstand system tract is placed between the erosive surface on O_4^5 and the top of the sandstone. A transgressive system tract is positioned between the flooding surface at the top of the sandstone and the maximal flooding surface O_7. A highstand system tract is placed between the maximal flooding surface and the base of the next sequence.

STRATIGRAPHY AND SEQUENCE STRATIGRAPHY OF THE C_3^3(P) AND THE LOWER PART OF THE P_1-KRT SUITE

LITHOSTRATIGRAPHY

Data are recorded from the AHIJ area (Fig. 1b, Fig. 5) near Artemovsk (MAKAROV, 1985). Three bore holes have been selected: A4756 in A, A4 in H, A530 in I and the Kalinovo cross-section in J. A cross-section has been surveyed in Kalinovo in J for checking the lithology and environments. MAKAROV (1985) presented a cross-section composed of fifteen boreholes in AHIJ area. This suite was defined between P_1 and Q_1 by Ukrainian stratigraphers and the boundary between Gzhelian and Asselian was placed in Q_1 by AISENVERG *et al.* (1960, 1975), KAGARMANOV & DONAKOVA (1990) and SOLOVIEVA *et al.* (1985a). However, new data published by DAVYDOV (1990, 1992) favour the position of the the Gzhelian / Asselian boundary in Q_5. The lower part of P_1-krt, the Kartamyshky suite will be

Source : MNHN, Paris

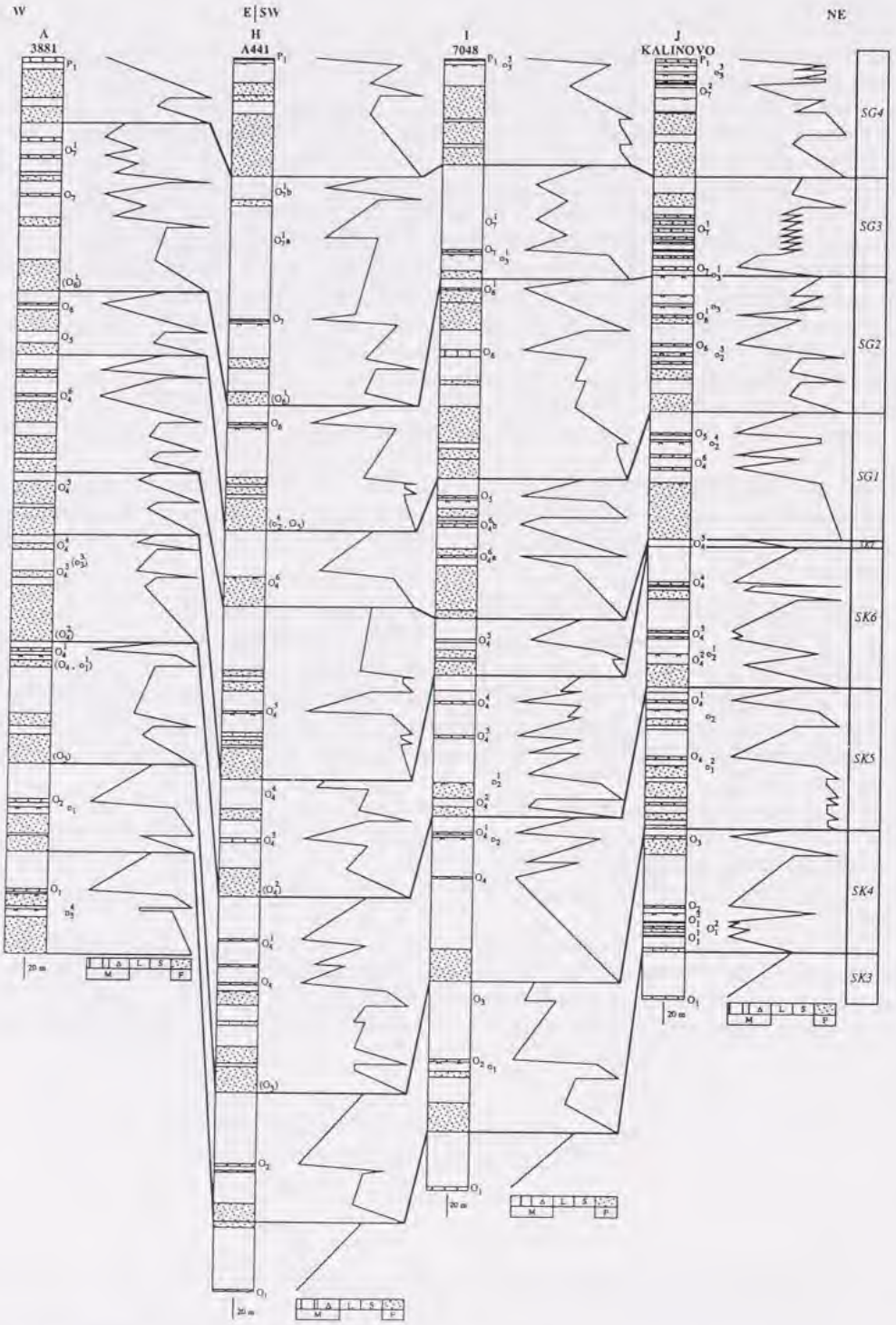

FIG. 4.— Lithostratigraphy and sequence stratigraphy of the C_3^2 (O) Suite in the southern transitional area AHI and in the northern transitional area J in Kalinovo. Legends and comments as in figure 2.

FIG. 4.— Lithostratigraphie et stratigraphie séquentielle de la Suite C_3^2(O) dans les zones de transition AHI et J à Kalinovo. Les légendes et les commentaires sont les mêmes que pour la figure 2.

Source : MNHN, Paris

described here too. Data on the P_1 suites near Artemovsk (profile, Fig. 1b) are recorded according to AISENVERG *et al.* (1975, Fig. 65), MOVSKOVICH & REDICHKIN (1980, Fig. 2, 1984), NESTERENKO & KIREEVA (1980) and LAPTCHIK (1970). The Ivano-darievka cross-section has been surveyed. comparison with the Pre-Donets Basin in bore hole 4199 (Fig. 1a) has been attempted by DAVYDOV (1990) and ALEKSEEVA *et al.* (1983). Figures 6 and 7 present the lithostratigraphy and the sequence stratigraphy of the P_1 Suites.

BIOSTRATIGRAPHY AND CHRONOSTRATIGRAPHY

FUSULINIDS.— These suites correspond to three Fusulinid biozones characterizing the middle and upper Gzhelian (Table 1). ALEKSEEVA *et al.* (1983) reported *Daixina ruzhencevi* from P_1 and DAVYDOV (1990) observed *Schagonella minor* in P_2. Numerous specimens of *Schagonella* and few *Jigulites* were found; however *Jigulites jigulensis* appears to be absent. These fusulinids are the same as those found in the *Jigulites jigulensis* biozone C_3D dated as middle Gzhelian, the Pavlovo-Posadian in the Moscow Basin.

DAVYDOV (1990) observed *Daixina* spp. in P_3, *Daixina sokensis* was found in P_3 and ALEKSEEVA *et al.* (1983) reported *Daixina enormis* and *Daixina* spp. from P_4. These fusulinids are typical for the *Daixina sokensis* biozone C_3E, dated as late Gzhelian, the Noginskian in the Moscow Basin.

No fusulinids were found in the lagoonal limestones near Artemovsk. However, ALEKSEEVA *et al.* (1983) and DAVYDOV (1990, 1992, 1993) studied the fusulinids of the bore hole 4199 (Fig. 6), located in the more marine Pre-Donets area eastwards (Fig. 1). They proposed correlations between the two areas: Q_7 is the same, but Q_8 in Pre-Donets is equivalent to Q_7 in Artemovsk. The Gzhelian / Asselian boundary is the subject of numerous discussions. DAVYDOV (1990) put the *Ultradaixina bosbytauensis - Daixina robusta* biozone C_3F at the Asselian base. In 1992, he dated this biozone as late Gzhelian, the Melekhovian in the Moscow Basin and the first Asselian biozone is therefore the *Sphaeroschwagerina fusiformis* biozone As1. The boundary between these two biozones represents the Gzhelian / Asselian boundary (DAVYDOV, 1992) and the potential Carboniferous / Permian boundary (JIN YU-GAN *et al.*, 1994). On the other hand, paleomagnetic data show a short-term normal polarity subzone (KHRAMOV, 1963) in the top of C_3F in Donets and Ural (KHRAMOV & DAVYDOV, 1984, 1993). In the Donets Basin, the normal polarity subzone is in the level of Q_8 / Q_7 and corresponds to the C_3F top according to SCHNEIDER *et al.* (1995). Note that there are uncertainties for the upper limit of this biozone in the Donets Basin. According to ALEKSEEVA *et al.* (1983), Q_9 in bore hole 4199 contains *Sphaeroschwagerina* cf.*fusiformis*. DAVYDOV (1992) placed the base of C_3F in P_5 and the top in Q_9 in bore hole 4199, being equivalent of Q_7 in Artemovsk. However, SCHNEIDER *et al.* (1995) regarded Q_1 as the base of C_3F and Q_5 as its top. We prefer an intermediate position with the base in P_5 and the top in Q_5, because this proposal takes into consideration the fusulinids with evolutive arguments and the paleomagnetism.

PLANTS.— For the plants, these suites correspond to three plants biozones characterizing upper Stephanian and Autunian. BOYARINA (submitted) defined below P_5^0 a megafloral local zone AO with *Asterotheca densifolia* and *Odontopteris osmundaeformis*. *Asterotheca densifolia* characterizes the upper Stephanian in the Saint-Etienne Basin (DOUBINGER *et al.*, 1995) and the Donets Basin. For the palynology, INOSOVA *et al.* (1976) defined IX and X palynological zones between P_2 and P_5^0 with Stephanian spores and 5% *Potonieisporites* sp. dated as late Stephanian-Autunian. The coal p_2 below P_3 shows a dominance of "Stephanian" forms with some *Potonieisporites* sp. A dominance of "Autunian" forms with *Potonieisporites* sp.is found in the claystone below the coal p_3. Furthermore, a claystone within the coal p_3 below P_4 shows a dominance of "Stephanian" palynomorphs with *Schopfipollenites ellipiticus*, *Columinisporites* sp. and *Potonieisporites* sp. The age is regarded to be late Stephanian with a coexistence of "Stephanian" forms in the coal and "Autunian" palynomorphs in the flood plain claystone. This coexistence of "Stephanian" and "Autunian" forms previously described from western Europe (BROUTIN *et al.*, 1986; BROUTIN *et al.*, 1990; BECQ-GIRAUDON, 1993) is now also recorded for the upper Stephanian of the Donets Basin. This coexistence is controlled by paleoenvironmental variations. The "Stephanian" flora consists of hygrophilous elements growing in marshes within the basin. The "Autunian" flora is typified by meso-xerophilous elements growing on topographic highs bordering the basin. The "Autunian" pollen came mainly by air and accumulated in the flood plain, lake or lagoon within the basin.

Source : MNHN, Paris

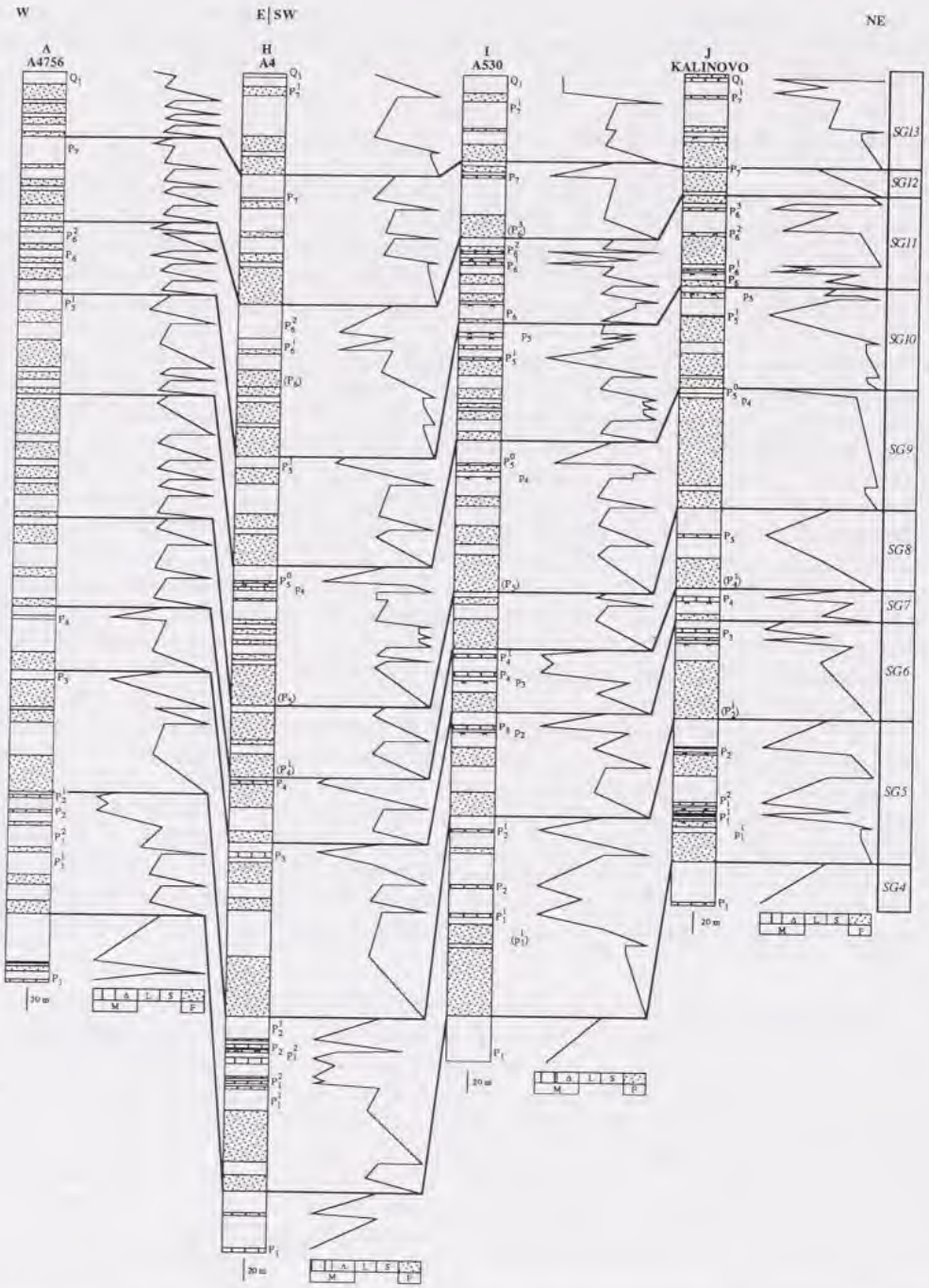

FIG. 5.— Lithostratigraphy and sequence stratigraphy of the $C_3^3(P)$ suite in the southern area AHI and in the northern transitional area J in Kalinovo. Legends and comments as in figure 2.

FIG. 5.— Lithostratigraphie et stratigraphie séquentielle de la Suite $C_3^3(P)$ dans les zones de transition AHI et J à Kalinovo. Les légendes et les commentaires sont les mêmes que pour la figure 2.

Source : MNHN, Paris

STSCHEGOLEV (1960, 1965, 1975), STSCHEGOLEV & KOSITSKAYA (1984) and BOYARINA (1994, submitted) found in the claystone below P_5 (Kalinovo, Fig. 5) meso-xerophilous Callipterid Pteridosperms. Abundant *Raminervia mariopteroides* grew in a moderately humid flood plain. Scarce *Rhachiphyllum schenkii*, *Dichophyllum cuneata*, *Autunia conferta*, *Lodevia nicklesii* grew in an elevated less humid part of the flood plain. In the roof of p_5, they found hygrophilous plants with *Asterotheca arborescens* and *Annularia stellata*. BOYARINA (submitted) defined megafloral local zones PRL between P_5^0 and P_6 and ASA between P_6 and Q_4. PRL is composed of *Pecopteris arcuata*, *Raminervia mariopteroides* and *Lodevia nicklesii*. ASA is composed of *Asterotheca daubreii* , *Sphenopteris germanica* and *Alethopteris subelegans*. *Raminervia mariopteroides* and *Dichophyllum cuneata* are taxa not known from other basins. *Autunia conferta* and *Lodevia nicklesii* are also known in some layers of the upper Stephanian in the Saint-Etienne Basin (DOUBINGER *et al.*, 1995). Therefore, this list of plants is too local and an age can not be attributed to these plants that can be upper Stephanian or Autunian. Based on the palynology, INOSOVA *et al.* (1976) defined the zone XI between P_5^0 and Q_1 with 10% *Potonieisporites* sp. and the zones I to IV of the Permian between Q_1 and Q_5 with 10% *Punctatisporites confusus*. The claystone below p_5, where Stschegolev described Callipterids, shows a dominance of "Autunian" forms with *Potonieisporites* spp. (above 80 %) and striate bisaccate pollen grains (*Protohaploxypinus* spp.). The bituminous coal p_5, the last coal of the Donets Basin, is characterized by a dominance of three "Stephanian" forms: *Calamospora* sp., *Laevigatosporites* sp., *Endosporites globiformis*. Furthermore, the claystone below P_7 shows "Stephanian" forms with *Crassispora kosankei*, *Tripartites aductus*, *Lundbladispora* sp. and pollen grains, e.g. *Marsupipollenites triradiatus*, *Gardenasporites* sp., striate bisaccates are absent. These beds are dated as Autunian with a coexistence of "Stephanian" and "Autunian" taxa, associated with the same paleoenvironmental variations during the late Stephanian and Autunian of the western Europe (BROUTIN *et al.*, 1990). INOSOVA *et al.* (*in* AISENVERG *et al.*, 1975, Fig. 6) and INOSOVA *et al.* (1976) showed the dominance of Autunian forms in Q_8, that is positioned near the Asselian base. The climatic change recorded at the limit between the Carboniferous and the Permian from wet to dry conditions with xerophilous taxa already occuring in the uppermost Carboniferous is evident in the Donets Basin like in the western Europe (BROUTIN *et al.*, 1990). So, there are two possibilities for the limit between Stephanian and Autunian: the first appearance of xerophilous plants in p_5 or their acme in Q_8. We choose the first solution. Such a choice implies that Lowermost Autunian would be latest Carboniferous in age. In conclusion, the base of the Autunian and of the C_3F zone of the upper Gzhelian are identical. And the base of Autunian and of the normal polarity subzone are identical. This solution agrees with MENNING *et al.* (1988) and SCHNEIDER *et al.* (1995) that reported the normal polarity subzone inside the lower Rotliegend near the base of the Manebach Formation in the Saale Basin, equivalent to the top of the Kusel Formation in the Saar Nahe Basin and lower part of the Autunian in the Autun Basin.

SEQUENCE STRATIGRAPHY

HIGH-FREQUENCY AND FOURTH ORDER SEQUENCES.— Nine sequences are proposed here for the C_3^3 suite (SG4 to SG12, Fig. 5, Fig. 3) and four (SG13 to SG16, Fig. 7) for the P_1-krt suite attributed to the Gzhelian. The duration of the Gzhelian was about five million years, the duration of these individual sequences is less than one million years, they are therefore fourth order sequences.

The sequences SG4 to SG13 present elementary sequences with four facies / paleoenvironments: a- sandstone (fluvial) - b- coal (swampy) - c- limestone (marine) - d- coal (swampy) during the aggradation and the retrogradation or three: a- coal (swampy) -b- claystone (lagoonal) - c- coal (swampy) during the progradation. The sequences SG14 to SG16 are composed of one or several elementary sequences with three facies / paleoenvironments: a- claystone (fluvial plain) - b- limestone (lagoonal) - c- claystone (fluvial plain) during the aggradation, the retrogradation and the progradation. Between Q_1 and Q_6, the marine trend is located at the top of the limestone and the continental trend at the base of the sandstone or in the middle of the claystone, because sandstone exists in this place in the Dnieper Basin (LAPTCHIK, 1970). So, these elementary sequences gather in a stacking pattern with erosion at their base, an aggradation for the fluvial sandstones in a lowstand system tract. There is little erosion at the base of the sequences SG5 and SG6 and of the sequences SG10 to SG16, strong erosion at the base of the sequences SG7, SG8 and SG9, as P_5 is eroded in the bore holes A530, A4, A4756. They include red fluvial sandstones between P_4 and Q_1, red claystones between Q_2 and Q_6 in Artemovsk area and fluvial sandstones between P_4 and Q_6 in the bore hole 4199. Then, a retrogradation in a transgressive system

Source : MNHN, Paris

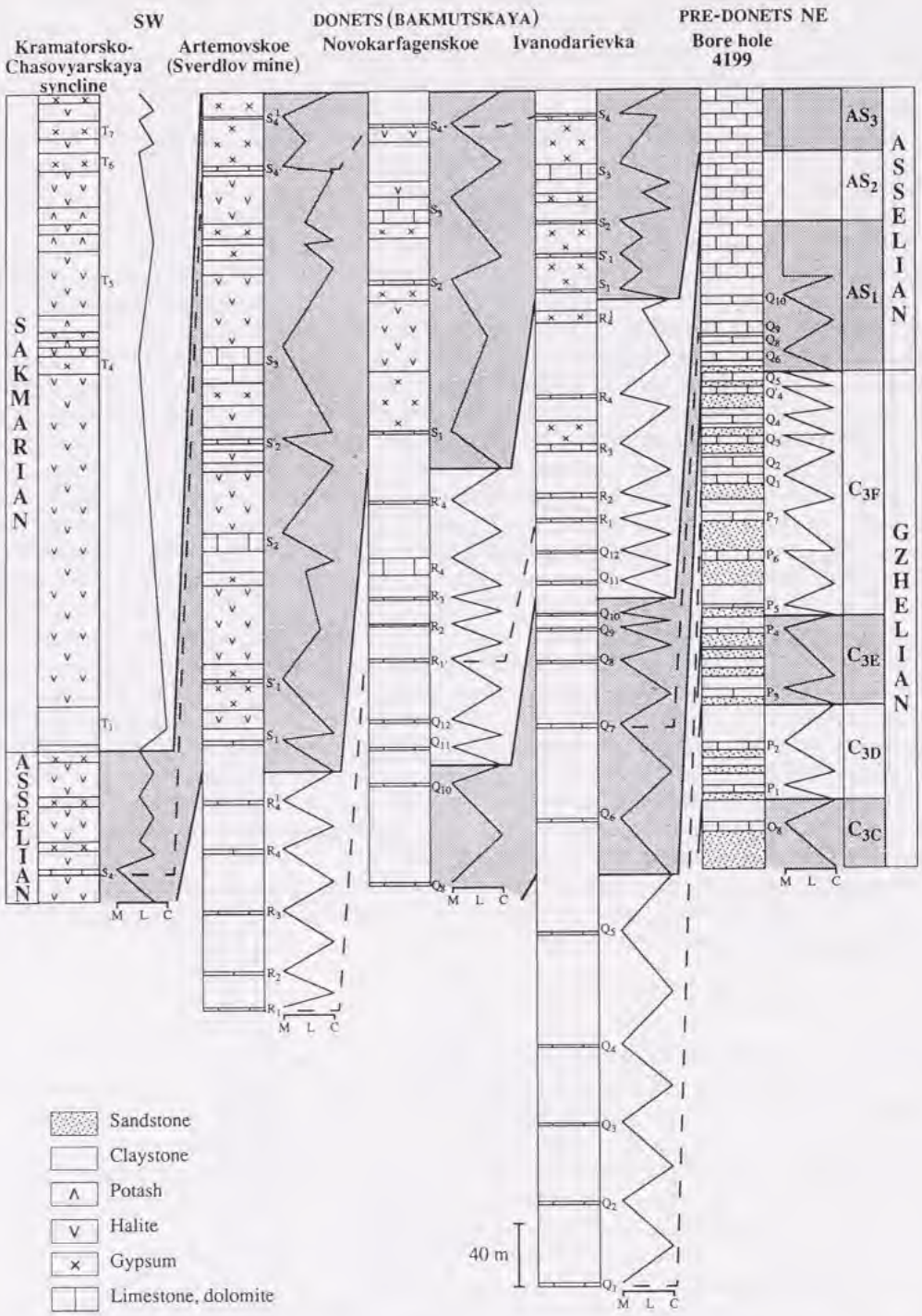

FIG. 6.— Lithostratigraphy and sequence stratigraphy of the upper Gzhelian and Lower Permian in the Donets Basin and Pre-Donets Basin in the bore hole 4199. M: marine environment. L: lagoonal environment. C: continental environment.

FIG. 6.— Lithostratigraphie et stratigraphie séquentielle du Gzhélien supérieur et du Permien inférieur dans les bassins du Donetz et du Pré-Donetz (forage 4199). M: environnement marin. L : environnement lagunaire. C : environnement continental.

Source : MNHN, Paris

tract is observed between the flooding surface, and the maximal flooding surface and a progradation in a highstand system tract between the maximal flooding surface and the base of the next sequence. The flooding surface is placed at the top of the sandstone for the sequence SG4 and on the first coal seam of the sequence in p_1^1 for the SG5, in p_2 for SG6, in p_3 for SG7, in the top of the sandstone for SG8, in p_4 for SG9, in the top of the sandstone for SG10 to SG12 and in the base of the limestone for SG13 to SG16. The maximal flooding surface is positioned at the top of the more transgressive limestone of the sequence with some uncertainty in comparing the logs, in P_1 for SG4, in P_2 for SG5, in P_3 for SG6, in P_4 for SG7, in P_5 for SG8, in P_5^0 for SG9, in P_5^1 for SG10, in P_6^1 for SG11, in P_7 for SG12, in Q_1 for SG13, in Q_3 for SG14, in Q_4 for SG15 and in Q_5 for SG16. So, for each sequence, these three system tracts form a fourth order sequence.

The thickness of these sequences increases towards the east and decreases towards the north, the thickness of sandstone increases westwards and northwards and the marine deposits increase eastwards. A strong erosion can be observed at the base of the fourth order sequence SG9, corresponding to the Autunian base.

THIRD ORDER SEQUENCES.— The fourth order sequences in these suites form three third order sequences (Fig. 3) belonging to the Gzhelian. The first is composed of two fourth order sequences. A fluvial lowstand system tract is placed between the erosive surface on O_7^1 and the top of the sandstone. A transgressive system tract is positioned between the flooding surface and the maximal flooding surface P_1. A highstand system tract is placed between the maximal flooding surface and the base of the next sequence.

The second third order sequence is composed of two fourth order sequences. A lowstand system tract is placed between the erosive on P_2 and top of the sandstone. A transgressive system tract is positioned between the flooding surface and the maximal flooding surface P_3. A highstand system tract is placed between the maximal flooding surface and the base of the next sequence below P_5.

The third third order sequence presents a strong erosion on P_5, but the lowstand system tract is positioned between the erosive surface on P_4 and the coal seam p_4 according to the paleontological argument. A transgressive system tract is placed between the flooding surface p_4 and the maximal flooding surface Q_1. A highstand system tract is positioned between Q_1 and the base of the next sequence in Q_6. The extension of the marine bands (Fig. 7) is lower between P_5 and Q_1, maximum in Q_1 and decreases between Q_1 and Q_5.

STRATIGRAPHY AND SEQUENCE STRATIGRAPHY OF THE LOWER PERMIAN SUITES

LITHOSTRATIGRAPHY

The same data as for P_1-krt are used here (Figs 6-7). Ukrainian stratigraphers defined the P_1-krt suite, named Kartamyshky, between Q_1 and R_1, the P_1-nk, named Nikitovsky, between R_1 and S_1, the P_1-sl, named Slaviansky, between S_1 and T_1, the P_1-krm, named Kramatorsky. P_1-krm, P_1-nk and P_1-sl are Asselian and P_1-krm is lower Sakmarian. The Dronovsky suite, composed of speckled claystone and sandstone is Tatarian (Upper Permian) and rests with an angular unconformity on the Sakmarian. Then, the conglomerate of Lower Triassic rests with an unconformity on the Tatarian (LAPTCHIK, 1970). So, a hiatus corresponding to an uplift or a compressive phase is located between the Sakmarian and Tatarian and another one between the Tatarian and Lower Triassic.

BIOSTRATIGRAPHY AND CHRONOSTRATIGRAPHY

FUSULINIDS.— LAPTCHIK (1970) described the Foraminifera of the Donets Basin. ALEKSEEVA *et al.* (1983) and DAVYDOV (1990, 1992) recognized the *Sphaeroschwagerina fusiformis* biozone As_1 (Table 1) between Q_7 and R_1 (lower Asselian in the Moscow and Ural basins). Davydov found also the *Sphaeroschwagerina moelleri* biozone As_2 between R_2 and S_1 (middle Asselian), the *Sphaeroschwagerina sphaerica* biozone As_3 from S_1 (upper Asselian). However, the "*Sakmarella" moelleri* biozone (lower Sakmarian) from T_1 is more problematical. In the Donets Basin near Artemovsk, fusulinids are absent because marine bands are dolomitic, except for Q_{11} where *Sphaeroschwagerina constans* of the As_2 biozone was found.

Source : MNHN, Paris

PLANTS.— The plants are rare in these red beds and indicate a xerophilous flora. BOYARINA (submitted) defined local floristic zones ASE between Q_4 and Q_8 and AL between Q_8 and R_4. The zone ASE is typified by *Alethopteris subelegans*, *Sphenopteris germanica*, *Ernestiodendron filiciformis*. The zone AL includes *Autunia conferta* and *Culmitzschia* (al. *Lebachia) angustifolia*. In the Autun Basin, BROUTIN *et al.* (1986) observed also the abundance of the xerophylous plants with *Autunia conferta* as in the Donets basin, the age of these taxa is Autunian unreservedly. INOSOVA *et al.* (1976) defined zones V and VI between Q_4 and Q_8 and zones VII to IX between Q_8 and R_4. They noted more 10% *Potonieisporites novicus* and 5% *Vittatina* in zones V and VI. They showed a dominance of Autunian forms in Q_8, placed near the Asselian base with *Vittatina* (up to 10%) and *Potonieisporites novicus* (10 to 50%). The climatic change in the Lower Permian results in the depositon of evaporites and red beds with a xerophilous flora.

SEQUENCE STRATIGRAPHY

HIGH-FREQUENCY AND FOURTH ORDER SEQUENCES.— Eleven sequences (SA1 to SA11, Figs 6-7) are proposed here for the Asselian and two for the Sakmarian (SS1, SS2). The duration of the Asselian was about six million years (MENNING, 1995), the duration of these individual sequences is less than the million years, they are therefore fourth order sequences.

In the Bakhmutskaya area of the Donets Basin, near Artemovsk, the sequences SA1 to SA11 begin in the middle of the claystone, passing laterally in a sandstone in the Dnieper Basin. For instance, the SA1 base corresponds to the palynological biozone V base below Q_6 (Fig. 7). In the bore hole 4199 of the Pre-Donets, the sequence SA1 begins at the base of the sandstone below Q_6, SA2 below Q_{10} and sequences can not be proposed for the limestones above without precise facies descriptions.

In the Donets Basin, these sequences represent one elementary sequence or several (e.i. Q_7-Q_9). They show a lowstand system tract and a transgressive system tract with red claystone in Q and R marine bands, green claystone in S marine bands or halite and potash, a maximal flooding with gypsum, limestone or dolomite, a highstand system tract with claystone. In the Pre-Donets Basin, the deposits are only limestones as in the Moscow and Ural basins. In the Dnieper Basin, LAPTCHIK (1970) reported sandstone at the Q_1, R_1, S_1 and T_1 base, sandstone in P_1-krt, gypsum, salt, dolomite and limestone in P_1-nk, P_1-sl and P_1-krm.

THIRD ORDER SEQUENCES.— The fourth order sequences can be gathered in three third order sequences for the Asselian corresponding to the biozones As_1, As_2 and As_3 and one for the Sakmarian. The first third order sequence presents a lowstand system tract below Q_6 with a minimum extension of the marine bands (Fig. 7), a transgressive system tract between Q_6 and Q_7, a maximal flooding surface in Q_7 corresponding to the maximum extension, a highstand system tract in Q_8, Q_9, Q_{10} with minimum extension. Note that for the sequence stratigraphy, there are two possibilities for the Asselian base corresponding to a minimum extension in Q_5 or in Q_8. The second third order sequence presents a lowstand system tract in Q_{11}-Q_{12} with a minimum extension of the marine bands, a transgressive system tract between Q_{11} and R_1, a maximal flooding surface in R_1 known in the Dnieper Basin and corresponding to the maximum extension, a highstand system tract in R_2, R_3, R_4 with minimum extension. The third third order sequence does not present a lowstand system tract and a transgressive system tract, but presents a maximal flooding surface in S_1 corresponding to the maximum extension and a highstand system tract between S_1 and T_1 with minimum extension.

The Sakmarian comprises only a single third order sequence that continues the highstand system tract of the Asselian before the closing of the Donets basin by uplift or compression, when eustatism continues in the Ural.

DISCUSSION ON THIRD AND SECOND ORDER SEQUENCES

Figures 3 and 7 present the sequence stratigraphy of the Kasimovian, Gzhelian and Asselian of the Donets Basin. The third order sequences of the Upper Carboniferous are arranged in two second order sequences that are equivalent to the Kasimovian and Gzhelian. The first second order sequence presents three third order sequences and shows a lowstand system tract with a strong erosion between the base of the sandstone on N_3 and the coal seam n_3^1 below N_4, a transgressive system tract between n_3^1 and O_2, a highstand system tract between O_2 and the base of the sandstone on O_4^5 . The middle and upper

Source : MNHN, Paris

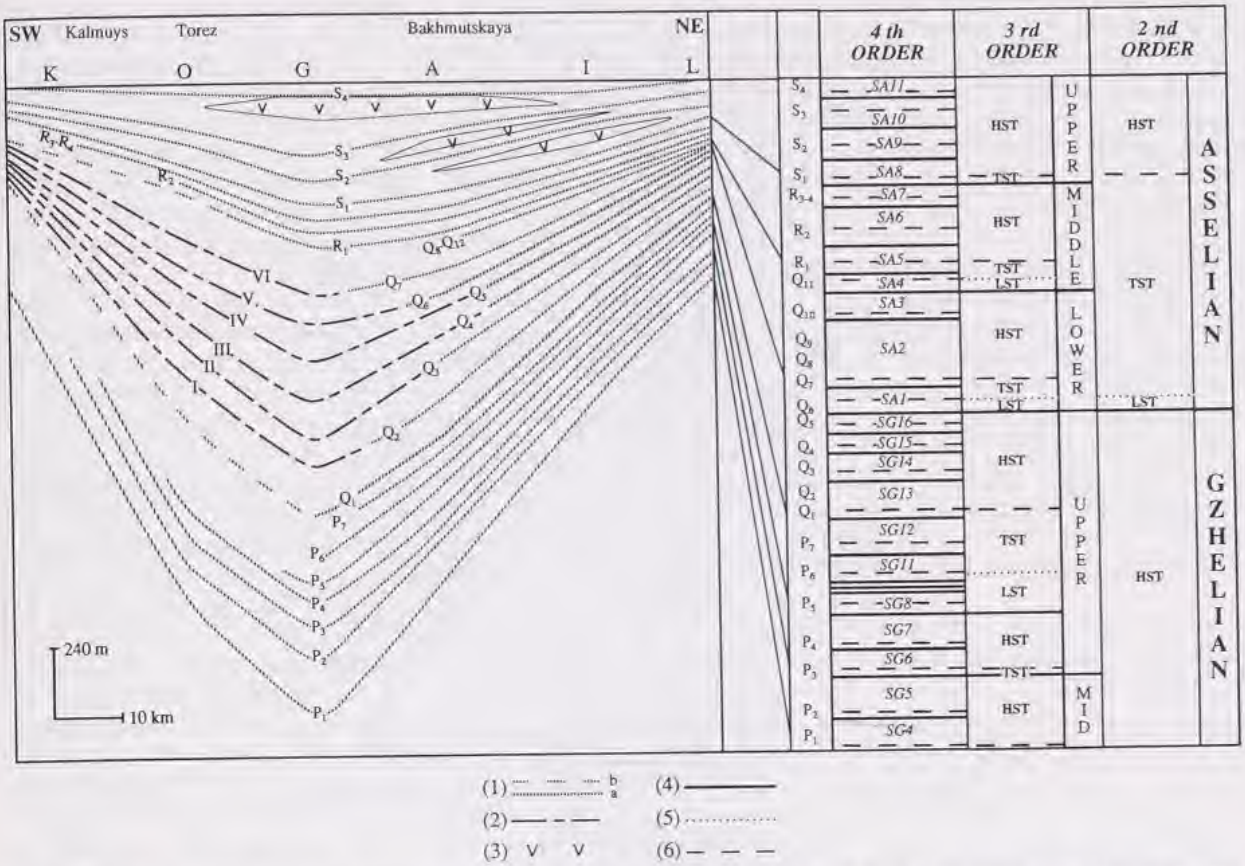

FIG. 7.— Lithostratigraphy and sequence stratigraphy of the upper Gzhelian and Lower Permian in the Donets Basin. A: Artemovsk. G: Gorlovka. I: Ivano-darievka. K: Khourakhovka. L: Lisitschansk. O: Otcheremuno. (1) Limestone, a: actual, b: supposed; (2) Palynological zone; (3) Halite; (4) Sequence boundary; (5) Flooding surface; (6) Maximal flooding surface.

FIG. 7.— Lithostratigraphie et stratigraphie séquentielle du Gzhélien supérieur et du Permien inférieur dans le bassin du Donetz. A : Artemovsk. G : Gorlovka. I : Ivano-darievka. K : Khourakhovka. L : Lisitschansk. O : Otcheremuno. (1) Calcaire, a : observé, b : supposé ; (2) biozone palynologique ; (3) Halite ; (4) limite de séquence ; (5) surface d'inondation ; (6) surface d'inondation maximale.

Kasimovian can present gaps in the Donets Basin. The second second order sequence presents four third order sequences and shows a lowstand system tract with a strong erosion between the base of the sandstone on O_4^5 and o_2^5 below O_6 a transgressive system tract between o_5^2 and O_7, a highstand system tract between O_7 and the base of the sandstone on Q_5.

The Asselian is a second order sequence with a lowstand system tract at the base, a transgressive system tract between Q_6 and S_1, a maximal flooding surface in S_1 known in the Dnieper Basin, a highstand system tract between S_1 and T_1. In the Ural Basin, work in progress shows that the Asselian is also a second order sequence with a highstand system tract in the third third order sequence. In the Donets Basin, only the lower Sakmarian is present and continues the Asselian sequence. Artinskian, Kungurian are absent and only Tatarian is present in the Upper Permian.

DISCUSSION ON THE GEOLOGICAL CONTROLS

The geological controls on the third and fourth order sequences are multiple. They include local and regional tectonic subsidence and uplift, sedimentary processes, climate and eustasy of glacial or plate-tectonics origin. The sequence periodicity does not allow separation of the glacio or tectonic eustasy for

Source : MNHN, Paris

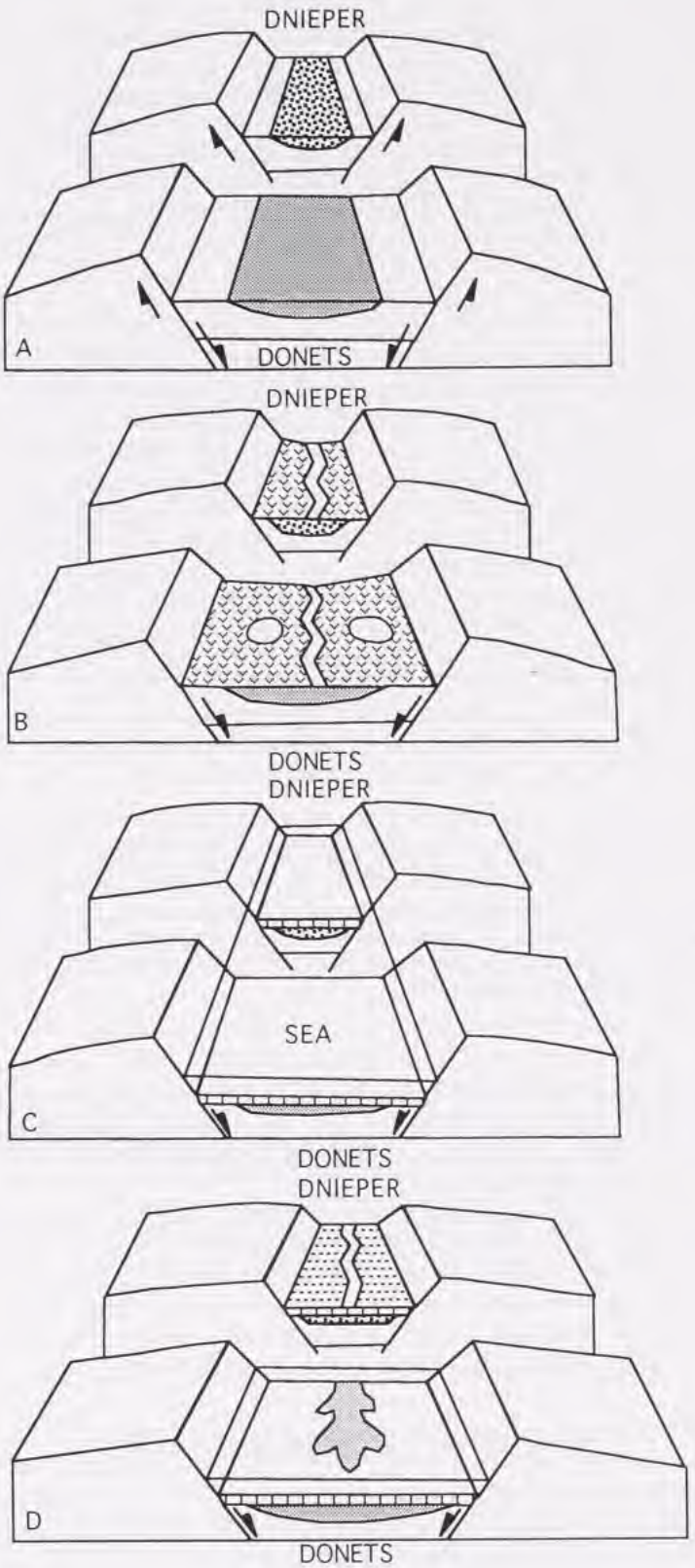

Source : MNHN, Paris

the third and fourth order sequences (CARTER *et al.*, 1991) as well as the effects of regional tectonics (DICKINSON *et al.*, 1994, p. 29). Using the spatial sequence amplitude, it is possible to separate local, regional and global events. The fourth, third and second order sequences have been identified all over the Donets Basin. The fourth order sequences are different in the transitional area and the more marine area. However, it should be possible to follow them and find their equivalents as well as their continuation in the Donets and Dnieper basins. For the elementary sequences we assume the continuity of the marine band, limestone becoming a lagoonal claystone westwards, indicating a maximal flooding surface. However, erosion has destroyed many elementary sequences in the more continental area and it is illusive to follow them far to the west across the continental area.

IZART & VACHARD (1994) hoped to separate tectonic and eustatic controls in comparing the Moscow Basin, which shows a little tectonic subsidence and is more sensitive to eustasy, with the Donets Basin where the tectonic subsidence is more important. Both basins are located on the same plate, the Russian plate and both basins have an open connection with the Tethys ocean. In the Moscow Basin, BRIAND *et al.* (in press) checked the validity of the fourth order sequences described by YABLOKOV *et al.* (1975). The same sequences were found in the Moscow and Donets basins. However, this result does not prove their glacio-eustatic origin because the Moscow basin became subjected to uplift of the Voronezh horst that separated the Donets Basin and the Moscow Basin. Numerous uplifts of the platform are recorded for the Moscow Basin during the Bashkirian and the lower Moscovian and regional tectonics could produce these sequences. However, each third order sequence corresponds to a biozone of fusulinids. Lithological and biological sequences are identical. Therefore, allocyclic factors including tectonic subsidence, eustasy and climate produce these evolutions.

TUCKER *et al.* (1993, p. 399) showed that during the "icehouse" time, when an icecap covered the pole, the third order sequences present a smaller amplitude than the fourth order sequence. During the Carboniferous, a polar ice cap existed on Gondwana (VEEVERS & POWELL, 1987; CROWELL, 1995) and could explain these fourth order sequences. The study of the sequence cyclicity by Walsh analysis (BEAUCHAMP, 1984) and comparison with Milankovitch periodicities (DE BOER & SMITH, 1994) allows to test this hypothesis. In that case, a better accuracy of time by the radiochronology is needed to calibrate the sequences of the Donets basin.

The drift of the Pangea into equatorial latitude during Carboniferous and tropical latitude near the Carboniferous / Permian boundary (SCOTESE & MCKERROW, 1990; SCOTESE & LANGFORD, 1995) explains the differences in climate (wet / dry), lithology (coal / evaporites, red beds) and plants (hygrophilous / xerophylous) between Carboniferous and Permian. The disappearance of coals, the appearance of red beds and evaporites in the Donets Basin are explained by the increase of dryness and establishment of monsoons induced by the perfect symmetry of continents forming Pangea approximately at the equator (BESLY, 1987; KUTZBACH & GALLIMORE, 1989; CECIL, 1990; BARRON & FAWCETT, 1995; PARRISH, 1995).

FIG. 8.— Blocks diagrams of the Dnieper-Donets rift during the genesis of a fourth order sequence in the Kasimovian and the Gzhelian time. **A**: Uplift of the Voronezh and Ukrainian horsts and / or global eustatic fall, erosion and fluvial deposition in the Dnieper-Donets graben. This period corresponds to a tectonic and/or eustatic lowstand system tract. **B**: Tectonic subsidence in the Dnieper-Donets graben and / or global eustatic rise with flooding that stops the fluvial deposits up-stream and allows the settlement of large swamp (coal). This period corresponds to a tectonic and / or eustatic transgressive system tract. **C**: Tectonic subsidence in the Dnieper-Donets graben and / or global eustatic rise with a maximal flooding and deposits of the marine limestones and claystones. This period corresponds to a tectonic and / or eustatic maximal flooding period. **D**: Tectonic subsidence in the Dnieper-Donets graben and / or filling by the deltas. At first, the environment is marine and then, gradually becomes lagoonal or lacustrine. This period corresponds to a tectonic and / or eustatic highstand system tract.

*FIG. 8.— Blocs diagrammes du rift du Dnieper-Donetz lors de la génèse d'une séquence du quatrième ordre pendant le Kasimovien et le Gzhélien. **A** : Soulèvement des horsts du Voronezh et de l'Ukraine et / ou chûte eustatique globale, erosion et dépôt fluviatile dans le graben du Dnieper-Donetz. Cette période correspond au cortège de bas niveau tectonique et / ou eustatique. **B** : Subsidence tectonique dans le graben du Dnieper-Donetz et / ou montée eustatique globale avec l'inondation qui bloque le dépôt fluviatile en amont et permet l'installation de marécage (charbon) sur de grande surface. Cette période correspond à un cortège transgressif tectonique et / ou eustatique. **C** : Subsidence tectonique dans le graben du Dnieper-Donetz et / ou montée eustatique globale avec une inondation maximale et des dépôts de calcaires et argilites marines. Cette période correspond à la période d'inondation maximale tectonique et / ou eustatique. **D** : Subsidence tectonique dans le graben du Dnieper-Donetz et / ou remplissage par les deltas. L'environnement est tout d'abord marin, et puis graduellement il devient lagunaire ou lacustre. Cette période correspond au cortège de haut niveau tectonique et / ou eustatique.*

Source : MNHN, Paris

Tectonic events at the scale of the Russian plate were the cause of these fourth order sequences with a superposition of glacio-eustatic oscillations. Figure 8 represents block diagrams of the Dnieper-Donets rift during a fourth order sequence in Late Carboniferous time. Each sequence presents four periods:

— the uplift of the Voronezh and Ukrainian horsts and / or the global eustatic fall, the erosion and the fluvial deposition in the Dnieper-Donets graben. This period corresponds to a tectonic and / or eustatic lowstand system tract.

— the tectonic subsidence in the Dnieper-Donets graben and / or global eustatic rise with a flooding that stops the fluvial deposits up-stream and allows the settlement of large swamp (coal seams). This period corresponds to a tectonic and / or eustatic transgressive system tract.

— the tectonic subsidence in the Dnieper-Donets graben and / or global eustatic rise with a maximal flooding and deposits of marine limestones and claystones. This period corresponds to a tectonic and / or eustatic maximal flooding period.

— the tectonic subsidence in the Dnieper-Donets graben and / or the filling by deltas. At first, the environment is marine and then, gradually becomes lagoonal or lacustrine. This period corresponds to a tectonic and / or eustatic highstand system tract.

An uplift or a tectonic inversion period occur between lower Sakmarian and Tatarian and between Tatarian and Lower Triassic.

CONCLUSION

New results concern the stratigraphy and the sequence stratigraphy of the Kasimovian, Gzhelian and Lower Permian in the Donets Basin and the geological controls in this basin. The Kasimovian corresponds to the lower Stephanian of the western Europe, the Gzhelian to the upper Stephanian and the lowermost Autunian, the Asselian to the uppermost Autunian. The Kasimovian, Gzhelian and Asselian are second order sequences and the fourth order sequences obscure the third order sequences in the Donets basin. This fact was yet known in the Moscow basin, the western Europe and the USA (IZART & VACHARD, 1994). Nevertheless, it is possible to distinguish three third order sequences equivalent to the lower, middle and upper Kasimovian, four third order sequences equivalent to the Gzhelian and three third order sequences equivalent to the Asselian, which can be further subdivided into fourth order sequences. The sequences are controlled by the regional tectonic subsidence in the graben and the uplift of the horsts and / or by eustasy with either a plate-tectonic or a glacial origin. Each third order sequence corresponds to a biozone of fusulinids. Lithological and biological sequences are identical. The thickness and tectonic subsidence decrease gradually between the Moscovian and Sakmarian. Hiatus exist betwen the Sakmarian and Tatarian and between Tatarian and Lower Triassic, corresponding to an uplift or a tectonic inversion period. The drift of the Pangea into equatorial latitude during Carboniferous and tropical latitude near the Carboniferous / Permian boundary explains the differences in climate, lithology and plants between Carboniferous and Permian.

ACKNOWLEDGEMENTS

We thank Professor STSCHEGOLEV, all the participants of the field mission during year 1994 in the Donets basin and N. ZHIKALIAK of the Donbass geological survey in Artemovsk. This study was carried out under a French-Ukrainian project financed by the Peri-Tethys program and BRGM. This note is a contribution of the IGCP 343, the Peri-Tethys program and of the UMR-CNRS 7566 G2R.

REFERENCES

AISENVERG, D.E., BRAZHNIKOVA, N.E., NOVIK, K.O., ROTAY, A.P. & SHULGA, P.L., 1960.— Carboniferous stratigraphy of the Donets Basin. *In*: *Compte Rendu du 4ème Congrès international sur la stratigraphie du Carbonifère, Heerlen, 15-20 septembre 1958*. Vol. 1. E. Van Aelst, Maestricht: 1-12.

AISENVERG, D.E., LAGUTINA, V.V., LEVENSTEIN, M.L. & POPOV, V.S., 1978.— Field excursion guidebook for the Donets Basin. *In*: *Compte Rendu du 8ème Congrès international sur la stratigraphie du Carbonifère, Moscow, 1975*. Nauka, Moscow: 1-360.

Source : MNHN, Paris

ALEKSEEVA, I.A., GLUSHENKO, N.V., IVANOV, V.K., INOSOVA, K.I., KALMYKEVA, M.A., KASHIK, D.S., KOSITSKAYA, R.J., KRUSINA, A.K.H., MOVSKOVICH, E.V., REDITCHIN, N.A. & SIVARTSMAN, E.G., 1983.— *Key Section of Boundary Carboniferous-Permian Beds of the South of Eastern European Platform (Gzhelian and Asselian Stages, Skosyrskaya Bore Hole N 4199).* Vol. 50. Nauka, Leningrad: 1-123 (in Russian).

BARON, E.J. & FAWCETT, P.J., 1995.— The climate of Pangaea: a review of climate model simulations of the Permian. *In*: P.A. SCHOLLE, T.M. PERYT & D.S. ULMER-SCHOLLE (eds), *The Permian of Northern Pangea*. Vol. 1. Springer, Berlin: 37-52.

BEAUCHAMP, K.G., 1984.— *Applications of Walsh and Related Functions; with an Introduction to Sequence Theory*. Academic Press, London: 1-308.

BECQ-GIRAUDON, J.-F., 1993.— Problèmes de la biostratigraphie dans le Paléozoïque supérieur continental (Stéphanien-Autunien) du Massif central. *Geodynamica Acta*, **6** (4): 219-224.

BESLY, B.M., 1987.— Sedimentological evidence for Carboniferous and Early Permian paleoclimates of Europe. *Annales de la Société géologique du Nord*, **106**: 131-143.

BOYARINA, N., (submitted).— Phytocoenosis characteristic of the Late Carboniferous-Early Permian for the Donets basin of Ukraine. *In*: *Comptes Rendus du 13ème Congrès international sur la stratigraphie du Carbonifère - Permien, Krakow, 1995.*

BOYARINA, N, 1994.— Callipterid pteridosperms from the Early Permian of Ukraine. *Acta Paleontologica Polonica*, **39** (1): 117-133.

BRIAND, C., IZART, A., VASLET, D., VACHARD, D., MAKHLINA, M., GOREVA, N., KOSSOVAYA, O. & JAROSHENKO, A., in press.— Sequence stratigraphy of the Moscovian, Kasimovian and Gzhelian in the Moscow basin. *Bulletin de la Société géologique de France*, **169** (1).

BROUTIN, J., DOUBINGER, J., FARJANEL, G., FREYTET, P., KERP, H., LANGIAUX, J., LEBRETON, M.-L., SEBBAN, S. & SATTA, S., 1990.— Le renouvellement des flores au passage Carbonifère Permien: approches stratigraphique, biologique, sédimentologique. *Comptes Rendus de l'Académie des Sciences, Paris*, **311** (II): 1563-1569.

BROUTIN, J., DOUBINGER, J., LANGIAUX, J. & PRIMEY, D., 1986.— Conséquences de la coexistence de flores à caractères stéphaniens et autuniens dans les bassins limniques d'Europe occidentale. *Mémoires de la Société géologique de France, Nouvelle Série*, **149**: 15-25.

CARTER, R.M., ABBOTT, S.T., FULTHORPE, C.S., HAYWICK, D.W. & HENDERSON, R.A., 1991.— Application of global sea-level and sequence-stratigraphic models in Southern Hemisphere Neogene strata from New Zealand. *In*: D.I.M. MCDONALD (ed.), Sedimentation, Tectonics and Eustasy. *Special Publications of International Association of Sedimentologists*, **12**: 41-65.

CECIL, C.B., 1990.— Paleoclimate controls on stratigraphic repetition of chemical and siliciclastic rocks. *Geology*, **18**: 533-536.

CHEKUNOV, A.V., KALUZHNAYA, L.T. & RYABCHUN, L.I., 1993.— The Dnieper-Donets Paleorift, Ukraine: deep structures and hydrocarbon accumulations. *Journal of Petroleum Geology*, **16** (2): 183-196.

CROWELL, J.C., 1995.— The ending of the Late Paleozoic ice age during the Permian period. *In*: P.A. SCHOLLE, T.M. PERYT & D.S. ULMER-SCHOLLE (eds), *The Permian of Northern Pangea*. Vol. 1. Springer, Berlin: 62-74.

DAVYDOV, V.I., 1990.— Biostratigraphic zones of the Gzhelian in the Donbas and Pre-Donets basins according to the Fusulinids. *In*: J.N. BOGDANOVA & E.M. BUGROVA (eds), *Problems of Modern Micropaleontology, Proceedings of the 34th Session of the All Union Palaeontology Society, Baku, 1988*: 52-69 (in Russian).

DAVYDOV, V.I., 1992.— Subdivision and correlation of Upper Carboniferous and Lower Permian deposits of the Donets basin and Pre-Donets trough based on fusulinids. *Soviet Geology*, **5**: 53-61 (in Russian).

DAVYDOV, V.I., 1993.— *New data on Correlation of Standart Scales of Upper Carboniferous and Lower Permian Marine and Continental Deposits (according to Donetz Basin Sections)*. Pangea, Calgary, Abstracts: 1-71.

DE BOER, P.L. & SMITH, D.G., 1994.— Orbital forcing and cyclic sequences. *In*: P.L. DEBOER & D.G. SMITH (eds), Orbital forcing and cyclic sequences. *Special Publications of International Association of Sedimentologists*, **19**: 1-14.

DICKINSON, W.R., SOREGHAN, G.S. & GILES, K.A., 1994.— Glacio-eustatic origin of Permo-Carboniferous stratigraphic cycles: evidence from southern cordilleran foreland region. *In*: J.M. DENNISON & F.R. ETTENSOHN (eds), Tectonic and eustatic controls on sedimentary cycles. *SEPM, Concepts in Sedimentology and Paleontology*, **4**: 25-34.

DOUBINGER, J., VETTER, P., LANGIAUX, J., GALTIER, J. & BROUTIN, J., 1995.— La flore fossile du bassin houiller de Saint-Étienne. *Mémoires du Muséum national d'Histoire naturelle*, **164**: 1-356.

HESS, J.C. & LIPPOLT, H.J., 1986.— $^{40}Ar / ^{39}Ar$ ages of tonstein and tuff sanidines: new calibration points for the improvement of the Upper Carboniferous time scale. *Isotope Geoscience*, **59**: 143-154.

INOSOVA, K.I., KRUZINA, A.H. & SCHVATSMAN, E.G., 1976.— *Atlas of Microspores and Pollens from the Upper Carboniferous and Lower Permian of the Donets Basin*. Nedra, Moscow: 1-176 (in Russian).

IZART, A. & VACHARD, D., 1994.— Subsidence tectonique, eustatisme et contrôle des séquences dans les bassins namuriens et westphaliens de l'Europe de l'Ouest, de la CEI et des USA. *Bulletin de la Société géologique de France*, **165** (5): 499-514.

IZART, A., BRIAND, C., VASLET, D., VACHARD, D., COQUEL, R. & MASLO, A., 1996.— Stratigraphy and sequence stratigraphy of the Moscovian in the Donets basin. *Tectonophysics*, **268**: 189-209.

Source : MNHN, Paris

JIN YU-GAN, SHENG JIN-ZHANG, GLENISTER, B.F., FURNISH, W.M., KOTLYAR, G.V., WARDLAW, B.R., KOZUR, H., ROSS, C.R. & SPINOSA, C., 1994.— Revised operational scheme of Permian chronostratigraphy. *Permophiles, Newsletter of SCPS*, **25**: 12-15.

KAGARMANOV, A.K. & DONAKOVA, L.M., 1990.— *Decisions of the Regional Stratigraphic Conference on the Middle and Upper Paleozoic of the Russian Platform, Leningrad 1988, Carboniferous System.* VSEGEI, 92 fig. (in Russian).

KHRAMOV, A.N. & DAVYDOV, V.I., 1984.— Paleomagnetism method and Stratigraphy. *Trudi VNIGRI, Leningrad*: 55-73 (in Russian).

KHRAMOV, A.N. & DAVYDOV, V.I., 1993.— Results of paleomagnetic investigations. *In*: V.A. CHERMYNKH, V.V. CHERNYKH & B.I. CHUVASHOV (eds), Permian system: guide to geological excursions in the uralian type localities. *Publications ESRJ, New Series*, **10**: 34-41.

KHRAMOV, A.N., 1963.— Paleomagnetic investigations of upper Paleozoic and Triassic in the western part of the Donets basin. *Trudi VNIGRI, Leningrad*, **204**: 96-117 (in Russian).

KOZITSKAYA, R.I., KOZENKO, Z.A., LIPIAGOV, O.M. & NEMIROVSKAIA, T.I.K., 1978.— *Conodonts of the Carboniferous of the Donets Basin*. Akademia Nauk Ukraine: 1-136 (in Russian).

KUTZBACH, J.E. & GALLIMORE, R.G., 1989.— Pangaean climates: megamonsoons of the megacontinent. *Journal of Geophysical Research*, **94**: 3341-3357.

LAPTCHIK, T.I. (ed.), 1970.— *Stratigraphy of the Permian of the Ukraine*. Vol. 6. Naukova Doumka, Kiev: 1-278 (in Russian).

LAVEINE, J.P., 1986.— La flore du bassin houiller du Nord de la France, biostratigraphie et méthodologie. *Annales de la Société géologique du Nord*, **106**: 87-94.

MAKAROV, I.A., 1982.— *Description of the Stratigraphic Cross-Sections of the Lower and Middle Carboniferous of the Donets Basin*. Ukraine Geology Ministery, PGO Donbas Geology, Artemovsk GPE (in Russian).

MAKAROV, I.A., 1985.— *Description of the Stratigraphic Cross-Sections of the Upper Carboniferous of the Donets Basin*. Ukraine Geology Ministery, PGO Donbas Geology, Artemovsk GPE (in Russian).

MENNING, M., 1995.— A numerical time scale for the Permian and Triassic periods: an integrated time analysis. *In*: P.A. SCHOLLE, T.M. PERYT & D.S. ULMER-SCHOLLE (eds), *The Permian of Northern Pangea*. Vol. 1. Springer, Berlin: 77-97.

MENNING, M., KATZUNG, G. & LÜTZNER, H., 1988.— Magnetostratigraphic investigations in the Rotliegende (300-252 Ma) of central Europe. *Zeitschrift fuer Geologische Wissenschaften*, **16**: 1045-1063.

MOVSKOVICH, E.V. & REDICHKIN, N.A., 1980.— The correlation of the Carboniferous-Permian boundary beds along margins of the Donets folded edifice. *In*: S.V. MEYEN (ed.), *Biostratigraphy of the Carboniferous-Permian boundary beds*. Akademia Nauk SSSR, Moscow: 23-29 (in Russian).

MOVSKOVICH, E.V. & REDICHKIN, N.A., 1984.— Correlation of Kasimovian, Gzhelian and Asselian in the Donets basin. *In*: V.V. MENNER & A.D. GRIGORIEVA (eds), *The Upper Carboniferous of the USSR*. Akademia Nauk SSSR, Moscow: 60-65 (in Russian).

NESTERENKO, L.P. & KIREEVA, G.D., 1980.— The stratigraphy and sedimentation of the Lower Permian (Asselian stage) of the Donets basin. *In*: S.V. MEYEN (ed.), *Biostratigraphy of the Carboniferous-Permian boundary beds*. Akademia Nauk SSSR, Moscow: 29-41 (in Russian).

ODIN, G.S., 1994.— Geologic time scale. *Comptes Rendus de l'Académie des Sciences, Paris*, **318** (2): 59-71.

PARRISH, J.T., 1995.— Geologic evidence of Permian climate. *In*: P.A. SCHOLLE, T.M. PERYT & D.S. ULMER-SCHOLLE (eds), *The Permian of Northern Pangea*. Vol. 1. Springer, Berlin: 54-61.

REMIZOVA, S.T., 1995.— Foraminifera and biostratigraphy of the Upper Carboniferous in North Timan. *Doklady Akademii Nauk SSSR*: 1-128 (in Russian).

SALVADOR, A. (ed.), 1995.— *International Stratigraphic Guide*. Second edition copublished by the International Union of Geological Sciences and The Geological Society of America: 1-214.

SCHNEIDER, J.W., RÖSSLER, R.R. & GAITSCH, B.G., 1995.— Proposal for a combined reference section of the central european continental Carboniferous and Permian for correlations with marine standard sections. *Permophiles, Newsletter of SCPS*, **26**: 26-32.

SCOTESE, C.R. & LANGFORD, R.P., 1995.— Pangea and the paleogeography of the Permian. *In*: P.A. SCHOLLE, T.M. PERYT & D.S. ULMER-SCHOLLE (eds), *The Permian of Northern Pangea*. Vol. 1. Springer, Berlin: 3-19.

SCOTESE, C.R. & MCKERROW, W.S., 1990.— Revised world maps and introduction. *In*: W.S. MCKERROW & C.R. SCOTESE (eds), Paleozoic paleogeography and biogeography. *Geology Society, Memoires*, **12**: 1-21.

SEMINA, S.A., 1984.— Correlation of some cross-sections of upper Carboniferous in the Donets basin with Fusulinids. *In:* V.V. MENNER & A.D. GRIGORIEVA (eds), *The Upper Carboniferous of the USSR*. Akademia Nauk SSSR, Moscow: 56-60 (in Russian).

SHANLEY, K.W. & MC CABE, P.J., 1994.— Perspectives on the sequence stratigraphy of continental strata. *American Association of Petroleum Geologists, Bulletin*, **78**: 544-568.

SOLOVIEVA, M.N., 1985.— Correction of the USSR general Carboniferous scale in connection with restudying the Moskovian stage stratotype and a new model for the correlation of the lower Moskovian substage. *In*: *Compte Rendu du 10ème Congrès international de stratigraphie et de géologie du Carbonifère, Madrid, 1983*. Vol. 1. Instituto geologico y minero de España, Madrid: 21-26.

Source : MNHN, Paris

SOLOVIEVA, M.N., CHIZHOVA, V.A., EINOR, O.L., GRIGORIEVA, A.D., REITLINGER, E.A. & VDOVENKO, M.V., 1985.— Review of recent data on the Carboniferous stratigraphy of the USSR. *In*: *Compte Rendu du 10ème Congrès international de stratigraphie et de géologie du Carbonifère, Madrid, 1983*. Vol. 1. Instituto geologico y minero de España, Madrid: 3-10.

SOLOVIEVA, M.N., FISUNENKO, O.P., GOREVA, N.V., BARSKOV, I.S., GUBAREVA, I.S., DZHENCHURAEVA, A.V., DALMATSKAIA, I.I., IVANOVA, E.A., POLETAEV, V.I., POPOV, A.V., RUMYANTSEVA, Z.S., TETERUK, V.K. & SHIK, E.M., 1985.— New data on stratigraphy of the Moskovian stage. *In*: *Compte Rendu du 10ème Congrès international de stratigraphie et de géologie du Carbonifère, Madrid, 1983*. Vol. 1. Instituto geologico y minero de España, Madrid: 11-20.

STEPHENSON, R.A. & the Europrobe intraplate tectonics and basin dynamics Dnieper-Donets working groups, 1993.— Continental rift development in Precambrian and Phanerozoic Europe: Europrobe and the Dnieper-Donets rift and Polish trough basins. *Sedimentary Geology*, **86**: 159-175.

STOVBA, S., STEPHENSON, R.A. & DVORIANIN, E., 1995.— Dnieper-Donets Basin, Ukraine: main observations from regional seismic reflection profiles. *Comptes Rendus de l'Académie des Sciences, Paris*, **321** (IIa): 1103-1110.

STSCHEGOLEV, A.K. & KOZITSKAYA, R.I., 1984.— The paleontological basis of the project of the Upper Carboniferous standart scale in the Europe and the central Asia. *In*: V.V. MENNER & A.D. GRIGOREVA (eds), *The Upper Carboniferous of the USSR*. Nauka, Moscow: 107-113 (in Russian).

STSCHEGOLEV, A.K., 1960.— From the middle Carboniferous to the Permian across the Flora. *Geological Journal*, **20**: 47-57 (in Russian).

STSCHEGOLEV, A.K., 1965.— Flora of the boundary between Carboniferous and Permian. *In*: D.L. STEPANOV & P.P. TIMOFEEV (eds), *Geology and Stratigraphy of the Carboniferous*. Nauka, Moscow: 234-243 (in Russian)

STSCHEGOLEV, A.K., 1975.— Die Entwicklung der Pflanzenbedeckung im Suden des Europäischen Teils der USSR, vom Ende des Mittelskarbons bis zum Perm. Umfang und Gliederung des oberen Karbons (Stefan). *In*: *Compte Rendu du 7ème Congrès international de stratigraphie et de géologie du Carbonifère, Madrid, 23-28 aug. 1971*. Vol. 4. Geolog. Landesamt Nordrhein-Westfalen, Krefeld: 275-280.

TUCKER, M.E., CALVET, F. & HUNT, D., 1993.— Sequence stratigraphy of carbonate ramps: system tracts, models and application to the Muschelkalk carbonate platforms of eastern Spain. *In*: H.W. POSAMENTIER, C.P. SUMMERHAYES, B.U. HAQ & G.P. ALLEN (eds), Sequence stratigraphy and facies associations. *Special Publications of International Association of Sedimentologists*, **18**: 397-415.

VAN WAGONER, J.C., POSAMENTIER, H.W., MITCHUM, R.H., VAIL, P.R., SARG, J.F., LOUTIT, T.S. & HARDENBOL, J., 1988.— An overview of the fundamentals of sequence stratigraphy and key definition. *In*: C.K. WILGUS (ed.), Sea-level changes - an integrated approach. *SEPM Special Publication*, **42**: 39-45.

VEEVERS, J.J. & POWELL, C.M.C.A., 1987.— Late Paleozoic glacial episodes in Gondwanaland reflected in transgressive-regressive depositional sequences in Euramerica. *Geological Society American Bulletin*, **98**: 475-487.

VILLA, E., DAVYDOV, V.I., KONOVALOVA, M.V. & REMIZOVA, S., 1993.— Studies on the base of the *Protriticites* zone. A report on SCCS project group 5. *Annales de la Société géologique de Belgique*, **116**: 323-331.

YABLOKOV, V.S., LEONENKO, V.S., MIKHAILOVA, E.V., BELSKAYA, T.N. & REITLINGER, E.A., 1978.— Field excursion guidebook for the Carboniferous sequences of the Moscow basin. *In*: *Compte Rendu du 8ème Congrès international sur la stratigraphie du Carbonifère, Moscow, 1975*. Nauka, Moscow: 1-176.

ZHEMCHUZHNIKOV, Y.A., YABLOKOV, V.S., BOGOLIOUBOVA, L.I., BOTVINKINA, L.I., FEOFILOVA, A.P., RITENBERG, M.I., TIMOFEEV, P.P. & TIMOFEEVA, Z.B., 1959-1960.— Structure and environment of the main coal-bearing suites and coal seams of the Middle Carboniferous of the Donetz basin. *Trudy Geological Institute, Akademia Nauk SSSR*, **15** (1): 1-332, (1959) and **2**: 1-347, (1960) (in Russian).

Source : MNHN, Paris

Source : MNHN, Paris

2

Stratigraphic correlations of the Upper Permian and Triassic beds from the Volga-Ural and Cis-Caspian

Edward A. MOLOSTOVSKY, Ija I. MOLOSTOVSKAYA & Maxim G. MINIKH

Saratov State University, Moskovskaya str., 161, 410750 Saratov, Russia

ABSTRACT

Correlation of the Upper Permian and Triassic deposits from the East of the Russian Plate, Cis-Ural Trough and the North of the Cis-Caspian Depression was performed on the basis of paleontologic, paleomagnetic and lithologic-facies data. Main sedimentation stages were distinguished, the influence of the geologic and climatic factors on sedimentation processes was analyzed. Of main importance in this respect were: hydrochemical regime of the Early Permian residual basin, transgressions of the Boreal Sea during the Kazanian, the Tethys transgressions in the Triassic and increased terrigenous drift from the region of the folded Urals during its tectonic activizations. Stratigraphic units were ranked according the scales and characters of accompanying geologic events.

RÉSUMÉ

Corrélations stratigraphiques dans le Permien supérieur et le Trias des régions Volga-Oural et Cis-Caspienne.

Les corrélations des dépôts du Permien supérieur et du Trias de l'Est de la Plate-forme russe, du Cis-Oural et du Nord de la Cis-Caspienne ont été réalisées sur la base de données paléontologiques, paléomagnétiques et faciologiques. Les principales étapes de la sédimentation sont distinguées, l'influence des facteurs géologiques et climatologiques sur les processus de sédimentation est analysée. De ce point de vue, les événements les plus importants sont le régime hydrochimique du bassin résiduel du Permien inférieur, les trangressions de la Mer Boréale durant le Kazanien, les transgressions de la Téthys au Trias et l'augmentation des apports détritiques depuis la région plissée de l'Oural lors de son activité tectonique. Les unités stratigraphiques sont organisées selon les échelles et les caractères des événements géologiques.

INTRODUCTION

The South Cis-Ural, Lower Volga and North Cis-Caspian regions include a vast area between the Volga River and the Ural Range, with the conventional southern border along the latitude of Inder and Baskunchak lakes (Astrakhan region) and the northern one - in the lower reaches of the Belaya River (Bashkiria). The boundaries of three major geostructures meet in this region: those of the Russian Plate, Cis-Ural Trough and Cis-Caspian Depression (Fig. 1). The main features of the Permo-Triassic sedimentation were determined by the development of these structures.

MOLOSTOVSKY, E.A., MOLOSTOVSKAYA, I.I. & MINIKH, M.G., 1998.— Stratigraphic correlations of the Upper Permian and Triassic beds from the Volga-Ural and Cis-Caspian. *In*: S. CRASQUIN-SOLEAU & E. BARRIER (eds), Peri-Tethys Memoir 3: stratigraphy and evolution of Peri-Tethyan platforms. *Mém. Mus. natn. Hist. nat.*, **177** : 35-44. Paris ISBN : 2-85653-512-7.

Source : MNHN, Paris

From a stratigraphic point of view, the Volga-Ural region is referential for the northern margin of the Tethys. Type sections for the majority of the continental Upper Permian and Triassic units are concentrated here; stratigraphic sequences of the index faunal groupings are studied thoroughly; a detailed magnetic zonality scheme has been produced.

The present paper is based upon geological, paleontological and paleomagnetic materials gained by the authors (MINIKH, 1972, 1977, 1995; MINIKH & MINIKH, 1985, 1995; MOLOSTOVSKAYA, 1987, 1993; MOLOSTOVSKY, 1983, 1995; BLOM *et al.*, 1982; LIPATOVA *et al.*, 1985) and on the research results obtained by a substantial number of geologists (GORSKY & GUSEVA (eds) 1990; SHISHKIN & OCHEV, 1992; TVERDOKHLEBOVA, 1991; ZAMARENOV *et al.*, 1969).

Facies variability of the red-bed sequences makes it difficult to correlate them according to lithologic features, which are of local importance. Regional and remote correlations are usually carried out according to the index fossil complexes; the most accurate results in some stratigraphic intervals are available by means of combined paleomagnetic and paleontologic definitions.

Ostracods are the leading stratigraphic group for the Upper Permian red-bed formation; they allow to divide and correlate the sequences at the stage and horizon levels (GORSKY & GUSEVA eds, 1990; MOLOSTOVSKAYA, 1987, 1993). Terrestrial vertebrates make it possible to recognize only the upper Tatarian substage, characterized by the Pareiasaur-Theriodont fauna. The more ancient, Dinocephalian fauna is common for the Ufimian and Kazanian stages, and for the lower Tatarian substage as well (GORSKY & GUSEVA eds, 1990).

Tetrapods and lungfish are of guiding stratigraphic importance for the Lower and Middle Triassic, palynoflora is important for the upper section (MINIKH & MINIKH, 1985, 1995; LIPATOVA, MINIKH, MOLOSTOVSKY *et al.*,1985; SHISHKIN & OCHEV, 1992). The paleomagnetic data become stratigraphically important in the upper Tatarian substage of the Permian and in the Triassic, where repeated changes of magnetic zonality are recorded. The Ufimian, Kazanian and lower Tatarian beds were formed during the stable period of reverse field (R-Kiama) and are not divisible according to paleomagnetic characteristics (MOLOSTOVSKY, 1983) .

The main regional and local units from various structural-facies zones are presented in figures 2 and 3 together with the guide fossil complexes and schemes of magnetic zonality. The figures were based upon the unified stratigraphic schemes for the Russian Plate, Cis-Ural Trough and Cis-Caspian Depression (GORSKY & GUSEVA eds, 1990; ZHAMOYDA, Lipatova & Romanovskaya (eds), 1982).

STRATIGRAPHIC CORRELATIONS

UPPER PERMIAN

In the most part of the territory considered, all the stages of the Upper Permian are represented in the sections.

The Ufimian stage in the south-east of the Russian Plate is composed of lacustrine-lagoonal deposits: red, more rarely grey clays, siltstones, sandstones, limestones, dolomites with anhydrite and gypsum interlayers (50-200 m thick). Mostly redstones, gypsinate in the lower portion of the section, occur to the east, where the Platform passes to the Trough (up to 190 m thick). Sandstones and coarse-pebble conglomerates prevail in the sections from the eastern part of the Trough (up to 700 m thick). In the north-eastern part of the Cis-Caspian Depression, the Akshatskaya formation (750 m thick), composed of alternating red and grey argillites and sandstones with anhydrite interlayers, is referred to the Ufimian stage.

The Ufimian sections of various facies are correlated according to ostracods belonging to the zonal complex of *Paleodarwinula abunda* (Mandelstam) and miospores of the zonal complex H2-*Granizospora vulgaris* (Naumova).

The Kazanian stage is subdivided into the lower and upper substages.

The lower Kazanian substage within the south-east of the Russian Plate, the western zone of the Cis-Ural Trough and the north-western part of the Cis-Caspian Depression, comprises various grey marine rocks up to 120-150 m thick. In the sections from the south-east of the Russian Plate, the lower Kazanian sequence is carbonate-halogenic; limestones and dolomites dominate, sandstones, halite and

Source : MNHN, Paris

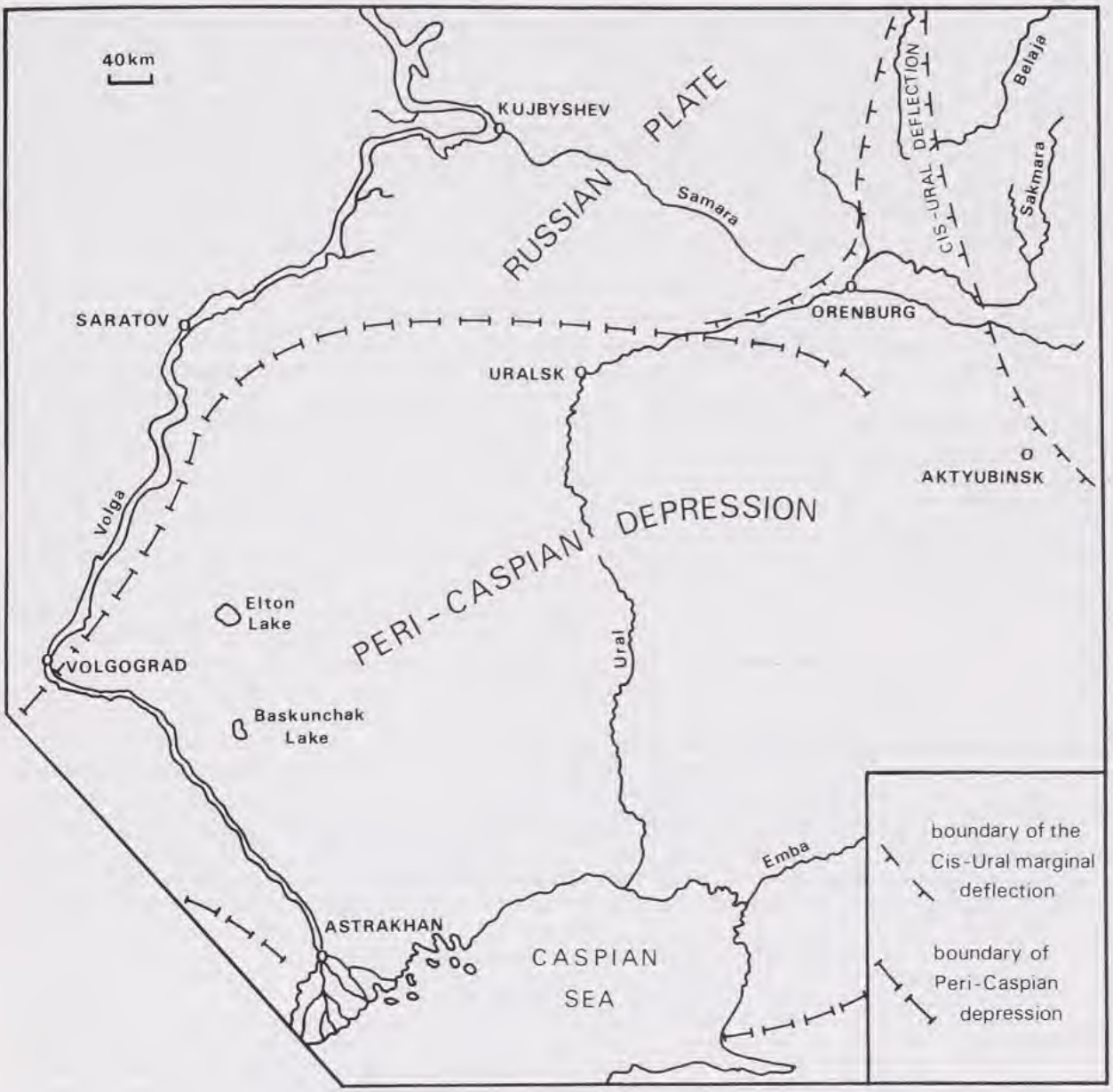

FIG. 1.— Key map of the Volga-Ural and Cis-Caspian regions.
FIG. 1.— Carte des régions Volga-Oural et Cis-Caspienne.

anhydrites are less common. According to the ratio of various lithotypes, the substage there comprises the Bajtuganskaya, Kamyshlinskaya and Barbashinskaya members (GORSKY & GUSEVA eds, 1990). In the western part of the Trough, clay-aleurolitic deposits with occasional interlayers of bioaccumulated limestones are common (70-100 m thick). In the axial zones, marine facies give way to lacustrine-lagoonal grey sandstones, siltstones and argilites containing charred plant detritus and rare marl interlayers (up to 600 m thick). In the eastern part of the Cis-Ural Trough, accumulations from saliferous lagoons occur: dolomites, anhydrites, gypsums with halitic interlayers (KULEVA, 1975).

The marine beds contain numerous remains of foraminifers, brachiopods, fish, leafy flora and miospores of the zonal complex J1 - *Striatopodocarpites tojmensis* Sedova. The palynocomplexes from

Source : MNHN, Paris

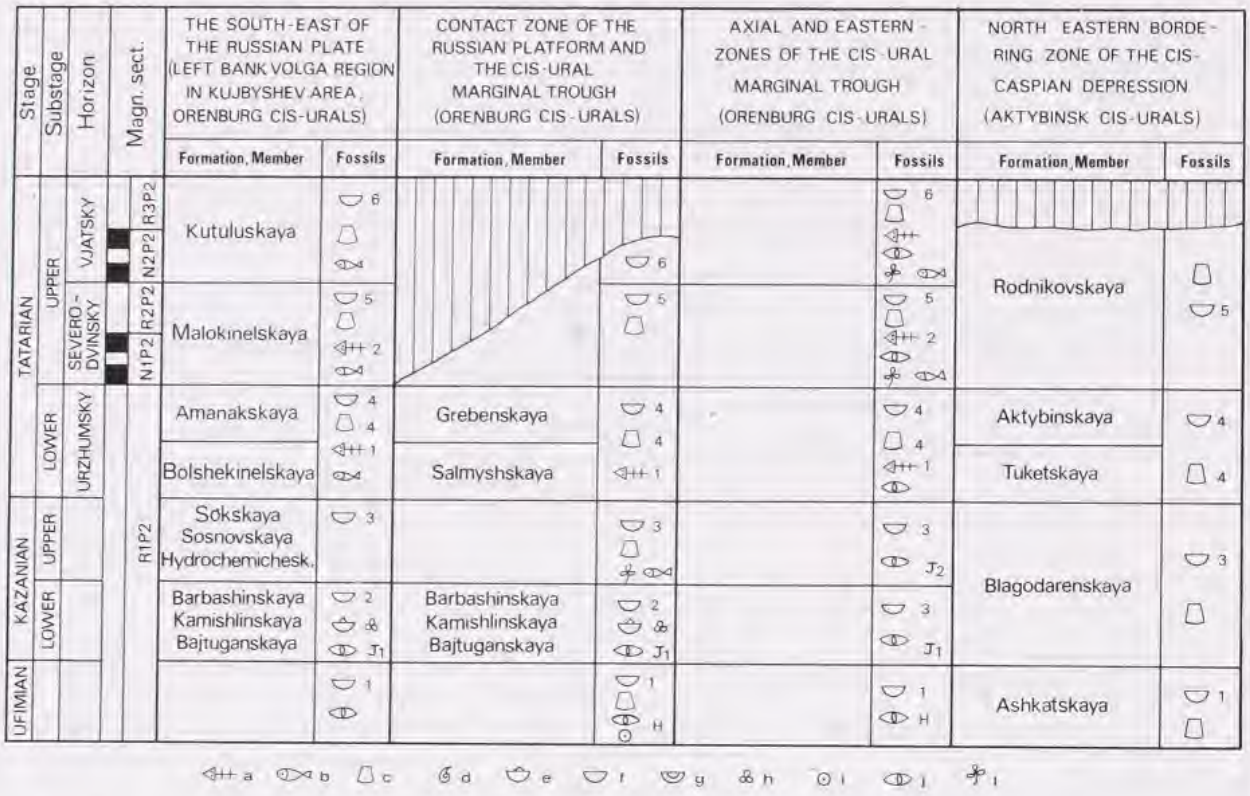

FIG. 2.— Correlation of the Upper Permian regional stratigraphic schemes.
Symbol for figures 2 and 3: **a**, tetrapods; **b**, fishes; **c**, bivalves; **d**, ammonites; **e**, brachiopods; **f**, ostracods; **g**, conchostracans; **h**, foraminifers; **i**, harofites; **j**, miospores; **l**, flora.
Guide fauna and flora groups in the Permian stratigraphy: Tetrapods: 1, *Dinocephalia*; 2, *Chroniosaurus dongusensis* Tverdochlebova; 3, *Chroniosuchus uralensis* Tverdochlebova. Bivalvia: 4, *Palaeomutela vjatkensis* Gusev. Ostracod: 1, *Paleodarwinula abunda* (Mandelstam); 2, *Amphissites tscherdynzevi* Posner; 3, *Paleodarwinula fainae* (Belousova); 4, *Paleodarwinula fragiliformis* (Kashevarova), *Suchonellina futshiki* (Kashevarova), *Suchonellina trapesoida* (Sharapova). Miospores: H, *Granizospora vulgaris* Naumova; J1, *Striatopodocarpites tojmensis* Sedova; J2, *Lueckisporites virkkia* Potonie & Kremp.

FIG. 2.— Corrélation des schémas stratigraphiques régionaux du Permien supérieur.
*Symboles pour les figures 2 et 3: **a**, tétrapodes; **b**, poissons; **c**, bivalves; **d**, ammonites; **e**, brachiopodes; **f**, ostracodes; **g**, conchostracés; **h**, foraminifères; **i**, harofites; **j**, miospores; **l**, flore.*
Groupes guides de la faune et la flore du Permien supérieur. Tétrapodes : 1, Dinocephalia ; *2*, Chroniosaurus dongusensis *Tverdochlebova* ; *3*, Chroniosuchus uralensis *Tverdochlebova*. *Bivalves* : 4, Palaeomutela vjatkensis *Gusev*. *Ostracodes : 1*, Paleodarwinula abunda (*Mandelstam*) ; *2*, Amphissites tscherdynzevi *Posner* ; *3*, Paleodarwinula fainae (*Belousova*) ; *4*, Paleodarwinula fragiliformis (*Kashevarova*), Suchonellina futshiki (*Kashevarova*), Suchonellina trapesoida (*Sharapova*). *Miospores* : *H*, Granizospora vulgaris *Naumova* ; *J1*, Striatopodocarpites tojmensis *Sedova* ; *J2*, Lueckisporites virkkia *Potonie & Kremp.*

the J1 zone serve as the most reliable correlatives in comparing the lower Kazanian non-marine beds with each other and with the marine analogues.

The upper Kazanian substage within the Platform is composed mostly of saliferous-lagoon sediments, subdivided from bottom to top into the hydrochemical (10-200 m thick), Sosnovskaya (30-125 m thick) and Sokskaya (up to 100 m thick) members. The lowermost member is composed of anhydrites and, to a lesser extent, of rock salt. The Sosnovskaya member is represented by anhydrites, dolomites and limestones. Red sandstones with gypsum lenses and nests prevail in the Sokskaya member. In the zone of the Platform/Trough contact and within the trough, the upper Kazanian sequence consists mainly of red siltstones and clays, interlayered with sandstones, marls and limestones (up to 700 m thick).

Source : MNHN, Paris

Ostracod zonal guide fossils *Darwinula fainae* (Belousova) and miospores of the palynozone J2 - *Lueckisporites virkkia* Potonie & Kremp are common for all the rocks of diverse geneses. As a whole, the non-marine facies present in the Kazanian stage, are characterized by guide fossil bivalves *Palaeomutela umbonata* (Fischer).

Recognition and division of the Kazanian deposits within the Cis-Caspian Depression is difficult due to poor paleontological description and insufficient data, especially from its western part. In the eastern side zone, the Kazanian stage contains the Blagodarnenskaya formation (750 m thick), built of alternating argilites, siltstones and sandstones interlayered by limestones. Red beds prevail in the upper part of the section; the lower half is dominated by grey rocks containing fossil conifer pollen, *Striatopodocarpites*, characteristic of the lower Kazanian substage from the Cis-Urals.

The Tatarian stage is divided into the lower and upper substages.

The lower Tatarian substage within the Urzhum Platform sections is subdivided from below upwards into the Bolshekinelskaya (50-100 m thick) and Amanakskaya (45-90 m thick) formations. The Bolshekinelskaya formation is composed of cross-bedded alluvial sandstones interlayered by red clays; the Amanakskaya one of clays and siltstones with rare marl and limestone layers.

In the zone of the Platform/Trough contact, the Salmysh sandstones and conglomerates (90-100 m thick) and the Grebenskaya clay-siltstones (80-100 m thick) are analogous to those mentioned above. In the Cis-Ural Trough, the Urhzum horizon is includes a thick (up to 800 m) red-bed sequence of sandstones, siltstones, conglomerates and clays interlayered with nodular limestones. In the north-eastern part of the Cis-Caspian Depression, the lower substage includes the Tuketskaya and Aktyubinskaya formations. The Tuketskaya one (up to 360 m thick) is composed of red sandstones, conglomerates, siltstones and clays; the Aktyubinskaya one (660 m thick) is of finer terrigenous composition. The substage is characterized by zonal guide fossils of ostracods *Paleodarwinula fragiliformis* (Kashevarova) and bivalves *Palaeomutela vjatkensis* Gusev.

The upper Tatarian substage is subdivided into the Severodvinsky and Vyatsky horizons, everywhere, except for the north-east of the Cis-Caspian Depression. In this part, the red-bed Rodnikovskaya formation composed of siltstones and sandstones, interlayered with limestones (820 m thick), corresponds to the undivided upper substage. In the Platform regions, the Severodvinsky horizon corresponds to the red-bed Malokinelskaya formation, composed of alternating clays, siltstones and sandstones interlayered with marls and limestones (up to 170 m thick). In the zone of the Platform/Trough contact, only terrigenous deposits occur: sandstones, conglomerates, siltstones (up to 100 m thick). In the Cis-Ural Trough, the Severodvinsky horizon (up to 700 m thick) has variable carbonate-terrigenous composition. The Severodvinsky horizon is distinguished on the basis of the zonal guide fossils of ostracods *Suchonellina futschiki* (Kashevarova) and the tetrapods *Chroniosaurus dongusensis* Tverdochlebova (TVERDOKHLEBOVA, 1991). In the paleomagnetic scale, zones N1P2 and R2P2 are equivalent to the Severodvinsky horizon (MOLOSTOVSKY, 1983). The Vyatsky horizon in the Platform, is represented by the Kutulukskaya formation composed of red and variegated clays, siltstones, marls, limestones with gravelstone and sandstone lenses (up to 100 m thick). In the Cis-Ural Trough, the horizon section is dominated by brown clays, siltstones and sandstones; grey and brown marls and limestones are less common (up to 460 m thick).

The Vyatkian deposits contain numerous remains of bivalves, conchostracans, charophytes and fishes. Ostracods *Suchonellina fragiloides* (Zekina), *Suchonella typica* Spisharsky and tetrapods *Chroniosuchus uralensis* Tverdochlebova are guide of stratigraphic importance. In the paleomagnetic scale, zones N2P2 and R3P2 correlate with Vyatkian horizon.

LOWER TRIASSIC

In the South Cis-Urals, the Lower Triassic is represented by the Blumental group and Petropavlovka formation.

The Blumental group includes the beds of three major cycles of alluvial sedimentation, corresponding (from bottom to top) to Kopanskaya (up to 590 m), Staritskaya (up to 370 m) and Kzylsajskaya (up to 330 m) formations. Each one of those is composed of three to seven rhythmic members, beginning with cross-bedded sandstones with conglomerate lenses. The upper parts of the

Source : MNHN, Paris

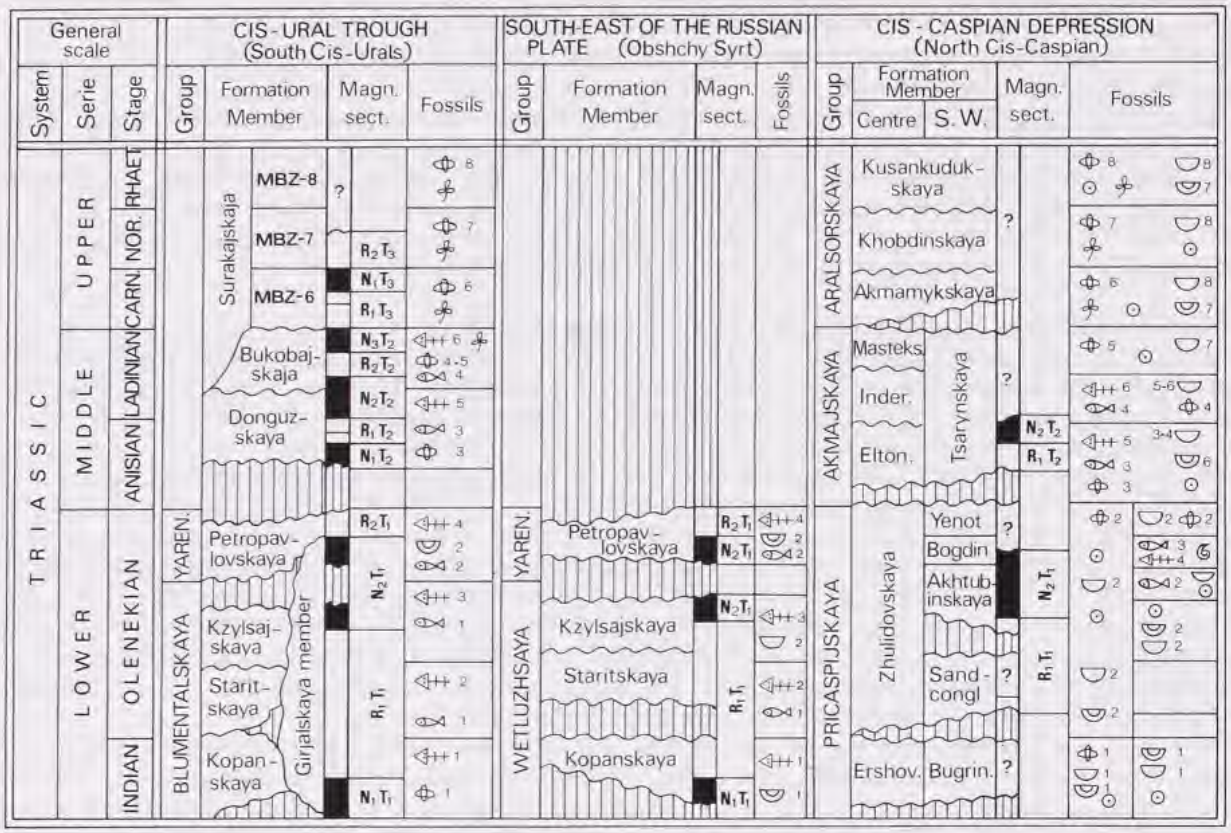

FIG. 3.— Correlation of the Triassic regional stratigraphic schemes.
Zonal guide fossil in the Triassic stratigraphy:
Tetrapods: 1, *Tupilakosaurus*; 2, *Benthosuchus*; 3, *Wetlugasaurus*; 4, *Parotosuchus*; 5, *Eryosuchus*; 6, *Mastodonsaurus*. Fishes: 1, *Gnathorhiza triassica* Minikh; 2, *Ceratodus multicristatus* Vorobjeva; 3, *Ceratodus gracilis* Vorobjeva; 4, *Ceratodus bucobaensis* Minikh. Ostracods: 1, *Darwinula ovalis* Glebova; 2, *Darwinula longissima* Belousova; 3, *Darwinula lauta* Schneider; 4, *Lutkevichinella bruttanae* Schneider; 5, *Glorianella inderica*; 6, *Pulviella aralsorica* Schneider; 7, *Gemanella schweyeri*; 8, the upper Triassic biozone. Conchostracans: 1, *Vertexia tauricornis* Lutkevich; 2, lower Baskunchak biozone; 3, Tananyk bio-assemblage; 4, Bogdo bio-assemblage; 5, upper Baskunchak bio-assemblage; 6, the Middle Triassic; 7, the upper Triassic biozone. Miospores: 1-8, Miospore biozone (MBZ).

FIG. 3.— Corrélations des schémas stratigraphiques régionaux du Trias.
Fossiles guides de la stratigraphie du Trias.
Tétrapodes : 1, Tupilakosaurus ; 2, Benthosuchus ; *3,* Wetlugasaurus ; *4,* Parotosuchus ; *5,* Eryosuchus ; *6,* Mastodonsaurus. *Poissons : 1,* Gnathorhiza triassica *Minikh* ; *2,* Ceratodus multicristatus *Vorobjeva* ; *3,* Ceratodus gracilis *Vorobjeva* ; *4,* Ceratodus bucobaensis *Minikh. Ostracodes : 1,* Darwinula ovalis *Glebova* ; *2,* Darwinula longissima *Belousova* ; *3,* Darwinula lauta *Schneider* ; *4,* Lutkevichinella bruttanae *Schneider* ; *5,* Glorianella inderica ; *6,* Pulviella aralsorica *Schneider* ; *7,* Gemanella schweyeri ; *8, Biozone du Trias supérieur. Conchostracés : 1,* Vertexia tauricornis *Lutkevich* ; *2, Biozone du Baskunchak inférieur ; 3, Bio-assemblage de Tananyk ; 4, Bio-assemblage de Bogdo ; 5, Bio-assemblage du Baskunchak supérieur ; 6, Le Trias moyen ; 7, Biozone du Trias supérieur.*
Miospores : 1-8, biozones à miospores (MBZ).

members are generally clayey. Less thick analogues of the suites mentioned, are recognized in the sections from the left bank of the Volga.

Some remains of neorachitomous labyrinthodonts, *Tupilakosaurus* sp., occur in the Kopanskaya formation; *Bentosuchus* cf. *sushkini* (Efremov) in the Staritskaya formation; *Wetlugasaurus angustifrons* Riabinin in the Kzylsajskaya formation. Remains of the dipnoan *Gnathorhiza triassica* Minikh are known from two upper formations. In the paleomagnetic scale, zones N1T1, R1T1 and partially R2T1 correspond to the Blumental group. According to the neorachitomous tetrapod fauna and magnetic zonality, the Blumental group correlates with the Vetluga supergroup from the Russian Plate and the Indian stage and the lower Olenekian substage from the Boreal region (SHISHKIN & OCHEV, 1992).

Source : MNHN, Paris

The Petropavlovskaya formation is composed of a number of rhythmic members opening with red-brown sandstones of alluvial-deltaic type and completed with lacustrine-floodplain siltstones and clays. The formation contains the parotosuchian tetrapod fauna and the Yarenian ichthyofaunal complex with *Ceratodus multicristatus* Vorobjeva. The lower part of the formation is normally magnetized and belongs to the zone N2T1, the upper part of the suite corresponds to the magnetozone R1T1.

In the east of the Cis-Ural Trough, the Lower Triassic includes the Girjalskaya member of sandstones and conglomerates of alluvial-proluvial origin (up to 420 m). In the north-eastern part of the Cis-Caspian Depression the red-bed terrigenous Pericaspian series of alluvial-deltaic type corresponds to the Lower Triassic (up to 1600 m); it consists of the Ershovskaya and Zhulidovskaya formations with peculiar freshwater zonal guide fossils of ostracods, conchostracans and charophytes.

In the south-western part of the depression, in the lower section, the following units are recognized (upwards): chiefly red-bed alluvial-deltaic, silto-arenaceous Bugrinskaya formation (up to 600 m), sand sequence (up to 55 m), sand-conglomerate sequence (up to 45 m) and silto-clayey (variegated in its upper part) Akhtubinskaya formation (up to 110 m), formed in shallow-water, littoral settings. These are overlain by the marine, grey-coloured clay-carbonate Bogdinskaya formation (up to 330 m), in its turn overlain by the variegated, sandy-clayey Yenotayevskaya formation (up to 200 m), accumulated under the conditions of near-shore plains. According to the faunas of ostracods and conchostracans, the Bugrinskaya member is referred to the Ershovs formation; the Akhtubinskaya, Bogdinskaya and Yenotayevskaya members form the Baskunchakskaya formation with its stratotype in Bolshoye Bogdo Mt. The Bogdinskaya member contains remains of the *Parotosuchus* fauna, the Yarenian ichthyofauna with *Ceratodus multicristatus* Vorobjeva, and ammonites (*Tirolites cassianus* Quenstedt) from the Olenekian *Columbites* zone.

In the paleomagnetic scheme the sand sequence and sand-conglomerate sequence corresponds to the zone R1T1, the Akhtubinskaya and preserved part of the Bogdinskaya members to the zone N2T1.

Middle Triassic

In the southern part of the Cis-Ural Trough, the Middle Triassic corresponds to the Donguzskaya, Bukobajskaya and the lowermost part of the Surokajskaya formation.

The Donguzskaya formation consists of variegated siltstones and clays of lacustrine origin with interlayers and lenses of grey cross-bedded sandstones (up to 360 m). The formation is characterized by tetrapods of *Eryosuchus* fauna, the Donguz Middle Triassic ichthyofauna with *Ceratodus gracilis* Vorobjeva, and the middle Anisian and early Ladinian guide fossil miospores (Fig. 3).

The Bukobajskaya formation consists of variegated siltstones and clays rich in plant remains; they alternate rhythmically with lenses of grey, cross-bedded sandstones (up to 600 m). The formation is characterized by tetrapods of *Mastodonsaurus* fauna, the Bukobajskaya zone of the Middle Triassic ichthyofauna with *Ceratodus bukobaensis* Minikh. According to its guide fossil flora and miospores, the Bukobajskaya formation correlates with the late Ladinian.

In the Cis-Caspian Depression, the Middle Triassic is recognized as the Akmajskaya series, which includes (from bottom to top) the Eltonskaya, Inderskaya and Masteksajskaya formations.

The Eltonskaya formation consists of littoral-marine variegated grey clays and limestones (up to 300 m) with guide fossil charophytes, ostracods and miospores, which allow to refer the formation to the Anisian. In the vicinity of Inder Lake, the formation contains occasional dipnoans *Ceratodus gracilis* Vorobjeva, from the Donguz zone (Fig. 3).

The Inderskaya formation (up to 220 m) is represented by marine grey clays and limestones with the Ladinian guide fossil charophytes, ostracods and miospore complexes. In the uppermost part of the formation, there are some remains of the Bukobajskaya dipnoan and the mastodonsaur tetrapod faunas.

The Masteksajskaya formation (up to 210 m) consists of dark-grey clays interlayered by siltstones and sandstones. Marine ostracods from the *Gemanella* zone and the late Ladinian miospores are characteristic of this formation.

Upper Triassic

The Surakajskaya formation (up to 300 m) corresponds to the Upper Triassic in the South Cis-Urals; it consists of lacustrine-marsh grey-coloured clays, siltstones and sandstones. According to the

Source : MNHN, Paris

palynologic data, the formation is composed of three biozones, MBZ-6,7,8, corresponding to the Carnian, Norian and Rhaetian stages, respectively (Fig. 3).

In the Peri-Caspian Depression, the Upper Triassic corresponds to the continental grey-coloured-variegated coal-bearing Aralsorskaya group (Fig. 3), comprising (from bottom to top) the Akmamykskaya (up to 425 m), Khobdinskaya (up to 380 m) and Kusankudukskaya (up to 300 m) formations. Each of them represents a sedimentary cycle starting with sandstones and ending with clays. All the formations include the Late Triassic zonal guide fossils of conchostracans and ostracods, and are correlated according to miospores with the Carnian, Norian and Rhaetian stages of the general scale, respectively.

PALEOGEOGRAPHIC RECONSTRUCTIONS

In the Upper Permian sections from the east of the Russian Plate and the west of the Trough, three lithologic-stratigraphic complexes are recognized: the Ufimian continental red-bed, the lower Kazanian marine grey-coloured and the upper Kazanian-Tatarian red-bed ones. A similarly composed three-member sequence is recognized in the east of the Cis-Caspian Depression and the central zone of the Cis-Ural Trough. The lower Kazanian marine formations, however, are replaced there by the coalified grey-coloured sequence of lacustrine-lagoonal and possibly littoral-marine sediments.

A certain continuity may be recognized in the spatial arrangement of the facies in the Ufimian and Kazanian sedimentation fields from the Russian Plate and the Cis-Ural Trough. This continuity consists in preferential concentration of the salt-bearing and carbonate sediments within the western regions of the Cis-Urals, and their gradual substitution by the terrigenous facies towards the folded Urals. It is worthy of note that the tendency is retained in the lower Kazanian marine basin that has drastically changed the sedimentation settings in the region.

For the Ufimian and upper Kazanian red-bed deposits, such continuity is caused by similar paleogeographic conditions: they were accumulating in shallow relict reservoirs, inherited from the Kungurian and lower Kazanian basins, relatively remote from the Ural sourcelands. The zones influenced by the latter ones, were characterized by dominating regime of terrigenous sedimentation. In the early Kazanian, similar arrangement of the facies was probably caused by uplifting mineralized waters from the westerly marine basin. On the whole, in all the territories considered, arid continental conditions were characteristic of the Late Permian sedimentation cycle. In the early Kazanian they were interrupted by a short-term boreal transgression accompanied by general humidization of the climate. During the whole of the Kazanian age, the character of sedimentation all over the Volga-Ural and Cis-Caspian regions was to a variable extent influenced by the Boreal Sea transgression.

With the start of the Triassic sedimentation cycle, independent formational sequences came into being in the Cis-Ural Trough and Cis-Caspian Depression. In the Cis-Caspian, the three-member series consisted of red-bed terrigenous, grey-coloured marine and coal-bearing lacustine-marsh formations. A three-member formational series appeared in the South Cis-Urals, as well: alluvial-proluvial, lacustrine and lacustrine-marsh coalified structures.

In the Early Triassic, the paleogeographic settings were arid everywhere, but the sedimentation processes were quite autonomous in every region. The relatively limited Olenekian transgression has not exerted any appreciable influence upon the continental sedimentation in the Cis-Urals, but the dynamic uplift of the Bogdinskian Sea has probably promoted the appearance of the deltaic facies in the Petropavlovskaya formation (SHISHKIN *et al.*, 1995).

The inter-regional geologic links became more evident in the Middle Triassic. The development of extensive Tethys transgression has coincided in time with general tectonic stabilization of the Urals, disappearance of the Lower Triassic alluvial-proluvial plain and setting of lacustrine sedimentation under more and more humid climatic conditions.

In the Late Triassic, similar landscape-climatic conditions have set in the vast areas of the South Cis-Urals, Trans-Urals and Cis-Caspian, which resulted in two associations of formations coming together; under the conditions of humid landscapes, a coalified terrigenous formation started to accumulate. It is represented by the coal-bearing Chelyabinskaya group in the middle Trans-Urals, Surakajskaya formation in the South Cis-Urals and the Aralsorskaya group in the Eastern Cis-Caspian.

Source : MNHN, Paris

CONCLUSION

The Late Permian and Triassic sedimentation was, on the whole, of arid character; it was as late as in the Late Triassic that lacustrine-marsh coal-bearing sediments started being generated in the vast plains of the Cis-Caspian and South Cis-Urals as the result of global increase of humidity.

Among the most important regional geologic factors influencing the formation of sedimentary rock complexes in the Upper Permian, were: residual salt-generating basins of the Lower Permian and the vast Kazanian transgression of the Boreal Sea, involving the whole of the eastern Russian Plate, the west of the Cis-Ural Trough and the north of the Cis-Caspian Depression.

In the end of the Early and in the Middle Triassic, sedimentation in the Cis-Caspian area was in many respects controlled by the Tethys eustatic oscillations. The peculiar character of the Late Permian and Early Triassic sedimentation within the Cis-Ural marginal trough was determined by intensive terrigenous drift from the regions of the folded Urals.

The materials available show that the stratigraphic boundaries of practically all the regional units of the Upper Permian and Triassic from the Volga-Ural and Cis-Caspian regions, are of event character, but record geologic events of diverse types and levels. This fact makes it possible to carry out research along various trends of geologic correlations: from detailed stratigraphic comparisons to comparative analyses of the large-scale reconstructions in paleogeography and geodynamics.

Of main importance in such research is the choice of reference correlation levels, marked with coincidence of geodynamic, paleogeographic, biotic, formational and geomagnetic boundaries. As far as the northern margin of the Tethys is concerned, in the Permo-Triassic part of the scale, the following boundaries meet this condition: those between the lower and the upper Tatarian substages, between the Permian and Triassic, and the Lower and Middle Triassic.

The rank and geologic importance of the last two boundaries are well-known. The boundary between the lower and upper Tatarian substages has not been considered properly, yet, and its current stratigraphic rank does not correspond to the significant reconstructions that have occurred at this level in the structure of the continental biota and in geomagnetic polarity regime. This boundary is marked by large-scale changes in tetrapod fauna: replacement of the dinocephalian grouping by the pareiasaur-theriodontid one (TVERDOKHLEBOVA, 1991; SHISHKIN & OCHEV, 1992). In the course of the Late Permian, fast change at the superfamily level occurred in ostracodes (MOLOSTOVSKAYA, 1987, 1993). There were significant changes in ichthyofauna systematic composition (MINIKH & MINIKH, 1995). In paleomagnetism evolution, the regime of stable reverse polarity field was replaced by an epoch of frequent reversals (MOLOSTOVSKY, 1983).

The above data offer profound grounds for regarding the upper Tatarian as an independent stage, more important in its extent and paleontologic distinctness than any of the currently known stages of the Upper Permian.

REFERENCES

BLOM, G.I., LOZOVSKY, V.R., MINIKH, M.G. *et al.*, 1982.— The general stratigraphic scale: Moscow, Mezen syneclise, Volga-Ural anteclise (scheme 1). *In*: A.I. ZHAMOYDA, V.V. LIPATOVA & G.M. ROMANOVSKAYA (eds), *Decision of the Interdepartment Stratigraphic Meeting on the Triassic from the East-European Platform (Saratov, 1979)*. Nedra, Leningrad: 20-35 (in Russian).

GORSKY, V.P. & GUSEVA, E.A. (eds), 1990.— Decision of the interdepartment regional stratigraphic meeting on the Middle and Upper Paleozoic from the Russian Platform: with regional stratigraphic charts. Leningrad, 1988. *In*: *The Permian system*. VSEGEI, Leningrad: 1-47 (in Russian).

KULEVA, G.V., 1975.— *The Upper Kazanian and Tatarian Continental Deposits from the Southern Part of Cis-Ural Marginal Deflection (within the Orenburg and south Bashkirian Cis-Urals)*. Saratov University Publication, Saratov: 1-164 (in Russian).

LIPATOVA, V.V., MINIKH, M.G., MOLOSTOVSKY, E.A. *et al.*, 1985.— Project of the unified scheme for the Triassic from the East-European Platform. *In*: V.V. LIPATOVA & V.G. OCHEV (eds), *Triassic Beds from the East-European Platform*. Saratov University Publication, Saratov: 10-28 (in Russian).

MINIKH, M.G., 1972.— Fishes. *In*: V.V. MENNER & V.V. LIPATOVA (eds), *Stratotype Section of the Lower Triassic Baskunchak Series from Bolshoye Bogdo Mountain*. Saratov University Publication, Saratov: 48-50 (in Russian).

Source : MNHN, Paris

MINIKH, M.G., 1977.— *Triassic Lungfish from the East of European USSR*. Saratov University Publication, Saratov: 1-96 (in Russian).

MINIKH, M.G., 1995.— Fishes. *In*: M.A. SHISHKIN (ed.), *Biostratigraphy of the Continental Triassic from the South Cis- Urals*. Nauka, Moscow: 38-56 (in Russian).

MINIKH, M.G. & MINIKH, A.V., 1985.— Division of the Triassic deposits from the East-European Platform according to ichthyofauna. *In*: V.V. LIPATOVA & V.G. OCHEV (eds), *Triassic Beds from the East-European Platform*. Saratov University Publication, Saratov: 44-52 (in Russian).

MINIKH, M.G. & MINIKH, A.V., 1995.— Division of the Permian and Triassic beds from European Russia according to ichthyofauna. *In*: *Proceedings of the All-Russia Meeting "Paleontology and Stratigraphy of the Continental Permian and Triassic from Northern Eurasia"*. PIN-RAS, Moscow: 23 (in Russian).

MOLOSTOVSKAYA, I.I., 1987.— To the division of the Upper Tatarian substage from the south-east of the Russian Platform by ostracods. *In*: V.I. ARTEMEV & G.I. BARULIN (eds), *Problems of Stratigraphy of the Paleozoic, Mesozoic and Cenozoic*. Saratov University Publication, Saratov: 47-57 (in Russian).

MOLOSTOVSKAYA, I.I., 1997.— Non-marine ostracods and paleobiogeographical distribution in the Late Permian basins in the east of Russian Plate. *In*: Contribution to Eurasia Geology. *Occasional Publications ESRJ, New Series, South Caroline University Publication*, **9**: 95-100.

MOLOSTOVSKY, E.A., 1983.— *Paleomagnetic Stratigraphy of the Upper Permian and Triassic from East of European Part of the USSR*. Saratov University Publication, Saratov: 1-168 (in Russian).

MOLOSTOVSKY, E.A., 1995.— Magnetostratigraphic section. *In*: M.A. SHISHKIN (ed.), *Biostratigraphy of the Continental Triassic from the South Cis-Urals*. Nauka, Moscow: 129-138 (in Russian).

SHISHKIN, M.A. & OCHEV, V.G., 1992.— The Permo-Triassic transition and the Early Triassic history of the Euramerican tetrapod fauna. *Bulletin of New Mexico Museum Natural History, Sciences*, **3**: 435-437.

SHISHKIN, M.A., OCHEV, V.G., TVERDOKHLEBOV, V.P. *et al.*, 1995.— *Biostratigraphy of the Triassic of Southern Cis-Urals*. Moscow, Nauka: 1-205 (in Russian).

TVERDOKHLEBOVA, G.I., 1991.— Tetrapod remain distribution in the Upper Tatarian substage from the East of the European Platform. *Bulletin of Moscow Naturalist Society*, **2**: 66-71 (in Russian).

ZAMARENOV, A.K., KUKHTINOV, D.A., ZAMARENOVA, E.N., ALEXEYEVA, V.I. & TARAN, L.V., 1969.— Stratigraphy, lithology and formation settings of the Upper Permian and Triassic deposits the eastern-border margin of the Peri Caspian Depression. *In*: V.N. VINOGRADOV (ed.), *The Permo-Triassic of the Russian Platform and its oil and gas content*. Nedra, Moscow: 191-201 (in Russian).

ZHAMOYDA, A.I., LIPATOVA, V.V. & ROMANOVSKAYA, G.M. (eds), 1982.— *Decision of the Interdepartment stratigraphic meeting on the Triassic from the East-European Platform (Saratov, 1979)*. Nedra, Leningrad: 1-64 (in Russian).

Source : MNHN, Paris

3

The Domanikoid facies of the Russian Platform and basin paleogeography

Valentina S. VISHNEVSKAYA

Institute of the Lithosphere, Russian Academy of Sciences, Staromonetny per., 22, Moscow 109180, Russia

ABSTRACT

The main purpose of the paper is a comparative analysis of the bituminous carbonate-siliceous deposits of the Devonian (Domanik) and Jurassic (Domanikoid) rift-type basins from the Russian platform to make their correlation, using an homogeneous chronometer (radiolarians). It compares the chemical composition and lithological types of sediments in order to understand the dynamics of subsidence and sedimentation, crustal tectonics of the region and to analyze the relationships between deep and shallow sedimentary basin evolution, as well as establishing the timing of events and, consequently, to elucidate more general geological processes such as paleoenvironments. We attempt to trace and to interprete the factors which controlled the sedimentation of domanikoid siliceous rocks enriched in P and C organic in rift basins, contributing to elaborate Jurassic paleogeographic maps.

RÉSUMÉ

Le faciès Domanikoid sur la Plate-forme russe et paléogéographie du bassin.

Le but de cet article est de présenter une comparaison entre les dépôts de carbonates siliceux bitumineux du Dévonien (Domanik) et du Jurassique (Domanikoid) dans les bassins de type rift de la Plate-forme russe pour établir des corrélations en utilisant un chronomètre homogène (radiolaires). On compare la composition chimique et le type sédimentologique des sédiments pour comprendre la dynamique de la subsidence et de la sédimentation, la tectonique crustale de la région et pour analyser les relations entre l'évolution des zones peu profondes et les zones de bassin aussi bien que pour établir la chronologie des événements et par conséquent pour élucider les processus géologiques plus généraux comme les paléoenvironnements. On essaie de tracer et d'interpréter les facteurs qui contrôlent la sédimentation des roches siliceuses du Domanikoid enrichies en P et C organique dans les bassins de rift, contribuant ainsi à élaborer les cartes paléogéographiques du Jurassique.

INTRODUCTION

The presence of domanikoid bituminous facies enriched in organic matter is very typical of Upper Jurassic strata of the North Peri-Tethys regions (Pechora, Sysola, Volga-Urals hydrocarbon provinces of the Russian platform). Similarly to the hydrocarbon Domanik Formation of the same area, the origin of these source rocks probably resulted from the post-rift subsidence events which took place at the rim of the Russian platform.

VISHNEVSKAYA, V.S., 1998.— The Domanikoid facies of the Russian Platform and basin paleogeography. *In:* S. CRASQUIN-SOLEAU & É. BARRIER (eds), Peri-Tethys Memoir 3: stratigraphy and evolution of Peri-Tethyan platforms. *Mém. Mus. natn. Hist. nat.*, **177** : 45-69. Paris ISBN : 2-85653-512-7.

Source : MNHN, Paris

The continuations of the largest Riphean aulacogens of the Russian platform are traced under Timan-Pechora and Volga-Urals basins (Fig. 1). The repeated tectonic splitting along the Timan-Pechora, Vyatka, Volga and Mid-Russian or Moscow (Fig. 2) depression took place during Middle-Late Devonian and Middle-Late Jurassic time periods. These rifting processes were probably connected to global world lithosphere plate reorganization at these times.

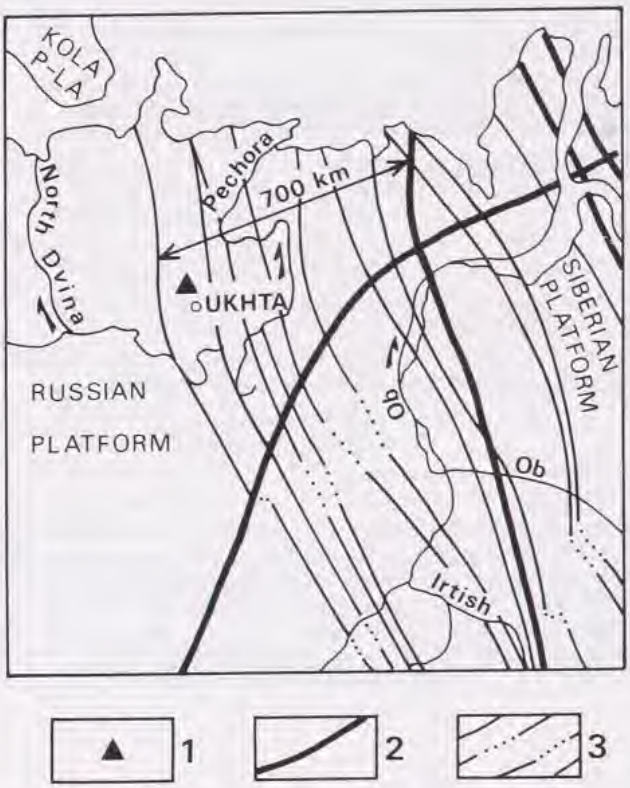

FIG. 1.— Location of studied samples from Domanik Horizon (1). The main Urals fault (2) and faults in basement of Siberian platform; pre-Paleozoic faults (3).

FIG. 1.— Localisation des échantillons étudiés dans l'horizon Domanik (1). Principale faille de l'Oural (2) et failles dans le soubassement de la Plate-forme sibérienne ; failles pré-Paléozoïques (3)

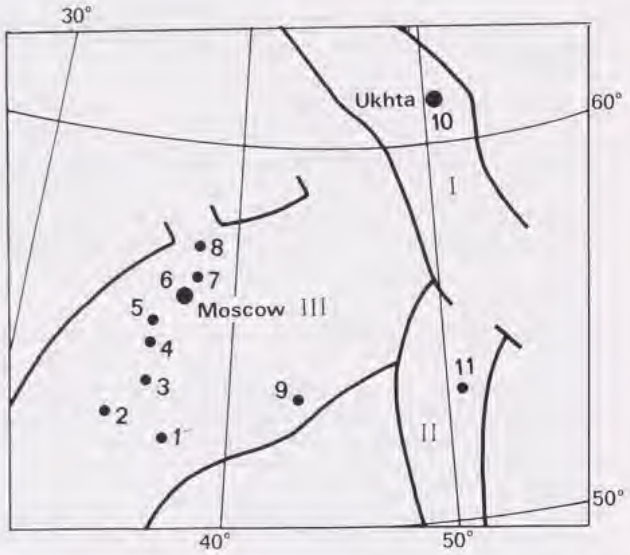

FIG. 2.— Location of investigated sites. I-II, Devonian paleorifts: I, Pechora, II, Vyatka; III, Riphean Mid-Russian aulacogen. Names of sites are given in legend of figure 3.

FIG. 2.— Localisation des sites étudiés. I-II, Paléorifts dévoniens : I, Pechora, II, Vyatka ; III, aulacogène riphéen de Russie centrale. Les noms des sites sont donnés sur la figure 3.

RIFTING AND GEOLOGICAL SETTING

As known, rift-basins are characterized by low crust thickness caused by mantle elevation and its evolution, higher heat flow values, high seismicity and steep gravity gradient. Measured from regional deep seismic sounding throughout the Timan-Pechora basin, the Moho depth reaches 36-40 km in its west part, 38-42 in its center and 34-36 in its north-eastern part (KOSTIUCHENKO, 1993). From Kostiuchenko's point of view, the spreading (rift) zone is located in the northern part of Timan-Pechora basin. The linear magnetic anomalies, the uplifting of the consolidated crust surface with a median valley, and the magnetic body penetrating the crust interpreted as the magma chamber, make the spreading zone similar to the mid-oceanic ridge. During the Middle and Late Devonian, complex systems of rift set up along the eastern and south-eastern margins of the European paleocontinent. They include the Pripyat-Dnieper-Donets, Peri-Caspian, Volga-Ural, Timan-Pechora, Eastern Barents Sea and Northern Kara Sea rift zones (NIKISHIN *et al.*, 1993).

Source : MNHN, Paris

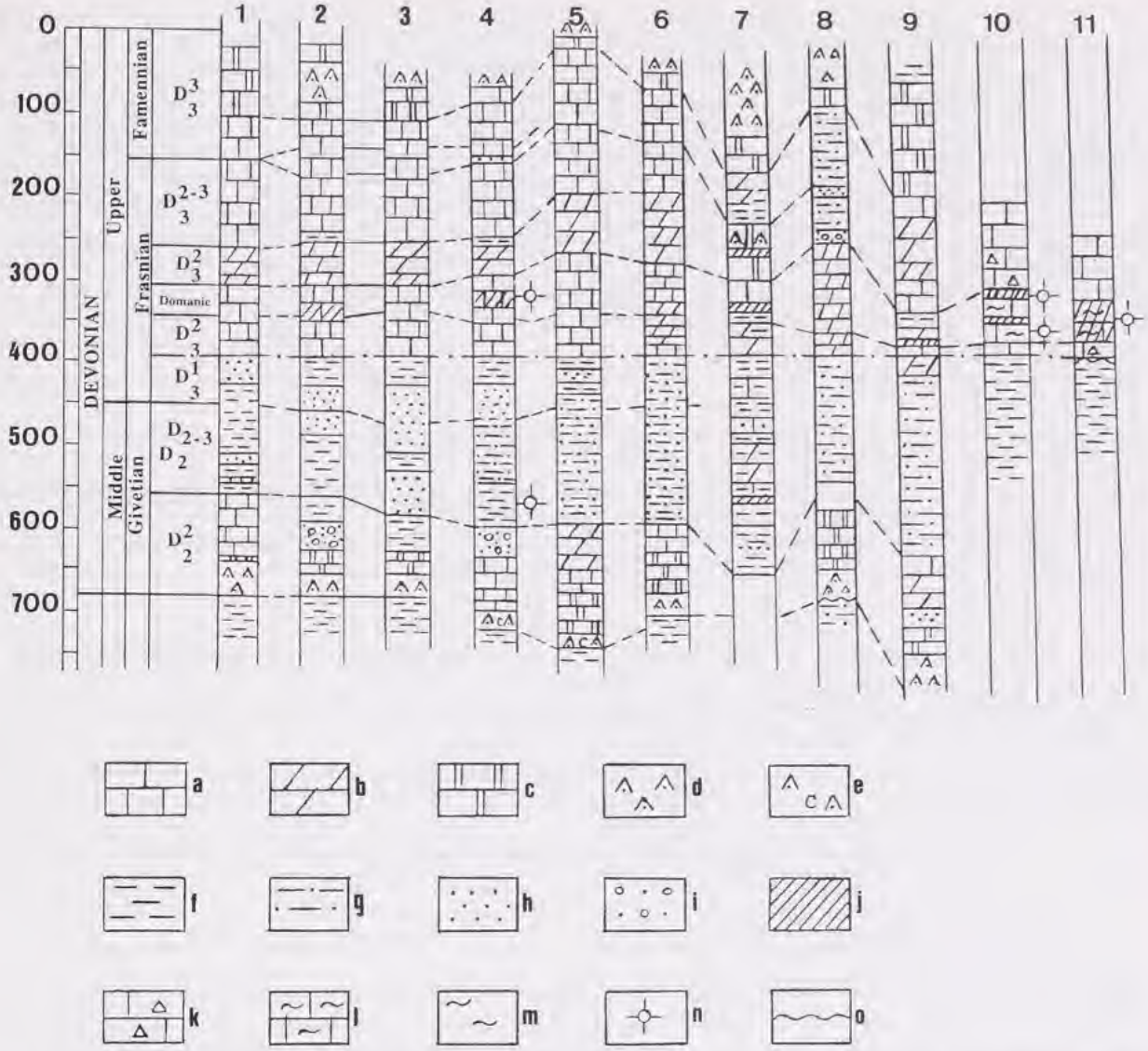

FIG. 3.— Distribution of the Devonian Domanik facies in the sections of the Russian platform. Sites or boreholes: 1, Plavsk; 2, Vorotinsk; 3, Pletenevka; 4, Kaluga; 5, Borovsk; 6, Moscow; 7, Povarovka; 8, Redkino; 9, Pachelma; 10, Ukhta; 11, Bugur.
Legend: 1, limestone; 2, marl; 3, dolomite; 4, anhydrite; 5, gypsum and salt; 6, clay; 7, siltstone; 8, sandstone; 9, conglomerate; 10, bituminous phtanite; 11, breccian limestone; 12, chert limestone; 13, chert; 14, radiolarian; 15, unconformity.

FIG. 3.— Distribution des faciès Domanik dans les coupes de la Plate-forme russe. Sites ou forages : 1, Plavsk; 2, Vorotinsk; 3, Pletenevka; 4, Kaluga; 5, Borovsk; 6, Moscow; 7, Povarovka; 8, Redkino; 9, Pachelma; 10, Ukhta; 11, Bugur.
Légende : 1, calcaires ; 2, marnes ; 3, dolomie ; 4, anhydrite ; 5, gypse et sel ; 6, argile ; 7, pélite ; 8, grès ; 9, conglomérat ; 10, phtanite bitumineuse ; 11, calcaire brêchique ; 12, calcaire à cherts ; 13, chert ; 14, radiolaires ; 15, discordance.

The foredeep basins of the Polar Urals and Pay-Khoy are situated in the eastern areas of Timan-Pechora. The well-known Pechora-Kolva Aulacogen is the axial suture of the Timan-Pechora basin (Fig. 1). It corresponds to a zone of reduced crustal thickness (36-38 km) and high crustal density (up to 2.9 gr/cm^3). The basement of the foredeep troughs is depressed up to a depth of 12-14 km (APLONOV & SHMELEV, 1993). The Devonian phase of an active rifting is distinguished in Pripyat trough too (KLUSHIN, 1992). The Kimmeridgian-Volgian phase is traced to the north into the Barents, Norway and

Source : MNHN, Paris

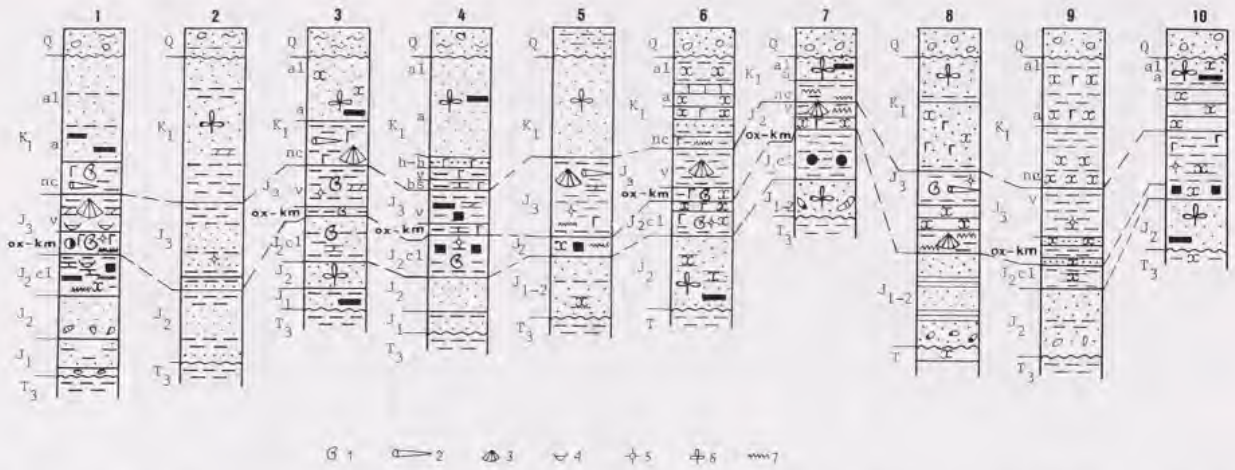

FIG. 4.— Distribution of the Jurassic domanikoid facies within the sections of the north-eastern part of the Russian platform. For location of boreholes, see figure 9; for lithology, see legend of figure 3.

FIG. 4.— Distribution du faciès domanikoid jurassique dans les coupes de la partie NE de la plate-forme russe. Pour la localisations des forages, voir figure 9 ; pour la lithologie voir figure 3.

North seas (DYER & COPESTAKE, 1989; KOZLOVA, 1994) and to the south into the Volga-Urals Basin. During Devonian time, the spreading rate of the Yapetus was rather high, about 8 cm/year (APLONOV, 1993) which caused a specific type of sedimentation. Rich energy resources are connected with Devonian and Jurassic rift basins. It is important to emphasize that during rift stages, a thick series of lacustrine alluvium and active marine marginal slope sediments (Figs. 2-4) locally oil and coal-bearing have been accumulated. There are numerous examples of lacustrine strata of the Late Devonian (ORMISTON, 1989) and Middle-Late Jurassic age (Fig. 4) which are excellent source rocks. Similar lacustrine strata have produced oil in the Beatrice field in the North Sea (ORMISTON, 1989). The tectonic setting in the distribution of the Jurassic domanikoid formations within the Timan-Pechora and Volga Basins shows resemblance with the same in the North Sea, where tectonic activity along graben bounding faults were also probably responsible for the character of the deposition of oil and others units (DYER & COPESTAKE, 1989).

In the North Sea tectonic rifting caused rapid subsidence which outpaced sedimentation to create basinal troughs or grabens and the basinal organic rich shales were accumulated in the graben axes during Kimmeridgian to Ryazanian times (DYER & COPESTAKE, 1989). The characteristic features of the Timan-Pechora and Volga-Urals rift-basins are also the presence of Domanik and domanikoid-type bituminous deposits.

DISTINCTIVE FEATURES AND PARTICULARITIES OF THE DOMANIKOID FACIES

Domanik means the Devonian source rocks (oil shales) enriched in organic carbon (kerogen) and term "domanikoid" is used for others rocks similar to Domanik. The Domanik facies has a special position in terms of paleogeographic conditions. There are many models for Domanik-type basins. One of the last was elaborated by ORMISTON (1993). It shows that interest to this problem is high and many aspects of phenomenon Domanik-type basin formation are still unclear. Oil of the Russian plate is mostly associated with Devonian Domanik-type rocks (for instance, Pripyat, Timan-Pechora, Volga-Urals Basins); fuel shale of Peri-Tethys is closely related to Jurassic siliceous bituminous rocks (Timan-Pechora, Volga-Urals Basins). The primary source of hydrocarbons is Domanik organic shales, domanikoid-type bituminous limestones and phtanites. The examples of the Ukhta Domanik facies (Domanik Creek of Ukhta region of Komi, Russia, Figs 2-3, section of site 10) and domanikoid shale of the Timan-Pechora Basin (Fig. 4, section 4) are given in order to consider this type of specific deposits.

Ukhta Domanik facies (60 m) is represented by grey to black phtanite and siliceous bituminous

Source : MNHN, Paris

limestone with little admixture of clay. The Ukhta middle Frasnian phtanites are oil shale rocks enriched in organic (kerogen) material. Content of TOC (total organic carbon) approaches 12-20%.

The Jurassic domanikoid-type of sediments is represented by fuel organic shale (Fig. 4, section 4) in the Volgian stage (up to 1 m in thick) or bituminous clay (Fig. 4, section 9) in the Kimmeridgian (2-3 m). However, the stratigraphic seccession shows that the Jurassic does not have a high TOC (5-10%). The flooding of former land areas toward the south probably released phosphate and nitrogen into adjacent waters where they favored the preservation of dead organisms and consequently the accumulation of TOC due to preservative character of phosphorus (MERTS *et al.*, 1990).

The chemical and normative composition of Ukhta Domanik facies (MERTS *et al.*, 1990) showed low Al and alkalies and higher P contents. Mineralogically, the quartz-calcedony prevailed. The secondary minerals are muscovite-hydromica, montmorillonite, calcite, pyrite, apatite and titanite. The Domanik oil shale are enriched in Mo, V, Ni. As geochemical indicator of the volcanic material in the phtanites the montmorillonite has been found. The low content of Mn probably points out the absence of stagnant environment in the Domanik sedimentary basin and confirms the deep slope condition (MERTS *et al.*, 1990).

The Jurassic clay of Pechora and Ukhta regions is enriched in glauconite and also montmorillonite. The glauconite (15-30%), montmorillonite (10-30%), hydromica (10-30%) and chlorite (5-10%) are dominating in the Kimmeridgian bituminous clay and glauconite (30-40%), kaoline (25-30%), montmorillonite (20-30%) are prevailing in the Volgian organic rich shale.

Contact of the Domanik facies with the underlying light clay (Fig. 3) is transgressive and begins with a stratum (about 0.5 m) composed of small pteropod and goniatite shells. The middle most productive part has a very thin flyschoid structure and in places resembles radiolarites, containing more than 50% radiolarian skeletons. Upper Devonian (middle Frasnian) sphaeroid-like *Entactinia* cf. *additiva* Foreman, *Astroentactinia paronae* (Hinde), *A.* cf. *crassata* Nazarov, *A.* cf. *stellata* Naz., *A.* aff. *tantilla* Naz., *Haplentactinia inaudita* Naz., *H. arrhinia* For., *H. rhinophyusa* For., *Polyentactinia circumretia* Naz., *P. kosistekensis* Naz., *Tetrentactinia* cf. *gracilispinosa* For., *Entactinosphaera grandis* Naz., *E. assidera* Naz., *E. echinata* (Hinde), *E. nigra* (Hinde), *E. variacanthina* For. (Fig. 5) and spicula-like forms *Paleoscenidium cladophorum* Deflandre, *Paleothalomnus* sp., *Ceratoikiscum spinosiarcuthum* For., *C. mertsi* sp. nov. (Fig. 6) were identified among radiolarians. Domanik radiolarians are associated with conodonts of *Polygnatus timanicum* zone. Conodonts *Palmatolepis gigas* Youngquist, *P. subrecta* Miller & Youngquist, *P. timanicus* Ovnatanova occur in the upper part of domanikoid Sopless suite. The *Palmatolepis punctata* conodont zone was determined by A. Yudina (MERTS, 1990) in the middle part of Domanik Horizon of Ukhta section.

Diversity of radiolaria, isotopic data from brachiopod shells and presence of corals in the neighbouring areas indicate very warm-water conditions for the Domanik basin. It is in a good agreement with the latitudinal location of the northern branch of the Yapetus in global reconstructions near the Equator (APLONOV, 1993). There are a lot of micro-algae *Tasmanites* in the Domanik facies. Recent bacteroids and micro-algae occur in abundance within vacuoles in the cytoplasm of living radiolaria. Older algae may also have been associated with radiolaria and could have existed far from the coastline for this reason (VISHNEVSKAYA *et al.*, 1993).

The major part of *Tasmanites* are found in areas located in the neighbourhood of deep faults (Timan-Pechora, Pyrgidan and Urengoy depressions). Synchronous mass extinction of radiolarians and micro-algae can be explained by sudden sharp transgressive-regressive events. The transgressive regime stimulated an accumulation of *Tasmanites* because the bulk of this genus was fixed under condition of transgression maximum (TALNOVA, 1995). For example, the mass deposition of *Tasmanites* was found in the delta-front trough of large paleorivers or paleorifts. The thick-walled tasmanitid prasinophyte algae *Tasmanites* (ORMISTON, 1989) and radiolarians had an excellent capacity to deliver lipids (ANDERSON, 1983) for a long time into the bottom sediments. The global affinity of *Tasmanites* to the source rocks is very famous (TELNOVA, 1995). On the background of standard methods the co-occurrence of *Tasmanites* and radiolaria can be used for prognosis of oil industry. The absence of foraminifera is regarded by ORMISTON (1993) as a result of anoxia, similarly to sediments of the Bonarelli level. The best preservation of radiolarians and algae is probably due to anoxia. The presence of phosphorus could be served as conservant too.

The upper part of Domanik is cross-bedded and consists of siliceous limestone with abundant micro- and macrofaunas or polydetritus limestone, and obviously shows a regressive character. The Kimmeridgian clay (5-45 m) from the Pechora and Ukhta regions has stratigraphic contact with the

Source : MNHN, Paris

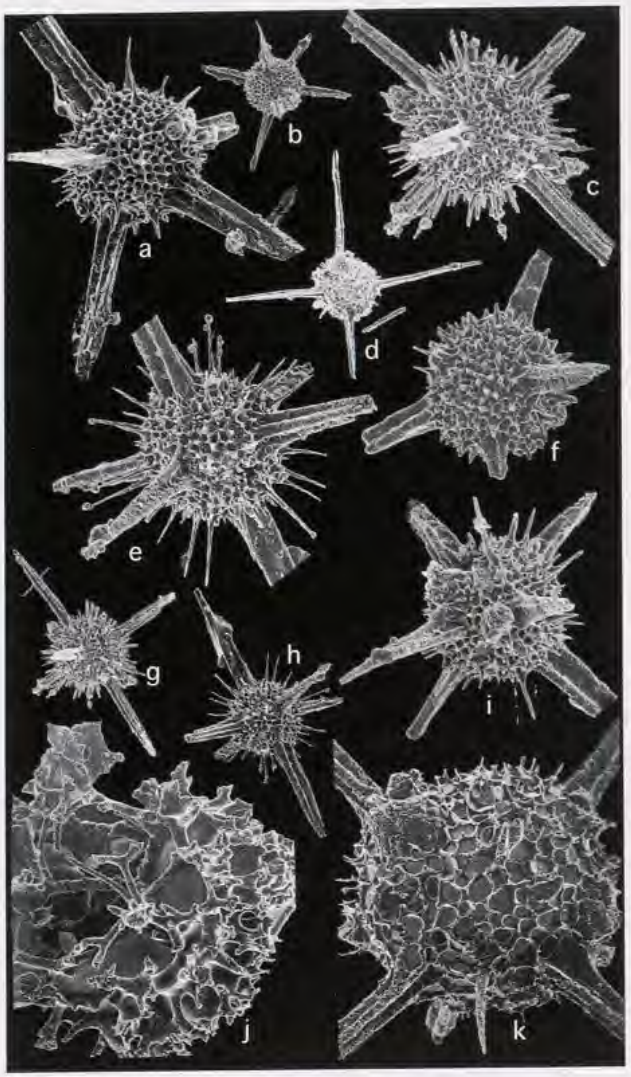

FIG. 5.— Sphaeroidal radiolariarians from Domanik Horizon (Domanik Section of Ukhta area, Sample 992). *Radiolaires sphaeroïdes de l'Horizon Domanik (coupe du Domanik de la région d'Ukhta, échantillon 992).* a, c, e, g, h, i: *Entactinosphaera grandis* Nazarov, a, c, e, i x128; g-h x64; b: *E.* sp. cf. *nigra* (Hinde), x64; d, k: *E. echinata* (Hinde), d x64; k x225; f: *E. assidera* Nazarov; j: *Haplentactinia inaudita* Nazarov, x200.

underlying strata (Fig. 4) and demonstrates the transgressive-regressive character towards Volgian strata. Radiolarians represent only a minor part of the total fauna. All taxa are known within the Boreal province of the Russian platform. The Kimmeridgian radiolarian assemblage of the Barents-Pechora-Ukhta region includes *Archaeocenosphaera ineaqualis* (Rust), *Praeconosphaera* ex gr. *sphaeroconus* (Rust), *Pseudocrucella* aff. *prava* Blome, *Crucella crassa* (Kozlova), *C. squama* (Kozlova), *C.* aff. *mexi-cana* Yang, *Orbiculiforma* cf. *iniqua* Blome, *O.* ? *retusa* (Kozlova), *Pantanellium tierra-blankaense* Pessagno & McLeod, *Parvicingula inornata* Blome, *P.* cf. *blowi* Pessagno, *P. haeckeli* (Pantanelli), *P. burnsensis* Pessagno & Whalen, *P. pizhmica* Kozlova, *P. pusilla* Kozlova, *P. papulata* Kozlova, *P. santabarbarensis* Pessagno, *P.* ? *enormis* Yang, *P.* ? *blackhornensis* Pessagno & Whalen, *Excingula* ? *bifaria* Kozlova.

The study of *Parvicingula* distribution shows the predominance of this genus in the Kimmeridgian of the Timan-Pechora and Barents regions. The species of this genus are represented by a wide range of morphotypes (Fig. 8). The co-occurence of Arcto-Boreal foraminiferal assemblages together with specific group of radiolarians and Buchia suggest the possibility to use *Parvicingula* as a Jurassic paleoclimatic indicator (VISHNEVSKAYA, 1996).

The Volgian strata has a transgressive character in the Pechora region. Within middle Volgian *Dorsoplanites panderi* ammonite Zone, among radiolarians *Parvicingula papulata* Kozlova, *P. conica* (Khabakov), *P. cristata* Kozlova, *P. rugosa* Kozlova, *P. simplicima* Kozlova are dominating species. Parvicingulids are up to 90% in the Barents-Pechora region, along with abundant ammonites, buchias and foraminiferas in these strata.

The uppermost part of the Volgian has a regressive character similar to the Ukhta Domanik Sections. Between Devonian and Jurassic levels, some similarity exists in the transgressive-regressive sequences and some difference in the composition of radiolarian assemblages and their paleoclimatic affinities. The bulk of Devonian radiolarians is represented by sphaeroid-like and spicula-like forms, which could be good deliverers of lipids (VISHNEVSKAYA *et al.*, 1993), in contrast to the Jurassic assemblages, where the parvicingulids, probably nassellarians of cold-water upwelling zones, were dominant. Radiolaria are the only planktic organisms known from Cambrian to recent, and are in great variety, although of their morphology, evolution, phylogeny and many paleoecological aspects are still unclear. One question is whether they were planktic, hemiplanktic or benthic during the whole Paleozoic? As we know, the first attempt of foraminifera to adopt the planktic mode of life started during Late Paleozoic and Triassic - Early Jurassic times, but appearance of definite planktic forms is Middle Jurassic (Bajocian) in age.

Source : MNHN, Paris

We do not know if and when radiolarians passed from benthic to planktic life. Possible planktic, benthic and transitionals forms could have existed simultaneously in the Middle-Late Devonian and possibly up to the Late Jurassic (VISHNEVSKAYA, 1993). This suggestion has certain significance for discussion about the time of appearance of recent oceans and the depth of the sedimentary domanikoid-type basins.

Bashkirian Domanik facies (30 m) has a similar structure and differs only by having phosphatic materials and rare glauconite, which can indicate a coeval volcanic activity, while Tatarian one (20 m) is characterized by abundant brachiopods in its lower and upper parts. To the north of Ukhta, the Kogva and Kolva Domanik facies (10-130 m) contain intraformational sandstone and silstone, indicating possible influence of islands, and is overlain by bituminous limestones with lenses of reef limestone debris.

The Jurassic domanikoid facies of Bashkiria and in the region of Syssola River contain abundant phosphate. The content of P_2O_5 reaches 25%, Al_2O_3 + Fe_2O_3 reaches 2-3% and C org. varies from 2 to 4-5% in the Kimmeridgian clay. The glauconite represents about 30% of the Kimmeridgian and Volgian clay. The content of P_2O_5 reaches 30%, Al_2O_3 and Fe_2O_3 is 3-4%, CaO is 40-45 % and C.org. is approximately 3-5% in the Volgian strata. In the region of the Syssola River in the Volgian Stage, KHUDYAEV (1931) recognized species belonging to *Parvicingula*: *(P.) multipora* Khudyaev, *P. susollaensis* Khudyaev, *P. khabakovi* Khudyaev, *P. zyrjanica* Khudyaev. The content of parvicingulides in the Syssola Basin is about 75%.

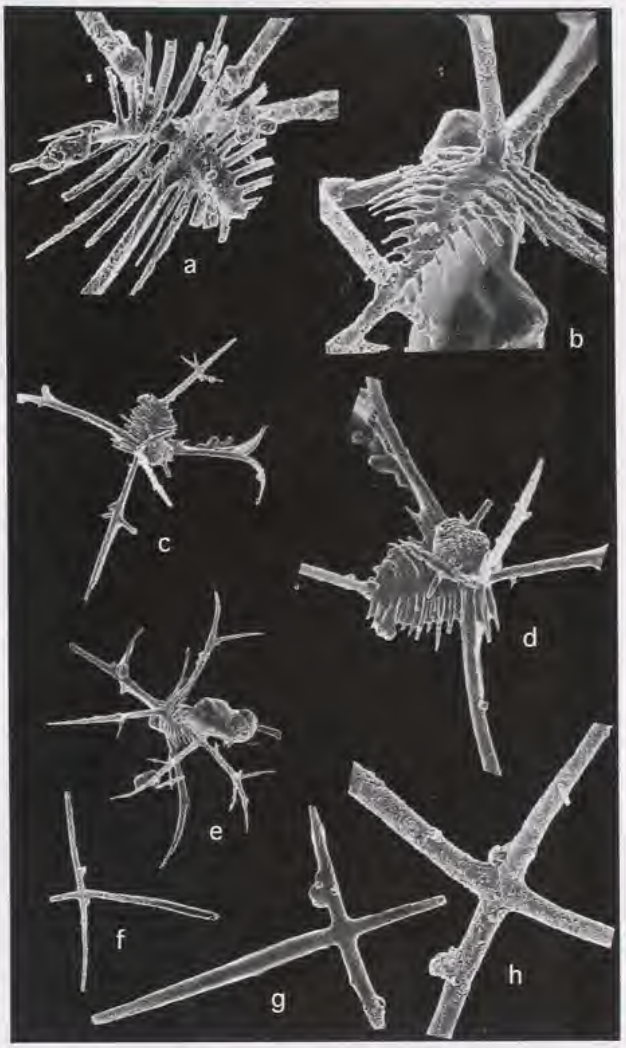

FIG. 6.— New species *Ceratoiskiscum mertsi* sp. nov. (a-e) and sponge spicules (f-h) from Domanik Section of Ukhta area, Sample 992. *Nouvelle espèce* Ceratoiskiscum mertsi *sp. nov. (a-e) et spicules d'éponges (f-h) de la coupe du Domanik dans la région de Ukhta.* a, b, h x225; c, e, f, g x64; d x96.

The Jurassic (Volgian) domanikoid facies of the Volga-Urals Basin are predominantly represented by bituminous clay with numerous fuel organic shale horizons (8-10 m, sometimes 15-25 m in thickness). The content of TOC is 10-55% in the Kashpir Section and 8-22% in the Gorodische Section. The admixture is composed of quartz, glauconite, foraminifers, sponge spicules and radiolarians. Among clay minerals of the Kashpir Section, hydromica (40-45%) is dominant. The distribution of the clay minerals in the Volgian organic rich strata of the Gorodische Section is as follows: montmorillonite (20-85%), hydromica (10-35%), kaolinite (10-45%), glauconite (5-40%). The maximum of montmorillonite is in the uppermost part of Volgian black shale. The Kimmeridgian clay minerals are represented by montmorillonite (15-30%), kaolinite (40-45%), hydromica (25-30%) and chlorite-glauconite (5-10%).

In the Gorodische section (Volga Basin), *Parvicingula jonesi* (Pessagno) is the dominant species within Kimmeridgian strata and *P. blowi* (Pessagno) is characteristic within Volgian strata. There, parvicingulid content reaches 50-60%. Within *Dorsoplanites panderi* ammonite Zone or the uppermost part of *Watznaueria communis* nannofossil Zone of the Gorodische Section radiolarians *Orbiculiforma* ex. gr. *mclaughlini* Pessagno, *Stichocapsa ? devorata* (Rust), *Phormocampe favosa* Khudyaev, *Parvicingula hexagonata* (Heitzer), *P. cristata* Kozlova, *P. conica* (Khabakov), *P.* aff. *alata* Kozlova,

Source : MNHN, Paris

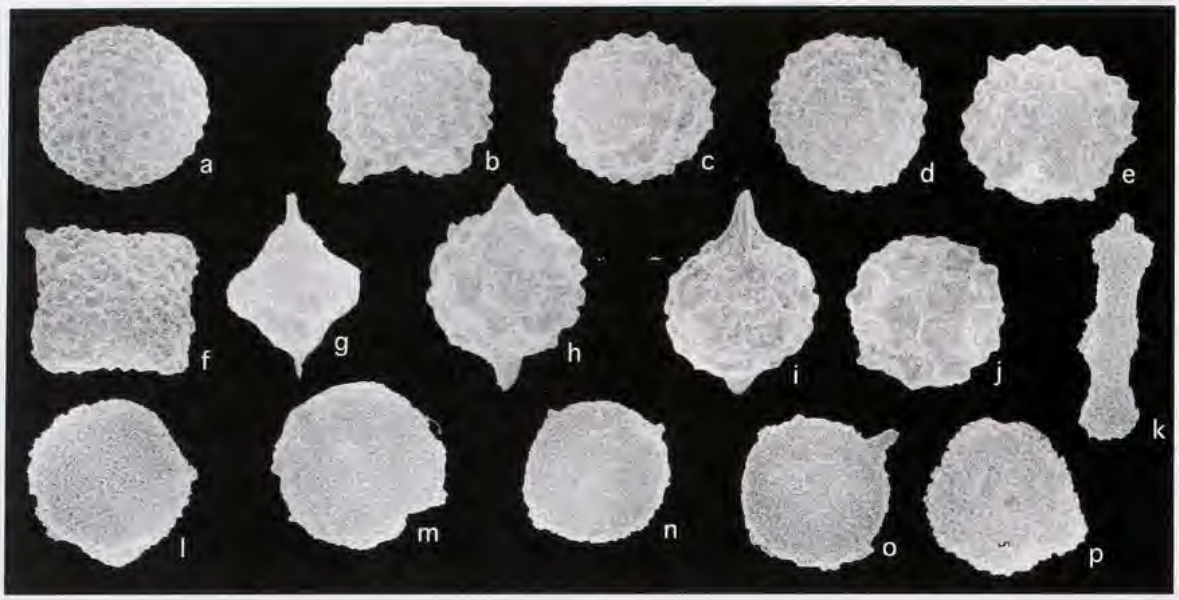

FIG. 7.— Kimmeridgian radiolarians of the Pechora Basin (Ukhta Section, Sample P).
Radiolaires kimmeridgiens du Bassin de Petchora (coupe de Ukhta, échantillon P). a: *Archaeocenosphaera ineaqualis* (Rust), x120; b,e: *Praeconosphaera* ex gr. *sphaeroconus* (Rust), b-d, x100, e, x200; f: *Crucella squama* (Kozlova), x200; g: *Pseudocrucella* aff. *prava* Blome, x200; h , j: *Pantanellium tierrablankaense* Pessagno & McLeod, x250; k: *Crucella* aff. *mexicana* Yang, x100; l: *Orbiculiforma* sp., x100; m: *O.* cf. *iniqua* Blome, x100; n,o: *O.* ? *retusa* (Kozlova), x100; p: *O.* sp., x100;

P. multipora (Khudyaev), *P.* aff. *haeckeli* (Pantanelli), *P.* aff. *spinosa* (Grill & Kozur), *Plathycryphalus* ? *pumilus* Rust, *Lithocampe* cf. *terniseriata* Rust were determined (Figs 9, 10). Tethyan species *P. boesii* (Parona) appears in the uppermost part of Volgian stage.

The Volgian strata of the Moscow district is represented by numerous phosphorite or phosphorite pebbles horizons where the content of TOC is low (less then 5%).

The main Kimmeridgian representatives of the Moscow region are *Parvicingula vera* Pessagno & Whalen, *P. inornata* Blome and *P. elegans* Pessagno & Whalen. Parvicingulids prevails, forming 50% of this assemblage and in the middle Volgian are represented by *P. haeckeli* (Pantanelli) and *P. hexagonata* (Heitzer) (BRAGIN, submitted).

South-western Saratov Domanikoid facies has organic-rich shale (13 m), while the Pachelma one (to 40 m) is characterized by bituminous clay with *Liorhynchus*, covered by the Famennian lagune-type deposits. The western Tambov-Tula Domanik level (40 m) is represented only by bituminous limestone and clay. To the west, the Devonian strata do not have oil-bearing character, only some coal beds occur. Kaluga and Moscow domanikoid facies (Fig. 3) are carbonaceous clays (5-38 m) with scarce organic matter. They are frequently underlain by sulphate complex with reworked spheroid-like radiolarians indicative of shallow shelf. Pripyat domanikoid facies also differs by numerous shallow-water spongy radiolarians. Devonian rifting was accompanied by basalt eruptions, as indicated at the Pripyat, Kaluga, Timan and Volga-Urals sites.

The Domanik basin is interpreted as a relatively shallow-water marginal sea (VISHNEVSKAYA, 1993), partly separated from Yapetus by an island arc and a barrier reef. Coeval volcanism confirms the active character of the Domanik basin. The formation of source rocks was concentrated in the Timan-Pechora and Volga-Urals basins of the Russian Plate, as is observed in the Jurassic rift-type basins. The organic shales were also accumulating in the same area. For this reasons, the Timan-Pechora and Volga-Urals Basins are of particular economic interest.

Source : MNHN, Paris

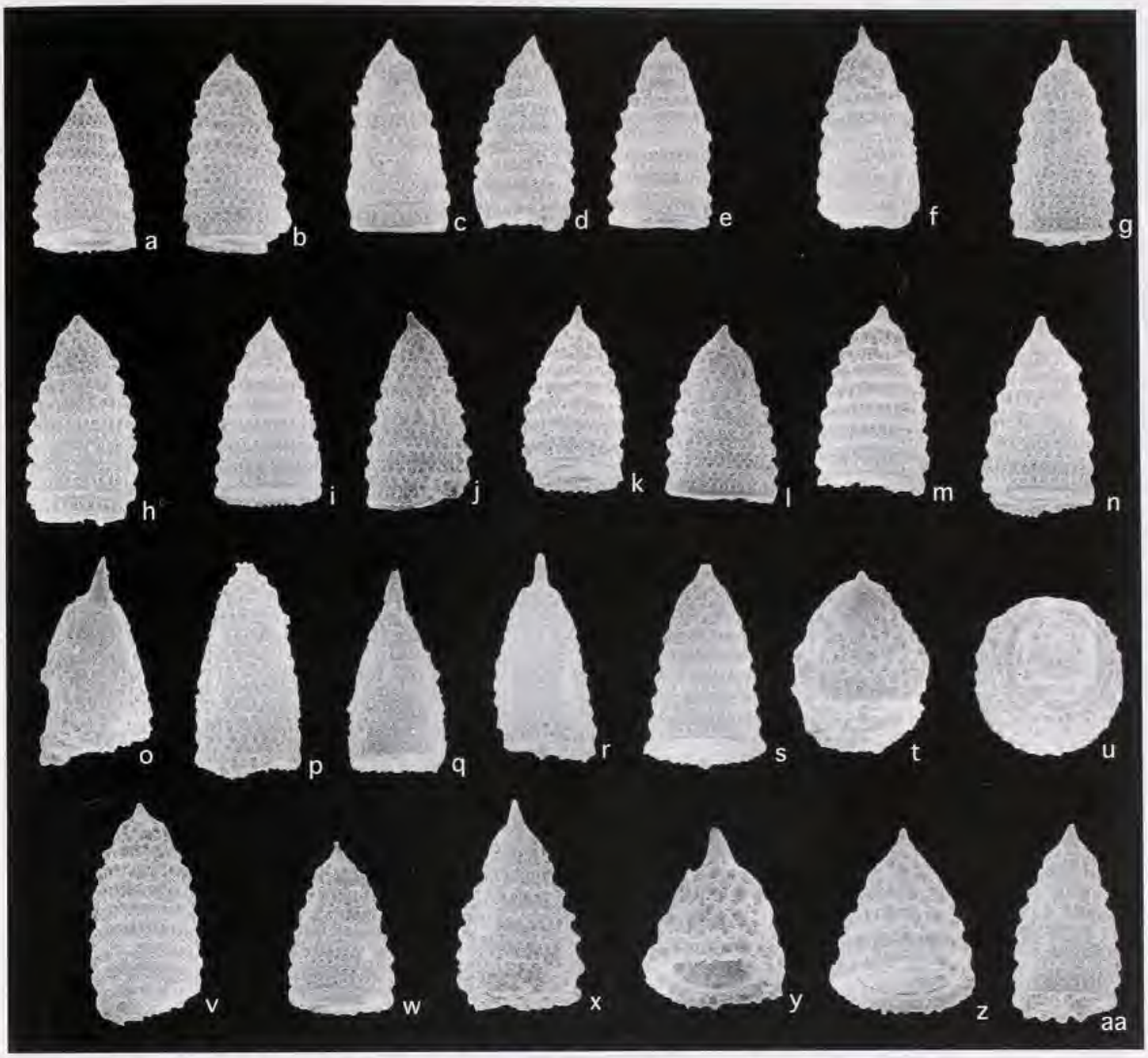

FIG. 8.— Kimmeridgian radiolarians of the Pechora Basin (Ukhta Section, Sample P).
Radiolaires kimmeridgiens du Bassin de Petchora (coupe de Ukhta, échantillon P). a: *Parvicingula inornata* Blome, x100; b,f: *P.* aff. *burnsensis* Pessagno & Whalen, b-c x100, d-f, x120; g: *P. haeckeli* (Pantanelli), x100; h: *P.* cf. *blowi* Pessagno, x100; i,k: *P. burnsensis* Pessagno & Whalen, x120; l: *P.* aff. *haeckeli* (Pantanelli), x100; m,n: *P. papulata* Kozlova, x120; o,p: *Excingula ? bifaria* Kozlova, o x150, p x100; q,r: *E.* ? sp., x100; s: *Parvicingula* ex gr. *burnsensis* Pessagno & Whalen, x120; t,u: *P.* sp., x150; v,w, aa: *P. ? enormis* Yang, x100; x,z: *P. ? blackhornensis* Pessagno & Whalen, x, x150, y-z, x200.

STRATIGRAPHIC CORRELATION OF THE JURASSIC DOMANIKOID FACIES

The lower Kimmeridgian *Parvicingula vera* Zone of the Barents-Timan-Pechora Basin (VISHNEVSKAYA & DE WEVER, 1996) is probably equivalent to the lower Kimmeridgian *Crucella crassa* Assemblage of KOZLOVA (1994) and correlates with the *Buchia concentrica* Zone, *A. kitchini* ammonite Zone and *Epistomina unzhensis* foraminiferal Zone as well. This interval may correspond to Kimmeridgian Clay Hydrocarbon Formation of the North Sea which contains abundant *P. jonesi* (DYER & COPESTAKE, 1989). Unfortunately, it is impossible to correlate the details of radiolarian assemblages and events as well as the stratigraphic distribution of individual taxa, because of confidentiality involving Britoil and its partners (DYER & COPESTAKE, 1989). For the same reasons, the distribution of samples within sites or boreholes was not figured.

Source : MNHN, Paris

The middle Volgian *Parvicingula haeckeli* Zone is closely correlated with the *Parvicingula papulata* Zone of Pechora Basin (KOZLOVA, 1994) and belongs to the *Dorsoplanites panderi* Zone which can be correlated with the *Evolutinella emeljanzevi-Trachammina septentrionalis* or *Saracenaria pravoslavlevi* foraminiferal Zone (KOZLOVA, 1994) in Pechora Basin and *Lenticulina biexcavata* Zone (LJUROV, 1994) in Syssola hydrocarbon Basin and *Parhabdolithus embergeri* nannoplankton Zone in Middle Volga hydrocarbon Basin. Due to microfossils we can trace this zone in Southern England and Northern France (VISHNEVSKAYA & DE WEVER, 1996).

Timan-Pechora and Volga Kimmeridgian-Volgian radiolarian assemblages are typically boreal in character in the presence of *Parvicingula* and the lack of *Mirifusus, Andromeda, Ristola, Acanthocircus diacranocanthos*, but subordinate development of Pantanellidae is fixed (Figs 8, 12). Nassellarian taxa are dominant in both (Figs 8, 9, 10) assemblages and diversity, mainly represented by species of *Parvicingula* and *Stichocapsa*.

FIG. 9.— Volgian radiolarians of the Volga-Urals Basin (Gorodische Section, Sample G).
Radiolaires volgiens du Bassin Volga-Oural (coupe de Gorodische, échantillon G). a,b: *Praeconosphaera* sp., a x120, b x150; c: *P.* ex gr. *sphaeroconus* (Rust), x150; d,f: *Orbiculiforma* ex gr. *mclaughlini* Pessagno, x150; g,h: *Stichocapsa ? devorata* (Rust), x150; i,k: *Phormocampe favosa* Khudyaev, x150; l: *Parvicingula hexagonata* (Heitzer), x150; m,r: *P. ? cristata* Kozlova, m x200, n-r x150; s,t: *Stichocapsa* sp., x150; u,v: *S.* sp. A, x150; w,x: *S.* sp. B, x150;

Source : MNHN, Paris

PALEOGEOGRAPHY OF THE VOLGIAN DOMANIKOID BLACK SHALE

The Jurassic stratigraphic sequences of the Timan-Pechora Basin (Fig. 4) show a clearly transgressive depositional system starting with Early-Middle Jurassic sands and deepening upward to the accumulation of the higher grade source rocks in the Volgian time. The mass extinction, observed there as well as in the Gorodische section of the Volga-Urals Basin (about 40 species of ammonites, 20 species of aucellids, 22 species of benthic and 20 species of planktonic foraminiferas, 10 species of belemnites, 5-40 taxa of calcareous nannofossils, 20 species of radiolarians and several species of algae were recognized within *Dorsoplanites panderi* Zone), possibly resulted from the cumulative effects of constant transgressive-regressive episodes (Fig. 4). The schematic paleogeographic reconstruction of the Volgian time suggests that the eastern rim of the shallow coastal sea had favorable environments for oil and fuel organic source rock accumulation (Fig. 11). As in recent marine environments, the maximal concentrations of phytoplankton, siliceous plankton and benthos, carbonaceous plankton, nekton and benthos were found in the water mass fringering the continent. The relative increase and good preservation in the bottom sediments of proportions of lipid rich organic matter was related to the preservative character of phosphorus.

In the Tethyan Realm, the genus *Parvicingula* is relatively rare, whereas more abundant in the Boreal (KHYDJAEV, 1931; SEDAEVA & VISHNEVSKAYA, 1995) and Australian provinces (VISHNEVSKAYA, 1996) reaches up to maximum. Owing to these data we can assume the cold water environments for the Jurassic domanikoid-bearing basin. Besides, the preponderance of parvicingulides can indicate an upwelling conditions which could exist along offshore.

PALEONTOLOGICAL DESCRIPTION

The description of some species from Ukhta Domanik Horizon and domanikoid shale is proposed.

Order SPUMELLARIA Ehrenberg, 1875

Family XIPHOSTYLIDAE Haeckel, 1881, *emend.* Pessagno & Yang, 1989

Genus ***ARCHAEOCENOSPHAERA*** Pessagno & Yang, 1989

Archaeocenosphaera inaequalis (Rust), 1898

Fig. 7, a

1898. *Cenosphaera inaequalis* Rust, pl. 26-1, fig. 6.

1994. *Archaeocenosphaera inaequalis* (Rust), KOZLOVA, pl. 1, figs 1, 2, 4-7.

RANGE AND OCCURRENCE— Late Jurassic (early Kimmeridgian), *Amoeboceras kitchini* ammonite zone, Ukhta section, Pechora River, Komi area, Russia, Sample P.

Family ACAENIOTYLIDAE Yang, 1993

Genus ***PRAECONOSPHAERA*** Yang, 1993

Praeconosphaera* ex gr. *sphaeroconus (Rust), 1898

Fig. 7, b-e; Fig. 9, c

1898. *Conosphaera sphaeroconus* Rust, p. 13, pl. 4, Fig. 8.

1993. *Praeconosphaera sphaeroconus* (Rust), YANG, p. 105, pl. 17, figs 2, 6, 12 ,16 ,23.

1994. *Praeconocaryomma sphaeroconus* (Rust), KOZLOVA, pl. 1, figs 9, 13.

Source : MNHN, Paris

RANGE AND OCCURRENCE— Late Jurassic (early Kimmeridgian), *Amoeboceras kitchini* ammonite zone, Ukhta section, Pechora River, Komi area, Russia, Sample P and late Volgian, *Craspedites subditus* ammonite zone, Gorodische standard Section of the Russian plate, Sample G.

***Praeconosphaera* sp.**

Fig. 9, a-b

RANGE AND OCCURRENCE— Late Volgian, *Craspedites subditus* ammonite zone, Gorodische standard Section of the Russian plate, Sample G.

Family PATULIBRACCHIDAE Pessagno, 1971, *emend.* Baumgartner, 1980

Genus ***CRUCELLA*** Pessagno, 1971

Crucella squama (Kozlova), 1971

Fig. 7, f

1971. *Hagiastrum squama* Kozlova, p. 1176, text-fig. 1: 10.
1994. *Crucella squama* (Kozlova), KOZLOVA, pl. 2, fig. 3.

RANGE AND OCCURRENCE.— Late Jurassic (early Kimmeridgian), *Amoeboceras ravni* ammonite zone, Ukhta section, Pechora River, Komi area, Russia, Sample P.

Crucella* aff. *mexicana Yang, 1993

Fig. 7, k

1993. *Crucella mexicana* Yang, p. 40, pl. 4, figs 10, 11, 14, 16; pl. 5, figs 10, 21.

RANGE AND OCCURRENCE.— Late Jurassic (early Kimmeridgian), *Amoeboceras ravni* ammonite zone, Ukhta section, Pechora River, Komi area, Russia, Sample P.

Family HAGIASTRIDAE Riedel, 1971, *emend.* Baumgartner, 1980

Genus ***PSEUDOCRUCELLA*** Baumgartner, 1980

Pseudocrucella* aff. *prava Blome, 1984

Fig. 7, g

1984. *Pseudocrucella prava* Blome, p. 352, pl. 3, figs 1-4, 6, 8-17; pl. 4, figs 1-4, 6-10, 12, 14-16, pl. 15, figs 16-17.

RANGE AND OCCURRENCE— Late Jurassic (early Kimmeridgian), *Amoeboceras kitchini* ammonite zone, Ukhta section, Pechora River, Komi area, Russia, Sample P.

Family PANTANELLIDAE Pessagno, 1977, *sensu* Pessagno & Blome, 1980

Genus ***PANTANELLIUM*** Pessagno, 1977, *sensu* Pessagno & Blome, 1980

Pantanellium tierrablankaense Pessagno & McLeod, 1987

Fig. 7, h-j

1987. *Pantanellium tierrablankaense* Pessagno & McLeod, p. 24, pl. 6, figs 5, 7, 8, 13-18.

RANGE AND OCCURRENCE— Late Jurassic (early Kimmeridgian), *Amoeboceras kitchini* ammonite zone, Ukhta section, Pechora River, Komi area, Russia, Sample P.

Source : MNHN, Paris

***Pantanellium* sp. A**

Fig. 12, a

Shell spherical without spines, with a mixture of large-sized pentagonal and hexagonal pore frames. Only three pore frames visible along diameter of shell.

RANGE AND OCCURRENCE— Late Jurassic (early Kimmeridgian), *Amoeboceras kitchini* ammonite zone, Ukhta section, Pechora River, Komi area, Russia, Sample P.

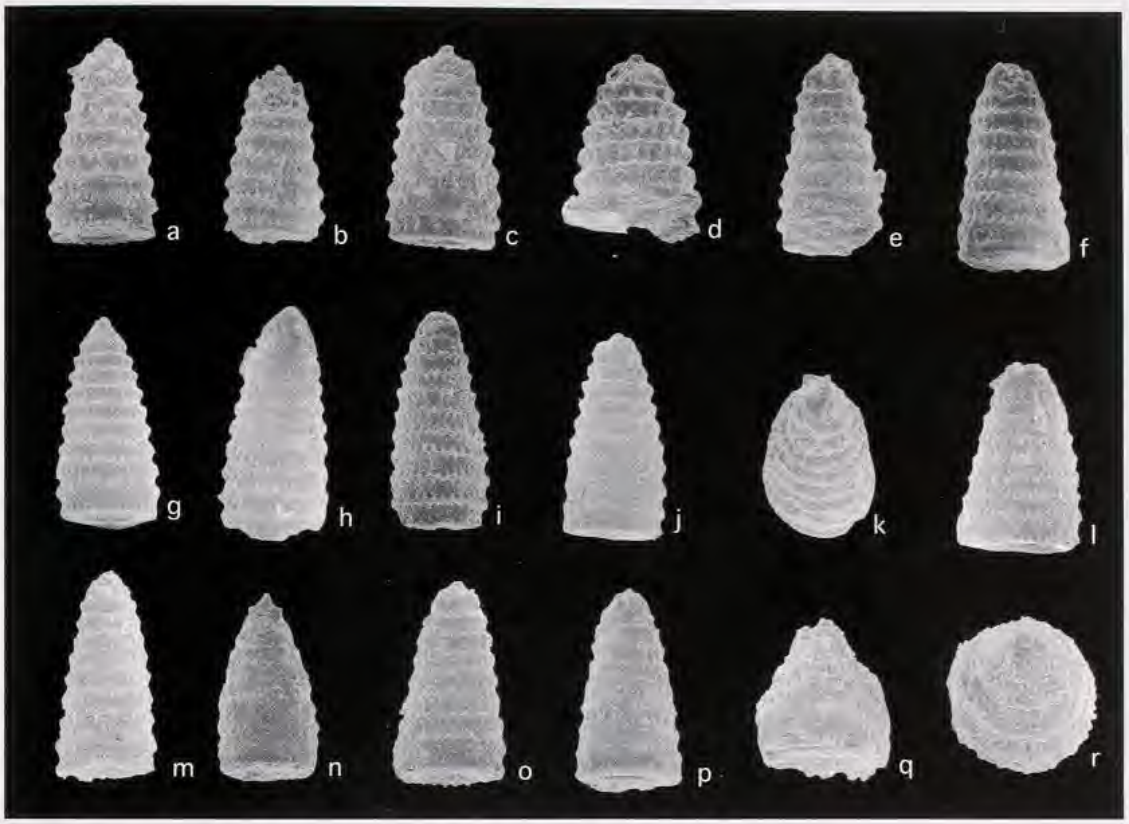

FIG. 10.— Volgian radiolarians of the Volga-Urals Basin (Gorodische Section, Sample G).
Radiolaires volgiens du Bassin Volga-Oural (coupe de Gorodische, échantillon G). a: *Parvicingula conica* (Khabakov), x150; b-f, h-j, m, o-p: *P.* aff. *alata* Kozlova, b-f, h, o-p x150, i-j, m x100; g: *P. multipora* (Khudyaev), x120; k: *P.* sp., x150; l: *P.* aff. *thomesensis* Pessagno, x150; n: *Parvicingula* aff. *spinosa* (Grill & Kozur), x100; q: *Platycryphalus ? pumilus* Rust, x150; r: *Lithocampe* cf. *terniseriata* Rust, x200.

Family ORBICULIFORMIDAE Pessagno, 1973

Genus ***ORBICULIFORMA*** Pessagno, 1973

Orbiculiforma* cf. *iniqua Blome, 1984

Fig. 7, m

1984. *Orbiculiforma iniqua* Blome, p. 353, pl. 5, figs 3, 4, 6, 7, 10, 11, 14-16.

RANGE AND OCCURRENCE— Late Jurassic (early Kimmeridgian), *Amoeboceras kitchini* ammonite zone, Ukhta section, Pechora River, Komi area, Russia, Sample P.

Source : MNHN, Paris

Orbiculiforma ? *retusa* (Kozlova), 1994

Fig. 7, n-o

1994. *Staurodictya retusa* Kozlova, pl. 2, figs 9-10.

RANGE AND OCCURRENCE— Late Jurassic (early Kimmeridgian), *Amoeboceras kitchini* ammonite zone, Ukhta section, Pechora River, Komi area, Russia, Sample P.

Orbiculiforma ex gr. *mclaughlini* Pessagno, 1977

Fig. 9, d-f

1977. *Orbiculiforma mclaughlini* Pessagno, p. 74, pl. 4, figs 4-7.
1989. *Orbiculiforma mclaughlini* Pessagno, DYER & COPESTAKE, p. 224, pl. 1, figs 3-4.

RANGE AND OCCURRENCE— Late Volgian, *Craspedites subditus* ammonite zone, Gorodische standard Section of the Russian plate, Sample G.

Orbiculiforma sp.

Fig. 7, l, p

RANGE AND OCCURRENCE— Late Jurassic (early Kimmeridgian), *Amoeboceras kitchini* ammonite zone, Ukhta section, Pechora River, Komi area, Russia, Sample P.

Family ENTACTINIIDAE Riedel, 1967, *emend.* Nazarov and Ormiston, 1984

Genus *ENTACTINOSPHAERA* Foreman, 1963

Entactinosphaera echinata (Hinde), 1899

Fig. 5, d, k

1899. *Heliosoma echinatum* Hinde, p. 50, pl. 9, figs 1-2.
1955. *Xiphosphaera echinatum* (Hinde), BYKOVA, p. 68, pl. 22, figs 4-5.
1963. *Entactinosphaera echinata* (Hinde), FOREMAN, p. 279, pl. 3, fig. 10; pl. 4, fig. 12.
1975. *Entactinosphaera echinata* (Hinde), NAZAROV, p. 60, pl. 3, figs 1-3; pl. 4, figs 1-4.
1983. *Entactinosphaera echinata* (Hinde), NAZAROV & ORMISTON, p. 458, pl. 1, figs 6-7.
1993. *Entactinosphaera echinata* (Hinde), AITCHISON, p. 115, pl. 5, figs 6, 11, 14; pl. 7, fig. 3.

RANGE AND OCCURRENCE.— Late Devonian (middle Frasnian), conodont zone *P. punctata*, Domanik Horizon, Ukhta section, Domanik Creek, Komi area, Russia, so far as known.

Entactinosphaera assidera Nazarov, 1975

Fig. 5, f

1975. *Entactinosphaera assidera* Nazarov, p. 64, pl. 5, figs 6-7; pl. 6, figs 6-8.

RANGE AND OCCURRENCE.— Late Devonian (middle Frasnian), conodont zone *P. punctata*, Domanik Horizon, Ukhta section, Domanik Creek, Komi area, Russia, so far as known.

Source : MNHN, Paris

Entactinosphaera grandis Nazarov, 1975

Fig. 5, a, c, e, g-i

1975. *Entactinosphaera grandis* Nazarov, pl. 5, figs 11-12; pl. 7, figs 1-4.
1988. *Entactinosphaera grandis* Nazarov, pl. 14, fig. 8.
1983. *Entactinosphaera grandis* Nazarov, NAZAROV & ORMISTON, p. 458, pl. 1, figs 4-5. 1993. Entactinosphaera grandis Nazarov, AITCHISON, p. 115, pl. 5, fig. 8.

RANGE AND OCCURRENCE.— Late Devonian (middle Frasnian), conodont zone *P. punctata,* Domanik Horizon, Ukhta section, Domanik Creek, Komi area, Russia, so far as known.

Entactinosphaera* sp. cf. *nigra (Hinde)

Fig. 5, b

RANGE AND OCCURRENCE.— Late Devonian (middle Frasnian), conodont zone *P. punctata*, Domanik Horizon, Ukhta section, Domanik Creek, Komi area, Russia, so far as known.

Family HAPLENTACTINIIDAE Nazarov, 1980

Genus ***HAPLENTACTINIA*** Foreman, 1963

Haplentactinia inaudita Nazarov, 1988

Fig. 5, j

1988. *Haplentactinia inaudita* Nazarov, pl. 14, fig. 6.

RANGE AND OCCURRENCE.— Late Devonian (middle Frasnian), conodont zone *P. punctata*, Domanik Horizon, Ukhta section, Domanik Creek, Komi area, Russia, so far as known.

Order NASSELLARIA Ehrenberg, 1875

Family PARVICINGULIDAE Pessagno, 1977

Genus ***EXCINGULA*** Kozlova, 1994

Excingula ? bifaria Kozlova, 1994

Fig. 8, o-p, Fig. 12, e

1994. *Excingula bifaria* Kozlova, pl. 5, figs 5-710.

RANGE AND OCCURRENCE— Late Jurassic (early Kimmeridgian), *Amoeboceras kitchini* ammonite zone, Ukhta section, Pechora River, Komi area, Russia, Sample P.

***Excingula* sp.**

Fig. 8, q-r

RANGE AND OCCURRENCE— Late Jurassic (early Kimmeridgian), *Amoeboceras kitchini* ammonite zone, Ukhta section, Pechora River, Komi area, Russia, Sample P.

Source : MNHN, Paris

Genus *PARVICINGULA* Pessagno, 1977

Parvicingula aff. *alata* Kozlova, 1994

Fig. 10, b-f, h-j, m, o-p

1994. *Parvicingula alata* Kozlova, pl. 8, Figs 1-3, 6.

RANGE AND OCCURRENCE— Late Volgian, *Craspedites subditus* ammonite zone, Gorodische standard Section of the Russian plate, Sample G.

Parvicingula antoshkinae sp. nov.

Fig. 12, h

1984. *Parvicingula* sp. A, BLOME, p. 364, pl. 9, fig. 10.

DIAGNOSIS.— Test elongate, subconical with nine to eleven chambers. Cephalis spherical smooth, slightly perforated, with thin and short pointed horn. Thorax, abdomen and first postabdominal chamber in form of discontinuous circumferential ridges, low and round, formed by rows of thick, parallel nodes or bars. Postabdominal chambers form subcylindrical part of shell with circumferential ridges. Each chamber with three rows of polygonal pore frames.

COMPARISON.— *Parvicingula antoshkinae* sp. nov. differs from *P. elegans* Pessagno & Whalen, 1982 by presence of nodes and worse development circumferential ridges.

MEASUREMENTS.— (8 specimens): in micrometers. High of test is 280-300, width in apical part (WA) is 80-90, width of the terminal tube is 135-145.

TYPE LOCALITY.— Clay of Pizhma Creek in Pechora River Basin, Sample P, near Siktivkar town, Komi area, Russia.

ETYMOLOGY.— Named in honour of Dr. A.I. Antoshkina for her contributions to the study of the Timan-Pechora faunas.

RANGE AND OCCURRENCE— Late Jurassic (early Kimmeridgian), *Amoeboceras kitchini* ammonite zone, Ukhta section, Pechora River, Komi area, Russia, Sample P.

Parvicingula ? blackhornensis Pessagno & Whalen, 1982

Fig. 8, x-z

1982. *Parvicingula blackhornensis* Pessagno & Whalen, p. 137, pl. 10, figs 10-12, pl. 13, Fig. 14.
1984. *Parvicingula blackhornensis* Pessagno & Whalen, BLOME, p. 357, pl. 9, figs 6, 11, 15, 22; pl. 15, Figs 3, 8.

RANGE AND OCCURRENCE— Late Jurassic (early Kimmeridgian), *Amoeboceras kitchini* ammonite zone, Ukhta section, Pechora River, Komi area, Russia, Sample P.

Parvicingula cf. *blowi* Pessagno, 1977

Fig. 8, h

1977. *Parvicingula blowi* Pessagno, p. 85, pl. 8, figs 11-14.
1984. *Parvicingula blowi* Pessagno, PESSAGNO *et al.*, p. 26, pl. 2, figs 14-15.
1989. *Parvicingula blowi* Pessagno, DYER & COPESTAKE, p. 227, pl. 2, figs 3-4.
1995. *Parvicingula blowi* Pessagno, HULL, p. 21, pl. 3, figs 6, 18, 22.

RANGE AND OCCURRENCE— Late Jurassic (early Kimmeridgian), *Amoeboceras kitchini* ammonite zone, Ukhta section, Pechora River, Komi area, Russia, Sample P.

Source : MNHN, Paris

Parvicingula burnsensis Pessagno & Whalen, 1982

Fig. 8, i-k

1982. *Parvicingula burnsensis* Pessagno & Whalen, p. 136, pl.
1992. *Parvicingula* cf. *bursnensis* Pessagno & Whalen, VISHNEVSKAYA, p. 27, pl. 1, fig. 15.
1994. *Parvicingula burnsensis* Pessagno & Whalen, KOZLOVA, pl. 3, figs 5-6.
1994. *Parvicingula burnsensis* Pessagno & Whalen, VISHNEVSKAYA, p. 217, figs 14-19.

RANGE AND OCCURRENCE— Late Jurassic (early Kimmeridgian), *Amoeboceras kitchini* ammonite zone, Ukhta section, Pechora River, Komi area, Russia, Sample P.

Parvicingula* aff. *burnsensis Pessagno & Whalen, 1982

Fig. 8, b-f

RANGE AND OCCURRENCE— Late Jurassic (early Kimmeridgian), *Amoeboceras kitchini* ammonite zone, Ukhta section, Pechora River, Komi area, Russia, Sample P.

Parvicingula* ex gr. *burnsensis Pessagno & Whalen, 1982

Fig. 8, s

RANGE AND OCCURRENCE— Late Jurassic (early Kimmeridgian), *Amoeboceras kitchini* ammonite zone, Ukhta section, Pechora River, Komi area, Russia, Sample P.

Parvicingula conica (Khabakov)

Fig. 10, a

1994. *Parvicingula conica* (Khabakov), KOZLOVA, pl. 8, figs 4, 8.

RANGE AND OCCURRENCE— Late Volgian, *Craspedites subditus* ammonite zone, Gorodische standard Section of the Russian plate, Sample G.

Parvicingula ? cristata Kozlova, 1994

Fig. 9, m-r

1994. *Parvicingula cristata* Kozlova, pl. 4, fig. 11.

RANGE AND OCCURRENCE.— Late Volgian, *Craspedites subditus* ammonite zone, Gorodische standard Section of the Russian plate, Sample G.

Parvicingula ? enormis Yang, 1993

Fig. 8, w-x, aa; Fig. 12, b

1993. *Parvicingula (?) enormis* Yang, p. 118, pl. 19, figs 6, 13, 18; pl. 20, figs 5, 6, 15, 22.

RANGE AND OCCURRENCE— Late Jurassic (early Kimmeridgian), *Amoeboceras kitchini* ammonite zone, Ukhta section, Pechora River, Komi area, Russia, Sample P.

Source : MNHN, Paris

Parvicingula genrietta sp. nov.

Fig. 12, f

DIAGNOSIS.— Test in form of low conical with short thin horn. Cephalis, thorax, abdomen and postabdominal chambers covered by irregular pores. Subsequent postabdominal chambers in form of circumferential ridges with three rows of hexagonal pore frames.

COMPARISON.— *Parvicingula genrietta* Vishnevskaya, n. sp., differs from *P. pizhmica* Kozlova, 1994 by the lack of circumferential ridges in the initial part of shell.

MEASUREMENTS.— (4 specimens) mean in micrometers. The high is 210-240, width of apical portion of the test (WA) is 100-110, maximum width of the terminal tube is 170-200.

TYPE LOCALITY.— Clay of Pizhma Creek in Pechora River Basin, Sample P, near Siktivkar town, Komi area, Russia.

ETYMOLOGY.— Named in honour of Dr. Genrietta Kozlova for her pioner contributions to the study of the Boreal radiolarians.

RANGE AND OCCURRENCE.— Late Jurassic (early Kimmeridgian), *Amoeboceras kitchini* ammonite zone, Ukhta section, Pechora River, Komi area, Russia, Sample P.

Parvicingula haeckeli (Pantanelli), 1898

Fig. 8, g, Fig. 12, c

1898. *Lithocampe haeckeli* Pantanelli, 1880, pl. 10, fig. 6.
1885. *Lithocampe haeckeli* Pantanelli, RUST, pl. 15, fig. 6.
1971. *Eucyrtidium haeckeli* (Pantanelli), KOZLOVA, p. 1176, text-fig. 1: 17.
1994. *Parvicingula haeckeli* (Pantanelli), KOZLOVA, pl. 3, figs 1-2; pl. 4, fig. 2.

RANGE AND OCCURRENCE.— Late Jurassic (early Kimmeridgian), *Amoeboceras kitchini* ammonite zone, Ukhta section, Pechora River, Komi area, Russia, Sample P.

Parvicingula aff. *haeckeli* (Pantanelli), 1898

Fig. 8, l

RANGE AND OCCURRENCE.— Late Jurassic (early Kimmeridgian), *Amoeboceras kitchini* ammonite zone, Ukhta section, Pechora River, Komi area, Russia, Sample P.

Parvicingula hexagonata (Heitzer), 1930

Fig. 9, l

1930. *Cyrtocalpis hexagonata* Heitzer, p. 391, pl. 1.

RANGE AND OCCURRENCE.— Late Volgian, *Craspedites subditus* ammonite zone, Gorodische standard Section of the Russian plate, Sample G.

Source : MNHN, Paris

Parvicingula inornata Blome, 1984

Fig. 8, a, Fig. 12, g

1984. *Parvicingula inornata* Blome, p. 360, pl. 9, figs 7, 17, 18; pl. 10, figs 2, 7, 9, 13.
1994. *Parvicingula inornata* Blome, KOZLOVA, pl. 4, fig. 1.
1994. *Parvicingula inornata* Blome, VISHNEVSKAYA, p. 217, figs 14-18.

RANGE AND OCCURRENCE— Late Jurassic (early Kimmeridgian), *Amoeboceras kitchini* ammonite zone, Ukhta section, Pechora River, Komi area, Russia, Sample P.

Parvicingula multipora (Khudyaev), 1931

Fig. 10, g

1931. *Dictyomitra multipora* Khudyaev, p. 23, pl. 1, fig. 52.

A regularly conical outline of shell with "a spine-like outgrowth"(KHUDYAEV, 1931) or an apical horn upon the cephalis and three rows of hexagonal pores decreasing in size toward cephalis, as well as presence of circumferential ridges at chamber joints allow to consider this species within genus *Parvicingula*.

RANGE AND OCCURRENCE— Late Volgian, *Craspedites subditus* ammonite zone, Gorodische standard Section of the Russian plate, Sample G.

Parvicingula papulata Kozlova, 1994

Fig. 8, m-n, Fig. 12, i

1994. *Parvicingula papulata* Kozlova, pl. 5, figs 5-7, 10.

RANGE AND OCCURRENCE— Late Jurassic (early Kimmeridgian), *Amoeboceras kitchini* ammonite zone, Ukhta section, Pechora River, Komi area, Russia, Sample P.

Parvicingula spinosa (Grill & Kozur), 1986

Fig. 10, n

1986. *Pseudodictyomitrella spinosa* Grill & Kozur, p. 253, pl. 7, figs 1-3.

The presense of conical shape with an apical horn and primitive arrangment of pores in horizontal rings rather indicates the belonging to *Parvicingula* than *Pseudodictyomitrella*.

RANGE AND OCCURRENCE— Late Volgian, *Craspedites subditus* ammonite zone, Gorodische standard Section of the Russian plate, Sample G.

Parvicingula aff. *thomesensis* Pessagno, 1977

Fig. 10, l

1977. *Parvicingula thomesensis* Pessagno, p. 49, pl. 8, figs 12, 25, 29.

RANGE AND OCCURRENCE.— Late Jurassic (late Volgian), *Craspedites subditus* ammonite zone, Gorodische standard Section of the Russian plate, Sample G.

Source : MNHN, Paris

Parvicingula sp. K

Fig. 12, d

REMARKS.— This form differs from all described *Parvicingula* by presence of well visible vertical and dorsal spines.

RANGE AND OCCURRENCE— Late Jurassic (early Kimmeridgian), *Amoeboceras kitchini* ammonite zone, Ukhta section, Pechora River, Komi area, Russia, Sample P.

Parvicingula sp.

Fig. 8, t-u, Fig. 10, k

RANGE AND OCCURRENCE— Late Jurassic (early Kimmeridgian), *Amoeboceras kitchini* ammonite zone, Ukhta section, Pechora River, Komi area, Russia, Sample P and Late Volgian, *Craspedites subditus* ammonite zone, Gorodische standard Section of the Russian plate, Sample G.

Family PHORMOCAMPIDAE Haeckel, 1887

Genus ***PHORMOCAMPE*** Haeckel, 1887

Phormocampe favosa Khudyaev, 1931

Fig. 9, h-k

1931. *Phormocampe favosa* Khudyaev, p. 41, pl. 1, fig. 33.

RANGE AND OCCURRENCE.— Late Jurassic (late Volgian), *Craspedites subditus* ammonite zone, Gorodische standard Section of the Russian plate, Sample G.

Family LITHOCAMPIDAE Haeckel, 1887

Genus ***LITHOCAMPE*** Ehrenberg, 1838

Lithocampe* cf. *terniseriata Rust, 1885

Fig. 10, r

1885. *Lithocampe terniseriata* Rust, p. 315, pl. 39, fig. 13.
1931. *Lithocampe terniseriata* Rust, KHUDYAEV, p. 25, pl. 1, fig. 44.

RANGE AND OCCURRENCE.— Late Jurassic (late Volgian), *Craspedites subditus* ammonite zone, Gorodische standard Section of the Russian plate, Sample G.

Genus ***PLATYCRYPHALUS*** Rust, 1885

Platycryphalus ? pumilus Rust, 1885

Fig. 10, q

1885. *Platycryphalus pumilus* Rust, p. 305, pl. 36, fig. 10.
1931. *Platycryphalus pumilus* Rust, KHUDYAEV, p. 39, pl. 1, fig. 17.

RANGE AND OCCURRENCE.— Late Jurassic (late Volgian), *Craspedites subditus* ammonite zone, Gorodische standard Section of the Russian plate, Sample G.

Source : MNHN, Paris

Genus ***STICHOCAPSA*** Haeckel, 1881

Stichocapsa ? devorata (Rust), 1885, ***sensu*** Dyer & Copestake, 1989

Fig. 9, g-h

1885. *Stichocapsa devorata* Rust, p. 318, pl. 41, figs 7-8.
1931. *Stichocapsa* aff. *devorata* Rust, KHUDYAEV, p. 45, pl. 1, fig. 46.
1989. *Stichocapsa devorata* Rust, DYER & COPESTAKE, p. 228, pl. 2, figs 9-11.

RANGE AND OCCURRENCE.— Late Jurassic (late Volgian), *Craspedites subditus* ammonite zone, Gorodische standard Section of the Russian plate, Sample G.

Stichocapsa sp. A

Fig. 9, u-v

RANGE AND OCCURRENCE.— Late Jurassic (late Volgian), *Craspedites subditus* ammonite zone, Gorodische standard Section of the Russian plate, Sample G.

Stichocapsa sp. B

Fig. 9, w-x

RANGE AND OCCURRENCE.— Late Jurassic (late Volgian), *Craspedites subditus* ammonite zone, Gorodische standard Section of the Russian plate, Sample G.

Stichocapsa sp.

Fig. 9, s-t

RANGE AND OCCURRENCE.— Late Jurassic (late Volgian), *Craspedites subditus* ammonite zone, Gorodische standard Section of the Russian plate, Sample G.

Order ALBAILLELLARIA Deflandre, 1953 *emend.* Holdsworth

Family CERATOIKISCIDAE Holdsworth, 1969

Genus ***CERATOIKISCUM*** Deflandre, 1953

Ceratoikiscum mertsi sp. nov.

Fig. 6, a-e

DIAGNOSIS.— Test as with family. Triangular frame is made by a-rod, b-rod and intersector spines. The a-rod has 12 pairs of caveal ribs. All rods are approximately equal in length. They are armed by the secondary spines in the post-triangle portions. The patagium and lamellar shell are absent.

COMPARISON.— This species can be distinguished from others due to the presence of numerous (12) caveal ribs.

MEASUREMENTS.— (3 specimens): mean (and range) in micrometers. The length of rods is 300 (290-330). The mean length of caveal ribs is 50.

Source : MNHN, Paris

FIG. 11.— Paleogeographic map of the Volgian stage.
1, sandstone and siltstone; **2**, clay; **3**, organic shale; **4**, coal and organic detritus; **5**, phosphate; **6**, land; **7**, location of sections from Fig. 4 (number in circle); **8**, location of outcrops (letter in circle).

FIG. 11.— Carte paléogéographique du Volgien.
***1**, grès et pélites ; **2**, argiles ; **3**, shale organique ; **4**, charbon et débris organique; **5**, phosphate ; **6**, terres emergées ; **7**, localisations des coupes de la figure 4 (nombres encerclés) ; **8**, localisation des affleurements (lettres encerclées).*

Source : MNHN, Paris

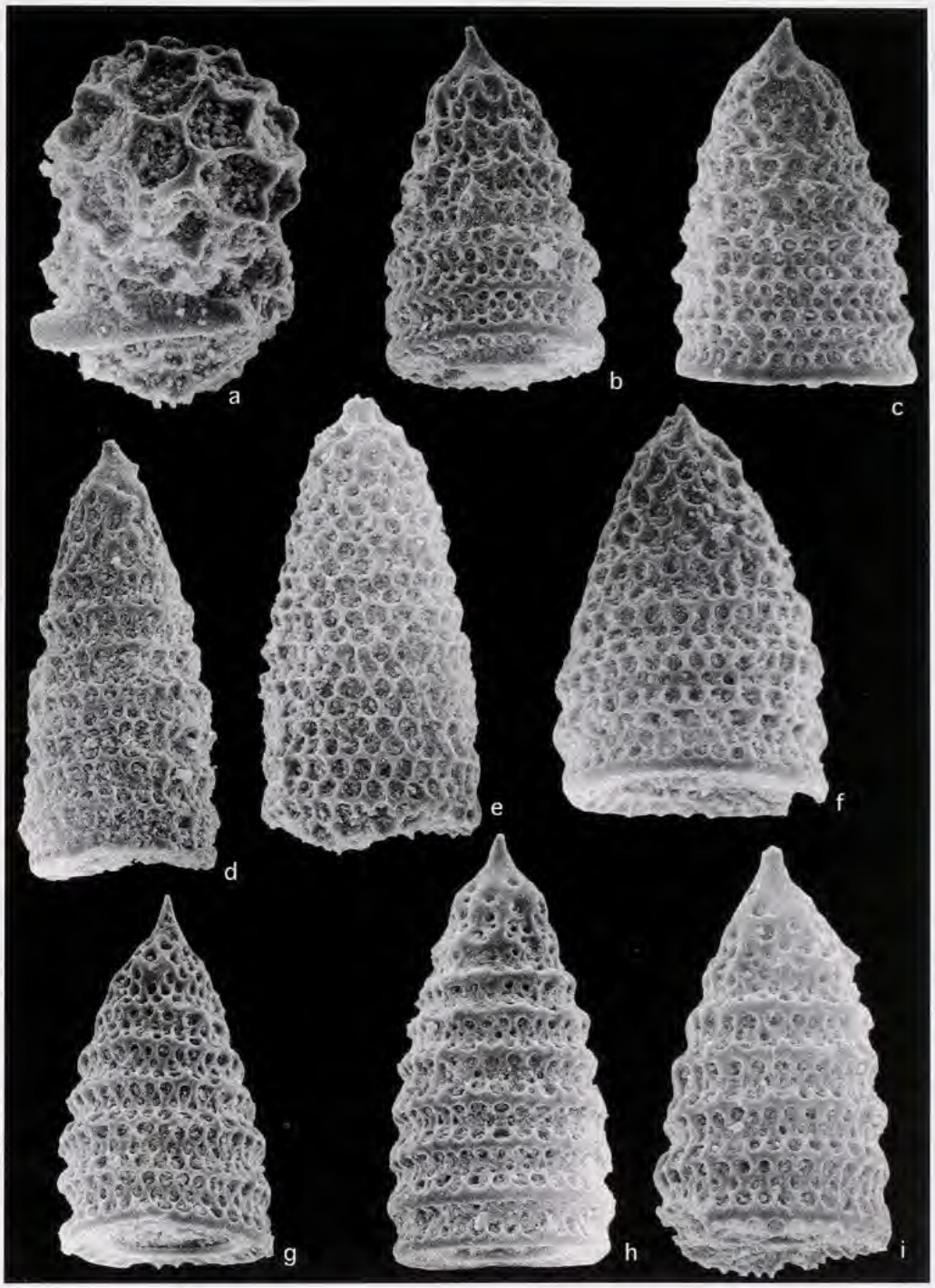

FIG. 12.— Some Kimmeridgian radiolarians of the Pechora Basin (Ukhta Section, Sample P).
Quelques radiolaires du Kimmeridgien du Bassin de Petchora (coupe de Ukhta, échantillon P). a: *Pantanellium* sp. A, x300; b: *Parvicingula ? enormis* Yang, x170; c: *P. haeckeli* (Pantanelli), x170; d: *P.* sp. K, x170; e: *Excingula ? bifaria* Kozlova, x170; f: *Parvicingula genrietta* sp. nov., x215; g: *P. inornata* Blome, x170; h: *P. antoshkina* sp. nov., x215; i: *P. papulata* Kozlova, x205.

Source : MNHN, Paris

TYPE LOCALITY.— Chert nodules in limestone of Domanik Creek (sample n. 922), near Ukhta town, Komi area, Russia.

ETYMOLOGY.— Named to honour geologist V. Merts, who first discovered this radiolarian locality.

RANGE AND OCCURRENCE.— Late Devonian (middle Frasnian), conodont zone *P. punctata*, Domanik Horizon, Ukhta section, Domanik Creek, Komi area, Russia, so far as known.

CONCLUSION

The Domanik and domanikoid facies have the following characteristics: a- decompensated subsidence on the periphery of Russian platform; b- transgressive-regressive regime; c- enriching in organic matter.

Domanik and domanikoid facies similar in lithological and geochemical composition but differ in character of organic matter. The deliverers of the Devonian Domanik were probably algae and radiolarians in contrast to the Jurassic domanikoid facies, where deliverers were represented by nannofossils as well as other groups of fauna and flora.

The Devonian Domanik was formed at the west periphery of warm-water Yapetus whereas Jurassic domanikoid facies were deposited along east rim of Russian Sea within the Boreal province.

Diverse siliceous microfossil assemblages have been obtained from the Volgian strata dated by ammonites and calcareous nannofossils. Radiolarian co-occurrence with calcareous nannofossils are of great interest. This description represents the first well-dated radiolarian assemblage of this age at such a high latitude of the Russian platform.

ACKNOWLEDGEMENTS

The author is grateful for constructive comments made by Fabrice CORDEY and an anonymous reviewer, which stimulated the improving of this paper. This work is part of the Peri-Tethys program. It was partly financially supported by the Peri-Tethys Grant N° 95-18 and N°95-96/18 and INTAS Grant N° 94-1099, RFFI-97-05-6555.

REFERENCES

ANDERSON, O.R., 1983.— *Radiolaria.* Springer, Berlin: 1-355.

APLONOV, S., 1993.— Determination of the paleo-oceanic crust age on the base of magnetic and paleomagnetic data: new examples from the deep sedimentary basin of Russian Arctic shelf. *In: L. P. Zonenshain Memorial Conference of Plate Tectonic, Moscow, november 17-20, 1993.* Geomar, Kiel: 30-31.

APLONOV, S. & SHMELEV, G., 1993.— Geophysical diagnosis of the suture in the Timan-Pechora basement. *In: L. P. Zonenshain Memorial Conference of Plate Tectonic, Moscow, november 17-20, 1993.* Geomar, Kiel: 31-32.

BRAGIN, N.Y., submitted.— Radiolaria from the phosphorites basal horizons of the Volgian Stage in the Moscow region. *Revue de Micropaléontologie.*

DYER, R. & COPESTAKE, P., 1989.— A review of latest Jurassic to earliest Cretaceous Radiolaria and their biostratigraphic potential to petroleum exploration in the North Sea. *Northwest European Micropaleontology and Palynology, London*: 214-235.

KHUDYAEV, J., 1931.— On the Radiolaria in phosphates in the region of the Syssola River. *Transactions of the Geological and Prospecting Service of USSR*, **46**: 1-48.

KLUSHIN, S.V., LEVASHOV, K.I., LIZANEZ, M.G. & PANKOVA ,V.V., 1992.— *The Separation of Gaps and Unconformity Boundaries on Seismic and Karatag Diagrammes. Gaps, Unconformities, Nonanticlinal Catchs.* Nauka; Technics, Minsk: 5-11.

KOSTIUCHENKO, S.L., 1993.— The continental plate tectonic model of the Timan-Pechora province based on integrated deep geophysical study. *In: L. P. Zonenshain Memorial Conference of Plate Tectonic, Moscow, november 17-20, 1993.* Geomar, Kiel: 85-86.

KOZLOVA, G.E., 1994.— Mesozoic radiolarian assemblage of the Timan-Pechora oil field. *Proceeding of Saint-Petersburg International Conference, Saint-Petersburg*: 60-75.

LJUROV, S.B., 1994.— Division of Jurassic sequences of the Middle Vichegda. *Abstracts of International Symposium Biostratigraphy of Oil Fields, Saint-Petersburg*: 59-60.

Source : MNHN, Paris

MERTS, A.V., YUDOVICH, YA.E., KETRIS, M.P. & STEINER, V.L., 1990.— On the geochemistry of middle Frasnian Ukhta Domanik. *Oil Shale*, **7** (3-4): 218-230.

NIKISHIN, A.M., MILANOVSKY, E.E., ZIEGLER, P.A., LOBKOVSKY, L.I., CLOETINGH, S. & FOKIN, P.A., 1993.— Devonian rifting along the eastern and south-eastern margins of European paleocontinent. *In: L. P. Zonenshain Memorial Conference of Plate Tectonic, Moscow, november 17-20, 1993*. Geomar, Kiel: 110.

ORMISTON, A.R., 1989.— *Factors Controlling the Deposition of Late Devonian to Early Carboniferous Oil Source Rocks: a Global Analysis*. Amoco Research Center, Tulsa (USA): 1-56.

ORMISTON, A.R., 1993.— The association of radiolarians with hydrocarbon source rocks. *Micropaleontology Special Publication, New-York*, **6**: 9-16.

SEDAEVA, G.M. & VISHNEVSKAYA, V.S., 1995.— Jurassic paleoenvironments of the North-Eastern European platform. *In: L. P. Zonenshain Memorial Conference of Plate Tectonic, Moscow, november 22-25, 1995*. Geomar, Kiel: 205.

TALNOVA, O.P., 1995.— Marine phytoplankton from the Devonian rocks of the Timan-Pechora province. *In*: Ecostratigraphy and fossil assemblages of Paleozoic and Mesozoic from North-Eastern Europa. *Trudy of Komi Scientific Center, Siktivkar*, **86**: 21-30.

VISHNEVSKAYA, V.S., 1993.— Model of sedimentary basin for the Domanik-type deposits: new version. *In: L. P. Zonenshain Memorial Conference of Plate Tectonic*. Vol. 86. Geomar, Kiel: 151-152.

VISHNEVSKAYA, V.S., 1996.— *Parvicingula* as indicator of Jurassic to Early Cretaceous paleogeographical and sedimentological paleoenvironments within North Peri-Tethys. *Abstracts of Moscow Peri-Tethys Workshop, Moscow*: 30-31.

VISHNEVSKAYA, V.S. & DE WEVER, P., 1996.— About possibility to correlate North Peri-Tethyan radiolarian events with others zonations. *Abstracts of Moscow Peri-Tethys Workshop, Moscow*: 31-32.

Source : MNHN, Paris

Source : MNHN, Paris

Paleomagnetism of Permian to Jurassic formations from the Turan Plate

Marie M. LEMAIRE [1], *Evgueni L. GUREVITCH* [2], *Khodjamourad NAZAROV* [3], *Michel WESTPHAL* [1], *Hugues FEINBERG* [4] & *Jean-Pierre POZZI* [4]

[1] École et Observatoire des Sciences de la Terre, UMR 7516, 5 rue R. Descartes 67084 Strasbourg Cedex, France

[2] V.N.I.G.R.I., Liteiny 39, 191104 St Petersburg, Russia

[3] Institute of Geology, Academy of Sciences, Ashkhabat, Turkmenistan

[4] École Normale Supérieure, URA 1316, Département de Géologie, 24 rue Lhomond 75231 Paris Cedex 05, France

ABSTRACT

Paleomagnetic studies have been started upon Upper Triassic-Early Jurassic volcanics and Permo-Triassic redbeds from the southwest of Turkmenistan. Application of the K/Ar method of dating on volcanic rocks from Turkmenbasi (40°N, 53°E) gives an homogeneous age of 200 Ma for 5 different lava flows and 227 Ma for an other one. These rocks, distributed among the two peninsula of Ufra and Turkmenbasi, have a complex magnetization, certainly related to the impressive tectonic history of the area. We identified a low-blocking temperature component close to the present field, which is probably a recent viscous or chemical magnetization. The high-blocking temperature component has a more complicated meaning. Declinations may be affected by possible rotations between sites, and we assume that the metamorphism affected differently the two peninsulas of Turmenbasi and Ufra. It follows from this that a synfolding component is identifiable among 8 sites from the peninsula of Turkmenbasi. It has been acquired after a folding of 70%: I=57° (±11°); pal.=37.6° (±6°). This inclination is in a good agreement with a possible remagnetization during the collision of Iran with the Turan plate in Jurassic time. A low inclination component, prefolding, with a high-blocking temperature, is identified on the peninsula of Ufra: I=28.9° (±3.5°); plat.=15.4° (±2°). It suggests a shortening of 13° at least, since the Upper Trias. Results from older rocks, Permian (Upper?) redbeds from Kizil Kaya (41°N, 55°E), suggest also the importance of the shortening. The high blocking temperature component isolated on these rocks gives us a reversed direction: D=230° I=-18° k=13 a95=6°; plat.=±9° (±3°); VGP: lat.=34°N long.=166°E (no fold test). Taking into account Permian-Triassic results from Mangyshlak (Kazakhstan), it is highly probable that a major shortening zone exists between the Turan plate and the stable Eurasian plate north of Caspian Sea.

RÉSUMÉ

Paléomagnétisme des formations permiennes à jurassiques de la Plaque de Turan.

L'étude paléomagnétique de séries du Permien-Trias et du Trias supérieur-Jurassique inférieur du sud ouest du Turkmenistan laisse supposer que d'importants raccourcissements ont eu lieu entre la plaque de Turan et l'Eurasie depuis le

LEMAIRE, M.M., GUREVITCH, E.L., NAZAROV, K., WESTPHAL, M., FEINBERG, H., & POZZI, J.P., 1998.— Paleomagnetism of Permian to Jurassic formations from the Turan Plate. *In:* S. CRASQUIN-SOLEAU & É. BARRIER (eds), Peri-Tethys Memoir 3: stratigraphy and evolution of Peri-Tethyan platforms. *Mém. Mus. natn. Hist. nat.*, **177** : 71-87. Paris ISBN : 2-85653-512-7.

Source : MNHN, Paris

Permien. Deux localités différentes ont été échantillonnées. La première se situe dans la région de Turkmenbasi (40°N, 53°E), en bordure de la mer Caspienne, à proximité du système de failles du Kopet Dagh. Les sites échantillonnés sont distribués sur deux péninsules, Ufra et Turkmenbasi, et sont composés de roches volcaniques calco-alcalines. Ces roches, dont l'âge a été attribué à 200-227 Ma par la méthode K/Ar, portent des directions d'aimantations difficiles à interpréter. Si la composante de basse température de blocage montrant une direction proche du champ actuel peut être interprétée comme une aimantation récente visqueuse ou chimique, la composante de haute température de blocage est plus complexe. Cependant nous pensons avoir identifié une composante syn-plissement sur 8 sites de la péninsule de Turkmenbasi. Cette composante aurait été acquise après un plissement de 70%: I=57° (±11°). La paléolatitude correspondante de 37.6 (±6°) indique que cette ré-aimantation pourrait s'être produite au cours de la collision de la plaque Iranienne avec la plaque de Turan au Jurassique. Une autre composante, montrant une faible inclinaison, a été isolée sur 5 sites de la péninsule d'Ufra: I=28.9° (±3.5°); pal.=15.4° (±2°). Cette composante, acquise avant le plissement ou bien après un faible plissement, suggère un raccourcissement de 13° au moins, depuis le Trias supérieur. La deuxième localité échantillonnée se situe dans la région du Tuarkyr près du village de Kizil-Kaya (41°N, 55°E). Les sites sont représentés par des grès rouges permo-triassiques. Une composante de haute température de blocage a été identifiée dans un site composé de 48 échantillons du Permien supérieur: D=230° I=-18° k=13 a_{95}=6°; plat.=±9° (±3°); VGP: lat.=34°N long.=166°E. Cette direction correspond à un raccourcissement de 16° (±6°) depuis la fin du Permien. Si nous considérons les résultats permo-triassiques de Mangyshlak (FEINBERG *et al.*, 1996), les résultats du Permien supérieur de Kizil Kaya, et les résultats du Trias supérieur de Turkmenbasi, alors il semblerait qu'une zone de raccourcissement soit présente au nord de la mer Caspienne entre la plaque de Turan et l'Eurasie.

INTRODUCTION

During Permian and Triassic times, the ocean formed between the Scythian-Turanian and Arabian plates during the last stage of the Pangea assembly, was affected by a major geodynamic evolution. Microplates, sometimes called "transit plates" (RICOU, 1995) left the northern margin of Gondwana and travelled northward, crossing the Paleo-Tethys. Subduction zones under the southern margin of Eurasia allowed for the disappearance of the former oceanic crust. Sea floor spreading to the south of these transit plates created the Neotethys. The so-called transit plates collided with the southern margin of Eurasia during the Late Triassic and Jurassic and were thus generally accounted as responsible for the Kimmerian phase. Nevertheless the regions east and west of the Caspian Sea were considered during a long time to be stable parts of the Eurasian plate.

Recently, FEINBERG *et al.* (1996) and WESTPHAL (1994) studied Permian-Triassic red beds from Mangyshlak (western Kazakhstan) and showed a large discrepancy between the measured paleolatitude (D= 12°, I=31° a_{95}=7°; plat.= 17°(±4°); VGP: 31°N, 206°E) and the expected one for stable Eurasia. The Mangyshlak area appeared to have moved northward about 10° since Lower Triassic. To obtain more accurate constraints on this crustal shortening we have undertaken paleomagnetic and magnetostratigraphic studies farther to the south, in Turkmenistan. Sampling was performed in Permian-Triassic redbeds from the Tuarkyr erosional window and in volcanics near Turkmenbasi city (formerly Krasnovodsk).

GEOLOGICAL SETTING

The general setting of the studied area corresponds to the apposition of northern and southern blocks, separated by a suture. The northern Variscan domain corresponds to the Turan plate, roughly located north of the Alborz and Kopet Dagh fold belts, and East of Caspian sea. The basement comprises mainly Lower Paleozoic to Upper Devonian sediments, folded and generally metamorphosed, intruded by granites dated from 360-370 Ma (ZONENSHAIN, 1990). On the adjoining Scythian plate, the occurrence of transgressive Carboniferous coal bearing deposits is noticeable. In contrast, the Southern Gondwanan domain, which corresponds to the Iran and Afghan blocks, is characterized by the complete lack of Devonian-Carboniferous folding (STAMPFLI, 1978; BERBERIAN & KING, 1981). The Infracambrian sedimentation is marked by evaporitic deposits, also known on the Arabic plate and in the Salt Range of Pakistan. Higher, Paleozoic sediments comprise mainly shallow water marine deposits, with scarce volcanics related to extensional tectonics. The similarity of Lower Devonian brachiopod faunas from the Arabic platform and from Bandar Abbas (Iran) demonstrates the close relationships between these two regions, which clearly belong to the same part of the North Gondawanan margin at this period (SAIDI, 1995). The suture separating the two domains is well documented in Iran from the west of the Caspian sea (Rasht area) to Aghdarband near Mashad with numerous remnants of obducted Paleozoic sea-floor (STÖCKLIN, 1974; ALAVI, 1991; BAUD *et al.*, 1991). Moreover, chemical analysis of ophiolites from Talesh and Mashad reveals that they were

Source : MNHN, Paris

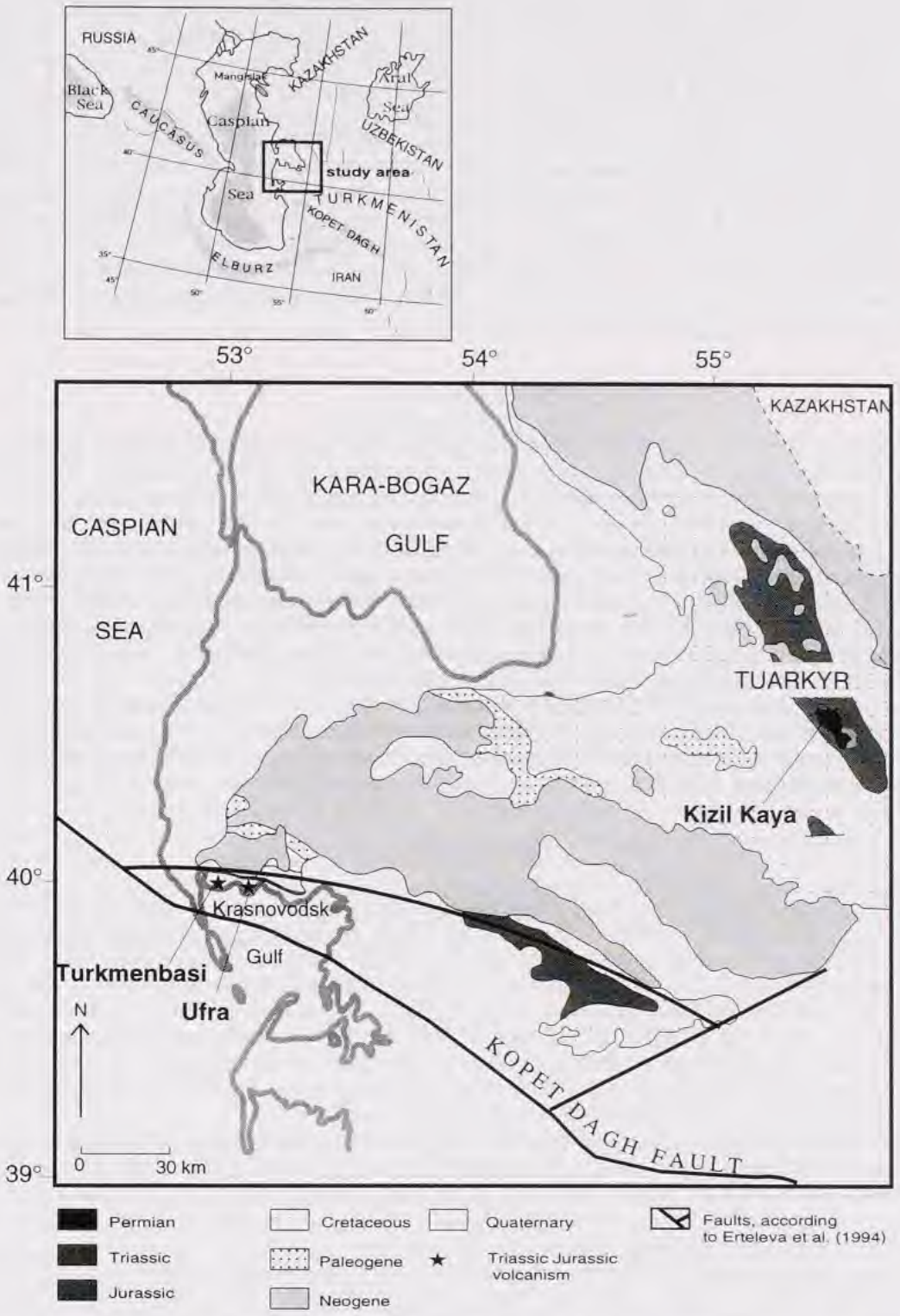

FIG. 1.— Geological outline of the studied area, according to KRIMOUS et al. (1989) and ERTELEVA*et al.* (1994).
*FIG. 1.— Carte géologique de la région étudiée, d'après KRIMOUS*et al. *(1989) et ERTELEVA*et al. *(1994).*

Source : MNHN, Paris

originally close to a subduction zone (WEBER-DIEFENBACH *et al.*, 1986). This suture was also recognized in northern Afghanistan in the Paropamisus mountains by BOULIN & BOUYX (1977 a,b).

After the Palaeozoic evolution described above, the Turan plate was affected during Late Permian (?) and Triassic times by a rapid subsidence, with the sedimentation of a thick molasse. At about the same time, the Southern margin of the plate experienced an important volcanic activity, with lava and pyroclastic deposits evolving from acidic (rhyolite-dacite) to andesitic type. This intra-plate volcanism is related to the subduction of Paleo-Tethys before and just after the 'docking' of the Iran block. On the Turan plate the first Kimmerian folding occured during the Late Triassic or Early Jurassic, and continued throughout Jurassic times (FEINBERG *et al.*, 1996). Recently, during the Pliocene tectonic phase, the southern part of the Turan plate has been truncated by a major fracture called the Kopet-Dagh-Balkan fault (Fig. 1), which corresponds to the overthrusting of the Kopet-Dagh structures on the Turan plate (ARTEMJEV & KABAN, 1994). This active fault, oriented N120° (LYBERIS *et al.*, 1995), plays an important seismic role with high magnitudes earthquakes (Krasnovodsk, 1895; Ashkhabad, 1948). The Kopet-Dagh fault has been sometimes presented as the southern boundary of the Turan plate, but this fault is in fact located 100 to 300 kilometers north of the northern border of the Gondwanan 'mega-terrane' which is the true limit.

SAMPLING

Sampling was carried out in two regions just north of the Kopet Dagh which have Mesozoic and Paleozoic outcrops (Fig. 1). The first region of Turkmenbasi and Ufra peninsulas, shows Triassic-Jurassic volcanics unconformably overlain by Jurassic sediments. Each site represents one or several units: a lava flow, a pyroclastic deposit, or a volcanoclastic deposit. The samples are distributed over several tens of meter of outcrop in order to avoid local tectonic or magnetic perturbations. Between 5 to 15 samples were cored with a portable drill or hand sampled. Orientation was done with a magnetic compass and the coordinates of the sites determined with a G.P.S. (Global Positioning System) receiver. After paleomagnetic analysis, some very close sites were grouped together into single statistical units. Bedding planes, fluidal structures were measured whenever it was possible. Separate hand samples of volcanics were also taken for age determination and geochemistry.

The second region, was near Kizil Kaya, in the Tuarkyr region (Fig. 1), where Permo-Triassic redbeds outcrop there. Sampling was organized into long stratigraphic section which covers the Amanbulak series (Permian) and the beginning of the Lower Triassic. The Amanbulak section has a thickness of 3 km at least. It is composed of sandstones, clays and conglomerates.

GEOCHEMISTRY

Six different lava flows from the Turkmenbasi area, were sampled in order to determine their radiometric ages with the K/Ar method. We selected, within the largest geographic scattering from Ufra and Turkmenbasi peninsulas, a representative fan of the various petrographic types. Chemical classification and nomenclature of the samples has been established on the basis of Na_2O+K_2O content, relative to the content of SiO_2 (LE BAS *et al.*, 1991). The acidic rocks are representative of a calcalkaline volcanism (BROUSSE, 1971; GIROD, 1978). Results of major- and trace-element analyses give a composition of the magmas similar to those which erupt at convergent plate boundaries (GILL, 1981). The sites selected have also significant paleomagnetic results. Two very close samples (UEA03 and UEB08) were chosen because they show opposite polarities.

Whole-rock analyses were obtained from the 100 to 160 µm sieve fraction. Potassium was measured by flame photometry with a lithium internal standard. Argon was extracted in a bakeable glass vacuum apparatus and determined by isotope dilution techniques (using ^{38}Ar as a tracer) in a MS 20 mass spectrometer. All samples were treated by the static method. The set constants recommended by STEIGER & JAEGER (1977) were used for age calculation.

K-Ar results are presented in Table1. Five samples show an homogenous age around 200Ma. Site TWA is older with an age of 226.8 Ma. Supplementary datations using $^{39}Ar/^{40}Ar$ methods are in process in order to control if this divergence is significant; wether it is real or related to the method of the K/Ar dating.

Source : MNHN, Paris

TABLE 1.— K/Ar dating of volcanic rocks from Turkmenbasi and Ufra (whole-rock). The nomenclature is based on the LE BAS *et al.* (1991) classification. wt.%: percent of weight.

TABLEAU 1.— Datation par la méthode K/Ar des roches volcaniques des péninsules de Turkmenbasi et Ufra. La nomenclature des roches est basée sur la classification de LE BAS et al. *(1991). wt.% : pourcentage du poids.*

Samples or sites	Location	Petrographic type	K_2O (wt.%)	$\frac{100.rad.^{40}Ar}{Total\ ^{40}Ar}$	$rad.^{40}Ar$ (10^{-11}mol/g)	Age(±σ) in Ma
UEA03	39°59'48"N-53°06'22"E	trachyte	2.936	96.9	86.44	193.7±4.4
UEB08	39°59'48"N-53°06'22"E	dacite-rhyolite	3.543	95.8	110.74	205.0±3.0
UWB06-07	39°58'27"N-53°03'27"E	rhyolite	3.482	97.1	103.36	195.2±2.9
TWA	40°01'18"N-52°55'44"E	dacite	2.222	96.6	77.32	226.8±5.2
TEA	40°00'46"N-52°56'59"E	dacite	2.936	97.6	87.21	195.3±4.5
TCA	40°00'28"N-52°57'04"E	rhyolite	4.535	97.9	141.43	204.6±3.0

PALEOMAGNETISM

PROCEDURES AND MEASUREMENTS

The drilled cores and hand samples were cut to the standard size of paleomagnetic specimens and measured in the Strasbourg and Paris paleomagnetic laboratories with a CTF cryogenic magnetometer or a modified Digico spinner with an equivalent noise level of 3.10^{-5} A/m. Susceptibilities were measured with a Digico bulk susceptibility bridge, with a sensitivity of $2\ 10^{-6}$(S.I.).

We tested both alternating field and thermal demagnetization methods on pilot specimens. With the A.F. method, parasitic magnetizations are often observed above 80mT and hamper the determination of the final magnetization. Therefore the thermal method was preferred for the main part of the samples. Fourteen steps of heating were made up to 590-600°C for Turkmenbasi, or up to 620°C for Kizil-Kaya. Susceptibilities were controlled every two steps to detect any mineral transformation which could alter the final direction. Demagnetization curves were analysed by principal component analysis on stereonets and on Zijderveld diagrams (ZIJDERVELD, 1967; KIRSCHVINK, 1980; KENT *et al.*, 1983). Fisher statistics (FISHER, 1953) were used to compute the average direction of each site and its statistical properties.

Within-site fold tests (MCELHINNY, 1964; WATSON & ENKIN, 1993) were usually not possible due to lack of attitude variation of strata within each site. However between-site fold tests were possible. A reversal test was possible in one volcanic site from Ufra.

RESULTS

TURKMENBASI AREA

Specimens distributed among 19 sites were demagnetized. Different behaviour was observed from one site to another. The NRM intensities vary globally from 10^{-3} A/m to 10A/m. In each site this intensity varies only by a factor 1 to 20. The Koenigsberger factor was calculated in order to identify any anomalous specimen; it varies from 0.1 to 4.

During thermal demagnetization one or two components of magnetization can be distinguished (Fig. 2). A low temperature component destroyed below 350°C is isolated at 5 sites. The average directions are reported in Table 2. They are close to the present field direction, which is: D=5° I=59°. Among the other 14 sites, the low component temperature, which sometimes appears, is too scattered to be analysed.

Source : MNHN, Paris

TABLE 2.— Low-blocking temperature components. Dg, declination in geographic coordinates; Ig, inclination in stratigraphic coordinates; kg, precision parameter in geographic coordinates; a95, semi-angle of the cone of 95% confidence in degree.

TABLEAU 2.— Composantes de basse température de blocage. Dg, déclinaison en coordonnées géographiques ; Ig, inclinaison en coordonnées géographiques ; a95, demi-angle du cône de confiance à 95%, en degrés.

SITE	number of samples	polarity	blocking temperature	Dg	Ig	kg	α_{95}
			TURKMENBASI				
TWC	6	N	200	10	53	8	24
TWE	5	N	200-250	336	55	65	9
IP	9	N		344	42	7	19
TEAB	19	N	200-250	345	68	22	7
			UFRA				
KP	7	N	<350	10	66	26	12
			KIZIL KAYA				
KC	70	N	<350	355	65	19	4
KD	11	N	<350	11	56	49	7
KG	5	N	<350	355	60	91	8
KM	21	N	<350	9	59	20	7
MEAN	number of sites : **9**	**N**		**357**	**59**	**57**	**7**

A high temperature component destroyed above 500°C is quite well defined for 13 sites (Table 3, Fig. 3, Fig. 4). It is carried by magnetite. Because of heterogeneous behaviour of some samples and scattered directions, the characteristic mean directions of 6 sites could not be isolated.

Twelve of the well defined final directions are normal. Site UEAB shows both normal and reversed directions (Fig. 5). A reversal test is possible on them. The antipodal angle lies between 160 and 170° (Table 4) and, according to MCFADDEN & MCELHINNY (1990), classifies this test as C. The test is positive, but the slight deviation indicates that a secondary contamination is still present in the primary magnetization. Nevertheless we are not in presence of a massive remagnetization.

We performed then a progressive fold test (WATSON & ENKIN, 1993) on mean directions from Ufra and Turkmenbasi (Fig. 6) all together. The best grouping is found for uncorrected or slightly corrected directions (Table 5). The k and a95 are not very satisfactory, but at this point of our analysis we could suppose that this mean is a secondary magnetization, and that the scattering is related to local rotations.

Then, to avoid the contribution of possible rotations, we performed the statistical analysis of inclination data only of ENKIN & WATSON (1996) (Fig. 7a). A different conclusion appears (Table 6). The strongest scattering is now in geographical coordinates. But it is meaningless to conclude from then on that the direction is primary. This progressive fold test is not conclusive.

Should we take into account the best grouping firstly found (Table 5), and then consider that all the samples have been remagnetized? The presence of a non negative reversal test and of an insignificant fold test on inclinations only, let us suppose that things are not so simple. The scattering could be related to an heterogeneous remagnetizing contribution.

We notice that the 5 sites from Ufra peninsula, representing independant flows, have a common behaviour; they all show inclinations lower than 40°, both before and after tectonic corrections (Fig. 4). The sites from Ufra are separated from Turkmenbasi ones by 7 km at least. For this reason, we decided to separate these two peninsula, supposing that metamorphism has affected differently these two localizations.

Source : MNHN, Paris

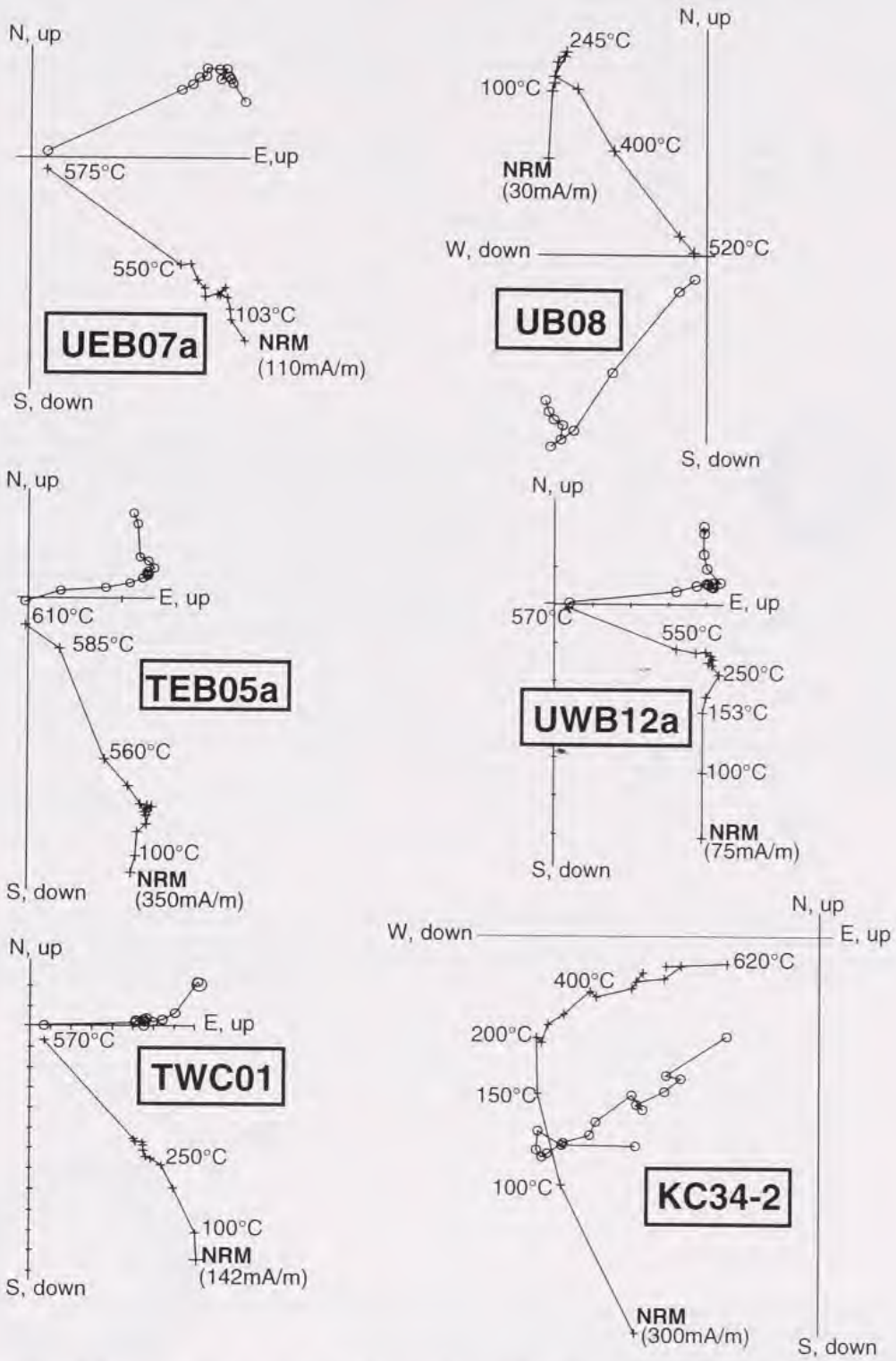

FIG. 2.— Examples of demagnetization curves. o, horizontal plane; +, East-West vertical plane. Characteristic temperatures are indicated.

FIG. 2.— Exemples de courbes de désaimantation. o, plan horizontal ; +, plan vertical Est-Ouest. Les températures caractéristiques sont indiquées.

Source : MNHN, Paris

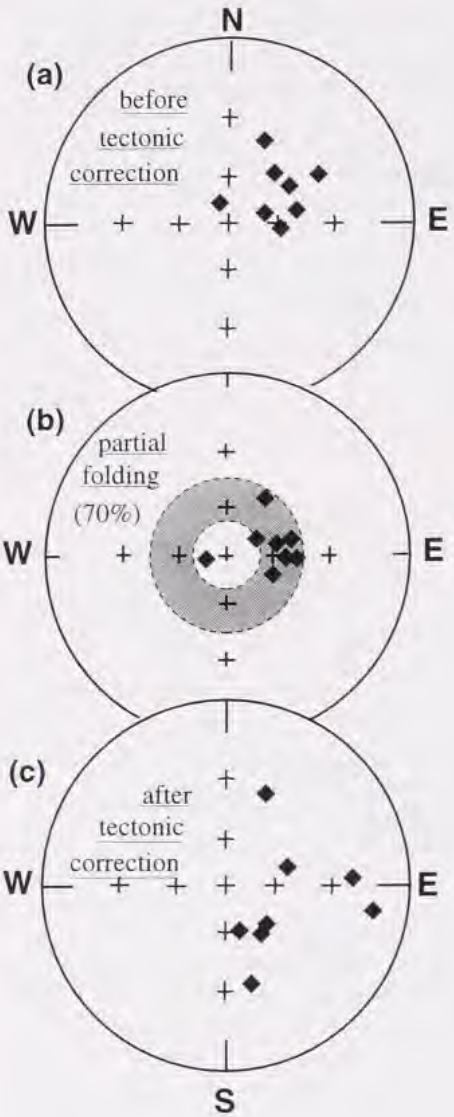

FIG. 3.— Distribution of the high blocking temperature component for 8 sites from the peninsula of Turkmenbasi, (a) before tectonic correction; (b) after a 70% folding; (c) after a complete tectonic correction. The grey circle indicates the mean inclination for a partial folding of 70%.

FIG. 3.— Distribution de la composante de haute température pour les 8 sites de la péninsule de Turkmenbasi, (a) avant la correction tectonique ; (b) après un plissement partiel de 70% (c) après la correction tectonique. Le cercle gris indique l'inclinaison moyenne pour un plissement partiel de 70%.

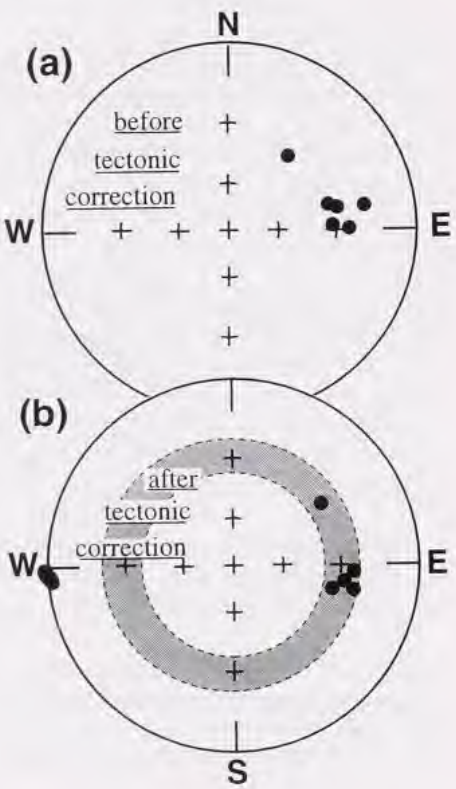

FIG. 4.— Distribution of the high blocking temperature component for 5 sites from the peninsula of Ufra before tectonic correction (a) and after tectonic correction (b). The grey circle indicates the mean inclination after the tectonic correction.

FIG. 4.— Distribution de la composante de haute tempértaure pour les 5 sites de la péninsule d'Ufra avec la correction tectonique (a) et après la correction tectonique (b). Le cercle gris indique l'inclinaison moyenne pour après correction de pendage.

Source : MNHN, Paris

TABLE 3.— High blocking temperature components. Dg/s, declination in geographic/ stratigraphic coordinates; Ig/s, inclination in geographic/ stratigraphic coordinates; ks, precision parameter in stratigraphic coordinates; a_{95}, semi-angle of the cone of 95% confidence, in degree, in stratigraphic coordinates; s, strike; d, dip.

TABLEAU 3.— Composantes de haute température de blocage. Dg/s, déclinaison en coordonnées géographiques / stratigraphiques; Ig/s, inclinaison en coordonnées géographiques / stratigraphiques ; a_{95}, demi-angle du cône de confiance à 95% en coordonnées stratigraphiques ; s, strike; d, dip.

SITE	position	number of samples	polarity	blocking temperature	Dg	Ig	Ds	Is	ks	α95	s	d
				TURKMENBASI								
TWA	40°01.3'N-52°55.7'E	13	N	580	62	33	144	55	55	6	115	70
TWC	40°01.2'N-52°55.9'E	6	N	570-580 80	50	166	34	38	11	115	75	
TWE	40°01'N-52°55.9'E	9	N	585	42	51	164	61	18	12	109	66
IP	40°00.7'N-52°57'E	13	N	580-600 75	68	100	13	202	3	24	59	
TA	40°00.7'N-52°57.1'E	9	N	590	23	39	72	52	265	3	62	46
TD	40°00.7'N-52°57.8'E	9	N	600	59	49	133	57	44	8	103	49
TEAB	40°00.8'N-52°57'E	23	N	585	97	59	86	21	86	3	344	40
TCA	40°00.5'N-52°57.1'E	5	N	590	329	77	23	33	115	7	115	48
				UFRA								
UWA	39°58.4'N-53°03.3'E	8	N	570-585 76	33	99	29	46	8	82	38	
UWB	39°58.5'N-53°03.3'E	5	N	570-585 79	29	102	24	68	9	82	38	
UOB	39°59.05'N-53°03.5'E	9	N	600	80	18	93	25	53	7	99	33
UCD	39°59'N-53°03.6'E	10	N	600	90	25	104	33	84	5	114	26
UEAB	39°59.8'N-53°06.4'E	20	35%R	500-520 39	37	55	31	15	8	33	25	
				KIZIL KAYA								
KC	40.5°N-55.5°E	48	92%R		230	10	230	-18	13	6	150	30

TABLE 4.— Reversal test on site UEAB. We use the MCFADDEN & MCELHINNY (1990) classification. For explanation of symbols see Table 2.

TABLEAU 4.— Test des inversions sur le site UEAB. Nous utilisons la classification de MCFADDEN & MCELHINNY (1990). Voir le tableau 2 pour l'explication des symboles.

Stratigraphic coordinates	Number of samples	Declination	Inclination	k	α_{95}
Reversed polarity	7	230	-30	14	16
Normal polarity	13	58	29.5	15	11
both	**20**	**55**	**31**	**15**	**8**
Angle between normal and reversed directions		(γo) 7.4°			
Critical angle		(γc) 18°			
Test classified Rc					

Source : MNHN, Paris

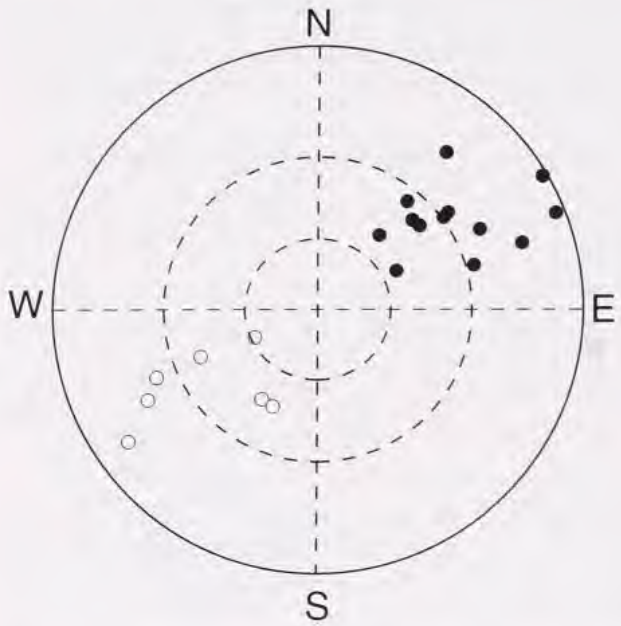

FIG. 5.— Distribution of the antipodal polarities of the samples from site UEAB.
FIG. 5. —Distribution des directions antipodales du site UEAB.

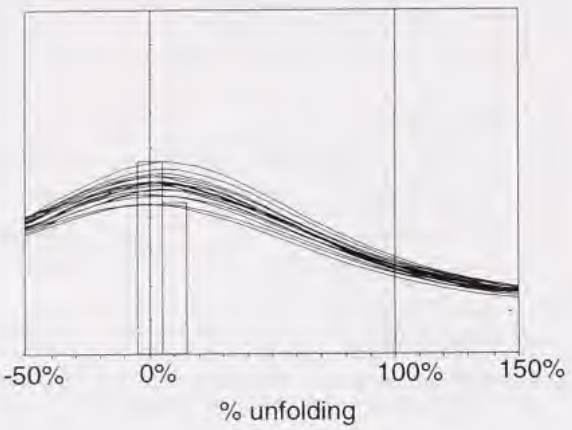

FIG. 6.— WATSON & ENKIN (1993) fold test on Turkmenbasi and Ufra peninsulas. Horizontal: unfolding ratio. The curves show 20 examples of variation of k (precision parameter). The histogram gives the position of the best unfolding ratio.
FIG. 6. —Test du pli de WATSON & ENKIN (1993) appliqué aux péninsules de Turkmenbasi et d'Ufra. Horizontalement : taux de déplissement. Les courbes représentent 20 exemples de variations de k, paramètre de précision. L'histogramme donne la position du meilleur taux de déplissement.

TABLE 5.— WATSON & ENKIN (1993) fold test on Turkmenbasi and Ufra peninsulas. For explanation of symbols see Table 2.
TABLEAU 5.— Test du pli de WATSON & ENKIN (1993), appliqué aux péninsules de Turkmenbasi et Ufra. Voir le Tableau 2 pour l'explication des symboles.

Number of sites **13**	Declination	Inclination	k	α_{95}
in situ	65.4	46.4	10.6	12.8
complete unfolding	117.5	46.9	5.4	17.9
partial unfolding, 4% (±10%)	67.1	47.3	10.6	12.8

Source : MNHN, Paris

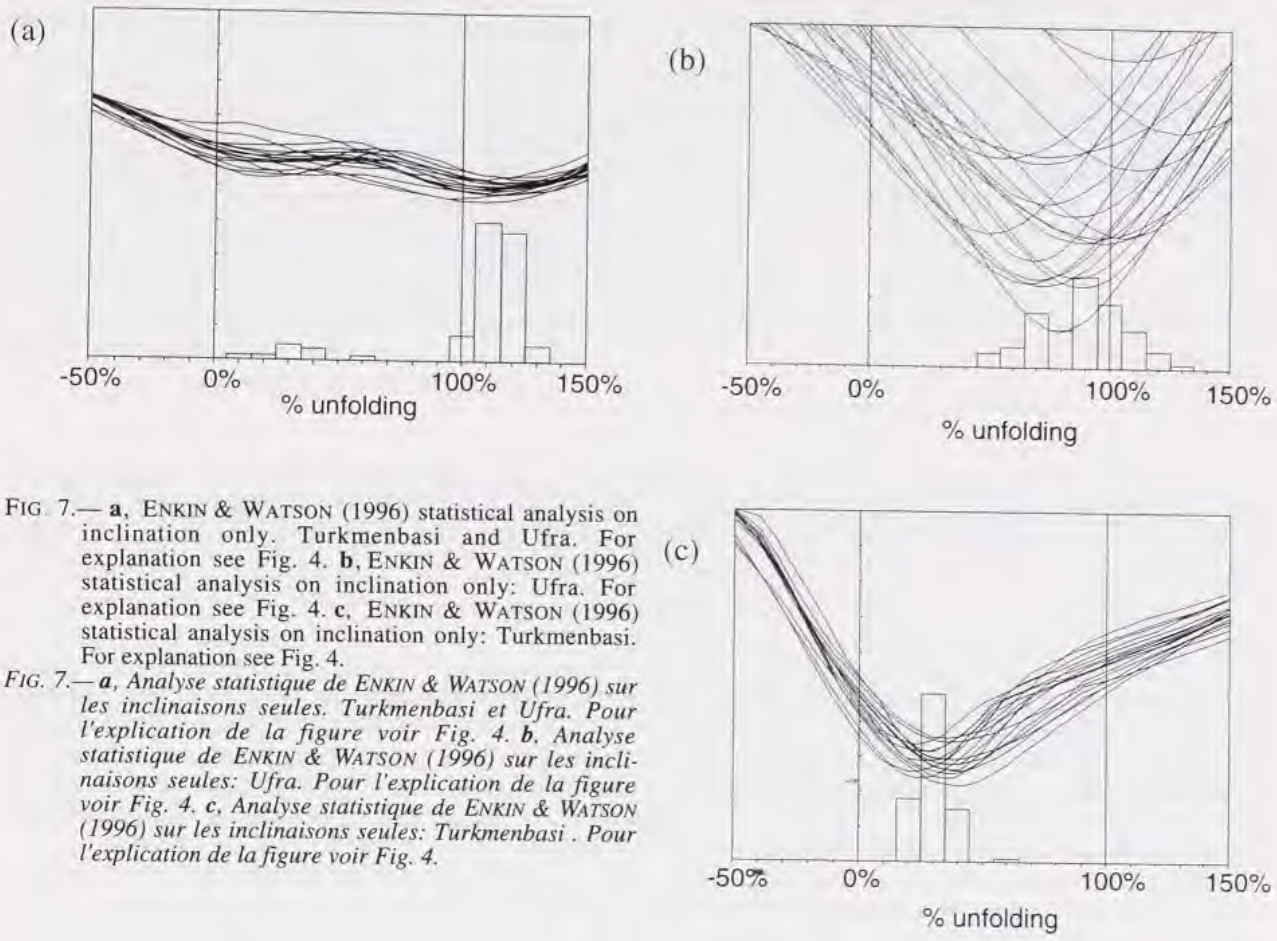

FIG. 7.— **a**, ENKIN & WATSON (1996) statistical analysis on inclination only. Turkmenbasi and Ufra. For explanation see Fig. 4. **b**, ENKIN & WATSON (1996) statistical analysis on inclination only: Ufra. For explanation see Fig. 4. **c**, ENKIN & WATSON (1996) statistical analysis on inclination only: Turkmenbasi. For explanation see Fig. 4.

*FIG. 7.— **a**, Analyse statistique de ENKIN & WATSON (1996) sur les inclinaisons seules. Turkmenbasi et Ufra. Pour l'explication de la figure voir Fig. 4. **b**, Analyse statistique de ENKIN & WATSON (1996) sur les inclinaisons seules: Ufra. Pour l'explication de la figure voir Fig. 4. **c**, Analyse statistique de ENKIN & WATSON (1996) sur les inclinaisons seules: Turkmenbasi . Pour l'explication de la figure voir Fig. 4.*

TABLE 6.— ENKIN & WATSON (1996) statistical analysis on inclination only; Ufra and Turkmenbasi peninsulas. σ, standard deviation.

TABLEAU 6.— Analyse statistique sur les inclinaisons seules d'après ENKIN & WATSON (1996) ; application aux péninsules d'Ufra et de Turkmenbasi. s, écart-type.

Number of sites **13**	Inclination	σ
in situ	43.7	17.3
complete unfolding	36.8	15.2
partial unfolding 106% (± 52%)	35.1	15.0

TABLE 7.— ENKIN & WATSON (1996) statistical analysis on inclination only; Ufra peninsula. σ, standard deviation.

TABLEAU 7.— Analyse statistique sur les inclinaisons seules d'après ENKIN & WATSON (1996) ; application à la péninsule d'Ufra. s, écart-type.

Number of sites **5**	Inclination	σ
in situ	28.4	7.3
complete unfolding	28.4	3.6
partial unfolding 88% (± 36%)	28.9	3.5

Source : MNHN, Paris

TABLE 8.— ENKIN A& WATSON (1996) statistical analysis on inclination only; Turkmenbasi peninsula. σ, standard deviation.

TABLEAU 8.— Analyse statistique sur les inclinaisons seules d'après ENKIN & WATSON (1996) ; application à la péninsule de Turkmenbasi. s, écart-type.

Number of sites 8	Inclination	σ
in situ	53.2	14.4
complete unfolding	42.2	17.5
partial unfolding 30% (± 13%)	57.1	11.0

UFRA PENINSULA.— The distribution of mean site directions from Ufra shows clearly that this distribution is not fisherian, neither before or after tectonic correction. Site UEAB has a similar inclination but a quite different declination indicating possible local tectonics rotations. We performed the Enkin and Watson test (1996) on the inclinations. The inclinations keep beeing low when we applied the tectonic correction. But the grouping improves (Fig. 7b) significantly for a partial or complete correction (Table 7). The mean inclination of 28.9° (±3.5°) could be either primary or synfolding.

TURKMENBASI PENINSULA.— The same procedure was done with Turkmenbasi results (Fig. 3). The best grouping is observed after a partial tectonic correction (Fig. 7c; Table 8). The mean inclination of 57.1° (±11°) is a remagnetization because the best grouping is found for a partial folding of 70% (±13%).

KIZIL KAYA

Five sites have been sampled and 120 specimens were demagnetized up to 620°C (Fig. 2). Only section KC, which is the longest, gave good results. This section represents a thickness of 1km almost, and is stratigraphicaly situated just below the Permian-Triassic boundary, in the upper part of the Amanbulak section. The NRM ranges from 1 to 500 mA/m. The first component has an unblocking temperature lower than 350°C. Its direction, well defined, is close to that of the present field (Table 2). It is probably a recent viscous or chemical remagnetization due to the weathering of the samples.

Above this temperature one or two components exist. Magnetization is heterogeneous: some samples see their magnetization disappearing below 580°C and for others 50% of the magnetization remains above 620°C. Only site KC gives consistent results. The large majority of the samples are of reversed polarity. A few samples are normal, but they are too few and the scatter is too large for a reversal test. An internal fold test is not significant because the bedding-plane attitudes are very similar. The characteristic magnetization direction is (Table 3) in stratigraphic coordinates: D=230° I=-18° k=13 a 9 5=6°; plat.=9°; PGV: lat.=34°N long.=166°E.

DISCUSSION

TURKMENBASI AREA

In view of the result of the progressive fold test on inclinations only (Fig. 7a), performed on the 13 final directions of Turkmenbasi and Ufra peninsulas, a pre-folding component is not identifiable. But this test neither proves that all these final directions have been remagnetized.

We consider another solution which is based on the heterogeneousness of the remagnetization. However, a detailed petrographic study must confirm the hypothesis of a different metamorphism in the Turkmenbasi and Ufra volcanic series.

Our reasoning is based on inclinations only. We cannot trust the declinations because of the eventful tectonic story of this area, close to the Ashkhabad fault (Fig. 1). The Enkin and Watson (1996) statistical analysis of paleomagnetic inclination data, allows us to isolate two components:

— a low inclination: 28.9° (±3.5°). This low inclination could either be prefolding or contemporary with the beginning of the folding (Table 7). It corresponds to a paleolatitude of 15.4° (±2°) (n°8 on Fig. 8).

Source : MNHN, Paris

— a synfolding inclination, 57.1° (±11°), which corresponds to a remagnetization at the end of the folding (folding of 70%). It implies a paleolatitude of 37.6°(±6°) (n°17).

We calculated the theoritical paleolatitudes for a point in the middle of the studied area (Turkmenbasi city: 41°N, 53°E). For Eurasia and Africa we used the apparent polar wander curve of BECK (1994) and draw the expected paleolatitudes since 280Ma (Fig. 8). We have to remind that a first folding occured before the Jurassic because the volcanics series from Turkmenbasi are unconformably overlain by Jurassic sediments. Therefore, we attribute an age comprised between 200 and 230 Ma, if we consider that the older age of 227Ma is significant, to the low inclination (n°8). It can be inferred that a shortenning of 13° at least, occured since this the Upper Triassic.

The synfolding component, corresponding to a paleolatitude of 37.6° (±6°), is in a good agreement with the hypothesis of a remagnetization of the volcanic series at the end of the collision of Iran with the Turan plate (Fig. 8).

KIZIL KAYA

Section KC, which is thought to be Upper Permian, has a main direction of: D=230° I=-18°; plat.= ±9° (±4°). The expected direction if this Tuarkyr region was part of Eurasia 260Ma ago is: D=45° I= 45° (BECK, 1994). Then a paleolatitude of -9° in the southern hemisphere corresponds to a shortenning of 25° (±6°) and to a rotation of 175° (±9°) with respect to Eurasia, in this case the main direction is reversed (D=230° I=-18°). Whereas a paleolatitude of +9° (±4°) corresponds to a shortenning of 16° (±6°) and to a rotation of 5° (±9°) only. In this case the main direction is normal (D=50° I=18°). We think that the second hypothesis, a paleolatitude in the northern hemisphere, is more likely because the Tuarkyr region isn't highly affected by tectonic movements: a rotation of 5° (±9°) seems to be more probable than a rotation of 175° (±9°).

Thus the main reversed direction observed probably represents one of the reversed zones within the Illawara mixed polarity zone and we assume that a shortening of 16° (±6°) occured since the Upper Permian between Turan plate and Eurasia.

CONCLUSION

We reported our results and also existing ones from the Iran and Turan plates (Table 9), for the Permian, Trias and Jurassic, on a diagram of the expected paleolatitudes (Fig. 8). According to SOFFEL & FÖRSTER (1980) and WENSINK (1981, 1982), we consider a belonging of Iran to the Gondwana during Permian and Post Permian times. Then the paleolatitudes for the Alborz (n°1 on Fig. 8), Abadeh & Jamal (n°2) and Sorkh Shales (n°7) results are drawn in the southern hemisphere (Fig. 8). The majority of the results are significantly below the theoretical curve of Eurasia. From the Permian to the Jurassic, the paleolatitudes increase progressively to join the curve of Eurasia at the end of the Jurassic. We gave two results for the Cretaceous from Kopet Dagh and Alborz, which show their belonging to Eurasia at this time.

Results n°5 and n°13 are distinct from the other. It isn't the aim of this paper to discuss the validity of the paleomagnetic data, but we have to notice that the previous results from Turkmenistan are heterogeneous. The paleomagnetic analysis are sometimes made on samples which are not demagnetized, and without any fold or reversal test.

Excluding results n°5 and n°13, we observe that the difference between results from the Turan plate and Iran is not large and may be not significant after the Permian. We suppose that a major shortenning zone between Iran, Turan and the stable Eurasian plate might exist somewhere north of the Caspian Sea.

ACKNOWLEDGEMENTS

Financial support was given by the Peri-Tethys program (94-27), INTAS (94-3036) and CNRS (MDRI). Geochemical analysis and K-Ar age determinations were made by the Centre de Géochimie de la Surface (CNRS-UPR 6251 Strasbourg). This is a contribution of CNRS, UMR 7516 and URA 1316.

Source : MNHN, Paris

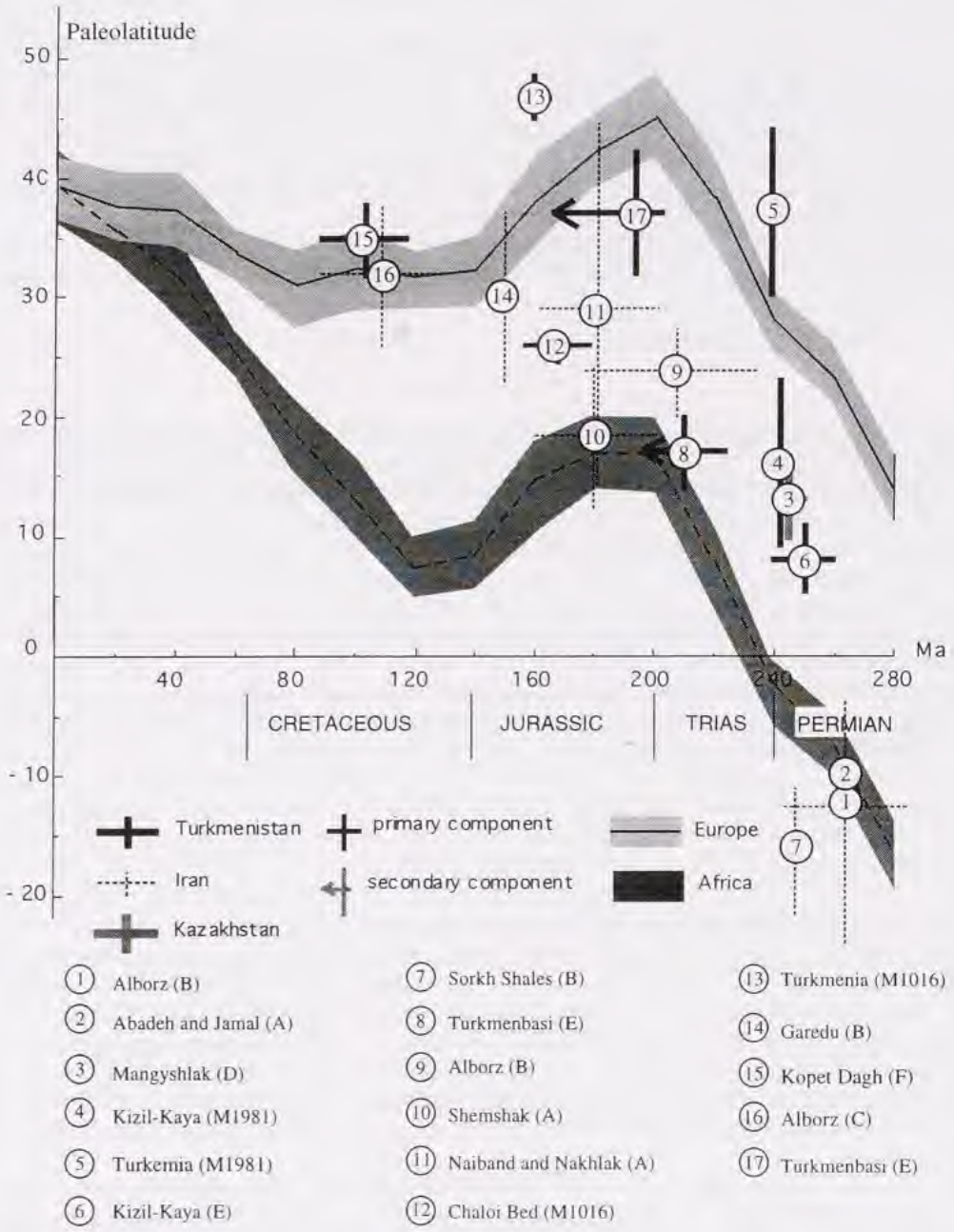

FIG. 8.— Theoretical paleolatitudes according to the apparent polar wander curves for Eurasia and Africa (BECK, 1994). Crosses show the values obtained in different places with errors. References in Table 9 are indicated by number 1 to 17. For further explanations see Table 9.

FIG. 8.— Paléolatitudes théoriques d'après les courbes de dérive des pôles d'Europe et d'Afrique (BECK, 1994). Pour plus d'informations voir le tableau 9.

Source : MNHN, Paris

TABLE 9.— Paleomagnetic results from Iran, Kazakhstan and Turkmenistan for Permian, Trias and Jurassic. The paleolatitudes were calculated for a point at the reference of Turkmenbasi. (I): Iran; (K): Kazakhstan; (T): Turkmenistan; ?: post-folding component; lat.: latitude; long.: longitude; paleolat.: paleolatitude; dpal.: error bar on the paleolatitude; ref.: reference of the pole; (A): SOFFEL & FÖRSTER , 1980; (B): WENSINK, 1979, 1982; (C): WENSINK & VARENKAMP, 1980; (D): FEINBERG *et al.*, 1996; (E): this paper; (F): BAZHENOV, 1987; M: MCELHINNY data base.

TABLEAU 9.— Résultats paléomagnétiques d'Iran, du Kazakhstan et du Turkmenistan pour le Permien, le Trias et le Jurassique. Les paléolatitudes (paleolat.) ont été calculées pour un point de référence situé à Turkmenbasi. (I) : Iran; (K) : Kazakhstan ; (T) : Turkmenistan ; ? : composante post-plissement; plat. : marge d'erreur sur la paléolatitude ; ref. référence des pôles ; (A) : SOFFEL & FÖRSTER, 1980 ; (B) : WENSINK, 1979, 1982; (C) : WENSINK & VARENKAMP, 1980; (D) : FEINBERG et al., *1996; (E) : cet article; (F) : BAZHENOV, 1987 ; M : base de données de MCELHINNY.*

REGION	Coordinates	Age (Ma)	Pole position				Turkmenbasi reference		ref.	on Fig.6
			lat.	long.	dp	dm	paleolat.	dpal.		n°
Alborz (I)	36.5°N-51.5°E	250-270	23°N	282°E	12	21	13	11	(B)	1
Abadeh and Jamal (I)	33°N-57°E	250-270	35°N	307°E	10	11	11	10	(A)	2
Mangyshlak (K)	44°N-52°E	240-250	61°N	208°E	4	5	13	4	(D)	3
Kizil-Kaya (T)	41°N-55°E	245-250	46°N	160°E	7	13	18	7	M1981	4
Turkemia (T)	41°N-55°E	241-245	45°N	128°E	11.9	16.2	37	8	M1981	5
Kizil-Kaya (T)	40.5°N-55.5°E	240-270	34°N	166°E	3	4	8	3	(E)	6
Sorkh Shales (I)	33.3°N-57.3°E	241-245	22°N	326°E	8	15	16	8	(B)	7
Turkmenbasi (T)	40°N-53°E	193-227					15.4	2	(E)	8
Alborz (I)	35.7°N-52.3°E	178-235	49°N	153°E	4	7	24	4	(B)	9
Shemshak (I)	33°N-57°E	185-200	38°N	314°E	7	7	18	7	(A)	10
Naiband and Nakhlak	33°N-57°E	160-200	15°N	349°E	22	22	29	22	(A)	11
Chaloi Beds (T)	40°N-54°E	157-178	76°N	225°E	2,4	3,8	26	2	M1016	12
Turkmenia (T)	41°N-56°E	157-164	74°N	109°E	2.7	3.3	47.3	2	M1016	13
Garedu (I)	34°N-57°E	145-155	79°N	217°E	10	17	30	11	(B)	14
Kopet Dagh (T)		"Middle" Cretaceous	75°N	153°E	5.4	5.4	35.6	3	(F)	15
Alborz (I)	36.3°N-51.8°E	Cretaceous	61°N	147.5°E	6.1	9.3	32.1	7	(C)	16
Turkmenbasi (T)	40°N-53°E	?					37.6	6	(E)	17

Source : MNHN, Paris

REFERENCES

ALAVI, M., 1991.— Sedimentary and structural characteristics of the Paleo-Tethys remnants in northeastern Iran. *Geological Society of America, Bulletin*, **103**: 983-992.

ARTMENJEV, M.E. & KABAN, M.K., 1994.— Density inhomogeneities, isostasy and flexural rigidity of the lithosphere in the Transcaspian region. *Tectonophysics*, **240**: 281-297.

BAUD, A. & STAMPFLI, G., 1991.— Tectonogenesis and evolution of a segment of the Cimmerides: the volcano-sedimentary Triassic of Aghdarband (Kopet Dagh, N.E. Iran). *In*: A.M.C. SENGÖR (ed.), *Tectonic Evolution of the Tethyan Region.* Kluwer, Dordrecht: 265-275.

BAZHENOV, M.L., 1987.— Paleomagnetism of Cretaceous and Paleogene sedimentary rocks from the Kopet-Dagh and its tectonic implications. *Tectonophysics*, **136**: 223-235.

BECK, F., 1994.— *Courbes de dérive des pôles du Permien à l'actuel pour les continents péri-atlantiques et indiens*. Thèse 3ème cycle, Université de Strasbourg, Strasbourg, France: 1-215.

BERBERIAN, M. & KING, G.C.P., 1981.— Towards a paleogeography and tectonic evolution of Iran. *Canadian Journal of Earth Science*, **18**: 210-265.

BOULIN, J. & BOUYX, E., 1977a.— Introduction à la géologie de l'Hindu Kouch occidental. *Mémoire hors série de la Société géologique de France*, **8**: 87-105.

BOULIN, J. & BOUYX, E., 1977b.— Sutures péri-indiennes successives et sutures d'Afghanistan. *Comptes Rendus de l'Académie des Sciences, Paris*, **284**: 785-798.

BROUSSE, R., 1971.— *Magmatologie du volcanisme néogène et quaternaire du Massif Central. "Symposium J. Jung, Plein-Air Service", Clermont-Ferrand*: 377-478

ENKIN, R.J. & WATSON, G.S., 1996.— Statistical analysis of paleomagnetic inclination data. *Geophysical Journal International*, **126**: 495-504.

ERTELEVA, O.O., YUNGA, S.L. & DANILOVA, M.A., 1994.— Mass identification of earthquake source mechanisms in Kopetdag seismic zone. *Physics of the Solid Earth*, **30**: 46-54.

FEINBERG, H., GUREVITCH, E.L., WESTPHAL, M., POZZI, J.P. & KRAMOV, A.N., 1996.— Palaeomagnetism of a Permian/Triassic sequence in Mangislak (Kazakhstan, CIS). *Comptes Rendus de l'Académie des Sciences, Paris*, **322**: 617-623.

FISHER, R.A., 1953.— Dispersion on a sphere. *Proceedings of the Royal Society*, **217 (A)**: 295-305.

GILL, J., 1981.— *Orogenic andesites and plate tectonics*. Springer, Berlin: 1-390.

GIROD, M., 1984.— *Les roches volcaniques: pétrologie et cadre structural*. Doin, Paris: 1-239.

KENT, D.V., BRIDEN, J.C., & MARDIA, K.W., 1983.— Linear and planar structure in ordered multivariate data as applied to progressive demagnetization of palaeomagnetic remanence. *Geophysical Journal (Royal Astronomical Society)*, **75**: 593-621.

KIRSCHVINK, J.L., 1980.— The least square line and plane and the analysis of paleomagnetic data. *Geophysical Journal (Royal Astronomical Society)*, **62**: 699-718.

KRIMOUS, V.N., AROSIMOVA, E.P., KALOUGIN, V.P., KAMICHEV, N.N., KRASILNIKOV, B.A., KORNIENKO, L.V., LOUKIN, I.N., MELNIKOVA, N.F., PACHAEV, M.S. & POPOVA, M.A., 1989.— Geological Map of the Independent State of Turkmenistan: 1:500 000. M.K. MIRZAHANOV (ed.).

LE BAS, M.J. & STRECKEISEN, A.L., 1991.— The IUGS systematics of igneous rocks. *Journal of the Geological Society of London*, **148**: 825-833.

LYBERIS, N., MANBY, G., KALOUGIN, YOUSOUPHOCAEV, H. & ASHIROV, T., 1995.— Mesozoic-present day tectonic and sedimentary evolution of the SE Peri-Caspian Margin (Turkmenistan). *Peri-Tethys Milano meeting*: 1-10.

MCELHINNY, M.W., 1964.— Statistical significance of the fold test in palaeomagnetism. *Geophysical Journal (Royal Astronomical Society)*, **8**: 338-340.

MCFADDEN, P.L. & MCELHINNY, M.W., 1990.— Classification of the reversal test in paleomagnetism. *Geophysical Journal International*, **103**: 725-730.

RICOU, E., 1995.— Tethys and transit plate patterns viewed against long-term periodicity of magnetic field reversal. *Physics of the Earth and Planetary Interior*, **87**: 255-265.

SAIDI, A., 1995.— *Calendrier de la migration Permo-Triassique et morcellement mésozoïque des éléments continentaux de l'Iran: apports de la subsidence et du paléomagnétisme*. Thèse de doctorat, Université Paris VI, Paris, France: 1-298.

SOFFEL, H.C. & FÖRSTER, H.G., 1980.— Apparent polar wander path of Central Iran and its geotectonic interpretation. *Journal of Geomagnetism and Geoelectricity*, **32**: 117-135.

STAMPFLI, G., 1978.— *Etude géologique générale de l'Elburz oriental au Sud de Gonbad-e-Qabus, Iran NW*. Thèse d'Université, Université de Genève, Genève, Suisse: 1-329.

STEIGER, R.H., & JAEGER, E., 1977.— Subcommission on geochronology: convention of the use of decay constants in geo and cosmochronology. *Earth and Planetary Science Letter*, **36**: 359-362.

Source : MNHN, Paris

STÖCKLIN, J., 1974.— Possible ancient continental margin in Iran. *In*: C.B.A.C. DRAKE (ed.), *The Geology of Continental Margins*. Springer, Berlin: 873-887.

WATSON, G.S. & ENKIN, R.J., 1993.— The fold test in paleomagnetism as a parameter estimation problem. *Geophysical Research Letters*, **20**: 2135-2137.

WEBER-DIEFENBACH, K., DAVOUDZADEH, M., ALAVI-TEHRANI, N. & LENSCH, G., 1986.— Paleozoic ophiolites in Iran. Geology, geochemistry and geodynamic implication. *Ofioliti*, **11**: 305-338.

WENSINK, H., 1979.— The implication of some palaeomagnetic data from Iran for its structural history. *Geologie en Mijnbouw*, **58** (2): 175-185.

WENSINK, H., 1981.— Le contact Gondwana-Eurasie en Iran d'après les recherches paléomagnétiques. *Bulletin de la Société géologique de France*, **6**: 547-552.

WENSINK, H., 1982.— Tectonic inferences of the paleomagnetic data from some mesozoic formations in Central Iran. *Journal of Geophysics*, **51**: 12-23.

WENSINK, H. & VARENKAMP, J.C., 1980.— Paleomagnetism of the basalts from the Alborz: Iran part of Asia in the Cretaceous. *Tectonophysics*, **68**: 113-129.

WESTPHAL, M., 1994.— Paleomagnetism of a Permo-Triassic section in Mangyslak (Kazahstan), typical problems. *Peri-Tethys News*, **1**: 3-4.

ZIJDERVELD, J.D.A., 1967.— Demagnetization: analysis of results. *In*: D. W. COLLINSON, K.M. CREER & S.K. RUNCORN (eds), *Methods in Paleomagnetism: Proceedings of the NATO Advanced Study Institute on Paleomagnetic Methods, held in the Physics Department of the University of Newcastle upon Tyne, April 1-10, 1964*. Elsevier, Amsterdam: 254-286.

ZONENSHAIN, L.P., KUZMIN, M.I. & NATAPOV, L.M., 1990.— Geology of the USSR: a plate-tectonic synthesis. *Geodynamic Series*, **21**: 1-242.

Source : MNHN, Paris

Source : MNHN, Paris

5

Reconstruction of paleostress fields in Crimea and the North West Caucasus, relationship with major structures

Aline SAINTOT, Jacques ANGELIER, Alexander ILYIN & Oleg GOUSHTCHENKO

Laboratoire Tectonique Quantitative, URA CNRS 1759, T26-E1, Case 129
Université P. et M. Curie, 75252 Paris Cedex 05, France

ABSTRACT

Between the East European platform and the Black Sea domain, major deformations occurred during the Mesozoic and Cenozoic times along the Crimea-Caucasus zone. Along the deformed boundary, especially in Crimea and NW-Caucasus, seven tectonic events were identified based on inversion of fault slip data sets. The observed chronological criteria allowed us to reconstruct the following succession of paleostress fields from youngest to oldest: (VII) Seismotectonic and tectonic studies indicate a compressional stress regime for the Present, with σ_1 trending N-S or NNW-SSE in NW-Caucasus, NW-SE in Crimea; (VI) a Early Pliocene NW-SE to WNW-ESE transpressional regime, with a counter-clockwise rotation of σ_1 trajectory from NW-Caucasus to Crimea; (V) a nearly E-W transpressional regime, with a counter-clockwise rotation of σ_1 trajectory from WNW-ESE in NW-Caucasus to ENE-WSW in Crimea, such as for the recent events; (IV) a Oligocene-Early Miocene multidirectional extensional regime perpendicular to the axes of maximum subsidence in peripheric troughs of the chains; we infer that these troughs developed during a post-compressional period following a lithospheric flexure. (III) a Late Eocene NE-SW compression which produced the fold-and-thrust belt of NW-Caucasus; (II) a Paleocene event, with a transtensional regime in NW-Caucasus related to the opening of the east Black Sea basin with σ_3 trending NE-SW, and a transpressional regime in Crimea with σ_1 trending NW-SE; (I) the oldest event that we could identify, at the limit between Early and Late Cretaceous, involves a N-S compressional regime in Crimea which resulted in north-vergent thrusting. We noted a deviation of stress trajectories from NW-Caucasian chain to Crimean chain after the major compressional event (post Eocene). The development of the N-S Kerch-Taman trough in the Oligo-Miocene time reflects the presence of a zone of weakness in the lithosphere, and probably explains the fan-shaped trajectory patterns of the subsequent stress fields from NW-Caucasus to Crimea.

RÉSUMÉ

Reconstruction des champs de contraintes en Crimée et dans le nord-ouest du Caucase, relation avec les structures majeures.

Entre la plate-forme est-européenne et le domaine de la Mer Noire, des déformations majeures ont eu lieu dans la zone Crimée-Caucase au cours du Mésozoïque et du Cénozoïque. Le long de la frontière déformée, plus spécifiquement, de la Crimée au Caucase nord-occidental, sept événements tectoniques ont pu être identifiés par l'inversion des mesures de failles à stries. Les critères chronologiques observés nous ont permis de reconstruire la succession suivante des champs de paléocontraintes, du plus jeune au plus ancien : (VII) un régime actuel compressif déterminé par des études tectoniques et

SAINTOT, A., ANGELIER, J., ILYIN, A. & GOUSHTCHENKO, O., 1998.— Reconstruction of paleostress fields in Crimea and the North West Caucasus, relationship with major structures. *In*: S. CRASQUIN-SOLEAU & É. BARRIER (eds), Peri-Tethys Memoir 3: stratigraphy and evolution of Peri-Tethyan platforms. *Mém. Mus. natn. Hist. nat.*, **177** : 89-112. Paris ISBN : 2-85653-512-7.

Source : MNHN, Paris

séismotectoniques, avec σ_1 dirigé N-S ou NNW-SSE dans le Caucase nord-occidental, et NW-SE en Crimée ; (VI) un régime transpressif NW-SE à WNW-ESE au Pliocene inférieur, avec une déviation anti-horaire de la trajectoire de σ_1 du Caucase nord-occidental à la Crimée ; (V) un régime transpressif, avec une déviation anti-horaire de la trajectoire de σ_1, comme dans le régime actuel, de WNW-ESE dans le Caucase nord-occidental à ENE-WSW en Crimée ; (IV) une extension multidirectionnelle durant l'Oligocène et le Miocène inférieur où l'axe σ_3 est perpendiculaire aux axes de subsidence maximale des dépressions périphériques à la chaîne. Ces fossés se développent dans une période post-compressive en réponse à la flexure de la lithosphère. (III) une compression NE-SW à l'Eocène supérieur à l'origine des plis et des charriages des séries de flysch du Caucase nord-occidental ; (II) au Paléocène, un régime transtensif dans le Caucase nord-occidental, relatif à l'ouverture du bassin oriental de la Mer Noire (σ_3, orienté NE-SW), et un régime transpressif en Crimée (σ_1, orienté NW-SE) ; (I) une compression N-S en Crimée. Il s'agit de l'événement le plus ancien que nous avons pu identifié, à la limite Crétacé inférieur-Crétacé supérieur, qui serait à l'origine des structures chevauchantes de la Crimée. Nous avons noté une déviation de la trajectoire des contraintes du Caucase à la Crimée après l'événement majeur compressif de l'Eocène supérieur. A l'Oligo-Miocène, le développement du fossé de Kerch-Taman entre les deux chaînes selon un axe N-S serait relatif à la présence d'une zone lithosphérique fragilisée de même orientation, qui perturberait les trajectoires de contraintes et expliquerait la distribution en éventail des trajectoires de σ_1 sur la zone étudiée.

INTRODUCTION

This study is located on the southern boundary of the east European platform, the Crimea and the northwest Great Caucasus and surrounding areas. The general geology of the Crimea and the NW-Caucasus has been studied since the end of the last century by works of numerous Russian and Soviet authors. In rocks Late Jurassic to Neogene in age, we found evidences of brittle deformation. We calculated local stress states by inversion of fault slip data sets. Groups of local stress states allow reconstruction of paleostress fields which are closely related with development of major structures of the deformed area. Moreover, the approach in term of paleostress reconstruction is an useful tool to constrain the chronology of the deformation in the belt. In this paper, we aim at better understanding the tectonic evolution of this area through identification of paleostress fields as indicated by brittle tectonic analysis.

GEOLOGICAL FRAMEWORK AND AGE OF DEFORMATION EVENTS

The Crimean and NW-Caucasian mountains are classically described as two meganticlinoria structures bordering the Eastern Black Sea Basin to the north. They correspond to the southern deformed boundary of the Scythian plate, as far as the Paleozoic history is concerned. The zone corresponding to present-day Crimea and Caucasus became part of Eurasia during the Namurian-Westphalian. During the Mesozoic, the convergence between the Tethys and the Eurasian craton resulted in subductions and collisions in the Crimean and Caucasian zones; the collision was continuing during the Cenozoic. The structural framework of this region is summarized in figure 1a.

NW-CAUCASUS

The NW-Caucasus is an area of widespread folding and thrusting affecting flysch formations Early Cretaceous to Paleocene in age. The fold axes trend NW-SE and the major thrusts associated are SW-vergent (Fig. 1b). In detail, some NW-SE faults perpendicular to the major folds and thrusts offset the northern thrust fronts, which is also the case offshore to the south. The Oligocene formations unconformably overlie the deformed flysch, indicating that the main folding event affecting the thick flysch series is late Eocene in age.

CRIMEA

The core of the Crimean chain (Fig. 1c) is constituted by high karstic plateaus of Jurassic massive limestones, forming thrusts sheets overthrusting series which include a parautochtonous flysch of the Late Triassic-Aalenian (Taurian group, extremely deformed, see POPADYUK *et al.*, 1991), as well as autochtonous series with ages up to the Albian. The general structure is shown in the cross-sections of figure 2. The cross-section in the Indol River Valley (Fig. 2c) let us to observe an imbrication of Valanginian-Hauterivian sandstones between to thrust planes to the feet of Agarmysh Mount. The recent structural mapping of GALKIN *et al.* (1994), in the area of the Salgir River Valley, reveals that

Source : MNHN, Paris

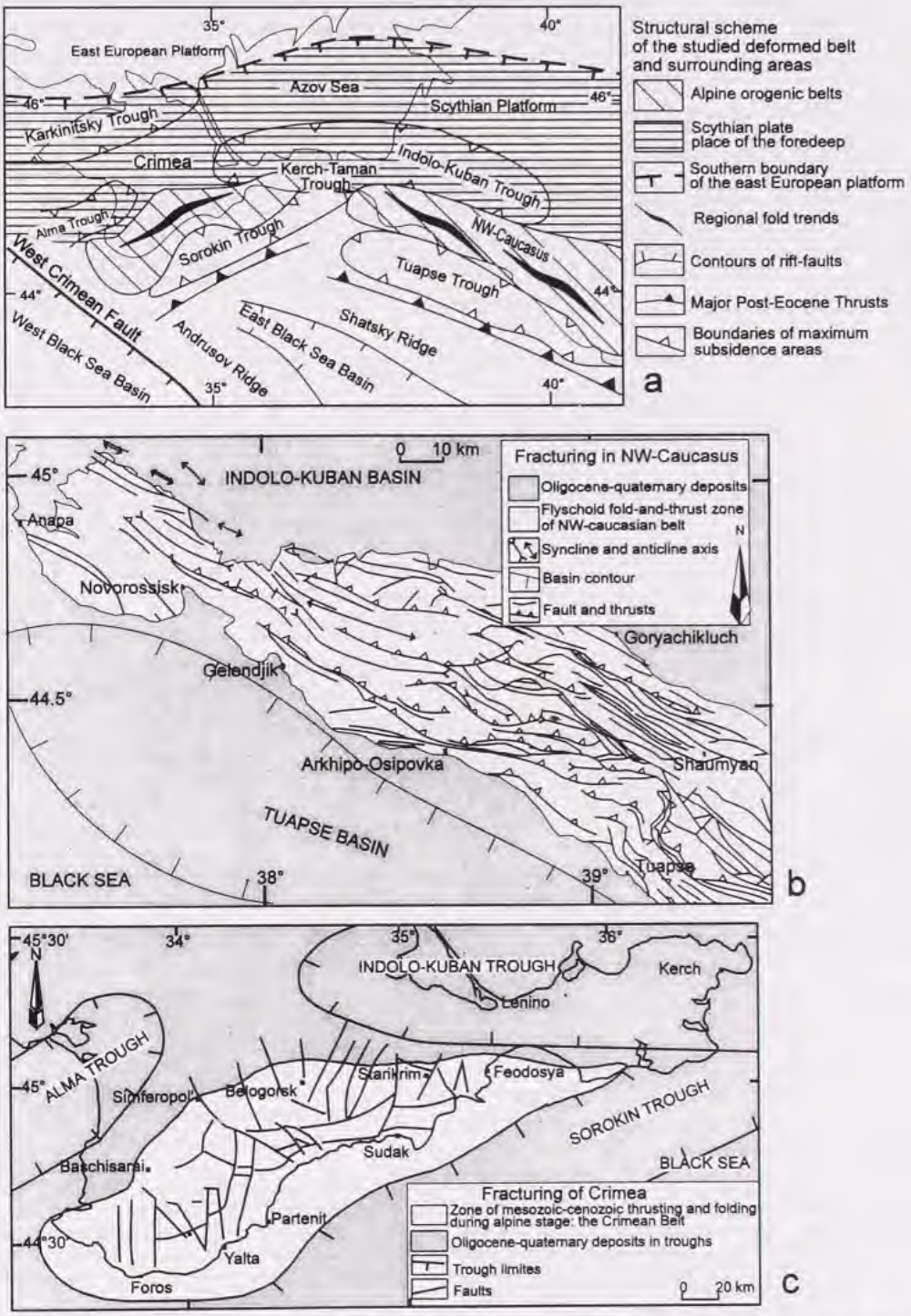

FIG. 1.— Structural framework: a, general map; b, fracturing and structure in NW-Caucasus; c, fracturing and structure in Crimea (from Geological map of the Great Caucasus, 1/500 000, anonymous, 198? and from Geological map of the Crimea and Caucasus, 1/1 500 000, anonymous, 198?).

FIG. 1.— Schéma structural : a, carte générale; b, fracturation et structures dans le Caucase nord occidental ; c, fracturation et structures en Crimée (d'après les cartes géologiques du Grand Caucase, 1/500 000, et de la Crimée, 1/1 500 000).

Source : MNHN, Paris

allochtonous units (Late Jurassic limestones and conglomerates) thrusted over the Early Cretaceous series of the autochtonous complex. Late Cretaceous formations seal the thrust front (POPADYUK *et al.*, 1991) on the northern flank of the belt. A major phase of structuration in Crimea has thus occurred between the Early Cretaceous and the Late Cretaceous (Fig. 2). The thrust sheets are north-vergent, with a total displacement larger than 20 km (POPADYUK *et al.*, 1991).

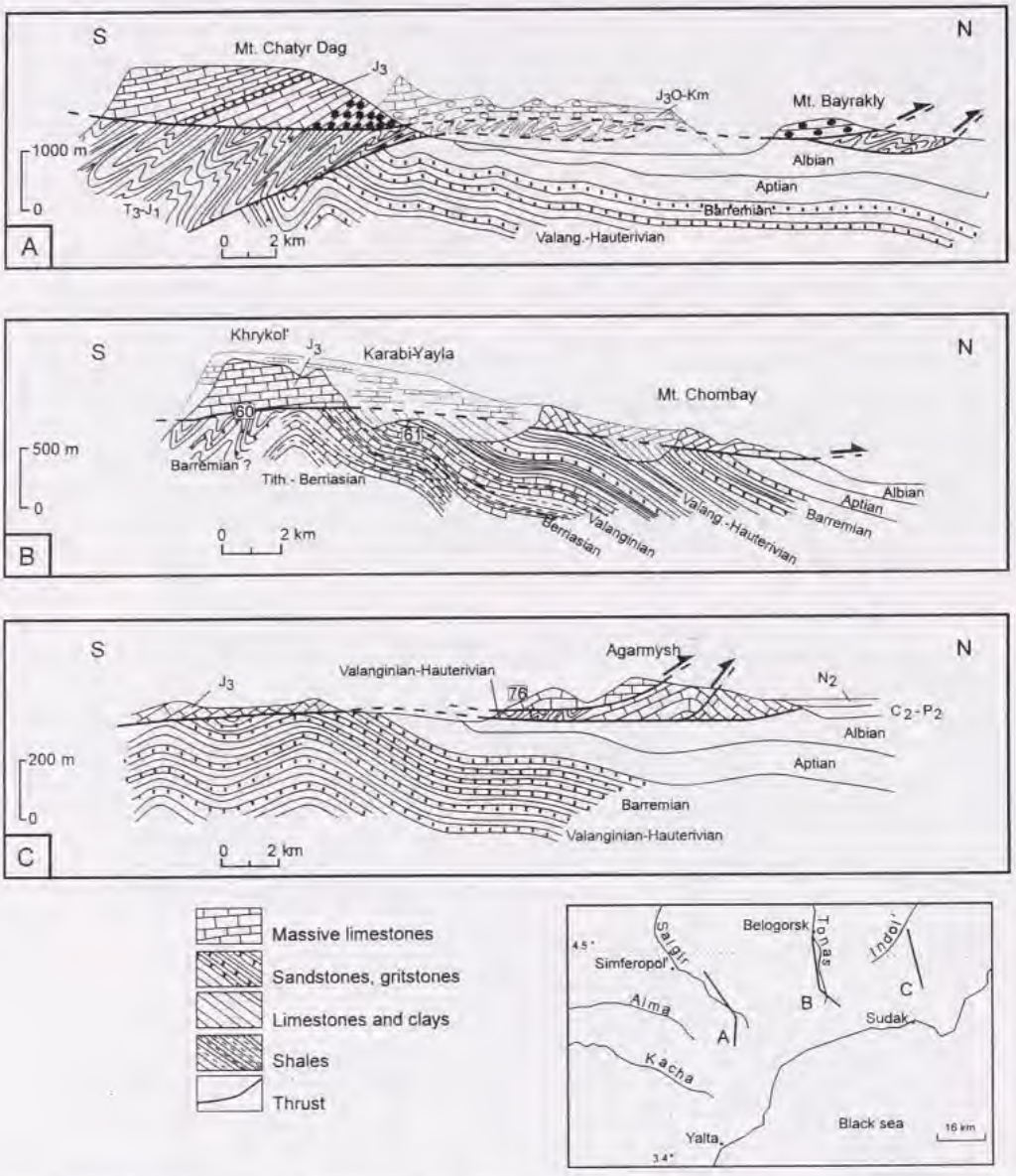

FIG. 2.— (from POPADYUK *et al.*, 1991). **A**: cross-section along the Salgir River Valley; **B**: cross-section along the Tonas River Valley (with sites 60 and 61); **C**: cross-section along the Sukhoy Indol River Valley (with site 76). Structures in background in grey. Allochtonous complex: J_3 O-Km, massive conglomerates of Oxfordian-Kimmeridgian; J_3, massive tithonian limestones (with imbrications of Valanginian-Hauterivian shales and sandstones along the Sukhoy Indol River Valley). Parautochtonous complex: T_3-J_1, terrigenous flysch of Taurian group. Autochtonous complex: Valanginian-Hauterivian to Albian formations; C_2-P_2, Late Cretaceous-Eocene; N_2, Late Neogene.

FIG. 2.— (d'après POPADYUK et al., 1991). ***A*** *: coupe de la vallée de la rivière Salgir ;* ***B*** *: coupe de la vallée de la rivière Tonas (avec les sites 60 et 61) ;* ***C*** *: coupe de la vallée de la rivière Sukhoy Indol (avec le site 76). Structures en arrière plan en grisé. Complexe allochtone : J_3 O-Km, conglomérats massifs de l'Oxfordien-Kimméridgien; J_3, calcaires massifs tithoniens (avec imbrications d'argiles et de grès du Valanginien-Hauterivien le long de la vallée de la rivière Sukhoy Indol). Complexe para-autochtone : T_3-J_1, flysch terrigène du groupe taurien. Complexe autochtone : formations du Valanginien-Hauterivien à l'Albien ; C_2-P_2, Crétacé supérieur-Eocène ; N_2, Néogène supérieur.*

Source : MNHN, Paris

The flyschs of the Taurian series (from Late Triassic to Aalenian) were strongly deformed during the Earlier-Middle Jurassic phase of compressional deformation (Bathonian, NIKISHIN *et al.*, this volume).

Concerning the Tertiary structure, outcrops of autochtonous terranes are present along the northern side of the belt, gently dipping to the north. The Oligocene formations unconformably overlie the Paleocene, indicating a late Eocene tectonic event also recognized in the NW-Caucasus. Three unconformities are observed in Neogene time: the Karaganian horizon (Langhian, middle Miocene), the Sarmatian formations (middle Miocene) and the Akchagylian series (late Pliocene) unconformably overlie the older formations (for local stratigraphy, i.e. Eastern ParaTethys, see Table 1 in annex). They are correlated with the period of maximum subsidence of basins (CHEKUNOV *et al.*, 1976; NIKISHIN *et al.*, this volume). In contrast, the southern flank of the Crimean belt is cut by large faults with the downthrown side to the south (KOGAN *et al.*, 1978; MURATOV *et al.*, 1984).

TABLE 1.— Correlation of Eastern Paratethys Stratigraphy with Tethys Stratigraphy (Neogene and Quaternary).
TABLE 1.— Stratigraphie de la Para-Téthys orientale (Néogène et Quaternaire).

CENOZOIC	QUATERNARY					0.50 Ma
					Bakunian	0.73 Ma
					Apcheronian	1.67 Ma
	NEOGENE	PLIOCENE	Upper	Piacenzian	Akchagylian	3.40 Ma
			Lower	Zanclean	Kimmerian	5.2 Ma
		MIOCENE	Upper	Messinian	Pontian	7.0 Ma
				Tortonian	Meotian	9.3 Ma
			Middle	Serravallian	Sarmatian	13.7 Ma
					Konkian	
				Langhian	Karaganian	
			Lower		Tchokrakian	16.5 Ma
				Burdigalian	Tarchanian	17.0 Ma
					Kozachurian	
				Aquitanian	Sakaraulian	
					Caucasean	

A major fracturating with dominating NE-SW and N-S trends (Fig. 1c) affects all terranes (including the Late Neogene in Crimea). These major faults clearly postdate the main thrusting discussed before, and are oblique relative to the preexisting, nearly E-W trending thrust faults.

NORTHEASTERN BLACK SEA BASIN (Fig. 1)

The southern edge of the deformed belt is the East Black Sea Basin (note that the Black Sea includes two major basin, eastern and western, separated by a horst, the Andrusov Ridge: KOGAN *et al.*, 1978; TUGOLESOV *et al.*, 1985). Numerous authors studied the development of the Black Sea through calculations of subsidence curves based on analyses of well and seismic reflection data.

Different interpretations exist concerning the timing of development of the Black Sea basins. All authors, however, concur to consider that the two basins did not develop simultaneously, the western basin appearing earlier than the eastern one (ISMAGILOV *et al.*, 1986; CHEKUNOV, 1990; OKAY *et al.*, 1994; NIKISHIN *et al.*, this volume). The geodynamic framework of the opening of the Black Sea basins suggests the opening of a back-arc basin related to a volcanic belt (the Pontides), as a response of the north-vergent subduction of southern oceanic domains related to the Tethys (LETOUZEY, 1977; ZONENSHAIN *et al.*, 1986; OKAY *et al.*, 1994).

The Maykopian series (Oligocene-early Miocene) unconformably overlie the earlier formations in basin flanks, indicating a pre-Oligocene age for the subsidence related to the main opening of the eastern basin (ISMAGILOV *et al.*, 1986). Accordingly, most authors consider a Late Cretaceous to early Paleocene age for the development of the East Black sea Basin (OKAY *et al.*, 1994; ROBINSON *et al.*, 1996)

Note that the northwestern segment of the Black Sea basin, south of Odessa shelf, is implied in north-vergent thrusting, west of Crimea, where a seismic reflection profile showed thrusts sealed by Oligocene formations (POPOVICH, 1989). The northern part of the shelf underwent reactivation during later tectonic episodes. Especially, the East Black Sea Basin was

Source : MNHN, Paris

TABLE 2.— Summary of paleostress results at all sites studied. n°, reference number of the site. Stress regimes: S, strike-slip faulting; R, reverse faulting; N, normal faulting. N, number of fault slip data. Trends and plunges of stress axes in degrees (with *, back rotated stress tensor). Methods as referred to ANGELIER (1991). Φ ratio of stress differences, $\Phi=(\sigma_2-\sigma_3)/(\sigma_1-\sigma_3)$. average angle between observed slip and computed shear in degrees. RUP, estimator as referred to ANGELIER (1991). Q, quality estimator (3, good; 2, fair; 1, poor).

*TABLE 2.— Solutions calculées pour les sites étudiés. n°, numéro de référence du site. Régime de contraintes : S, décrochant ; R, inverse ; N, normal. N, nombre de failles pour le calcul du tenseur des contraintes. Directions et plongements des axes de contraintes en degrés (avec *, tenseur des contraintes basculé). INVD ou R4DT : Méthodes d'inversion (ANGELIER, 1991). $\Phi=(\sigma_2-\sigma_3)/(\sigma_1-\sigma_3)$. angle moyen entre la strie réelle et la strie calculée en degré. RUP, estimateur moyen de qualité de la méthode INVD (ANGELIER, 1991). Q, critère de qualité (3, bon ; 2, moyen ; 1, bas).*

moving to the NNW and plunged below the Crimean and NW-Caucasian belts, resulting in widespread folding of the Maykopian series (ISMAGILOV *et al.*, 1986). Thus, a south-vergent thrust zone developed, which may indicate an incipient subduction context.

FOREDEEP BASINS

North of the belt, the E-W Indolo-Kuban basin probably represents the Maykopian foredeep basin of the NW-Caucasus (NIKISHIN *et al.*, this volume), following the major compressional event, late Eocene in age. Likewise, the Alma basin, north west of the Crimean, probably represents the mid-Tertiary foredeep. Although these two basins are deep (Fig. 1a), large subsidence occurred during the Oligocene-Miocene times along the northern side of the whole belt.

SOUTHERN TROUGHS

Along the southern side of the Crimea-NW-Caucasus belt, the Sorokin and Tuapse troughs probably represent flexural basins related to south-vergent thrusting. Especially, the Tuapse trough developed along the northern slope of the eastern Black Sea Basin, parallel to the NW-SE trend of the major fold-and-thrust structures of the NW-Caucasus, during the Oligocene-Miocene, as a consequence of the major compressional event of the late Eocene; similarly, the development of the Sorokin trough is Oligocene-Miocene in age (TUGOLESOV *et al.*, 1985, ISMAGILOV *et al.*, 1986; NIKISHIN *et al.*, this volume). In addition, a late folding phase affected the Oligo-Miocene sedimentary infills of these troughs (MEYSNER *et al.*, 1981; ISMAGILOV *et al.*, 1986; TEREKHOV *et al.*, 1989).

Note that despite this relative regional continuity of the southern troughs, a transverse area of subsidence developed between the two folded areas (Crimea and Caucasus) with a N-S orientation: the Kerch-Taman trough. Asymmetric mud volcanoes of Maykopian-Plio-Quaternary sediments developed in the Kerch and Taman peninsulas, and in the Sorokin and Tuapse troughs as well. In the Kerch-Taman areas, these mud volcanoes are elongated along E-W trends with steep flanks to the north indicating that they formed at ramp fronts which correspond to the activation of deeper thrusts (KAZANTSEV *et al.*, 1988). Drilling in the Kerch peninsula revealed north-vergent thrusting of late Eocene age at depth of about 3.5 km (KAZANTSEV *et al.*, 1988). The diapirism of clay material, which resulted in later volcanism, is related to later reactivations of these thrusts, under compressional regimes, and is now active.

NIKISHIN *et al.* (this volume) point out that the subsidence phases related to the development of these troughs was not accompanied by major normal faulting, which supports the interpretation in terms of Mid-Cenozoic flexural basins. A geochemical study (AL'BOV *et al.*, 1974) in the Kerch Taman rocks revealed high concentrations of elements, deep crustal or mantellic in origin, which suggests that deep-seated faults are involved, which is consistent with the probable presence of a crustal zone of weakness beneath the Kerch-Taman segment of the belt.

Source : MNHN, Paris

Localities	Lat./Long. in degrees	Age of formation	n°	Stress regime	N	σ_1 trend	σ_1 plunge	σ_2 trend	σ_2 plunge	σ_3 trend	σ_3 plunge	Meth.	Φ	α	% RUP	Q
Baschisarai	44.77/33.99	Middle Jur.	1	S	9	180	26	312	54	078	23	INVD	0.1	13	38	3
			*	S		003	02	269	60	094	30	INVD	0.1	13	36	3
			1	S	9	144	14	253	52	044	34	INVD	0.1	12	40	2
			1	R	14	194	06	103	01	002	84	INVD	0.5	12	22	3
			1	Dykes with E-W trends												
	44.72/33.85	Paleogene	2	S	7	100	08	288	82	190	01	INVD	0.6	04	17	3
			2	S	15	129	01	031	84	220	06	INVD	0.4	11	37	3
	44.77/33.87	Paleogene	3	S	25	131	04	294	86	041	01	INVD	0.5	09	29	3
	44.77/33.98	Sant./Camp.	4	S	5	177	34	045	44	287	26	INVD	0.6	07	30	1
			4	Crushed zone with N115 trends												
	44.78/33.75	Sarmatian	23	Tension gashes σ'_3= 080												
			23	Tension gashes σ'_3= 150												
	44.75/33.85	Late Eoc.	25	S	18	318	08	059	52	222	37	INVD	0.1	12	38	3
			25	N	4	184	49	337	38	078	14	INVD	0.9	05	24	1
			25	N	8	127	77	222	01	313	13	INVD	0.3	04	11	3
			25	N	9	109	75	286	15	016	01	INVD	0.4	09	24	3
			25	Tension gashes σ'_3= 045												
			25	Tension gashes σ'_3= 145												
	44.73/33.92	Tur./Coniac.	38	Stylolites σ'_1= 150												
	44.80/34.02	Middle Jur.	39	Tension gashes σ'_3= 080												
			39	Pre-tilting : Tension gashes σ'_3= 120												
	44.80/34.01	Middle Jur.	40	Stylolites and associated stylolitic planes σ'_1= 170												
	44.80/34.00	Middle Jur.	41	R	19	190	09	100	01	006	81	INVD	0.6	11	22	3
			41	S	14	171	20	345	70	080	02	INVD	0.4	11	25	3
			41	S	8	112	10	224	65	018	22	INVD	0.5	14	35	2
			41	R	6	135	01	225	02	016	87	INVD	0.4	11	35	2
			41	S	6	340	46	131	40	234	15	INVD	0.7	09	28	1
			41	R	12	214	03	305	19	115	71	INVD	0.2	15	35	3
Simferopol'	44.96/33.62	Neogene	17	Tension gashes σ'_3= 180												
	44.95/34.17	Middle Jur.	32	N	18	317	79	217	02	127	11	INVD	0.5	10	24	3
			32	S	17	074	01	339	77	164	13	INVD	0.4	12	34	3
			32	S	9	178	21	311	60	080	20	INVD	0.6	05	26	2
Foros	44.41/33.70	Late Jur.	8	N	43	175	77	270	01	360	13	INVD	0.4	12	29	3
			8	S	6	247	21	103	65	343	13	INVD	0.5	08	36	2
	44.37/33.68	Late Jur.	9	R	4	246	33	149	10	045	55	INVD	0.4	09	31	1
			9	S	13	142	42	322	48	052	00	INVD	0.6	11	36	2
			9	S	10	066	11	209	77	334	08	INVD	0.3	10	32	3
	44.37/33.68	Late Jur.	47	S	30	304	15	178	66	039	19	R4DT	0.2	12	30	3
			47	R	6	281	03	013	21	183	69	INVD	0.6	03	11	1
			47	S	14	023	06	139	78	292	11	INVD	0.4	20	44	2
			47	R	5	143	01	233	12	049	78	INVD	0.6	05	12	1
	44.48/33.88	Late Jur.	48	N	7	130	83	270	05	001	04	INVD	0.3	12	33	2
	44.42/33.82	Late Jur.	49	N	14	142	71	306	18	038	05	INVD	0.5	08	27	3
Yalta	44.40/34.07	Late Jur.	45	R	20	336	01	245	60	066	30	R4DT	0.1	13	66	2
			45	N	9	283	80	044	05	134	09	INVD	0.3	07	17	3
			45	N	18	340	81	090	03	180	08	INVD	0.5	09	26	3
			45	S	15	252	15	064	75	161	02	INVD	0.6	19	35	2
			45	S	9	202	14	053	74	294	08	INVD	0.4	08	32	2
	44.57/34.07	Late Trias. Early Mid. Jur.	50	N	9	023	78	215	12	124	02	INVD	0.5	06	24	3
	44.49/34.02	Late Jur.	51	S	8	235	05	342	73	144	16	INVD	0.3	10	35	2
			51	Stylolites σ'_1= 040												

Source : MNHN, Paris

Localities	Lat./Long. in degrees	Age of formation	n°	Stress regime	N	σ_1 trend	σ_1 plunge	σ_2 trend	σ_2 plunge	σ_3 trend	σ_3 plunge	Meth.	Φ	α	% RUP	Q
Yalta	44.52/34.22	Late Trias. Early Jur.	52	S	8	112	02	005	83	203	06	INVD	0.6	13	39	2
			58	Stylolites σ'_1= 150												
	44.53/34.03	Late Jur.	58	Stylolites σ'_1= 040												
			58	Tension gashes σ'_3= 090												
	44.52/33.98	Late Jur.	59	S	6	348	09	148	80	257	03	INVD	0.6	06	15	2
Partenit	44.57/34.33	Middle Jur.	43	S	5	253	14	073	75	343	00	INVD	0.3	10	28	1
	44.60/34.33	Middle Jur.	44	Pre-tilting tension gashes σ'_3= 100												
	44.62/34.32	Middle Jur.	53	S	8	180	15	000	75	090	00	INVD	0.4	08	21	2
Belogorsk	45.06/34.62	Midldle Eoc.	28	Tension gashes σ'_3= 060												
	45.07/34.67	Midldle Eoc.	30	N	18	297	82	177	04	087	07	INVD	0.3	10	27	3
			30	S	8	216	39	054	50	314	09	INVD	0.7	15	43	2
	44.85/34.67	Late Jur.	60	S	5	197	14	097	35	305	51	INVD	0.3	13	55	1
	44.87/34.63	Neocomian	61	S	8	347	32	171	58	078	02	INVD	0.7	04	13	2
	44.97/34.63	Tithonian	63	S	14	164	01	066	80	254	10	INVD	0.4	16	34	3
			63	S	17	008	14	142	70	274	13	INVD	0.4	13	28	3
	45.05/34.60	Early Mid. Eoc.	84	S	5	327	46	141	44	234	03	R4DT	0.8	01	18	1
Stari Krim	44.97/34.98	Late Jur.	76	S	7	282	37	076	50	182	13	INVD	0.3	07	27	1
			76	S	12	208	50	048	39	310	10	INVD	0.3	11	37	2
			76	S	21	359	13	258	41	103	47	INVD	0.3	08	22	2
	45.00/35.07	Cretaceous ?	79	N	14	309	72	195	08	103	16	INVD	0.5	09	34	3
			79	S	15	338	17	212	63	075	21	INVD	0.4	12	34	3
			Associated stylolites													
			79	S	18	014	07	258	74	106	15	INVD	0.5	10	26	3
			79	R	6	247	05	156	05	021	83	INVD	0.1	07	24	1
			Associated stylolites													
Sudak	44.80/34.94	Late Jur.	5	N	5	148	68	263	10	357	19	INVD	0.6	04	16	1
			*	S		107	33	265	55	010	11	INVD	0.6	04	15	1
			5	R	8	182	21	273	04	015	69	INVD	0.2	12	30	2
			5	Tension gashes and associated mineral fibers σ'_3= 120												
			5	Tension gashes and associated mineral fibers σ'_3= 45												
	44.79/34.92	Late Jur.	6	Tension gashes σ'_3= 155												
			6	Tension gashes σ'_3= 020												
	44.87/35.08	Late Jur.	10	S	5	276	37	084	53	182	06	INVD	0.7	06	12	1
			10	Tension gashes σ'_3= 100												
	44.86/35.07	Late Jur.	11	R	13	218	04	128	04	351	84	INVD	0.6	10	25	3
			11	Tension gashes σ'_3= 105												
	44.85/35.08	Late Jur.	64	S	14	172	18	047	61	270	22	INVD	0.5	15	34	2
			64	N	7	129	70	006	12	273	17	INVD	0.4	08	25	1
	44.84/35.08	Late Jur.	65	S	6	330	64	152	26	062	01	INVD	0.7	07	25	1
	44.86/35.08	Late Jur.	66	N	21	293	84	151	05	061	03	INVD	0.1	18	57	2
	44.90/35.13	Late Jur.	67	N	4	201	74	028	16	297	02	INVD	0.6	07	22	2
Feodosya	44.93/35.18	Middle Jur.	68	R	20	213	06	303	01	039	84	INVD	0.5	14	34	3
	44.95/35.27	Late Jur.	81	S	21	018	22 01	156	61	281	17	INVD	0.6	09	28	3
			*	S	21	017		111	75	287	15	INVD	0.6	09	28	
Kerch	45.32/36.34	Neogene	12	R	19	124	08	033	02	290	82	INVD	0.5	11	39	3
			12	R	16	160	11	251	05	004	78	INVD	0.5	08	30	3
			12	R	6	047	02	138	20	312	70	INVD	0.6	14	31	1
	45.37/36.26	Late Mid. Mioc.	74	R	10	212	06	303	10	093	79	INVD	0.4	10	38	3
	45.40/36.42	Meotian	78	S	5	278	13	106	76	009	02	INVD	0.4	10	31	1
			78	R	4	354	12	084	02	182	77	INVD	0.6	04	9	1
Lenino	45.32/35.67	Meot./Pont.	70	N	4	028	58	181	29	278	12	INVD	0.7	10	26	1
	45.40/35.73	Meotian	71	N	21	214	83	001	06	091	04	INVD	0.3	10	30	3
	45.27/36.02	Middle Mioc.	75	S	8	068	02	175	81	338	08	INVD	0.6	18	42	1

Source : MNHN, Paris

Localities	Lat./Long. in degrees	Age of formation	n°	Stress regime	N	σ_1 trend	σ_1 plunge	σ_2 trend	σ_2 plunge	σ_3 trend	σ_3 plunge	Meth.	Φ	α	% RUP	Q
Anapa	44.87/37.33	Late Maas.	97	N	5	174	73	031	14	299	10	INVD	0.6	16	47	1
			*	N	5	288	87	029	01	119	03	INVD	0.6	15	46	1
			97	Tension gashes σ'_3= 005												
			97	Tension gashes σ'_3= 120												
	44.92/37.40	Danian	98	Tension gashes σ'_3= 135												
	45.02/37.47	Early Paleocene	99	S	6	285	09	187	41	025	48	INVD	0.7	05	31	1
			*	S	6	122	22	289	67	031	05	INVD	0.9	09	28	1
Novorossisk	44.70/37.86	Late Cretaceous	13	N	13	202	86	298	00	028	04	INVD	0.5	16	38	3
			*	R	13	214	10	122	10	348	76	INVD	0.5	16	38	3
			14	Tension gashes σ'_3= 165												
			14	Tension gashes σ'_3= 070												
	44.67/37.56	Early Paleocene	14	S	10	250	11	354	51	152	37	INVD	0.3	06	26	3
			*	S	10	249	06	350	63	156	26	INVD	0.3	06	25	3
			14	N	7	052	66	296	11	202	21	INVD	0.4	06	34	1
			*	N	7	067	70	291	14	198	13	INVD	0.4	07	33	1
			14	R	34	218	07	308	01	045	83	INVD	0.5	10	37	3
			*	R	34	038	03	308	06	152	83	INVD	0.5	10	37	3
	44.72/37.60	Maas.?	15	S	7	359	28	240	42	111	36	INVD	0.4	06	27	2
			*	S	7	195	07	343	82	104	04	INVD	0.4	03	12	2
	44.75/37.75	Late Cretaceous	16	R	7	212	11	309	30	104	58	INVD	0.5	08	33	1
			16	N	25	029	69	206	21	296	01	INVD	0.2	09	24	3
			*	N	23	218	80	039	10	309	00	INVD	0.3	07	21	3
	44.88/37.90	Paleogene?	94	Tension gashes σ'_3= 120												
	44.82/37.93	Coniacian Santonian	95	N	5	334	75	164	15	073	02	INVD	0.6	07	15	2
			*	N	5	033	78	153	06	244	10	INVD	0.4	07	15	2
			95	Pretilting tension gashes σ'_3= 090												
			95	S	12	112	02	283	88	022	00	INVD	0.4	14	35	3
			95	Pretilting stylolites and associated stylolitic planes σ'_1= 045												
	44.83/37.07	Coniacian Santonian	96	S	5	034	51	232	38	135	09	INVD	0.6	12	34	1
			*	S	5	033	09	271	73	125	14	INVD	0.6	12	37	1
			96	R	7	158	02	248	06	051	84	INVD	0.3	10	24	3
			96	N	10	257	84	148	02	058	06	INVD	0.4	12	33	3
Gelendjik	44.53/38.15	Late Campanian	85	R	18	355	13	263	12	131	73	INVD	0.4	06	15	3
			*	R	18	176	08	268	14	057	74	INVD	0.5	06	15	3
			85	S	8	338	04	181	85	069	02	INVD	0.7	08	29	3
			85	R	7	329	10	061	12	200	75	INVD	0.8	11	27	3
			*	R	7	137	09	228	05	344	80	INVD	0.7	11	26	3
			Stylolites and associated stylolitic planes													
			85	R	5	033	08	301	11	158	76	INVD	0.7	02	11	2
			*	R	5	214	10	305	02	044	79	INVD	0.6	02	10	2
			85	N	4	252	83	147	02	057	07	INVD	0.5	02	17	1
	44.55/38.17	Coniacian	91	Stylolites and associated stylolitic planes σ'_1= 110												
		Santonian	91	R	12	202	26	295	06	036	63	INVD	0.8	08	22	2
			92	R	10	206	05	116	00	023	85	INVD	0.7	07	15	3
			Associated bedding plane fault													
	44.54/38.15	Coniacian Santonian	92	R	10	165	07	256	09	036	78	INVD	0.2	10	24	3
			Associated bedding plane fault													
			92	S	9	132	04	280	85	042	03	INVD	0.4	11	41	2
			Associated bedding plane fault													
	44.55/38.13	Coniacian Santonian	93	R	21	280	08	186	23	027	66	INVD	0.7	16	34	3
			Associated stylolites													
	44.57/38.10	Late Campanian	102	S	12	290	07	138	82	020	04	INVD	0.6	12	34	3
			102	Synfolding bedding plane fault during NE-SW compressional event												

Source : MNHN, Paris

Localities	Lat./Long. in degrees	Age of formation	n°	Stress regime	N	σ_1 trend	σ_1 plunge	σ_2 trend	σ_2 plunge	σ_3 trend	σ_3 plunge	Meth.	Φ	α	% RUP	Q
Arkhipo-Osipovka	44.47/38.40	Coniacian Santonian	87	S	5	194	11	307	64	099	23	INVD	0.6	15	32	1
			87	R	9	288	14	019	02	115	76	INVD	0.1	11	30	3
	44.46/38.38	Late Cretaceous	88	R	17	089	16	182	11	305	71	INVD	0.2	10	28	3
								Associated stylolites								
	44.52/38.32	Late Campanian	89	R	30	108	02	217	82	018	07	INVD	0.2	17	37	3
			89	R	13	140	00	050	11	231	79	INVD	0.5	10	22	2
	44.38/38.53	Coniacian Santonian	86	S	5	024	07	118	33	283	56	INVD	0.1	10	29	1
			86	N	10	272	82	006	01	097	08	INVD	0.4	06	12	2
	44.25/38.85	Late Maas.	120	N	11	143	75	287	12	018	08	INVD	0.4	06	27	3
			120	R	14	143	11	052	06	294	78	INVD	0.7	12	29	2
	44.27/38.82	Late Maas.	121	R	15	002	18	093	02	189	72	INVD	0.8	10	24	2
	44.28/38.79	Late Camp.	122	S	7	321	07	219	59	056	30	INVD	0.2	12	39	1
	44.30/38.77	Late Cret.	123	S	16	159	02	344	88	249	00	INVD	0.2	10	30	3
	44.33/38.70	Late Maas.	124	S	8	331	31	217	34	092	40	INVD	0.3	12	41	2
			*	S	8	155	21	287	60	056	20	INVD	0.3	12	41	2
			124	S	7	087	54	326	20	225	28	INVD	0.3	18	51	1
Tuapse	44.17/39.22	Late Campanian	109	S	16	015	05	144	83	285	06	INVD	0.4	19	39	3
			109	S	6	336	03	182	87	066	01	INVD	0.4	13	41	2
			109	N	9	202	60	010	29	103	05	INVD	0.3	10	29	2
			*	N	9	152	82	359	07	268	04	INVD	0.4	10	23	2
	44.15/39.18	Coniacian Santonian	110	S	27	190	07	334	81	100	05	INVD	0.2	12	34	3
			110	N	8	219	70	008	17	101	10	INVD	0.5	12	25	2
			*	N	8	016	77	187	13	278	02	INVD	0.6	12	24	2
			110	S	11	338	11	215	70	071	16	INVD	0.3	14	36	3
			*	S	11	158	05	048	76	249	13	INVD	0.2	11	35	3
	44.14/39.14	Coniacian Santonian	111	R	19	031	26	124	06	225	63	INVD	0.7	13	37	3
			*	R	19	224	02	134	05	334	84	INVD	0.6	10	25	3
						Pretilting stylolites and associated stylolitic planes σ'_1= 040										
	44.12/39.05	Early Paleoc.	112	N	7	068	87	320	01	230	03	INVD	0.4	10	26	2
	44.14/39.05	Late Camp. Early Maas.	113	R	12	172	09	268	33	068	55	INVD	0.3	10	25	3
			*	S	12	347	01	228	87	077	02	INVD	0.3	12	27	3
	44.15/39.02	Early Paleocene	114	S	4	081	18	210	63	344	19	INVD	0.5	05	27	2
			114	N	5	229	63	136	02	045	27	INVD	0.4	05	22	2
			114	N	4	009	64	209	25	115	08	INVD	0.3	03	23	2
			*	S	4	015	07	266	70	107	19	INVD	0.2	03	22	2
			114	R	7	096	11	195	38	353	50	INVD	0.6	07	26	3
			*	S	7	091	13	308	74	183	09	INVD	0.6	09	25	3
	44.16/39.02	Late Maas.	115	S	7	130	06	230	59	036	30	INVD	0.4	07	38	3
			115	R	11	084	08	178	22	335	66	INVD	0.8	07	24	3
			*	N	11	163	57	340	33	071	02	INVD	0.8	07	22	3
	44.17/39.00	Early Paleocene	116	S	7	158	24	358	65	252	07	INVD	0.7	12	30	2
			116	S	11	108	23	237	56	007	23	INVD	0.5	13	34	3
			*	S	11	285	02	021	76	194	14	INVD	0.4	10	30	3
			116	S	5	356	64	207	22	112	12	INVD	0.4	02	20	2
			*	S	5	016	17	186	72	285	03	INVD	0.6	02	13	2
			116	R	7	248	13	151	27	000	59	INVD	0.8	07	34	1
			*	N	7	195	80	288	00	018	10	INVD	0.8	08	22	1
	44.17/38.97	Early Paleoc.	117	S	7	081	20	220	64	346	16	INVD	0.2	06	23	3
	44.18/38.92	Late Cretaceous	118	S	8	074	21	304	60	172	21	INVD	0.3	15	41	2
			*	R	8	287	00	017	07	195	83	INVD	0.3	17	40	2
	44.19/38.89	Late Maas.	119	N	12	250	69	114	16	019	14	INVD	0.6	11	34	3
Goryachikluch	44.61/39.08	Early Paleoc.	103	S	10	199	10	335	77	108	09	INVD	0.4	15	34	2
	44.55/38.98	Valanginian?	105	N	15	331	78	125	11	216	05	INVD	0.4	12	30	3
			*	R	15	209	06	300	05	069	82	INVD	0.4	12	31	3
Shaumyan	44.35/39.23	Valanginian?	106					Tension gashes and associated mineral fibers σ'_3= 080								
	44.30/39.30	Late Camp.?	107	N	4	278	70	130	17	037	10	INVD	0.8	10	34	1
	44.28/39.28	Late Cretac.	108	N	8	058	64	297	14	201	22	INVD	0.4	15	45	2

Source : MNHN, Paris

PALEOSTRESS FIELDS

METHODS FOR PALEOSTRESS FIELD DETERMINATION

Numerous brittle structures have been observed. By inversion of faults slip data (ANGELIER, 1975, 1984, 1991), we determined both the attitude of the three principal stress axes (σ_1, σ_2, σ_3, with $\sigma_1 \geq \sigma_2 \geq \sigma_3$ and pressure counted positive) and the value of the Φ ratio between principal stress differences: $\Phi = (\sigma_2 - \sigma_3)/(\sigma_1 - \sigma_3)$. In each site, we separated subsets of fault slip data consistent with different stress tensors. The quality of each determination was determined based on the number of data, on the angle between the calculated shear and observed striae for each fault, and on the estimators 'RUP' (as defined by ANGELIER, 1991). Note that as the misfit increases, a ranges from 0° to 180° whereas 'RUP' ranges from 0° to 200°.

For the regional synthesis, local stress states were grouped based on consideration of both the type-orientation of the corresponding regimes (extensional, compressional or strike-slip) and the chronological constraints. We thus reconstructed seven successive paleostress fields which are consistent in terms of regimes and timing (SAINTOT *et al.*, 1996).

In detail, relative chronology between successive paleostress were obtained by using criteria such as successive striations on a fault plane, crosscutting relationships, reactivation of conjugate fault planes. Consideration of the relative ages of faulting and folding was of large help, because it allowed distinction of pre-folding, syn-folding and post-folding paleostresses. Compilation of such relative chronology criteria brought constraints on regional successions of events through correlation of local results. The stratigraphic ages of affected terranes also imposed major constraints in dating.

REGIONAL RESULTS: CRIMEA AND NW-CAUCASUS BELTS

The studied region was divided in three parts based on regional geology, with 69 sites in the Crimean chain, 11 sites in Kerch peninsula and 44 sites in the NW-Caucasus. 140 local stress states were determined, and their characteristics are listed in table 2. The regional synthesis allowed characterization of seven main paleostress fields. We describe them thereafter, from the latest to the oldest. Note that in some cases, the tectonic regimes in Crimea may differ from those in NW-Caucasus, as the result of large differences in the orientation of structural grains.

THE PRESENT-DAY STRESS FIELD (Fig. 3a, 3b, 3c).— The southern boundary of the east-european platform is seismically active, so that the present-day stress field could be determined through inversion of focal mechanisms of earthquakes (GOUSHTCHENKO *et al.*, 1993a, b). In the studied area, the direction of the principal horizontal stress axes widely varies (Fig. 3a). From the westernmost part of Crimea to the eastern part of the NW-Caucasus, the trend of σ_1 trajectories deviates from NW-SE to N-S, the attitude of σ_2 axes is E-W trending in the NW-Caucasus and vertical in western Crimea, while σ_3 axes are SW-NE in Crimea and vertical in the NW-Caucasus. We conclude that the Crimean belt is presently dominated by a strike-slip regime, whereas the NW-Caucasus undergoes a pure compressional regime (Fig. 3a).

Concerning geological data (Fig. 3b, 3c), in the Kerch peninsula, we collected slip data on reverse faults (sites 12, 78; Fig. 3c) associated to a pure compressional regime like in NW-Caucasus (sites 85, 92, 96, 121; Fig. 3b). This Quaternary regime affects Crimea where strike-slip faults were observed (sites 1, 3, 41, 48, 61, 63, 79, 84). We include in this tectonic phase stress states which show E-W extension (sites 25, 28, 30, 71, 86, 106). This may be due to a release of confining pressure for the compressional N-S event, or to a permutation of σ_1 and σ_2 axes under the strike-slip regime that we observed in sites in Crimea (sites 1, 3, 41, 48, 61, 63, 79, 84); we note that in Crimea this phenomenon is localized on the northern flank of the belt, with development of numerous tension gashes (sites 23, 25, 28).

Note also that the reactivation of the thrusting defined of late Eocene in age and which produces the

Source : MNHN, Paris

recent mud volcanism in the Kerch-Taman peninsula could be related to this compressional phase (ANGELIER *et al.*, 1994; SAINTOT *et al.*, 1995).

THE EARLY PLIOCENE (KIMMERIAN) COMPRESSIONAL STRESS FIELD (Fig. 4a, 4b).— As the Quaternary event described above, we observed a deviation of the trends of σ_1 trajectories from NW-SE in NW-Caucasus to WNW-ESE in Crimea (Fig. 4a, 4b).

The strike-slip regime dominated in NW-Caucasus (sites 14, 85, 92, 115, 116, 122, 123) but reverse faulting was observed locally (sites 89, 120). This event affected, with formation of reverse and strike-slip fault sets, the Neogene series in the Kerch area in sites 12,78 (ANGELIER *et al.*, 1994). In the Crimean belt, the strike-slip regime was observed in six sites (2, 5, 10, 41, 52, 76); one site (47) was marked by pure compression southwest of Crimea. Development of tension gashes was associated with this event (sites 6, 17) and near Bashisarai (site 25) extension occurred perpendicular to the trend of compression.

THE NEARLY E-W COMPRESSIONAL STRESS FIELD (Fig. 5a, 5b).— Along the NW-Caucasian coast from Gelendjik to Tuapse, we observed development of reverse faults (sites 93, 88) and strike-slip faults (sites 87, 89, 95, 102, 114, 117) in the Cretaceous to Paleocene series relative to a nearly E-W compressional event (Fig. 5a). In this tectonic setting, the NW-Caucasian margin underwent a sinistral strike-slip movement.

In the western Crimean belt, in Jurassic limestones, a strike-slip regime with σ_1 trending WSW-ENE occurred (sites 8, 9, 32, 43, 45, 51), with local development of stylolites. In eastern Crimean belt, this compressional regime is poorly recorded (site 79). In the Neogene series of the Kerch Peninsula (sites 12, 70, 74, 75), we observed a local deviation in the trend of σ_1 trajectories, from WSW-ENE to NE-SW. In this tectonic setting, the Crimean boundary probably underwent a sinistral strike-slip movement.

The age of this event is attributed to the Sarmatian; unconformities observed in Crimea and NW-Caucasus and the period of subsidence defined by NIKISHIN *et al.* (this volume) support the age of this event.

THE MULTIDIRECTIONAL EXTENSIONAL STRESS FIELD (Fig. 6a, 6b).— This extensional regime probably occurred from Oligocene to early Miocene time (Maykopian), in agreement with the development of peripheric basins of the Crimean and NW-Caucasian belt. The trend of σ_3 trajectory was thus perpendicular of the axes of maximum subsidence in the troughs.

Along the NW-Caucasian coast (Fig. 6a), Cretaceous and Paleocene series are affected by NE-SW extensional regime related to the development of the Tuapse trough (sites 85, 96, 112, 114, 119, 120, 124). A NE-SW extensional regime is also observed in the northern flank of the NW-Caucasus (sites 107, 108), in agreement with the development of the Kuban foredeep (Fig. 6a).

A NW-SE extensional regime related to the development of the Alma trough is marked in the

---

FIG. 3.— Present-day Quaternary stress fields; a, computed by inversion of focal mechanisms of earthquakes (from GOUSHTCHENKO *et al.*, 1993a, b); b and c, computed by inversion of fault slip data sets in NW-Caucasus and Crimea respectively. Stereoplots in figure 3b-c: examples of faults consistent with the paleostress field illustrated. Schmidt's projection, lower hemisphere. Fault planes as thin lines, bedding planes as doted lines, striae as small arrows (inward directed=reverse, outward directed=normal, strike-slip striae as couple of thin arrows). Computed stress axes as 5-, 4- and 3- branch stars (σ_1, σ_2 and σ_3 respectively). Trend of compression: inward directed large arrows; trend of extension: outward directed large arrows. Couples of arrows in map: sites where we reconstructed the tectonic regime illustrated. Trend of compression: inward directed arrows; trend of extension: outward directed arrows; trend of σ_1 axis in strike-slip regime: inward directed triangles. Brittle features associated with faults: JX, tension gashes; LP, stylolites; JP, stylolitic pressure-solution seams. (For locations, see figures 1b and 1c for NW-Caucasus and Crimea respectively).

FIG. 3.— Champ de contraintes quaternaire et actuel ; a, déterminé par l'inversion des mécanismes au foyer des séismes (d'après GOUSHTCHENKO et al., 1993a, b) ; b et c, déterminé par l'inversion des glissements sur les plans de failles respectivement dans le Caucase nord-occidental et en Crimée. Stéréogrammes (Fig. 3b-c): exemples de failles compatibles avec le champ de contraintes illustré. projection de Schmidt hémisphère inférieur. Plans de failles : lignes continues, plans startigraphiques : lignes en pointillé, stries : petites flèches (convergentes = inverses, divergentes = normales, stries décrochantes: couples de flèches). Axes de contraintes calculés : étoiles à 5-, 4- et 3- branches, σ_1, σ_2 et σ_3 respectivement. Direction de compression : grandes flèches convergentes; direction d'extension : grandes flèches divergentes. Couples de flèches sur les cartes : sites où le régime tectonique a été déterminé. Direction de compression = flèches convergentes ; direction d'extension= flèches divergentes ; direction de l'axe σ_1 dans les régimes décrochants = triangles convergents. Structures cassantes associées aux failles : JX, fentes de tension ; LP, stylolites ; JP, plans stylolitiques. (pour la localisation, voir figure 1b pour le Caucase nord occidental et 1c pour la Crimée).

Source : MNHN, Paris

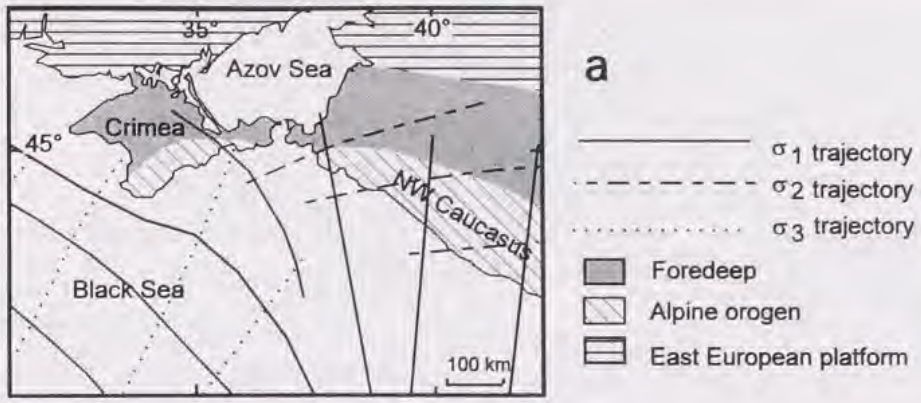

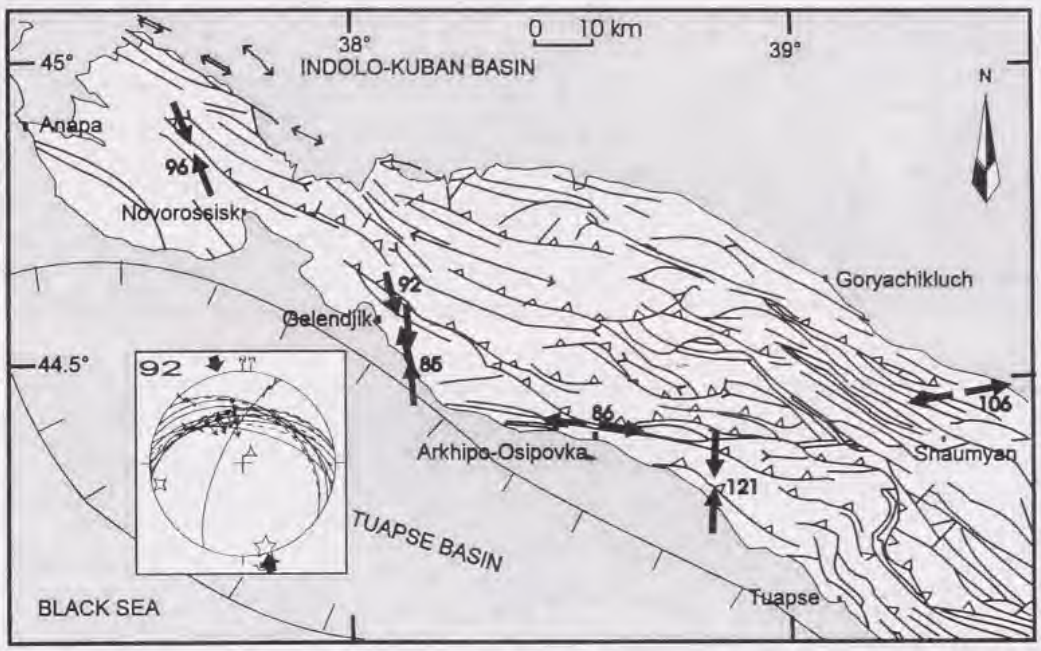

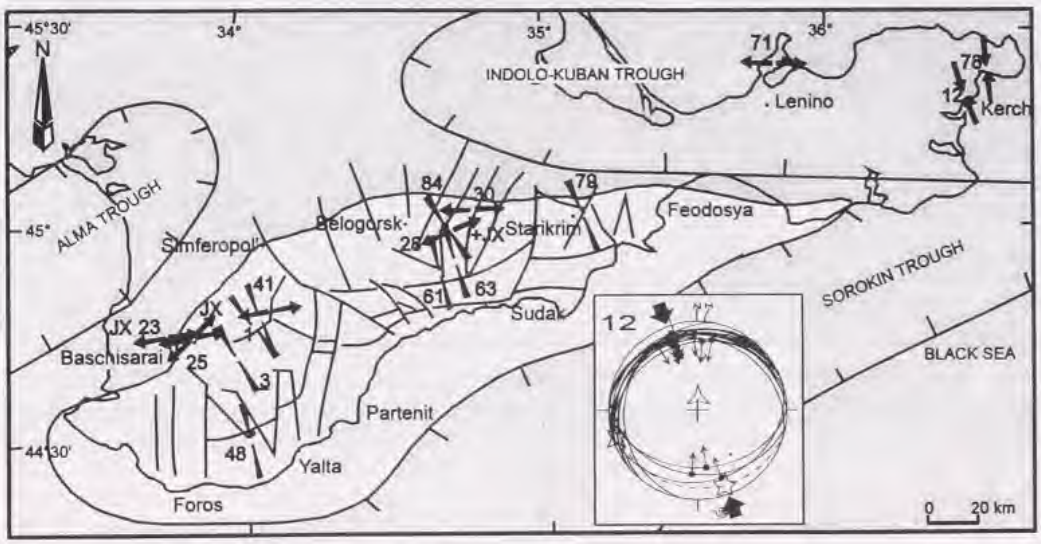

Source : MNHN, Paris

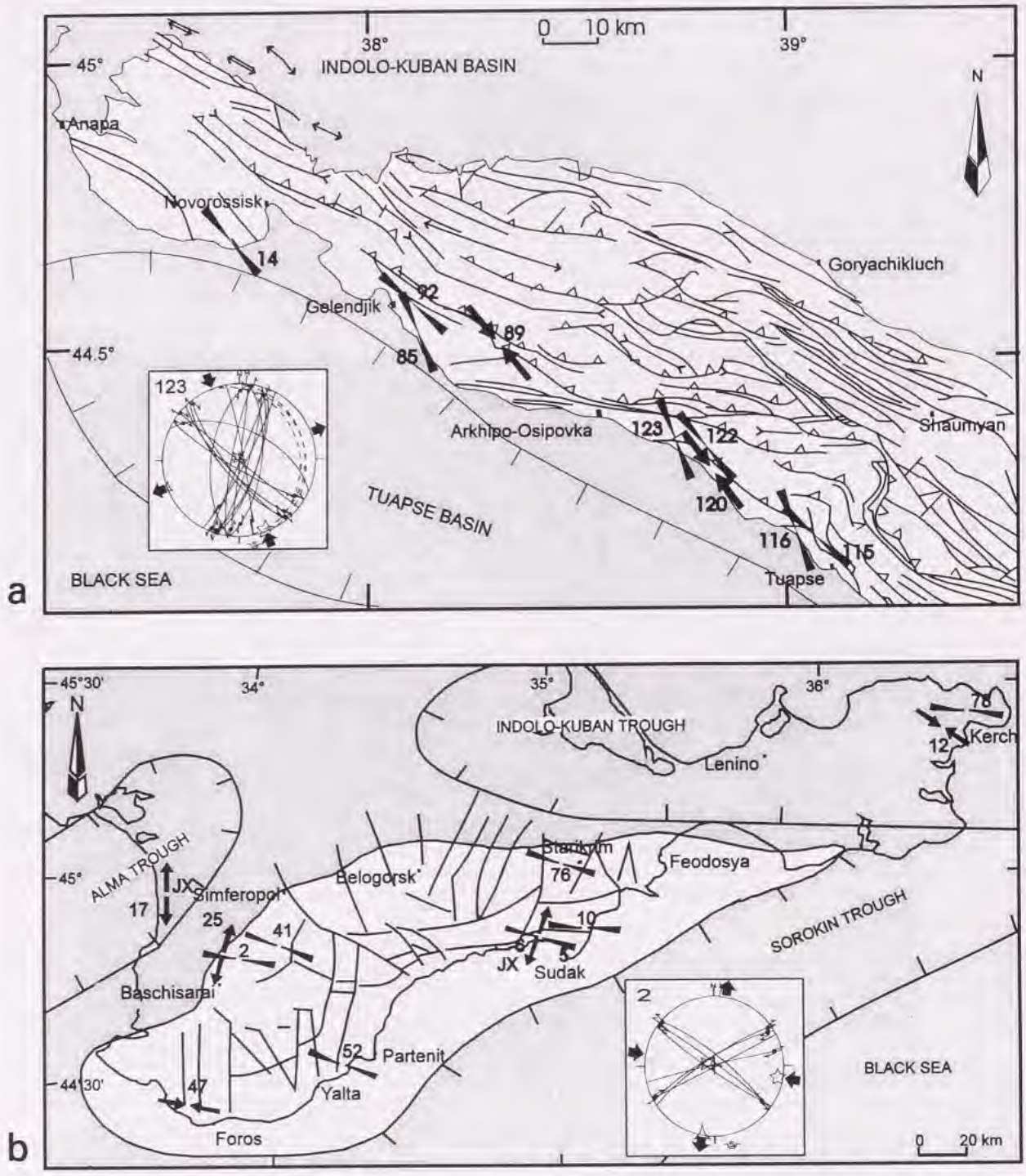

FIG. 4.— Kimmerian (early Pliocene) stress field; a, in NW-Caucasus; b, in Crimea; symbols as for figures 3b-c.
FIG. 4.— Champ de contraintes cimmérien (Pliocène inférieur) ; a, dans le Caucase nord occidental; b, en Crimée ; mêmes symboles que pour les figures 3b-c.

Source : MNHN, Paris

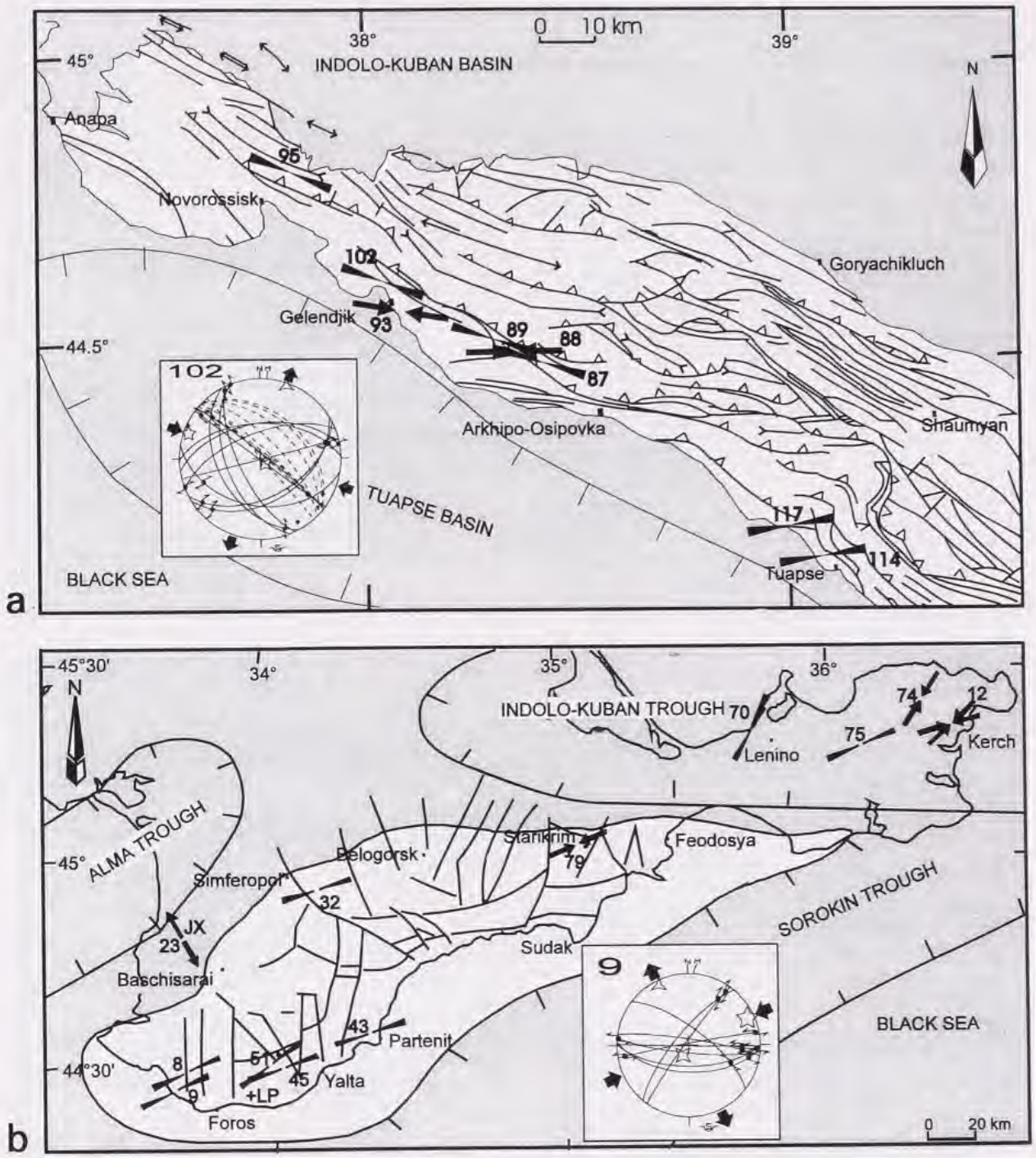

FIG. 5.— Sarmatian (middle-late Miocene) stress field; a, in NW-Caucasus; b, in Crimea;
FIG. 5.— Champ de contraintes sarmatien (Miocène moyen-supérieur) ; a, dans le Caucase nord occidental ; b, en Crimée ; mêmes symboles que pour les figures 3b-c.

Source : MNHN, Paris

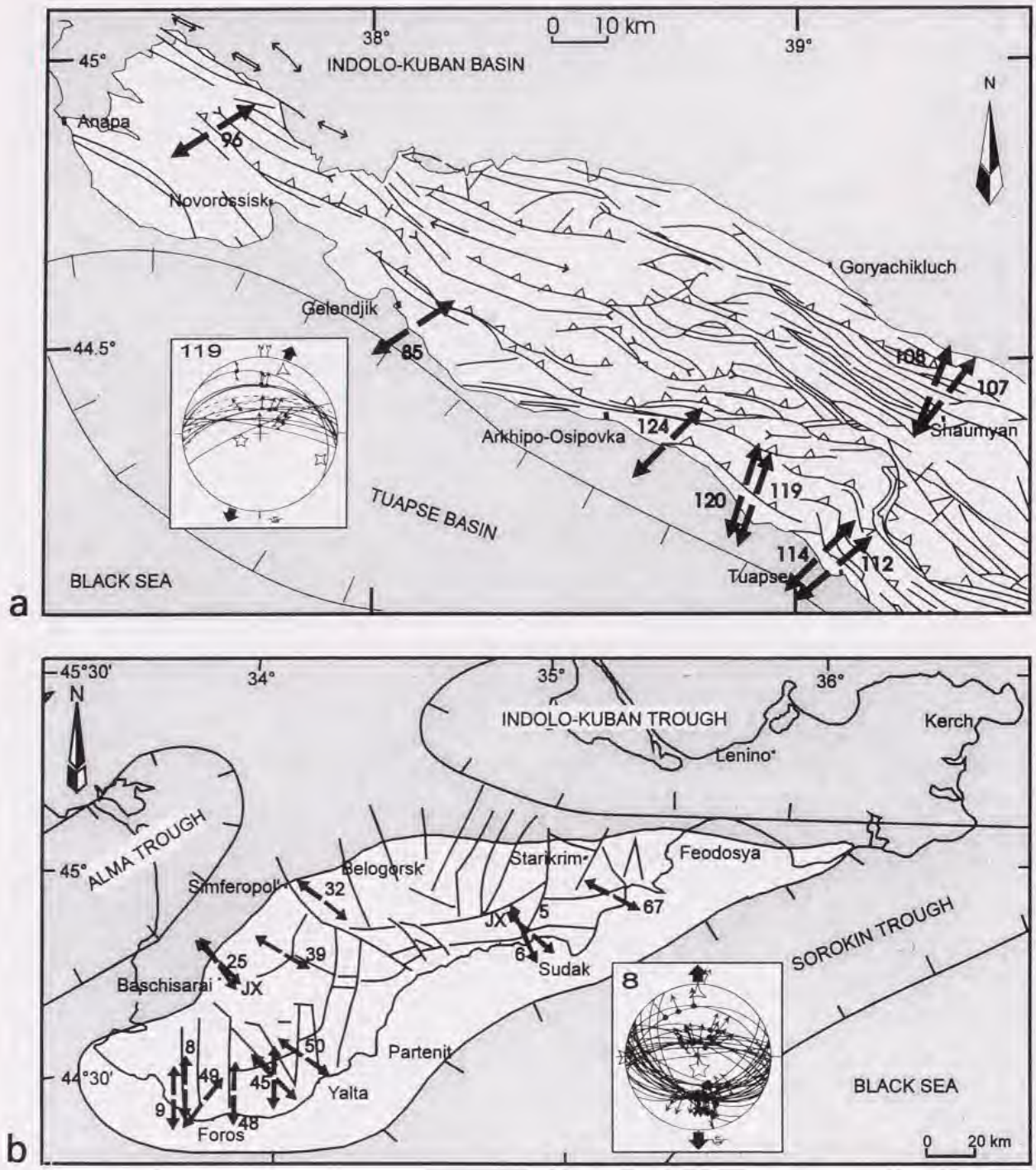

FIG. 6.— Oligocene-early Miocene stress field; a, in NW-Caucasus; b, in Crimea; symbols as for figures 3b-c.
FIG. 6.— Champ de contraintes de l'Oligocène- Miocène inférieur ; a, dans le Caucase nord occidental ; b, en Crimée ; mêmes symboles que pour les figures 3b-c.

Source : MNHN, Paris

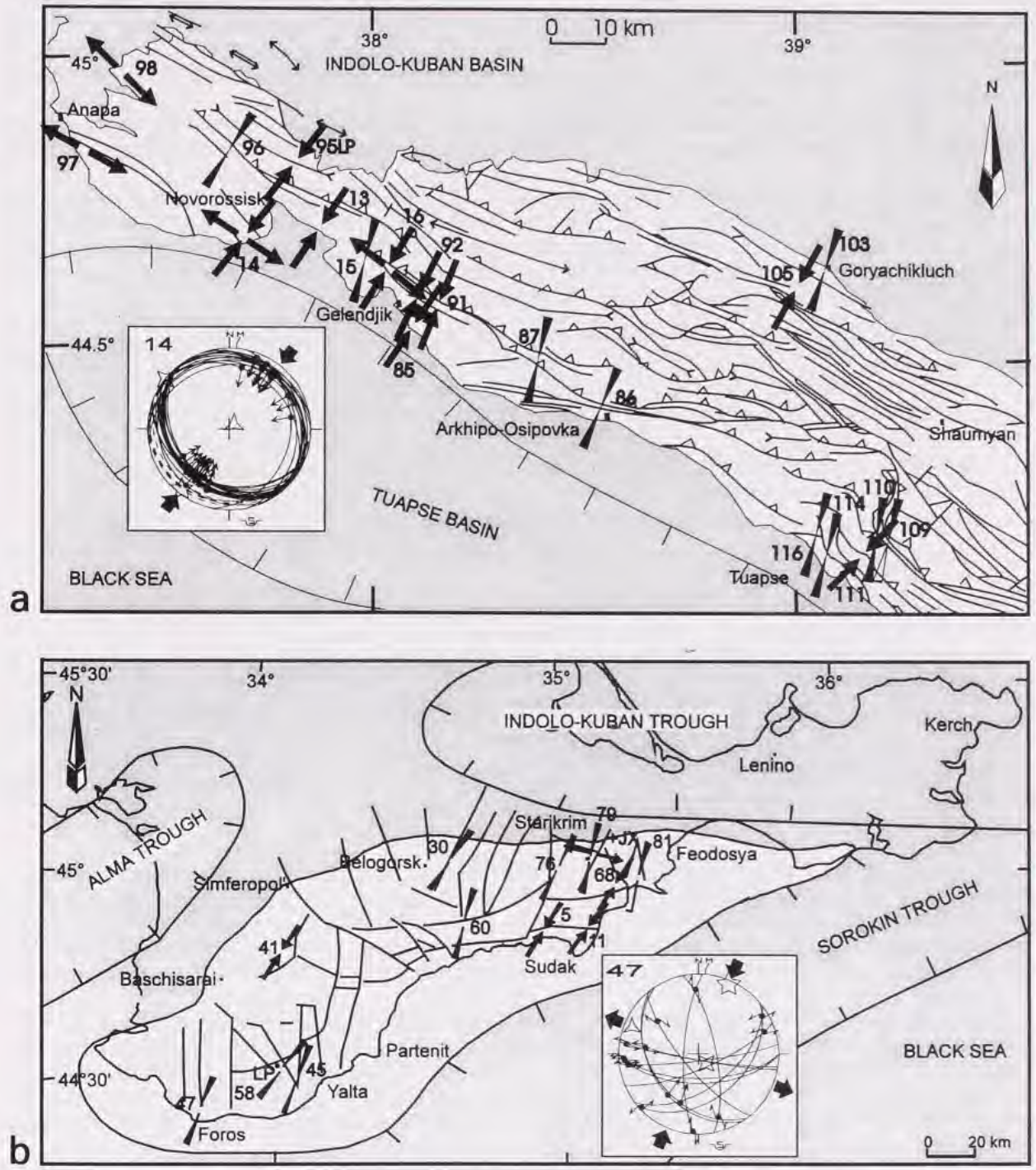

FIG. 7.— Late Eocene stress field; a, in NW-Caucasus; b, in Crimea; symbols as for figures 3b-c.
FIG. 7.— Champ de contraintes de l'Eocène terminal ; a, dans le Caucase nord occidental ; b, en Crimée ; mêmes symboles que pour les figures 3b-c.

Source : MNHN, Paris

northwestern flank of the Crimean belt (sites 25, 32, 39), with sets of normal faults and tension gashes. The $\sigma 3$ trajectories determined along the south coast of the Crimea follows the curve of the Sorokin trough from N-S near Foros to NW-SE from Yalta to Sudak (Fig. 6b). The subsidence of the southern flank of the Crimean mountain, along large step-like normal faults (illustrated in figure 10), is contemporaneous with this tectonic framework.

The origin of the development of the peripheric trough may lie in an important flexuring process affecting the lithosphere (NIKISHIN *et al.*, this volume) after the late Eocene compressional event described below.

We found some traces of an E-W extensional event (not illustrated) relative to the formation of the N-S Kerch-Taman trough (SAINTOT *et al.*, 1995) but this trough is a branch between the Indolo-Kuban trough to the North and the Sorokin trough to the South of Crimea (Fig. 1a). The existence of a N-S oriented weak lithospheric zone is inferred, and might have permitted propagation of the Sorokin trough to the North and the propagation of the Indolo-Kuban trough to the South.

THE NE-SW COMPRESSIONAL STRESS FIELD (Fig. 7a, 7b).— In NW-Caucasus, the NE-SW compression (ANGELIER *et al.*, 1994) is very well marked in the series of flysch from Cretaceous to Paleocene (sites of Paleocene formations: 14, 103). The characteristics of this compressional event (Fig. 7a) are in agreement with the general direction of thrusting and folding (SAINTOT *et al.*, 1995). This event occurred:

— before folding in sites 13, 14, 105, 111, with development of reverse faults sets, and in sites 15, 96, 114, 116 with strike-slip faults;

— syn-folding, with associated bedding slips (site 92);

— after folding in sites 16, 91 with reverse fault system, and in sites 14, 86, 87, 103, 109, 110 with associated conjugate strike-slip faults.

Near Gelendjik (sites 95) and near Tuapse (sites 111), this event resulted in the development of stylolites and associated stylolitic pressure solution seams before tilting.

The northwestern tip of the NW-Caucasian belt was affected, during this tectonic event, by an extensional regime with $\sigma 3$ trajectories trending NW-SE (sites 14, 16, 97, 98). This local area may have been affected by a release of the confining pressure within the frame of a general compressional regime.

The tectonic activity related to this major compressional event in NW-Caucasus affected Crimea with a strike-slip regime (sites 30, 45, 47, 58, 60, 76, 79, 81). However, a permutation of $\sigma 3$ and $\sigma 2$ axes occurred in site 79, which produced a local extensional regime perpendicular in trend to the average compression. Reverse faults (sites 5, 11, 41, 68), tension gashes (site 79) and stylolites (site 58) locally developed (Fig. 7b).

THE EXTENSIONAL-STRIKE-SLIP STRESS FIELD IN NW-CAUCASUS AND THE COMPRES-SIONAL-STRIKE-SLIP STRESS FIELD IN CRIMEA (Fig. 8a, 8b, 8c).— An early NE-SW extensional-strike-slip event affected flysch formation in NW-Caucasus at least up to the Early Paleocene epoch (formations of site 14 affected); this event occurred before the late Eocene folding phase. Strike-slip faults developed in this tectonic setting (sites 14, 99, 114, 116), with a permutation of $\sigma 1$ and $\sigma 2$ stress axes occurring in site 116 (Fig. 8a).

From the Cretaceous to the Paleocene time, a deep trough with flysch deposits developed in the NW-Caucasus, along NW-SE trends (which were folded in late Eocene compressional event), nearly parallel to the east Black Sea basin (NIKISHIN *et al.*, this volume). The extension was probably related to a transtensional overall mechanism. The whole region was affected by an important strike-slip extensional regime, and the interpretation of this event suggests that the opening of the east Black Sea basin occurred until the early Paleocene.

A nearly E-W extensional regime is clearly defined in sites 109, 110, 115 and it is associated to a strike-slip regime in sites 124, 113, 110, 109 (Fig. 8b). This event occurred before the folding event of

FIG. 8.— Paleocene stress field; a, b in NW-Caucasus; c, in Crimea; symbols as for figures 3b-c.

FIG. 8.— Champ de contraintes paléocène ; a, b dans le Caucase nord occidental ; c, en Crimée ; mêmes symboles que pour les figures 3b-c.

Source : MNHN, Paris

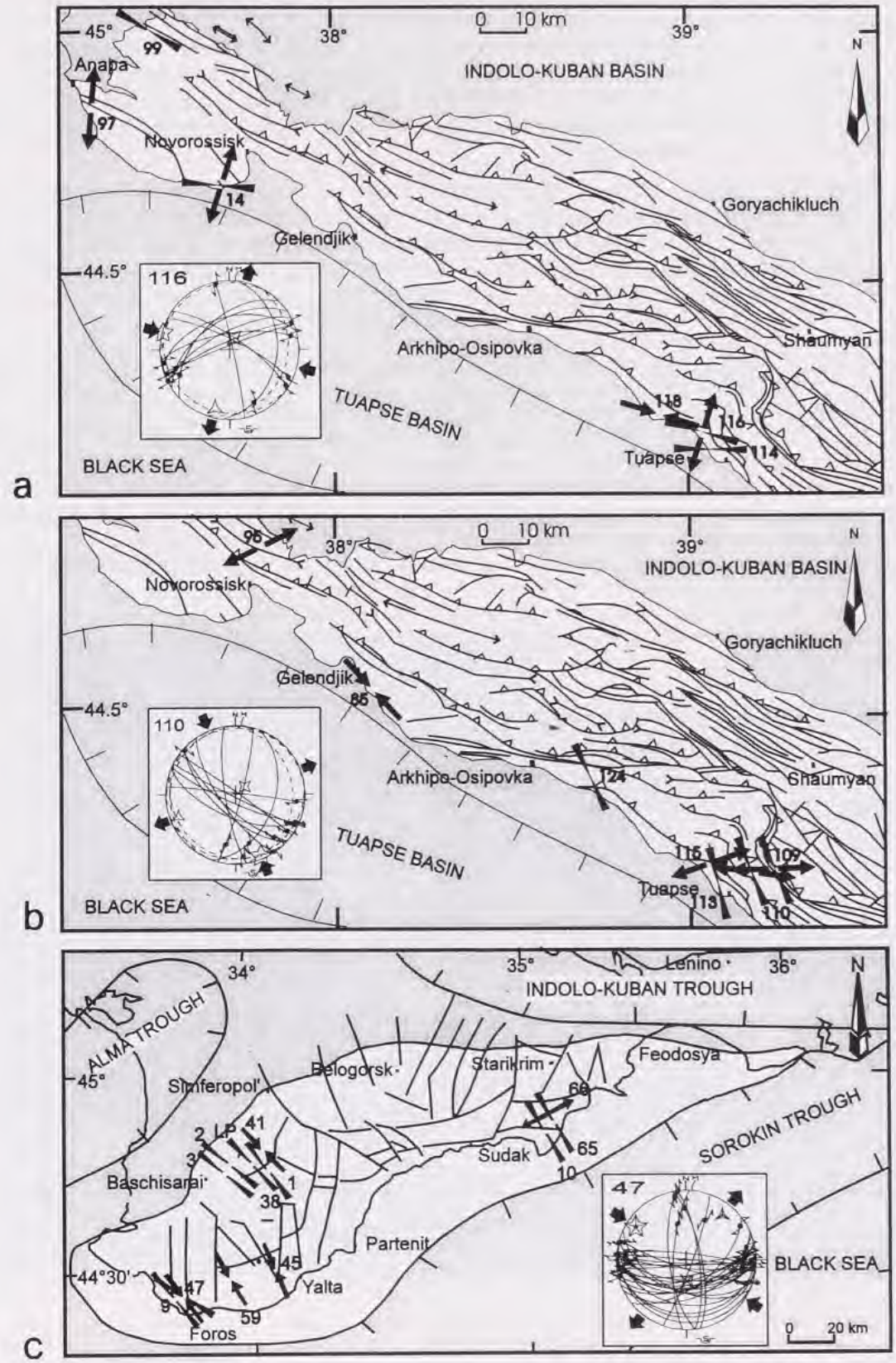

Source : MNHN, Paris

late Eocene and it affected NW-Caucasian Paleocene flysch, so that it is difficult to distinguish this event from the NE-SW extensional strike-slip discussed before (Fig. 8a).

Simultaneously, Crimea was affected by a compressional strike-slip regime with σ_1 trending NW-SE (Fig. 8c). In this event, reverse faults (sites 41, 45, 47, 59) and strike-slip faults (sites 1, 2, 3, 9, 10, 15, 38, 47) developed. Normal faults were only identified in site 66. Note the homoaxiality of stress in Crimea and NW-Caucasus, and the change in strike-slip regime which was transpressional in Crimea and transtensional in NW-Caucasus.

THE OLDEST N-S COMPRESSIONAL STRESS FIELD (Fig. 9).— In Crimea, the massive jurassic limestones formed the high plateaus (Karabi Yayla, Chatyr Dag plateaus and others, Fig. 2) and are strongly fractured along N-S directions. The N-S compressional event is recorded in these formations by reverse conjugate fault systems (sites 1, 5, 40, 41). The compressional N-S event was associated with the development of thrust sheet structures in Crimea. A strike-slip regime is associated to this event (observed in sites 1, 32, 41, 53, 63, 64, 76) with development of stylolites in site 76.

Near Bachisarai (sites 1, 41), in the northern-western flank of the Crimean chain, dykes of dioritic rocks crop out, they are elongated in E-W direction, and shows a dip of 70° to the north. They formed in Middle Jurassic time within the Tauric series (volcano-terrigenous flysch of the Late Triassic-Aalenian) during an earlier N-S extensional event that we could not identify. We assume that these dykes developed along vertical planes, indicating that they were later tilted during the N-S compressional event (which produced strike-slip faults before tilting and reverse faults after tilting, with again a permutation between σ_2 and σ_3 principal stress axes).

Concerning the age of the N-S compressional event, the affected limestones are Middle and Late Jurassic in age. It is possible to assume that this event is related to the development of north-vergent thrust sheet structures, in Crimea which occured after Early Cretaceous time, according to POPADYUK *et al.* (1991) and GALKIN *et al.* (1994). Moreover, the Late Cretaceous limestones and clays seals the thrust-front in the northern flank of Crimea (POPADYUK *et al.*, 1991). This tectonic event occured in the limit between Early Cretaceous and Late Cretaceous. To confirm this point of view, it is necessary to collect more fault slip data sets in Cretaceous formations in Crimea.

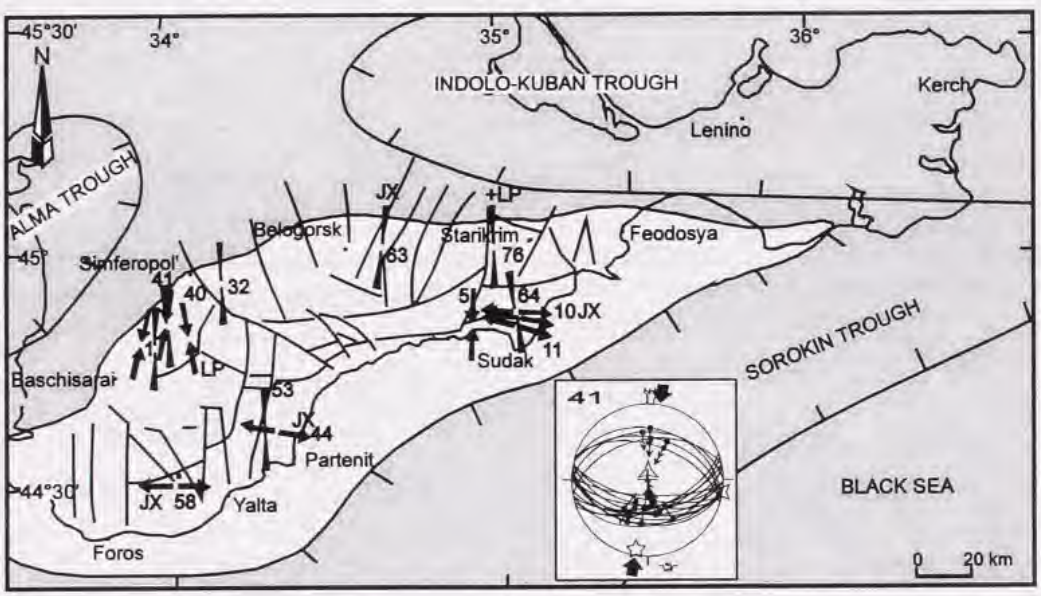

FIG. 9.— Early Cretaceous/Late Cretaceous stress field in Crimea; symbols as for figures 3b-c.

FIG. 9.— Champ de contraintes Crétacé inférieur/ Crétacé supérieur en Crimée ; mêmes symboles que pour les figures 3b-c.

Source : MNHN, Paris

DISCUSSION AND CONCLUSION

RELATIONS TO MAJOR EVENTS

Summarizing, we reconstructed several paleostress fields related to major steps in the evolution of the Crimea and the NW-Caucasus region. We present them below, in the stratigraphic order (Fig. 11):

— The N-S compressional event induced strike-slip faulting and north-vergent major thrusting, resulting in structuration of Crimea in the Early Cretaceous/Late Cretaceous time (Fig. 9). No paleostress state could be determined in the NW-Caucasus for this event.

— In the Paleocene time, a transtensional regime was active in NW-Caucasus region, with σ_3 trending nearly NE-SW. This regime was probably related to the rifting of the east Black Sea basin, which is Late Cretaceous/Paleocene in age (Fig. 8a, 8b). In the Paleocene time, a transpressional regime was active in Crimea with σ_1 trending NW-SE. This regime reactivated N-S directed fracturing in a strike-slip regime in Crimea (Fig. 8c).

— The late Eocene NE-SW compressional event resulted in major structural development of the NW-Caucasus (Fig. 7a), with folding of the flysch mass and south-vergent thrusting of numerous units. A transpressional regime with σ_1 trending NE-SW occurred in Crimea, and this margin underwent and overall in sinistral strike-slip regime (Fig. 7b).

FIG. 10.— Photography illustrating the Oligocene-early Miocene event with a normal step-like fault near Foros (site 8) in the southern coast of Crimea.

FIG. 10.— Faille normale au miroir décamétrique près de Foros (site 8) sur la côte Sud de la Crimée illustrant l'événement oligocène-miocène inférieur.

Source : MNHN, Paris

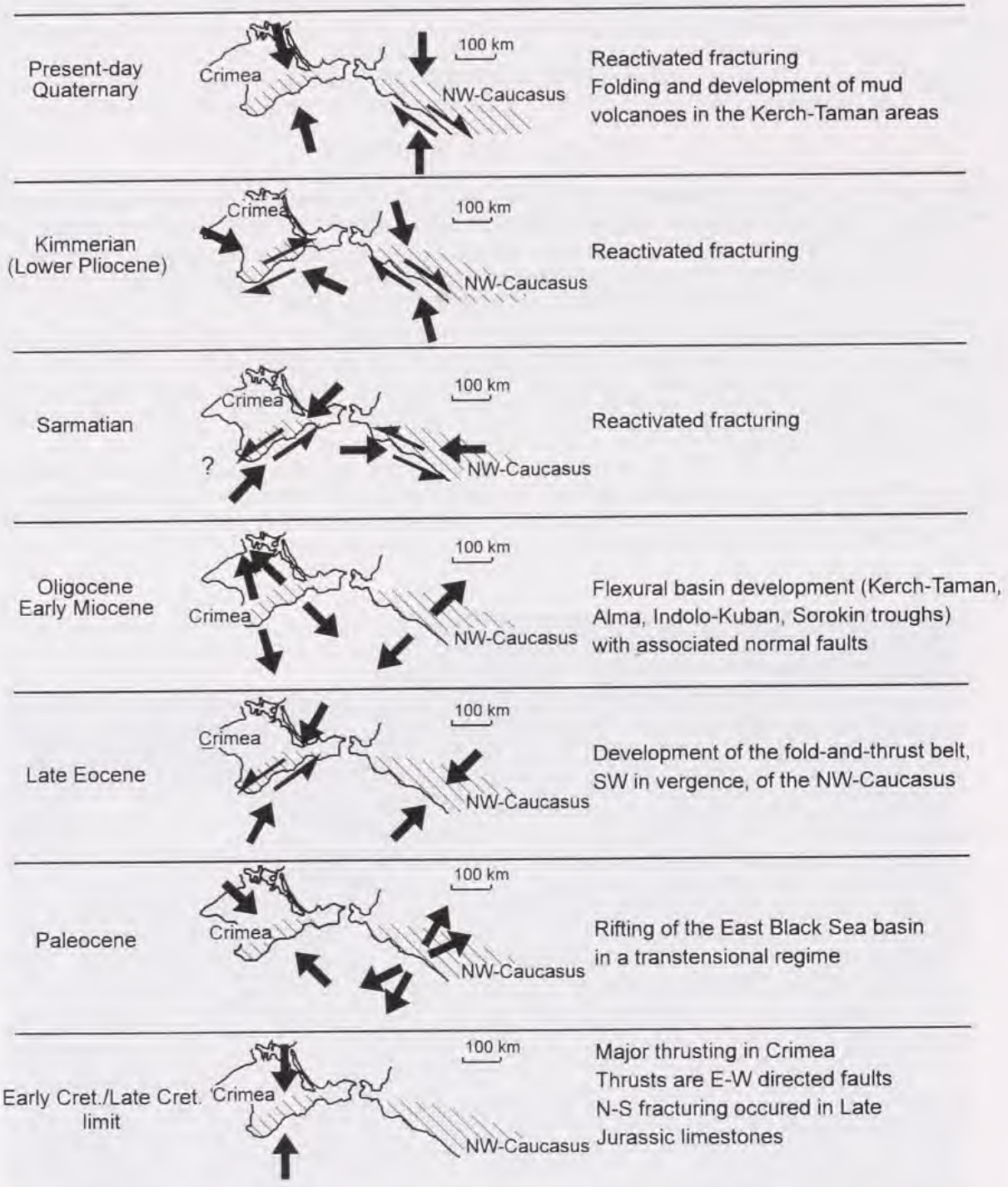

FIG. 11.— Tectonic evolution of the NW-Caucasus and Crimea in the light of successive reconstructed paleostress fields. Directions of compression, extension and lateral shear shown as couples of arrows. For details, see figures 3, 4, 5, 6, 7, 8, 9.

FIG. 11.— Évolution tectonique du Caucase nord occidental et de la Crimée déduite de la succession des champs de contraintes. Directions de compression, d'extension schématisées par des couples de flèches. Pour plus de détails, voir les figures 3, 4, 5, 6, 7, 8, 9.

Source : MNHN, Paris

— A multidirectional extensional event related to the development of peripheric basins of the belt occurred in the Oligocene-early Miocene times. The trend of $\sigma 3$ trajectories was perpendicular to the axes of maximum subsidence in the nearest troughs (Fig. 6a, 6b).

— A nearly E-W strike-slip regime, not very well constrained, seems to have been active in the Sarmatian time (Fig. 5a, 5b). The NW-Caucasian margin underwent sinistral strike-slip movement; the sinistral movement of the Crimean margin was unclear. A deviation in the trend of $\sigma 1$ trajectory occurred, from E-W in the NW-Caucasus to ENE-WSW in the Crimea.

— The Kimmerian event is well defined and from Crimea to NW-Caucasus the margin was in a general dextral strike-slip regime. The dextral transpressional reactivation of the belt probably uplifted Crimea as a 'push-up' structure between the West Crimean Fault (Fig. 1a) and the NW-Caucasian margin (SAINTOT *et al.*, 1995). We note that a deviation of the trend of $\sigma 1$ trajectories from NW-SE in NW-Caucasus to WNW-ESE in Crimea (Fig. 4a, 4b).

— The Quaternary-Present Day stress field determined by inversion of seismic focal mechanisms and recent fault slip data is characterized by a NW-SE tranpressional regime in Crimea, whereas a N-S compressional regime prevailed in the NW-Caucasus (Fig. 3a, 3b, 3c). As for the previous Sarmatian and Kimmerian events, we observed a counter-clockwise deviation in the trend of $\sigma 1$ trajectories, from the NW-Caucasus to the Crimea. This phenomenon is probably due to the presence of a N-S trending zone of lithospheric weakness which separated the Crimea and the NW-Caucasus, as indicated by the development of the N-S Kerch-Taman trough in Oligocene-early Miocene time.

The latest tectonic events (Sarmatian, Kimmerian and Quaternary-Present day) were marked by unconformities both on flank of Crimean belt and NW-Caucasian mountains.

An important feature of the whole area studied is the large number of strike-slip faulting occurrences. We infer that during the Alpine tectogenesis, the southern boundary of the southern part of the east European Platform mainly underwent alternating transpressive and transtensive regimes.

AKNOWLEDGEMENTS

We thank Russian participants in the first field trip, and Ms Carla MULLER for the systematic dating of rock samples. This work was supported by the Peri-Tethys program and thesis grants were supported by the French Embassy in Moscow (A. ILYIN) and the French M.R.E. (A. SAINTOT).

REFERENCES

AL'BOV, S.V., 1974.— Geochemical environment in the Kerch-Taman region and nearby areas. *Doklady Akademii Nauk SSSR, Earth Sciences Section*, **208**: 222-224.

ANGELIER, J., 1975.— Sur l'analyse de mesures recueillies dans des sites faillés: l'utilité d'une confrontation entre les méthodes dynamiques et cinématiques. *Comptes Rendus de l'Académie des Sciences, Paris*, **281** (D): 1805-1808, (Erratum: 1976.— *Ibid.*, **283** (D): 466).

ANGELIER, J., 1984.— Tectonic analysis of fault slip data sets. *Journal of Geophysical Research*, **89** (B7): 5835-5848.

ANGELIER, J., 1991.— Inversion directe et recherche 4-D: comparaison physique et mathématique de deux modes de détermination des paléocontraintes en tectonique des failles. *Comptes Rendus de l'Académie des Sciences, Paris*, **312** (II): 1213-1218.

ANGELIER, J., GOUSTCHENKO, O.I., SAINTOT, A., ILYIN, A., REBETSKY, Y., VASSILIEV, N., YAKOVLEV, F. & MALUTIN, S., 1994.— Relations entre champs de contraintes et déformations le long d'une chaîne compressive-décrochante: Crimée et Caucase (Russie et Ukraine). *Comptes Rendus de l'Académie des Sciences, Paris*, **319** (II): 341-348.

ANONYMOUS, 198?.— *Geological map of the great Caucasus. 1/500 000.*

ANONYMOUS, 198?.— *Geological map of the Crimea and Caucasus. 1/1 500 000.*

CHEKUNOV, A.V., 1990.— Problems of the Black Sea depression. *Geophysical Journal*, **9** (4): 471-507.

GALKIN, V.A., FËDOROV, Ye.V. & BAKHOR, K., 1994.— The interrelationships and structure of the Upper Jurassic and Lower Cretaceous deposits in the Salgir River Valley. *Transactions (Doklady) of the Russian Academy of Sciences, Earth Science Sections*, **326** (7): 55-60.

GOUSTCHENKO, O.I., MIKHAILOVA, A.V., MOSTRJUKOV, A.O. & PETROV, V.A., 1993a.— The regional stress-monitoring and the mechanism of deforming Caucasus-Iranic seismoactive zone. *Terra Abstract, supplement n°1 to Terra Nova*, **5**: 218.

Source : MNHN, Paris

GOUSTCHENKO, O.I., REBETSKY, Y.L., MIKHAILOVA, A.V., GOUSTCHENKO, N.Y., KUOK, L.M.& RASSANOVA, G.V., 1993b.— The recent regional field of stresses and the mechanism of the lithosphere deformation of seismoactive East-Asia region. *Terra abstract, supplement n°1 to Terra Nova*, **5**: 259.

ISMAGILOV, D.F. & SHLEZINGER, A.Ye., 1986.— Sedimentary cover of the bottom of the Caucasus section of the Black Sea. *Oceanology*, **26** (4): 486-491.

KAZANTSEV, Yu.V. & BEKHER, N.I., 1988.— Allochtonous structures of the Kerch Peninsula. *Geotectonics*, **22** (4): 346-355.

KOGAN, L.I., MALOVTSKIY, Ya. P., MOSKALENKO, V.N. & SHIMKUS, K.M., 1978.— New data on structure of the sedimentary layer of the Black Sea floor south of Crimea. *Doklady Akademii Nauk SSSR*, **233**: 88-90.

LETOUZEY, J., 1977.— Synthèse des données géophysiques et géologiques de la Mer Noire. *Publication de l'Institut français du Pétrole, Géologie*, **n°21773**.

MEYSNER, L.B. & TUGOLESOV, D.A., 1981.— Late Cenozoic troughs on the Northeastern Black Sea. *Geotectonics*, **15** (6): 538-545.

MURATOV, M.V., ARKHIPOV, I.V & USPENSKAYA, Y.A., 1984.— Structural evolution of the Crimea Mountains and comparison with the Western Caucasus and the Eastern Balkan Ranges. *International Geological Review*, **26** (11): 1259-1266.

NIKISHIN, A.M., CLOETINGH, S., BARABOSHKIN, E.Yu., BOLOTOV, S.N., KOPAEVICH, L.F., NAZAREVICH, B.P., PANOV, D.I., BRUNET, M.F., ERSHOV, A.V., KOSOVA, S.S., IL'INA, V.V. & STEPHENSON, R.A., 1998.— Scythian platform: chronostratigraphy and stages of tectonic history. *In*: S. CRASQUIN-SOLEAU & É. BARRIER (eds), Peri-Tethys Memoir 3: stratigraphy and evolution of Peri-Tethyan platforms. *Mémoires du Muséum national d'Histoire naturelle*, **177**: 00-000.

NIKISHIN, A.M., CLOETINGH, S., BRUNET, M.F., BOLOTOV, S.N. & ERSHOV, A.V., 1998.— Scythian platform, Caucasus and Black Sea region: Mesozoic-Cenozoic tectonic history and dynamics. *In*: S. CRASQUIN-SOLEAU & É. BARRIER (eds), Peri-Tethys Memoir 3: stratigraphy and evolution of Peri-Tethyan platforms. *Mémoires du Muséum national d'Histoire naturelle*, **177**: 00-000.

OKAY, A.I., SENGÖR, A.M.C. & GÖRÜK, N., 1994.— Kinematic history of the opening of the Black Sea and its effect on the surrounding regions. *Geology*, **22**: 267-270.

POPADYUK, I.V. & SMIRNOV, S.Y., 1991.— The problem of the structure of the Crimean Mountain region: traditional ideas and reality. *Geotectonics*, **25** (6): 489-497.

POPOVICH, S.V., 1989.— Structural characteristics of the mezosoic-cenozoic deposits of the northwestern shelf of the Black Sea. *Geotectonics*, **23** (6): 530-537.

ROBINSON, A.G., RUDAT, J.H., BANKS, C.J. & WILES, R.L.F., 1996.— Petroleum geology of the Black Sea. *Marine and Petroleum Geology*, **13** (2): 195-223.

SAINTOT, A., ANGELIER, J., GOUSTCHENKO, O., ILYIN, A., REBETSKY, Y., VASSILIEV, N., YAKOVLEV, F. & MALUTIN, S., 1995.— Paleostress reconstruction and major structures in Crimea and NW-Caucasus. Communication to the EUG VIII, Strasbourg, 9-13 April 1995. *Abstract Supplement n°1 to Terra Nova*, **7**: 269.

SAINTOT, A., ANGELIER J. & ILYIN, A., 1996.— *Champs de contraintes en Crimée et dans le Caucase nord-occidentale: 16th Earth Sciences meeting, 10-12 April 1996, Orléans.* Société géologique de France, Paris, Abstract in special volume.

TEREKHOV, A.A. & SHIMKUS K.M., 1989.— Young sediments and young overthrust structures in the Peri-Crimean and Peri-Caucasus zones of the Black Sea Basin. *Geotectonics*, **23** (1): 54-59.

TUGOLESOV, D.A., GORSHKOV, A.S., MEYSNER, L.B., SOLOV'YEV, V.V. & KHAKHALEV, Ye.M., 1985.— The tectonics of the Black Sea trough. *Geotectonics*, **19** (6): 435-445.

ZONENSHAIN, L.P. & LE PICHON, X., 1986.— Deep basins of the Black Sea and Caspian Sea as remnants of Mesozoic back-arc basins. *Tectonophysics*, **123**: 181-211.

Source : MNHN, Paris

Neogene evolution of the Carpathian foothills: insights from the romanian diapir fold area

Jean-Claude HIPPOLYTE [1] *& Mircea SANDULESCU* [2]

[1] Laboratoire de Tectonique Quantitative, CNRS URA 1759, T26-E1, Case 129
Université P. et M. Curie, 75252 Paris Cedex 05, France

[2] Institut Géologique de Roumanie, Str. Caransebes 1, Sector 1, 78344 Bucarest, Roumanie

ABSTRACT

In the diapir fold area of Romania, the frontal part of the Carpathian foothills is characterized by folds and minor thrusts formed during the Pliocene-Quaternary 'Wallachian phase'. Most Wallachian folds and thrusts are not located at the outermost front of the Carpathians, but are more internal structures. Consequently, the location of the deformation during the 'Wallachian phase' contrasts with the Cretaceous-middle Miocene piggy-back thrust sequence of the East Carpathians. This difference results from a modification in the stress field, with a direction of compression changing during late Miocene from NW-SE to NS. Structural observations and the stratigraphic dating of the paleostress change indicate that the Wallachian tectonics was not a brief event but lasted from middle Tortonian to early Pleistocene, with major deformations at the end of this period. The building of the inner margin of the foredeep was contemporaneous with the strong subsidence of this basin and with the filling of few piggyback syn-tectonic basins.

RÉSUMÉ

Evolution néogène du contrefort des Carpates : aperçu de la zone des plis diapirs de Roumanie.

Dans la zone des plis diapirs de Roumanie, la partie frontale du contrefort des Carpates est caractérisée par la présence de structures compressives, formées durant la phase Wallache d'âge Plio-Quaternaire. La plupart de ces structures ne sont pas localisées sur le front externe des chevauchements miocènes, mais sont situées à l'intérieur des nappes miocènes. La localisation de la déformation pendant la phase Wallache contraste donc avec la séquence d'apparition des chevauchements antérieurs au Crétacé-Miocène moyen des Carpates orientales. Cette différence est liée ici à une modification du champ de contraintes, puisque la direction de compression est passée de NW-SE à N-S durant le Miocène supérieur. La présence de plis synsédimentaires et la datation stratigraphique des états de contraintes successifs montrent que la tectonique Wallache n'est pas un événement bref, mais a durée du Tortonien moyen au Pléistocène inférieur, avec une déformation majeure à la fin de cette période. La construction de la marge interne de l'avant-fosse actuelle fut contemporaine de la forte subsidence de ce bassin et du remplissage de quelques bassins syn-compressifs de type "piggyback".

INTRODUCTION

The Carpathian fold and thrust belt results from the closure of the Tethyan oceanic basin and its continental margins. The 'Main Tethyan Suture' runs across the Carpathian area (Fig. 1). It separates

HIPPOLYTE, J.-C. & SANDULESCU, M., 1998.— Neogene evolution of the Carpathian foothills: insights from the romanian diapir fold area. *In*: S. CRASQUIN-SOLEAU & É. BARRIER (eds), Peri-Tethys Memoir 3: stratigraphy and evolution of Peri-Tethyan platforms. *Mém. Mus. natn. Hist. nat.*, **177** : 113-127. Paris ISBN : 2-85653-512-7.

Source : MNHN, Paris

Fore-Apulian tectonic units (Inner Dacides) to the west from European units (Median, Outer and Marginal Dacides plus Moldavides) to the east and southeast. The Dacides show Cretaceous tectogenesis, while the Moldavides show Miocene tectonism (SANDULESCU, 1980; 1989). Since the age of the formations of the thrust units and the age of their thrusting decrease from the internal to the external areas (DUMITRESCU & SANDULESCU, 1970) there is a typical piggy-back sequence of thrusting in this fold and thrust belt.

Each period of tectogenesis (Cretaceous and Miocene) was followed by flexural subsidence of the foreland (ELLOUZ & ROCA, 1993). In front of the Cretaceous thrust belt, a migrating foredeep basin was filled with Cretaceous to Miocene flyschs. These flysch sediments now constitute the moldavian nappes emplaced during Miocene (SANDULESCU, 1980; 1989). The present foredeep basin which follows the curvature of Carpathians (Fig. 1) is partly filled by middle Miocene sediments and by the outermost Carpathian nappe. In the southern areas it also includes a thick late Miocene to Early Quaternary sedimentary sequence, and it ranges 9000 metres depth in the Focsani Depression (DUMITRESCU & SANDULESCU, 1970) (Fig. 1).

The outer part of this foredeep basin lies above the foreland Mesozoic carbonate platforms (Fig. 1) and is largely covered by Late Quaternary eolian and fluviatile deposits. Its inner part is complex

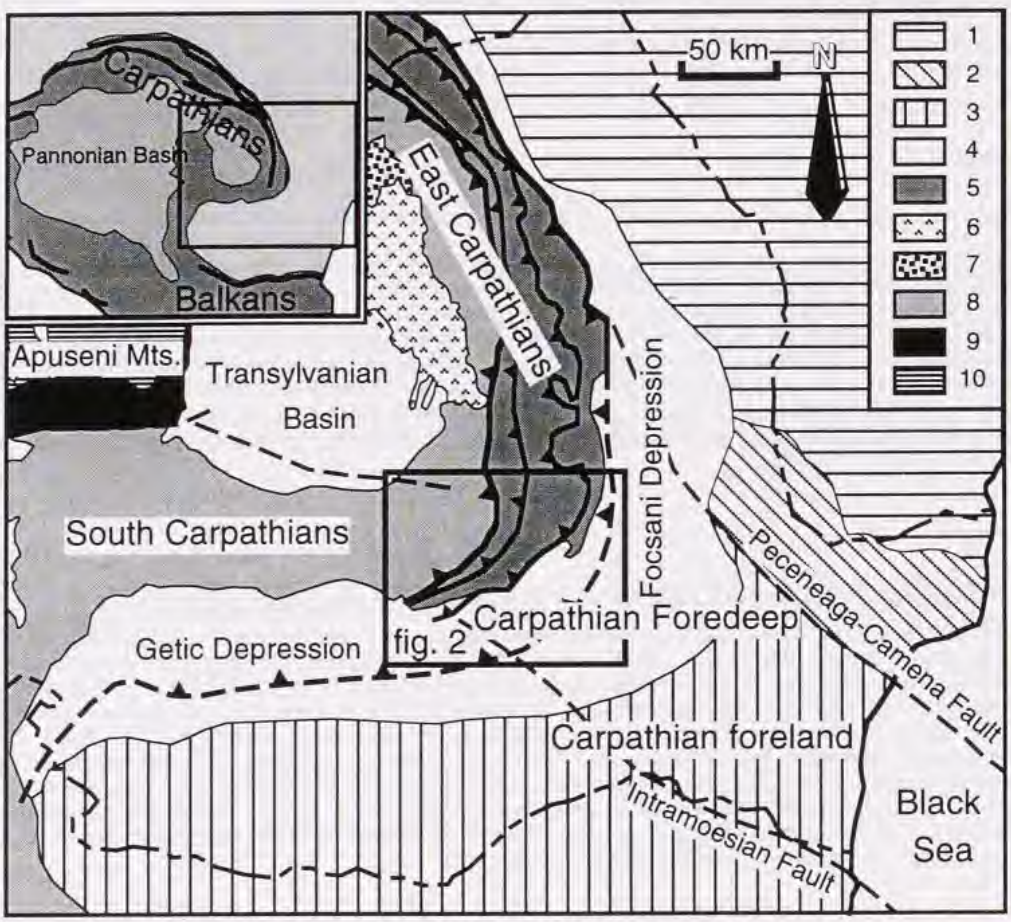

FIG. 1.— Geological sketch of Romania, with location of the area of interest. **1**, East European and Scythian platforms; **2**, North Dobrogea Cimmerian orogen; **3**, Moesian platform; **4**, middle Miocene-Quaternary depressions; **5**, Moldavides; **6**, Neogene volcanic arc; **7**, Eocene-early Miocene post-tectonic cover; **8**, Median, Outer and Marginal Dacides (European units); **9**, Transylvanides and Pienides (Tethyan Suture); **10**, Inner Dacides (Fore-Apulian units).

*FIG. 1.— Schéma géologique de la Roumanie avec situation de la zone d'étude. **1**, Plate-forme est européenne et plate-forme scythique ; **2**, Orogène cimmérien de la Dobrogea septentrionale ; **3**, Plate-forme Moesienne ; **4**, Bassins du Miocène moyen-Quaternaire ; **5**, Moldavides ; **6**, Arc volcanique néogène ; **7**, Couverture post-tectonique éocène-miocène inférieur ; **8**, Dacides médianes, externes et marginales (unités européennes) ; **9**, Transylvanides et Pienides (suture téthysienne) ; **10**, Dacides internes (unités pré-Apuliennes).*

Source : MNHN, Paris

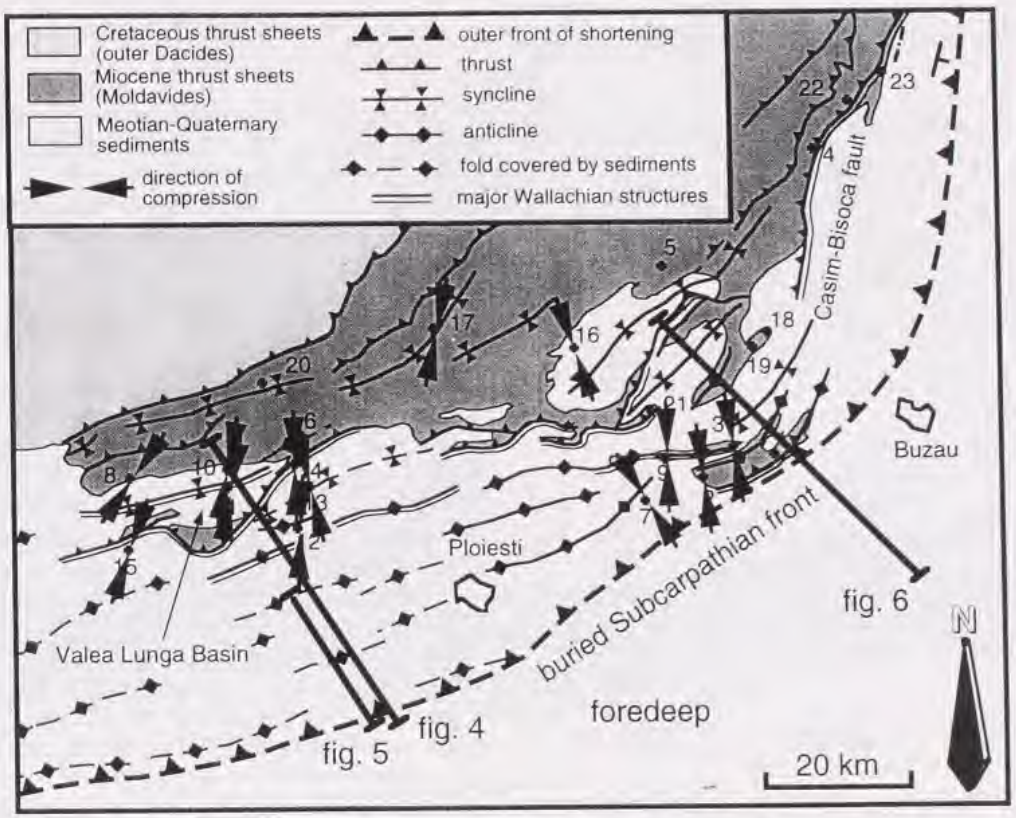

FIG. 2.— Directions of compression of Wallachian age (Meotian-early Pleistocene). Structural sketch from DUMITRESCU & SANDULESCU (1970). The compression directions are dated of this period because they are computed with faults measured in the Meotian-early Pleistocene sequence (sites 7, 10, 11, 12, 13, 14, 15, 16), or correlated using relative chronologies (sites 8, 9 and 17), or correlated to an adjacent site with same trend of compression (sites 2 and 3).

FIG. 2.— Directions de compression d'âge Valaque (Méotien-Pléistocène inférieur). Schéma structural d'après DUMITRESCU & SANDULESCU (1970). Les directions de compression sont datées de cette période car elles ont été calculées à partir de plans striés mesurés dans les dépôts du Méotien-Pléistocène inférieur (sites 7, 10, 11, 12, 13, 14, 15, 16), ou parce qu'elles sont corrélées grâce à des observations de chronologies relatives (sites 8, 9, 17), ou bien parce qu'elles sont corrélées à des sites voisins mieux datés et qui présentent la même direction de compression (sites 2 et 3).

because in places it is partly underthrust beneath the Carpathian thrust front (Fig. 1), whereas in other places it partially rests above the compressional structures of the outer Carpathians (Figs 1, 2). In northern Romania for instance, the Sarmatian deposits (Serravallian-early Tortonian of the eastern Paratethys chronostratigraphy, figure 3, STEININGER *et al.*, 1988) of the foredeep margin are largely overthrust by the frontal nappe of the Carpathians (Fig. 1). In the south, along the inner foredeep margin, the late Sarmatian to Quaternary sediments of the foredeep sequence dip to the east, with sub-vertical bedding planes close to the outcropping thrust units (Fig. 2). Still farther south, in the Carpathian bend area of Romania, the late Sarmatian to Pleistocene foredeep sediments rest unconformably above the outer Carpathian nappes (Figs 1, 2, 4). There, folds and minor faults of Wallachian age (early Pleistocene, DUMITRESCU & SANDULESCU, 1968) characterize the diapir fold area (Figs 2, 4). Westward (Getic Depression, Fig. 1), the foredeep of the South Carpathians has also largely covered the Miocene nappes, but no Wallachian fold is described there, the Pliocene-early Pleistocene sediments of the foredeep gently dipping to the south.

To determine the way this complex margin was created, we made structural analyses supported by fault-slip measurements primarily in the east Carpathians bend area (Fig. 2), where the Wallachian phase was first defined (STILLE, 1924). Using the stress inversion technique (ANGELIER, 1989), we will tentatively relate the observed structures to their causative tectonic forces.

Source : MNHN, Paris

Myr	Eastern Paratethys	Mediterranean
	Pleistocene	Pleistocene
	Romanian	Pliocene
	Dacian	
5.6	Pontian	Messinian
8.5	Meotian	Tortonian
	Sarmatian	Serravallian
13.6	Badenian	Langhian
16.5		

FIG. 3.— Correspondence between Eastern Paratethys and Mediterranean ages (from STEININGER *et al.*, 1988).

FIG. 3.— Corrélation entre les âges de la Paratéthys orientale et ceux de la Méditerranée (d'après STEININGER et al., 1988).

STRUCTURES

In the East Carpathians bend area (Fig. 2), seismic profiles show that the outermost thrust sheet (Subcarpathian Nappe) is thrust above Badenian and in places early Sarmatian deposits (Figs 4, 5) (STEFANESCU, 1984; MOCANU & RADULESCU, 1994; DICEA, 1995). Being sealed by late Sarmatian deposits (Fig. 5) (DUMITRESCU & SANDULESCU, 1968), this thrusting ended in Sarmatian. However, a Sarmatian to Quaternary foredeep sequence rests above the outer Carpathian thrust sheets (Fig. 5), and folds and thrusts affecting sediments as young as early Pleistocene exist also in this area (Fig. 4). Therefore we can distinguish the pre-late Sarmatian structures from the more recent ones (Wallachian structures).

We can note in the cross-section of figure 4 that the amplitude of the Wallachian folds increases from the outer to the inner foredeep, where thrust faults even merge to the surface. It is a general feature in the bend area, the most important Wallachian folds and thrusts constitute the compressive inner margin of the foredeep basin (Fig. 2).

In figure 2, one can note that the Wallachian structures (structures that affect the Meotian to Quaternary sequence) are all located behind the front of the Subcarpathian nappe. Taking into account the age of this frontal thrust (intra-Sarmatian), we conclude that the Wallachian (Pliocene-Quaternary) thrusts are in overstep sequence. In more details, seismic profiles show that in the late Sarmatian to Quaternary deposits, the more internal the faults are, the younger they are (STEFANESCU & DICEA, 1995).

The most important Wallachian thrusts, underlined on figure 2, constitute the compressive inner margin of the foredeep. This margin extends from Valea Lunga to Buzau (Fig. 2) and trends E-W. It is oblique to the front of the Subcarpathian nappe which trends NE-SW in this area (Fig. 2). In the cross-section of figure 4, this margin (area of the Valea Lunga basin) is more than 30 km internal to this front, while in the cross-section of figure 6, this margin is only a few hundred metres internal.

Along the Focsani depression (Fig. 1), as mentioned before, the inner limb of the foredeep basin is tilted to the east (Fig. 2). This regional tilt can result either from of a back shear motion of the late Miocene-Pliocene molasse decoupled at the top of the Subcarpathian nappe (ELLOUZ *et al.*, 1996) (the front of this nappe forming a triangle zone in a cross section view), or from the activity of an out-of-sequence east-vergent thrust fault (the Casim-Bisoca fault) (Fig. 6) (STEFANESCU, 1984; ELLOUZ *et al.*, 1996). In this later solution, we can note that the Casim-Bisoca fault has the same characteristics as the thrust faults of the Valea Lunga-Buzau compressive margin. This faults is effectively in overstep sequence compared with the front of the Subcarpathian nappe unconformably overlain by the late Sarmatian to Pliocene sequence, and it constitutes the inner margin of the foredeep basin (Fig. 2). It constitutes therefore the prolongation to the north of the Valea Lunga-Buzau compressive margin which, north of Buzau, has the same trend as the front of the Subcarpathian nappe.

The obliquity of the Valea Lunga-Buzau compressive margin and the overstep sequence of thrusting are the main characteristics of the foreland basin that we tried to explain.

Source : MNHN, Paris

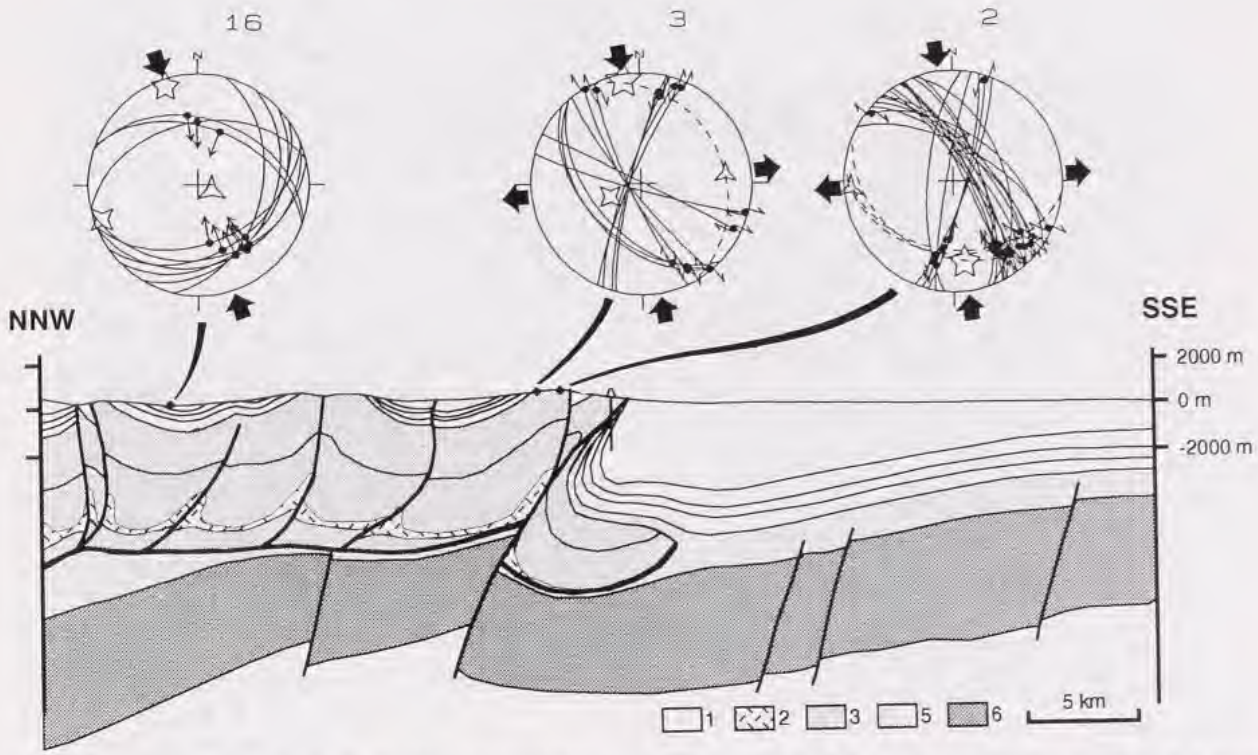

FIG. 4.— Cross-section 1, in the Wallachian fold and thrust area (location in Fig. 2; from STEFANESCU, 1984) with Schmidt diagrams (lower hemisphere) of Wallachian striated fault planes (thin lines), computed stress axes (5-, 4- and 3- branch stars represent σ1, σ2 and σ3 respectively) and bedding planes (broken lines). Site 14 is in the thrust contact between Badenian (Langhian-early Serravallian) and Meotian sediments. **1**, Meotian (middle Tortonian) to Quaternary foredeep sediments; **2**, diapir of early Miocene salt; **3**, Oligocene-Sarmatian (middle-late Miocene); **4**, Cretaceous-Eocene; **5**, autochtonous Miocene; **6**, autochtonous Paleozoic-Paleogene.

*FIG. 4.— Coupe 1, dans la zone des chevauchements et plis Valaques (voir figure 2 pour la localisation ; d'après STEFANESCU, 1984) avec diagrammes (projection Schmidt, hémisphère inférieur) de plans de failles striés d'âge Valaque, axes de contraintes calculés (étoiles à 5, 4 et 3 branches représentant σ1, σ2 et σ3 respectivement) et plans de stratification (tirets). Le site 14 est situé au contact chevauchant entre les sédiments d'âge badénien (Langhien-Serravallian inférieur) et ceux d'âge méotien. **1**, sédiments d'avant-fosse d'âge méotien (Tortonien moyen) à Quaternaire ; **2**, diapir de sel miocène moyen ; **3**, Oligocène-Sarmatien (Miocène moyen-supérieur) ; **4**, Crétacé-Eocène ; **5**, Miocène autochtone ; **6**, Paléozoïque-Paléogène autochtone.*

PALAEOSTRESS ORIENTATIONS

In an attempt to determine why the Valea Lunga-Buzau foredeep margin is oblique to the front of the Carpathians and why the recent thrusts are in overstep sequence, we first measured fault planes with slickensides and then computed the successive stress axes that account for the observed deformation. Indeed two successive stress fields are reconstructed thus indicating NW-SE and N-S trends of compression. The N-S trending compression (Fig. 2) is the most recent. It is the only compression found in the Meotian to Quaternary foredeep sequence. Even the early Pleistocene sediments are affected (site 13, Figs 2, 4 and table 1). Therefore, this N-S trend of compression, identified in the main structures of the inner foredeep margin, characterize the Wallachian phase (STILLE, 1924).

The stress regime is reverse (site 7, 10, 12, 13, 14 and 16, table 1) or strike-slip (sites 2, 3, 9, 11, 15 and 17, table 1) depending on the location (geographic stress permutation, HIPPOLYTE *et al.*, 1992). Moreover, the existence of both reverse and strike-slip stress regimes in a same site (site 8, table 1), results from a temporal stress permutation (HIPPOLYTE *et al.*, 1992), probably during a unique event.

This N-S compression is sometimes perpendicular to the Pliocene-Quaternary folds axes, but it is often slightly oblique, suggesting that some of them may be Moldavian structures reactivated during the

Source : MNHN, Paris

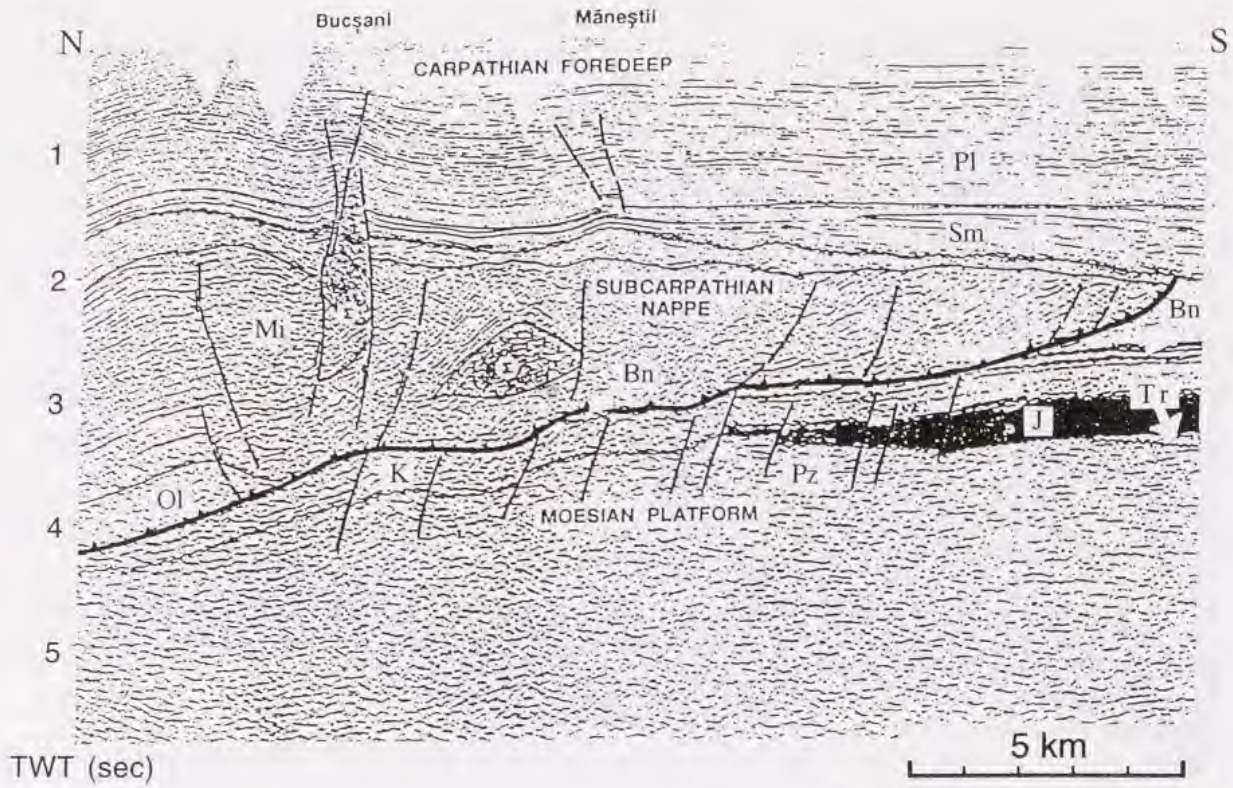

FIG. 5.— Seismic profile in the inner Carpathian foredeep (location in Fig. 2; from MOCANU & RADULESCU, 1994, and DICEA, 1995). The frontal thrust of the Carpathians (Subcarpathian Nappe) is buried under foredeep sediments. Whereas the tectonic contact between this nappe and the early foredeep sediments is sealed by Sarmatian deposits, the Pliocene foredeep sediments are folded in the inner zones. PZ: Paleozoic, Tr: Triassic, J: Jurassic, K: Cretaceous, Ol: Oligocene, Mi: Miocene, Σ: Miocene salt, Bn: Badenian, Sm: Sarmatian, Pl: Pliocene.

FIG. 5.— Profil sismique dans l'avant-fosse interne des Carpathes (voir figure 2 pour la localisation ; d'après MOCANU & RADULESCU, 1994 ; DICEA, 1995). Le chevauchement frontal des Carpathes (Nappe Subcarpatique) est enfoui sous les sédiments de l'avant-fosse. Bien que les sédiments Sarmatiens scellent le contact de cette nappe avec les dépôts inférieurs de l'avant-fosse, les sédiments pliocènes de cette avant-fosse sont déformés dans les zones internes. PZ : Paléozoïque, Tr : Trias, J : Jurassique, K : Crétacé, Ol : Oligocène, Mi : Miocène, Σ : Sel miocène, Bn : Badénien, Sm : Sarmatien, Pl : Pliocène.

Wallachian phase (Fig. 2). This N-S compression also created the thrusts of Wallachian age bordering the foredeep basin to the north (Fig. 2). Northwest of Ploiesti, the Valea Lunga depocentre is partly isolated from the main foredeep basin (Fig. 2). This depocentre is located on the hanginwall of a thrust fault. As measurements at site 14 (Fig. 4) indicate that this thrust moved to the south, the direction of thrusting is found parallel to the direction of compression. The NE-trending segment of this thrust (Fig. 2) is an oblique ramp with a left lateral component of movement. The Valea Lunga basin, only deformed by compression, is probably a piggyback syn-compressive basin (ORI & FRIEND, 1984) dating both the thrust activity and the N-S compression as Meotian-early Pleistocene in age. Thinning of the foredeep sedimentary sequence over numerous anticline hinges in the East Carpathians bend area (Fig. 2), confirms this age (STILLE, 1953; PARASCHIV, 1975; STEFANESCU, 1984). In figure 6, the large thinning of the Meotian-Quaternary sequence from the south to the north of a large broken anticline is a clear example of syn-depositional tectonics.

In contrast to the foredeep sequence, the Paleogene to Sarmatian sediments of the outer Moldavian nappes have recorded two compressional trends: N-S (Fig. 2) and NW-SE (Fig. 7). As the NW-SE compression does not affect the Meotian to Quaternary sediments, we concluded that it is the older Cenozoic event. Moreover, this stratigraphic dating of the stress orientation indicates that the NW-SE compression ended in Sarmatian and was replaced at this time by the N-S compression, syn-depositional of the Meotian-early Pleistocene stratigraphic sequence. Observations of slickensides superposition

Source : MNHN, Paris

TABLE 1.— Paleotress tensors computed from fault-slip data (Schmidt diagrams in annex). Sites of figs 2 and 7. S = State of stress: S = strike-slip stress regime, C = compressional regime, E = extensional regime. N = number of faults used for paleostress calculation. σ1, σ2, σ3: trend (N to E) and plunge of stress axes (°). Φ = (σ2-σ3)/(σ1-σ3). ANG = average angle between computed shear stress and observed slickenside lineation (°).

TABLEAU 1.— Paléocontraintes calculées à partir de mesures de plans de failles striés (diagrammes en annexe). Sites des figures 2 et 7. S = Type d'état de contraintes : S = régime décrochant, C = régime compressif, E = régime extensif. N = nombre de failles utilisées dans le calcul des paléocontraintes. σ1, σ2, σ3 : direction et plongement en ° des axes de contraintes. Φ = (σ2-σ3)/(σ1-σ3). ANG = angle moyen entre la contrainte cisaillante calculée et la strie mesurée (°).

Site	Type of rock	Age	S	N	σ 1	σ 2	σ 3	Φ	ANG
1	limestone	Late Sarmatian	S	23	124 09	349 77	216 09	0.39	13
2	limestone	Late Sarmatian	S	24	173 27	009 62	066 07	0.38	09
3	limestone	Late Sarmatian	S	12	351 06	248 65	084 24	0.24	09
4	hard volcanic tuff	Badenian	C	10	129 04	219 05	003 84	0.58	09
5	marl	Oligocene	C	11	295 40	205 00	115 50	0,52	09
5	same faults backtilted		C	11	125 09	216 09	351 77	0.52	09
6	sandstone	Burdigalian-Langhian	C	27	306 01	036 15	210 75	0.57	10
6			S	12	305 05	056 77	214 12	0.32	08
6			E	09	285 81	036 03	126 08	0.17	07
7	clay	Romanian	C	15	148 17	053 16	281 66	0.06	18
8	marl	Burdigalian-Langhian	S	29	138 50	331 39	236 07	0.18	13
8	same faults backtilted		S	29	316 08	188 77	047 10	0.18	13
8			E	16	341 75	076 01	166 15	0.32	14
8			C	20	216 11	124 11	351 74	0.83	11
8			S	10	039 01	307 53	130 37	0.21	12
9	limestone	Late Sarmatian	C	12	118 40	249 38	002 27	0.24	15
9	same faults backtilted		C	12	142 03	234 24	047 66	0.24	15
9			S	08	121 43	006 24	256 37	0.48	14
9	same faults backtilted		S	08	139 03	038 76	230 14	0.48	14
9			S	11	186 06	074 75	277 14	0.48	08
9B	Northern limb of anticline 9		S	24	004 06	119 76	273 13	0.32	13
9B	Northern limb of anticline 9		E	06	220 80	000 08	091 06	0.23	16
10	sandstone	Meotian	C	07	198 41	094 15	349 45	0.47	13
10	same faults backtilted		C	07	011 07	279 11	132 78	0.47	13
11	marl	Romanian	S	09	190 28	030 60	284 09	0.46	11
11			E	06	146 70	027 10	294 18	0.39	09
12	clay	Dacian	C	28	183 27	075 32	305 46	0.05	13
12			E	14	054 82	175 04	266 07	0.39	06
13	conglomerate	Early Pleistocene	C	07	347 13	078 06	193 75	0.33	08
14	marl	Meotian	C	06	179 06	271 17	071 72	0.64	11
15	clay	Pontian	S	19	200 01	297 78	110 12	0.45	11
15			E	13	023 53	185 36	282 08	0.05	11
16	clay	Romanian	C	10	341 07	250 08	113 79	0.54	08
17	hard volcanic tuff	Badenian	E	18	315 41	054 10	154 47	0.40	08
17	same faults backtilted		E	18	216 67	058 21	325 08	0.40	08
17			E	05	319 27	142 60	253 12	0.45	09
17	same faults backtilted		E	05	032 74	139 05	231 15	0.45	09
17			C	07	084 23	195 40	332 42	0.63	05
17	same faults backtilted		C	07	288 09	018 01	117 81	0.63	05
17			C	11	134 00	044 02	225 88	0.41	08
17			E	07	145 78	321 12	051 01	0.42	10
17			S	05	192 21	331 63	096 16	0.51	08
18	limestone	Late Sarmatian	S	09	311 01	216 75	041 15	0.14	06
18			E	06	211 76	309 02	040 14	0.02	03
19	limestone	Late Sarmatian	S	28	109 06	353 76	201 12	0.38	09
20	marl	Burdigalian-Langhian	C	05	113 31	354 39	228 35	0.05	01
21	limestone	Late Sarmatian	C	14	349 34	253 08	152 55	0.26	11
21	same faults backtilted		C	14	148 03	238 01	346 87	0.26	11
22	sandstone	Badenian	S	20	114 25	316 63	208 09	0.38	08
23	sandstone	Sarmatian	C	28	190 51	069 23	325 30	0.16	07
23	same faults backtilted		C	28	136 06	226 01	326 84	0.16	07

Source : MNHN, Paris

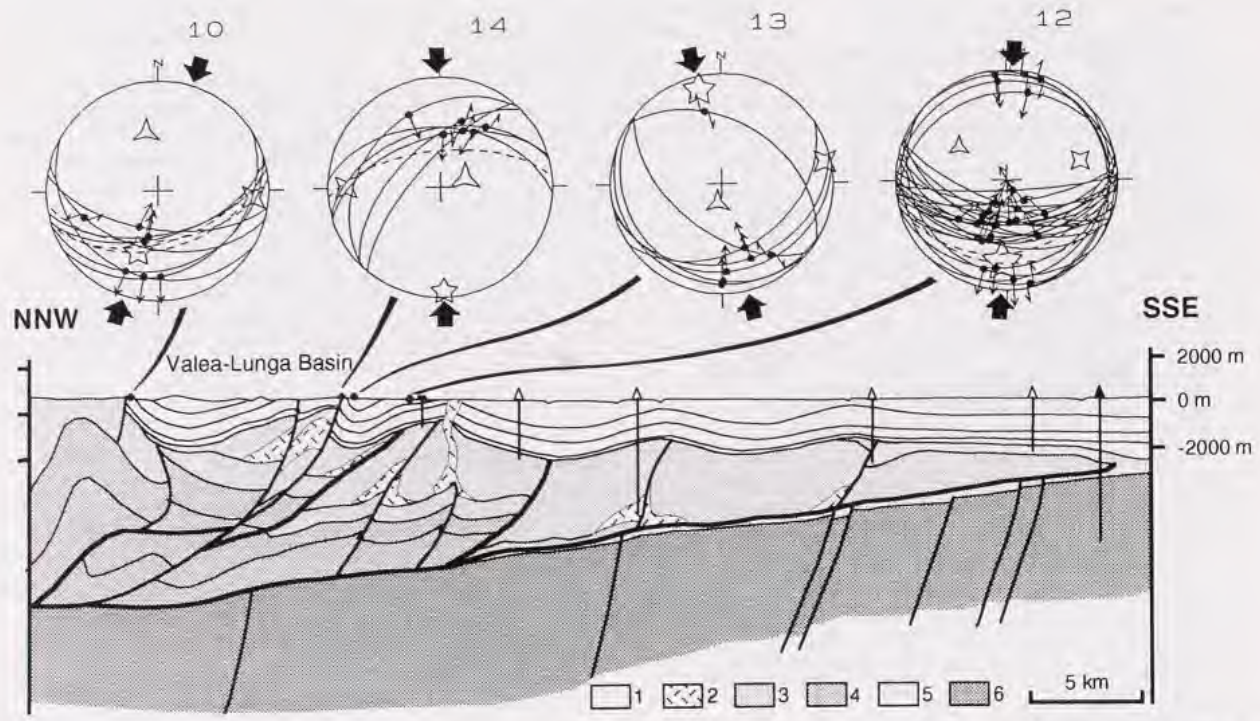

FIG. 6.— Cross-section 2, in the Wallachian fold and thrust area (location in Fig. 2; from STEFANESCU, 1984, modified) with Schmidt diagrams (lower hemisphere) of Wallachian striated fault planes and computed stress axes (bedding planes as broken lines). Same legend as figure 4.

FIG. 6.— Coupe 2, dans la zone des chevauchements et plis Valaques (localisation en figure 2 ; modifié d'après STEFANESCU, 1984) avec diagrammes (projection Schmidt, hémisphère inférieur) de plans de failles striés d'âge Valaque, axes de contraintes calculés. Même légende que figure 4.

confirm the chronology between these two compressional trends. This chronology is also confirmed by simple geometrical relationships between computed stress axes and bedding planes. For example, the stress axes of the NW-SE compression are tilted at sites 9 and 17 (table 1 and annex) (the compression faulted the rocks before bed-tilting), while in the same sites, the stress axes of the N-S compression are not tilted and therefore postdate bed-tilting.

The NW-SE compression predating Meotian time characterizes the Moldavian 'phase' (SANDULESCU, 1980) when large nappe emplacement occurred. This compression was also responsible for folding. In site 17, the pre-tilt and post-tilt characteristics of the stress axes of the NW-SE compression indicate that the folding of this area was completed before the N-S Meotian-early Pleistocene compression. As for the Wallachian event, during this NW-SE compression the stress regime was either reverse (sites 4, 5, 17, 20, 21, 23, table 1) or strike-slip (sites 1, 8, 18, 19, 22, table 1) and temporal stress permutations, between reverse and strike-slip regimes, also occurred (sites 6 and 9, table 1 and annex).

For both the N-S and the NW-SE compression, the temporal stress permutations could lead to normal faulting with extension perpendicular to the direction of compression (sites 9B, 11, 12, 15, 17, 18, table 1 and annex). This is a common feature which is no more frequent in this foothill area, than for example in autochtonous foreland carbonate platforms. One cannot conclude that this extension results from diapir tectonics, since it is not found above diapirs (MRAZEC, 1927) and, on the contrary, it is sometimes found in synclines (sites 11, 15, 17). This phenomenon only affects reduced areas of some outcrops. Its local development within major compressional structures indicates that these stress permutations probably reflect lateral variations in the confining pressure during the deformation, rather than a general extensional event.

The two directions of compression are very different (Figs 2, 7). The existence of block rotations could not be controlled in this area by paleomagnetism because the tested Neogene rocks gave week and

Source : MNHN, Paris

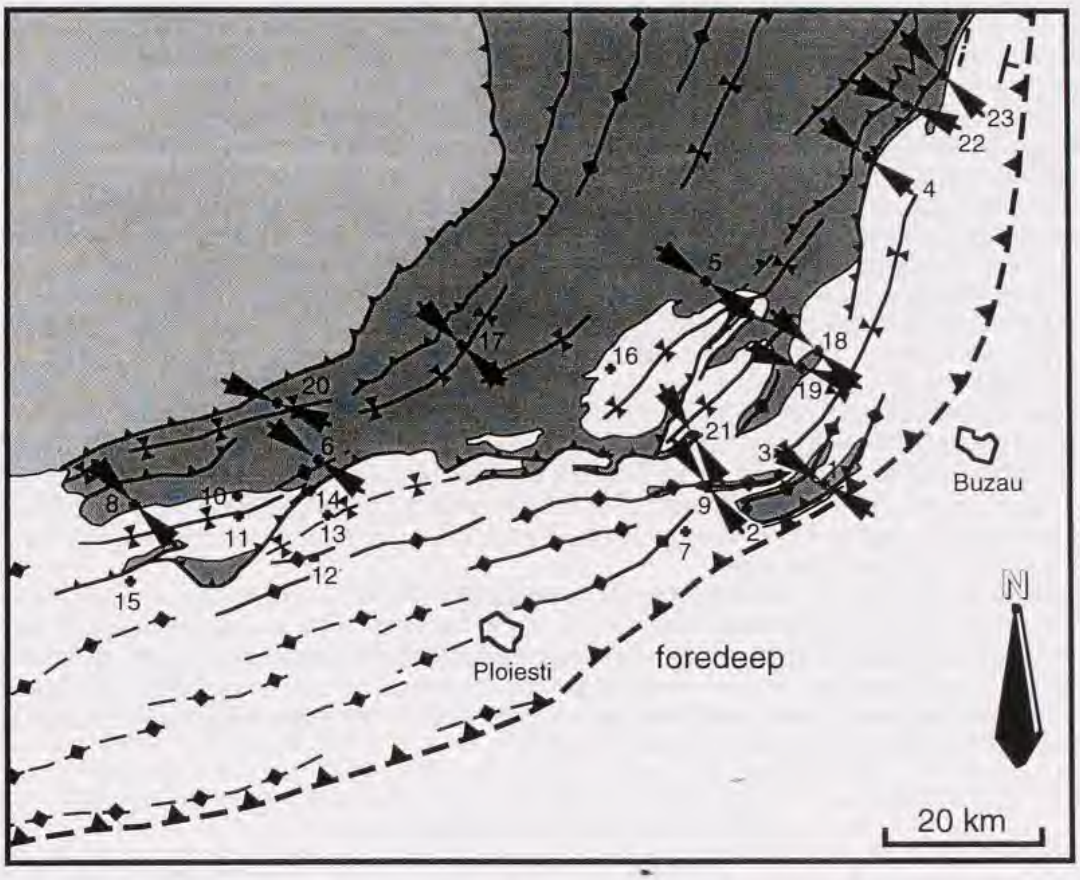

FIG. 7.— Direction of compression of Moldavian age (early Miocene-Sarmatian). Same legend and location as fgure 2.
FIG. 7.— Direction de compression d'âge Moldave (Miocène inférieur-Sarmatien). Même légende et localisation que pour la figure 2.

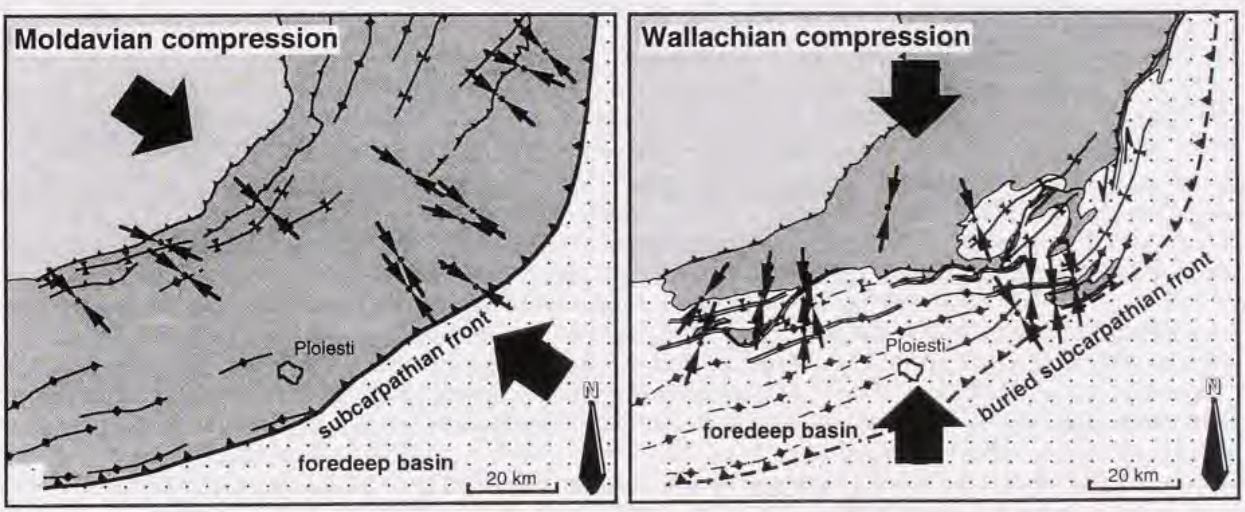

FIG. 8.— Neogene evolution of the Romanian diapir fold area. a) End of the nappe emplacement of the Moldavides controled by the NW-SE Miocene compression. b) Thrusting and folding in the Moldavides during the Wallachian (late Miocene, Pliocene and early Quaternary) tectonic phase. The foredeep develops partly above the Moldavian nappes. It is bounded to the north by an E-W trending folded belt superposed on the arcuate Moldavian thrust pile.
FIG. 8.— Évolution Néogène de la zone des plis diapir. a) Fin de la mise en place des nappes Moldaves sous l'action d'une compression miocène orientée NW-SE. b) Chevauchement et plissement des Moldavides pendant la " phase Valaque " (Miocène supérieur, Pliocène et Pléistocène inférieur). L'avant-fosse se forme en partie au dessus des nappes. Elle est limitée au nord par une chaîne plissée d'orientation E-W superposée à l'arc des nappes moldaves.

Source : MNHN, Paris

unstable natural remanent magnetization. The hypothesis that these two different trends of compression could result from rotations of fractured blocks within a single stress field is unlikely. The chronology of the two trends of compression (NW-SE, first and N-S second) indicates that the rocks affected by the N-S compression would have undergone a counter-clockwise rotation during Neogene to obtain the NW-SE trend. However the existing paleomagnetic data in Miocene and older rocks in the south-east Carpathians (BAZHENOV *et al.*, 1993), South Carpathians (PATRASCU *et al.*, 1992) and the Apuseni mounts (BORDEA *et al.*, 1993; PATRASCU *et al.*, 1994) all indicate clockwise rotations.

Moreover, we can consider that the older trend of compression that was characterized (NW-SE Miocene event) may have undergone the larger rotation. However, this Miocene event is characterized with the same trend until central-south Carpathians (RATSCHBACHER *et al.*, 1993). Close to this area, the Paleogene and Neogene andesites of the South Apuseni Mountains (Fig. 1) allowed a paleomagnetic control of the block rotations, showing that no rotation occurred in rocks of middle-late Miocene age (15 to 9 My, PATRASCU *et al.*, 1994). In the non-rotated andesites of this area, we characterize a strike-slip deformation that has also a NW-SE trend of compression, and is dated of Badenian-Sarmatian by the filling of pull-apart basins nearby. We conclude that the NW-SE Miocene trend of compression was not rotated after the middle Miocene in the South Apuseni mounts. On the same way, the Miocene compression that is trending NW-SE in the South Carpathians and the Southeast Carpathians may have usually undergone only minor rotations after the middle Miocene. As our measurements, in the diapir fold area, are made mostly in Late Neogene rocks, the possible block rotations may not have change the stress orientations in a significant way.

In conclusion, despite the second order extension generated by local stress perturbations, the paleostress analysis confirms that the inner margin of the foredeep basin is compressive. The structures of this margin are polyphase, however, their present dominant E-W orientation results mainly from the Wallachian N-S compression. The overstep sequence of thrusting and the obliquity of the foredeep margin with the outer thrust front result from the change in the compression direction from NW-SE to N-S, during late Sarmatian-Meotian (Tortonian, Fig. 3).

DISCUSSION AND CONCLUSION

The nappe emplacement in the outer Carpathians (Moldavides) lasted during most of Miocene and ended in middle Sarmatian with the emplacement of the Subcarpathian nappe. In the diapir fold area, the NW-SE compression affects the Tertiary stratigraphic sequence until the late Sarmatian deposits. Therefore, it is this compression that generated the nappes of the outer Carpathians (Fig. 8a). Since we did not found this compression in more recent formations, we conclude that this stress field ended in late Sarmatian, just after the end of the nappe emplacement.

After the nappe emplacement, the foredeep subsided strongly in the southern areas (Fig. 1). In the diapir fold area (Fig. 2), the foredeep inner margin was built by the N-S compression (Fig. 8b). On this margin, probable piggyback syn-compressive basins (as the Valea Lunga Basin) began to form in Meotian time. The climax of this compression, in the early Pleistocene, has allowed the definition of the Wallachian phase (STILLE, 1924; DUMITRESCU & SANDULESCU, 1968).

In contrast to the previous NW-SE compression, the N-S Wallachian compression was not responsible for large nappe emplacement, but created thrust faults with unprecedented vertical movements (Figs 4, 6) accounting for the trap of sediments in piggyback basins and the thick sediment accumulations in the foredeep basin (Fig. 6). In the area north of Buzau, where the trend of the margin curves to the north, the foredeep margin could be transpressive with a left lateral component of movement in accommodation of a N-S shortening (Fig. 8b). Further paleostress determinations will aim at determining if the tilt of the inner margin of the Getic Depression (east-trending non folded segment of the foredeep basin, Fig. 1) also results from a N-S compression, coeval to the NNE-SSW compression identified in Paleogene and Early Neogene rocks of central South Carpathians (RATSCHBACHER *et al.*, 1993). In the study area, the change of the stress orientation from NW-SE to N-S explains the overstep sequence of thrusting (Fig. 8b).

A southward movement of the thrust stack could be the reason for the change in the stress field. During early and middle Miocene the NW-SE compression was related to the eastward escape of the Tisza intra-Carpathian block (ROYDEN *et al.*, 1982, CSONTOS *et al.*, 1992; LINZER, 1996) or a foreland underthrusting (SANDULESCU, 1989). Afterward, a blocking along the NNW-trending part of the East

Source : MNHN, Paris

Carpathians could have produced this southward movement of the thrust stack, in the not yet blocked southeast Carpathians.

At the front of the East Carpathians bend area, the inner margin of the foredeep basin is thus a compressive margin formed by N-S compression. Its compressional structures are superposed on Miocene nappes and are in internal position (Fig. 8b). This location and the correlative overstep sequence of thrusting result from a change in the stress orientation, from NW-SE during the outer Carpathian thrusting (early Miocene to Sarmatian) to N-S during Meotian-early Pleistocene (Fig. 8). During this latter period, folding and thrusting mostly generated vertical movements. This characteristic of the deformation must be linked to the contemporaneous thick accumulation of sediments in the foredeep and explain the formation of piggyback basins in the foredeep inner margin.

ACKNOWLEDGEMENTS

This work was supported by the Peri-Tethys Program. We are grateful to F. ROURE and L. FODOR for their helpful comments on this paper. We thank H. RON for the paleomagnetism analysis of samples of Neogene sediments. We also thank D. BADESCU, N. BADESCU, P. CONSTANTIN and M. TURTURANU for their help during the field work and their constructive discussions of the results.

REFERENCES

ANGELIER, J., 1989.— From orientation to magnitudes in paleostress determinations using fault slip data. *Journal of Structural Geology*, **11**: 37-50.

BAZHENOV, M., BURTMAN, V. & SANDULESCU, M., 1993.— Paleomagnetism of the Upper Cretaceous rocks and its bearing on the origin of the Romanian Carpathian arc. *Romania Journal of Tectonic and Regional Geology*, **75**: 9-14.

BORDEA, S., SURMONT, J. & SANDULESCU, M., 1993.— Paléomagnétisme des séries sédimentaires mésozoiques de l'unité de Bihor (Monts Apuseni septentrionaux, Roumanie); conséquences paléotectoniques. *Romania Journal of Tectonic and Regional Geology*, **75**: 15-25.

CSONTOS, L., NAGYMAROSY, A., HORVATH, F. & KOVAC, M., 1992.— Tertiary evolution of the Intra-Carpathian area: a model. *Tectonophysics*, **208**: 221-241.

DICEA, O., 1995.— The structure and hydrocarbon geology of the Romanian East Carpathian border from seismic data. *Petroleum Geoscience*, **1**: 135-143.

DUMITRESCU, F. & SANDULESCU, M., 1968.— Problèmes structuraux fondamentaux des Carpates roumains et de leur avant-pays. *Anuarul Comitetului de Stat al Geologiei Romania*, **36**: 195-218.

DUMITRESCU, F. & SANDULESCU, M., 1970.— Carta tectonica scara 1:1.000.000, Romania. *In*:*Atlas Geologic foaia 6*. Institutul Geologic, Bucuresti.

ELLOUZ, N. & ROCA, E., 1994.— Palinspastic reconstructions of the Carpathians and adjacent areas since the Cretaceous: a quantitative approach. *In*: F. ROURE (ed.), *Peri-Tethyan Platforms: Proceeding of the IFP Peri-Tethys Research Conference held in Arles, France, March 23, 1993*. Technip, Paris: 51-77.

ELLOUZ, N., ROURE, F., SANDULESCU, M. & BADESCU, D., 1996.— Balanced cross-sections in the eastern Carpathians (Romania): a tool to quantify Neogene dynamics. *In*: F. ROURE *et al.* (eds), *Geodynamic Evolution of Sedimentary Basins: Proceedings of the International Symposium held in Moscow, May 18-23, 1992*. Technip, Paris.

HIPPOLYTE, J.-C., ANGELIER, J. & ROURE, F., 1992.— Les permutations de contraintes: exemples dans des terrains quaternaires du sud de l'Apennin (Italie). *Comptes Rendus de l'Académie des Sciences, Paris*, **315** (II): 89-95.

LINZER, H.-G., 1996.— Kinematics of retreating subduction along the Carpathian arc, Romania. *Geology*, **24**: 167-170.

MOCANU, V.I. & RADULESCU, F., 1994.— Geophysical features of the Romanian territory. *In*: T. BERZA (ed.), *Alcapa II, field guidebook*. Geological Institute of Romania: 17-36.

MRAZEC, L., 1927.— Les plis diapirs et le diapirisme en général. *Comptes Rendus des Séances de l'Institut géologique de Roumanie*, **6** (1914-1915): 215-255.

ORI, G.G. & FRIEND, P.F., 1984.— Sedimentary basins formed and carried piggyback on active thrust sheets. *Geology*, **12**: 475-478.

PARASCHIV, D., 1975.— Geologia zacamintelor de hidrocarburi din Romania. *Prospectiuni si explorari geologice, seria A*, **10**: 1-363.

PATRASCU, St., BLEAHU, M., PANAIOTU, C. & PANAIOTU, C.E., 1992.— The paleomagnetism of the Upper Cretaceous magmatic rocks in the Banat area of the South Carpathians: tectonic implications. *Tectonophysics*, **213**: 341-352.

PATRASCU, St., PANAIOTU, C., SECLAMAN, M. & PANAIOTU, C.E., 1994.— Timing of rotational motion of the Apuseni Mountains (Romania): paleomagnetic data from Tertiary magmatic rocks. *Tectonophysics*, **233**: 163-176.

Source : MNHN, Paris

RATSCHBACHER, L., LINZER, H-G., MOSER, F., STRUSIEVICZ, R.-O., BEDELEAN, H., HAR, N. & MOGOS, P.A., 1993.— Cretaceous to Miocene thrusting and wrenching along the central South Carpathians due to a corner effect during collision and orocline formation. *Tectonics*, **12** (4): 855-873.

ROYDEN, L.H., HORVATH, F. & BURCHFIELD, B.C., 1982.— Transform faulting, extension and subduction in the Carpathian Pannonian region. *Geological Society of America, Bulletin, New-York*, **93** (8): 717-725.

SANDULESCU, M., 1980.— Analyse géotectonique des chaînes alpines situées autour de la Mer Noire occidentale. *Annuarul de Institute Geologie si Geofizica*, **56**: 5-54.

SANDULESCU, M., 1989.— Structure and Tectonic history of the Northern Margin of Tethys between the Alps and the Caucasus. *Mémoires de la Société géologique de France, Nouvelle Série*, **154**: 3-16.

STEFANESCU, M., 1984.— *Elaborarea profilelor, scara 1:200.000 pentru completarea imaginii geologice a teritoriului R. S. Romania: A17, A18, A19, A20.* Institutul de Geologie si Geofizica, Bucuresti.

STEFANESCU, M. & DICEA, O., 1995.— Multiple thrust events at the Carpathian orogen/foreland contact in Romania. Abstract of the Association Round Table. *In: American Association of Petroleum Geologists, International Conference. Nice, september 10-13, 1995*: 1250.

STEININGER, F.F., MÜLLER, C. & RÖGL, F., 1988.— Correlation of Central Paratethys, Eastern Paratethys, and Mediterranean. Neogene stages. *In*: L. H. ROYDEN & F. HORVATH (eds), The Pannonian basin. A study in basin evolution. *American Association of Petroleum Geologists, Memoir*, **45**: 79-87.

STILLE, H., 1924.— *Grundfragen der vergleicherrden.* Tektonik; Borntraeger, Berlin.

STILLE, H., 1953.— Der geotektonische Werdegang der Karpaten. *Beihefte zum Geologischen Jahrbuch*, **8**: 1-239.

Source : MNHN, Paris

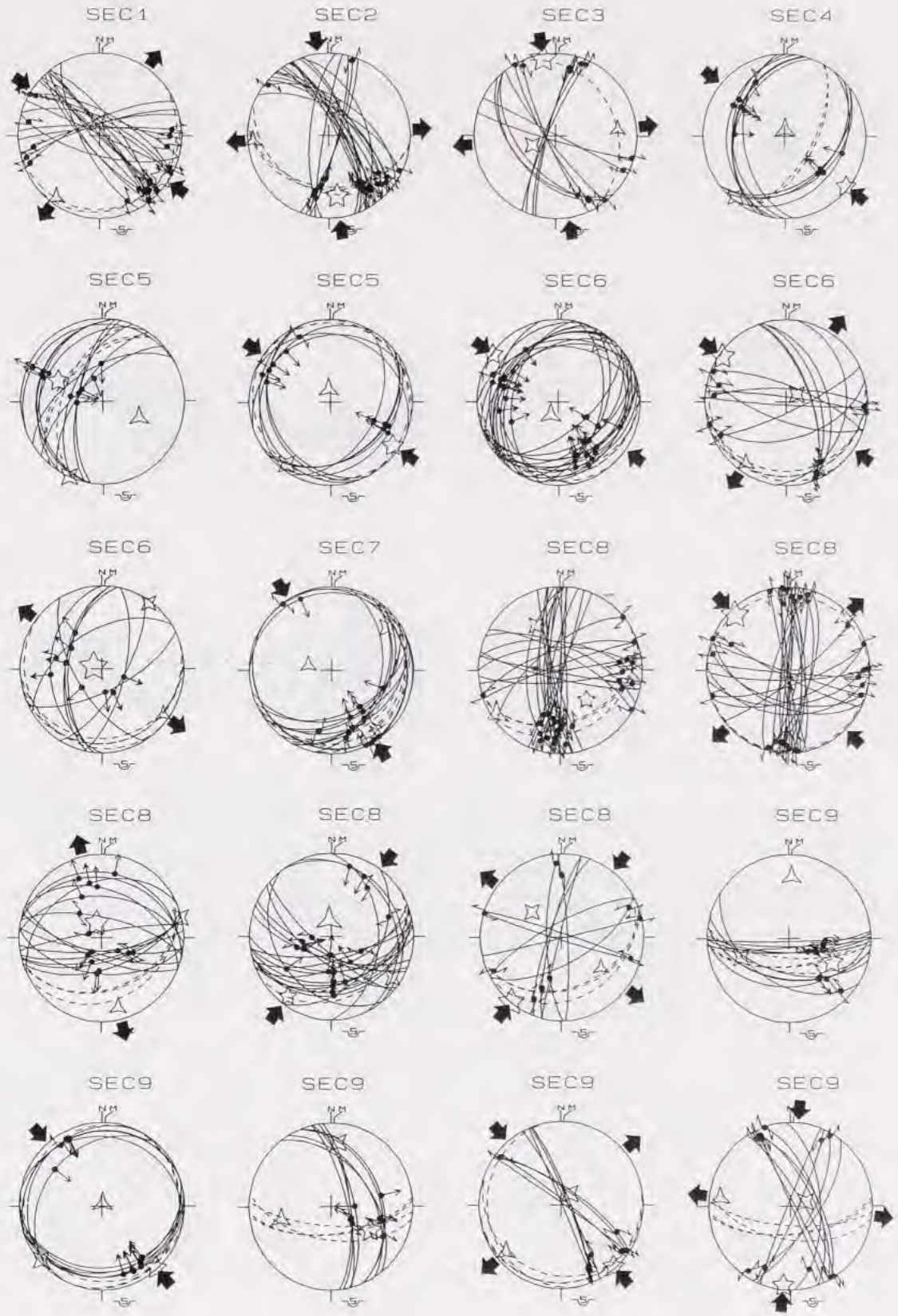

Source : MNHN, Paris

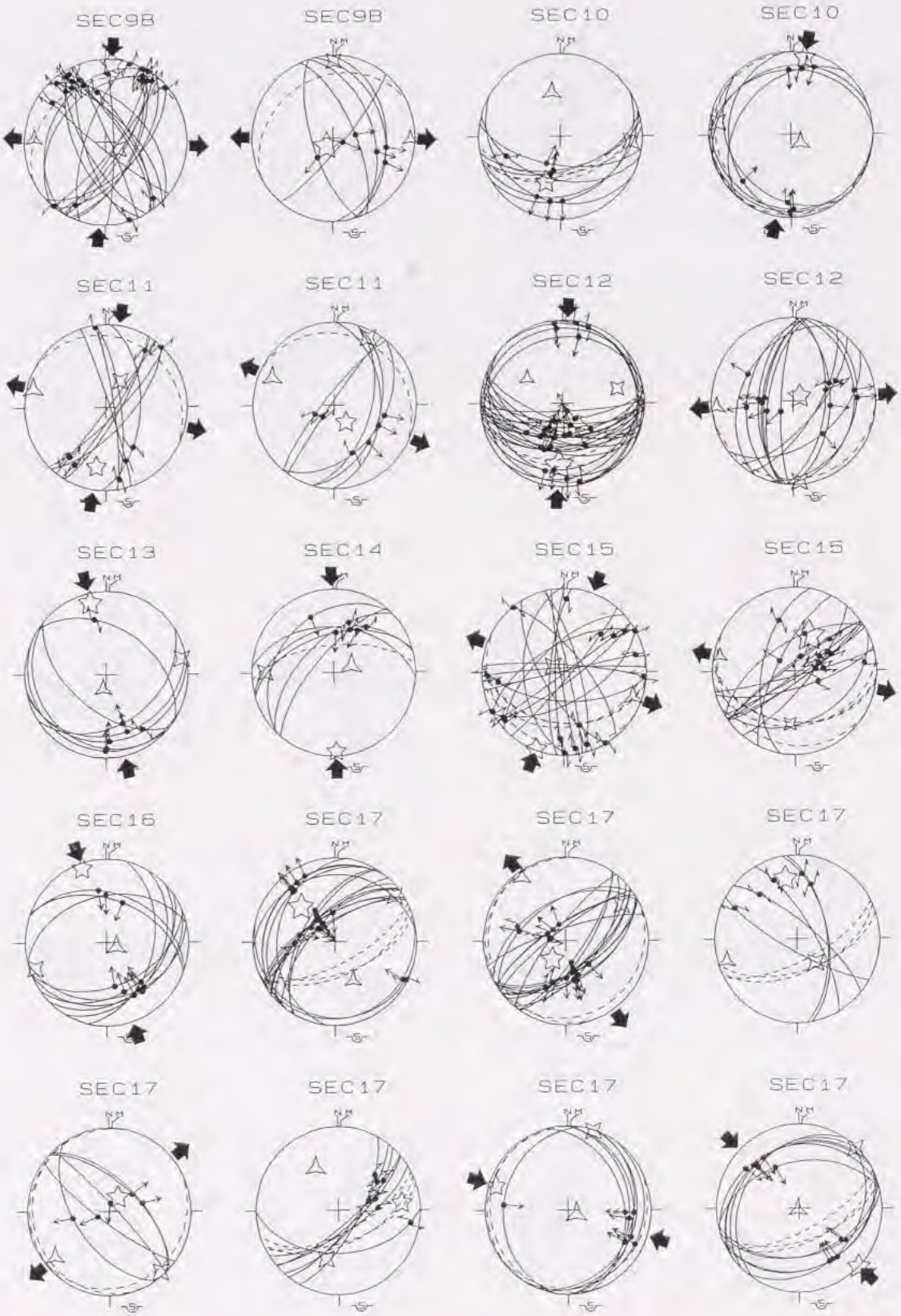

Source : MNHN, Paris

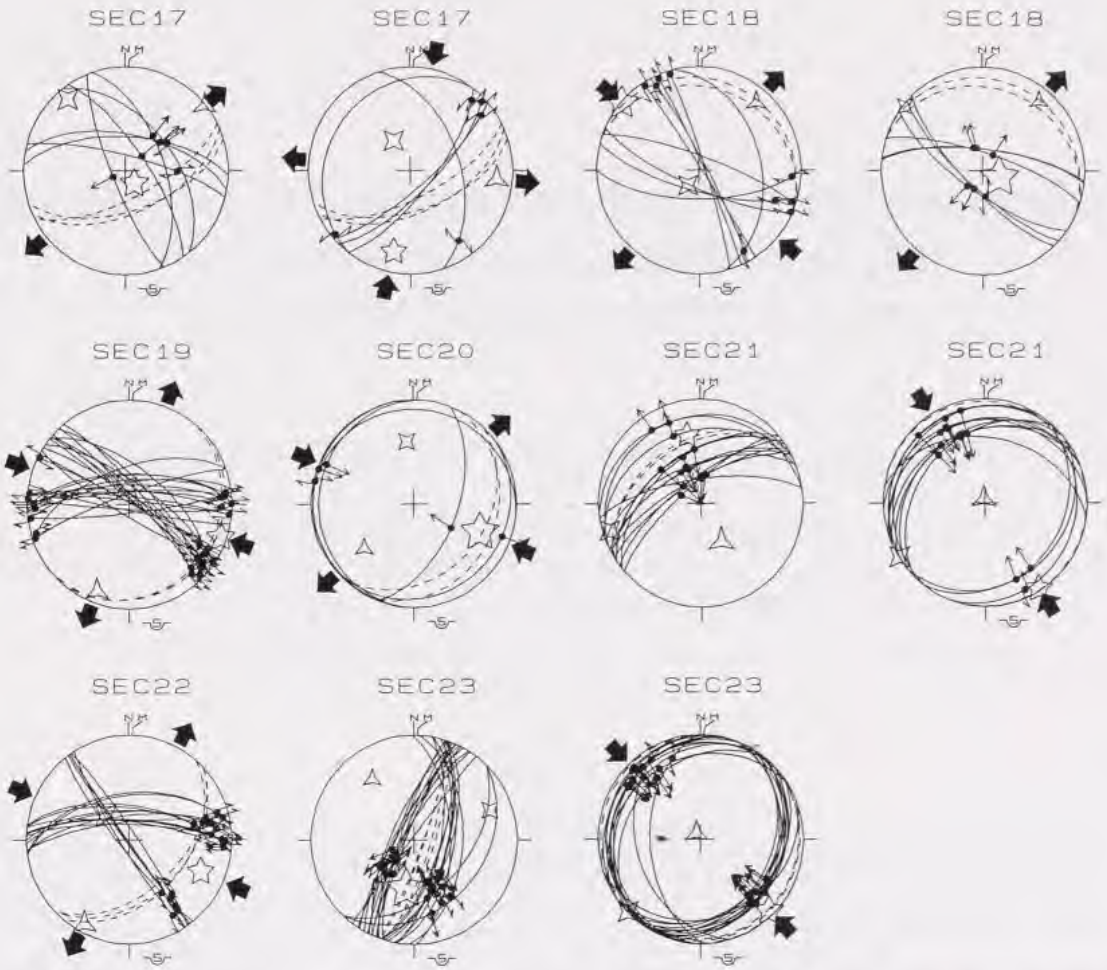

Annex: Schmidt diagrams (lower hemisphere) of striated fault planes and computed stress axes (references in table 1; same legend as for figure 4). Note that in the cases where faulting occurred before folding, the fractures are presented in two diagrams: one for the present fault attitude (the bedding planes, the faults and the stress axes are tilted) and one for the original fault attitude (the bedding planes and two stress axes are horizontal).

Annexe : Diagrammes (projection Schmidt, hémisphère inférieur) de plans de failles et d'axes de contraintes calculés (références dans le tableau 1 ; même légende que pour la figure 4). Remarquer que dans les cas où la fracturation a précédé un plissement important, les failles sont représentées dans deux diagrammes : un pour la géométrie actuelle (plans stratigraphiques, failles et axes de contraintes basculés) et un pour la géométrie originelle (plans de stratification et deux axes de contraintes sont horizontaux).

Source : MNHN, Paris

Source : MNHN, Paris

The Moesian Platform as a key for understanding the geodynamical evolution of the Carpatho-Balkan alpine system

Françoise BERGERAT [1], *Pierre* MARTIN [2] & *Dimo* DIMOV [3]

[1] Département de Géotectonique, CNRS URA 1759, case 129, Université P. et M. Curie
75252 Paris Cedex 05, France

[2] SGN/I2G/GEO, B.R.G.M., B.P. 6009, 45060 Orléans Cedex 2, France

[3] Geology and Geography Faculty, St-Kliment Ohridski University, 15 Tzar Osvoboditel Bd.
1000 Sofia, Bulgaria

ABSTRACT

From the Mesozoic to Present, Moesia has been a foreland platform regardless of the configuration of the Alpine orogen. The analysis of brittle structures characterizes the successive paleostress fields related to the different Alpine tectonic events of the Balkan area. Several main fault systems have been identified. A rather extensional phase, N-S to NNE-SSW, characterized by strike-slip and normal faulting, is of post-Aptian and pre-Maastrichtian age. A N-S to NNE-SSW compressional stress, characterized by strike-slip and reverse faulting, corresponds to a tectonic phase at the end of the middle Eocene. Another NNE-SSW compressional stress is of Pliocene age. An E-W extensional stress may by related to the N-S compression of middle Eocene age (permutation of stresses) or to a Miocene phase. The question of possible rotation and / or translation of the Moesian platform is discussed taking into account paleomagnetic data. A major rotation has not occurred. No data can confirm or invalidate a westward translation of Moesia. The main identified tectonic events are connected both to the Black Sea opening and to the Eurasian and Arabo-African plates convergence.

RÉSUMÉ

La plate-forme moésienne, clé pour la compréhension de l'évolution géodynamique alpine du système Carpates-Balkans.

Du Mésozoïque à l'Actuel, la Moésie a constitué une plate-forme d'avant pays de l'orogène alpin. L'analyse des structures cassantes caractérise les paléo-champs de contrainte successifs liés aux différents événements tectoniques alpins des Balkans. Plusieurs systèmes de failles majeurs ont été identifiés. Une phase à dominante extensive, N-S à NNE-SSW, caractérisée par des décrochements et des failles normales, est d'âge post-Aptien et anté-Maastrichtien. Une compression N-S à NNE-SSW, caractérisée par des décrochements et des failles inverses, correspond à une phase tectonique datée de la fin de l'Eocène moyen. Une autre compression NNE-SSW est d'âge pliocène. Une contrainte extensive E-W peut être liée soit à la compression N-S de l'Eocène moyen, par un phénomène de permutation de contraintes, soit à une phase miocène. La question de la rotation et / ou de la translation de la Moésie est discutée en prenant en compte les données du paléomagnétisme. Aucune rotation majeure n'a pu se produire. Aucune donnée ne permet de confirmer ou d'infirmer une translation vers l'ouest de la plate-forme moésienne. Les mouvements tectoniques majeurs identifiés sont attribués à la fois à l'ouverture de la Mer Noire et à la convergence Afrique / Eurasie.

BERGERAT, F, MARTIN, P. & DIMOV, D., 1998.— The Moesian Platform as a key for understanding the geodynamical evolution of the Carpatho-Balkan alpine system. *In*: S. CRASQUIN-SOLEAU & É. BARRIER (eds), Peri-Tethys Memoir 3: stratigraphy and evolution of Peri-Tethyan platforms. *Mém. Mus. natn. Hist. nat.*, **177** : 129-150. Paris ISBN : 2-85653-512-7.

Source : MNHN, Paris

INTRODUCTION

Various geological synthesis have been proposed for Tethyan and peri-Tethyan chains, platforms and basins (e.g. DERCOURT *et al.*, 1985, 1986; RICOU *et al.*, 1985, 1986). In these syntheses, the position occupied by the Moesian platform brings up several questions regarding its relationships with the neighboring chains of the Carpathian Mountains and the Balkan (Fig. 1). One of the main questions concerns its possible rotation or translation relative to stable Europe.

The present Moesian platform is part of a foreland of the Carpatho-Balkan chain. In Romania, it consists essentially of the Carpathian fore-deep, where Pliocene and Miocene molassic formations are largely developed. In Bulgaria, it is represented in its central and western parts by Cretaceous and Paleocene formations that have mostly subhorizontal bedding dips. The Miocene and Pliocene formations crop out to the North-West and in the East of the platform in two depressions that have formed since the middle Miocene.

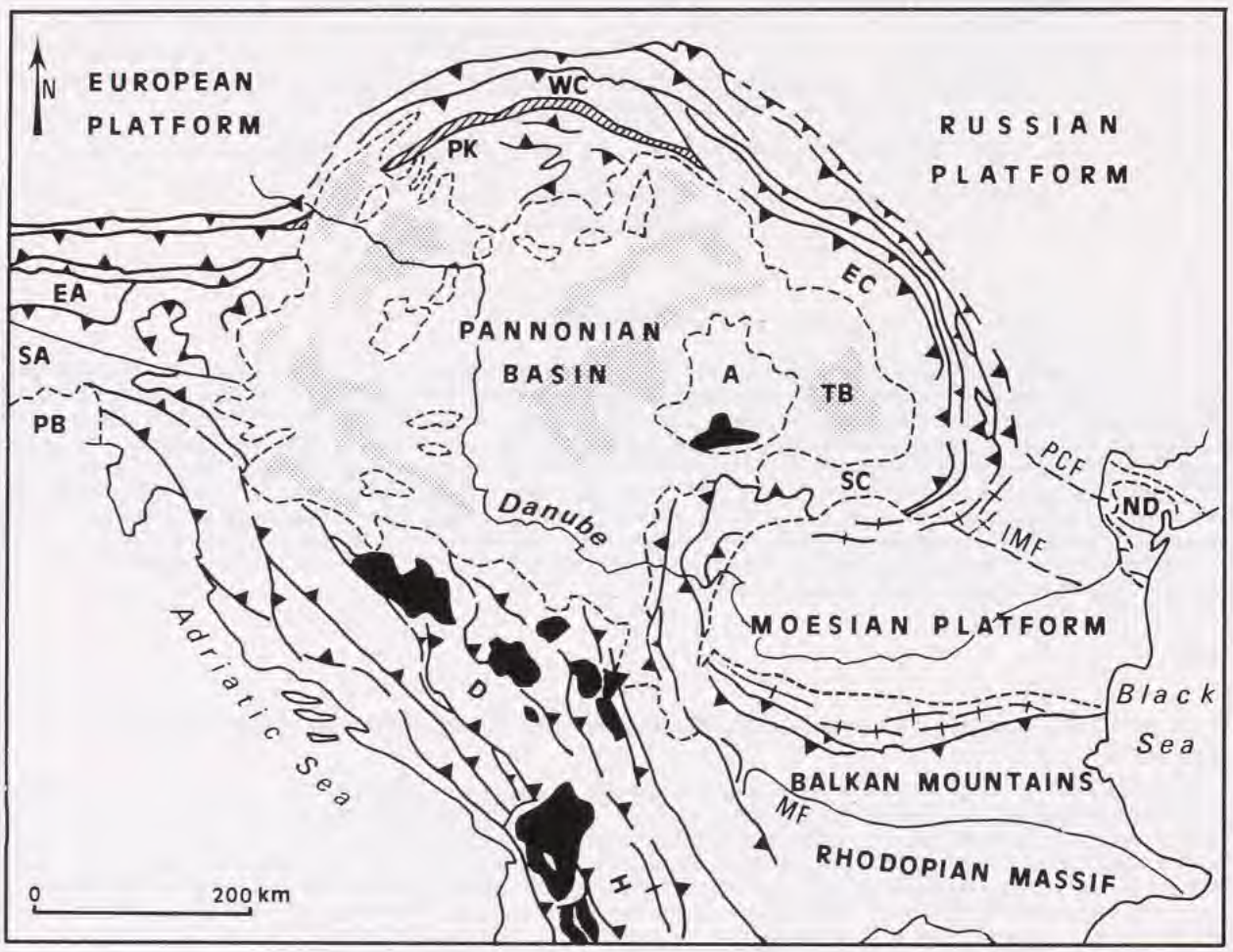

FIG. 1.— Tectonic sketch map of the Central European Alpine System. Abbreviations are as follows: A, Apuseni Mountains; EA, Eastern Alps; EC, Eastern Carpathians; IMF, Intra-Moesian Fault; MF, Maritsa Fault; ND, Northern Dobrogea; PB, Pô Basin; PCF, Peceneaga-Camena Fault; PK, Pieniny Klippen zone (hatched area), SC, Southern Carpathians; TB, Transylvanian Basin; WC, Western Carpathians.

FIG. 1.— Carte tectonique schématique du système alpin d'Europe Centrale. A, Monts Apuseni ; EA, Alpes orientales ; EC, Carpates orientales ; IMF, faille intra-moesienne ; MF, faille de la Maritsa ; ND, Dobrogée-Nord ; PB : bassin du Pô ; PCF, faille de Peceneaga-Camena ; PK, zone des klippes piennines (hachures) ; SC, Carpates méridionales ; TB, bassin transylvain ; WC, Carpates occidentales.

Source : MNHN, Paris

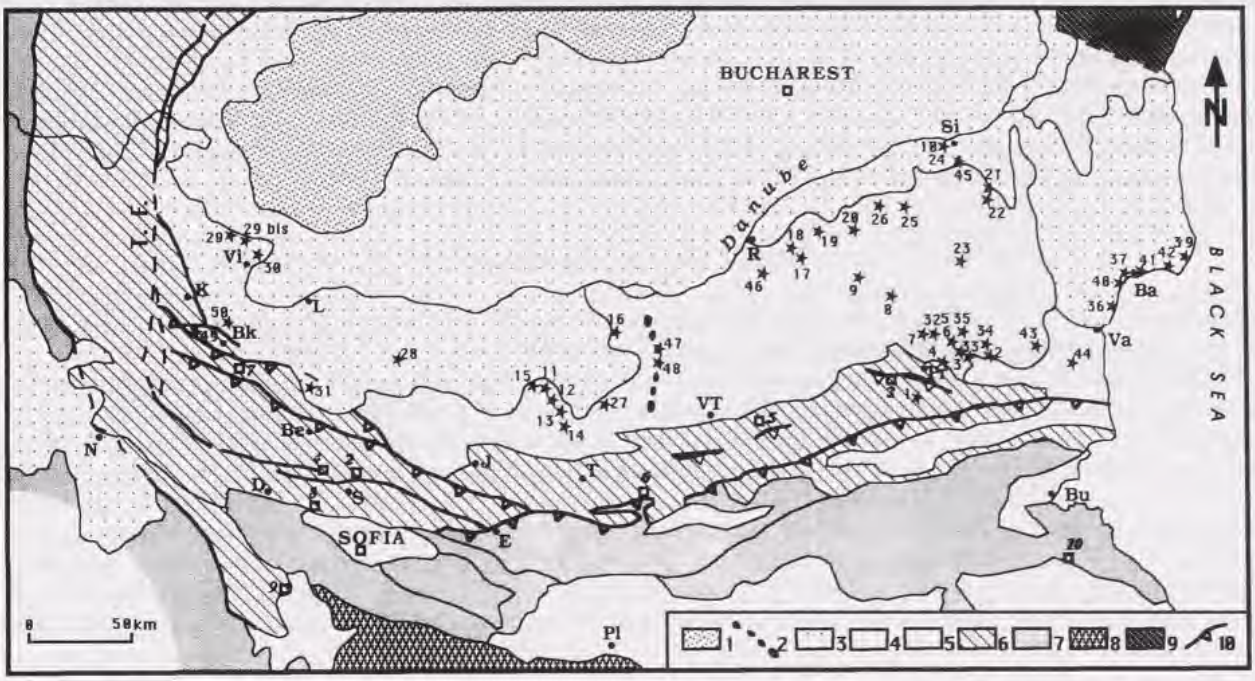

FIG. 2.— Simplified geological map of the Moesian platform and Balkan domain (after the International Geological map of Europe, 1:1,500,000, 1969-1983 and geological maps of Bulgaria 1:500,000, 1989 and 1:1,000,000, 1978).
Location of microtectonic measurements sites (stars, 1 to 50) and samples collection for paleomagnetic studies (squares, 1 to 9). Numbers refer to the following: **1**, Plio-Quaternary; **2**, Plio-Pleistocene basalts; **3**, Mio-Pliocene of Lom and Vidin depressions and of the Carpathian foredeep; **4**, Cenozoic intra-Balkan basins; **5**, Cretaceous of the Moesian platform; **6**, Fore-Balkan and Stara Planina; **7**, Sredna Gora; **8**, Rhodope-Strandza; **9**, Precambrian and Paleozoic of Dobrogea; **10**, major thrusts.
Abbreviations are as follows: Ba, Balcik; Be, Bercovica, Bk, Belogradcik; Bu, Burgas; D, Dragoman; E, Etropole; J, Jablanica; K, Kula; L, Lom; N, Nis; Pr, Preslav; PL, Plovdiv; R, Russe; S, Svoge; Si, Silistra; T, Trojan; Va, Varna; Vi, Vidin; VT, Veliko Tarnovo; TF, Timok Fault.

FIG. 2.— Carte géologique simplifiée de la plate-forme moesienne et du domaine balkanique (d'après la carte géologique internationale de l'Europe à 1/1 500 000, 1969-1983, et les cartes géologiques de Bulgarie à 1/500 000, 1989 et 1/1 000 000, 1978).
*La localisation des sites de mesures microtectoniques est indiquée par des étoiles (numérotées de 1 à 50), celle des échantillons pour les études de paléomagnétisme par des carrés (numérotés de 1 à 9). **1**, Plio-Quaternaire ; **2**, basaltes plio-pleistocènes ; **3**, Mio-Pliocène des dépressions de Lom et de Vidin et de l'avant-fosse carpathique ; **4**, bassins cénozoïques intra-balkaniques ; **5**, Crétacé de la plate-forme moesienne ; **6**, Prébalkan et Stara Planina ; **7**, Sredna-Gora ; **8**, Rhodope-Strandza ; **9**, Précambrien et Paléozoïque de la Dobrogée ; **10**, chevauchements majeurs.*

The classic division of Bulgaria was established by BONCEV (1940) and is still used (e.g. BONCEV, 1988; IVANOV, 1988). South of the Moesian platform and the small triangle of Kula attributed to the Southern Carpathians (Fig. 2), three main zones occur, the Fore-Balkan, the Stara-Planina (including the subzone of Luda Kamcija) and the Sredna Gora. The Rhodope is located to the South of the Sredna Gora. However, these various zones and subzones correspond to superposed alpine configurations (DERCOURT & RICOU, 1987). Therefore these names will only represent tectonic zones here if an age is associated. In the opposite case, they will have only a meaning of geographical sector.

The main tectonic and paleogeographical configurations, from the Jurassic to the Tertiary, are clearly oblique to one another. Furthermore, several of these paleogeographical elements have played a major role in the Alpine development of Bulgaria. The basin of Nis-Trojan of Upper Jurassic-Lower Cretaceous age, and the magmatic axis of the Upper Cretaceous are included with these elements (DERCOURT & RICOU, 1987). These major structures have influenced later deformations. The inherited structure and the obliquity of successive tectonic configurations, make the structure of the Balkan extremely complex.

In northern Bulgaria, the zone corresponding presently to the Moesian platform has always

Source : MNHN, Paris

represented a foreland platform in the different tectonic settings from the Mesozoic to the Present. The analysis of brittle deformations, can be used to characterize the paleostress fields associated to the different Alpine tectonic events.

The aims of this paper are a- to describe and interpret in terms of paleostress tensors the different fault systems that affect the Cretaceous to Pliocene formations of the Moesian platform, b- to examine the possible rotation and / or translation of this platform, and c- to discuss the paleostresses deduced in the framework of Black Sea opening and Africa-Eurasia convergence.

ALPINE DEVELOPMENT OF THE MOESIA-BALKAN DOMAIN

In the Triassic, a continental platform developed on the post-Hercynian peneplain. The same subsiding platform facies can be observed from the foreland to the Central Sredna Gora.

In the latest Jurassic-Lower Cretaceous, the Nis-Trojan flysch basin (3000 m of Lower Cretaceous) developed at the south-eastern margin of the platform (Fig. 3). It separates the Moesian platform to the North from a series of horsts to the South. The Jablanica line (NICOLOV & KRISHEV, 1965), also called the Etropole line, represents zone of variable width of facies changing. For DERCOURT & RICOU (1987), this line is a transform fault linked to the opening of the basin. IVANOV (pers. comm.) believes the basin is bounded to the SSE by a strike-slip fault, separating it from fragments of the Serbo-Macedonian massif. The basin disappears in the Aptian. During the Albian, an important tectonic phase is characterized by folds approximately E-W and thrust faults verging North (IVANOV, 1988). This tectonic event appears to copy almost exactly the previous setting because the deformed zone front corresponds approximately to the ancient Nis-Trojan basin (DERCOURT & RICOU, 1987).

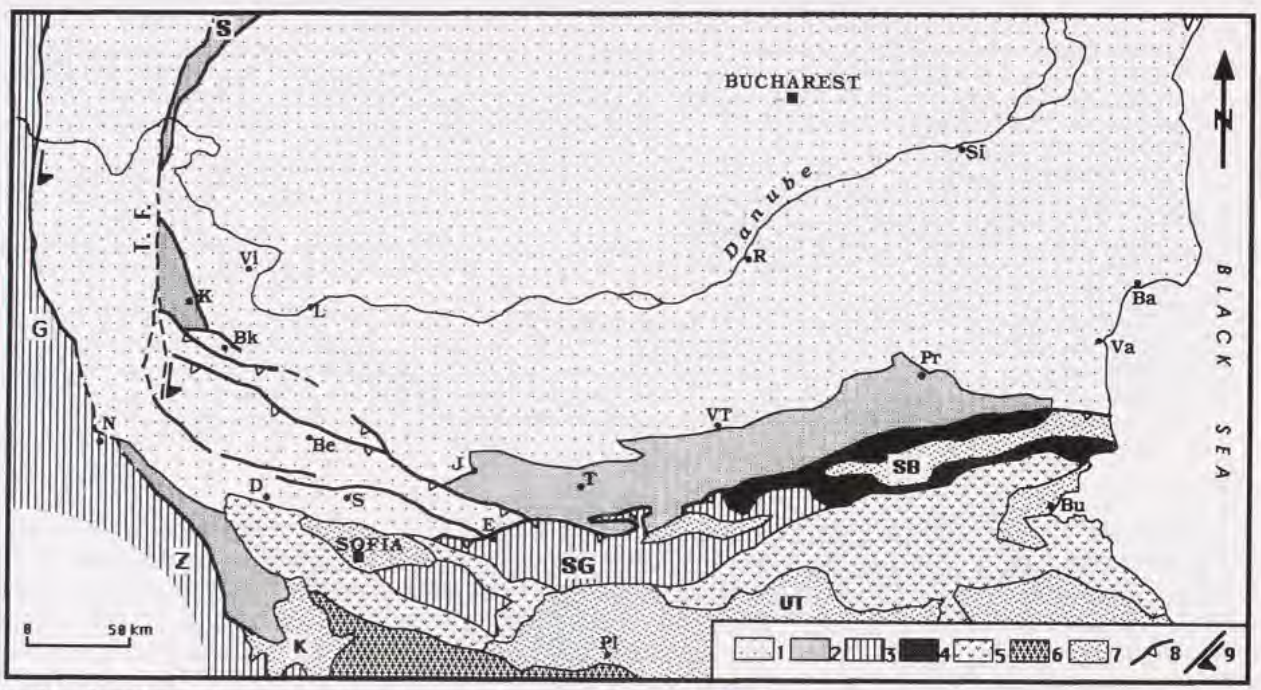

FIG. 3.— Superimposed tectonic and paleogeographic settings in the Moesian platform and Balkan domain.
Numbers refer to the following features: **1**, Eo-Cretaceous Moesian platform (including Fore-Balkan); **2**, Nis-Trojan basin, Severin (S) and Kraina-Kula Klippes; **3**, Neo-Cretaceous Getic (G) domain , and of Zemen (Z) and Sredna Gora (SG); **4**, Luda Kamcija basin; **5**, Neo-Cretaceous magmatic axis; **6**, Rhodope-Strandza; **7**, Cenozoic intra-Balkan basins, K, Kraiste, SB, South-Balkan, UT, Upper Thrace; **8**, major Eocene thrusts; **9**, major Miocene strike-slip faults. Abbreviations for towns as for figure 2.

FIG. 3.— Tectoniques et paléogéographies superposées dans la plate-forme moesienne et le domaine balkanique.
***1**, plate-forme moesienne éo-crétacée (incluant le Prébalkan) ; **2**, bassin de Nis-Trojan, Klippes de Severin (S) et Kraina-Kula ; **3**, domaines néo-crétacés gétique (G), de Zemen (Z) et de Sredna Gora (SG) ; **4**, bassin de Luda Kamcija ; **5**, axe magmatique néo-crétacé ; **6**, Rhodope-Strandza ; **7**, bassins cénozoïques intra-balkaniques ; **8**, chevauchements éocènes majeurs ; **9**, décrochements miocènes majeurs.*

Source : MNHN, Paris

Starting during the Senonian, a new flysch basin developed (NACHEV, 1977, 1978, 1980) in the Eastern and Northern part of the Stara Planina (Fig. 3). It constitutes the subzone of Luda Kamcija (flysch of Emine of Turonian-lower Paleocene age). During the same period to the South of this zone, significant calc-alkaline magmatism, active especially during the Coniacian-Santonian (more than 6000 m of volcano-clastic sediments), occurs in the Srednogorian rift (Fig. 3). The volume of volcanogenic rocks and their potassium content increase towards the Black Sea, but the neocretaceous magmatic axis can be recognized throughout Bulgaria, from Dragoman to Burgas (Fig. 3). This axis is superposed obliquely upon the ancient structures. Furthermore, the non-volcanic facies (flysch of Emine) are known only to the North of the axis and to the East of the Etropole line. Elsewhere in the Stara Planina as well as in the Fore-Balkan, a platform style sedimentation prevailed.

During the lower and middle Eocene, a vast molassic depression, trending NW-SE to E-W, extending from Serbia to the Black Sea (NACHEV, 1980) developed. These molasse deposits have been folded after the middle Eocene. The formation of folds in the Stara Planina and the Fore-Balkan has been immediately followed by significant thrusting to the North (Fig. 3) (IVANOV, 1988). These folds and thrusts characterize another major tectonic phase. The most significant thrust is the so-called Stara Planina thrust (thrusting of the Sredna Gora over the Stara Planina). Some other thrusts also accommodate the shortening on the northern flanks of the Svoge, Bercovica and Belogradcik anticlines (Fig. 3).

From Neogene to Quaternary, the post-tectonic configuration superposed on the various alpine elements. Several systems of troughs exist (Fig. 3). a- The kraistides trend N 150°-160° and separate Serbo-Macedonian and Rhodope. b- The South-Balkan is oriented E-W and occurs between Stara Planina and Sredna Gora. c- The depression of Upper Thrace has an irregular form and masks the boundary between Sredna Gora and Rhodope.

BRITTLE DEFORMATION AND PALEOSTRESSES IN THE MOESIAN PLATFORM

Except for domes and depressions, the deformation of the Moesian platform is essentially characterized by brittle tectonics (BERGERAT & PIRONKOV, 1994). The most ancient exposed rocks suitable for tectonic analysis are of Lower Cretaceous age and the most recent are of Pliocene age. The brittle deformation study has been carried out in 50 sites of which 22 are in calcareous formations of Lower Cretaceous age (Valanginian to Aptian), 9 are in Maastrichtian-Paleocene calcareous formations, 12 are in Miocene formations and 7 are in the Pliocene. All sites of measurements were located in the platform itself, except 1 in the Fore-Balkan (Fig. 2).

Joints, tension gashes, tectonic stylolites and faults all occur at 45 sites. Most sites contain evidence of several tectonic events. The various populations of faults were separated by using the mechanical coherence criteria and chronological observations in the field (BERGERAT, 1994) such as crosscutting structures, tilting of early-formed structures and superposition of slickenside lineations on the same plane (Figs 4, 5). This analysis allowed us to distinguish 5 main fault systems (including 2 geometrically identical, but of different ages) that have been analyzed in terms of paleostresses (INVDIR method; ANGELIER, 1990).

E-W TO ESE-WNW COMPRESSION AND N-S TO NNE-SSW EXTENSION

A right-lateral strike-slip system with an azimuth 40° to 60° and a left-lateral one with an azimuth 150° to 160° have been identified in 25% of the measured sites in the Moesian platform (Fig. 6). These sites are all located in limestones of Valanginian to Aptian age with subhorizontal bedding dips. This fault system has not been observed in formations of Upper Cretaceous age or more recent. Moreover chronological criteria commonly indicate that it is prior to the approximately N-S compression and / or E-W extension.

Only 5 sites present a sufficient number of faults to obtain a stress tensor of good quality. The azimuth of the maximal principal stress $\sigma 1$ varies from 95° to 120° and is horizontal (Table 1).

Source : MNHN, Paris

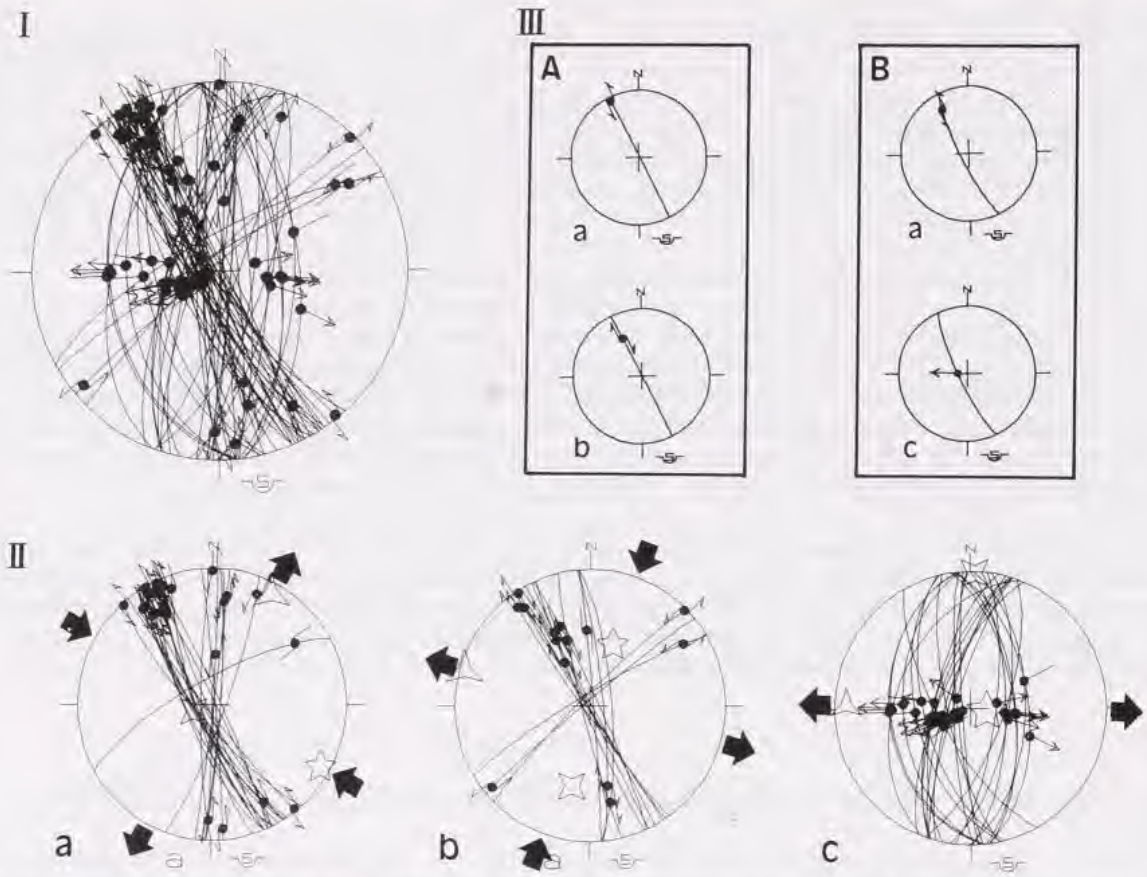

FIG. 4.— Analysis of the Carev Brod quarry (site 4, Hauterivian-Valanginian limestones), a polyphased site (after BERGERAT & PIRONKOV, 1994). Separation of the different stress states and relative chronological criteria.
I. Entire fault-slip data population represented on stereographic projections of fault planes (great circles) and slickenside lineations (divergent arrows for normal slip, convergent arrows for reverse slip, double arrows for strike-slip). Data are plotted on lower hemisphere, equal-area projections.
II. Separation of the entire population into three sets of stress tensors (cf. tables). a, Strike-slip faults compatible with ESE-WNW compression/NNE-SSW extension. b, Strike-slip faults compatible with a NNE-SSW compression/ESE-WNW extension. c, Normal faults compatible with a E-W extension. Five, four and three-prong stars represent $\sigma 1$, $\sigma 2$ and $\sigma 3$ respectively. Large black arrows indicate inferred directions for compression and extension.
III. Examples of fault planes bearing two generations of slickenside lineations. A: NNW-SSE trending fault plane with early horizontal striations showing left-lateral motion (set a) and a second one showing right-lateral motion (set b); B: Another fault plane with the same trend showing early left-lateral horizontal striations (set a) and a later dip-slip one showing normal motion (set c).

FIG. 4.— Exemple de site polyphasé : la carrière de Carev Brod (site 4, calcaires de l'Hauterivien-Valanginien) (d'après BERGERAT & PIRONKOV, 1994). Séparation des différents états de contrainte et critères de chronologie relative.
I. Lot de données brutes : projections cyclographiques des plans de failles et de leurs stries (canevas de Schmidt, hémisphère inférieur, symbolisé sur les diagrammes par un S dans un demi-cercle), flèches centrifuges : failles normales, flèches centripètes : failles inverses, doubles flèches : décrochements.
II. Séparation de la population entière de failles en trois familles. Analyse en termes de tenseurs des contraintes (cf. tableaux), a, décrochements compatibles avec une compression ESE-WNW et une extension NNE-SSW, b, décrochements compatibles avec une compression NNE-SSW et une extension ESE-WNW, c, failles normales compatibles avec une extension E-W. Étoiles à 5, 4 et 3 branches : $\sigma 1$, $\sigma 2$ et $\sigma 3$ respectivement, grosses flèches noires : directions probables de compression et d'extension.
III. Exemples de plans de failles portant deux générations de stries, A : plan de direction NNW-SSE portant une première striation, horizontale, caractéristique d'un jeu senestre (famille a) et une seconde également horizontale, postérieure, caractéristique d'un jeu dextre (famille b) ; B : autre plan de même direction portant également une première striation horizontale montrant un jeu senestre (famille a) et une seconde "dip-slip" indiquant un mouvement normal (famille c).

Source : MNHN, Paris

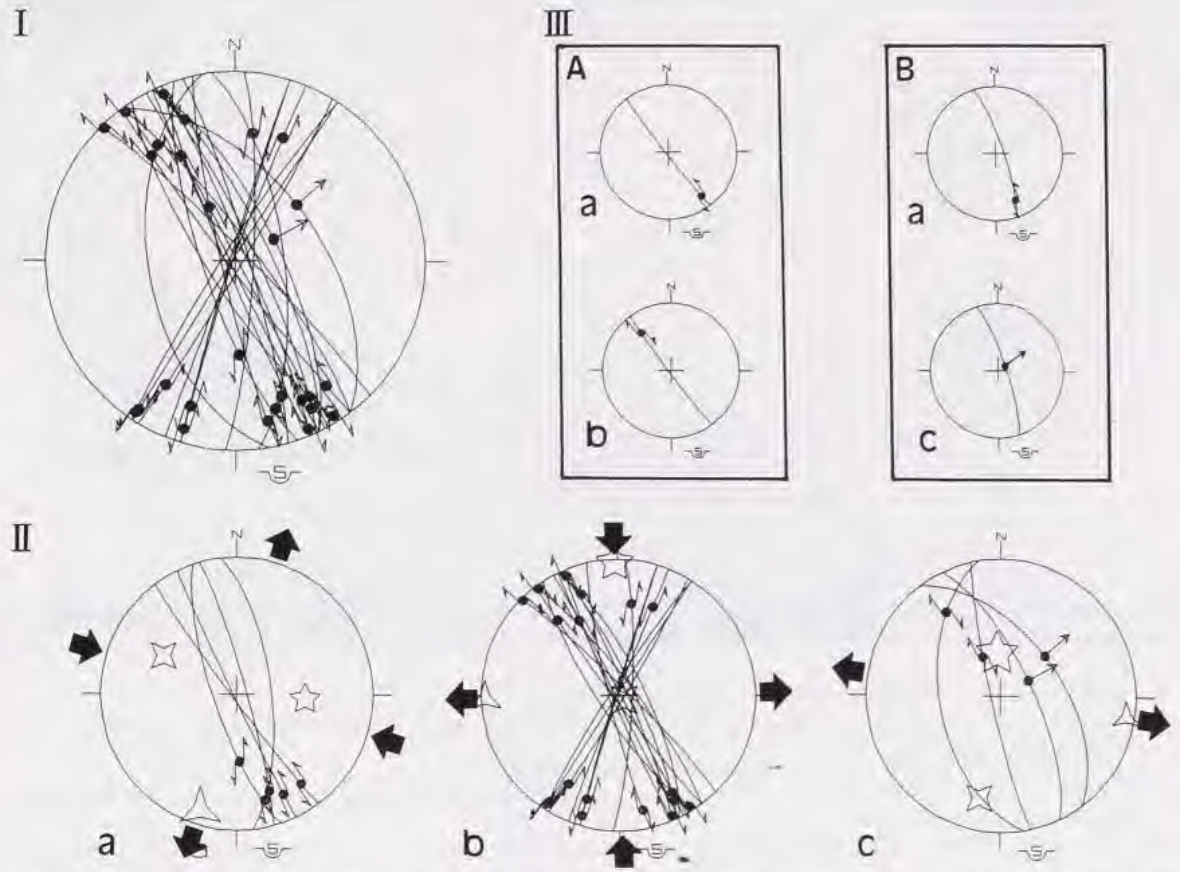

FIG. 5.— Example of polyphased site at roadcut near Devnja (site 43, Hauterivian-Valanginian limestones). Separation of the different stress states and relative chronological criteria.
I. Entire fault-slip data population.
II. Separation of the entire population into three sets. Analysis done in terms of stress tensors (cf. tables). a, Strike-slip faults compatible with a ESE-WNW compression/NNE-SSW extension. b, Strike-slip faults compatible with a N-S compression/E-W extension. c, Normal faults compatible with an E-W extension.
III. Examples of fault planes bearing two generations of slickenside lineations. A: NW-SE trending fault plane bearing early horizontal striations showing left-lateral motion (set a) and a second one showing a right lateral motion (set b). B: A NNW-SSE trending fault plane showing early left-lateral horizontal striations (set a) and dip-slip striations showing a normal motion (set c).

FIG. 5.— Exemple de site polyphasé : bord de route près de Devnja (site 43, calcaires de l'Hauterivien-Valanginien). Séparation des différents états de contrainte et critères de chronologie relative.
I. Lot de données brutes
II. Séparation de la population entière de failles en trois familles. Analyse en termes de tenseur des contraintes (cf. tableaux). a, décrochements compatibles avec une compression ESE-WNW et une extension NNE-SSW, b, décrochements compatibles avec une compression N-S et une extension E-W, c, failles normales compatibles avec une extension E-W.
III. Exemples de plans de failles portant deux générations de stries. A : plan de direction NW-SE portant une première striation, horizontale, caractéristique d'un jeu senestre (famille a) et une seconde, également horizontale, postérieure, caractéristique d'un jeu dextre (famille b). B : plan de direction NNW-SSE portant une première striation, horizontale, montrant un jeu senestre (famille a) et une seconde "dip-slip" indiquant un mouvement normal (famille c).

NNW-SSE TO NNE-SSW COMPRESSION AND ENE-WSW TO WNW-ESE EXTENSION

In 50% of the sites of the Moesian platform many strike-slip faults give a state of stress with horizontal compressive stress axis NNW-SSE to NNE-SSW. Many horizontal stylolitic peacks, trending NNE-SSW, accompany commonly the strike-slip system (Fig. 7). Identified in all formations of

Source : MNHN, Paris

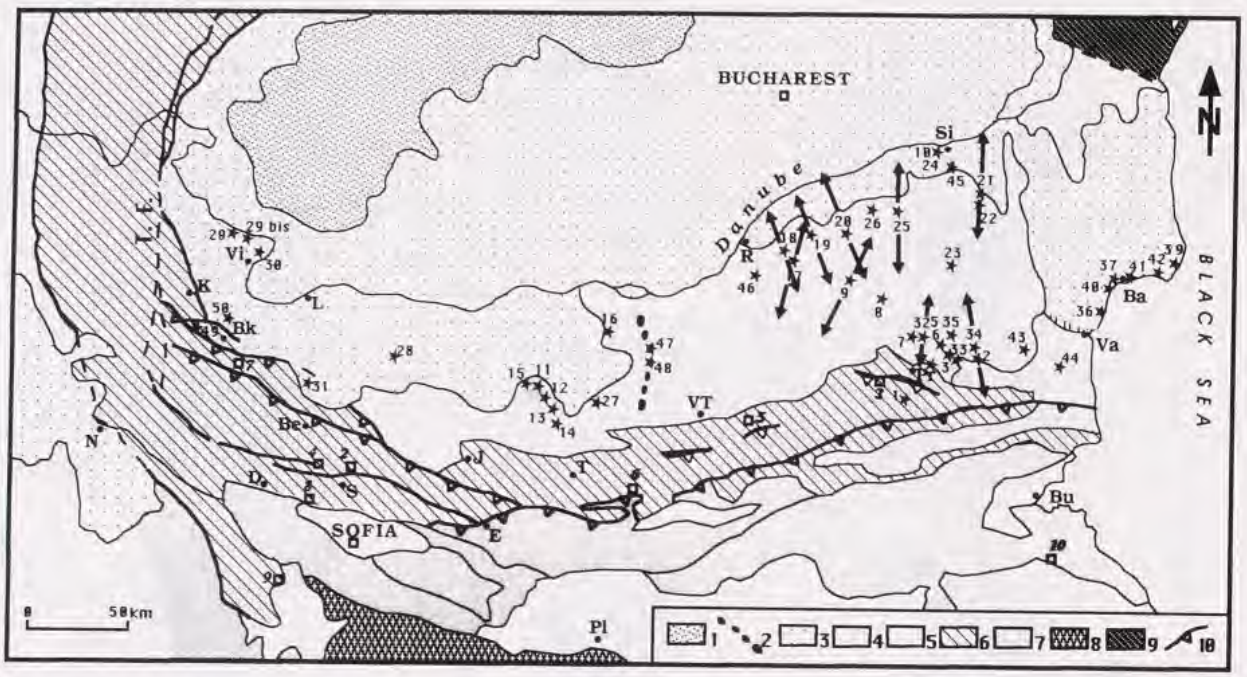

FIG. 6.— ESE-WNW to E-W compression in the Moesian platform.
Large black arrows show computed directions of compression, small black arrows show estimated directions of compression.

FIG. 6.— Compression ESE-WNW à E-W dans la plate-forme moesienne.
Les grandes flèches noires indiquent les directions de compression calculées, les petites flèches noires, les directions de compressions estimées.

N°	Locality	Age	N	σ1	σ2	σ3	Φ	α	RUP
5-6	CAREV BROD	Valanginian-Hauterivian	23	120-8	250-78	28-7	0.7	14	30
7	GARA HITRINO I	Valanginian-Hauterivian	5	94-5	285-85	184-1	0.4	7	24
9	TOPCII	Aptian	8	272-10	80-80	181-2	0.2	28	49
35	ZLATNA	Berriasian-Barremian	7	306-15	123-75	215-1	0.4	13	47
43	DEVNJA	Valanginian-Hauterivian	5	94-48	297-39	197-12	0.7	5	7

TABLE 1.— Paleostress tensor computations based on fault slip data analysis for the ESE-WNW to E-W compression.
The columns contain from left to right: Site number on figure 2 (N°) and name of the closest locality; age of the rocks; number of fault slip data (N); trend and plunge of the principal stress axes σ1, σ2, σ3 (in degrees); ratio $\Phi = (\sigma2-\sigma3) / (\sigma1-\sigma3)$; average angle between computed shear stress and observed slickenside lineation (α in degrees); ratio "upsilon" (RUP) of the INVDIR method (cf. ANGELIER, 1990). Possible values of RUP range from 0 to 200%. Average RUP values below 50% correspond to good fits between actual fault slip data distribution and computed shear stress distribution.

TABLEAU 1. — Résultats des calculs des tenseurs de paléo-contraintes pour la compression ESE-WNW à E-W. De gauche à droite : numéro du site (N°, voir localisation figure 2) et nom de la localité la plus proche ; âge des roches, nombre de failles à stries (N) ; directions et prolongements des axes de paléo-contraintes σ1, σ2 et σ3 (en degrés) ; rapport des contraintes principales $\Phi = (\sigma2 - \sigma3)/(\sigma1 - \sigma3)$; angle moyen entre strie calculée et strie réelle (α en degrés) ; rapport "upsilon" (RUP) de la méthode INVDIR (cf. ANGELIER, 1990). Valeurs possibles de RUP comprises entre 0 et 200%. Des valeurs moyennes de RUP inférieures à 50% correspondent à une bonne cohérence entre la strie réelle observée et la contrainte tangentielle calculée.

Source : MNHN, Paris

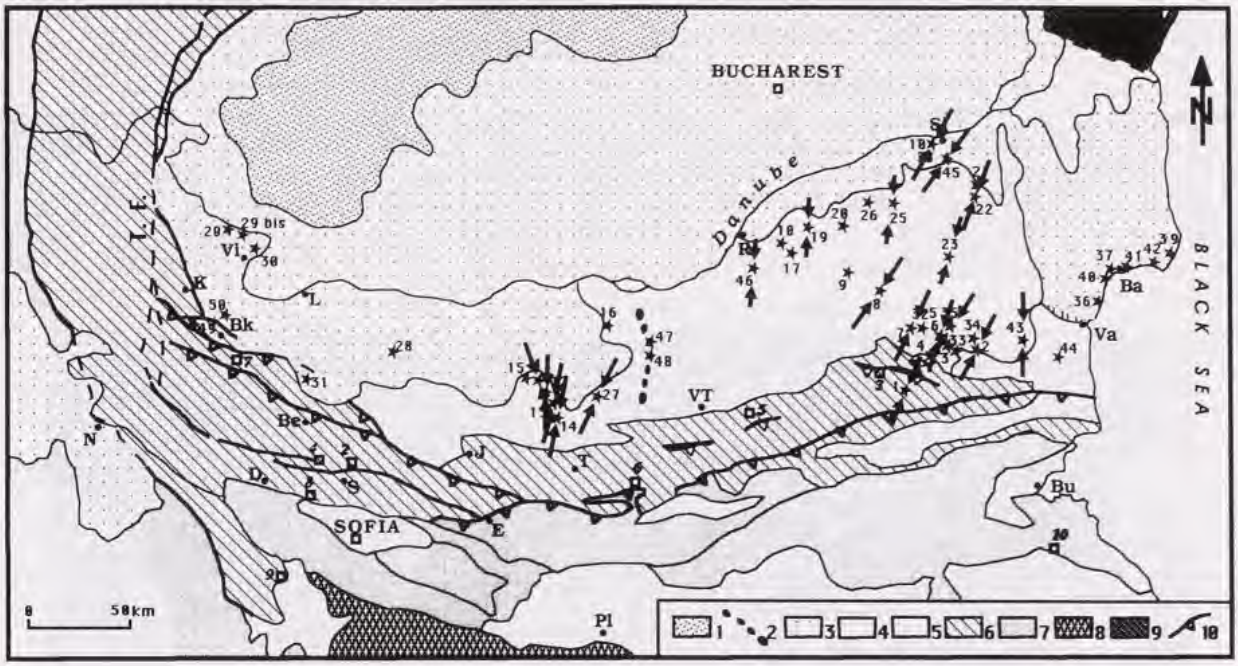

FIG. 7.— NNW-SSE to NNE-SSW compression in the Moesian platform.
Arrows as for figure 6.
FIG. 7.— Compression NNW-SSE à NNE-SSW dans la plate-forme moesienne.
Légende : voir figure 6.

Valanginian to Paleocene age, this state of stress is represented by a right-lateral fault system with an azimuth 160°-200° and a left-lateral one with an azimuth 50°-90°. Near the Fore-Balkan as well as in the Preslav anticline (Fore-Balkan, Fig. 2), these strike-slip faults are associated with many reverse faults with an azimuth 90°-135°. The inferred directions of σ1 are practically identical if we separately compute the stress tensor for strike-slip faults and for reverse faults, except for a stress permutation of σ2 and σ3 (Fig. 8). In detail at the Fore-Balkan site, strike-slip faults are clearly tilted with the layering and predate the reverse faults indicating an evolution from a strike-slip regime to a purely compressive regime during the same compression phase.

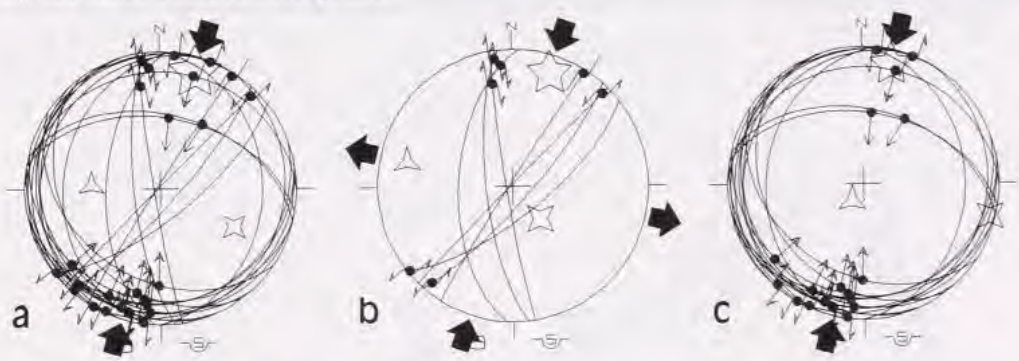

FIG. 8.— Example of σ2/σ3 stress permutations at Preslav site.
The entire fault population has been back-tilted around an average bedding plane N 115°-40°S. This fault slip data population characterizing a NNE-SSW compression (a) may be divided in two sets with (b) strike-slip faulting (σ1 and σ3 horizontal) and (c) reverse faulting (σ1 and σ2 horizontal).
FIG. 8.— Exemples de permutations des contraintes σ2 et σ3 dans le site de Preslav.
La population entière de failles (a) peut être divisée en deux familles : décrochements caractérisant une compression NNE-SSW et une extension ESE-WNW, avec σ1 et σ3 horizontaux (b), et failles inverses caractérisant une compression NNE-SSW, avec σ1 et σ2 horizontaux (c).

Source : MNHN, Paris

TABLE 2.— Paleostress tensor computations based on fault slip data analysis for the NNW-SSE to NNE-SSW compression. See caption of table 1 for definitions.

TABLEAU 2.— Résultats des calculs de tenseurs de paléo-contraintes pour la compression NNW-SSE à NNE-SSW. Légende voir tableau 1.

N°	Locality	Age	N	σ1	σ2	σ3	Φ	α	RUP
1	PRESLAV	Valanginian-Hauterivian	16	014-12	105-4	214-77	0.3	4	36
			7	019-14	140-64	283-21	0.2	8	33
2	KASPICAN	Valanginian-Hauterivian	21	33-12	228-77	123-3	0.6	13	37
5-6	CAREV BROD	Valanginian-Hauterivian	10	16-40	188-50	283-4	0.7	15	32
7	GARA HITRINO I	Valanginian-Hauterivian	9	211-10	37-79	301-1	0.5	12	33
8	RAZGRAD	Barremian	19	33-13	177-74	301-9	0.4	23	43
11	PLEVEN	Maastrichtian-Paleocene	7	351-1	229-87	81-2	0.4	17	36
12	RALOVO	Maastrichtian	16	184-17	351-73	93-4	0.7	21	50
13	TODOROVO	Maastrichtian	14	196-3	354-87	106-1	0.4	7	27
14	BEJANOVO	Maastrichtian	14	15-9	106-13	252-74	0.4	9	22
21-22	BOGOROVO	Aptian	9	18-14	236-72	110-10	0.1	13	30
10-24	SREBARNA	Pliocene	6	27-1	118-65	296-25	0.2	6	30
27	MERKOVO	Danian	9	32-8	194-82	302-2	0.6	7	27
			11	11-21	119-39	260-44	0.2	5	25
35	ZLATNA	Berriasian-Barremian	6	341-2	244-72	72-18	0.3	9	30
			6	210-14	5-75	118-6	0.9	7	17
43	DEVNJA	Valanginian-Hauterivian	18	359-3	131-86	269-3	0.5	15	38
45	PROF. ICHIRKOVO	Pliocene	4	34-11	186-78	303-6	0.5	1	29

FIG. 9.— Azimuthal dispersion of the maximal principal stress for the N-S to NNE-SSW compression (18 stress tensors computed).

FIG. 9.— Dispersion azimutale de la contrainte principale maximale pour la compression N-S à NNE-SSW (18 tenseurs calculés).

Source : MNHN, Paris

The direction of σ1 varies in all the Cretaceous-Paleocene sites of the Moesian platform between NNW-SSE and NNE-SSW with two maxima at N 15° and N 30° (Fig. 9, Table 2). However, the data do not support the presence of two distinct tectonic episodes.

A NNE-SSW compressional state of stress has also been recognized in two sites located in the Pliocene limestones of the region of Silistra (North-East of the Moesian platform; Fig. 2). Despite the poor quality of these limestones (terrestrial facies unfavorable to a good preservation of the movement indicators), one can observe left-lateral strike-slip faults of azimuth 50°-70° and right-lateral ones of azimuth 5°-10°, as well as horizontal reverse faults of azimuth 115°-120° (Fig. 10). These data allow one to define a horizontal maximum principal stress σ1 with an azimuth 30° (Table 2). A disrupted fold with an E-W trending axis in Sarmatian limestones near Balcik (site 37, Fig. 2) also shows this compression.

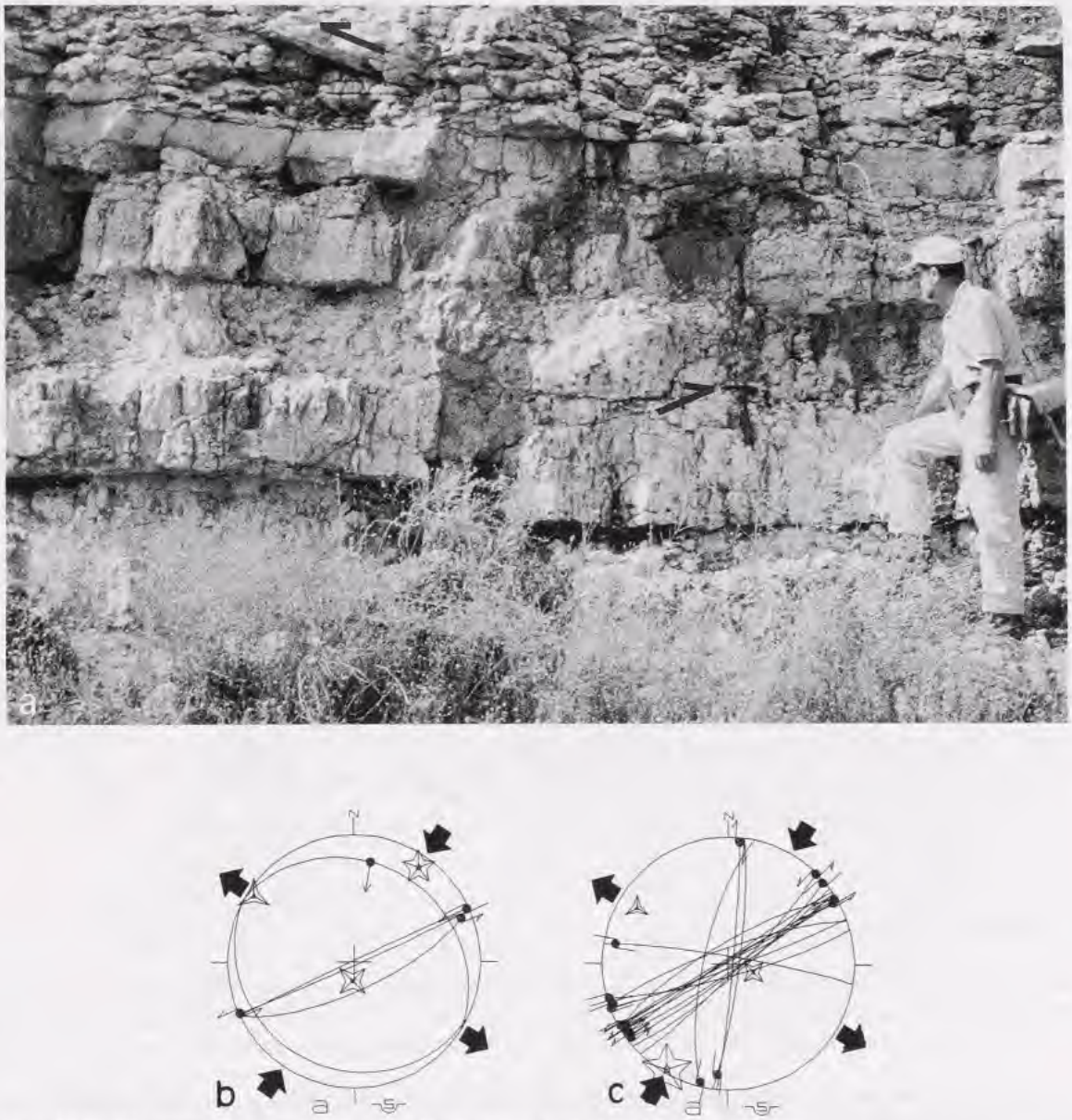

FIG. 10.— NNE-SW compression in the Pliocene, Northeastern part of the Moesian platform.
a, Reverse faults at Professor Ichirkovo; b, Stereographic projection of faults planes at Professor Ichirkovo roadcut; c, Stereographic projection of faults planes at Srebarna roadcut.

FIG. 10.— Compression NNE-SSW dans le Pliocène de la partie nord-est de la plate-forme moesienne.
a, failles inverses à Professor Ichirkovo ; projections stéréographiques des plans de failles et contraintes principales à Professor Ichirkovo (b) et à Srebarna (c).

Source : MNHN, Paris

NNW-SSE TO NNE-SSW EXTENSION

Many normal faults with an azimuth 70° to 130° have been observed in 30% of the sites, exclusively in rocks of Valanginian to Aptian age (Fig. 11) and characterize an approximately E-W σ3 axis. These normal faults predate the approximately N-S strike-slip compression, as well as the E-W extension. On the other hand, no chronological relationship has been found between the E-W compression and the approximately N-S extension.

The direction of extension σ3 resulting from the computation of stress tensors varies from N 160° to N 200° following the dominance of the set of faults with an azimuth 70°-80° or that with an azimuth 120°-130° (Table 3). There is currently no evidence to support 2 distinct fracture sets. Given the lack of chronological relations between the N-S compression and the E-W extension and the general compatibility of these two stress regimes, it is likely that they represent a single phase with a permutation of σ2 and σ3 (Fig. 12).

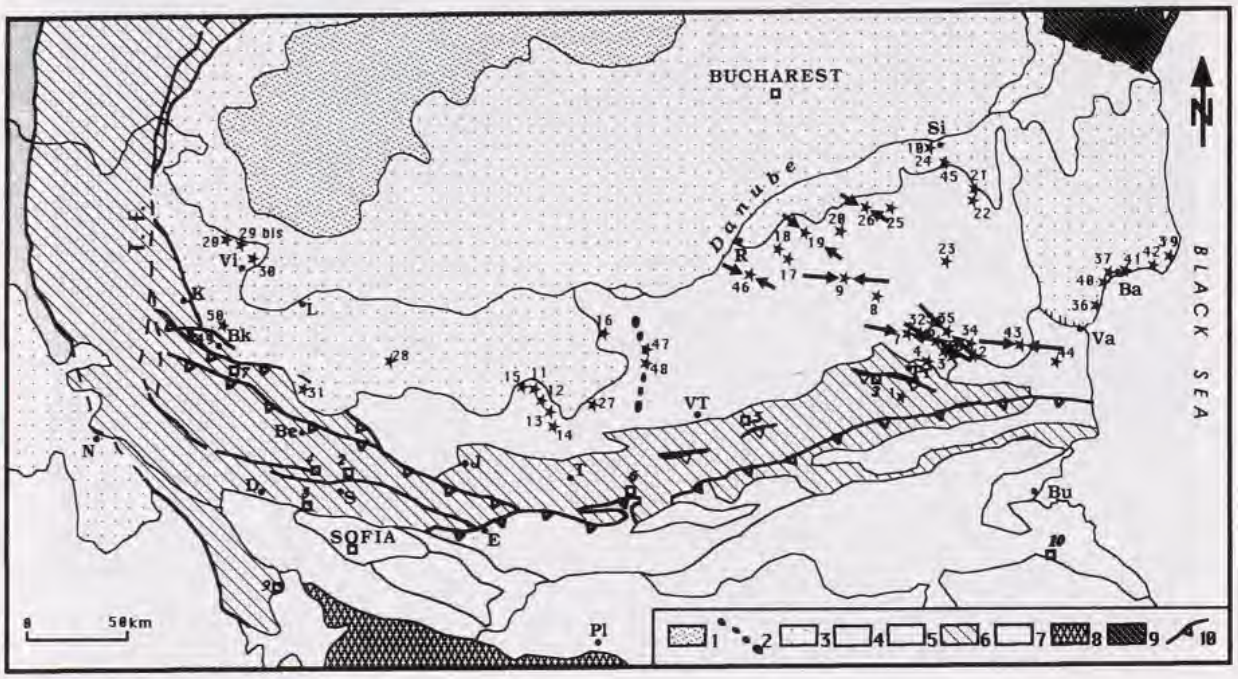

FIG. 11.— NNW-SSE to NNE-SSW extension in the Moesian platform.
Large black arrows show computed directions of extension, small black arrows show estimated directions of extension.

FIG. 11.— Extension NNW-SSE à NNE-SSW dans la plate-forme moesienne.
Les grandes flèches noires indiquent les directions d'extension calculées, les petites flèches noires, les directions d'extension estimées.

E-W TO WNW-ESE EXTENSION

Normal faults with an azimuth 170°-200° are present in 49% of the sites of Valanginian to Paleocene age and allow the characterization of a state of extensional stress E-W to WNW-ESE (Fig. 13). In most sites, the direction of extension is close to N100°-110°, with extreme values of N80° and N135° (Table 4).

The systematic presence of both strike-slip and normal faults corresponding to a same direction of σ3 in most of the sites (Table 1), as well as the systematic absence of chronological criteria between these 2 fracture sets, suggest that the difference between these extensional and strike-slip regimes is a permutation of stress σ2 and σ3 (Fig. 12).

Nevertheless one station in the Sarmatian of the region of Vidin (North-West of the Moesian platform; Fig. 2) also recorded an E-W trending extension (Fig. 14) that is necessarily younger than the

Source : MNHN, Paris

TABLE 3.— Paleostress tensor computations based on fault slip data analysis for the NNW-SSE to NNE-SSW extension. See caption of table 1 for definitions.

TABLEAU 3.— Résultats des calculs de tenseurs de paléo-contraintes pour l'extension NNW-SSE à NNE-SSW. Légende voir tableau 1.

N°	Locality	Age	N	σ1	σ2	σ3	Φ	α	RUP
9	TOPCII	Aptian	6	354-71	114-10	207-16	0.2	5	18
17	CERVEN	Aptian	4	41-71	289-8	196-17	0.5	4	33
18	NICOVO	Aptian	7	358-72	256-4	164-17	0.3	3	12
19	TITOVO	Aptian	14	277-81	76-9	166-3	0.2	21	55
20	TERTER	Aptian	9	39-85	249-5	159-3	0.2	10	34
21-22	BOGOROVO	Aptian	15	310-77	183-8	91-10	0.0	11	34
25	GLAVINICA	Aptian	8	23-74	277-5	186-16	0.3	6	17
34	STOJAN MIHAJ.	Berriasian-Barremian	5	133-85	260-3	351-4	0.4	13	41

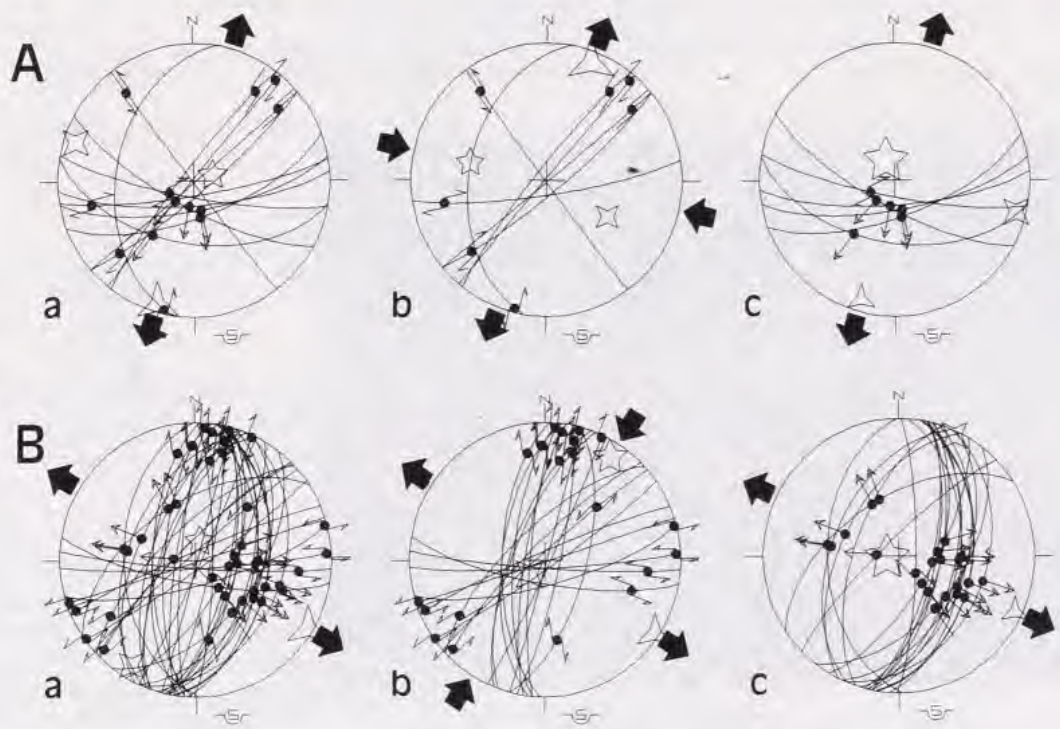

FIG. 12.— Examples of σ1/σ2 permutations. sites of Topcii (A) and Kaspican (B).
In each site, the entire fault slip data population characterizing NNE-SSW extension (A, a) or ESE-WNW extension (B, a) may be divided into two sets with (b) strike-slip faulting (σ1 and σ3 horizontal) and (c) normal faulting (σ2 and σ3 horizontal).

FIG. 12.— Exemples de permutations des contraintes σ1 et σ2 : sites de Topcii (A) et Kaspican (B).
Dans chaque site la population entière de failles caractérisant une extension NNE-SSW (Aa) ou ESE-WNW (Ba) peut-être divisée en deux familles : des décrochements avec σ1 et σ3 horizontaux (b) et des failles normales, avec σ2 et σ3 horizontaux (c).

Source : MNHN, Paris

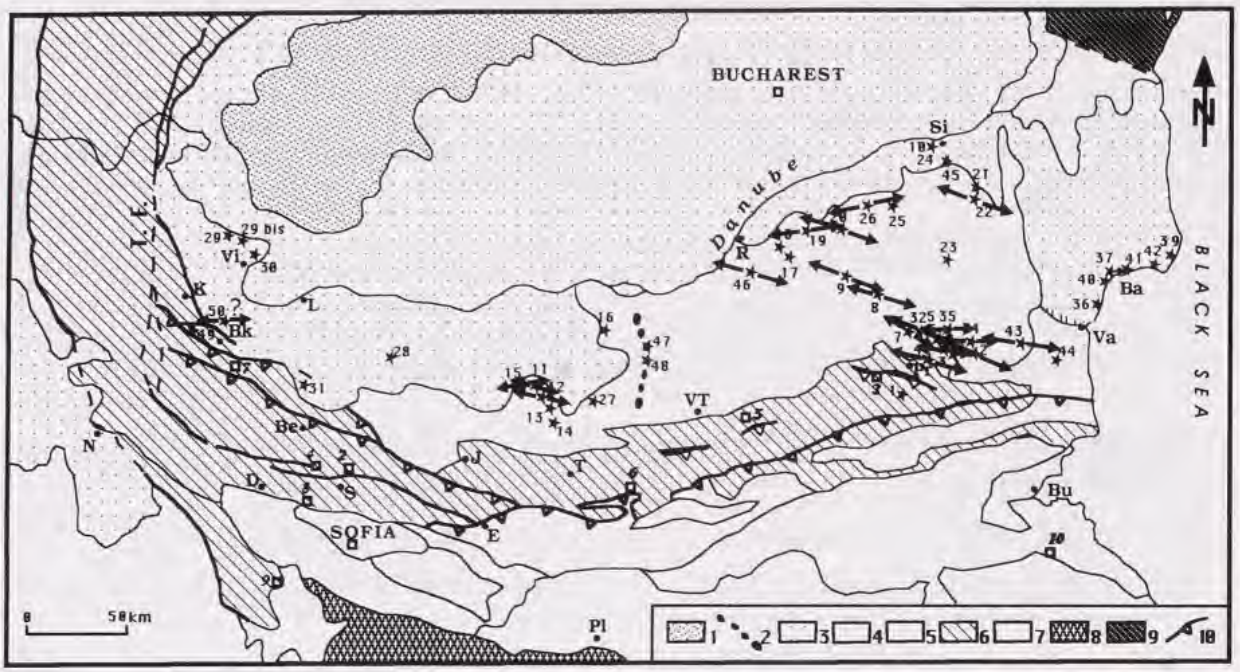

FIG. 13.— E-W to WNW-ESE extension in the Moesian platform.
Arrows as for figure 11.
FIG. 13.— Extension E-W à WNW-ESE dans la plate-forme moesienne.
Légende : voir figure 11.

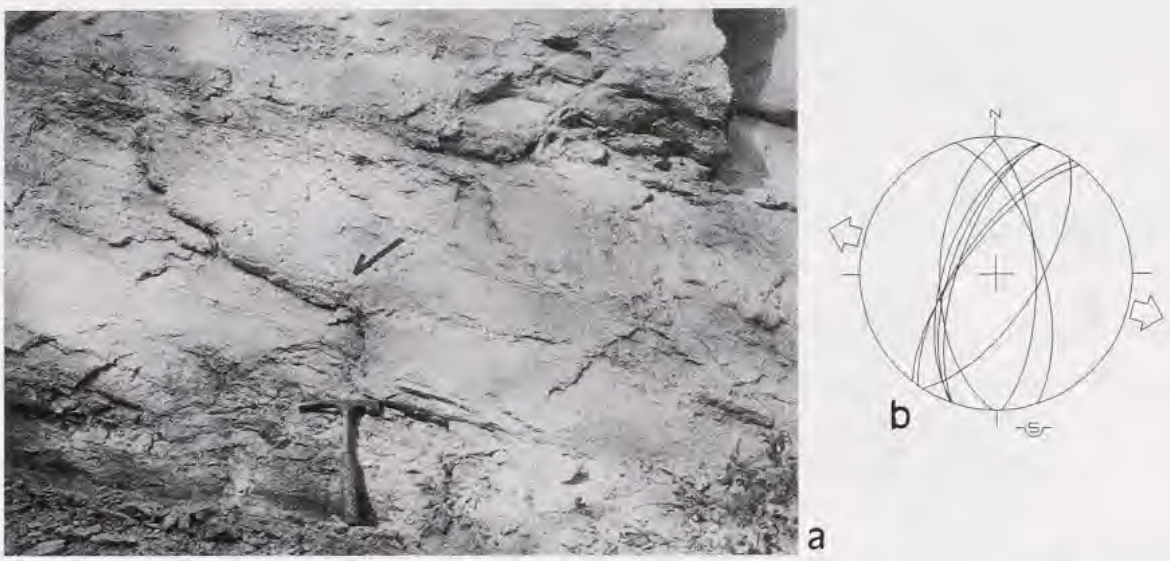

FIG. 14.— E-W extension in the middle Miocene at Dimovo.
a- Normal faults in tilted sandstone layers (average bedding plane N 180°-20°E), b- Stereographic projection of fault planes after back-tilting. White arrows as estimated direction of extension.
FIG. 14.— Extension E-W dans le Miocène moyen à Dimovo.
a : failles normales dans les couches gréseuses basculées (plan de stratification moyen : N 180°-20°E), b : projections stéréographiques des plans de failles après remise à l'horizontale de la stratification. Les flèches blanches indiquent la direction d'extension estimée.

Source : MNHN, Paris

TABLE 4.— Paleostress tensor computations based on fault slip data analysis for the E-W to ESE-WNW extension. See caption of table 1 for definitions.
TABLEAU 4.— Résultats des calculs de tenseurs de paléo-contraintes pour l'extension à ESE-WNW. Légende voir tableau 1.

N°	Locality	Age	N	σ1	σ2	σ3	Φ	α	RUP
2	KASPICAN	Valanginian-Hauterivian	22	263-83	25-4	115-6	0.2	11	2
3	MATNICA	Valanginian-Hauterivian	8	264-77	5-3	96-13	0.1	10	32
4	SUMEN	Senonian	7	276-82	17-2	107-8	0.4	4	8
5-7	CAREV BROD	Valanginian-Hauterivian	26	100-81	2-1	272-9	0.4	9	33
7	GARA HITRINO 1	Valanginian-Hauterivian	10	287-71	42-8	135-17	0.2	9	27
8	RAZGRAD	Barremian	11	160-87	20-2	290-2	0.5	13	31
9	TOPCII	Aptian	13	287-78	195-1	104-12	0.2	9	30
19	TETOVO	Aptian	24	226-73	354-10	86-13	0.2	12	37
20	TERTER	Aptian	11	85-73	188-4	279-17	0.4	6	19
21-22	BOGOROVO	Aptian	8	359-82	197-8	107-3	0.2	13	47
26	BELICA	Aptian	9	45-77	168-7	259-11	0.3	19	46
32	GARA HITRINO 2	Valanginian-Hauterivian	9	111-78	209-2	299-12	0.3	6	21
34	TOJAN MIHAJ.	Berriasian-Barremian	14	77-83	182-2	272-7	0.3	9	24
35	ZLATNA	Berriasian-Barremian	8	272-84	7-1	97-6	0.5	4	15
43	DEVNJA	Valanginian-Hauterivian	4	355-65	192-24	99-7	0.3	20	56
46	BACARBOVO	Berriasian-Barremian	7	108-74	199-0	289-16	0.4	17	41

deformation discussed above. Obviously we cannot assert from a single site located in the northwest extremity of the platform that this deformation represents the same tectonic phase because no normal faults have been observed in the Miocene of the Balcik-Varna area.

DISCUSSION

The strike-slip stress state characterized by a horizontal maximal principal stress σ1 E-W to ESE-WNW has never been identified in rocks younger than the Aptian. Moreover, in sites of Valanginian to Aptian age where it could be demonstrated, relative chronology criteria (Fig. 4) indicate that it is prior to states of stress in compression approximately N-S and / or extension approximately E-W, which affect not only the Lower Cretaceous, but also the Upper Cretaceous-Paleocene.

Similar remarks may be made concerning the state of stress characterized by normal faults and a NNW-SSE to NNE-SSW horizontal principal minimal stress σ3. This one is also only observable in rocks of Valanginian to Aptian age and always predates the N-S compression and the E-W extension. The age and directions of σ3 are identical for these two states of stress implying that it concerns a single phase characterized by an ENE-WSW to ESE-WNW maximal horizontal stress (σH max = σ1 or σ2) and a NNW-SSE to NNE-SSW minimal horizontal stress (σH min = σ3). This phase therefore corresponds to an extensional strike-slip tectonic regime. However, in the field, normal faults are clearly more abundant that strike-slip ones (Figs 6, 11) which would imply a dominantly extensional phase.

Source : MNHN, Paris

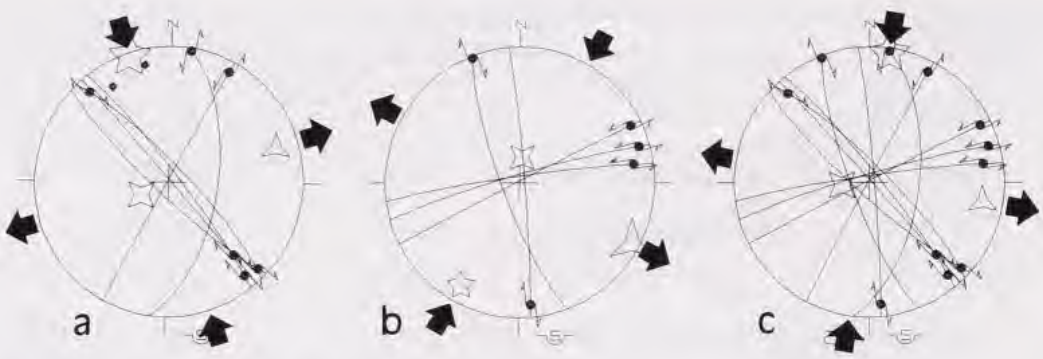

FIG. 15.— Zlatnaniva quarry (Berriasian-Barremian limestones),
This site shows NNW-SSE (a) and NNE-SSW (b) compression characterized by strike-slip faulting. The stress tensor computation for both sets shows a N-S compression (c), but some faults do not fit with the average stress tensor (due to the large dispersion in azimuth of each family, especially the left-lateral one: dispersion angle close to 90°).

FIG. 15.— Analyse de la carrière de Zlatnaniva (calcaires du Berriasien-Barremien).
Le site montre des compressions NNW-SSE (a) et NNE-SSW (b) caractérisées par des décrochements. Le calcul du tenseur des contraintes pour la population totale montre une compression N-S (c), mais plusieurs failles ne sont pas en bon accord avec ce tenseur (en raison de la grande dispersion azimutale de chaque famille, les failles senestres en particulier montrant un angle de dispersion de près de 90°).

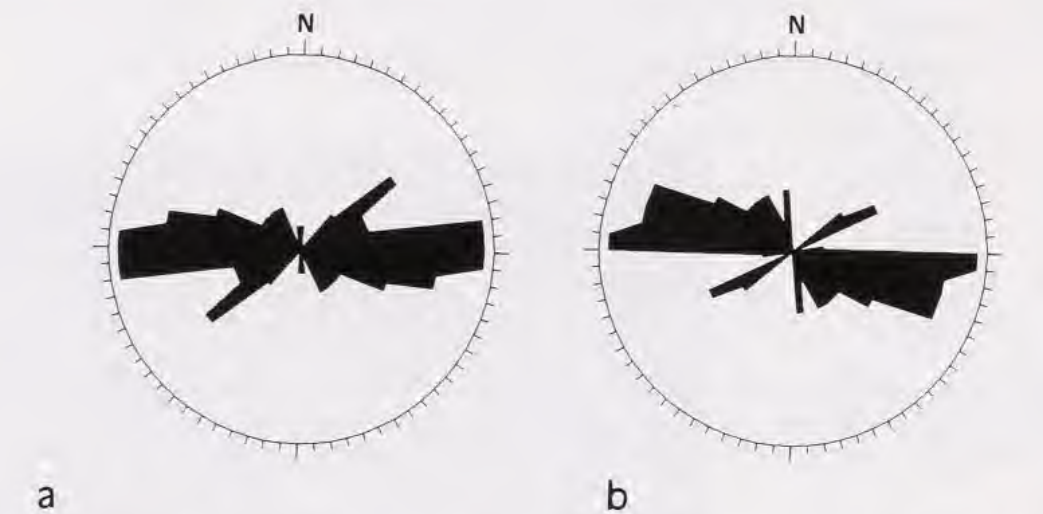

FIG. 16.— Joint directions in the Miocene (a, 49 measurements) and the Pliocene (b, 34 measurements) in the eastern part of the Moesian platform

FIG. 16.— Directions de diaclases dans le Miocène (a : 49 mesures) et le Pliocène (b : 34 mesures) de la partie orientale de la plate-forme moesienne.

The state of stress characterized by strike-slip faulting and, near the Fore-Balkan, by reverse faulting with a NNW-SSE to NNE-SSW maximal principal stress $\sigma 1$ has been recognized in all formations ranging in age from the Lower Cretaceous to the Paleocene. At the end of the middle Eocene, the folding and thrusting of the Stara-Planina and Fore-Balkan area were induced by a major compressional phase (IVANOV, 1988). The progressive change from North to South (from the Danube river to the front of the Fore-Balkan) of a strike-slip regime to a purely compressive regime with reverse faulting (Figs 7, 8) suggests that this state of stress characterizes here the same compressional phase.

Does the NNW-SSE to NNE-SSW azimuthal dispersion of the horizontal $\sigma 1$ axis (Fig. 9) correspond to a single roughly N-S compressive state of stress with temporal or local variations or does it

Source : MNHN, Paris

TABLE 5.— Paleomagnetic data from Bulgaria. The columns contain from left to right: Area of sampling; N°, site number on figure 2; Locality; age of the sampled formation; D(°), mean declination; I (°), mean inclination; authors.
TABLEAU 5.— Données paléomagnétiques de Bulgarie. De gauche à droite : région d'échantillonnage, numéro du site (N°, voir localisation figure 2), localité, âge de l'échantillon, déclinaison D(°) et inclinaison I(°), références.

Area	N°	Locality	Age	D(°)	I(°)	Reference
Fore-Balkan	1	SMOLIANOVCI	Permian-Triassic	18.72	27.15	Nozharov *et al.*, 1980
	2	BOV	Triassic	26.07	39.35	*id.*
	3	TARGOVISTE	Bajocian-Bathonian	7.4	59.2	Surmont *et al.*, 1991
Stara-Planina	4	GINCI 1	Kimmeridgian-Tithonian	7.6	53.8	*id.*
	4	GINCI 2	Tithonian-Berriasian	2.9	51.3	*id.*
	5	ELENA	Tithonian-Valanginian	8.6	56.3	*id.*
	6	NESHKOVCI	Toarcian	14.5	52	Kruczyk *et al.*, 1988
	6	KURT HISAR	Aalenian	3.7	43.3	*id.*
	6	CHIFLIK	Kimmeridgian	30.3	59.5	*id.*
	7	DOLNI LOM	Bathonian	10.8	57.4	*id.*
	7	MITROVCI	Callovian	37.3	59.4	*id.*
	7	BELI MEL	Callovian	24	68	*id.*
Sredna Gora	8	GRADEC	Bajocian-Callovian	296	67	Kruczyk *et al.*, 1990
Kraiste	9	ZABLANO	Pliensbachian	158	79	*id.*
Strandza	10	BLIZNAK	Callovian-Kimmeridgian	351	22	*id.*

correspond to two distinct stress states? Only one site out of 18 seems to have recorded two distinct stress states: One NNW-SSE (σ1: az. 341°), the other NNE-SSW (σ1: az. 210°) (Table 2, Fig. 15).

As previously shown, the state of stress characterized by normal faults and an E-W trending extension could be attributed to the same tectonic phase, characterized by strike-slip faults and both N-S trending compression and E-W trending extension. The two states of stress could then be explained by a simple permutation of stresses σ1 and σ2 (Fig. 13). However this hypothesis is based solely on mechanical coherence criteria. It would therefore consist of a tectonic phase characterized by a strike-slip compressive regime near the chain, changing into a strike-slip extensional regime within the platform to the North. No chronological criterion invalidates or confirms the synchronism of normal and strike-slip faults. One notes elsewhere that this extension has practically never been observed west of a Ruse-Veliko Tarnovo line (Fig. 12), whereas the N-S trending compression was recognized over the whole platform.

The NNE-SSW trending compression recognized in the Pliocene around Silistra (Fig. 10) would correspond to a phase syn-or post-Pliocene in age. This phase has been recognized in the Carpathians (SANDULESCU, 1988) and shown to have a N-S to NNE-SSW horizontal σ1 (HIPPOLYTE & SANDULESCU, 1996). The coaxiality of the two phases (Eocene and Pliocene) makes it difficult to know wheter all the faults measured in the Cretaceous and the Paleocene are related to the Eocene phase ; they could partly be syn-or post-Pliocene.

Finally, brittle structures other than joints are not present in any of the 8 sites studied in the Miocene of the eastern part of the platform. Although relatively distributed in direction, these joints nevertheless

Source : MNHN, Paris

show a well marked E-W maximum (Fig. 16a). One finds this same E-W trend for joints measured in the Pliocene limestones in Professor Ichirkovo (Fig. 16b), which would imply a quite recent age for these fractures.

The majority of these joints are extension fractures but small part may be hybrid-fractures. They can be related to regional stress field and are parallel or subparallel to the direction of greatest horizontal stress (HANCOCK, 1991). That supposes here a horizontal $\sigma 3$ axis close to N-S. It is difficult to interpret this recent direction of extension in the framework of the Carpatho-Balkan domain.

CONSTRAINTS FROM PALEOMAGNETISM

The most discussed question regarding the Moesian platform is whether it underwent rotation (and/or translation). For some authors (e.g. SENGÖR *et al.*, 1984), the Balkan and the Moesian platform have not undergone any post-Hercynian rotation relative to stable Europe. For others (e.g. HSÜ *et al.*, 1977), they have undergone an important counterclockwise rotation. The microtectonic analysis alone does not discriminate between these two hypotheses. Thus we have analyzed the available paleomagnetic data (Fig. 2). The data considered come from rocks of Permian to Lower Cretaceous age in the Fore-Balkan (NOZHAROV *et al.*, 1980; SURMONT *et al.*, 1991), the Stara Planina (KRUCZYK *et al.*, 1988; SURMONT *et al.*, 1991) and the Sredna Gora, Kraiste and Strandza zones (KRUCZYK *et al.*, 1990).

The results of analyses undertaken by NOZHAROV *et al.* (1980) in the Northwestern part of the Fore-Balkan are compatible with values obtained for the Moesian platform. Similarly, sites analyzed in the whole Stara Planina by KRUCZYK *et al.* (1988) show neither relative rotation between its western and central parts, nor rotation relative to stable Europe.

Paleomagnetic studies realized by SURMONT *et al.* (1991) in the western part of the Fore-Balkan and the central and eastern parts of the Stara Planina indicate that these zones have undergone a low amplitude counterclockwise rotation (about 10°-15°) as compared to the Eurasia. This result was obtained using the theoretical evolution of the declination of a site centered on the external Balkanides, assuming it was rigidly linked to Eurasia, and the curve of pole drift of the Eurasia established by WESTPHAL *et al.* (1986). The use of the synthetic curve proposed for Eurasia by these authors lead to a much smaller rotation. According to SURMONT *et al.* (1991) the rotation occurred during the Eocene phase.

The investigations led by KRUCZYK *et al.* (1990) on Jurassic sediments of Sredna Gora, Kraiste and Strandza, and compared to reference data for the European platform imply a counterclockwise rotation of southern Bulgaria of approximately 10° to 20°. These results compared to those obtained on magmatic rocks of the Sredna Gora, of Santonian-Campanian age (NOZHAROV *et al.*, 1987), suggest that Jurassic rocks have acquired their post-folding magnetic remanence at the end of the Upper Cretaceous (KRUCZYK *et al.*, 1990). The difference between the magnetic declination and the geomagnetic field expected for the Upper Cretaceous in Southern Bulgaria (by using the curve of pole drift of WESTPHAL *et al.*, 1986) indicates a counterclockwise rotation of 10° to 20° with respect to Eurasia.

If one considers the all of these results together, despite differences of interpretation according to authors, the whole Moesian platform, Fore-Balkan and Stara Planina area, including even the Sredna Gora, has undergone a small or null rotation (maximum counterclockwise rotation: 20°) by reference to stable Europe. This postulated rotation may have occurred at the end of the Upper Cretaceous, as suggested by KRUCZYK *et al.* (1990), since the direction of the Eocene compression characterized by the analysis of microtectonic data in the Moesian platform is close to that recognized, for the same period, immediately westward in the Pannonian Basin (FODOR *et al.*, 1992), as well as in the whole western European platform (LETOUZEY *et al.*, 1986; BERGERAT, 1985, 1987).

A major rotation of the Moesian-Balkan domain did not occur according to existing paleomagnetic data.

A study of Mesozoic series of the Unit of Bihor (Apuseni Mountains, Romania) by SURMONT (1989) has shown a remagnetization in the Upper Cretaceous-Paleocene. During and after this remagnetization, the Bihor Unit has undergone a clockwise rotation of approximately 60° as compared to the Eurasia, that SURMONT (1989) interprets, at least partly, as due to the pushing of Moesia. This Unit belongs to the South-Pannonian block (Tisza), as well as the Mecsek and Villany Mountains in Hungary. The position of this block at the beginning of the Tertiary is poorly constrained and controversial (BALLA, 1985; CSONTOS *et al.*, 1992; CSONTOS, 1995). In the present state of our knowledge, one can neither confirm

Source : MNHN, Paris

nor invalidate the hypothesis of a westward translation of Moesia, nor constrain its role in the rotation of the Tisza.

CONCLUSION

No compressive event recorded in the Moesian platform can, by its direction or by its age, correspond to the major phase that has affected parts of the Sredna Gora and the Strandza-Eastern Rhodope during the Albian.

The oldest tectonic phase that seems to have affected the Moesian platform since the beginning of the Cretaceous is the post-Aptian and pre-Maastrichtian phase with an E-W to ESE-WNW trending compression and a N-S to NNE-SSW trending extension. Although characterized both by strike-slip and normal faults, the abundance of normal faults and their systematic presence in most sites show that this phase is dominantly extensional. It is thus tempting to relate deformation of the Moesian platform to extension that occurred since the Senonian in the Eastern Stara Planina (flysch of Emine).

The major phase dating from the end of the middle Eocene (IVANOV, 1988), has been recorded in all rocks of Cretaceous and Paleocene age of the Moesian platform. This phase corresponds to the formation of significant in the Balkan and the Rhodope. According to NACHEV (1980), the formation of structures was generated in two episodes, one after the lower Paleocene and one after the middle Eocene. One can perhaps see in the distribution of $\sigma 1$ directions (NNW-SSE to NNE-SSW) the trace of these two episodes.

Finally, the last recognizable tectonic phase, affecting Pliocene limestones in the Northwestern part of the platform, corresponds probably to a phase well known in the Romanian Carpathians (SANDULESCU, 1988) and little mentioned in Bulgaria until now (BERGERAT & PIRONKOV, 1994). This phase, has a direction of compression close to N-S, that is practically identical to the Eocene phase in the Bulgarian part of the Moesian platform. In the Southern Carpathians in contrast the same direction of compression is present in the Late-Miocene and Pliocene, but is quite different in the early-middle Miocene (HIPPOLYTE & SANDULESCU, 1996). This therefore demonstrates a notable geodynamical change during the Miocene in the Carpathians area.

The Alpine evolution of the Moesian platform can be characterized in terms of stages, from the beginning of the Upper Cretaceous to the Pliocene, related both to the opening of the Black Sea and to the convergence of the Eurasian and Arabo-African plates.

The timing and mechanism of the formation of the Black Sea basin have been long debated and contradictory models for its origin have been proposed (e.g. ADAMIA *et al.*, 1974; BOCCALETTI *et al.*, 1974; BRINKMANN, 1972; HSÜ *et al.*, 1977; FINETTI, 1995; FINETTI *et al.*, 1988; LETOUZEY *et al.*, 1977; MANETTI *et al.*, 1988; OKAY *et al.*, 1994; ZONENSHAIN & LE PICHON, 1986). However, the latest geological and geophysical data indicate that the western Black Sea has an oceanic nature and confirm its interpretation as a back arc basin, behind the Rhodope-Pontide arc. Subduction initiated in the Aptian-Cenomanian of the neo-Tethys ocean northward beneath the Eurasian margin (Fig. 17a) caused the development of the arc and the basin (SENGÖR & YILMAZ, 1981; GÖRUR, 1988; OKAY *et al.*, 1994). Using this model, some authors (HSÜ *et al.*, 1977; OKAY *et al.*, 1994) proposed that the Senonian Sredna Gora rifting is related to that of the Black Sea (Fig. 17a).

The extensional phase ($\sigma 3$ NNW-SSE to NNE-SSW) in the Moesian platform, post-Aptian-pre-Maastrichtian in age, may also be related to this extension. Some of the normal faults produced during this extensional event, are preserved and evident on seismic reflection lines of the Moesian platform area where one can see that the normal fault activity terminated before the end of the Cretaceous (FINETTI *et al.*, 1988).

At the end of the Paleocene, the opening of the western Black Sea was completed.

The consumption of the Tethyan oceanic crust produced an important compressive tectonic event that affected the Great Caucasus, Crimea and Balkanides (FINETTI, 1995).

The Rhodope fragment, collided with the Southern edge of the Eurasian plate inducing the development of nappes originating from the Rhodope basement, followed by thrusting farther to the North in the Balkan (Fig. 17b).

This compressive phase, of middle Eocene age in the Balkan, has also been recorded in the Moesian platform, dominantly by strike-slip faulting in a NNW-SSE to NNE-SSW compressive stress field.

Source : MNHN, Paris

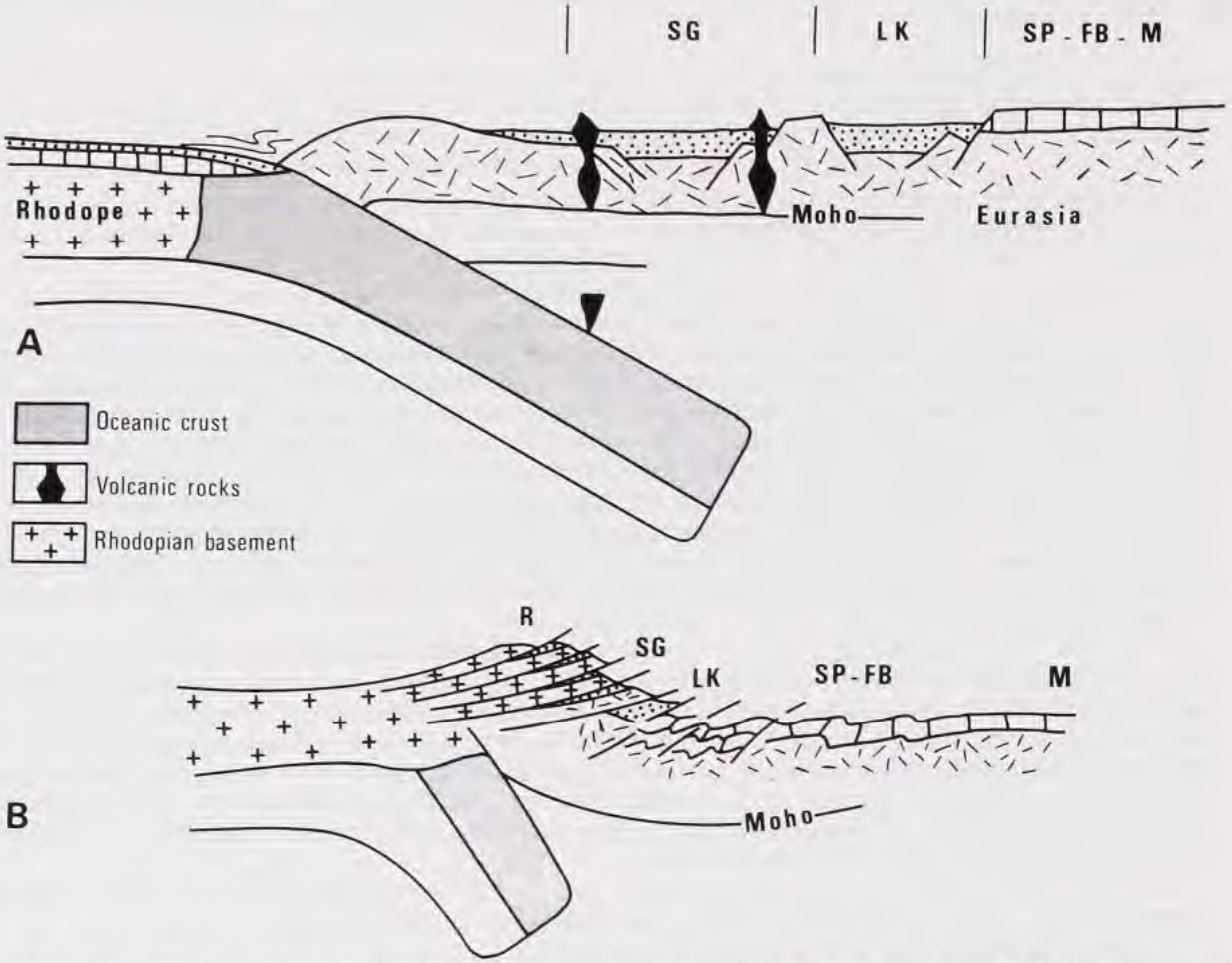

FIG. 17.— Upper Cretaceous (A) and middle Eocene (B) geodynamical stages of the Balkanides (modified after DERCOURT in DURAND-DELGA *et al.*, 1988; IVANOV, 1988).
Abbreviations are as follows: R, Rhodope; SG, Sredna Gora; LK, Luda Kamcija; SP, Stara Planina; FB; Fore-Balkan; M, Moesian platform.

FIG. 17.— Géodynamique des Balkanides au Crétacé supérieur (A) et à l'Eocène moyen (B) (modifié d'après DERCOURT in DURAND - DELGA et al., 1988 ; IVANOV, 1988).
R : Rhodope, SG : Sredna Gora, LK : Luda Kamcija, SP : Stara Planina, FB : Prébalkan, M : plate-forme moesienne.

Finally, continuing convergence caused compression, as shown by the small reverse and strike-slip faults yielding a NNE-SSW compression in the Pliocene of the Moesian platform.

ACKNOWLEDGEMENTS

This study was carried out as part of the Peri-Tethys program. Special thanks are given to Z. IVANOV for his constructive observations and to P. HANCOCK for his review. We acknowledge V. CARRERE and M. GORDON for improving the English of this paper.

REFERENCES

ADAMIA, S.A., GAMKRELIDZE, I.P., ZAKARIADZE, G.S. & LORDKIPANIDZE, M.B., 1974.— Adjaro-Trialetian depression and problem of formation of deep basin of the Black Sea. *Geotectonika*, **1**: 78-94 (in Russian).

Source : MNHN, Paris

ANGELIER, J., 1990.— Inversion of field data in fault tectonics to obtain the regional stress. II: a new rapid direct inversion method by analytical means. *Geophysical Journal International*, **103**: 363-376.

BALLA, Z., 1984.— The Carpathian loop and Pannonian basin: a kinematic analysis. *Geophysical Transactions*, **30** (4): 313-353.

BERGERAT, F., 1985.— *Déformations cassantes et champs de contrainte tertiaires dans la plate-forme européenne*. Thèse de Doctorat d'État ès Sciences naturelles, Université Pierre et Marie Curie, Paris, France. Also published as *Mémoires des Sciences de la Terre*, **85-07**: 1-315.

BERGERAT, F., 1987.— Stress fields in the European platform at the time of Africa-Eurasia collision. *Tectonics*, **6** (2): 99-132.

BERGERAT, F., 1994.— From inversion methods to paleostress field reconstructions in platforms, chains and basins: an overview. Some examples in Western and Central Europe. *In*: F. ROURE (ed.), *Peri-Tethyan Platforms: Proceeding of the IFP Peri-Tethys Research Conference held in Arles, France, March 23, 1993*. Technip, Paris: 159-178.

BERGERAT, F. & PIRONKOV, P., 1994.— Déformations cassantes et contraintes crétacées à actuelles dans la plate-forme Moesienne (Bulgarie). *Bulletin de la Société géologique de France*, **165** (5): 447-458.

BOCCALETTI, M., GOCEV, P. & MANETTI, P., 1974.— Mesozoic isopic zones in the Black Sea Region. *Bollettino della Società de Geologia Italiana*, **93**: 547-565.

BONCEV, E., 1940.— Aus der alpidischen Tectonik Bulgariens. *Zeitschrift der Bulgarischen geologischen Gesellschaft*, **12** (3): 157-247.

BONCEV, E., 1988.— Notes sur la tectonique alpine des Balkans. *Bulletin de la Société géologique de France*, **4** (2): 241-249.

BRINKMANN, R., 1974.— Geologic relations between Black Sea and Anatolia. *In*: E.T. DEGENS & D.A. ROSS (eds), The Black Sea - Geology, chemistry and biology. *American Association of Petroleum Geologists, Memoir*, **20**: 63-76).

CSONTOS, L., 1995.— Tertiary tectonic evolution of the intra-carpathian area: a review. *Acta Vulcanologica*, **7**: 1-13.

CSONTOS, L., NAGYMAROSY, A., HORVATH, F. & KOVAC, M., 1992.— Tertiary evolution of the Intra-Carpathian area: a model. *Tectonophysics*, **208**: 221-241.

DERCOURT, J. & RICOU, L.E., 1987.— Discussion sur la place de la Bulgarie au sein du système alpin. *Review of the Bulgarian Geological Society*, **48** (3): 1-14.

DERCOURT, J., ZONENSHAIN, L.P., RICOU, L.E., KAZMIN, G.V., LE PICHON, X., KNIPPER, L.A., GRANDJACQUET, C., SBORSHCHIKOV, M.I., BOULIN, J., SOROKHTIN, O., GEYSSANT, J., LEPVRIER, C., BIJU-DUVAL, B., SIBUET, J. C., SAVOSTIN, A. L., WESPHAL, M. & LAUER, J.P., 1985.— Présentation de neuf cartes paléogéographiques au 1/20 000 000 s'étendant de l'Atlantique au Pamir pour la période du Lias à l'Actuel. *Bulletin de la Société géologique de France*, **1** (5): 637-653, 9 cartes h.t.

DERCOURT, J., ZONENSHAIN, L.P., RICOU, L.E., KAZMIN, V.G., LE PICHON, X., KNIPPER, A.M., GRANDJACQUET, C., SBORSHCHIKOV, I.M., GEYSSANT, J., LEPVRIER, C. & PECHERSKY, D.H., 1986.— The geological evolution of the Tethys belt from the Atlantic to the Pamir since the Liassic. *Tectonophysics*, **123**: 241-315.

FINETTI, I.R., 1995.— Geophysical study of the Black Sea. *Peri-Tethys Meeting, Milan*, Abstract Volume: 1.

FINETTI, I., BRICCHI, G., DEL BEN, A., PIPAN, M. & XUAN, Z., 1988.— Geophysical study of the Black Sea. *Bollettino di Geofisica Teorica ed Applicata*, **30** (117-118): 197-324.

FODOR, L., MAGYARI, A., KAZMER, M. & FOGARASI, A., 1992.— Gravity-flow dominated sedimentation on the Buda paleoslope (Hungary): record of Late Eocene continental escape of the Bakony unit. *Geologische Rundschau*, **81** (3): 695-716.

GÖRÜR, N., 1988.— Timing of opening of the Black Sea basin. *Tectonophysics*, **147**: 247-262.

HANCOCK, P.L., 1991.— Determining contemporary stress directions from neotectonic joint systems. *Philosophical Transactions of the Royal Society of London*, **337** (A): 29-40.

HIPPOLYTE, J.C. & SANDULESCU, M., 1996.— Paleostress characterization of the "Wallachian phase" in its type area (Southeastern Carpathians, Romania). *Tectonophysics*. **263**: 235-248.

HSÜ, K.J., 1977.— Tectonic evolution of the Mediterranean basins. The Eastern Mediterranean. *In*: A.E.M. NAIRN & W.H. KANES (eds), *The Ocean Basins and Margins*. Vol. 4A: *The Eastern Mediterranean*. Plenum Press, New-York: 29-75.

IVANOV, Z., 1988.— Aperçu général sur l'évolution géologique et structurale du massif des Rhodopes dans le cadre des Balkanides. *Bulletin de la Société géologique de France*, **4** (2): 227-240.

KRUCZYK, J., KADZIALKO-HOFMOKL, M., NOZHAROV, P., PETKOV, N., & NACHEV, I., 1988.— Paleomagnetism of Jurassic sediments from Balkan, Bulgaria. *Acta Geophysica Polonica*, **37** (1): 49-62.

KRUCZYK, J., KADZIALKO-HOFMOKL, M., NOZHAROV, P., PETKOV, N. & NACHEV, I., 1990.— Paleomagnetic studies on sedimentary Jurassic rocks from southern Bulgaria. *Physics of the Earth and Planetary Interiors*, **62**: 82-96.

LETOUZEY, J., 1986.— Cenozoic paleo-stress pattern in the Alpine Foreland and structural interpretation in a platform basin. *Tectonophysics*, **132**: 215-231.

LETOUZEY, J., BIJU-DUVAL, B., DORKEL, A., GONNARD, R., KRISTCHEV, K., MONTADERT, L. & SUNGURLU, O., 1977.— The Black Sea: a marginal basin. Geophysical and geological data. *In*: B. BIJU-DUVAL & L. MONTADERT (eds), *International Symposium on Structural History of Mediterranean Basins*. Technip, Paris: 363-376.

MANETTI, P., BOCCALETTI, M. & PECCERILLO, A., 1988.— The Black Sea: remnant of a marginal basin behind the Srednogorie-Pontides Island- Arc system during the upper Cretaceous- Eocene times. *Bollettino di Geofisica Teorica ed Applicata*, **30** (117-118): 39-51.

Source : MNHN, Paris

NACHEV, I., 1977.— Olistostromes in the Tithonian flysch of Bulgaria. *Review of the Bulgarian Geological Society*, **37** (1): 43-52 (in Bulgarian).

NACHEV, I., 1978.— On the Upper Cretaceous basin model in the Srednogorie zone. *Comptes Rendus de l'Académie bulgare des Sciences*, **31** (2): 213-216.

NACHEV, I., 1980.— Island arc model and alpine evolution of Bulgaria. *Review of the Bulgarian Geological Society*, **41** (3): 230-247 (in Bulgarian).

NICOLOV, T. & KRISCHEV, K., 1965.— Principles of the stratigraphy and lithology of the lower Cretaceous in the Fore-Balkan. *Bulletin of the Geological Institute, Series stratigraphy and tectonics*, **6**: 77-115.

NOZAROV, P., DOLAPCHIEVA, M. & KRUSTEV, N., 1987.— Paleomagnetism and rocks physical properties from the Gutzal plutonium (Bulgaria). *Bulgarian Geophysical Journal*, **13** (1): 85-91.

NOZHAROV, P., PETKOV, N., YANEV, S., KROPACEK, V., KRS, M. & PRUNER, P., 1980.— Paleomagnetism and Magnetic Anisotropy of Stephanian-Triassic sediments from NW Bulgaria. *Bulgarian Geophysical Journal*, **6** (2): 97-104.

OKAY, A.I., SENGOR, A.M.C. & GÖRÜR, N., 1994.— Kinematic history of the opening of the Black Sea and its effect on the surrounding regions. *Geology*, **22**: 267-270.

RICOU, L.E., DERCOURT, J., GEYSSANT, J., GRANDJACQUET, C. & LEPVRIER, C., 1986.— Geological constraints on the Alpine evolution of the Mediterranean Tethys. *Tectonophysics*, **123**: 83-122.

RICOU, L.E., ZONENSHAIN, L.P., DERCOURT, J., KAZMIN, V., LE PICHON, X., KNIPPER, A., GRANDJACQUET, C., SBORSHCHIKOV, M.I., GEYSSANT, J., LEPVRIER, C., PECHERSKY, M., BOULIN, J., SIBUET, J.C., SAVOSTIN, L.A., SOROKHTIN, O., WESTPHAL, M., BAZHENOV, M.L., LAUER, J.P. & BIJU-DUVAL, B., 1985.— Méthodes pour l'établissement de neuf cartes paléogéographiques de l'Atlantique au Pamir depuis le Lias. *Bulletin de la Société géologique de France*, **1** (5): 625-635.

SANDULESCU, M., 1988.— Cenozoic tectonic history of the Carpathians. *In*: L.H. ROYDEN& F. HORVATH (eds), the Pannonian basin. A study in basin evolution. *American Association of Petroleum Geologists, Memoir*, **45**: 17-25.

SENGÖR, A.M.C., 1984.— The Cimmeride Orogenic system and the tectonics of Eurasia. *Geological Society of America, Special Paper*, **195**: 181-241.

SENGÖR, A.M.C. & YILMAZ, Y., 1981.— Tethyan evolution of Turkey: a plate tectonic approach. *Tectonophysics*, **75**: 181-241.

SURMONT, J., 1989.— *Etude paléomagnétique des chaînes alpines de la Méditerranée moyenne (Hellénides, Carpathes, Balkanides): conséquences paléogéographiques*. Thèse, Université Pierre et Marie Curie, Paris, France. Also published as *Mémoires des Sciences de la Terre*, **89-19**: 1- 289.

SURMONT, J., NIKOLOV, T., THIERRY, J., PEYBERNES, B. & SAPUNOV, I., 1991.— Paléomagnétisme des formations sédimentaires jurassiques et éocrétacées des zones de Stara Planina-Prébalkan et de Luda Kamcija (Balkanides externes, Bulgarie). *Bulletin de la Société géologique de France*, **162** (1): 57-68.

WESPHAL, M., BAZHENOV, M.L., LAUER, J.P., PECHERSKY, D.M. & SIBUET, J.C., 1986.— Paleomagnetic implications on the evolution of the Tethys belt from the Atlantic ocean to the Pamirs since the Triassic. *Tectonophysics*, **123**: 37-82.

ZONENSHAIN, L.P. & LE PICHON, X., 1986.— Deep basins of the Black Sea and Caspian Sea as remnants of mesozoic back-arc basins. *Tectonophysics*, **123**: 181-211.

Source : MNHN, Paris

8

Scythian Platform: chronostratigraphy and polyphase stages of tectonic history

Anatoly M. NIKISHIN [1], *Sierd CLOETINGH* [2], *Sergey N. BOLOTOV* [1], *Evgenij Yu. BARABOSHKIN* [1], *Ludmila F. KOPAEVICH* [1], *Bronislav P. NAZAREVICH* [1], *Dmitry I. PANOV* [1], *Marie-Françoise BRUNET* [3], *Andrei V. ERSHOV* [1], *Vera V. ILINA* [1], *Svetlana S. KOSOVA* [4] & *Randell A. STEPHENSON* [2]

[1] Geological Faculty, Moscow State University, 119899 Moscow, Russia

[2] Vrije Universiteit, De Boelelaan 1085, 1081 HV Amsterdam, The Netherlands

[3] Département de Géotectonique, CNRS URA 1759, case 129, Université P. et M. Curie 75252 Paris Cedex 05, France

[4] Central Geophysical Expedition, Moscow, Russia

ABSTRACT

The tectonic history of the Scythian Platform, overlying the pre-Mesozoic folded basement, is presented on the basis of chronostratigraphic and subsidence history data. The following stages can be recognized: Early Triassic-Carnian - origin of continental rift system; pre-Norian-Hettangian - syncollisional orogeny; Sinemurian-early Aalenian - synrift uplift; late Aalenian-pre-Callovian - syncompressional regional subsidence with pre-Callovian uplift; Callovian-Tithonian - synrift subsidence and uplift; early Berriasian - compressional deformations; late Berriasian-Barremian - regional subsidence; Aptian-Albian - continental rift system origination; Late Cretaceous-Eocene - thermal regional subsidence complicated by stress events; Oligocene-early Miocene - syncompressional regional subsidence; middle Miocene-Quaternary - syncollisional molasse basin formation with five main compressional phases.

RÉSUMÉ

La plate-forme Scythe : chronostratigraphie et histoire tectonique polyphasée.

L'histoire tectonique de la plate-forme Scythe, reposant sur un socle plissé anté-mésozoïque est présentée sur la base de données de reconstitution de la chronostratigraphie et de la subsidence. On peut reconnaître les étapes suivantes : Trias inférieur-Carnien - origine du système de rift continental; pré-Norien-Hettangien - orogenèse syncollisionelle ; Sinémurien-Aalénien inférieur - soulèvement synrift; Aalénien supérieur-pré-Callovien - subsidence régionale syncompression accompagnée d'un soulèvement d'âge pré-Callovien; Callovien-Tithonique - subsidence synrift et soulèvement; Berriasien inférieur - déformations en compression ; Berriasien supérieur-Barrémien - subsidence régionale ; Aptien-Albien - origine du système de rift continental ; Crétacé supérieur-Eocène - subsidence régionale d'origine thermique, compliquée par des variations des contraintes tectoniques ; Oligocène-Miocène inférieur - subsidence régionale syncompression ; Miocène moyen-Quaternaire - formation de bassins molassiques syncollisionels avec cinq phases principales de collision.

NIKISHIN, A.M., CLOETINGH, S., BOLOTOV, S.N., BARABOSHKIN, E.Y., KOPAEVICH, L.F., NAZAREVICH, B.P., PANOV, D.I., BRUNET, M.-F., ERSHOV, A.V., ILINA, V.V., KOSOVA, S.S. & STEPHENSON, R.A., 1998.— Scythian Platform: chronostratigraphy and polyphase stages of tectonic history. *In*: S. CRASQUIN-SOLEAU & É. BARRIER (eds), Peri-Tethys Memoir 3: stratigraphy and evolution of Peri-Tethyan platforms. *Mém. Mus. natn. Hist. nat.*, **177** : 151-162. Paris ISBN : 2-85653-512-7.

Source : MNHN, Paris

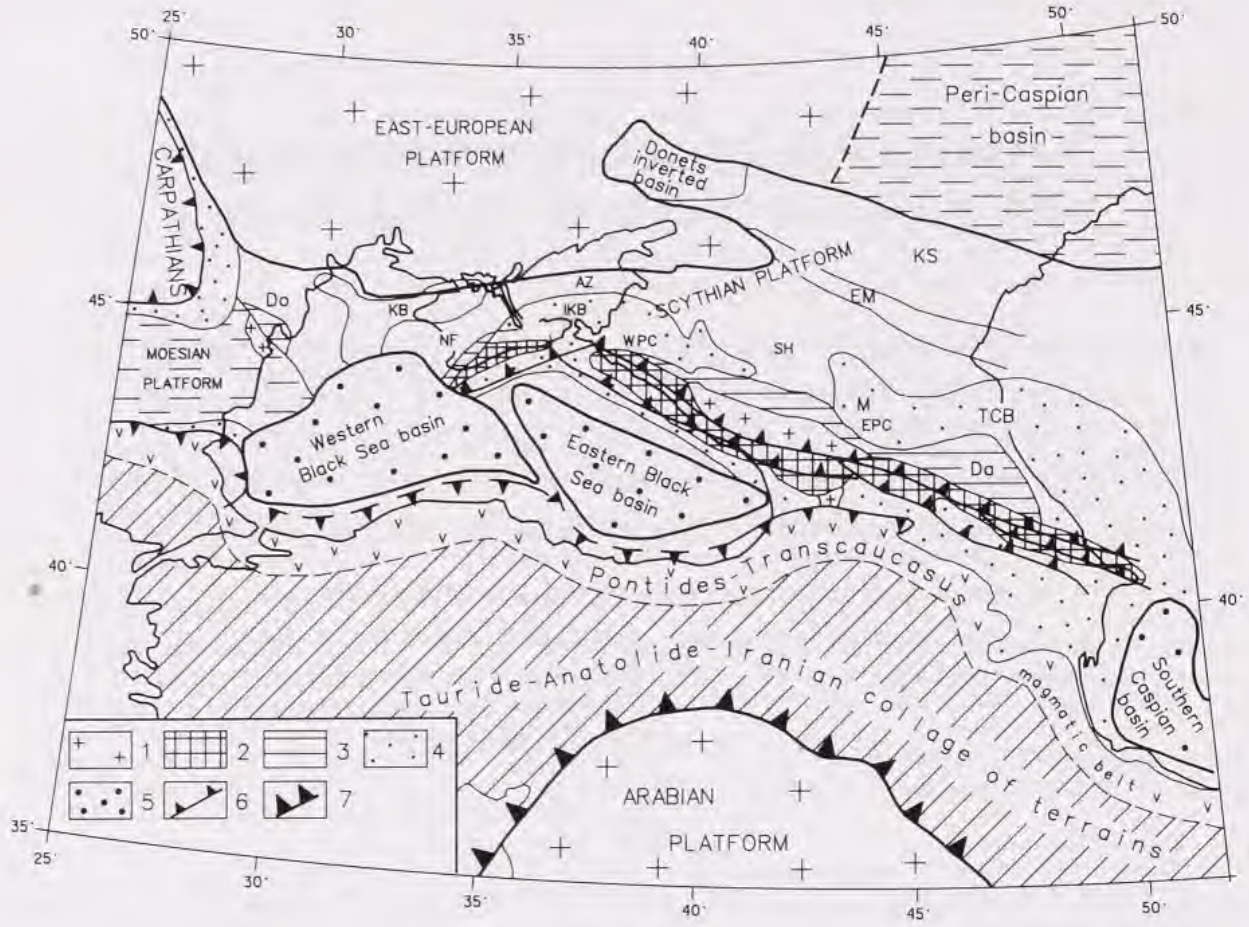

FIG. 1.— Tectonic position of the Scythian Platform. **1-3**, Great Caucasus-Southern Crimea-Dobrogea orogen: **1**, pre-Mesozoic basement; **2**, intensively folded / thrusted Mesozoic and (or) Cenozoic; **3**, gently deformed Mesozoic and (or) Cenozoic (deformed margins of the Scythian Platform); **4**, Late Cenozoic molasse basin; **5**, basin with oceanic or very thinned continental crust; **6**, thrust zone; **7**, zone of continental subduction in Zagros. Some basins and other tectonic units: Az - Azov Basin (recent Azov Swell), Da - Dagestan basin, Do - Dobrogea orogen, EM - East Manych basin, EPC - Eastern Pre-Caucasus basin (includes western part of the Terek-Kuban basin, Mozdok basin and in pre-Neogene times - Dagestan basin), IKB - Indol-Kuban molasse basin, K - Kayasula basin, KB - Karkinitsky (Northern Crimea) basin, KS - Karpinsky Swell, M - Mozdok basin, NF - Novo-Fedorovsk basin, SH - Stavropol High, TCB - Terek-Caspian molasse basin, WPC - Western Pre-Caucasus basin (includes Indol-Kuban molasse basin).

*FIG. 1.— Carte tectonique de la Plate-forme Scythe. **1-3**, Orogène Grand Caucase-Crimée méridionale-Dobrogée : **1**, socle anté-Mésozoïque ; **2**, Mésozoïque et (ou) Cénozoïque intensément plissé / chevauché ; **3**, Mésozoïque et (ou) Cénozoïque faiblement plissé / chevauché (marges déformées de la Plate-forme Scythe) ; **4**, bassin molassique Cénozoïque supérieur ; **5**, bassin avec une croûte océanique ou une croûte continentale très amincie ; **6**, zone de chevauchement ; **7**, zone de subduction continentale dans le Zagros. Quelques bassins et autres unités tectoniques : Az - bassin d'Azov (récemment ride d'Azov), Da - bassin du Dagestan, Do - Dobrogée, orogène, EM - bassin du Manych oriental, EPC - bassin oriental du Pré-Caucase (comprenant la partie occidentale du bassin Térek-Kuban, le bassin de Mozdok et à l'anté-Néogène - le bassin du Dagestan), IKB -bassin molassique d'Indol-Kuban, K - bassin de Kayasula, KB - bassin de Karkinitsky (Crimée septentrionale), KS - ride de Karpinsky, M - bassin de Mozdok, NF - bassin de Novo-Fedorovsk, SH - Haut de Stavropol, TCB - bassin molassique Térek-Caspien, WPC - bassin occidental du Pré-Caucase (comprenant le bassin molassique d'Indol-Kuban).*

Source : MNHN, Paris

INTRODUCTION

The Scythian Platform is located between the Great Caucasus-South Crimea orogen to the South, and the East European Platform to the North (Fig. 1). It includes the Scythian Platform itself underlain by a Late Paleozoic folded basement and covered by the Terek-Caspian and Indol-Kuban foreland molasse basins of the Great Caucasus-Southern Crimea orogen.

This region is relatively well investigated (MILANOVSKY & KHAIN, 1963; MILANOVSKY, 1968; CHEKUNOV *et al.*, 1976; KORONOVSKY *et al.*, 1987; GOFMAN *et al.*, 1988; ROSTOVTSEV, 1992; LETAVIN, 1980; KUNIN *et al.*, 1989). The thickness of sedimentary basin cover is typically more than 5 km and up to 12 km. The following lithostratigraphic complexes make up the sections of the Scythian Platform: Triassic, Jurassic-Eocene, Oligocene-lower Miocene, middle Miocene-Quaternary.

CHRONOSTRATIGRAPHY OF THE SCYTHIAN PLATFORM

The stratigraphy of the Scythian Platform is based on the data from a few hundreds of wells.

These data are summarized on the chronostratigraphic profiles located in the eastern Pre-Caucasus area and Crimea area (Figs 2-4).

Early-Middle Triassic-early Carnian: Lower-Middle Triassic and lower Carnian strata are located in a few rift-type basins and were folded and partially eroded in pre-Norian and pre-Aalenian-Bajocian times. Two main sedimentary basins, the East-Pre-Caucasus basin and West-Pre-Caucasus-Crimea basin

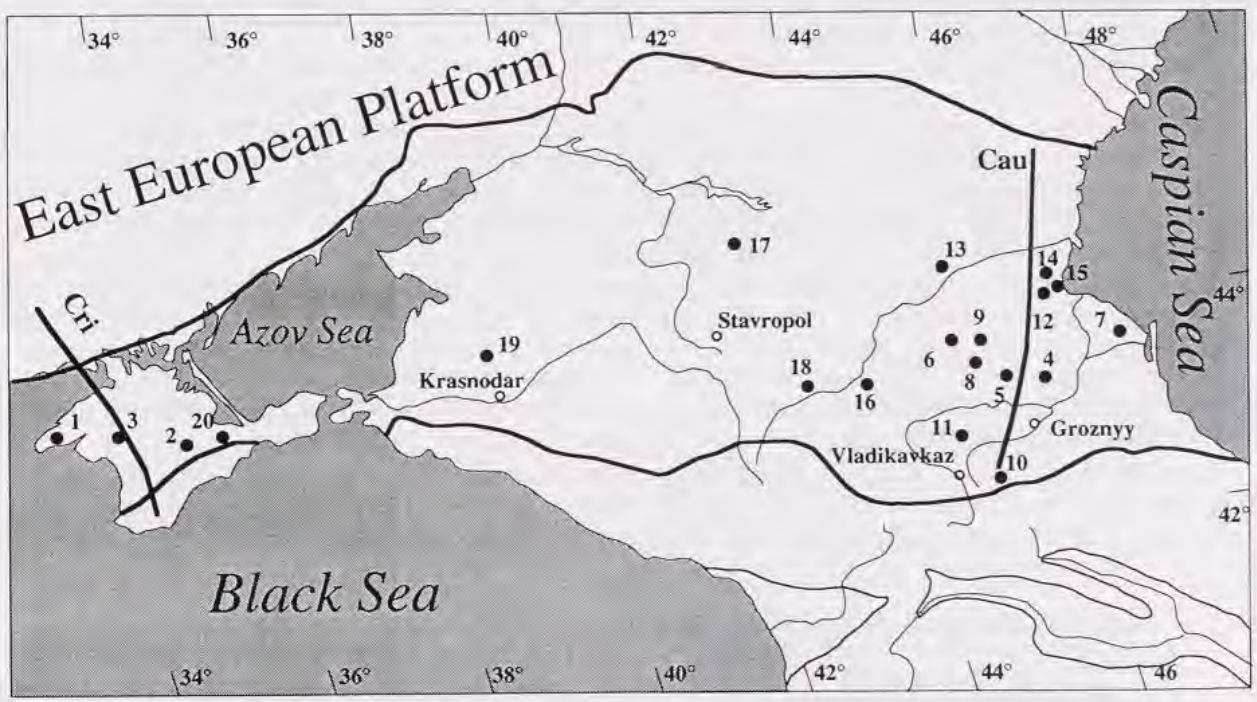

FIG. 2.— Location map. Solid lines: Cau. - location of the chronostratigraphic profile for the eastern Pre-Caucasus region (see figure 3), Cri. - location of the chronostratigraphic profile for the Central-Northern Crimea (see figure 4). Numbers - location of wells used for backstripping analysis (see figure 5).

FIG. 2.— Carte de localisation. Trait plein: Cau. - localisation du profil chronostratigraphique de la région orientale du Pré-Caucase (voir figure 3), Cri. - localisation du profil chronostratigraphique de la région centrale du nord de la Crimée (voir figure 4). Chiffres - localisation des forages utilisés pour l'analyse du " backstripping " (voir figure 5).

Source : MNHN, Paris

were separated by the Central-Pre-Caucasus (Stavropol) High. The East-Pre-Caucasus basin was represented by a water covered rift system. It is possible to recognize at least three paleorift troughs of East-West trend: East Manych to the North, Mozdok to the South and Kayasula in the middle (NAZAREVICH *et al.*, 1986; NIKISHIN *et al.*, 1994). A few remnants of other rift valleys can be proposed too. The East Manych trough was a shallow and then a relative deep-water trough with clay, marl, carbonate uncompensated sedimentations and volcanic centres. Kayasula trough had a same paleogeography, but was shallower and carbonate sedimentation dominated together with volcanism. Underwater high between East Manych and Kayasula troughs was covered by carbonatic reef belt. Preliminary data of flysch-like sediments in the Mozdok basin suggest that this trough was a part of an Early-Middle Triassic passive margin.

Reliable stratigraphic data on the West-Pre-Caucasus-Crimean area are absent. It was a marine sedimentary basin with Northern-Crimea-Azov and Novo-Fedorovsk rift-like troughs with carbonate, clay and clastic depositions (SLAVIN, 1986; BOIKO, 1993; BOIKO *et al.*, 1986). The Lower-Middle Triassic of the West-Kuban (West-Pre-Caucasus) basin is represented by carbonates and clastic deposits. The paleowater-depth increased to the direction of recent Great Caucasus (BOIKO *et al.*, 1986). Possibly uplift, erosion and deformation took place in a pre-Norian time.

Late Triassic: three main Late Triassic sedimentary basins in the Scythian Platform can be recognized: the East-Pre-Caucasus or Nogaisk basin, West-Pre-Caucasus or West Kuban basin and the Crimea region. The Nogaisk basin originated at the site of the former Early-Middle Triassic rift system. It covers East Manych-Kayasula-Mozdok rifted basins. The Nogaisk basin was a continental volcanogenic-molasse basin of the Norian-Rhaetian age (NAZAREVICH *et al.*, 1986). It was filled by sands, silts, conglomerates and volcanics (andesites, rhyolites, ignimbrites, tuffs). The Karpinsky Swell zone was upthrusted to the Nogaisk basin (NAZAREVICH *et al.*, 1986; NIKISHIN *et al.*, 1994; SOBORNOV, 1995). The Great Caucasus region and Karpinsky Swell zone were main sources of clastic material. The Central Pre-Caucasus (Stavropol) area was an uplifted (mountain-?) region. The West-Pre-Caucasus basin underwent structural changes; flysch, bioherm and shallow-water clastic sediments formed in different subzones of the former basin (BOIKO, 1993; PRUTSKY & LAVRISCHEV, 1989). At the margin of the Great Caucasus basin a carbonate reef belt originated (BOIKO *et al.*, 1986). The former Azov-Northern-Crimea rift basin suffered inversion tectonics. The data on Central-Northern Crimea are very poor (SLAVIN, 1986); in a few wells Late Triassic dacites, andesites and intrusions of diorites have been drilled.

In all these basins Late Triassic complexes unconformably overlie older sediments. The Late Triassic is mainly represented by Norian-Rhaetian. The presence of the early Carnian is more local, restricted probably to Carnian marine sediments. Hettangian sediments are not documented in the Scythian Platform. It appears that the main orogenic deformations took place in the late Carnian-pre-Norian time, at the Rhaetian / Hettangian boundary and in Hettangian.

Early Jurassic: the Scythian Platform was an uplifted area during the Hettangian, probably as a result of syncompressional tectonics. The Sinemurian is absent as well, possibly due to thermal synrift uplift (the rifting took place in the zone of recent Great Caucasus). Sinemurian sedimentation took place along the Great Caucasus trough. Pliensbachian and Toarcian strata are located in a few rift-like troughs with a typical width of about 30 km and thickness of sediments (mainly claystones and siltstones with possible Pliensbachian dacites and rhyolites) about 150-200 meters (STAFEEV *et al.*, 1995).

Aalenian-Bathonian: during the late Aalenian-early Bathonian a regional subsidence of the Scythian Platform took place (KORONOVSKY *et al.*, 1987; PANOV & GUSCHIN, 1987). The main sedimentary basins were the following: the Kalmyksky basin (in the Karpinsky Swell zone), East-Pre-Caucasus

---

FIG. 3.— Chronostratigraphic profile for the Eastern Pre-Caucasus region, for location see figure 2 (solid line Cau.). Lithology is simplified: **1**, limestones; **2**, marls mainly; **3**, clays; **4**, siltstones; **5**, sandstones; **6**, conglomerates; **7**, evaporites; **8**, deep-water turbidites; **9**, basalts mainly; **10**, volcanic arc complex (volcanites, flysch, clastic sediments); **11**, acidic volcanites and molasse; **12**, erosional boundary; **13**, orogenic event with folding / thrusting and uplift; **14**, rift phase; **15**, compressional phase.

*FIG. 3.— Profil chronostratigraphique de la région orientale du Pré-Caucase, position figure 2 (ligne Cau.). La lithologie est simplifiée : **1**, calcaires ; **2**, marnes ; **3**, argiles ; **4**, microgrès ; **5**, grès ; **6**, conglomérats ; **7**, évaporites ; **8**, turbidites d'eau profonde ; **9**, principalement basaltes ; **10**, complexe d'arc volcanique (volcanites, flysch, sédiments clastiques) ; **11**, volcanites acides et molasse ; **12**, limite d'érosion ; **13**, événement orogénique avec plissement / chevauchement et soulèvement ; **14**, phase extensive ; **15**, phase compressive.*

Source : MNHN, Paris

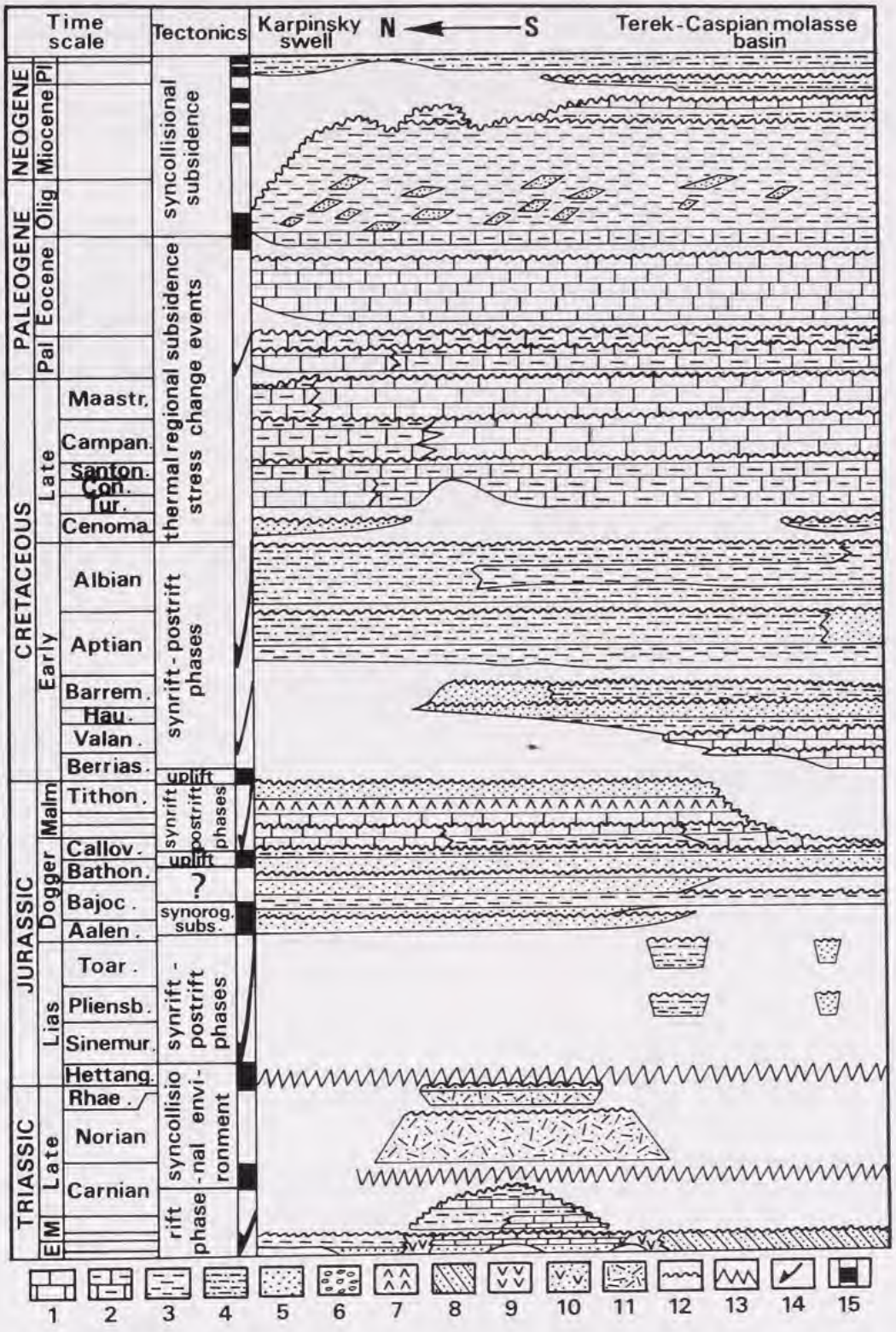

Source : MNHN, Paris

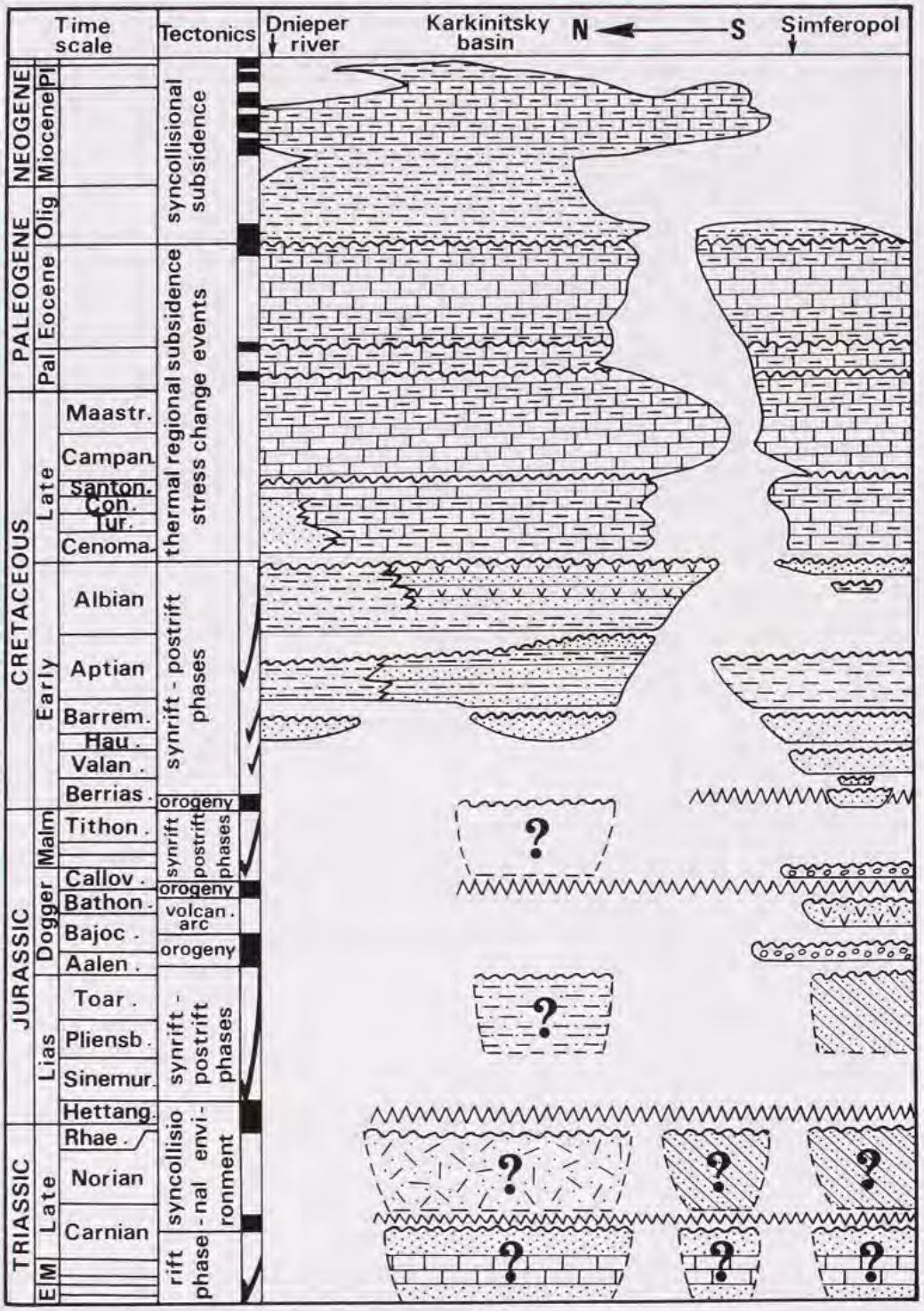

FIG. 4.— Chronostratigraphical profile for the Central-Northern Crimea, for location see figure 2 (solid line Cri.). Lithology is simplified. For legend, see figure 3.

FIG. 4.— Profil chronostratigraphique de la région centrale du nord de la Crimée, position figure 2 (ligne Cri.); la lithologie est simplifiée. Pour la légende voir figure 3.

Source : MNHN, Paris

basin, East-Kuban basin and West-Kuban basin in the West-Pre-Caucasus area, and the Southern-Crimea-Great Caucasus deep-water trough (orogenic zone). All the basins were filled by clay and silt deposits mainly. During late Aalenian-Bajocian-earliest Bathonian time, main epoch of the Scythian Platform subsidence occurred. It was a time of major subduction-related magmatism in the Transcaucasus area and orogenic activity inside the Great Caucasus belt. The East-European Craton was the main source of the clastic material supply. The basins water-depths were not deep, and coal-bearing sediments originated in several places. The late Bathonian-early Callovian is mainly a gap in the stratigraphy being a time of syncompressional uplift and minor erosion.

Callovian-Tithonian: the Callovian-Late Jurassic was the next epoch of the Scythian Platform history. Although sedimentary basins were nearly the same as in the Middle Jurassic, configurations and structure of the basins changed. Shallow-water sedimentation dominated during the Callovian-early Oxfordian, with deposition of clays, silts, conglomerates and carbonates. A few more deep areas were located in the central parts of the basins. In the middle-late Oxfordian, the paleogeography was nearly the same. Reef belts began to grow around the deep parts of the basins, and uncompensated sedimentation took place in the central portions of the basins. In the Kimmeridgian-Tithonian, after the changes of basin configuration and uplift of the southern marginal zone of the Scythian Platform, evaporite sedimentation dominated. This phase marks the most important evaporite event in the Scythian Platform history. Callovian-Upper Jurassic sedimentations had a great diversity and were very heterogeneous. At the end of the Tithonian and in the Berriasian, a change of paleogeography took place together with a weak uplift and compressional tectonics (MILEEV *et al.*, 1995). An angular unconformity can be recognized in a few seismic profiles at the Jurassic / Cretaceous boundary or intra-Berriasian.

Early Cretaceous: the Early Cretaceous was the following stage of the platform cover formation. It was a time of unstable tectonic environments inside the Scythian Platform. The following sedimentary basins can be recognized: the East-Pre-Caucasus (Dagestan) basin, West-Pre-Caucasus (Kuban) basin, Northern Crimea (Karkinitsky) basin, South-Western Crimea (Western Pre-Yaila) basin, South-Eastern Crimea (Eastern Pre-Yaila) basin, the Salgir Graben in the centre of the Southern Crimea, and the Great Caucasus deep-water trough. Carbonate and terrigenous shallow-water sediments dominated in the Early Cretaceous of the Scythian Platform. We can recognize two main substages of history in the Early Cretaceous: late Berriasian-Barremian, and Aptian-Albian. During the first substage shallow-water sedimentation dominated but although the tectonic setting is not clear, a tensional regime is probable. The Aptian-Albian was a time of continental rifting, but more accurate stratigraphical and structural data are required to recognize different events in this history. The Salgir Graben in the Southern Crimea originated in the Aptian-early Albian (MURATOV, 1969). Karkinitsky (Northern Crimea) deep graben (more than 3 km of sediments) was active in Aptian-Albian with volcanism in the middle-late Albian (MURATOV, 1969; CHEKUNOV *et al.*, 1976; GRIGORIEVA *et al.*, 1981), but subsidence started in the Barremian or late Hauterivian. Belogorsk (or Eastern-Pre-Yaila) graben (more than 1 km of sediments) originated in the Aptian-Albian in the south-eastern portion of the Crimea. Kuban basin and Dagestan basin suffered rapid subsidence. Volcanism took place in a number of regions in the middle-late Albian-earliest Cenomanian (GRIGORIEVA *et al.*, 1981).

Late Cretaceous: the Late Cretaceous consists of a carbonate platform cover on the Scythian Platform and the southern part of the Russian Platform. The relatively deepest parts of the basin were close to the Great Caucasus trough and overlying some Early Cretaceous rifted basins (for example - the Karkinitsky basin). The Great Caucasus trough was the deep-water basin with a flysch sedimentation mainly.

Paleocene-Eocene: the Paleocene-Eocene paleogeography was nearly the same as in the Late Cretaceous. Carbonate shallow-water sedimentation dominated round the Scythian Platform. The deepest portions of the basins were close to the Great Caucasus trough, and some changes of basins configuration can be observed in the Platform, pointing to some changes of tectonics in the Paleocene and at the Paleocene / Eocene boundary.

Oligocene-early Miocene (Maykop time): during the Oligocene - early early Miocene time, the Maykop formation had been formed. The Maykop formation is widespread in areas of the Scythian Platform, Great Caucasus trough, Black Sea basin, and the Turan Platform. It has been formed in the large marine basin known as Paratethys (MILANOVSKY, 1968; SCHERBA, 1987; KORONOVSKY *et al.*, 1987; POPOV *et al.*, 1993). The early Oligocene basins sometimes cross outlines the former basins and follow closely to the configurations of younger molasse basins.

Source : MNHN, Paris

The thickness of Maykop formation is up to 1-3 km in the Scythian Platform, filling a deep-water basin with water-depths up to 400-1000 meters. The Maykop formation is represented mainly by clay and sandstones, including series of clinoforms southwardly dipping toward the Caucasus (KUNIN *et al.*, 1989). The water depths have increased to the south. Deep water basin originated very rapidly in the early Oligocene. Limited evidence exists that at the northern slope of the Great Caucasus clinoforms dip to the north, and there are a few proposed latest Eocene-early Oligocene thrusts to the Scythian Platform from the Caucasus belt.

Extensional faults at the bottom of Maykop formation cannot be recognized on the seismic profiles (KUNIN *et al.*, 1989). Deep-water basins have formed mainly due to vertical subsidence without significant role of faults. Gravitational olistostrome sedimentary bodies moving to the inner portions of the Maykop basin are well established on seismic profiles and field outcrops in the lower part of Maykop formation (SCHERBA, 1987; KUNIN *et al.*, 1989).

Late early Miocene-Quaternary: in the late early Miocene-early middle Miocene (Tarkhanian-Konka, 17-13.7 Ma ago) the Scythian Platform was filled by marine and continental sediments (MILANOVSKY, 1968). Uplift evidence exists of a central part of the Great Caucasus since the Chokrakian (16.5 Ma ago) (GONTSHAROVA & SCHERBA, 1996). In the Sarmatian time (late middle Miocene - early late Miocene) a large supply of molasse sediments started from the Great Caucasus. In the late Sarmatian time, the Great Caucasus existed as mountains (MILANOVSKY, 1968; KUNIN *et al.*, 1989). The uplift of Great Caucasus was irregular in time during the Miocene, Pliocene and Quaternary; phases of rapid uplift alternated with tectonically more quiet epochs (MILANOVSKY, 1968).

Zones with a different geological history are seen in the eastern part of North Caucasus basin in Miocene-Quaternary. Examples are the Terek-Caspian basin, East-Manych basin, zone of Karpinsky Swell, Stavropol High. The Terek-Caspian basin underwent subsidence up to 2-4 km and was filled by molasse sediments. These molasses make up large scale clinoforms of alluvial to marine sediments.

The Karpinsky Swell zone has undergone an uplift up to 0.5 - 1 km in Miocene; at the end of Pliocene - Quaternary time its eastern part has subsided and was covered by a sedimentary cover, at the same time its western part has continued slow uplift (MILANOVSKY, 1968).

The East Manych basin zone was a topographically low depression filled by molasse in Pliocene-Quaternary time. The molasse clinoforms progradated toward this basin both from the Great Caucasus Mountains to the south and Karpinsky Swell to the north. The Stavropol High has undergone slow uplift in Miocene-Quaternary.

ONE DIMENSION BURIAL HISTORY MODELLING OF THE SCYTHIAN PLATFORM

We used computer modelling to investigate the burial history of the Scythian Platform (NIKISHIN *et al.*, 1994) using the data from 128 wells and sections. A number of curves of tectonic subsidence rates are shown on figure 5. The analysis of the model shows the following features:

Early-Middle Triassic-Carnian: rapid subsidence event for many wells; possible interpretation: rift phase and post-rift subsidence;

Triassic / Jurassic boundary: uplift event for a few wells; possible interpretation - inversion compressional tectonics;

End of the Early Jurassic: a few wells show rapid subsidence event at this time; possible interpretation - weak rift phase coeval with main phase of opening of the Great Caucasus trough;

Late Aalenian-Bajocian-early Bathonian: subsidence phase; possible interpretations: syncompressional foreland-type subsidence or postrift subsidence accelerated by compression;

Pre-Callovian changes of subsidence curves: possible compressional event;

Late Jurassic: rapid subsidence, possible extensional phase;

Jurassic / Cretaceous boundary: changes of subsidence curves; possible compressional event;

Cretaceous-Paleocene-Eocene: gentle thermal subsidence accelerated in Mid-Cretaceous time in many areas by possible tension events; changes of subsidence curves at the Cretaceous / Paleocene and Paleocene / Eocene boundaries for many areas show proposed changes in a stress field;

Source : MNHN, Paris

Oligocene: rapid subsidence phase, syncompressional subsidence;

Middle Miocene-Quaternary: five rapid subsidence events: 16.6-15 Ma ago (Tschokrakian-Karaganian); 12.4-9.7 Ma ago (Sarmatian); 7-5 Ma ago (at the Meotian / Pontian boundary-Pontian); 3.7-1.8 Ma ago (Akchagylian); 1.6-0 Ma; these rapid subsidence phases coincide with the main deformational compressional phases in the Great Caucasus; hence it appears that they are related to collisional phases; some areas underwent syncompressional uplift during the late phases of collision.

TECTONIC HISTORY OF THE SCYTHIAN PLATFORM

The proposed tectonic history of the Scythian Platform is based on geological data (including data from the Great Caucasus-Southern Crimea orogen and other surrounding areas) and inferences from the computer burial history. The short scenario of the proposed history is represented below (Figs 3-4).

Early-Middle Triassic-Carnian: a major continental rift system covered by post-rift cover originated along the former Late Paleozoic orogen; it includes the East Manych basin, Kayasula basin, Mozdok basin, Kiliya-Karkinitsky-Azov belt of basins, Tulcea (Dobrogea) basin, rift basins of the Moesian platform and Turan platform, activated Dnieper basin. Rift related magmatism took place in many rifted basins. Compressional tectonics took place in pre-Norian time.

Norian-Rhaetian. Compressional tectonics, origin of molasse basins, orogenic magmatism.

Triassic / Jurassic boundary and Hettangian: collisional orogeny (possible collision with Transcaucasus terrane, Iran terrane, Western and Eastern Pontides terranes).

Sinemurian-early Aalenian: high stand of the Scythian Platform, origin of a Great Caucasus deep-water rifted trough and weak rifting in the uplifted Scythian Platform.

Late Aalenian-early Bajocian: collisional orogenic events in the Crimea, weak compressional events in the Great Caucasus and regional subsidence of the Scythian Platform.

Late Bajocian-Bathonian: during the Bajocian a large subduction-related magmatic belt was active in the Transcaucasus-Pontides area. Intra-Bajocian inversion tectonics took place along the Great Caucasus-South Crimean belt. This inversion tectonics continued to Bathonian and had a culmination at the end of Bathonian-beginning of the Callovian as an orogeny along the Great Caucasus-South Crimean belt. Regional subsidence of the Scythian Platform took place in Bajocian-early Bathonian and was terminated by pre-Callovian uplift.

Callovian-mid-Berriasian: a new rift phase took place in the Callovian-Tithonian along the Great Caucasus-South Crimean belt, in the Dobrogea and the Moesian Platform. The rifting was accompanied by subsidence of the Scythian Platform.

Berriasian: orogenic events, uplift and thrusting-folding took place in the Crimea and Scythian Platform.

Late Berriasian-Barremian: a new system of sedimentary basin configuration originated in the Scythian Platform, possibly in response to a new weak tension phase. Uplift in pre-Aptian time.

Aptian-Albian: a system of rifted basins originated in the Scythian-Black Sea-Caucasus area.

Late Cretaceous: postrift subsidence and stress events in the Scythian Platform and Great Caucasus.

Paleocene-Eocene: regional thermal subsidence of the Scythian Platform modulated by stress events.

Eocene / Oligocene boundary: rapid syncompressional subsidence of the Scythian platformand orogenic activity in the Caucasus region.

Oligocene-early Miocene (Maykop time): rapid syncompressional subsidence of the southern part of the Scythian Platform led to origin of deep-water basins which were filled by clay and sandstones. At the end of the Maykop time relative compensation by sediments took place in the Scythian Platform.

Middle Miocene-Quaternary: Arabia-Europe continent-continent collision led to collision tectonics and orogeny in the Caucasus-South Crimea region, and a few molasse basins originated to the north and south of the Great Caucasus-South-Crimean orogen. The North Caucasus Indol-Kuban and Terek-

Source : MNHN, Paris

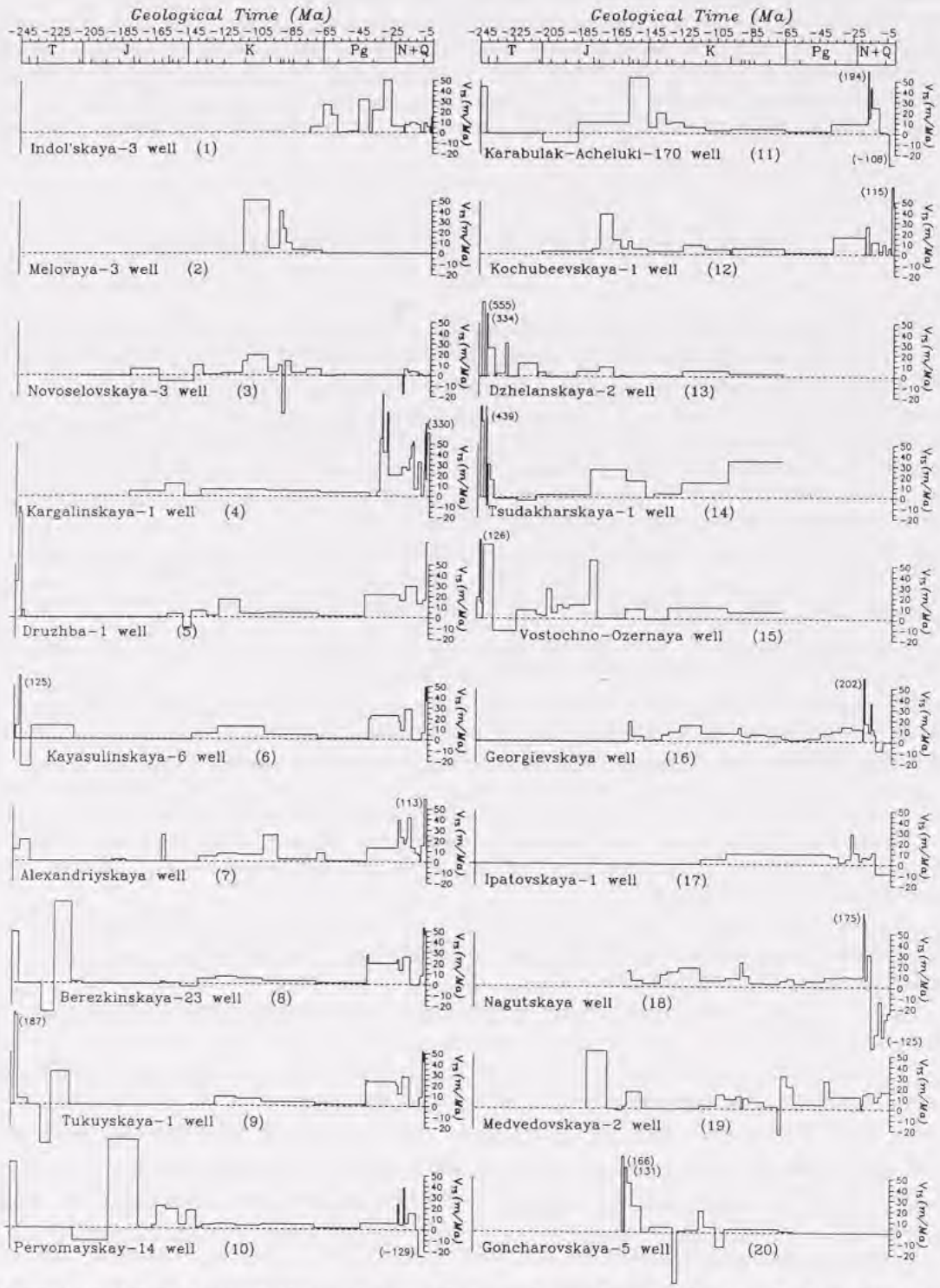

FIG. 5.— Comparison of the tectonic subsidence rate curves for some deep wells on the Scythian Platform. Location of wells (numbers) are given in figure 2.

FIG. 5.— Comparaison des taux de subsidence tectonique pour quelques forages profonds de la Plate-Forme Scythe. La position des forages (chiffres) est donnée figure 2.

Source : MNHN, Paris

Caspian molasse basins underwent five rapid subsidence phases: 16.5-15, 12.4-9.7, 7-5, 3.7-1.8 and 1.6-0 Ma ago. These times coincide with the main phases of thrusting in the Caucasus. Since the middle Miocene a syncompressional bulge has been uplifted along the belt of Karpinsky Swell-Donets Basin-Ukrainian Shield.

CONCLUSIONS

The Mesozoic-Cenozoic subsidence history of the Scythian platform was very complex. It was controlled by many synrift subsidence or uplift phases, postrift thermal subsidence epochs, syncompressional phases and epochs of subsidence or uplift (see figures 3, 4). The recent platform cover is an integrated result of a succession of different tectonic processes with a complex thermal history.

ACKNOWLEDGEMENTS

The work was funded by the Peri-Tethys program. International programmes IGCP-369, INTAS, EUROPROBE and LITHOSPHERE supported our communications and discussions. Russian Geological Survey (ROSKOMNEDRA) sponsored our many-years field works. We thank E.E. MILANOVSKY, V.E. KHAIN, A.S. ALEKSEEV, J. DERCOURT, P. ZIEGLER, J.-P. CADET, V.G. KAZMIN, W. CAVAZZA, B. FOUKE, N.V. KORONOVSKY, A.N. STAFEEV and E. GRADINARU for fruitful discussions. Netherlands Research School of Sedimentary Geology contribution n° 960412.

REFERENCES

BOIKO, N.I., 1993.— *Lithology of the Mesozoic Carbonates of the Western Pre-Caucasus Region.* Doctor of Science Dissertation, Moscow State University, Moscow, Russia: 1-425 (in Russian).

BOIKO, N.I., PUSHKARSKY, E.M. & SEDLETSKY, V.A., 1986.— Triassic carbonate formations of the western Pre-Caucasus region. *In*: *Formations of Sedimentary Basins.* Nauka, Moscow: 104-114 (in Russian).

CHEKUNOV, A.V., VESELOV, A.A. & GILKMAN, A.I., 1976.— *Geological Structure and History of the Peri-Black Sea Basin.* Naukova Dumka, Kiev: 1-164 (in Russian).

GOFMAN, E.A., SOROKINA, I.E., EGOYAN, V.L. *et al*, 1988.— *Mesozoic-Cenozoic Complexes of the Peri-Caucasus Region (Structure and Correlations).* Nauka, Moscow: 1-94 (in Russian).

GONTSHAROVA, I.A. & SCHERBA, I.G., 1996.— Tarkhanian-Karaganian stage of development of the Euxinian-Caspian Basin of the Paratethys. *In*: *Peri-Tethys Programme in Moscow. Moscow Workshop, January 16-17, 1996.* Geological Faculty, Moscow State University, Moscow, Abstracts: 15-16.

GRIGORIEVA, V.A., KAMENETSKY, A.E., PAVLYUK M.I., PALINSKY, P.V. & PLAKHOTNY, L.G., 1981.— *Formations and Oil and Gas Potential of the Cretaceous Sediments of the Southern Ukraine.* Naukova Dumka, Kiev: 1-140 (in Russian).

KORONOVSKY, N.V., KOZHEVNIKOV, A.V., PANOV, D.I. *et al.*, 1987.— The history of geologic development and structure formation of the central part of Terek-Caspian trough. *In*: E.E. MILANOVSKY & N.V. KORONOVSKY (eds), *Geology and Mineral Resources of the Great Caucasus.* Nauka, Moscow: 147-174 (in Russian).

KUNIN, N.Ya., KOSOVA, S.S. & BLOKHINA, G.Yu., 1989.—*Recognition of the Non-Anticline Traps for Oil and Gas Based on Seismostratigraphic Analysis (on the Example of the Eastern Peri-Caucasus Region).* VNIIOENG, Moscow: 1-43 (in Russian).

LETAVIN, A.I., 1980.— *Basement of the Young Platform of the Southern USSR.* Nauka, Moscow: 1-150 (in Russian).

MILANOVSKY, E.E., 1968.— *Neotectonics of the Caucasus.* Nedra, Moscow: 1-638 (in Russian).

MILANOVSKY, E.E. & KHAIN, V.E., 1963.— *Geological Structure of the Caucasus.* Moscow University Press, Moscow: 1-357 (in Russian).

MILEEV, V.S., ROZANOV, S.B., BARABOSHKIN, E.Yu., NIKITIN, M.Yu. & SHALIMOV, I.V., 1995.— The position of the Upper Jurassic deposits in the structure of the Mountain Crimea. *Bulletin MOIP, Geologia*, **70** (1): 22-31 (in Russian).

MURATOV, M.V. (ed.), 1969.— *Geology of the USSR.* VIII: *Crimea.* (1), *Geology.* Nedra, Moscow: 1-576 (in Russian).

NAZAREVICH, B.P., NAZAREVICH, I.A. & SHVYDKO, N.I., 1986.— Nogaysk (Upper Triassic) volcanogenic-sedimentary formation of the Eastern Peri-Caucasus region: composition, structure, and relations with pre- and post-Nogaysk volcanites. *In*: *Formations of Sedimentary Basins.* Nauka, Moscow: 67-86 (in Russian).

NIKISHIN, A.M., BOLOTOV, S.N., ERSHOV, A.V., NAZAREVICH, B.P., CLOETINGH, S., LOBKOVSKY, L.I. & STEPHENSON, R., 1994.— Geodynamic analysis of the North-Caucasus sedimentary basin according to the data of burial history computer modelling. *In*: Yu.G. LEONOV, A.F. MOROZOV & L.N. SOLODILOV (eds), *Tectonics and Magmatism of the East-European Platform.* KMK, Moscow: 85-93 (in Russian).

Source : MNHN, Paris

PANOV, D.I. & GUSCHIN, A.I., 1987.— Structural-formational tectonic subdivisions of the Great Caucasus region for the Early and Middle Jurassic time, and the local Early-Middle Jurassic stratigraphy. *In*: E.E. MILANOVSKY & N.V. KORONOVSKY (eds), *Geology and Mineral Resources of the Great Caucasus.* Nauka, Moscow: 124-139 (in Russian).

POPOV, S.V, AKHMETIEV, M.A., ZAPOROZHETS, N.I., VORONINA, A.A. & STOLYAROV, A.S., 1993.— History of the Eastern Paratethys in the Late Eocene-Early Miocene. *Stratigrafiya. Geologicheskaya Korrelyatsiya,* **1** (6): 10-39 (in Russian).

PRUTSKY, N.I. & LAVRISCHEV, V.A., 1989.— Northwestern Caucasus in Mesozoic. *In*: A.A. BELOV & M.A. SATIAN (eds), *Geodynamics of the Caucasus.* Nauka, Moscow: 92-98 (in Russian).

ROSTOVTSEV, K.A. (ed.), 1992.— *Jurassic of the Caucasus.* Nauka, Saint-Petersburg: 1-192 (in Russian).

SCHERBA, I.G., 1987.— Olistostromes and problems of Cenozoic tectonics of the Caucasus. *In*: E.E. MILANOVSKY & N.V. KORONOVSKY (eds), *Geology and Mineral Resources of the Great Caucasus.* Nauka, Moscow: 191-200 (in Russian).

SLAVIN, V.I., 1986.— Geological history of the Crimea peninsula in the Triassic. *Bulletin MOIP, Geologia*, **61** (6): 46-50 (in Russian).

SOBORNOV, K., 1995.— Structural evolution of the Karpinsky swell, Russia. *Comptes Rendus de l'Académie des Sciences, Paris*, **321** (II a): 161-169.

STAFEEV, A.N., PANOV, D.I., YUTSIS, V.V., SMIRNOVA, S.B. &GUSHCHIN, A.I., 1995.— Eastern Peri-Caucasus Lias: unsolved problems of the stratigraphy, paleostructure and geodynamics. *In*: *5th Zonenshain Conference OF Plate Tectonic. Moscow, November 22-25, 1995.* Geomar, Kiel, Programme and Abstracts: 91-92.

Source : MNHN, Paris

Scythian Platform, Caucasus and Black Sea region: Mesozoic-Cenozoic tectonic history and dymanics

Anatoly M. NIKISHIN [1], *Sierd CLOETINGH* [2], *Marie-Françoise BRUNET* [3], *Randell A. STEPHENSON* [2], *Serguey N. BOLOTOV* [1] & *Andrei V. ERSHOV* [1]

[1] Geological Faculty, Moscow State University, 119899 Moscow, Russia

[2] Vrije Universiteit, De Boelelaan 1085, 1081 HV Amsterdam, The Netherlands

[3] Département de Géotectonique, CNRS URA 1759, case 129, Université P. et M. Curie 75252 Paris Cedex 05, France

ABSTRACT

Collision orogeny in the Caucasus-Scythian area took place at the Triassic / Jurassic boundary. During the Jurassic-Eocene times the region was in back-arc tectonic environments with many phases of back-arc extension and compression. At the Eocene / Oligocene boundary the subduction system was transformed into a zone of collision, and during the Oligocene-Quaternary the region was subjected to polyphase collisional tectonics. The Scythian Platform subsidence / uplift is a result of superimposed different subsidence mechanisms: synrift-postrift subsidence, foreland syncompressional subsidence and subduction-related subsidence of a broad region.

RÉSUMÉ

Plate-forme Scythe, Caucase et région de la Mer Noire : histoire tectonique et géodynamique au Mésozoïque et Cénozoïque.

L'orogenèse est arrivée au stade de collision dans la zone Caucase-plate-forme Scythe à la limite Trias-Jurassique. Durant la période comprise entre le Jurassique et l'Éocène, la région était située dans un environnement tectonique d'arrière-arc sujet à de nombreuses phases d'extension et de compression. À la limite Éocène / Oligocène, le système de zone de subduction a été transformé en une zone de collision, et durant l'Oligocène-Quaternaire, la région a été soumise à une tectonique collisionnelle polyphasée. Les subsidence / soulèvement de la plate-forme Scythe résultent de la superposition de différents mécanismes de subsidence : une subsidence synrift et post-rift, une subsidence syncompression de bassin d'avant-pays et la subsidence d'une vaste région reliée à la subduction.

NIKISHIN, A.M., CLOETINGH, S., BRUNET, M.-F., STEPHENSON, R.A., BOLOTOV, S.N. & ERSHOV, A.V., 1998.— Scythian Platform, Caucasus and Black Sea region: Mesozoic-Cenozoic tectonic history and dymanics. *In*: S. CRASQUIN-SOLEAU & É. BARRIER (eds), Peri-Tethys Memoir 3: stratigraphy and evolution of Peri-Tethyan platforms. *Mém. Mus. natn. Hist. nat.*, **177** : 163-176. Paris ISBN : 2-85653-512-7.

Source : MNHN, Paris

INTRODUCTION

The Scythian Platform-Caucasus-Black Sea region has a complicated Mesozoic-Cenozoic history (SENGÖR & YILMAZ, 1981; DERCOURT *et al.*, 1993; KAZMIN & SBORSCHIKOV, 1989; LORDKIPANIDZE, 1980; FINETTI *et al.*, 1988; ZIEGLER, 1990; BAZHENOV & BURTMAN, 1990; OKAY *et al.*, 1994; STAMPFLI & MARCHANT, 1995). We discuss new reconstructions of the regional tectonic history based mainly on a new scheme of tectonic events in the whole area. We will discuss separately tectonic history of the Scythian Platform, Great Caucasus, Southern Crimea orogen, Dobrogea, Moesian Platform, Pontides-Transcaucasus-Alborz magmatic belt and the Black Sea.

MESOZOIC-CENOZOIC HISTORY OF THE SCYTHIAN PLATFORM

The Scythian Platform is located between the Great Caucasus-Southern Crimea orogen to the South, and the East European Platform to the North. The geological history of the Scythian Platform is described in NIKISHIN *et al.*, (this volume), and a summary is presented below (Figs 1-8):

Early-Middle Triassic-Carnian: a major continental rift system originated along the former Late Paleozoic orogen. Rift related magmatism took place in many rifted basins. Compressional tectonics took place in pre-Norian time.

Norian-Rhaetian: compressional tectonics, molasse basins origin accompanied by orogenic magmatism.

Triassic / Jurassic boundary and Hettangian: collisional orogeny.

Sinemurian-early Aalenian: weak rifting in the uplifted Scythian Platform.

Late Aalenian-early Bathonian: regional subsidence of the Scythian Platform, pre-Callovian uplift.

Callovian-mid-Berriasian: a new rift phase took place in the Callovian-Tithonian along the Great Caucasus-South Crimean belt, in the Dobrogea and the Moesian Platform. The rifting was accompanied by subsidence of the Scythian Platform.

Berriasian: orogenic event, uplift and thrusting-folding.

Late Berriasian-Barremian: a new system of sedimentary basin configuration originated in the Scythian Platform; possibly in response to a new weak tensional phase.

Aptian-Albian: a system of rifted basins originated in the Scythian Platform area.

Late Cretaceous: postrift subsidence and tensional events in the Scythian Platform.

Paleocene-Eocene: regional subsidence of the Scythian Platform modulated by stress events.

Eocene / Oligocene boundary and Oligocene-early Miocene (Maykop time): rapid syncom-pressional subsidence of the southern part of the Scythian Platform led to the formation of deep-water basins which were filled by clay and sandstones.

Middle Miocene-Quaternary: a continent-continent collision has led to collisional tectonics and orogeny in the Caucasus-South Crimea region, and a few molasse basins originated to the north and south of the Great Caucasus-Southern-Crimea orogen. North Caucasus Indol-Kuban and Terek-Caspian molasse basins underwent rapid subsidence phases: 16.5-15, 12.4-9.7, 7-5, 3.7-1.8 and 1.6-0 Ma ago. Since the middle Miocene a syncompressional bulge has been uplifted along the belt of Karpinsky Swell-Donets Basin-Ukrainian Shield.

MESOZOIC-CENOZOIC HISTORY OF THE GREAT CAUCASUS

Many different views exist on this issue (MILANOVSKY & KHAIN, 1963; BELOV & SATIAN, 1989; LORDKIPANIDZE, 1980; DERCOURT *et al.*, 1993; SHARAFAN, 1995). Below we will discuss a recently developed working model of the Great Caucasus history:

Triassic / Jurassic boundary: origin of the collisional orogen nearly along the recent Great Caucasus (KAZMIN & SBORSCHIKOV, 1989);

Source : MNHN, Paris

Sinemurian-early Pliensbachian: the formation of the continental rift-like sedimentary basin (data of PANOV & GUSCHIN, 1987) in a back-arc environment (?);

Late Pliensbachian-Toarcian-early Aalenian: the development of the deep-water Great Caucasus trough with rifted, very thin continental crust and basalt volcanism (or local spreading of the oceanic crust in the Toarcian) (data of PANOV & GUSCHIN, 1987; LORDKIPANIDZE, 1980).

Late Aalenian-Bajocian-Bathonian: development of the major subduction-related magmatic belt along the southern margin of the Great Caucasus trough (LORDKIPANIDZE, 1980; PANOV & GUSCHIN, 1987), inversion deformations inside the Great Caucasus trough;

End of the Bathonian: peak of inversion tectonics, thrusting and folding inside the trough (PANOV & GUSCHIN, 1987; KORONOVSKY *et al.*, 1987);

Late Jurassic-Eocene: development of the deep-water flysch trough along the southern part of the recent Great Caucasus (MILANOVSKY & KHAIN, 1963; BELOV & SATIAN, 1989); The flysch trough underwent a complex stress history; for example a tensional phase took place in the Late Jurassic (origin of the trough); basalt rift-like magmatic and tensional events took place along the trough possibly in Albian-Cenomanian (LOMIZE, 1969; LORDKIPANIDZE, 1980); during the late Paleocene Great Caucasus trough underwent a phase of rapid subsidence (possibly due to extension) (BENIJAMOVSKY & SCHERBA, 1995); a weak compressional event took place in the early-middle Berriasian;

Eocene / Oligocene boundary and early Oligocene: compressional tectonics, folding and thrusting at least along the northern portion of the trough (MILANOVSKY, 1968; ADAMIA *et al.*, 1989);

Oligocene-early early Miocene: compressional tectonics in the relative deep-water Great Caucasus trough;

Late early Miocene-Quaternary: polyphase collisional tectonics, formation of the mountains (possibly since 16.5 Ma ago) and asymmetric fold-thrust belt (MILANOVSKY, 1968).

MESOZOIC-CENOZOIC HISTORY OF THE SOUTHERN CRIMEA OROGEN

Our model of the geological history of the south-western portion of the orogen is based on a new interpretation of former and our new data (MURATOV, 1969; SLAVIN, 1986; SLAVIN *et al.*, 1983; MAZAROVICH & MILEEV, 1989 a, b; PANOV *et al.*, 1994):

Early-Middle Triassic (formations are absent in the folded complex, there are olistoliths in younger sediments and data on Scythian Platform rifted basins): origin of a rifted basin or passive margin;

Carnian-Norian (data of SLAVIN, 1986 mainly in our interpretation): syncompressional formation of flysch complex, shallow-water clastic sediments and acidic volcanism;

Rhaetian-Hettangian-early Sinemurian (?) (data of SLAVIN, 1986; PANOV *et al.*, 1994, mainly in our interpretation): proposed orogenic phase, folding, uplift followed by formation of shallow-water carbonate cover;

Late Sinemurian(?)-Pliensbachian-Toarcian-early Aalenian(?): development of the deep-water trough with turbidite sedimentation in the deepest parts (SLAVIN, 1986; SLAVIN *et al.*, 1983; MAZAROVICH & MILEEV, 1989 a; PANOV *et al.*, 1994);

Aalenian-early Bajocian: intensive orogenic event, thrusting and folding; origin of the Bitak molasse basin filled by conglomerates (up to 4 km) in the belt between Southern-Crimea orogen and Scythian Platform (data of MURATOV, 1969; SLAVIN & CHERNOV, 1981 in our interpretation); development of the Beshuy coal-bearing molasse basin inside the orogen (ROMANOV *et al.*, 1987);

Late Bajocian-Bathonian: development of the subduction-related volcanic island arc, volcanism (mainly in the late Bajocian), formation of shallow-water to turbidite sediments (data of MURATOV, 1969; MAZAROVICH & MILEEV, 1989 a, b);

Pre-Callovian time: intensive orogenic event, thrusting and folding (data of SLAVIN, 1986; MURATOV, 1969);

Callovian-middle Berriasian: development of the marine basin in the rift-like trough along the former orogenic belt, filling of the basin by shallow to relative deep water carbonates, conglomerates

Source : MNHN, Paris

and flysch-like deposits (MURATOV, 1969); fold-thrust deformations in the Berriasian (MILEEV *et al.*, 1995);

Late Berriasian-Eocene: relatively stable tectonics, covering by shallow-water sediments;

Oligocene-Quaternary: uplift of the area.

MESOZOIC-CENOZOIC HISTORY OF DOBROGEA

North Dobrogea is located between Scythian and Moesian platforms (to the North-East of the Peceneaga-Camena Fault) and is an uplifted basement of the Scythian platform with the Late Paleozoic basement (SANDULESCU *et al.*, 1995). The data on the geology of the Dobrogea are summarized *in* SANDULESCU *et al.* (1995) and KRUGLOV & TSYPKO (1988). The following stages of the geological history in the Mesozoic-Cenozoic can be recognized:

Early Triassic-Carnian: continental rifting;

Norian-Rhaetian-Hettangian: postrift subsidence modulated possibly by compressional (?) events;

Sinemurian-Callovian: origin of a relative deep-water rift-like trough with turbidite sedimentation, a complex history of the trough is not excluded, folding in the pre-Oxfordian time;

Oxfordian-Kimmeridgian: new rift phase, pre-Hauterivian (possibly intra-Berriasian) inversion tectonics, thrusting ; pre-Late Cretaceous uplift;

Latest late Albian-Campanian: platform subsidence; post-Cretaceous uplift.

MESOZOIC HISTORY OF THE MOESIAN PLATFORM

We will discuss the history of the Varna block located at the eastern part of the Moesian Platform and the shelf of the Black Sea using data of DACHEV, STANEV & BOKOV *in* BELOUSSOV & VOLVOVSKY (1989). Triassic sediments compile a few basins with sediments partly eroded at the Triassic / Jurassic boundary times. It is possible that the Triassic sediments formed rifted basins or part of a passive margin. Orogenic deformations and uplift took place at the Triassic / Jurassic boundary. The Early-Middle Jurassic is presented by shallow-water clastic sediments. The Upper Jurassic-Valanginian consists of carbonate cover; an uncompensated sedimentation took place in a relatively deep water rifted basin along the eastern and southern margins of the Varna block. Barremian-Upper Cretaceous forms a platform cover.

PONTIDES-TRANSCAUCASUS-ALBORZ MAGMATIC BELT

The history of the subduction-related magmatic belts of the Caucasus-Black Sea region is very complex (DERCOURT *et al.*, 1993; LORDKIPANIDZE, 1980; STAMPFLI & MARCHANT, 1995; OKAY *et al.*, 1994; ROBINSON *et al.*, 1995). Two Mesozoic-Cenozoic magmatic belts can be recognized in the Caucasus-Black Sea region: a Triassic magmatic belt with hypothetical position and remnants of the belt in Northern Iran (STAMPFLI & MARCHANT, 1995), North Caucasus-Turkmenia- North Afghanistan (KHAIN, 1979) and possible in the Western-Central Pontides (USTAOMER & ROBERTSON, 1994), and a Jurassic-Eocene Pontides-Transcaucasus-Alborz magmatic belt (LORDKIPANIDZE, 1980). The history of the Triassic magmatic belt is not well constrained.

The Pontides-Transcaucasus-Alborz magmatic belt trends at least from the Srednegorie to West Pontides and East Pontides, and to Transcaucasus- Alborz (LORDKIPANIDZE, 1980). During the Jurassic-Barremian it is possible to separate a number of events in the magmatic belt history (LORDKIPANIDZE, 1980; TVALCHRELIDZE & MIKHAILOV, 1985; SENGÖR & YILMAZ, 1981; ROBINSON *et al.*, 1995). The climax of volcanism took place in the Transcaucasus during the Bajocian (PANOV & GUSCHIN, 1987; MILANOVSKY, 1991).

During the Aptian-Late Cretaceous the magmatic belt was well developed from Bulgaria to northern Iran. In the Srednegorie (Bulgaria) volcanism initiated in the Campanian (TVALCHRELIDZE &

Source : MNHN, Paris

MIKHAILOV, 1985), in the Western Pontides: since the Coniacian (well documented) or even Aptian-Albian to Campanian or Maastrichtian (GÖRÜR *et al.*, 1993), in the Eastern Pontides - since Turonian to Maastrichtian (ROBINSON *et al.*, 1995), in the Transcaucasus belt - since Aptian-Albian to early Turonian (and locally - to the early Maastrichtian) (TVALCHRELIDZE & MIKHAILOV, 1985; LORDKIPANIDZE, 1980), in the Alborz - in the late Barremian-Aptian-early Senonian (WENSINK & VAREKAMP, 1980).

During Paleogene times subduction-related magmatic belt is known in the Eastern Pontides, Transcaucasus belt, and in the Alborz (LORDKIPANIDZE, 1980). The volcanism took place in the Eocene and locally early Oligocene; there are no well documented Paleocene volcanites (LORDKIPANIDZE, 1980; TVALCHRELIDZE & MIKHAILOV, 1985; MILANOVSKY, 1991; ROBINSON *et al.*, 1995, 1996). The climax of the volcanism occurred in the mid-Eocene time.

HISTORY OF THE BLACK SEA BASIN

The Black Sea deep-water basin originated as a back-arc extensional structure (ZONENSHAIN & LE PICHON, 1986; GÖRÜR, 1988; FINETTI *et al.*, 1988). The main problem is a timing of the opening and geometry of the opening. Western Black Sea Basin originated in the Mid-Late Cretaceous (FINETTI *et al.*, 1988; GÖRÜR *et al.*, 1993), but Eastern Black Sea Basin originated or in Mid-Late Cretaceous (FINETTI *et al.*, 1988; BELOUSSOV & VOLVOVSKY, 1989; OKAY *et al.*, 1994), or in Paleocene (ROBINSON *et al.*, 1995, 1996), or in Eocene (LORDKIPANIDZE, 1980). We have the following constraints on the timing of the Black Sea Basin origin based on continental geology:

— during the Aptian-Albian continental rifting took place in Crimea region (Karkinitsky rift system) and in Western Pontides (GÖRÜR *et al.*, 1993), weak proposed rift events took place in the Hauterivian-Barremian in the Crimea too;

— in Bulgaria just to the north of Srednegorie subduction-related volcanic belt rifting took place in Cenomanian-Turonian (TVALCHRELIDZE & MIKHAILOV, 1985);

— in Georgia to the north of the Transcaucasus subduction-related volcanic belt back-arc late Turonian-Santonian alkaline basalts are formed (LORDKIPANIDZE, 1980);

— inside the Great Caucasus trough basaltic volcanism of probably back-arc origin took place in Albian-Cenomanian (LOMIZE, 1969; LORDKIPANIDZE, 1980);

— weak continental rifting took place in Late Cretaceous to the north of Crimea (CHEKUNOV *et al.*, 1976);

— during the Eocene the Transcaucasus magmatic belt suffered intra-arc rifting with basaltic volcanism;

— the southern part of Crimea underwent uplift possibly associated with rift shoulder development during the early-middle Albian; thermal regional subsidence in the Crimea (our data), Western Pontides (GÖRÜR *et al.*, 1993) and Dobrogea (SANDULESCU *et al.*, 1995) started since the latest late Albian-Cenomanian;

— inside the Scythian Platform stress changes took place at the Cretaceous / Paleocene boundary;

— the Eastern Pontides were possibly thermally uplifted in Paleocene times (ROBINSON *et al.*, 1995).

Data on rifting around the Black Sea and on the history of subduction-related volcanic belts show that the continental rifting in the Western and Eastern Black Sea basins took place in Aptian-Albian (proposed weak rift event could be in Hauterivian-Barremian); ocean crust spreading took place since the latest late Albian-Cenomanian to the Late Cretaceous in the Western Black Sea Basin. Eastern Black Sea Basin suffered at least two stages of rifting: during the Aptian-Late Cretaceous, and, according to ROBINSON *et al.* (1995) in the mid-Paleocene.

The Black Sea Basin underwent a number of compressional phases in the Cenozoic. During the middle Eocene collision of the Rhodope terrane with Moesian Platform and West Black Sea basin took place (FINETTI *et al.*, 1988; BELOUSSOV & VOLVOVSKY, 1989). During the Oligocene-early Miocene (Maykop time) syncompressional deep-water basins originated at the margins of the East Black Sea Basin: Sorokin Basin just to the south of Crimea, Tuapse Basin at the boundary between Black Sea and recent Great Caucasus and Guria Basin to the north of East Pontides (TUGOLESOV *et al.*, 1985; FINETTI

Source : MNHN, Paris

et al., 1988). During the Neogene-Pleistocene, Black Sea underwent compression and thrusting along the margins together with molasse basin formation (TUGOLESOV *et al.*, 1985; FINETTI *et al.*, 1988).

PALEOTECTONIC RECONSTRUCTIONS

Our paleotectonic reconstructions for the region are shown on figures 1 to 8. The geometry of reconstructions is very simplified. We can recognize the following stages:

Early Triassic-early Carnian: origin of a major continental rift system in the Scythian-Dobrogea-Moesian region, possibly in a back-arc tectonic environment.

Carnian / Norian boundary-Hettangian: collisional tectonics along the eastern Moesia-Scythian-Crimea-Great Caucasus-Alborz region. The collision took place between the Eurasia and some continental terranes (possibly Transcaucasus terrane, Alborz terrane, Western and Eastern Pontides terranes) (KAZMIN & SBORSCHIKOV, 1989; OKAY *et al.*, 1994; ROBINSON *et al.*, 1995; STAMPFLI & MARCHANT, 1995).

Sinemurian-Toarcian: the Transcaucasus-Pontides subductional magmatic belt originated (may be close to position of the former Triassic magmatic belt) possibly in the Sinemurian-Toarcian with north-dipping subduction. A major back-arc rifting phase took place and deep-water rifted basin was formed along the belt Great Caucasus-Southern Crimea-recent margin between Moesian Platform and Western Black Sea basin-southern margin of the Moesian Platform; rift events took place in the Scythian Platform and Dobrogea.

Aalenian history: during the Aalenian and at the Aalenian / Bajocian boundary compressional tectonics took place, orogeny in the Crimea, orogeny and uplift in the Pontides (ROBINSON *et al.*, 1995), and proposed weak compressional deformations in the Great Caucasus Trough (PANOV & GUSCHIN, 1987).

Bajocian-Bathonian history: during the Bajocian a major subductional magmatic belt was active in the Transcaucasus-Pontides area (LORDKIPANIDZE, 1980; TVALCHRELIDZE & MIKHAILOV, 1985; PANOV & GUSCHIN, 1987; ROBINSON *et al.*, 1995). Intra-Bajocian inversion tectonics took place along the Great Caucasus-Southern Crimea basins. This inversion tectonics continued to Bathonian times and culminated at the end of Bathonian-beginning of the Callovian as an orogeny along the Great Caucasus-Southern Crimea belt. Regional subsidence of the Scythian Platform and southern half of the Russian Platform was initiated since the late Aalenian and especially since the late Bajocian. It was simultaneously with the maximum of the late Bajocian subduction related volcanism in the Transcaucasus-Pontides belt and inversion tectonics inside the Great Caucasus Trough.

Callovian-mid-Berriasian history: a new rifting phase took place in the Callovian-Tithonian along the Great Caucasus-Southern Crimea belt, in the Dobrogea area and along the eastern and southern margin of the Moesian Platform; rift volcanism also occurred in Dobrogea and southern part of the Great Caucasus. The Transcaucasus-Pontides volcanic belt was active in this time, suggesting a back-arc origin of the rifting.

Berriasian orogenic event: during the Berriasian time or at the Jurassic / Cretaceous boundary an orogenic event and associated thrusting took place in the Southern Crimea basin; in the Dobrogea (?), and in the western Pre-Caucasus area of the Scythian Platform.

Late Berriasian-Barremian history: during this time a new configuration of sedimentary basins was formed in the Scythian platform; possibly in response to a new weak tensional phase.

Aptian-Late Cretaceous history: major subductional volcanic arcs were active in this time along the Srednegorie-Western Pontides-Eastern Pontides-Transcaucasus-Alborz belt. A system of back-arc rifted basins originated to the North of this volcanic belt: the West Black Sea basin, East Black Sea basin, extension of the Great Caucasus Trough, and the formation of the rift system in the Northern-Crimea region. The rifting took place partially along the former magmatic belts: for example remnants of the same Bajocian volcanic arc exist in the Eastern Pontides and in the southern Crimea. Kinematic restoration of the Black Sea opening is problematic (FINETTI *et al.*, 1988; OKAY *et al.*, 1994; DERCOURT *et al.*, 1993). Constraints are required from restoration of the Caucasus region using precise paleomagnetic data whereas large scale strike-slip movements cannot be excluded. At present different

Source : MNHN, Paris

phases of rifting can be recognized but it is impossible to carry out a kinematic restoration; a number of rifting phases occurred - hypothetical Hauterivian-Barremian, Aptian-Albian (especially middle-late Albian), Cenomanian-Turonian, Senonian. Ocean crust spreading took place in the West Black Sea Basin in the latest late Albian-Cenomanian-Turonian and possibly later. Tensional events took place all around the Scythian Platform in Mid-Cretaceous time.

Paleocene-Eocene history: in the Paleocene, subductional volcanism was very weak (or absent) in the Transcaucasus-Pontides belt; a possible rift phase took place in the Eastern Black Sea basin (ROBINSON *et al.*, 1995). During the Eocene (especially mid-Eocene), Transcaucasus-Eastern Pontides subductional volcanic belt was very active (LORDKIPANIDZE, 1980); at the time of the maximum subductional volcanism, a relative rapid platformal subsidence of the Scythian and East European platforms took place.

Orogeny at the Eocene / Oligocene boundary-early Miocene: at the Eocene / Oligocene boundary the north-dipping subduction system was changed by collision of the Pontides-Transcaucasus-Alborz area with Tauride-Anatolide (SENGÖR & KIDD, 1979; ADAMIA *et al.*, 1989; ROBINSON *et al.*, 1995) and Central-East Iran-Lut terrane (SAIDI, 1995). It led to the uplift of the Transcaucasus region and to compressional tectonics along the Black Sea-Scythian area.

Middle Miocene-Quaternary orogeny: Arabia / Europe Miocene-Quaternary continent-continent collision (SENGÖR & KIDD, 1979) lead to collision tectonics and orogeny in the Caucasus south Crimea region, and to syncompressional subsidence of the Black Sea basin.

GEODYNAMICAL HISTORY OF THE SCYTHIAN PLATFORM

The following three main driving mechanisms are proposed for the Scythian Platform subsidence in the Jurassic-Eocene.

Rifting and postrift thermal subsidence. This model of the subsidence is relatively well constrained as we have a number of rift stages occurring: after every of the rift phase a postrift subsidence took place.

Loading by a new orogen and compressional stresses. Real regional subsidence of the Scythian Platform started in the Aalenian and mainly Bajocian simultaneously with orogenic events in the Caucasus-South Crimean belt. Hence the start of the foreland-type subsidence was connected with the orogeny.

Subduction-related subsidence of a broad region. The maximum of the volcanic activities of the Pontides-Transcaucasus-Alborz subduction magmatic belt took place in the Bajocian, Albian-Late Cretaceous and Eocene. At the same times maximum subsidence of the Scythian Platform and southern part of the Russian Platform takes place. This supports a causal connections between activity of the subductional magmatism and subduction itself with a broad platformal subsidence.

During the Oligocene-Neogene-Quaternary, the dynamics of the Scythian Platform was controlled by collision tectonics. Two main collisional epochs can be separated: Oligocene-early Miocene and middle Miocene-Quaternary. During the Oligocene-early Miocene two different processes took place:

— compression due to collision with Tauride-Anatolide-Iranian terranes and

— possible roll-back of the subducted lithosphere followed by detachment of the subducted slab. During the middle Miocene-Quaternary new collisional epoch took place after a short break. The collision took place between the Europe and Arabia. The collision was irregular with five main phases of shortening: 16.5-15, 12.4-9.7, 7-5, 3.7-1.8 and 1.6-0 Ma ago. Each compressional event was accompanied by rapid subsidence of molasse basins followed usually by clinoform sedimentation. The syncompressional bulge to the north of the Scythian Platform molasse basins suffered uplift since the early Miocene. The distance between the bulge axis and orogen axis is nearly 350 km. The largest compressional event took place in the Sarmatian (13.6-9.7 Ma ago): at this time compressional folding and thrusting occurred inside the Russian Platform up to 1200 km to the north of the Great Caucasus.

Source : MNHN, Paris

FIG. 1-8.— Series of paleotectonic maps illustrating the Mesozoic-Cenozoic history of the Scythian-Caucasus-Black Sea region.
FIG. 1-8.— Série de cartes paléotectoniques illustrant l'histoire méso-cénozoïque de la région plate-forme Scythe-Caucase-Mer Noire.

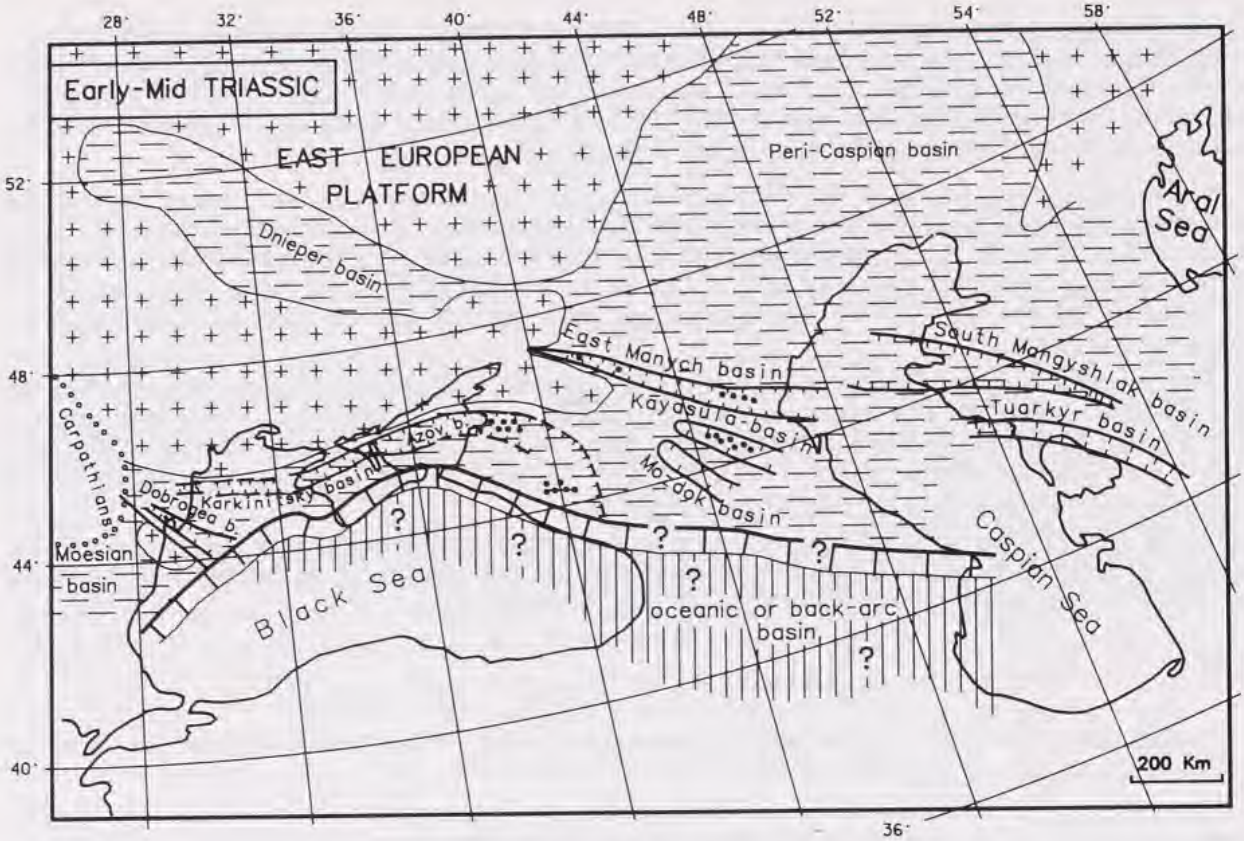

FIG. 1.— Early-Mid Triassic. See legend in figure 8.
FIG. 1. — *Trias inférieur et moyen. Légende, voir figure8.*

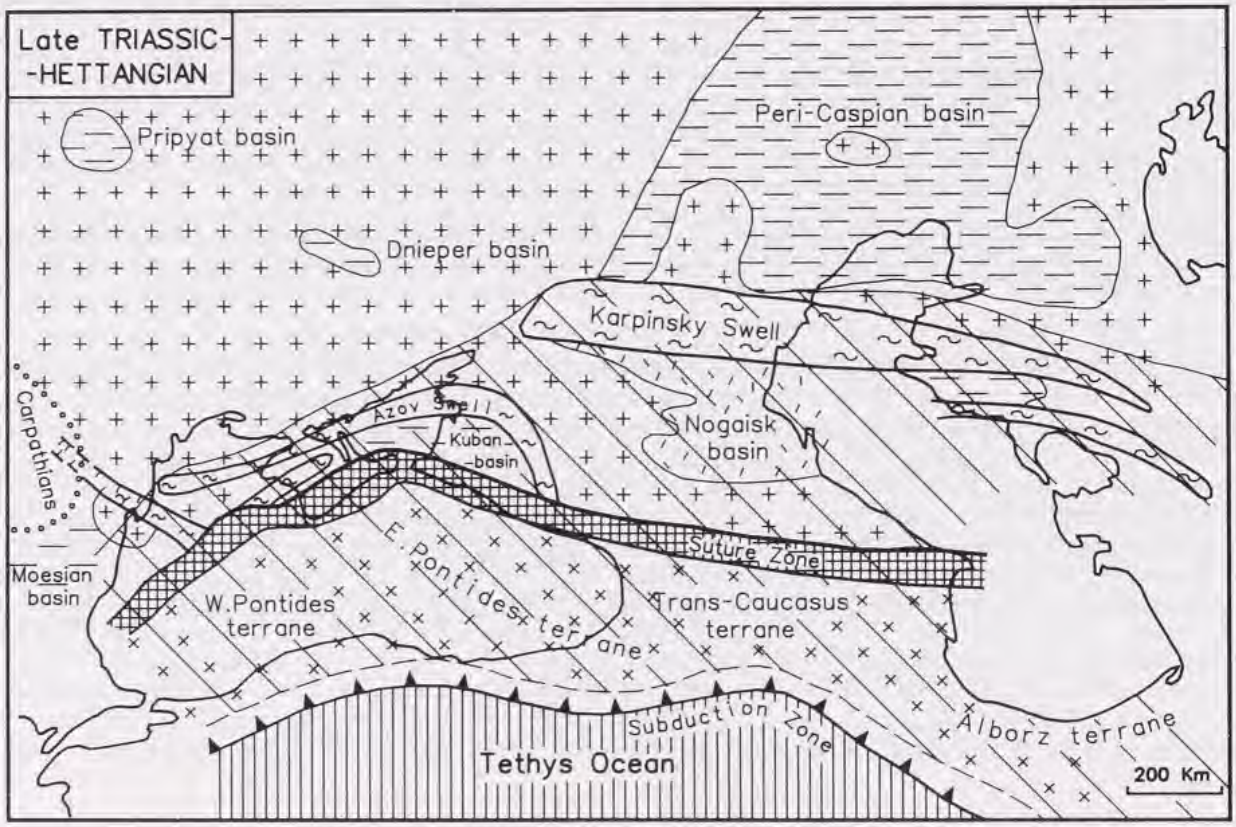

FIG. 2.— Late Triassic-Hettangian. See legend in figure 8.
FIG. 2.— Trias supérieur-Hettangien. Légende, voir figure 8.

Source : MNHN, Paris

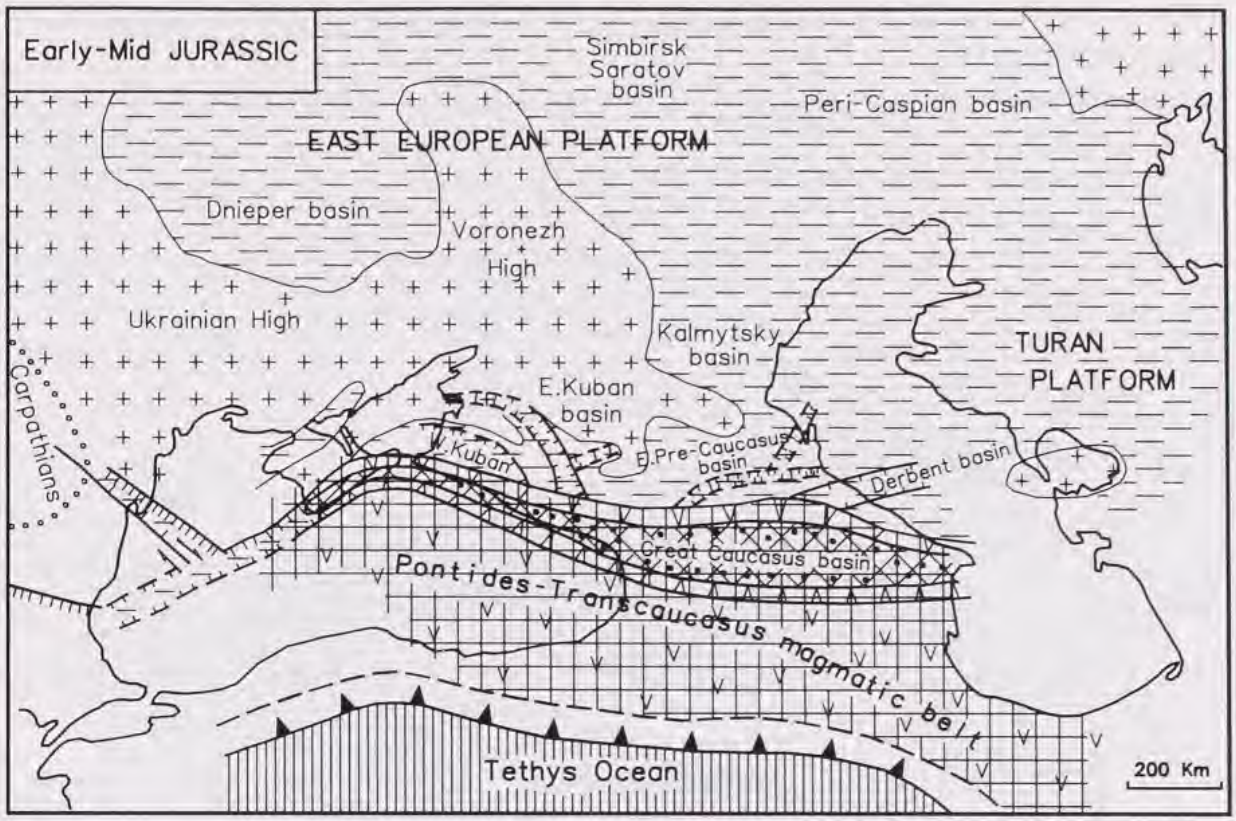

FIG. 3.— Early-Mid Jurassic. See legend in figure 8.
FIG. 3.— Jurassique inférieur et moyen. Légende, voir figure8.

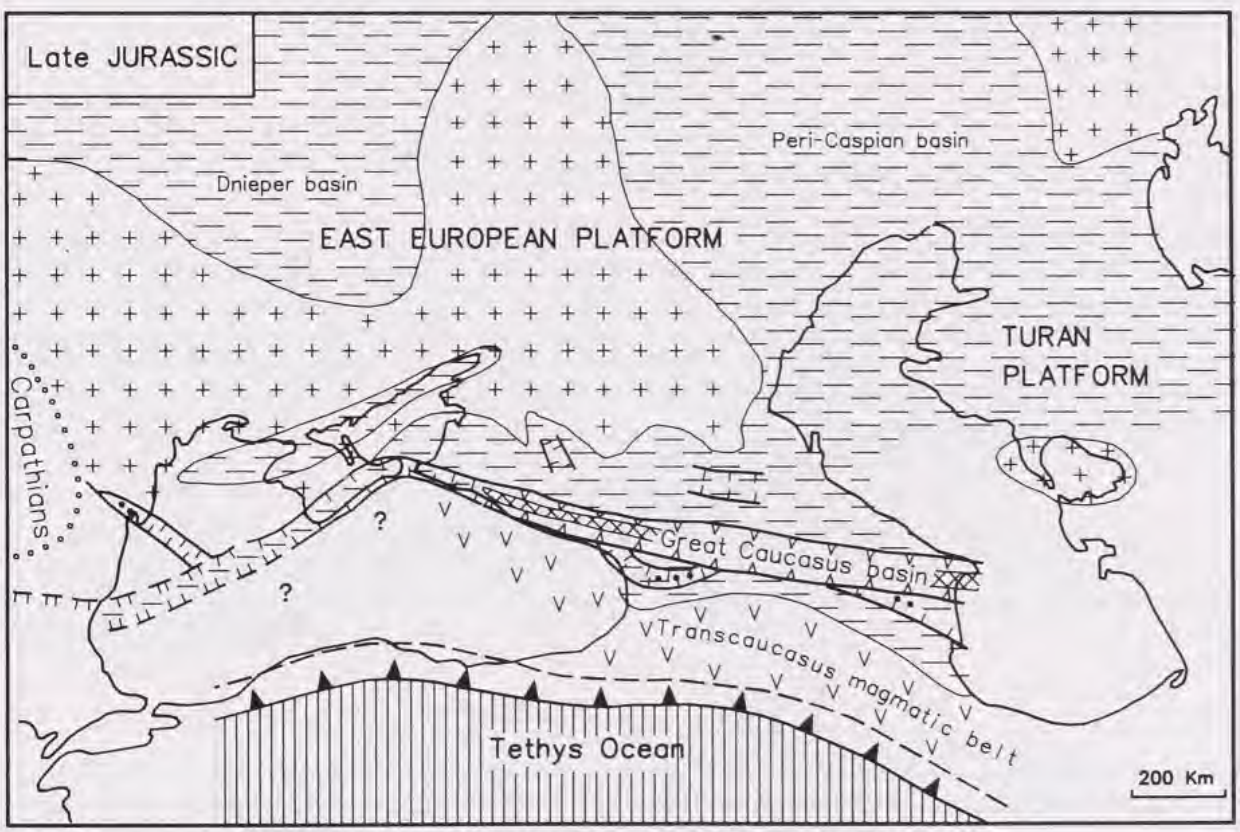

FIG. 4.— Late Jurassic. See legend in figure 8.
FIG. 4.— Jurassique supérieur. Légende, voir figure8.

Source : MNHN, Paris

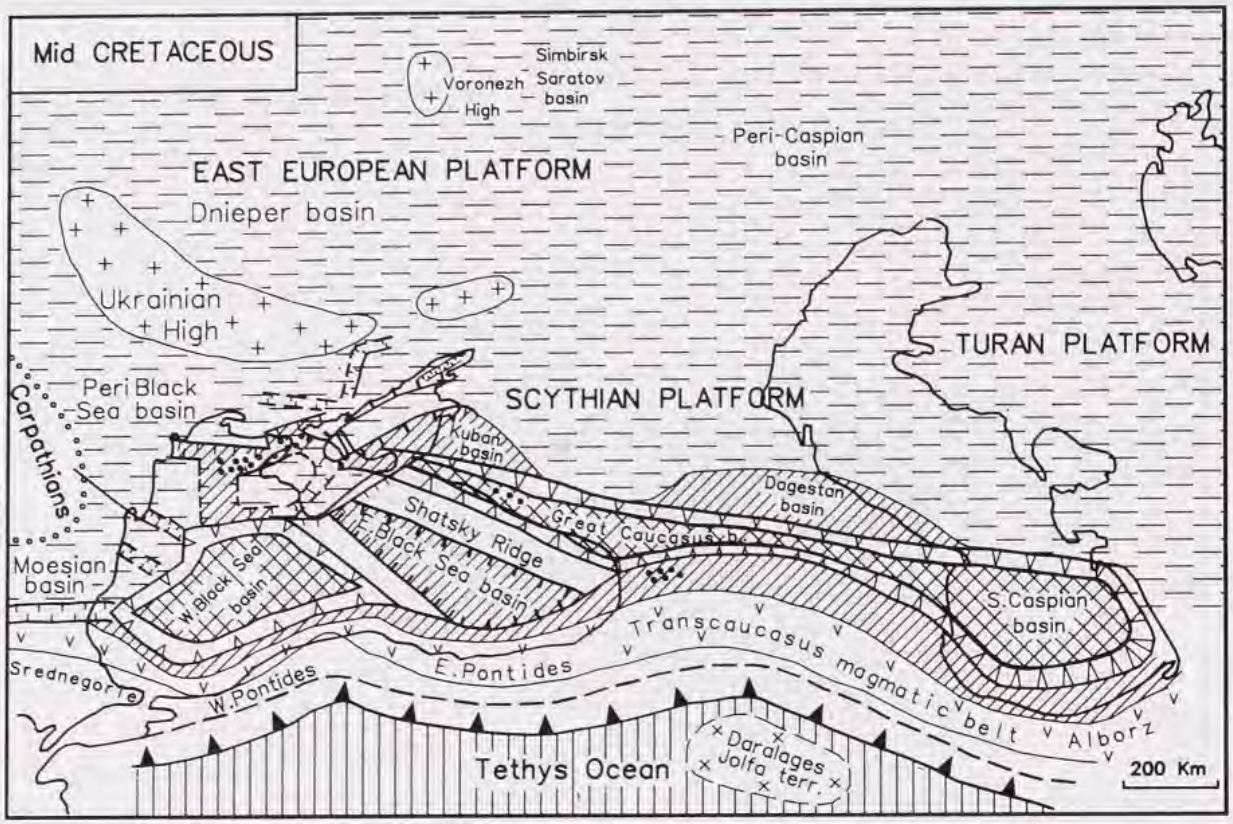

FIG. 5.— Mid-Cretaceous. See legend in figure 8.
FIG. 5.— Crétacé moyen. Légende, voir figure 8.

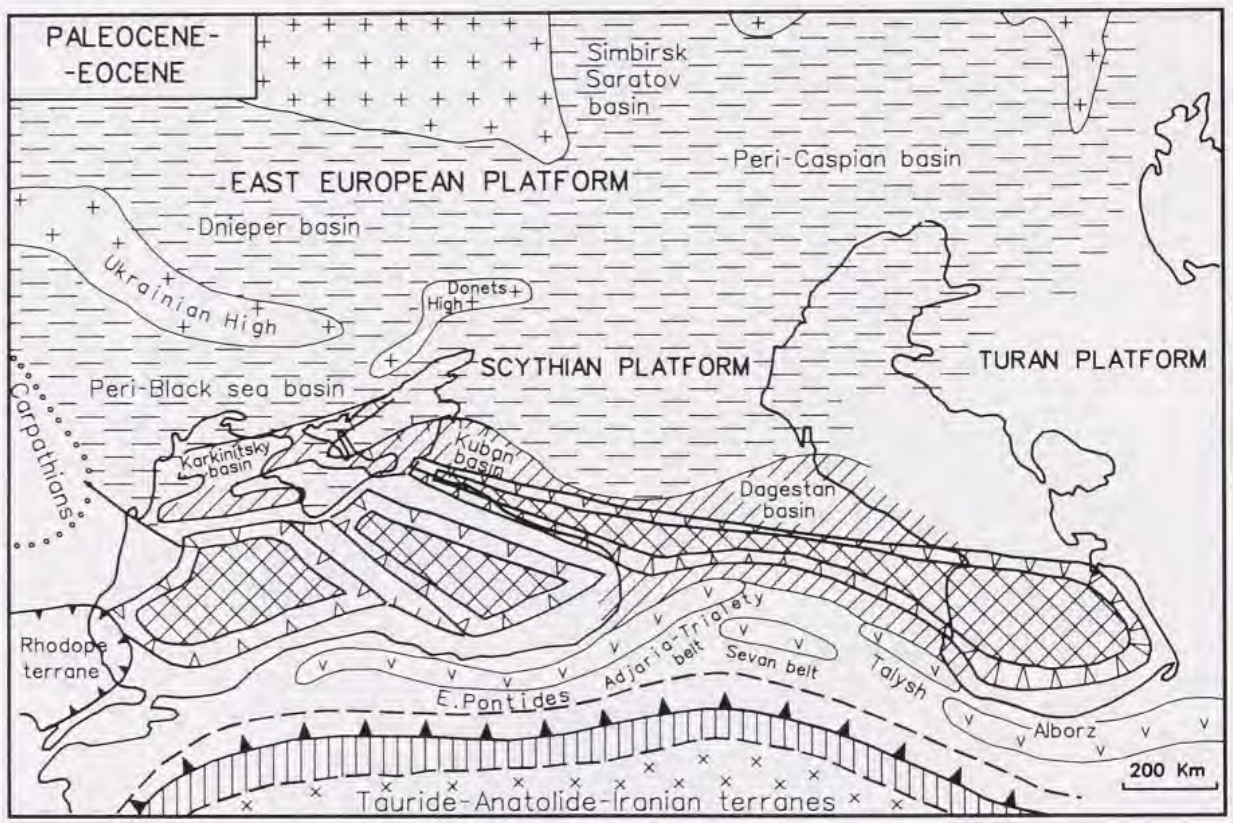

FIG. 6.— Paleocene-Eocene. See legend in figure 8.
FIG. 6.— Paléocène-Eocène. Légende, voir figure 8.

Source : MNHN, Paris

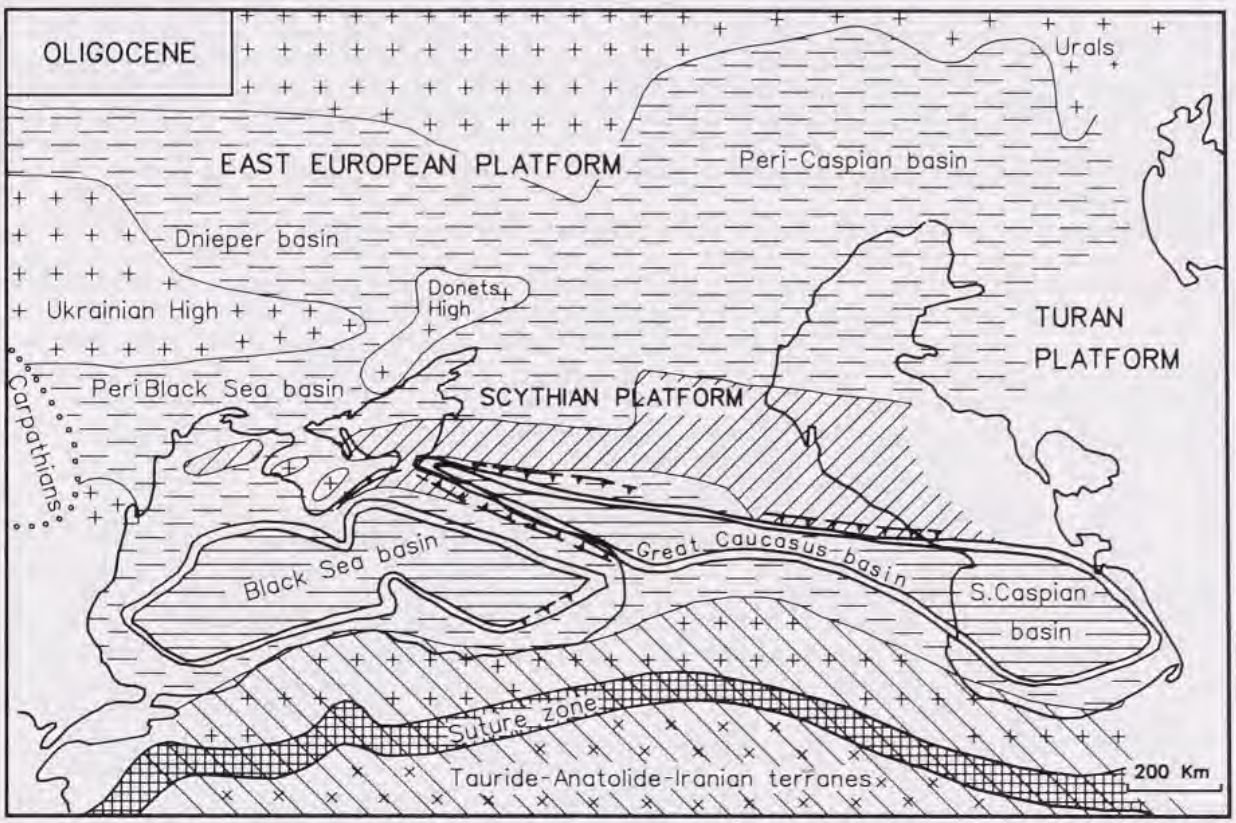

FIG. 7.— Oligocene. See legend in figure 8.
FIG. 7.— Oligocène. Légende, voir figure8.

CONCLUSION

Major continental rift system originated in the Early-Mid Triassic to the south of the East-European Platform. Collision orogeny in the Caucasus-Scythian area took place at the Triassic / Jurassic boundary.

During the Jurassic-Eocene times permanent subduction system was relatively stable, and subduction related magmatic belt was active along the Pontides-Transcaucasus-Alborz belt; the Caucasus-Scythian region was in a back-arc tectonic environment with many phases of back-arc extension and compression; polyphase subsidence complicated by uplift events of the Scythian Platform took place.

At the Eocene / Oligocene boundary the subduction system was transformed into a collision zone, syncollisional subducted slab roll-back followed by slab detachment took place together with the early Oligocene wide spread rapid subsidence event in the Scythian-Black Sea area.

During the Neogene - Quaternary the region underwent polyphase collision tectonics.

The Scythian Platform subsidence / uplift is a result of superimposed different subsidence mechanisms: synrift-postritf subsidence, foreland syncompressional subsidence; subduction-related subsidence of a broad region and so on.

ACKNOWLEDGEMENTS

The work was funded by the Peri-Tethys Program. The international programmes IGCP-369, INTAS, EUROPROBE and LITHOSPHERE supported our communications and discussions. Russian Geological Survey (ROSKOMNEDRA) sponsored our many years field works. We thank E.E. MILANOVSKY, V.E.

Source : MNHN, Paris

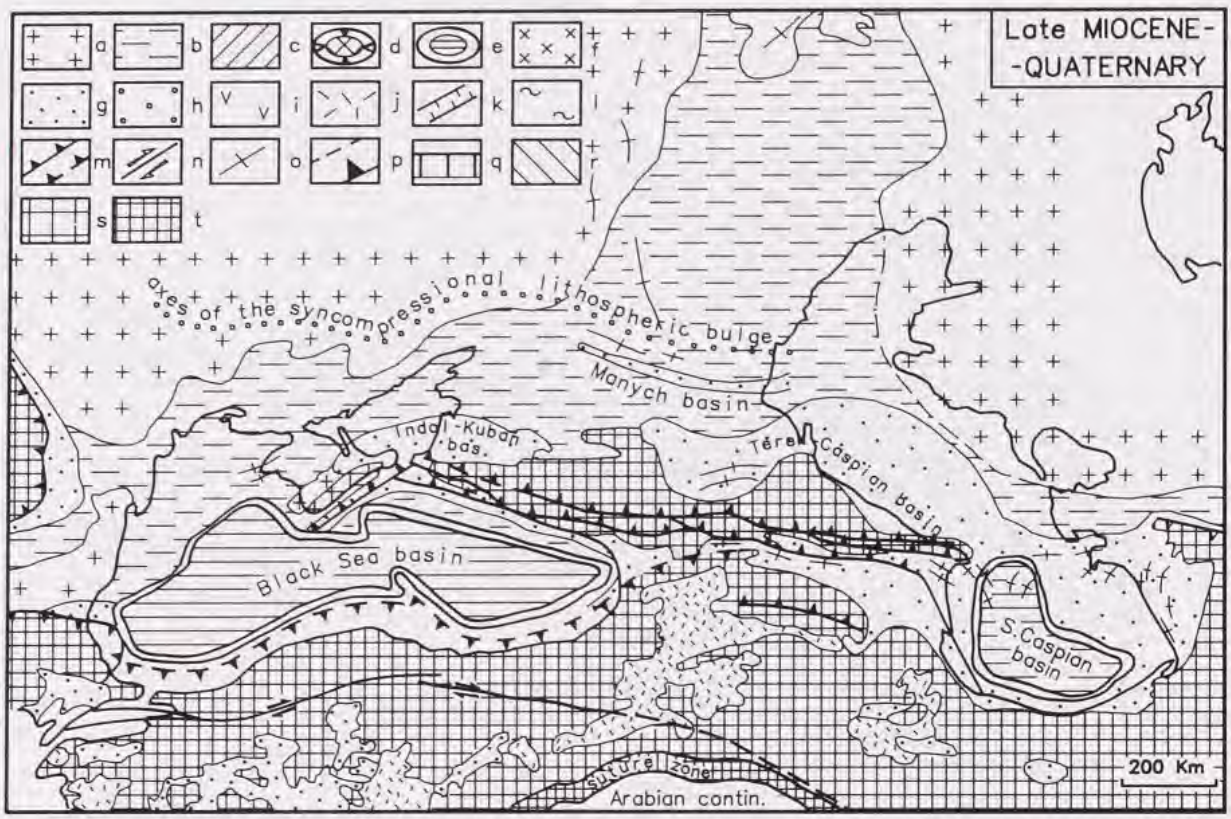

FIG. 8.— Late Miocene-Quaternary. Legende: **a**, land, mainly plains; **b**, shallow-water and continental sedimentary basins mainly; **c**, relative deep shelf marine sedimentary basin; **d**, back-arc deep-water basin with oceanic or very thin continental crust in tensional environment, dominantly; **e**, remnant deep-water back arc basin; **f**, continental terrane accreted to Europe; **g**, molasse basin; **h**, intraplate volcanites, mainly basalts; **i**, subduction related magmatic belt; **j**, syn-orogenic intracontinental volcanites; **k**, rift basin; **l**, inverted former rift basin; **m**, thrust belt; **n**, strike-slip fault; **o**, anticline fold; **p**, subduction zone; **q**, passive continental margin; **r**, areas which underwent syncompressional deformations and mainly uplift during the Late Triassic-Hettangian and Oligocene; **s**, areas with syncompressional deformation in the Aalenian and (or) pre-Callovian times; **t**, Alpine uplifted orogen. Other symbols are explained on the maps.

*FIG. 8.— Miocène supérieur-Quaternaire. Légende : **a**, terre émergée, principalement des plaines ; **b**, bassins sédimentaires d'eau peu profonde et continentaux ; **c**, bassin sédimentaire marin côtier relativement profond ; **d**, bassin arrière arc d'eau profonde avec une croûte océanique ou une croûte continentale très fine en environnement extensif dominant ; **e**, bassin arrière arc résiduel d'eau profonde ; **f**, "terrane" continental accrété à l'Europe ; **g**, bassin molassique ; **h**, volcanisme intraplaque, principalement des basaltes ; **i**, chaîne magmatique liée à une zone de subduction ; **j**, volcanisme intracontinental syn-orogénique ; **k**, bassin de rift ; **l**, bassin de rift inversé ; **m**, chaîne de chevauchement ; **n**, faille de décrochement ; **o**, pli anticlinal ; **p**, zone de subduction ; **q**, marge continentale passive ; **r**, zone ayant subi des déformations syn-compression et principalement des soulèvements durant la période Trias supérieur-Hettangien et Oligocène ; **s**, - zone ayant subi des déformations syn-compression à l'Aalénien et (ou) au pré-Callovien ; **t**, chaîne alpine soulevée. Les autres symboles sont expliqués sur les cartes.*

KHAIN, E.Yu. BARABOSHKIN, L.F. KOPAEVICH, B.P. NAZAREVICH, D.I. PANOV, M.G. LOMIZE, J. DERCOURT, P. ZIEGLER, W. CAVAZZA, V.G. KAZMIN, J.P. CADET, L.E. RICOU, G. STAMPFLI, E. GRADINARU, M. WILSON for fruitful discusions. Netherlands Research School of Sedimentary Geology contribution number 960413.

REFERENCES

ADAMIA, Sh.A., GABUNIA, G.L., KUTELIA, Z.A.,KHUTSYSHVILI, O.D. & TSYMAKYRIDZE G.K., 1989.— Characteristic features of Caucasus tectonics. *In:* A.A. BELOV & M.A. SATIAN (eds), *Geodynamics of Caucasus.* Nauka, Moscow: 3-15 (in Russian).

BAZHENOV, M.L. & BURTMAN, V.S., 1990.— *Structural Arc of the Alpine Belt: Carpathians, Caucasus, Pamir.* Nauka, Moscow: 1-165 (in Russian).

Source : MNHN, Paris

BELOV, A.A. & SATIAN, M.A. (eds), 1989.— *Geodynamics of Caucasus*. Nauka, Moscow: 1-215 (in Russian).

BELOUSSOV, V.V. & VOLVOVSKY, B.S. (eds), 1989.— *Structure and Evolution of the Earth's Crust and Upper Mantle of the Black Sea*. Nauka, Moscow: 1-208 (in Russian).

BENIJAMOVSKY, V.N. & SCHERBA, I.G., 1995.— About the deep-water structural zones on the Caucasus in the Paleocene according to the new micropaleontological data. *In*: V.YA. SHARAPAN (ed.), *Main Problems of the Geological Structure and Economical Geology of the Northern Caucasus*. Roscomnedra, Essentuki: 207-208.

CHEKUNOV, A.V., VESELOV, A.A. & GILKMAN, A.I., 1976.— *Geological Structure and History of the Peri-Black Sea Basin*. Naukova Dumka, Kiev: 1-164 (in Russian).

DERCOURT, J., RICOU, L.E. & VRIELYNCK, B. (eds), 1993.— *Atlas Tethys, Palaeoenvironmental Maps*. Gauthier-Villars, Paris: 1-307, 14 maps, 1 pl.

FINETTI, I., BRICCHI, G., DEL BEN, A., PIPAN, M. & XUAN, Z., 1988.— Geophysical study of the Black Sea area. *Bolletino di Geofisica Teorica ed Applicata*, **30** (117-118): 197-324.

GÖRÜR, N., 1988.— Timing of opening of the Black Sea basin. *Tectonophysics*, **147**: 247-262.

GÖRÜR, N., TÜYSÜZ, O., AYKOL, A., SAKINÇ, M., YIGITBAÇ, E. & AKKÖK, R., 1988.— Cretaceous red pelagic carbonates of northern Turkey: their place in the opening history of the Black Sea. *Eclogae Geologicae Helveticae*, **86**: 819-838.

KAZMIN, V.G. & SBORSCHIKOV, I.M., 1989.— Paleozoic and Early Mesozoic deformations on the Caucasus, and their place in the Tethys history. *In*: A.A. BELOV& M.A. SATIAN (eds), *Geodynamics of the Caucasus*. Nauka, Moscow: 46-54 (in Russian).

KHAIN, V.E., 1979.— North-Caucasus-Turkmenia-North-Afghanistan Late Triassic volcanic-plutonic belt, and opening of the Northern Tethys Zone. *Doklady Akademii Nauk SSSR*, **249** (5): 1189-1192 (in Russian).

KORONOVSKY, N.V., KOZHEVNIKOV, A.V., PANOV, D.I. *et al.*, 1987.— The history of geologic development and structure formation of the central part of Terek-Caspian trough. *In*: E.E. MILANOVSKY & N.V. KORONOVSKY (eds), *Geology and Mineral Resources of the Great Caucasus*. Nauka, Moscow: 147-174 (in Russian).

KRUGLOV, S.S. & TSYPKO, A.K. (eds.), 1988.— *Tectonics of the Ukraine*. Nedra, Moscow: 1-254 (in Russian).

LOMIZE, M.G., 1969.— *Volcanism of the North-Western Caucasus and its Connection with Tectonics*. Moscow State University Press, Moscow: 1-220 (in Russian).

LORDKIPANIDZE, M.B., 1980.— *Alpine Volcanism and Geodynamics of the Central Segment of the Mediterranean Fold Belt*. Metsniereba, Tbilisi: 1-162 (in Russian).

MAZAROVICH, O.A. & MILEEV, V.S. (eds), 1989a.— *Geological Structure of the Kacha Upland of the Mountain Crimea. Stratigraphy of the Mesozoic*. Moscow State University Press, Moscow: 1-168 (in Russian).

MAZAROVICH, O.A. & MILEEV, V.S. (eds), 1989b.— *Geological Structure of the Kacha Upland of the Mountain Crimea. Stratigraphy of the Cenozoic, Magmatism and Metasomatism*. Moscow State University Press, Moscow: 1-160 (in Russian).

MILANOVSKY, E.E., 1968.— *Neotectonics of the Caucasus*. Nedra, Moscow: 1-638 (in Russian).

MILANOVSKY, E.E., 1991.— *Geology of the USSR*. Vol. 3. Moscow State University Press, Moscow: 1-272 (in Russian).

MILANOVSKY, E.E. & KHAIN, V.E., 1963.— *Geological Structure of the Caucasus*. Moscow State University Press, Moscow: 1-357 (in Russian).

MILEEV, V.S., ROZANOV, S.B., BARABOSHKIN, E.Yu., NIKITIN, M.Yu. & SHALIMOV, I.V., 1995.— The position of the Upper Jurassic deposits in the structure of the Mountain Crimea. *Bulletin MOIP, Geologia*, **70** (1): 22-31 (in Russian).

MURATOV, M.V. (ed.), 1969.— *Geology of the USSR*. VIII: *Crimea. Part 1, Geology*. Nedra, Moscow: 1-576 (in Russian).

NIKISHIN, A.M., CLOETINGH, S., BOLOTOV, S.N., BARABOSHKIN, E.Yu., KOPAEVICH, L.F., NAZAREVICH, B.P., PANOV, D.I., BRUNET, M.-F., ERSHOV, A.V., IL'INA, V.V., KOSOVA, S.S. & STEPHENSON, R., 1998.— Scythian Platform: chronostratigraphy and polyphase stages of tectonic history. *In*: S. CRASQUIN-SOLEAU & É. BARRIER (eds), Peri-Tethys Memoir 3: stratigraphy and evolution of Peri-Tethyan platforms. *Mémoires du Muséum national d'Histoire naturelle*, **177**: 00-000.

OKAY, A.I., SENGÖR, A.M.C. & GÖRÜR, N., 1994.— Kinematic history of the opening of the Black Sea and its effect on the surrounding regions. *Geology*, **22**: 267-270.

PANOV, D.I. & GUSCHIN, A.I., 1987.— Structural-formational tectonic subdivisions of the Great Caucasus region for the Early and Middle Jurassic time, and the local Early-Middle Jurassic stratigraphy. *In*: E.E. MILANOVSKY & N.V. KORONOVSKY (eds), *Geology and Mineral Resources of the Great Caucasus*. Nauka, Moscow: 124-139 (in Russian).

PANOV, D.I., GUSCHIN, A.N., SMIRNOVA, S.B. & STAFEEV, A.N., 1994.— New data on geological structure of the Triassic and Jurassic sediments in the Lozovoe Zone in the Crimea, basin of the Bodrak river. *Vestnik Moscow State University, Geologia*, **3**: 19-29 (in Russian).

ROBINSON, A.G., BANKS, C.J., RUTHERFORD, M.M. & HIRST, J.P.P., 1995.— Stratigraphic and structural development of the Eastern Pontides, Turkey. *Journal of the Geological Society of London*, **152**: 861-872.

ROBINSON, A.G., RUDAT, J.H., BANKS, C.J. & WILES, R.L.F., 1996.— Petroleum geology of the Black Sea. *Marine and Petroleum Geology*, **13**: 95-223.

ROMANOV, L.F., TESLENKO, Yu.V. & YANOVSKAYA, G.G., 1987.— Aalenian organic remnants in the coal-bearing deposits of the Bushuy Mine in the Crimea (biofacial analysis). *In*: *Biostratigraphy and Paleontology of the Sedimentary Cover of the Ukraine*. Naukova Dumka, Kiev: 86-90 (in Russian).

Source : MNHN, Paris

ROSTOVTSEV, K.A. (ed.), 1992.— *Jurassic of the Caucasus*. Nauka, Saint-Petersburg: 1-192 (in Russian).

SAIDI, A. 1995.— *Migration Éocimmérienne et morcellement Mésozoïque des éléments continentaux de l'Iran*. Thèse, Université Pierre et Marie Curie, Paris, France: 1-280.

SANDULESCU, M., SEGHEDI, A., OAIE, G., GRADINARU, E. & RADON, S., 1995.— *Central and North Dobrogea, Romania. Field Guidebook, October 1-4, 1995 (IGCP Project n° 369)*. Geological Institute of Romania and University of Bucharest, Bucharest: 1-75.

SENGÖR, A.M.C. & KIDD, W.S.F., 1979.— Post-collisional tectonics of the Turkish-Iranian plateau and a comparison with Tibet. *Tectonophysics*, **55**: 361-376.

SENGÖR, A.M.C. & YILMAZ, Y., 1981.— Tethyan evolution of Turkey: a plate tectonic approach. *Tectonophysics*, **75**: 181-241.

SHARAFAN, V.Ya. (ed.), 1995.— *Main Problems of the Geological Investigations and Economical Geology of the Northern Caucasus*. Roscomnedra, Essentuki: 1-494 (in Russian).

SLAVIN, V.I., 1986.— Geological history of the Crimea peninsula in the Triassic. *Bulletin MOIP, Geologia*, **61** (6): 46-50 (in Russian).

SLAVIN, V.I., BYZOVA, S.L. & DOBRYNINA, V.Ya., 1983.— Geological structure of the Lozovoe zone in the mountain Crimea. *Bulletin MOIP, Geologia*, **58** (1): 43-53 (in Russian).

SLAVIN, V.I. & CHERNOV, V.G., 1981.— Geological structure of the Bitak formation (Toarcian-Middle Jurassic) in the Crimea. *Izvestiya Vuzov, Geologia i Razvedka*, **7**: 24-34 (in Russian).

STAMPFLI, G.M. & MARCHANT, R.H., 1995.— Plate configuration and kinematics in the Alpine region. *In*: R. POLINO & R. SACCHI (eds), *Rapporti Alpi-Appennino (e guide alle escursioni). Peveragno (CN), 31 Maggio- 1 Giugno 1994*. Accademia nazionale delle Scienze, Roma: 147-166.

TVALCHRELIDZE, G.A. & MIKHAILOV, A.E. (eds), 1985.— *South-Black-Sea Volcanic Belt and its Metallogeny*. Nauka, Moscow: 1-96 (in Russian).

TUGOLESOV, D.A., GORSHKOV, A.S., MEYSNER, L.B. *et al.*, 1985.— *Tectonics of the Mesozoic Sediments of the Black Sea Basin*. Nedra, Moscow: 1-215 (in Russian).

USTAOMER, T. & ROBERTSON, A.H.F., 1994.— Palaeozoic marginal basin and subduction-accretion, the Palaeotethyan Kure Complex, Central Pontides, northern Turkey. *Journal of the Geological Society of London*, **151**: 291-305.

WENSINK, H. & VAREKAMP, J.C., 1980.— Paleomagnetism of basalts from Alborz: Iran part of Asia in the Cretaceous. *Tectonophysics*, **68**: 113-129.

ZIEGLER, P., 1990.— *Geological Atlas of Western and Central Europe*. 2nd ed., Shell International Petroleum Mij., Den Haag: 1-239.

ZONENSHAIN, L.P. & LE PICHON X., 1986.— Deep basins of the Black Sea and Caspian Sea as remnants of Mesozoic back-arc basins. *Tectonophysics*, **123**: 181-211.

Source : MNHN, Paris

10

Triassic series on the Saharan Platform in Algeria; Peri-Tethyan onlaps and related structuration

Hamid AÏT SALEM [1], *Sylvie BOURQUIN* [2], *Louis COUREL* [2], *Berrached FEKIRINE* [1], *Cherif HELLAL* [1], *Leïla MAMI* [1] & *Mohamed TEFIANI* [3]

[1] SONATRACH, CRD, avenue du 1er novembre, 35000 Boumerdès, Algérie

[2] Centre des Sciences de la Terre de l'Université de Bourgogne
UMR CNRS 5561, 6, boulevard Gabriel, 21000 Dijon, France

[3] Institut des Sciences de la Terre de l'Université Houari Boumédienne
BP 32, 16111 El Alia Alger, Algérie

ABSTRACT

The aim of this paper is to understand the pattern of the Triassic deposits over the Algerian Saharan Platform and thus to establish a basis for structural hypothesis. Review of biostratigraphic and some unpublished palynologic data may open new perspectives. Palynologic assemblages are described from Ladinian / Carnian boundary in the east and from upper Carnian to Norian in the north. In the south-eastern part of the Algerian Sahara, new references about Anisian vertebrates remains allow to date the earliest Triassic series. More generally Triassic deposits commence earlier in the eastern part of the platform. Two cross-sections in the north of the Saharan Platform were studied, based on high-resolution sequence stratigraphy correlations. Seven minor stratigraphic cycles recording a complete cycle of base-level fall-to-rise, are observed in these series. They are part of the general base-level rise trend of a major stratigraphic cycle, i.e. a retrogradational trend. Main results concern the diachronism of the boundaries of the traditional Triassic lithostratigraphic units. During the Carnian, the dolomitic sebkha deposits grade westward, i.e. landward, into fluvial environments. During the Norian-Rhaetian, the evaporite series migrate in the same direction, while fluvial sandstones step landward in a transgressive pattern. The variations in thickness and facies of the Triassic series are controlled in details by pre-Triassic paleoreliefs and synsedimentary fracturation. Investigations were carried out by isopach map analysis, used with circumspection. Isopach plots of the lower series provide evidence of pre-Triassic paleotopography, mainly in the southern part of the platform. Later reactivation of these fractures was progressively associated with Triassic NE directions, mainly in the northern part of the platform. In the northern domain, during the Carnian / Norian stage, NE oriented trough persist, associated with a more regular surface, dipping very gently eastward, toward the marine peritethyan domain in Tunisia. The E-W elongated S4 salt formation with its first salt deposits above the clastic Triassic sediments seems to characterize Late Triassic / Jurassic opening of the Atlantic / Alpine Tethys domain.

AÏT SALEM, H., BOURQUIN, S., COUREL, L., FEKIRINE, B., HELLAL, C., MAMI, L. & TEFIANI, M., 1998.— Triassic series on the Saharan Platform in Algeria; Peri-Tethyan onlaps and related structuration. *In*: S. CRASQUIN-SOLEAU & É. BARRIER (eds), Peri-Tethys Memoir 3: stratigraphy and evolution of Peri-Tethyan platforms. *Mém. Mus. natn. Hist. nat.*, **177** : 177-191. Paris
ISBN : 2-85653-512-7.

Source : MNHN, Paris

RÉSUMÉ

Séries triasiques sur la plate-forme saharienne en Algérie ; onlaps péri-téthysiens et structuration associée.

Cette note vise à comprendre la géométrie et l'organisation des dépôts triasiques sur la Plate-forme saharienne en Algérie et à établir ainsi une base pour des hypothèses structurales. Une revue biostratigraphique et des données palynologiques inédites ouvrent des perspectives stratigraphiques nouvelles. Des cortèges palynologiques sont décrits, datés de la limite Ladinien / Carnien dans l'Est et du Carnien supérieur au Norien au Nord. Dans la partie sud-est de la Plate-forme saharienne, des données bibliographiques nouvelles concernant des restes de vertébrés permettent de dater de l'Anisien les plus anciennes séries triasiques de la Plate-forme. Plus généralement, les séries triasiques sont plus anciennes dans la partie orientale. Deux profils ont été étudiés dans le Nord de la Plate-forme saharienne, à partir de corrélations basées sur la stratigraphie séquentielle haute-résolution. Sept cycles stratigraphiques mineurs ont été reconnus dans ces séries, représentant un cycle complet de baisse à montée du niveau de base. Ils s'intègrent dans la tendance générale de montée du niveau de base d'un cycle stratigraphique majeur rétrogradant. Ainsi est établi le diachronisme des limites des unités lithostratigraphiques traditionnelles du Trias algérien. Au cours du Carnien, les dépôts dolomitiques de Sebkha gagnent vers l'Ouest, en direction amont, au dépens des environnements fluviatiles. Au cours du Norien-Rhétien, les séries évaporitiques migrent dans la même direction, pendant que les grès fluviatiles gagnent vers l'amont selon un modèle transgressif. Les variations d'épaisseur et de faciès des séries triasiques sont contrôlées dans le détail par les paléo-reliefs anté-triasiques et la fracturation syn-sédimentaire. Ces résultats sont basés sur une étude critique des cartes d'isopaques. La géométrie des isopaques des séries inférieures met clairement en évidence la paléo-topographie anté-triasique, principalement dans la partie sud de la plate-forme. La réactivation postérieure des fractures anciennes est progressivement associée à des directions NE, surtout dans le Nord de la plate-forme. Dans le domaine septentrional, pendant la période Carnien / Norien, une gouttière persistante d'orientation NE présente un fond plus régulier très légèrement incliné vers l'Est, en direction du domaine péri-téthysien marin en Tunisie. L'allongement E-W de la formation salifère S4, avec ses premiers dépôts salifères au dessus des sédiments clastiques triasiques, semble caractériser l'ouverture d'âge Trias supérieur / Jurasique du domaine téthysien atlantique / alpin.

INTRODUCTION

The Mesozoic Saharan Platform in Algeria is a vast Peri-Tethyan epicratonic domain bounded to the north by the "Saharan Flexure" or "Atlasic Flexure" (BUSSON, 1971). Two types of domain occurred north of this boundary in Triassic times, northern allochthonous series and southern autochthonous series (Fig. 1). The allochthonous series of the Maghrebides — the Kabyle Ridge — are part of the Tethyan domain in palaeogeographical terms (TEFIANI *et al.*, 1991; TEFIANI *et al.*, 1994; DURAND-DELGA & TEFIANI, 1994). The autochthonous Triassic series deposited north of the Saharan Flexure are poorly known in eastern Algeria. A few outcrops along the Tunisian border are related to diapirs (VILA, 1994; PERTHUISOT, 1994) or in the Baborian Zone of Tell (BOURMOUCHE *et al.*, 1996). In the Saharan Atlas, because of the depth of burial, there is only seismic data to indicate Triassic series about one thousand metres thick beneath several kilometres of Mesozoic cover (VIALLY *et al.*, 1994). Despite the scarcity of data and analogies with the Algerian (VIALLY *et al.*, 1994), Moroccan (BEAUCHAMP *et al.*, 1995) and Tunisian Triassic series, the autochthonous north domain is distinguished from the Saharan Platform by important and rapid thickness variations, in relation with synsedimentary structuration.

The Triassic Saharan Platform stands out as a vast area of relatively thin series (not exceeding 500 m) compared with the supposed thick deposits of the Saharan Atlas tectonic trough. The platform is open to the east, beyond the Tunisian border, but closed to the south and west where the Triassic deposits become thinner and even pinch out locally. To the north the Saharan Flexure marks the boundary of accessible Triassic deposits (*in situ* Triassic series deeper than 5,000 m). This paper attempts to highlight the characteristics of clastic and evaporitic sedimentation on the platform and its possible relations with the eastern marine domain. The significance of structural control will be revealed.

PERSPECTIVES

Following the pioneering works of Saharan geologists and rare oil industry publications, BUSSON (1967, 1970, 1971) proposed a stratigraphical, structural and palaeogeographical synthesis of the Triassic of the Saharan Platform in Algeria which remains a work of reference. Advances have been made in various fields since.

Biostratigraphical data by ACHAB (1970) and REYRE (1973) have been supplemented by oil industry reports that unfortunately are unpublished in part. Works by JALIL (1993, 1994), JALIL & TAQUET

Source : MNHN, Paris

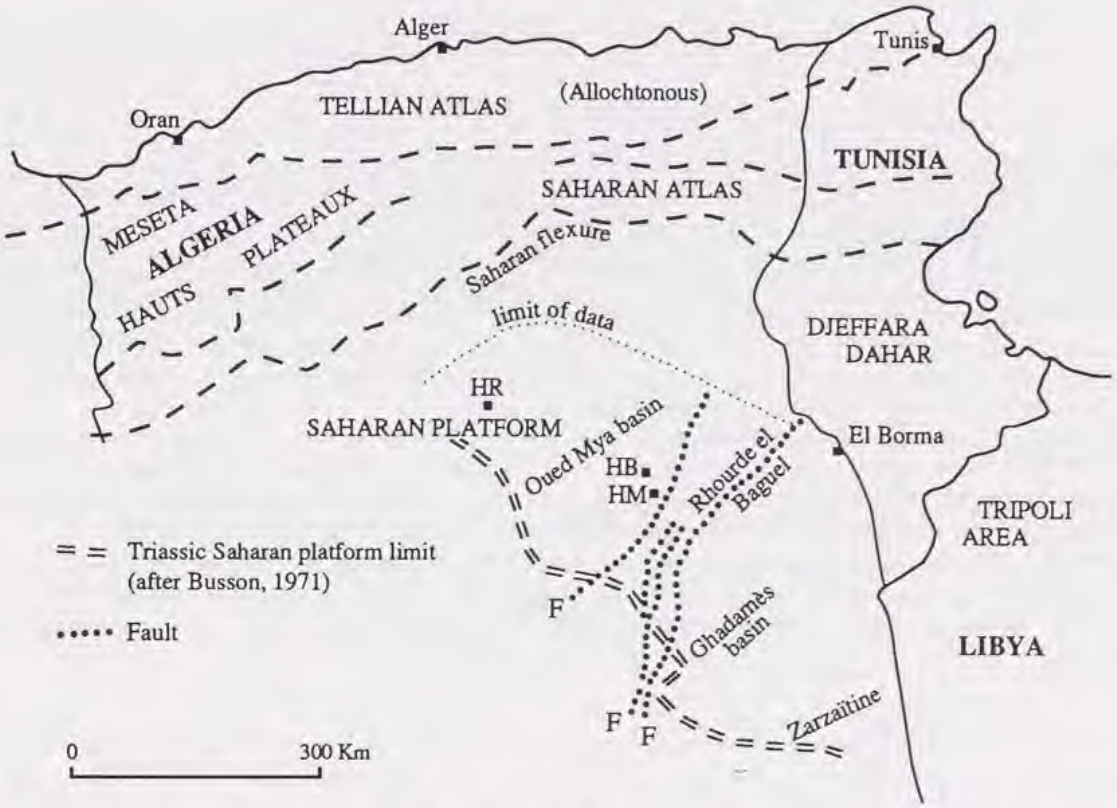

FIG. 1.— Triassic palaeogeographical sketch of Algeria; location map and major structural elements. HR- Hassi R'Mel, HB- Haoud Berkaoui, HM- Hassi Messaoud.

FIG. 1.— Carte paléogéographique schématique du Trias d'Algérie. HR- Hassi R'Mel, HB- Haoud Berkaoui, HM- Hassi Messaoud.

(1994) and JALIL *et al.* (1995) on vertebrate remains provide new evidence concerning the central issue of dating the Zarzaïtine Sandstones.

Sedimentological works (BENAMRANE, 1987; HAMEL, 1988; AÏT SALEM, 1992; AÏT SALEM & HELLAL, 1993; BAYARASSOU, 1994) and oil industry papers (DJARNIA, 1991; JONES & TURNER, 1993; DANIELS *et al.*, 1994; DEAKINS & DANIELS, 1994) have attempted to establish correlations between proximal and distal clastic continental series, transit directions and interpretations of relations with the marine domain.

Detailed investigations of the variations in facies and thickness of the Triassic series have proved the control of platform structuration. The influence of the Palaeozoic structural legacy was discussed by AÏT OUALI & NEDJARI (1994) and NEDJARI (1994). Fracturation has been particularly well studied in the oil reservoir areas (BOUDJEMA, 1987; HAMEL, 1988; AÏT SALEM, 1992; BOUDJEMA *et al.*, 1994; BAYARASSOU, 1994). Progress can now be made in interpreting the Triassic structuration of the Peri-Tethyan Platform.

This work focuses on clastic Triassic deposits and covers series older than what is known as the d2 dolomite. This series, with its southern argillaceous lateral equivalents, is so far the first reliable level of correlation above the pre-Triassic basement on a large part of the Saharan Platform in Algeria. Below this level BUSSON (1971) already presumed diachronism between clastics and evaporites in some instances. We seek to open up new perspectives on Peri-Tethyan Triassic onlaps, without claiming to provide an exhaustive synthesis of the Triassic series. Therefore, for methodological reasons, we shall attribute no value a priori to long distance correlations between the lithostratigraphical formations currently used ("Série inférieure", T1, T2, etc.). Our aim is to understand the relationships between proximal and distal clastics and between clastics and evaporites during advances of the Triassic sedimentation domain over the Saharan Platform.

Source : MNHN, Paris

REGIONAL FRAMEWORK

The Palaeozoic legacy is clearly marked in the morphology of the base of the Triassic. AÏT OUALI & NEDJARI (1994) and NEDJARI (1994) emphasised the structuration of the Triassic Platform into SW-NE or SSW-NNE oriented strips in relation with the reactivation of Panafrican and / or Late Palaeozoic fractures. The occurrence of emerged palaeoreliefs that were gradually buried beneath the base of the Triassic series has been clearly demonstrated, as for example on the Hassi-R'Mel structure, by BUSSON (1971), BENAMRANE (1987), BOUDJEMA (1987), HAMEL (1988), DJARNIA (1991), BOUDJEMA *et al.* (1994) and BAYARASSOU (1994). The same workers, however, emphasised the likely reactivation of fractures during the deposition of the Triassic of Hassi-R'Mel. Similar conclusions have been drawn for other sites, especially at Hassi-Messaoud (AÏT SALEM, 1992).

Thorough knowledge of structuration of the Saharan Platform in the Triassic would require a combined study of isopach maps at successive time intervals, a sedimentological analysis across the entire domain and also a subsidence analysis. At this stage, a preliminary examination of the isopach maps based on lithostratigraphic correlations can be used to outline the platform structure:

— Westward thinning, inferred from analysis of the "Série inférieure" Formation isopachs (Fig. 2). The isopach data are confined to the north of the platform but other data point to the same trend further south. The "Série inférieure" clearly thins out on the highs of Hassi-R'Mel, Hassi-Messaoud and Talemzane.

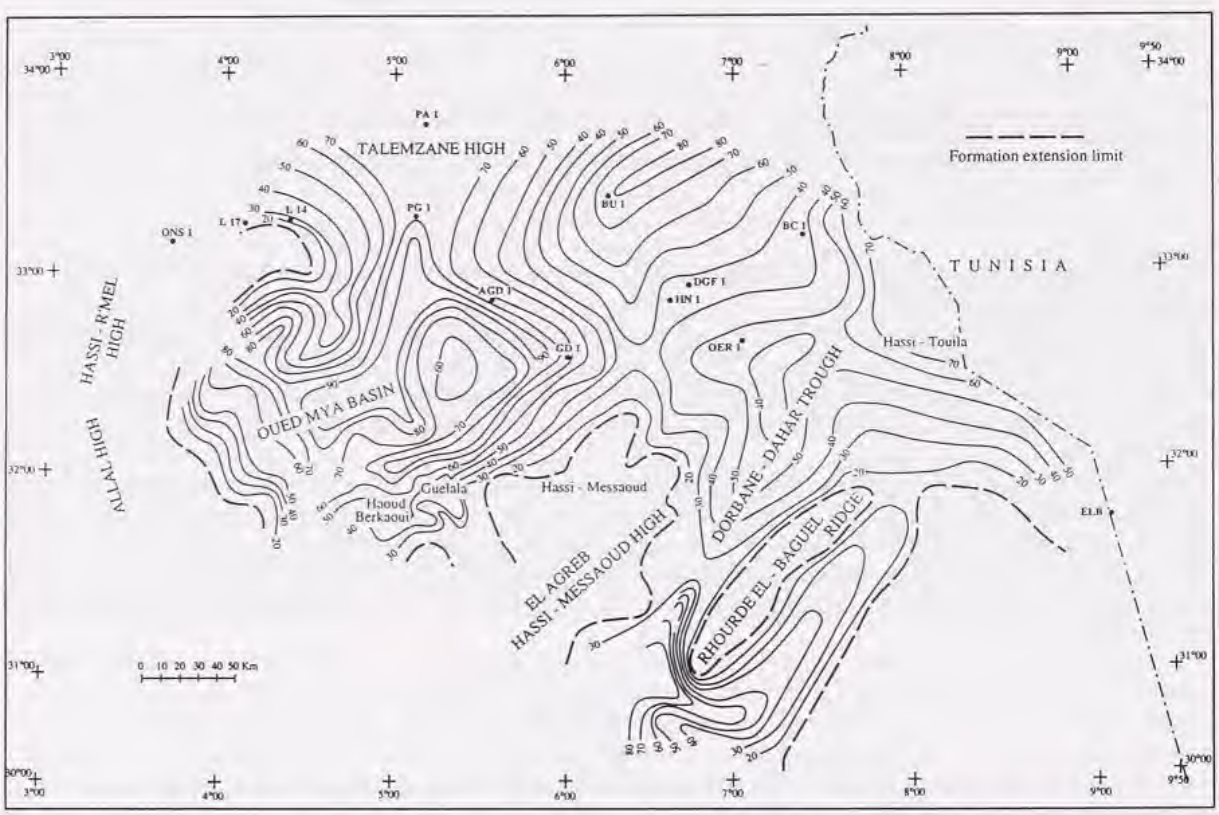

FIG. 2.— Isopach map of the "Série inférieure", northern part of the Saharan Platform; isopach values in meters (HELLAL, FEKIRINE & AÏT SALEM, Sonatrach doc.)

FIG. 2.— Carte des isopaques de la Série inférieure, partie nord de la Plate-forme saharienne ; valeurs des isopaques en mètres (HELLAL, FEKIRINE & AÏT SALEM, documents Sonatrach)

Source : MNHN, Paris

— The distribution and geometry of depocentres and the highs separating them is mapped (Fig. 3) mainly from detailed studies (well-logs, seismic and gravimetric) of thickness variations at the edges of the highs. On this scale, N-S alignments predominate in the south whereas SW-NE alignments occur in the north.

— A large N-S fracture belt crosses the platform from Hassi-Messaoud to El Biod, as reported by BUSSON (1971), BOUDJEMA (1987), AÏT SALEM (1992), BAYARASSOU (1994), HAMEL (1988). It includes highs and fractures. These are essential features in the division of the platform into two separate areas of sedimentation: the Ghadames Basin to the east and the Oued Mya Basin to the west.

Based on this outline of the regional setting, sequence stratigraphy correlations along two transects provide new data on facies distribution across the platform during the Triassic. First though it is essential to define a chronological framework despite the inherent difficulties where continental clastic series are concerned.

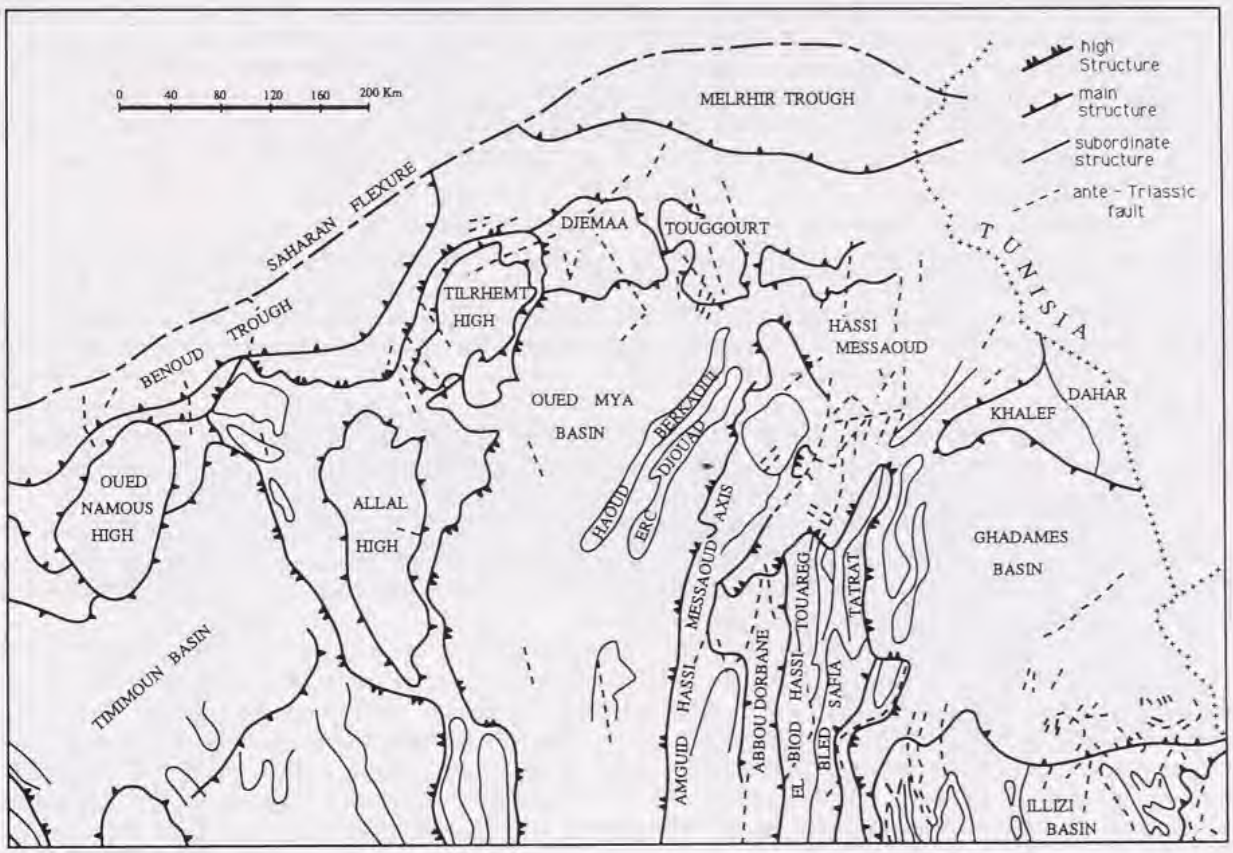

FIG. 3.— Structural sketch of the Saharan Platform under the Triassic cover. After SONATRACH geophysic and drilling data.
FIG. 3.— Carte structurale schématique de la Plate-forme saharienne sous la couverture triasique. D'après données de forages et géophysiques de la SONATRACH.

BIOSTRATIGRAPHIC DATA AND CHRONOLOGICAL FRAMEWORK

Palynology is the main biostratigraphical tool in what are essentially sandy / silty and argillaceous series. Works by BIARD (1963), ACHAB (1970) and REYRE (1973) form a starting point. Their chronological framework was used by BEICIP (1978), Total (1979) and SONATRACH in-house reports (MAMI, 1980; BOURMOUCHE, 1982; MAMI, 1989; MAMI & BOURMOUCHE, 1994). Nevertheless biostratigraphy has still not established a single correlation level. Worse still, the Triassic / Liassic

Source : MNHN, Paris

boundary is still not precisely defined by any fossil assemblage or localised in the series. For practical purposes, since ACHAB (1970) and BUSSON (1971) the Hettangian d2 marker acts as the ceiling to supposed Triassic series although the biostratigraphic upper boundary of the Triassic has not been defined. Below, only the Upper Triassic has been formally identified by palynology. REYRE (1973) did describe, though, a *Disacites* assemblage that was not *striatiti* and was devoid of *Classopolis* (or with a few rare individuals) (zone 1) which "might be characteristic of the Middle Triassic plus perhaps part of the Upper Triassic" in the Gassi-Touil area. In this same eastern region close to the Tunisian border Busson suggested the presence of a Middle Triassic series primarily on the basis of lithological correlations with Tunisia.

Unpublished palynological works (Mami, SONATRACH) report the following points:

— At the DAS-1 well (Figs 4, 5) at the Hassi-R'Mel site (2259 - 2262 m) the assemblage of *Enzonalasporites vigens*, *Tsugaepollenites oriens*, *Ovalipollis pseudoalatus*, disaccates of the genus *Alisporites* and the persistence of *Circulina* are indicative of late Carnian / early Norian age.

— The upper Carnian was recognized in a number of wells by a rich and well preserved assemblage with *Camesporites secatus* and the occurrence of *Brodispora striata* in conjunction with *Patinasporites densus*, *Vallasporites ignacii*, *Enzonalasporites vigens*, *Praecirculina granifer* and *Duplicisporites granulatus*. This assemblage was collected from wells EBW1 (El Borma region on the Tunisian border, Fig. 1, 2316 - 2414.50 m), RHA1 (Rhourde el Baguel Trough region, Fig. 1, 3089.90 - 3106.50 m) and also from wells whose sedimentology is studied below (section Fig. 4): LI4 (2986.50 - 3033.50 m), PG1 (3470 - 3555.90 m) and PH1 (3815.70 - 3854 m) on the Talemzane high.

— A third assemblage was found in well EBW1 (2419 - 2504 m) (El Borma region on the Tunisian border, Fig. 1). The microflora is characterised by the absence of *Brodispora striata* and persistence of smaller quantities of *Camerosporites secatus* and *Duplicisporites granulatus*. Bisaccates predominate, especially the genera *Pityosporites*, *Sahnites* and *Ellipsovelatisporites*. Sparse spores are found of the genera *Verrucosisporites* and *Reticulosisporites*. *Camerosporites secatus* was reported from the Middle and Upper Triassic by SCHEURING (1970, 1978), SCHURMAN (1977), VISSHER & KRYSTYN (1978), VISSHER & BRUGMAN (1981) and VAN DER EEM (1983). The oldest report of *C. seccatus* comes from Ladinian (MOY & TRAVERSE, 1986). This third Saharan assemblage suggests an upper-Ladinian / Carnian age, which are the earliest reported in wells of the Algerian Sahara, and which is consistent with the findings of REYRE (1993) referred to above.

In view of the location of the assemblages described for the wells, these new palynological data confirm that the Triassic series commence earlier in the east (EBW1 well). The chronological framework defined by palynology is, however, too loose to allow correlations between the lower and upper boundaries of the clastic or evaporitic formations.

Vertebrate remains are known from outcrops of the Zarzaïtine series in the extreme south-east of the Algerian Triassic domain. Since LEHMAN (1957) collections have been increased and datings revised but the fauna have still not been clearly located in the gritty series. Two assemblages, however, can be distinguished palaeontologically and chronologically. They are thought to be superposed but in the same hundred metre high cliff. Work is underway to attempt to resolve the question of their location. The most recent datings by JALIL (1993, 1994), JALIL & TAQUET (1994) and JALIL *et al.* (1995) are now very informative. Remains of Capitosaurids, Trematosaurids and Brachyopoids collected from the cliff base are dated as early Anisian (Spathyan age is no longer mentioned in the latest publications). Above, the other assemblage has yielded *Aetosaurus* and *Phytosaurus* dated as late Carnian to early Norian (JALIL *et al.*, 1995). It is now ascertained that the Middle Triassic occurs in the south-east part of the Saharan Platform in Algeria. The significance of this finding will be discussed later.

HIGH-RESOLUTION SEQUENCE STRATIGRAPHY OF THE NORTHERN PART OF THE ALGERIAN SAHARAN PLATFORM: STRATIGRAPHIC CYCLE GEOMETRY

This study was carried out on two cross-sections in the north of the Saharan Platform: an E-W section between the Tunisian border and the Hassi-R'Mel area (Fig. 4) and a N-S section within the Hassi-R'Mel area (Fig. 5). All the series are part of the Upper Triassic, Carnian to Hettangian. The transects are bounded at the top by a dolomitic unit, named d2, which is dated as Hettangian.

Source : MNHN, Paris

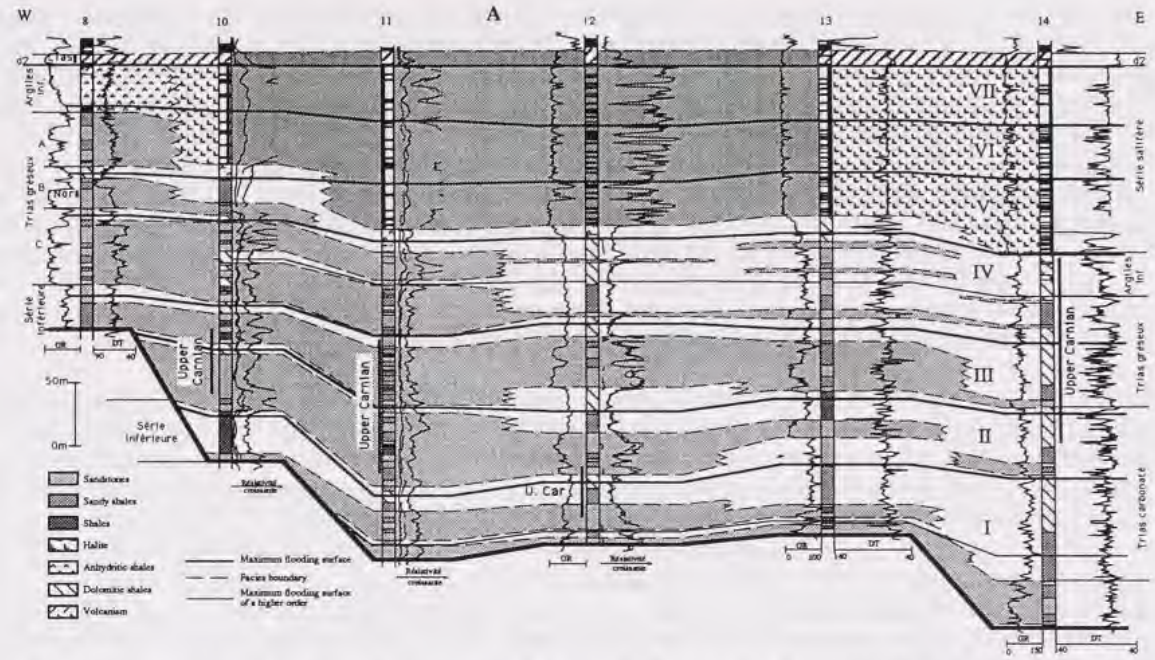

FIG. 4.— Triassic east-west stratigraphic cycles geometries between the Tunisian border and the Hassi R'Mel area. Nor: Norian; I to VII: stratigraphic minor cycles. See figure 5 for the location.

FIG. 4.— Géométrie des cycles stratigraphiques dans le Trias selon une section est-ouest, de la frontière tunisienne à la région d'Hassi R'Mel : Nor: Norien; I à VII : cycles stratigraphiques mineurs. Voir figure 5 pour la localisation.

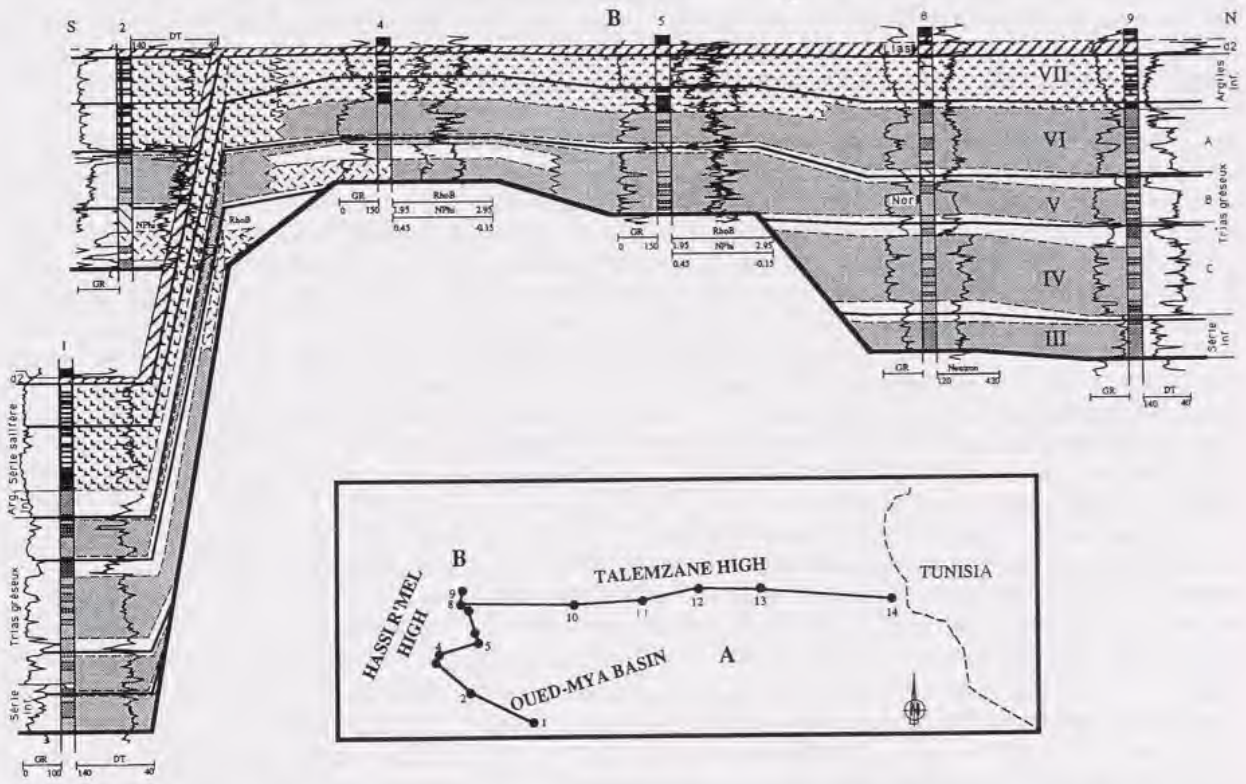

FIG. 5.— Triassic north-south stratigraphic cycles geometries within the Hassi R'Mel area. See figure 4 for the keys.

FIG. 5.— Géométrie des cycles stratigraphiques dans le Trias selon une section nord-sud, dans la région d'Hassi R'Mel : Voir figure 4 pour la légende.

Source : MNHN, Paris

BUSSON (1971) proposed lithostratigraphic correlations and supposed that the sandstone deposits are more recent at the west of the Saharan Platform and that the upper part of the "Trias gréseux" Formation might be the equivalent of the lower part of the salt deposits in the centre and east of the platform. Only high-resolution sequence stratigraphy could establish correlations between the basin-centre evaporite series and the basin-margin clastic series.

Correlations within the Triassic series of the north of the Saharan Platform are based on high-resolution sequence stratigraphy, where stratigraphic cycles of different scales and durations are recognised. Correlations and cycle ranks are based on the identification of the smallest stratigraphic units, i.e. genetic sequences recorded in well logs, calibrated on cores, and their grouping on larger scales by stacking pattern analysis (CROSS, 1988; HOMEWOOD *et al.*, 1992; CROSS *et al.*, 1993). Genetic sequences are defined as packages of strata representing a complete base-level cycle of sediment accumulation (BUSCH, 1971) with no further details as to base-level cycle origin, cycle duration or cycle symmetry.

Within the predominantly continental Triassic strata, base-level rise-to-fall turnaround surfaces or maximum flooding surfaces can be correlated easily across the basin (BOURQUIN & GUILLOCHEAU, 1993; BOURQUIN & GUILLOCHEAU, 1996; COUREL *et al.*, 1994). In such instances, each genetic sequence is bounded by base-level rise-to-fall turnaround surfaces and records a complete cycle of base-level fall and rise. By observing whether the stacking arrangement of genetic sequences are successively more landward (or deeper or thicker) or more seaward (or shallower or thinner, or more amalgamated) different scales of stratigraphic cycles are identified.

In the E-W section, the Triassic series are made up of four lithostratigraphic units in the west: the "Série inférieure", "Trias gréseux", "Argiles inférieures" and "Série salifère" (Fig. 4). The facies are more distal to the east and the fluvial sandstones grade laterally eastward into dolomitic sabkha (Fig. 4). Westward a carbonate unit is more-or-less developed within the "Trias gréseux" Formation (Fig. 4). Within the Hassi-R'Mel area, Triassic series are made up of three lithostratigraphic units (Fig. 5): "Série inférieure", "Trias gréseux", comprising three units — C, B and A — and the "Argiles inférieures" (gypseous or anhydritic shales). The "Série inférieure" Formation and unit C are dated as upper Carnian, while units, B, A and the "Argiles inférieures" Formation are dated as Norian to Rhaetian (HAMEL, 1988). The three sandstone units start with fluvial deposits overlain by lagoonal dolomitic or anhydritic shales (HAMEL, 1988). A volcanic episode occurred within this area the Hassi-R'Mel High where Triassic series are not complete.

Correlations of the two cross-sections (Figs 4, 5) show that the boundaries of the Triassic lithostratigraphic units are diachronous. Seven stratigraphic minor cycles (I to VII), bounded by maximum flooding intervals within dolomite shales, are observed within these series (Fig. 4). These cycles record a complete cycle of base-level fall-to-rise. The turnaround surface from base-level fall-to-rise on the scale of these cycles cannot be characterized easily either at the base or in the lower part of fluvial deposits in the absence of core data from all the wells. Within the salt series, each genetic sequence is made up of halite and shale couples, and the three minor cycles (V, VI, VII) display vertical evolution where the genetic sequences are increasingly argillaceous. These seven minor cycles are part of the general base-level rise trend of a major cycle, i.e. a retrogradational trend, that cannot be further characterized in the study area, exhibiting the transition from fluvial sandstone to halitic sabkha deposits and then to dolomitic deposits. The biostratigraphic data obtained from some wells (Fig. 4) confirm that the first four cycles are part of the upper Carnian. However, the lower part of the first cycle could be older, especially in the eastern wells.

Correlations on the N-S section reveal five stratigraphic minor cycles, bounded by maximum flooding intervals within lagoonal shales (Fig. 5). On the high, where wells HR9, HR150 and HR177 are correlated, Triassic sedimentation began with the fluvial sandstones of unit B. Two episodes of volcanism may have occurred in the south of this area (Fig. 5). High-resolution sequence stratigraphy correlations indicate that the first two cycles of the E-W section are missing in the Hassi-R'Mel area (Figs 4, 5). Unit C, dated as upper Carnian, is equivalent to the third cycle. Unit B, dated as Norian, represents the lateral landward equivalent of the base of the "Série salifère" in the east and can be correlated with the fifth cycle (first salt cycle). The sixth cycle (second salt cycle) grades westward into the fluvial deposits of unit A. In the seventh cycle, the halitic deposits migrate westwards into anhydritic or dolomitic deposits devoid of fluvial sandstones.

These high-resolution sequence stratigraphy correlations establish stratigraphic cycle geometries. The Triassic series of the north of the Saharan Platform feature seven cycles which are part of a general

Source : MNHN, Paris

base-level rise trend of a major cycle, i.e. retrogradational trend. Four cycles occurred during the late Carnian. In the east these cycles are essentially composed of dolomitic sabkha deposits and grade westward, i.e. landward, into fluvial depositional environments ("Série inférieure", "Trias gréseux", "Argiles inférieures" and unit C of the Hassi-R'Mel area). During the Norian-Rhaetian, the evaporite series migrate westward, or landward, while fluvial sandstones of units B and A step landward in a transgressive pattern. Vertical aggradation predominates towards the top of the salt series, with lateral transition of the halitic deposits into anhydritic or dolomitic deposits. These high-resolution sequence stratigraphy correlations could allow correlations in the Saharan Platform between Algerian and Tunisian Triassic series.

TRIASSIC STRUCTURATION OF THE SAHARAN PLATFORM IN ALGERIA

Reconstructing the structural history of the Saharan Platform in Triassic times in Algeria requires sound knowledge of the nature and geometry of sedimentary bodies but also involves situating them in their chronological framework. Biostratigraphic data are unfortunately of little help and sequence stratigraphy correlations are confined to transects where detailed studies have been undertaken. The proposed scheme of the distribution of clastic and evaporitic sedimentary series over space and time is still only an outline but may serve as a basis for structural hypotheses.

First it should be noted that the earliest Triassic deposits on the Mesozoic Saharan Platform are thought to date from the Middle Triassic and to be located in the Zarzaïtine region, close to the Libyan border (Fig. 1). Detailed isopach maps by BUSSON (1971) of the region of the south-east of Hamada de Tinrhert exhibit a series of bands suggesting sedimentation troughs generally open towards the ENE. The earliest Algerian Triassic deposits are thought to join up with an eastern domain. Marine facies of the same age are known in Libya and in the Arabian peninsula. Further north, BUSSON (1971) and more recent works (BOUAZIZ, 1988; BEN ISMAIL, 1991; CHANDOUL *et al.*, 1993) show that the Triassic series of southern Tunisia could have been deposited from Scythian times onwards and that Carnian marine strata are known in the Mekhraneb Dolomite.

In the northern region of the Saharan Platform, BUSSON's proposal (1971) ascribing the greater thickness of the "Série gréseuse inférieure" in the east to earlier subsidence in the east than in the west is confirmed by our description of a progressive retrogradation.

The variations in thickness and in facies of the Triassic series are controlled in detail by pre-Triassic palaeorelief and synsedimentary fracturation. They are investigated by isopach map analyses. Unfortunately, these are based on lithostratigraphic correlations and not on time-lines. They must therefore be used with circumspection. They are confined to the northern part of the platform (Fig. 6) and are designed to highlight structures on the scale of a hundred kilometres within a limited time interval. This local information must be supplemented by the map that extends further south (Fig. 3). This map covers, for all the Triassic series, the major features of thickness variations, whose contours are smoothed to try to depict the main depocentres and highs.

Isopach plots of the lower series (Fig. 2) are the ones most likely to represent diachronous formations. They provide clear evidence of the pre-Triassic palaeotopography. Whereas the directions inherited from Panafrican and Hercynian times are clearly N-S in the southern part of the platform, these orientations which subsist in the northern area bend for the most part to NE, from the Rhourde el Baguel Ridge to the Hassi-R'Mel Dome via the Dorbane-Dahar Trough, the El Agreb / Hassi-Messaoud Horst and the Oued Mya Basin (AÏT SALEM, 1992). It should be noticed that these orientations mark extensions of sedimentary units and may include orientations of different fractures or flexuration.

Isopach plots of the formation located between the two sets of volcanic flows (Fig. 7) concern a poorly defined time interval, given that the flows are probably but not definetly of the same age on the scale of the same field, but that their ages may vary from field to field. The occurrence of fissure type volcanism and highly contrasted thickness variations are, however, probable indicators of substantial fracturation. The NE orientation of the extensions of sedimentary units appears more plainly than before in a domain where subsidence was probably faster and more irregular.

Isopach plots T1 and T2 on the scale of a vast northern domain (Fig. 8) exhibit two types of characteristic. South of the region on the map, the transit system via NE oriented troughs persists, especially in the Oued Mya Basin and the Dorbane Basin. To the north, a much more regular surface seems to stand out, dipping very gently eastwards towards Tunisia, where subsidence is clearly more

Source : MNHN, Paris

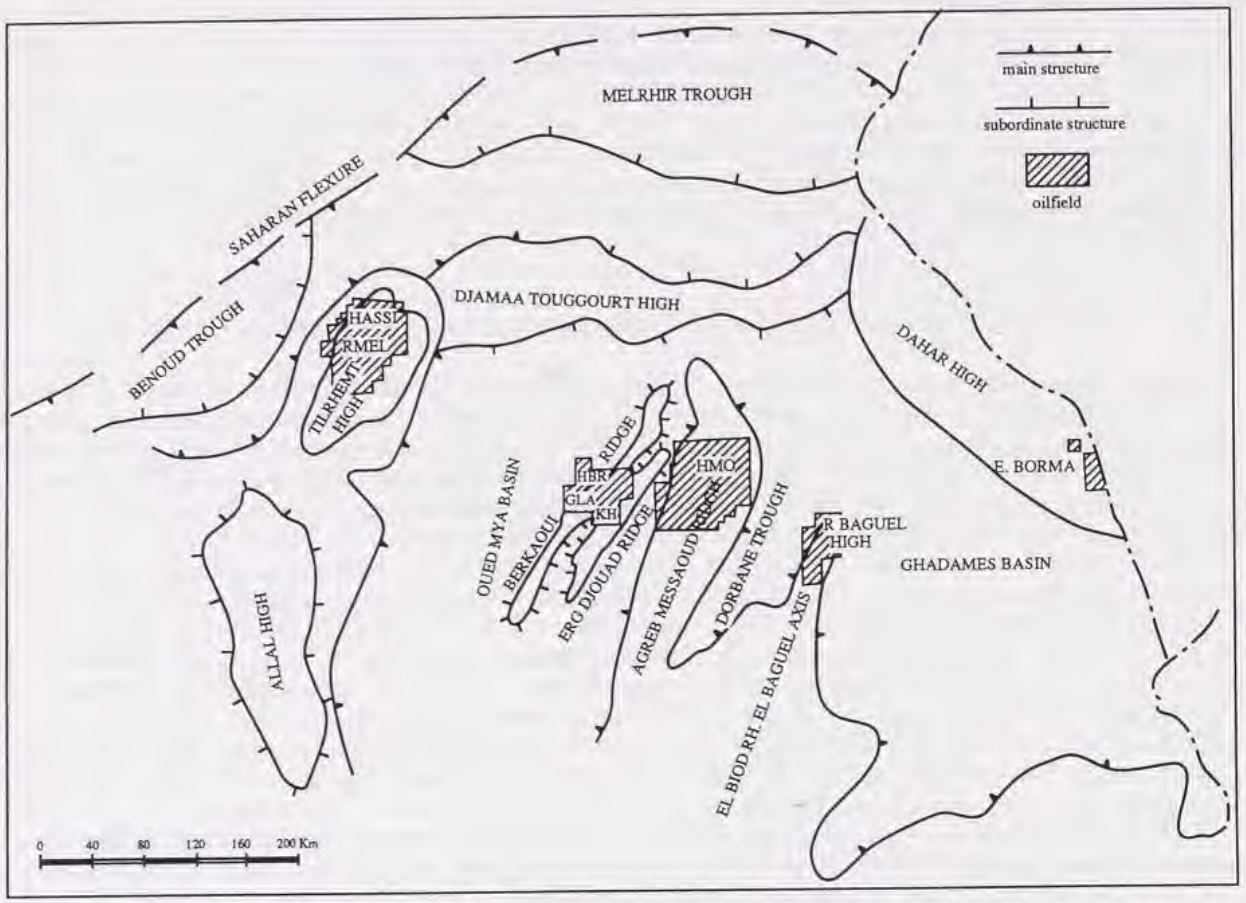

FIG. 6.— Structural sketch of the northern part of the Saharan Platform (details of the figure 4) under the Triassic cover. After SONATRACH geophysic and drilling data.

FIG. 6.— Carte structurale de la partie nord de la Plate-forme saharienne (détails de la figure 4) sous la couverture triasique. D'après données de forages et géophysiques de la SONATRACH.

marked (310 m of sediment on the Tunisian border). By contrast, the series thins out westwards on the edges of the Talemzane, Hassi-R'Mel, Allal and Hassi-Messaoud Highs.

The S4 Salt Series (Fig. 9) is clearly bounded to the south but its northward extent is unknown. It shows series of even thickness and thinning of the salt serie towards the west. This thinning results from halitic facies passing laterally into basin-margin fluviatile sandstones in a retrogradational pattern.

By adding the thicknesses of all the Triassic formations, the lines would mask the stages in the development of structuration over time. These stages do appear though in the examination of successive isopach maps, which, however, omit a large southern area of the Saharan Platform. The Mesozoic structuration is progressively established on the basis of the pre-Triassic legacy in the form of NS-oriented reactivated fractures and overall palaeotopography. Sedimentary transit orientations bend first eastward and then NE-oriented fractures are clearly established, in conjunction with fissure type volcanism in the Hassi-Messaoud and Rhourde el Baguel fields. A vast domain of sedimentation with series that progressively thicken eastwards, where maximum subsidence occurs, is then established throughout a large northern region. The salt series towards the east was laid down in a vast E-W trough bounded abruptly to the south.

Before concluding it should be recalled that the interpretation of the isopach plots is questionable as thickness cannot be converted directly into subsidence values. Isopach maps merely provide indications about the geometry of faciological units, which is evidence nevertheless of morpho-structural parameters. The stress fields responsible for this pattern of development cannot be read directly from the isopach plots. It is fairly clear though that the WSW-ENE fracturation directions characteristic of the

Source : MNHN, Paris

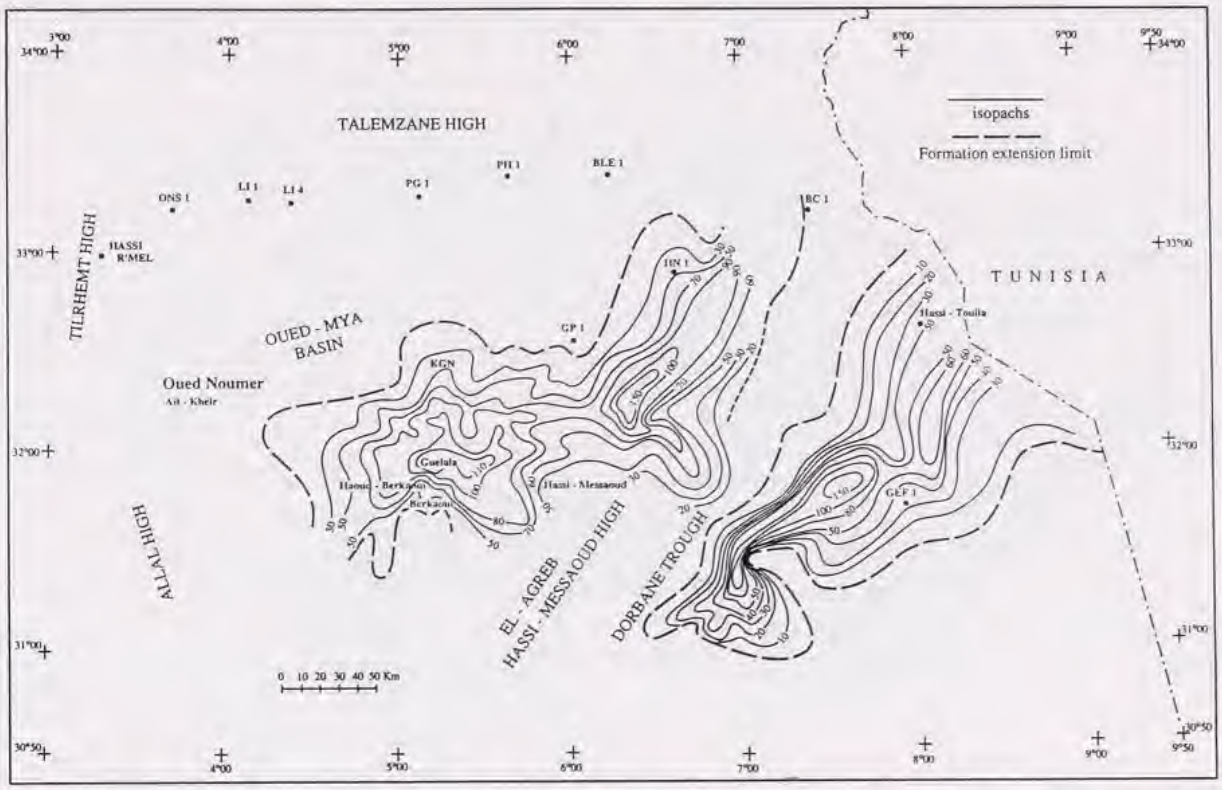

FIG. 7.— Sopach map of the "Trias éruptif" Formation, northern part of the Saharan Platform; isopach values in meters (HELLAL, FEKIRINE & AÏT SALEM, Sonatrach doc.)

FIG. 7.— Carte des isopaques de la formation du Trias éruptif, partie nord de la Plate-forme saharienne ; valeurs des isopaques en mètres (HELLAL, FEKIRINE & AÏT SALEM, documents Sonatrach)

Atlas Trough and the major Mesozoic fractures of the north of the African Craton appeared progressively in the course of the Triassic with a NE opening to the Tethys Ocean (BEAUCHAMP *et al.*, 1995; JACKSON *et al.*, 1995). The fissure eruptions on the Saharan Platform in Algeria are thought to be associated with differences in subsidence and the development of NE-oriented fractures. The first volcanic eruptions are thought to date from Carnian times when the Triassic fractures of the Algerian Sahara were initiated. The S4 salt serie with its E-W extension is believed to be representative of Jurassic structuration.

CONCLUSION

On the Mesozoic Saharan Platform, in view of the vertebrate remains, the earliest middle Triassic deposits have been located in the Zarzaïtine region, close to the Libyan border. In the northern part of the platform, according to the palynologic assemblages, the Triassic series commence earlier in the east (Tunisian border): at the Ladinian / Carnian boundary, east of the Ghadamès Basin. In the west, younger deposits (upper Carnian) directly lie on the basement. Lower Triassic sediments were deposited in the north-east trending depocenters only.

According to high resolution sequences stratigraphy correlations, seven minor stratigraphic cycles, part of the general base-level-rise trend, i.e. retrogradational trend, are observed in these series. In the lower part, during the Carnian, eastern dolomitic sebkha deposits grade westward, i. e. landward, into fluvial environments. In the upper part, during the Norian, evaporite series migrate westward or landward, while fluvial sandstones step landward in an onlapping pattern. Vertical aggradation predominate towards the top of the salt series, with lateral transition of the halite deposits into anhydrite

Source : MNHN, Paris

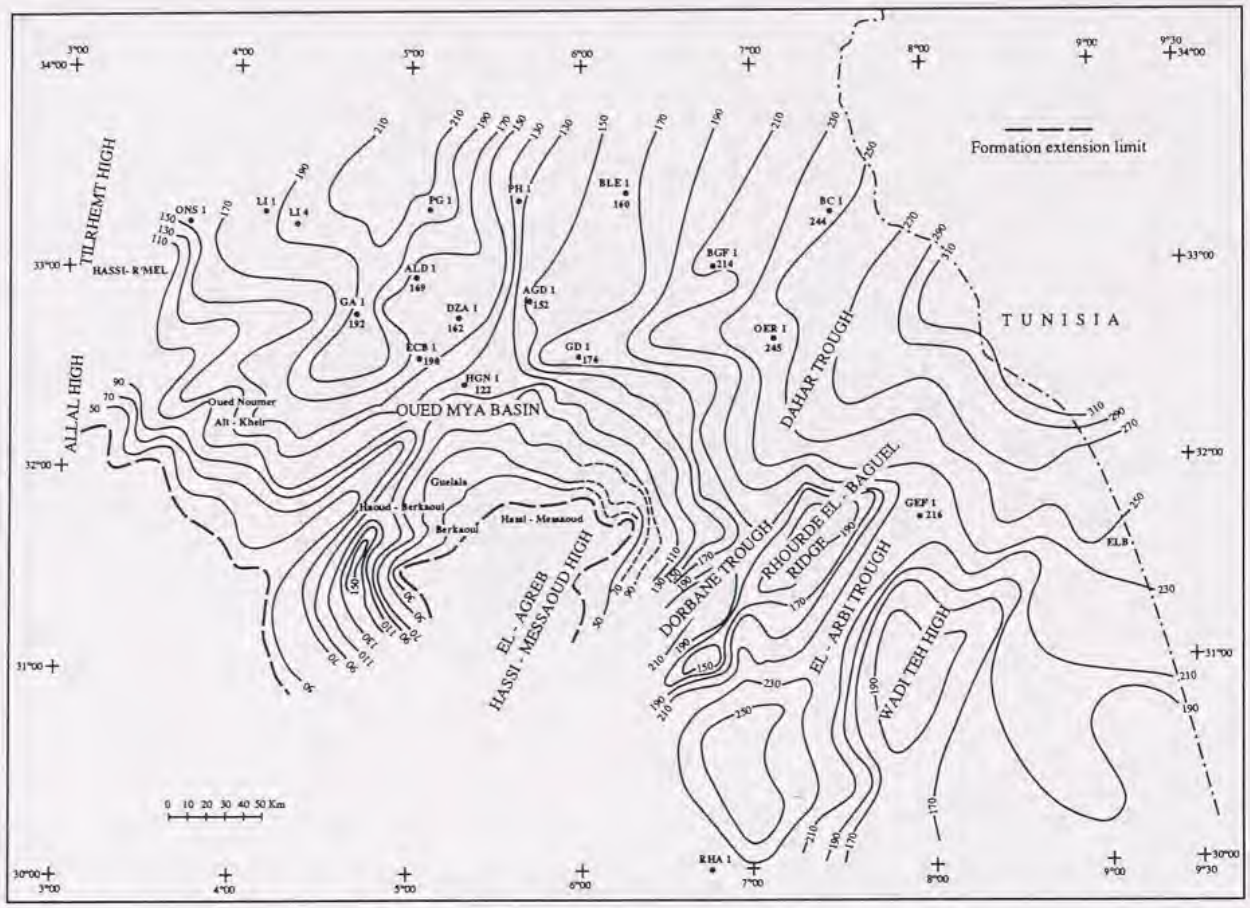

FIG. 8.— Isopach map of the "T1 and T2" Formations, northern part of the Saharan Platform; isopach values in meters (HELLAL, FEKIRINE & AÏT SALEM, Sonatrach doc.)

FIG. 8.— Carte des isopaques des formations T1 et T2, partie nord de la Plate-forme saharienne; valeurs des isopaques en mètres (HELLAL, FEKIRINE & AÏT SALEM documents Sonatrach)

or dolomitic deposits. The description of the progressive retrogradation can be understood by the development of subsidence area towards the external domain of the platform.

Isopach maps have been analysed across four lithostratigraphic units. Such units are obviously diachronous but allow to investigate Triassic Saharan Platform structuration. Direction inherited from Panafrican and Variscan times are clearly N-S in the south. This orientation subsits in the north but bend for the most part to NE. Contrasted thickness variations, linked with fissure volcanism fracturations, are good indicators of younger (Carnian) NE directions. North of the Algerian Platform, NE oriented sedimentation troughs coexist with a much more regular surface in the Ghadamès basin, dipping very gently eastward, toward the marine peritethyan domain in Tunisia. The S4 salt series at the top of the Triassic series is clearly EW bounded to the south.

The NE opening seems to correspond to the opening of the Neo-Tethys / East Mediterranean system initiated in Permian time (STAMPFLI *et al.*, 1991). In the Djeffara (South Tunisia) where a continuous Permian-Triassic marine sequence is known, rifting is at least Permian or older. A thermal contraction of the thinned crust could have generated the onlap of the Triassic sequence in the Saharan domain. The Carnian fracturation is found all around the Atlantic-Alpine area and could be related to the Pangea break-up. This second cycle is superimposed to the thermal subsidence and correspond to the Late Triassic / Jurassic opening of the Atlantic / Alpine Tethys (STAMPFLI *et al.*, 1991).

Source : MNHN, Paris

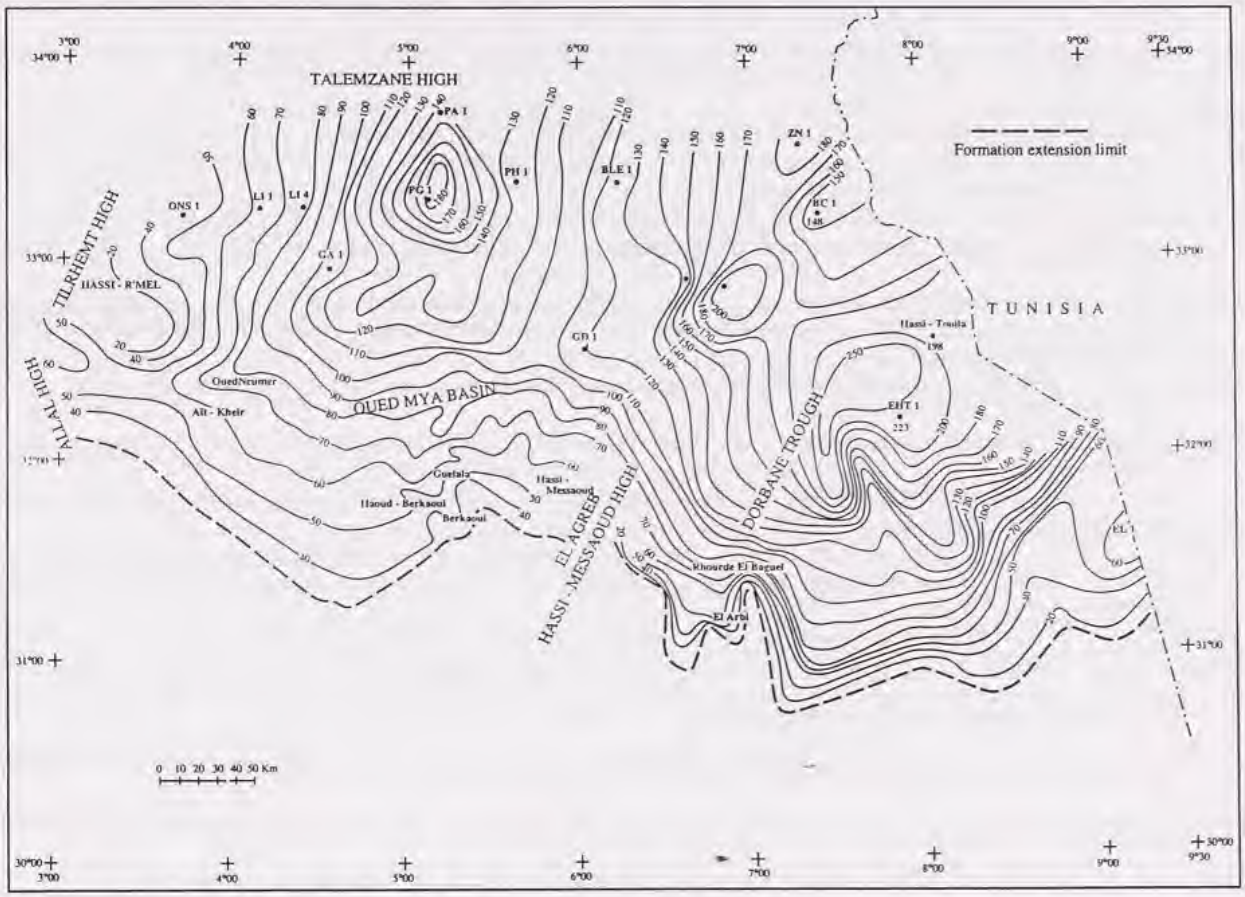

FIG. 9.— Isopach map of the "Série salifère S4" Formation, northern part of the Saharan Platform; isopach values in meters (HELLAL, FEKIRINE & AÏT SALEM, Sonatrach doc.)

FIG. 9.— Carte des isopaques de la Série salifère S4, partie nord de la Plate-forme saharienne ; valeurs des isopaques en mètres (HELLAL, FEKIRINE & AÏT SALEM, documents Sonatrach).

ACKNOWLEDGEMENTS

Critical review provided by G. STAMPFLI improved the manuscript. We gratefully acknowledge SONATRACH for allowing us to study the subsurface data. We thank also the Peri-Tethys Program for its financial support. This paper is a contribution to the theme "Enregistrement des phénomènes biologiques et sédimentaires" of the UMR CNRS 5561 "Paléontologie analytique et Géologie sédimentaire".

REFERENCES

ACHAB, A., 1970.— *Le Permo-Trias saharien. Associations palynologiques et leurs applications en stratigraphie*. Thèse 3ème cycle, Université d'Alger, Alger, Algérie: 1-144.

AÏT OUALI, R. & NEDJARI, A., 1994.— La province triasique: vingt ans d'informations géologiques. Un bilan critique. *CRD Sonatrach*: 1-38.

AÏT SALEM, H., 1992.— Le Trias détritique de l'Oued Mya (Sahara algérien); sédimentation estuarienne, diagenèse et porogenèse, potentialités pétrolières. *Documents, Département des Sciences de la Terre, Université Claude Bernard, Lyon, France*, **120**: 1-165.

Source : MNHN, Paris

AÏT SALEM, H. & HELLAL, C., 1993.— La série de Zaraïtine. Sédimentologie (Edjelleh-Tiguentourine-La reculée). Trias, *Livret-guide d'excursion; Société Algérienne des Sciences Géologiques et Sonatrach*, **4**: 1-8.

BAYARASSOU, S., 1994.— *Étude dynamique du Trias et du Lias du Bassin de l'Oued Mya (Sahara algérien). Sédimentologie, compaction, subsidence, sismique.* Thèse, Université Claude Bernard, Lyon, France: 1-244.

BEAUCHAMP, J., BENAOUISS, N. & COUREL, L., 1995.— Où était donc le domaine marin dans le Maroc africain au Trias supérieur?, *Comptes Rendus de l'Académie des Sciences*, Paris, **321** (II a): 1033-1040.

BEICIP, 1978.— Étude géologique du champ d'Hassi-R'Mel. Étude sismique et structurale (1ère partie); étude géologique des réservoirs (2ème partie). *Sonatrach*, Rapport inédit.

BEN ISMAIL, M. H., 1991.— *Les bassins mésozoïques (Trias-Aptien) du Sud de la Tunisie: stratigraphie intégrée, caractéristiques géophysiques et évolution géodynamique*. Thèse de Doctorat ès-Sciences, Université de Tunis, Tunis, Tunisie: 1-466.

BENAMRANE, O., 1987.— *Diagraphies et sédimentologie: une combinaison efficace pour l'étude des bassins et l'exploration des pièges stratigraphiques d'hydrocarbures (Trias du Bassin de Oued Mya- Algérie).* Thèse, Université Pierre et Marie Curie, Paris, France: 1-181.

BIARD, A., 1963.— *Contribution à l'étude palynoplanctologique du Permo-Trias en France et en Afrique du Nord*. Thèse 3ème cycle, Université de Dijon, Dijon, France: 1-187.

BOUAZIZ, S., 1986.— *La déformation dans la Plate-forme du Sud tunisien (Dahar et Jeffar): approche multiscalaire et pluridisciplinaire*. Thèse 3ème cycle, Université de Tunis, Tunis, Tunisie: 1-180.

BOUDJEMA, A., 1987.— *Évolution structurale du bassin pétrolier "triasique" du Sahara nord-oriental (Algérie).* Thèse, Université Paris XI, Orsay, France: 1-279.

BOUDJEMA, A., GAUTHIER, F. & LOUNIS, R., 1994.— The structural evolution of the Ghadames and Ilizi basins during the Paleozoic, Mesozoic and Cenozoic: petroleum implications. *Ghadamès 94, International Conference on Oil, Ghadamès*, Abstract: 6-7.

BOURMOUCHE, R., 1982.— Étude palynologique du sondage HEB-1. *CRD Sonatrach*, Rapport n°385-1-20-55.

BOURMOUCHE, R., DURAND-DELGA, M., LACHKAR, G. & VILA, J.M., 1996.— Découverte de palynoflores du Trias supérieur (Carnien moyen-supérieur) dans les grès rouges du Djebel Mcid Aïcha (zone tellienne, Algérie nord-orientale). *Comptes Rendus de l'Académie des Sciences, Paris*, **322** (IIA): 765-772.

BOURQUIN, S. & GUILLOCHEAU, F., 1993.— Géométrie des séquences de dépôt du Keuper (Ladinien à Rhétien) du Bassin de Paris: implications géodynamiques. *Comptes-Rendus de l'Académie des Sciences, Paris*, **317**: 1341-1348.

BOURQUIN, S. & GUILLOCHEAU, F., 1996.— Keuper stratigraphic cycles in the Paris Basin and comparison with cycles in other Peri-Tethyan basins (German Basin and Bresse-Jura Basins). *Sedimentary Geology*, **105**: 159-182

BUSCH, D.A., 1971.— Genetic units in delta prospecting. *American Association of Petroleum Geologists, Bulletin*, **55** (8): 1137-1154.

BUSSON, G., 1967.— Le Mésozoïque saharien. 1ère partie: l'Extrême Sud-Tunisien. *Publication CRZA, Géologie*, **8**: 1-194.

BUSSON, G., 1970.— Le Mésozoïque saharien. 2ème partie: essai de synthèse des données des sondages algéro-tunisiens. *Publication CRZA, Géologie*, **11**: 1-811.

BUSSON, G., 1971.— *Principes, méthodes et résultats d'une étude stratigraphique du Mésozoïque saharien*. Thèse, Université Pierre et Marie Curie, Paris, France: 1-441.

CHANDOUL, H., BUROLLET, P. F., BEN FERJANI, A. & MEMMI, L., 1993.— Recueil des coupes types de Tunisie. I: Trias et Jurassique. *ETAP, Mémoire*, **4**: 1-95.

COUREL, L., POLI, E. & BOURQUIN, S., 1994.— Corrélations dans les bassins triasiques à dominante clastique et évaporitique; exemples d'utilisation des relations génétiques entre clastiques, évaporites et carbonates dans les cortèges sédimentaires (Systems tracts) dans l'Est de la France. *Mémoires du Service géologique de l'Algérie*, **6**: 85-97.

CROSS, T.A., 1988.— Controls on coal distribution in transgresive-regressive cycles. *In*: C.K. WILGUS, B.S. HASTINGS, C.G.ST.C. KENDALL, H.W. POSAMENTIER, C.A. ROSS & J.C. VAN WAGONER (eds), Sea-level change: an integrated approach. *Society of Economic Paleontologists and Mineralogists, Special Publication*, **42**: 371-380.

CROSS, T.A., BAKER, M.R., CHAPIN, M.A., CLARK, M.S., GARDNER, M.H., HANSON, M.S., LESSENGER, M.A., LITTLE, L.D., MCDONOUGH, K.-J., SONNENFELD, M.D., VALAZEK, D.W., WILLIAMS, M.R. & WITTER, D.N., 1993.— Applications of high-resolution sequence stratigraphy to reservoir analysis. *In*: R. ESCHARD & B. DOLIGEZ (eds), *Subsurface Reservoir Characterization from Outcrop Observations, IFP Exploration and Production Research Conference*. Technip, Paris: 11-33.

DANIELS, R.P., HOOK, R.C., SORENSEN, P.R. & EMME, J.J., 1994.— Triassic depositional system and reservoir development Ghadames basin, Algeria. *Ghadamès 94, International Conference on Oil, Ghadamès*, Abstract: 11.

DEAKINS, R.J. & DANIELS, R.P., 1994.— Hydrocarbon seal capacity of the Triassic carbonate Ghadames basin, Algeria. *Ghadamès 94, International Conference on Oil*, Abstract: 11-12.

DJARNIA, M.R., 1991.— *Étude des conditions de formation d'un éventuel anneau à huile dans le gisement de Hassi-R'Mel (Algérie).* Thèse, Université Louis Pasteur, Strasbourg, France: 1-175.

DURAND-DELGA, M. & TEFIANI, M., 1994.— Problèmes posés par le Trias des zones internes des Maghrébides et des Cordillères béthiques. *Mémoires du Service géologique de l'Algérie*, **6**: 41-56.

Source : MNHN, Paris

HAMEL, A., 1988.— *Étude géologique des grès triasiques du gisement pétrolier de Hassi R'Mel (Algérie); caractérisation, extension et milieu de dépôt*. Thèse, Université de Franche-Comté, Besançon, France: 1- 190.

HOMEWOOD, P., GUILLOCHEAU, F., ESCHARD, R. & CROSS, T.A., 1992.— Corrélations haute résolution et stratigraphie génétique: une démarche intégrée. *Bulletin des Centres de Recherche Exploration-Production Elf-Aquitaine*, **16**: 357-381.

JACKSON, J.S., MOORE, S.R. & QUARLES, A.I., 1995.— Tethys- and Atlas-related Deformations in the Triassic basin (Algeria). *American Association of Petroleum Geologists Meeting*, Nice, Abstract.

JALIL, N., 1993.— *Les vertébrés triasiques de la série de Zarzaïtine (Algérie): étude anatomique et phylogénétique des Amphibiens Temnospondyles et des Diapsides*. Thèse, Université Paris VII, Paris, France: 1-179.

JALIL, N., 1994.— Sur la présence de Brachyopoidea (Vertebrata, Tetrapoda, Remnospondyli) dans la série de Zarzaïtine (Trias, Algérie). *Comptes Rendus de l'Académie des Sciences, Paris*, **318**: 1687-1691.

JALIL, N., & TAQUET, P., 1994.— Les vertébrés triasiques de la série de Zarzaïtine (Algérie). Liste faunique et implications stratigraphiques. *Mémoires du Service géologique de l'Algérie*, **6**: 99-104.

JALIL, N., LUCAS, S.G. & HUNT, A.P, 1995.— Biochronological significance of Aetosaurs and phytosaurs (Reptilia, Archosauromorpha) in the Triassic Zarzaïtine series of Algeria. *Neues Jahrbuch für Geologie und Palaeontologie, Monatshefte*, **3**: 173-181.

JONES, M. & TURNER, P., 1993.— Triassic of Algeria. Integration into an international petroleum context. *In*: Comptes Rendus Colloque Trias d'Algérie, Boumerdès 1993. *CRD Sonatrach*: 19.

LEHMAN, J.P., 1957.— Les Stégocéphales sahariens. *Annales de Paléontologie*, **43**: 139-146.

MAMI, L. & BOURMOUCHE, R., 1994.— Résultats palynostratigraphiques des formations triasiques de la région d'El Biod. *CRD Sonatrach*, Rapport n°44.

MAMI, L., 1980.— Étude palynologique du sondage REH-1. *CRD Sonatrach*, Rapport n°162-9-20.

MAMI, L., 1989.— Étude palynologique des sondages HEB-1, RN-11, RHA-1, REK-1, EKR-1. *CRD Sonatrach*, Rapport n°28.

MOY, C. & TRAVERSE, A., 1986.— Palynostratigraphy of the subsurface Eagle Mills Formations (Triassic) from a well in East-central Texas, USA. *Palynology*, **10**: 225-234.

NEDJARI, A., 1994.— Images et évènements fini hercyniens de l'Ouest du Maghreb (Algérie, Maroc). *Mémoires du Service géologique de l'Algérie*, **6**: 13-40.

PERTHUISOT, V., 1994.— Structures et géométrie des diapirs maghrébins. Essai de synthèse. *Mémoires du Service géologique de l'Algérie*, **6**: 153-159.

REYRE, Y., 1973.— Palynologie du Mésozoïque saharien. *Mémoires du Muséum national d'Histoire naturelle*, **27** (C): 1-284.

SCHEURING, B.W., 1970.— Palynologische und palynostratigraphische Untersuchungen des Keupers im Bölchentunnel (Solothurner Jura). *Mémoires Suisses de Paléontologie*, **88**: 1-119.

SCHEURING, B.W., 1978.— Mikrofloren aus den Meridekalken des Mte San Giorgio (Kanton Tessin). *Mémoires suisses de Paléontologie*, **100**: 1-205.

SCHURMAN, W.M.L., 1977.— Aspects of Late Triassic palynology. 2: Palynology of the "Grès et schistes à Avicula contorta" and "Argiles de Levallois" (Rhaetian) of Northeastern France and Southern Luxembourg. *Review of Palaeobotany and Palynology*, **23** (3): 159-253.

STAMPFLI, G., MARCOUX, J. & BAUD, A., 1991.— Tethyan margins in space and time. Palaeogeography, *Palaeoclimatology, Palaeoecology*, **87**: 373-409.

TEFIANI, M., BAUDELOT, S. & BOURMOUCHE, R., 1991.— Datations palynologiques du Trias du Djurdjura (Algérie). Implications géodynamiques. *Comptes Rendus de l'Académie des Sciences*, Paris, **313**: 451-456.

TEFIANI, M., PEYBERNES, B., HAGDORN, H. & LACHKAR, G., 1994.— Le Trias des zones internes d'Algérie: repères biostratigraphiques et géodynamiques dans les séries du Djurdjura (Dorsale kabyle). *In*: *1er Congrès Français de Stratigraphie, Toulouse*: 73-74.

VAN DER EEM, J.G.L.A., 1983.— Aspects of Middle and Late Triassic palynology. 6: palynological investigations in the Ladinian and Lower Carnian of the Western Dolomites, Italy. *Review of Palaeobotany and Palynology*, **39** (3/4): 189-300.

VIALLY, R., LETOUZEY, J., BENARD, F., HADDADI, N., DESFORGES, G., ASKRI, H. & BOUDJEMA, A., 1994.— Basin inversion along the North African Margin. The Saharan Atlas (Algeria). *In*: F. ROURE (ed.), *Peri-Tethyan Platforms: Proceeding of the IFP Peri-Tethys Research Conference held in Arles, France, March 23, 1993*. Technip, Paris: 79-118.

VISSHER, H. & KRYSTYN, L., 1978.— Aspects of Late Triassic palynology. 4: a palynological assemblages from Ammonoid-controlled Late Carnian (Tuvalian) sediments of Sicily. *Review of Palaeobotany and Palynology*, **26** (2/4): 93-112.

VISSHER, H. & BRUGMAN, W.A., 1981.— Ranges of selected palynomorphs in the Alpine Triassic of Europe. *Review of Palaeobotany and Palynology*, **34**: 115-128.

VILA, J.M., 1994.— Mise au point et données nouvelles sur les terrains triasiques des confins algéro-tunisiens: Trias allochtone, "glaciers de sel" sous-marins et vrais diapirs. *Mémoires du Service géologique de l'Algérie*, **6**: 105-152.

Source : MNHN, Paris

Source : MNHN, Paris

11

New data on the Jurassic and Neogene sedimentation in the Danakil Horst and Northern Afar Depression, Eritrea

Mario SAGRI [1], *Ernesto* ABBATE [1], *Augusto* AZZAROLI [1], *Maria Laura* BALESTRIERI [1], *Marco* BENVENUTI [1], *Piero* BRUNI [1], *Milvio* FAZZUOLI [1], *Giovanni* FICCARELLI [1], *Marta* MARCUCCI [1], *Mauro* PAPINI [1], *Giulio* PAVIA [2], *Viviana* REALE [1], *Lorenzo* ROOK [1] & *Tewelde Medhin* TECLE [3]

[1] Dipartimento Scienze della Terra, Università di Firenze, Via G. La Pira 4, 50122 Firenze, Italy

[2] Dipartimento Scienze della Terra, Università di Torino, Via Accademia delle Scienze 5, 10123 Torino, Italy

[3] Department of Mines, Asmara, Eritrea

ABSTRACT

The Jurassic Antalo Limestone in the Danakil Horst sedimentary cover, the Neogene volcano-sedimentary suite of the Sahel (Massawa) area and the coeval sedimentary filling of the northern Afar (Danakil) Depression have been examined. Composite sections, totalling about 1.100 m, have been measured in the Antalo Limestone resting above the continental Adigrat Sandstones. Six units have been described and their depositional environments have been related to a carbonate ramp system. Basinal conditions, marked by dark grey marls and shales, have been recognized in the middle-lower portion of the succession. Seven depositional sequences, separated by important boundary surfaces, display well-developed system tracts. Ammonites, foraminifers and calcareous nannofossils allow to assign a late Callovian to early Kimmeridgian age to the studied sections. A new geological map evidences a complex fault pattern in the northern Danakil Horst. It is likely that, besides normal faulting, the small Danakil continental block also experienced strike-slip deformation during its detachment from the Nubian plate. In the Sahel area at the foot of the Eritrean escarpment and above Oligocene Trap Basalts a volcano-sedimentary succession (Dogali Formation), 550 m thick, consists at its base of lacustrine siliceous deposits interbedded with basalt flows. Fluviodeltaic sands and gravels prevail in the upper portion with intervening evaporites and patch reef limestones. They are cyclically arranged and constitute at least four depositional sequences. A proboscidian (*Deinotherium*) remain has been found at the base of the Dogali Formation and indicates an early Miocene age. These syn-rift deposits within the Southern Red Sea rift basin are truncated by post-rift Boulder Beds fanglomerates. A 500 m thick succession in the upper portion of the Danakil Formation in the Northern Afar Depression exhibits fluviodeltaic and lacustrine deposits. An early to middle Pleistocene human skull and rich vertebrate faunas have been found. These fossil findings together with the sedimentologic features of the deposits provide evidence of a savannah environment prospicient to swamps and shallow lakes. The syn-rift Danakil Formation is unconformably overlain by post-rift Boulder Beds. The Sahel and Northern Afar Neogene sediments record the deformational history at the hinge zone between the Eritrean escarpment and the adjacent subsiding lowlands.

SAGRI, M., ABBATE, E., AZZAROLI, A., BALESTRIERI, M.L., BENVENUTI, M., BRUNI, P., FAZZUOLI, M., FICCARELLI G., MARCUCCI, M., PAPINI, M., PAVIA, G., REALE, V., ROOK, L. & TECLE, T.M., 1998.— New data on the Jurassic and sedimentation in the Danakil Horst and Northern Afar Depression, Eritrea. *In:* S. CRASQUIN-SOLEAU & É. BARRIER (eds), Peri-Tethys Memoir 3: stratigraphy and evolution of Peri-Tethyan platforms. *Mém. Mus. natn. Hist. nat.*, **177** : 193-214. Paris ISBN : 2-85653-512-7.

Source : MNHN, Paris

RÉSUMÉ

Nouvelles données sur la sédimentation du Jurassique et du Néogène dans le Horst du Danakil et dans la dépression du Nord de l'Afar, Erythrée.

Trois séries sédimentaires ont été étudiées : les calcaires jurassiques d'Antalo de la couverture sédimentaire du Horst Danakil, les formations volcano-sédimentaires néogènes de la région du Sahel (Massawa) et le remplissage sédimentaire de la partie septentrionale de la dépression de l'Afar (Danakil). Des sections composites d'une longueur totale de 1100 m ont été mesurées dans les calcaires d'Antalo, recouvrant les grés continentaux d'Adigrat. Six unités sont décrites et leurs conditions de dépôts sont misent en relation avec un système de rampes carbonatées. Des conditions de dépôts de bassin, caractérisées par des marnes grises et des shales, ont été reconnues dans les parties inférieure et moyenne de la série. Sept séquences de dépôts, séparées par des limites franches, présentent des " system tracts " bien développés. L'étude des ammonites, des foraminifères et des nannofossiles permettent d'attribuer un âge callovien supérieur à kimméridgien aux séries étudiées. Une nouvelle cartographie de la partie septentrionale du Horst Danakil a mis en évidence une tectonique complexe, essentiellement par failles normales liées au détachement du bloc Danakil de la plaque nubienne. Cette tectonique distensive est associée à des mouvements décrochants. Au pied de l'Erythrée, dans la région du Sahel, une série volcano-sédimentaire de 550 m d'épaisseur se développe sur les trapps basaltiques oligocènes. Elle est constituée à sa base de dépôts lacustres siliceux interstratifiés avec des coulées de basalte. Des sables et des graviers fluvio-deltaïques dominent dans la partie supérieure de la série où existent également des évaporites et des calcaires récifaux. Ils constituent au moins quatre séquences de dépots. Un reste de proboscibien (*Deinotherium*) trouvé à la base de la formation de Dogali indique un âge Miocène inférieur. Ces dépôts syn-rifts du bassin méridional de la Mer Rouge sont tronqués par des fanglomérats post-rifts. La série lacustre et fluvio-deltaïque, épaisse de 500 m, située dans la partie supérieure de la Formation Danakil dans la dépression de l'Afar septentrional, a été attribuée au Pléistocène inférieur et moyen à partir de riches faunes de vertébrés et en particulier de restes humains. Ces fossiles, trouvés avec les figures sédimentaires de dépôt, indiquent un environnement de savane. La formation syn-rift Danakil est recouverte en discordance par des conglomérats deltaïques post-rifts.

INTRODUCTION

During two field expeditions in Eritrea (November 1994 and December 1995), three geologic sections through the Danakil Horst and the Northern Afar (Danakil) Depression were surveyed (Fig. 1). They cross various stratigraphical and structural settings that can be traced on a wide area for which recent studies are lacking.

We focussed our attention on: (a) the Mesozoic sedimentary cover of the northern portion of the Danakil Horst; (b) the Miocene to Pleistocene succession near Dogali, west of Massawa; (c) the Plio-Pleistocene portion of the so-called Red Series near Buia, Northern Afar Depression.

The study area of research theme (a) has been the Danakil Horst, that is a continental block left behind in the progressive detachment of Arabia from Nubia. It has been rotated by some 30° counterclockwise (BUREK, 1970; SICHLER,1980) and is presently bounded on its SW side by the northern termination of the Afar Depression. Toward NW the latter makes transition into the Southern Red Sea coastal plain (Sahel) at the foot of the Eritrean escarpment (Fig. 1).

As to the Mesozoic successions of the Danakil Horst, our specific aim was to gain information on significant events (such as the inception of marine deposition, the age of clastic inflows and of the anoxic events) that could be correlated with coeval occurrences in Northern Somalia, Ethiopia and Arabia.

Research lines (b) and (c) cover areas that straddle accross the Southern Red Sea and the Northern Afar Depression (Fig. 1). Their geological setting is similar since they expose prevailingly clastic, Neogene successions that can be envisaged as syn- and post-rift deposits within rift basins. The latter are the Southern Red Sea basin for the Dogali-Massawa area, and the Afar Depression for the Buia region. The Neogene deposits were investigated in order to provide chronological and paleoenvironmental data on the different rifting stages in these two transects.

LITHO-, BIO- AND SEQUENCE-STRATIGRAPHY OF THE ANTALO LIMESTONE

The occurrence of the Antalo Limestone in the Danakil Horst has been reported since a long time in the pioneering works by VINASSA DE REGNY (1924, 1931). We have been carrying out a detailed study of this formation in the northern areas close to the Adeilo village (Figs 2, 3) and only a reconnaissance survey between Amarti and Edd (Fig. 1). Owing to intense tectonic disturbances affecting the Adeilo area, the Antalo Limestone could not be examined in a single continuous section. Thus, six partial sections have been measured and vertical reconstructions and lateral correlations are presented in figure 3.

Source : MNHN, Paris

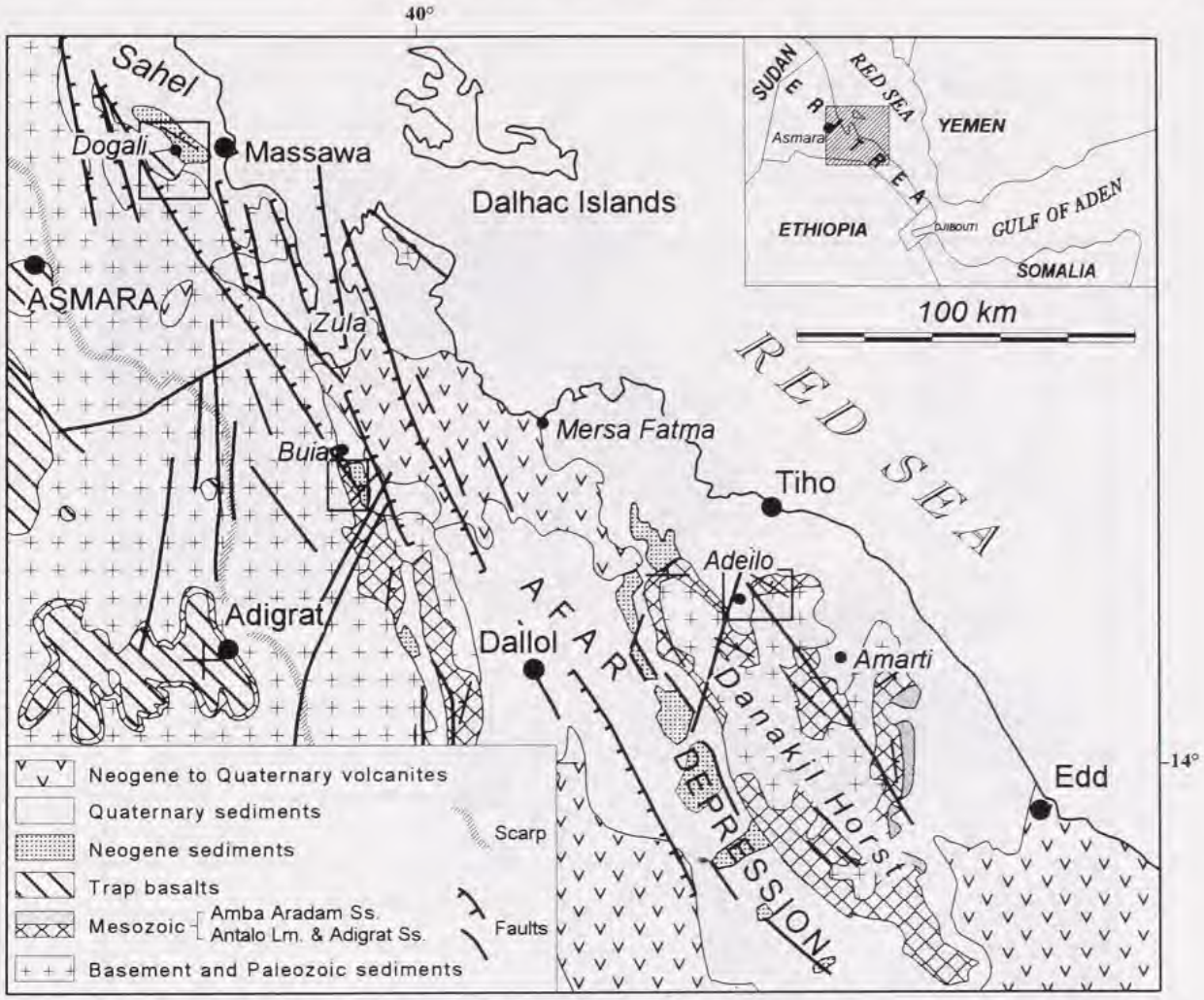

FIG. 1.— Simplified geological map of the Danakil Horst, Northern Afar Depression and adjoining Eritrean-Ethiopian Plateau, with the indication of the study areas (Dogali, Buia, Adeilo). Modified after KAZMIN (1975), MERLA *et al.* (1979), GARLAND (1980), DRURY *et al.* (1994).

FIG. 1.— Carte géologique simplifiée du horst Danakil, de la dépression de l'Afar septentrional et du Plateau érythréo-éthiopien, avec la localisation des zones d'étude (Dogali, Buia, Adeilo). Modifié d'après KAZMIN (1975), MERLA et al. *(1979), GARLAND (1980), DRURY* et al. *(1994).*

It should be noted that while the transition to the underlying Adigrat Sandstones is frequently found, that to the overlying Amba Aradam Sandstones is not exposed in the northern part of the Danakil Horst. According to cursory reconnaissance, the latter transition crops out only in the eastern and southern areas and is probably marked by marly levels.

Another problem we have been facing is the stratigraphic position of the highly tectonized 50 m-thick gypsum level which outcrops near Adeilo. Its stratigraphic position surmised in figure 3 derives from loose regional correlations (south of Amarti, gypsum beds occupy a similar position) and from a tentative correlation with the Simi Koma key bed (see below).

THE ANTALO LIMESTONE IN THE ADEILO AREA

More than 1,000 m have been measured in detail close to Adeilo and six main rock assemblages (" Units ") (from A to F) have been provisionally distinguished (Fig. 4). Their thickness varies from a few tens (Unit B) to a few hundreds of meters (Unit C). Each unit is composed of different lithofacies that have been grouped under different subunits (e.g. A1, A2).

Source : MNHN, Paris

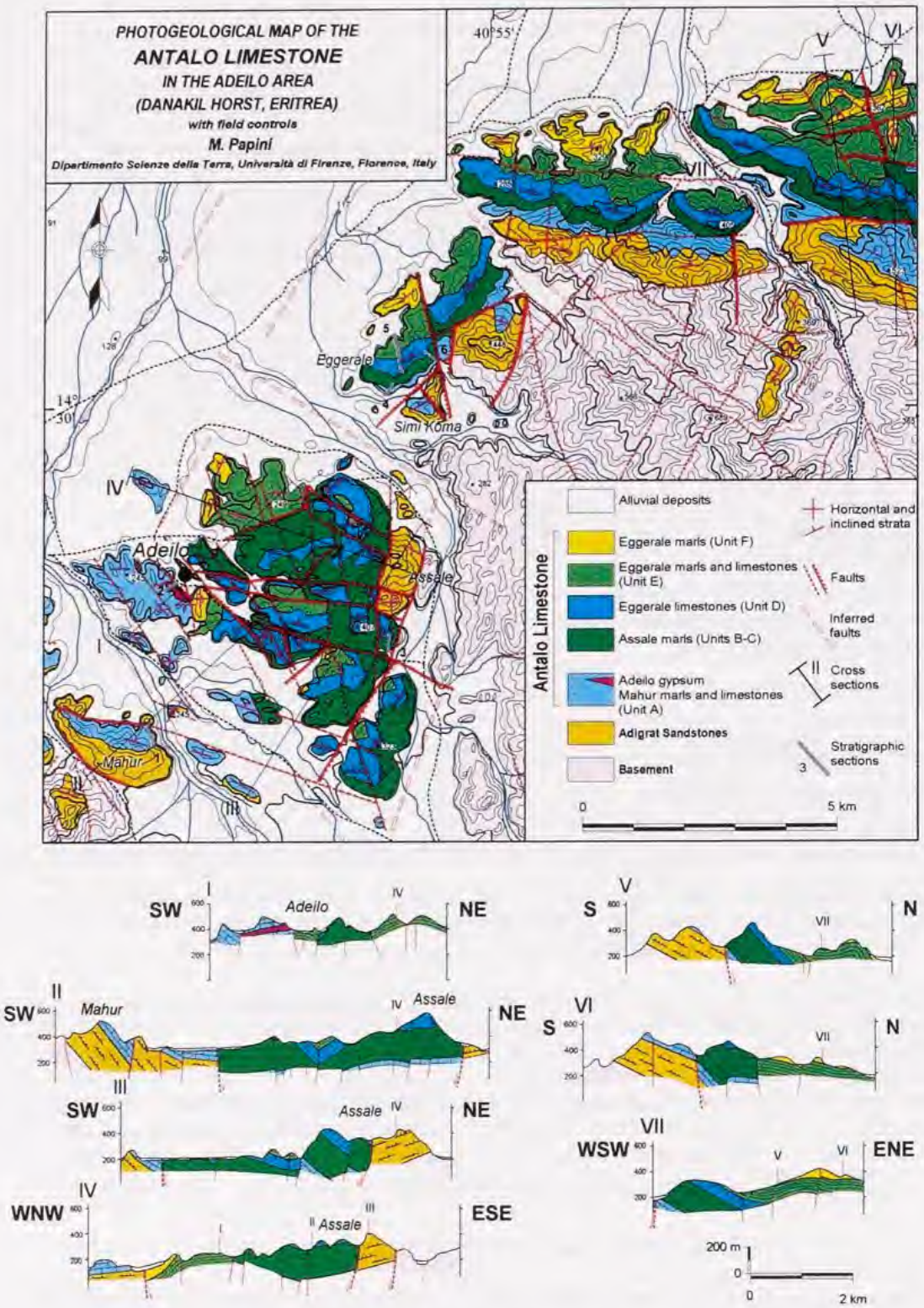

FIG. 2.— Photogeological map and cross sections of the Adeilo area.
FIG. 2.— Carte photogéologique et coupes du secteur d'Adeilo.

Source : MNHN, Paris

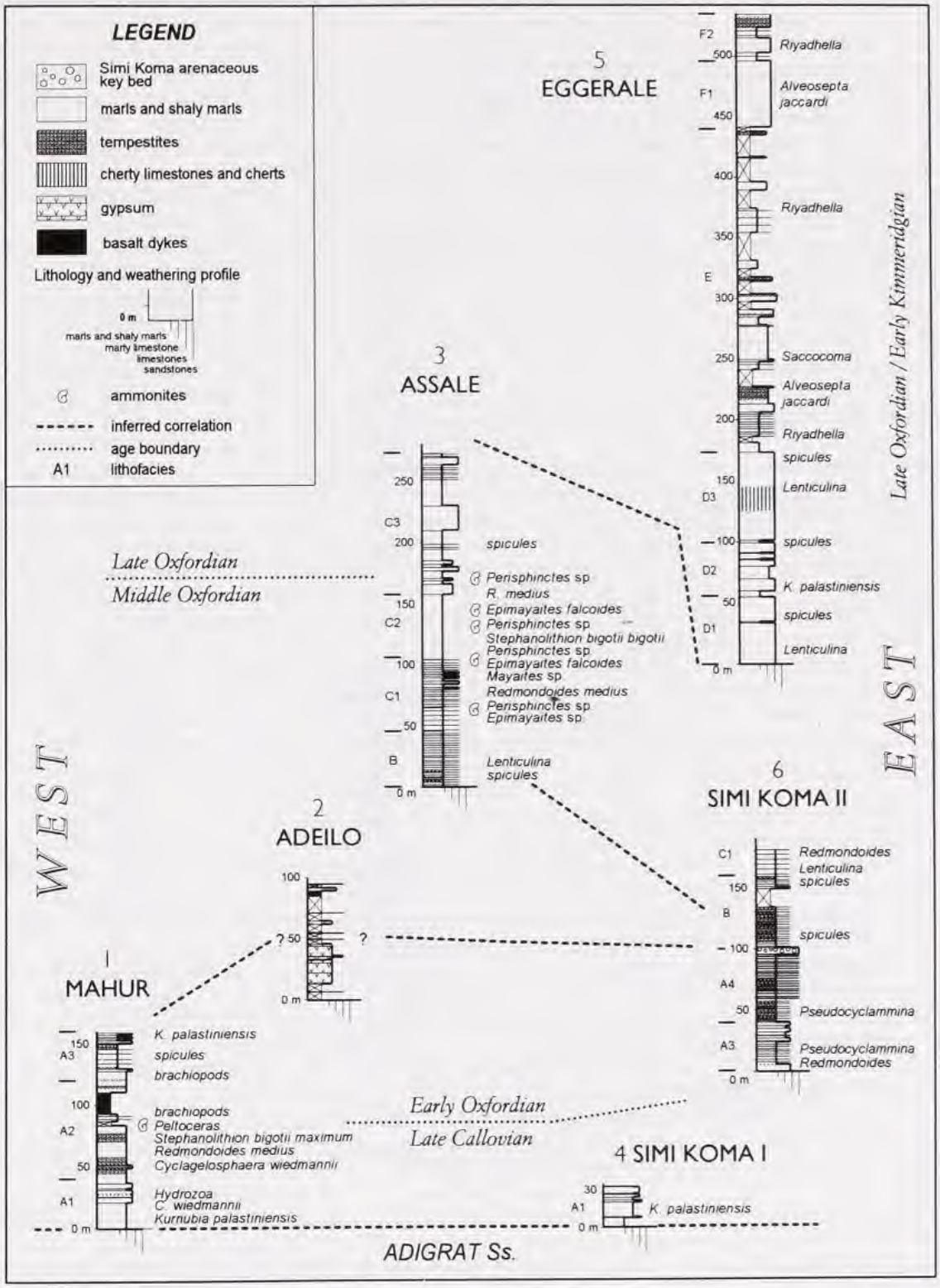

FIG. 3.— Detailed sections of the Antalo Limestone in the Adeilo area. For location see figure 2.
FIG. 3.— Coupes détaillées des calcaires d'Antalo dans le secteur d'Adeilo (localisation figure 2).

Source : MNHN, Paris

Unit A (Mahur and Simi Koma I and II sections, Fig. 3; 0-220 m, Fig. 4). Unit A (220 m thick) consists predominantly of lithologies varying between blueish limestones and dark grey-blueish marls. Moreover, it is characterized by the occurrence of more or less frequent bioclastic levels. Shells are generally broken (coquinas), but also many levels with unbroken shells (lumachellas) are present. Within marly intervals, coquina levels are generally thin and the shells are completely embedded in a muddy matrix. If carbonate increases and calcilutitic levels become more frequent, the bioclastic beds are thicker, coarser, often graded and with an erosional base. In other occurrences, monotypic, well-sorted and well-cemented lumachellas have been observed. In siliciclastic beds, graded bedding, horizontal, wavy and hummocky laminations also occur. All these features are consistent with those of deeper to shallower storm layers (BURCHETTE & WRIGHT, 1992). Unit A can be subdivided in four subunits (Figs 3, 4). Subunit A1 (0-40 m, Fig. 4) exhibits in its lower part prevailing dark gray, fetid marly limestones, sometimes nodular and bioturbated, alternating with well-bedded calcilutites and calcarenites. Bedding joints are generally stylolitic. Bioclasts, in particular pelecypods and brachiopods, are abundant. In the upper part thick beds of bioclastic calcarenites and, subordinately, of calcilutites with *Hydrozoa* are present. They contain cherty nodules and beds, and stylolitized bedding joints. Fossils: a typical *Hydrozoa* horizon has been found in this subunit and can be compared with occurrences at the same stratigraphic level reported in other areas (e.g. Somalia, BRUNI & FAZZUOLI, 1976).The microfauna is rather rich in benthic foraminifers with the classical late Callovian to Oxfordian assemblage *Kurnubia palastiniensis* Henson, *Nautiloculina oolithica* Mohler, *Lenticulina* sp. and *Cyclammina* sp. Gastropods, echinoid spines and sponge spicules are also present. The calcareous nannofossil assemblage is scarce, poorly preserved and not well diversified. It is dominated (Plate 1) by the *Watznaueria* genus (*W. barnesae* (Black), *W. britannica* (Stradner), *W. communis* (Reinhardt), *W. fossacincta* (Black) and *W. manivitae* (Bukry)) and includes *Cyclagelosphaera margerelii* Noël, *C. wiedmannii* Reale & Monechi and very rare *Lotharingius* cf. *crucicentralis* (Medd) and *Polypodorhabdus* spp. *C. wiedmannii* Reale & Monechi is indicative of a Callovian age (REALE & MONECHI,1994). Subunit A2 (40-120 m, Fig. 4) consists of bioclastic calcareous-marly levels alternating with thinly bedded marly limestones. In the lower part are present calcilutites and numerous tempestite lumachella beds. Fossils: *Peltoceras (Unipeltoceras)* sp. indicating a late Callovian age and numerous brachiopods have been found in the middle portion of this subunit. In the lower part the late Callovian to Oxfordian assemblage with *Kurnubia palastiniensis* Henson, *Nautiloculina oolithica* Mohler, *Redmondoides medius* (Redmond), *R. inflatus* (Redmond), *Pseudocyclammina* sp. and *Glomospira* sp. has been recognized. The calcareous nannofossil content is similar to that of A1, but, because of the greater frequence of marly levels, it is richer and somewhat better preserved. In addition to those species found in A1, the assemblage includes *Biscutum* sp., *Crepidolithus* sp., *Cyclagelosphaera lacuna* Varol & Girgis, *Discorhabdus (Palaeopontosphaera) dorsetensis* Varol & Girgis, *Podorhabdus grassei* Noël, *Zeugrhabdotus erectus* (Deflandre) and *Zeugrhabdotus* spp. In the middle portion of A2 the presence of *Stephanolithion bigotii maximum* Medd indicates a latest Callovian / early Oxfordian age (KAENEL *et al.*, 1996). Subunit A3 (120-160 m, Fig. 4) is made up mostly by dm-thick, blueish calcilutitic beds alternating with thinner dark gray to blackish, marly interbeds, often with *Thalassinoides*-type bioturbation and tempestitic lumachella (in particular small ostreids) beds. At the top of the section thick beds of bioclastic calcarenites appear. Fossils: particularly toward the top, this subunit is relatively rich in sponge spicules and subordinately in brachiopods. *Redmondoides medius* (Redmond) and *Bathysiphon* sp. have been determined. Biomicrites at the top of this subunit contain *Kurnubia palastiniensis* Henson and *Nautiloculina oolithica* Mohler, that are indicative of a late Callovian to Oxfordian age. In the lower half of A3 the calcareous nannofossil assemblage is again scarce, poorly preserved, not diversified and dominated by *Watznaueria* as in A1. The disappearance of *Cyclagelosphaera wiedmannii* Reale & Monechi possibly indicates an Oxfordian age. In the upper half the nannofossils are almost absent and just few *Watznaueria* persist. Very rare and questionable *Mitrolithus* sp. are also present. In the lower part of subunit A4 (160-220 m, Fig. 4) a regular alternance of dm-thick beds of more or less marly limestone, often including lumachella beds and of marls, sometimes nodular, is present. In the upper part lumachella beds are gradually replaced by thin siltstone beds and then by thicker calcareous terrigenous sandstones. The upper part of this subunit, organized in thickening- and coarsening-up cycles, consists of dm-thick beds of calcareous sandstones with horizontal, cross and hummocky lamination and thin silty-marly interbeds, passing upwards to a 5 m-thick coarse terrigenous calcareous sandy bed-set (the Simi Koma key bed). The latter includes cm- to dm-sized calcarenite clasts and nodules and lenses of blackish chert. Horizontal, cross and wavy

Source : MNHN, Paris

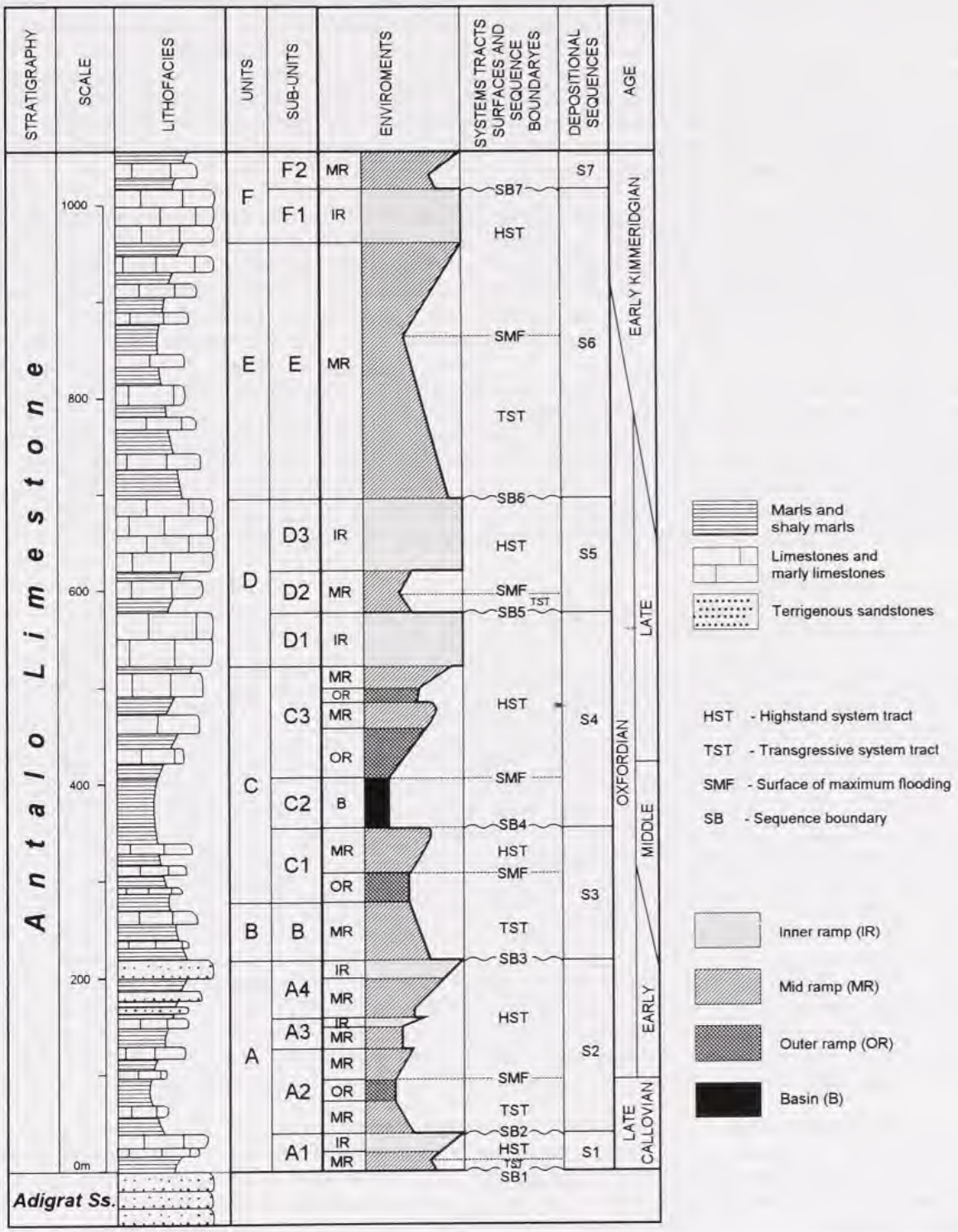

FIG. 4.— Composite section summarizing the logs of Fig. 3, with the environment and the sequence stratigraphy interpretation. Units and sub-units as in figure 3.

FIG. 4.— Coupe synthétique des logs de la figure 3, avec les paléoenvironnements et l'interprétation en termes de séquences stratigraphiques. Même unités et sous-unités que figure 3.

Source : MNHN, Paris

laminations are well evident as well as a thickening and coarsening up pattern that we relate to the progradation of a silicoclastic deltaic body. Fossils: foraminiferal assemblages are rather poor in this subunit, with the exception of some levels particularly rich in *Redmondoides* sp. together with *Pseudocyclammina* sp. and *Ammodiscidae*. The calcareous nannofossil assemblage is present only in the lower portion, although it is scarce and poorly preserved with very rare *Cyclagelosphaera margerelii* Noël, *C. lacuna* Varol & Girgis, *Watznaueria barnesae* (Black) and *Polypodorhabdus* spp. Age of Unit A: the above mentioned ammonites and the calcareous nannofossils content indicate a late Callovian age from the middle part of subunit A2 downward, and an early Oxfordian age upward. The foraminiferal assemblages are consistent with these datings.

Unit B (Simi Koma II and Assale sections, Fig. 3; 220-280 m, Fig. 4). In its lower and middle parts dm-thick beds of blueish calcilutites alternate regularly with more or less silty dark grey marls, tempestitic lumachella beds and with rare thin beds of calcareous, hummocky-laminated, sandstones. In the upper part the storm layers become rare and eventually disappear. The thickness of the intercalated marly levels increases, whereas the thickness and the frequency of the calcilutitic beds decrease. Calcilutites and marls with their dark colour and abundant small sulphide crystals indicate hypoxic to anoxic conditions of the sedimentary environment. These conditions are present also in the lower part of the overlying subunit C1. Fossils: fragments of pelecypods, brachiopods, benthic foraminifers and sponge spicules are often present. *Lenticulina* sp. occurs at the base of the Assale section. As to the calcareous nannofossils, they are absent in the lowermost portion of B of the Simi Koma section, but they appear upward in the succession with *Crepidolithus* sp., *Cyclagelosphaera margerelii* Noël, *Lotharingius hauffii* Grün & Zweili, *Watznaueria barnesae* (Black), *W. britannica* (Stradner), *W. communis* (Reinhardt). The assemblage is indicative of a generic Middle to Late Jurassic age. Age: the age of Unit B is possibly early to middle Oxfordian based on its stratigraphic position.

Unit C (Assale and Simi Koma II sections, Fig. 3; 280-520 m, Fig. 4). Subunit C1 (280-360 m, Fig. 4) is composed by 10-20 cm thick beds of dark grey, sulphide-rich, calcilutites and dark grey marly, often yellowish, interbeds. Subunit C2 (360-400 m, Fig. 4) consists of yellowish-grey, splintery marls with rare levels of marly limestones. In subunit C3 (400-520 m, Fig. 4) the calcareous content increases and levels, that are prevailingly marly, alternate with calcareous marls. They are both yellowish-pink. Fossils: C1 yielded some *Perisphinctes* sp. and *Epimayaites* sp., while *Perisphinctes* sp. was found at the base of C3. Subunit C2 contains abundant ammonites. The most significant are *Epimayaites falcoides* Spath, *"Perisphinctes" orientalis* Siemiradzki and *"Perisphinctes"* aff. *subcolubrinus* Siemiradzki that indicate the middle / late Oxfordian boundary. Pelecypods, ostracods and echinoderms often appear as bioclasts. In the C Unit, foraminifers are scarce and represented only by some *Redmondoides medius* (Redmond), *R. inflatus* (Redmond), *Spirillinidae* and *Eponides* sp. Particularly in the middle portion of Unit C, the calcareous nannofossils are quite abundant and diversified and moderately preserved. Their assemblage is dominated by the *Watznaueriaceae* (*Watznaueria barnesae* (Black), *W. britannica* (Stradner), *W. communis* (Reinhardt), *W. contracta* (Bown & Cooper), *W. manivitae* (Bukry), and less abundant *Cyclagelosphaera margerelii* Noël, *C. lacuna* Varol & Girgis, *Lotharingius* cf. *crucicentralis* Medd, *L. velatus* Bown & Cooper, *L. hauffii* Grün & Zweili) and includes, among others, *Biscutum dubium* (Noël), *Crepidolithus* sp., *Discorhabdus* (*Palaeopontosphaera*) *dorsetensis* Varol & Girgis, *Polypodorhabdus* spp., *Stephanolithion bigotii bigotii* Deflandre, *Zeugrhabdotus erectus* (Deflandre) and *Zeugrhabdotus* spp. The presence of *Stephanolithion bigotii bigotii* Deflandre in the middle portion of Unit C indicates an age younger than early Callovian. Age: the age of Unit C is middle to late Oxfordian based on ammonites.

Unit D (Eggerale section, Fig. 3; 520-700 m, Fig. 4). In the lower part (D1: 520-580 m, Fig. 4) blue-greyish calcilutites are prevailing. They are fetid, sulphide-rich, dm-thick beds, with rare and thin marly interbeds. In the field they constitute a prominent cliff. The middle part (D2: 580-620 m, Fig. 4) consists of thickening- and coarsening-up cycles of calcilutites and calcarenites in beds. 30-60 cm thick alternating with marls. In the upper part (D3: 620-700 m, Fig. 4) calcilutitic beds, 30-60 cm thick, are present and form a second steep cliff. Upwards, the bed thickness decreases and there are nodules and lenses of chert and marly intercalations. Fossils: sponge spicules and late Callovian to Oxfordian benthic foraminifers (*Kurnubia palastiniensis* Henson, *Nautiloculina oolithica* Mohler, *Ammodiscidae* and *Lituolidae)* and rare radiolarians are present.The calcareous nannofossil assemblage, indicative of a Middle to Late Jurassic age, is scarce, poorly preserved and not diversified. The genus *Watznaueria* is

Source : MNHN, Paris

still the most abundant with *W. barnesae* (Black), *W. britannica* (Stradner), *W. communis* (Reinhardt) and *W. manivitae* (Bukry). Very rare *Lotharingius velatus* Bown & Cooper, *L. hauffii* (Grün & Zweili) and *Cyclagelosphaera margerelii* Noël are also present. Age: the age of Unit D is possibly late Oxfordian - early Kimmeridgian, based on its stratigraphic position.

Unit E (Eggerale section, Fig. 3; 700-960 m, Fig. 4). Marly limestones and marls alternate with thin bed-sets of calcilutites and bioclastic calcarenites. The marly limestones are often bioclastic and lumachella beds are present as well. The marls show yellowish or pink-violet colour and evident fixility or nodularity. Calcilutites are dark grey, sometimes yellowish or reddish, due to oxidation of small sulfide crystals. Bioturbation is often present. Fossils: bioclasts of pelecypods, gastropods, echinoderms and rare radiolarians, benthic foraminifers, encrusting foraminifers, serpulids, ostracods occur. As to the foraminifers, *Alveosepta jaccardi* (Schrodt), *Riyadhella* sp., *Lenticulina* sp. and *Ammodiscidae* are present. *Saccocoma* sp., sponge spicules and crinoidal spines have been also found. In both units E and F almost all the samples are barren of calcareous nannofossils. Only sporadic *Discorhabdus* sp. and *Watznaueria* sp. have been recognized. Age: late Oxfordian - early Kimmeridgian on the base of the *Alveosepta jaccardi* occurrence.

Unit F (Eggerale section, Fig. 3; 960-1080 m, Fig. 4). Subunit F1 (960-1020 m, Fig. 4) consists of often reddish calcilutites in dm-thick beds and subordinate bioclastic calcarenites with thin marly interbeds. Marly levels and sets of dm-thick calcilutitic beds characterize subunit F2 (1020-1080 m, Fig. 4); in its upper part bioclastic calcarenites and dm-thick tempestitic beds with fragments of pelecypods and gastropods are frequent. All calcarenite samples contain abundant silt- to sand-size quartz grains. Fossils: the poor foraminiferal assemblage includes *Alveosepta jaccardi* (Schrodt), *Riyadhella* sp., *Paraurgonina* sp. and *Ataxophragmiidae*. Age: late Oxfordian - early Kimmeridgian on the base of *Alveosepta jaccardi* (Schrodt) occurrence.

ENVIRONMENTAL INTERPRETATION AND SEQUENCE STRATIGRAPHY

In the Adeilo area the Antalo Limestone is prevailingly made up by calcareous and marly beds arranged in 1 to 10 m thick asymmetric cycles. These cycles, that are exclusively subtidal, exhibit the following attributes: a- within each cycle shaly-marly beds are prevailing at the base and calcareous beds at the top; b- tempestite beds and / or calcarenites are present in the upper portion of several cycles; c- the thickness of the calcareous beds increases upward whilst that of the marly beds decreases. These features indicate upward shallowing cycles. Since the base of each cycle records an increase in water depth, the cycles can be envisaged as parasequences (VAN WAGONER *et al.*, 1988).

These features support the inference that the Antalo Limestone was deposited in a shaly and calcareous homoclinal ramp (*sensu* BURCHETTE & WRIGHT, 1992). Since slumpings and breccia bodies as well as evidence of synsedimentary faulting are lacking, the floor of the ramp should have been very gentle. This is suggested also by the extensive areal occurrence of sedimentary units with the same characteristics.

The variability of the lithological and sedimentological features of the parasequences led to recognize four sub-environments such as those that appear in the schematic inner ramp to basin section of figure 5. These sub-environments are: a- an inner ramp with prevailing high-energy, carbonate, bioclastic sandy barrier; b- a mid ramp with frequent calcareous bioclastic storm layers, alternating with marly and shaly beds; c- an outer ramp with rare storm reworking, abundance of shaly and marly levels, and d- a basin with shaly-marly sediments and pelagic faunas (radiolarians, ammonites).

We can refer our subunits in the Adeilo succession to these sub-environments (Fig. 4). Starting from the bottom, subunit A1 is a shoaling up sequence deposited at first on a mid ramp with hypoxic conditions and then on an inner ramp with medium to high turbulence. Features in subunit A2 indicate a deepening toward an outer ramp environment, followed by fluctuations within a mid ramp. The environment in subunit A3 exhibits again a shallowing up evolution from a mid ramp to a restricted inner ramp. Subunit A4 can be referred, at first, to a mid ramp shallowing upward to an inner ramp, and, according to the thickening- and the coarsening-up pattern, to the progradation of a siliciclastic delta (Simi Koma key bed). During the sedimentation of Unit B a progressive deepening occurred, although limited to a mid ramp environment.

In subunit C1 an initial outer ramp gave place to mid ramp; in C2 basinal conditions, marked by

Source : MNHN, Paris

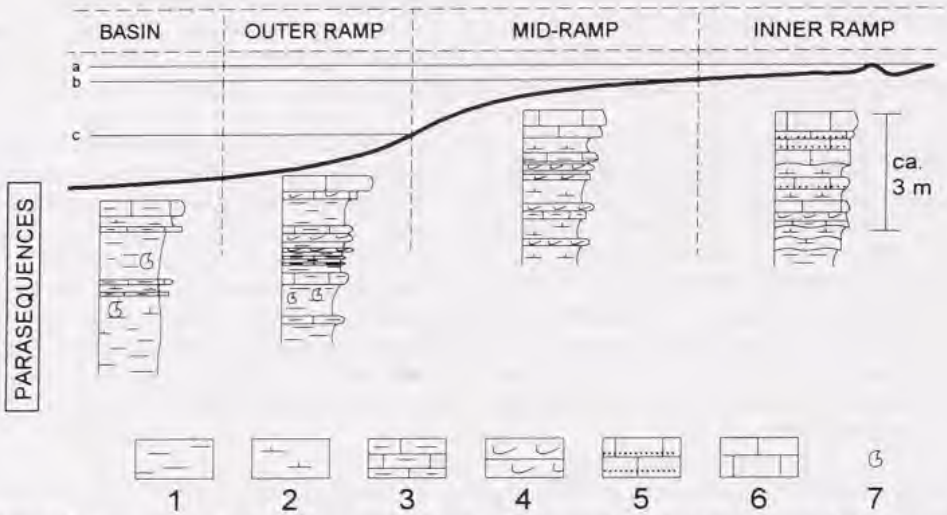

FIG. 5.— Lithology of parasequences and different sub-environments in a schematic inner ramp to basin cross-section. Legend: 1, shales; 2, marls; 3, marly limestones; 4, tempestitic coquina beds; 5, calcarenites; 6, calcilutites; 7, ammonites, a, mean sea level; b, fair-weather wave base; c, storm wave base.

FIG. 5.— Lithologie des paraséquences et des sub-environements dans une rampe interne schématique. 1, shales ; 2, marnes ; 3, marno-calcaires ; 4, calcaires coquillers ; 5, calcarénites ; 6, calcilutites ; 7, ammonites, a, principaux niveaux marins ; b, limite d'action des vagues ; c, limite d'action des vagues de tempêtes.

marly lithologies and extensive occurrences of ammonites, prevailed. Later on, conditions changed back to mid ramp through some fluctuations (C3).

As to unit D, the environment varies from an inner, restricted ramp in the lower part (D1) to a mid-inner ramp in the median part (D2), and, finally, again to an inner ramp (D3). A mid ramp environment with a relative deepening in the median portion is recognizable in unit E, and a variation from inner ramp to mid ramp in unit F.

A cyclic repetition of sub-environments is thus evident in the succession that also includes larger-scale cycles framed between major surfaces (SB 1 to 7, Fig. 4). In the field these surfaces correspond to morphological contrasts since they are placed where there is an abrupt change between more calcareous bed packets and the overlying shaly / marly portions. Accordingly, the depositional environment shifts upsection toward a relevant deepening. These surfaces, sometimes with unconformity features, comprise bed packages from several tenth to several hundred meters thick and cover a time span of one up to some million years. They can be regarded as sequence boundaries framing depositional sequences, possibly of the third order.

From bottom to top, the oldest surface (SB1) corresponds to the boundary surface between the Adigrat Sandstones and the Antalo Limestone. The second surface (SB2) occurs at the top of subunit A1, above the level with Hydrozoa and corals. The third surface (SB3) is placed on the top of the Simi Koma thick arenaceous bed packet, the deltaic body probably connected laterally with the evaporites of the Adeilo section. The fourth surface (SB4) is present at top of subunit C1, and the fifth surface (SB5) on the top of the lower limestone cliff correnspponding to the subunit D1. The sixth surface is placed at the top of the upper limestone cliff corresponding to the subunit D3, and the seventh surface (SB7) at the top of calcareous subunit F1.

According to this interpretation, these surfaces bound six depositional sequences, namely S1 (40 m thick), S2 (170 m thick), S3 (130 m thick), S4 (230 m thick), S5 (120 m thick) and S6 (330 m thick) (Fig. 4). These sequences show more or less developed intervals with a retrogradational arrangement of parasequences, that are considered as transgressive system tracts, and generally thicker intervals with progradational arrangement of parasequences (highstand system tract).

It is to be noted that in the sequence S4 the whole transgressive system tract corresponds to the bacinal C2 subunit and its surface of maximum flooding corresponds to a large-scale relative deepening.

Unfortunately, available chronostratigraphic data are not adequate for a precise dating of the sequence boundary surfaces and do not allow a close comparison with the global sequence boundaries (VAIL *et al.*, 1984; HALLAM, 1988).

Source : MNHN, Paris

CHRONOSTRATIGRAPHIC CONSIDERATIONS AND CORRELATIONS WITH ADJOINING REGIONS IN EAST AFRICA

In the study area the Antalo Limestone was deposited in a time span extending from late Callovian to early Kimmeridgian. Some comments can be added to these age attributions. As to the lower age limit, that is the invasion of the Antalo sea above the terrestrial to transitional Adigrat Sandstones, we can observe that this transgression is widespread in the whole East Africa as well as in Arabia (the so called *Eligmus* fauna of ARKELL, 1951). For its large areal extension we can assume that it was connected with an outstanding eustatic rise. During the Callovian there is an important phase of coastal onlap at 155 Ma (HAQ *et al.*, 1988). Even if the datings of the lower and upper boundaries of the Callovian are uncertain (see HARLAND *et al.*, 1982; ODIN & ODIN, 1990), we are inclined to relate the basal flooding surface of the Antalo Limestone in Adeilo to this 155 Ma old rise because of the *Peltoceras* (uppermost Callovian, ca. 152 Ma) occurrence 80 m above the base of the studied succession.

It is noteworthy that the greatest deepening of the basin was reached at ca. 148 Ma (middle / late Oxfordian boundary) as suggested by the marls with ammonites of Unit C, 400 m above the base.

The data obtained from the Antalo Limestone in the northern Danakil Horst can be matched with those from Ethiopia, Somalia and NE Kenya. We have seen that the inception of marine sedimentation occurred in the late Callovian in the Adeilo area and we assumed that this event can be framed in the large-scale marine transgression in the whole East Africa. Some well-known sections, such as Sa Wer (ABBATE *et al.*, 1974) and Bihendula (BUSCAGLIONE & FAZZUOLI, 1987; ABBATE *et al.*, 1994) in Somalia, the Blue Nile gorge (FICCARELLI, 1968; RUSSO *et al.*, 1994), Mekele (BOSELLINI *et al.*, 1995) and Dire Dawa (FICCARELLI *et al.*, 1975) in Ethiopia can be taken for reference. It has to be added that some local differences (from late Bathonian to early Oxfordian) exist in dating the first marine episodes, but they can be imputed to a heterochronous transgression or, more likely, to poor biostratigraphic calibrations. However, a well documented precocious transgression occurred during the early Toarcian (SOEC, 1954; CANUTI *et al.*, 1983; BOSELLINI, 1989; LUGER *et al.*, 1990) limitedly to some areas (e.g. Ahl Mado in northern Somalia and Lugh-Mandera basins in southern Somalia / northeastern Kenya).

A closer comparison between the Antalo Limestone at Adeilo and in other East Africa successions shows that the late Callovian *Hydrozoa* limestones at the top of subunit A1 (Mahur section, Fig. 3) can be correlated with the lithologically similar and possibly coeval level at the top of the Bihen Limestones at Bihendula (BRUNI & FAZZUOLI, 1976).

Further correlations can be traced among levels showing remarkable deepenings of the basin. The middle / upper Oxfordian marls with ammonites of Unit C of the Adeilo area correspond to coeval and similar basinal deposits with belemnites and / or ammonites, that are common in East Africa (see Warandab depositional sequence of BOSELLINI, 1989).

At a very short distance from the Adeilo area, the Mekele outlier in Tigrai (MERLA & MINUCCI, 1938; ARKIN *et al.*, 1971; BEITH, 1972; BOSELLINI *et al.*, 1995) share some common features with the succession described in this paper. In both areas marly and calcareous lithotypes are arranged in parasequences with frequent storm layers denoting a ramp environment. Moreover, a thick marly interval with ammonites occurs in the middle portion of both sections, but siliciclastic and / or evaporitic intercalations are lacking in the lower to middle portion of the Mekele section. Interestingly, the total thickness of the Antalo Limestone increases from the Mekele area to the Danakil Depression.

STRUCTURAL COMMENTS ON THE ADEILO AREA

A photogeological map at 1: 100,000 scale (Fig. 2) with several field controls is presented for the Adeilo area. It was meant to trace lateral and vertical extension of the sedimentary units distinguished in the Antalo Limestone and to provide information on the structure of this area for which detailed mapping is still lacking. The photogeologic study, together with field observations, testifies at least for the Adeilo area, a quite complex structural setting. On the basis of reconnaissance work a similar complexity seems to be common also in the eastern and southeastern slopes of the Danakil block (see MOHR, 1967). In the mapped area different structural situations can be distinguished.

Source : MNHN, Paris

The northern side shows a homoclinal structure with bedding slightly (max. 15°) tilted toward north and, limitedly to the Mt. Eggerale area, toward NW. This structure is affected by syntethic E-W trending normal faults with northern downthrown blocks. An important NW-SE trending family of faults has a possible left transcurrent component suggested by block offsets, rectilinear traces of regional extension and a few observed striated mesofaults. Large knee folds are locally present (see sect. V, Fig. 2).

The Mt. Assale topographic high is a large downfaulted block bounded to the east by a NNE-SSW fault system and to the SW by a NW-SE fault system. Only in proximity of the main fault systems the dipping becomes variable and steeper. The structure is further complicated by a normal fault system with an E-W trend.

SYN- AND POST- RIFT DEPOSITS IN THE SAHEL AND IN THE NORTHERN AFAR REGIONS

The syn- and post-rift Neogene deposits of the Sahel coastal plain and Northern Afar Depression record important tectonic events that affected these zones and the surrounding regions. They outcrop on both sides of the Afar Depression and in the hills west of Massawa (Fig. 1) above Tertiary Trap basalts, Mesozoic sediments and Precambrian basement (DAINELLI, 1943; FRAZIER, 1970).

The succession comprises predominantly continental deposits with an exposed thickness of several hundreds of meters (DAINELLI, 1943; BANNERT *et al.*, 1970; KAZMIN, 1975; GARLAND, 1980).

The sedimentary units recognized are generally bounded by sharp erosional surfaces, paleosols and angular unconformities.

THE SAHEL AREA

In this area a 650 m thick volcano-sedimentary succession (Dogali Formation) rests above Oligocene (28 Ma, DRURY *et al.*, 1994) Trap basalts and is unconformably overlain by Desset Boulder Beds (PORRO, 1935; KAZMIN, 1975) (Fig. 7).

The Dogali and Desset formations merge laterally offshore into the shallow marine, up to 7,000 m thick, sediments of the Habab, Dunishub and Amber salt formations (CARELLA & SCARPA, 1962; SESTINI, 1965; KAZMIN, 1975).

THE DOGALI FORMATION

Composite sections, totalling 500 m, have been measured in the Dogali, Desset and Gabeichelti areas (Fig. 7). They show that the lower portion of this formation (lower Dogali Formation) is predominantly siliceous, while the upper one (upper Dogali Formation) consists mainly of pebbly sands, conglomerates, reefal limestones and gypsum beds. More in particular, the lower portion is made up by siliceous, fine grained, yellow, brown and dark grey laminated or nodular clays and silts in 0.2-0.5 m thick beds with rusty hematitic coats. The silty beds are graded and contain root marks and leaf prints. Volcanoclastic green sandy beds, 0.2-1.5 m thick, massive or horizontally laminated are interbedded in the siliceous lacustrine deposits. They are graded and contain reed fragments, leaf prints and clay clasts. These lithofacies may be interpreted as deposited in fresh-water ponds during volcanic quiescence with reduced clastic inflows.

A lenticular, 0.5-1.5 m thick level of brown massive or cross-stratified pebbly sandstones is also present toward the base of this formation. It contains well-rounded pebbles derived from Trap basalts and associated acidic volcanites, silicified tree trunks, mammalian bones among which a newly discovered *Deinotherium* remain (a fragment of lower jaw with teeth).

The lower Dogali Formation with a total thickness of 350 m consists in its upper part of 200 m of basalts.

The upper Dogali Formation shows diversified lithologies that are cyclically:

— gravelly facies. Massive, normal and reverse graded pebbles with abundant reddish sandy matrix. Clasts are rounded, imbricated and polymodal in size. Horizontal and trough cross lamination are common features of the pebbly beds that are 1-2 m thick. Locally, they are amalgamated and lie on erosional surfaces. Clasts up to 40 cm are polymictic and derive from basement rocks, basalts and acidic

Source : MNHN, Paris

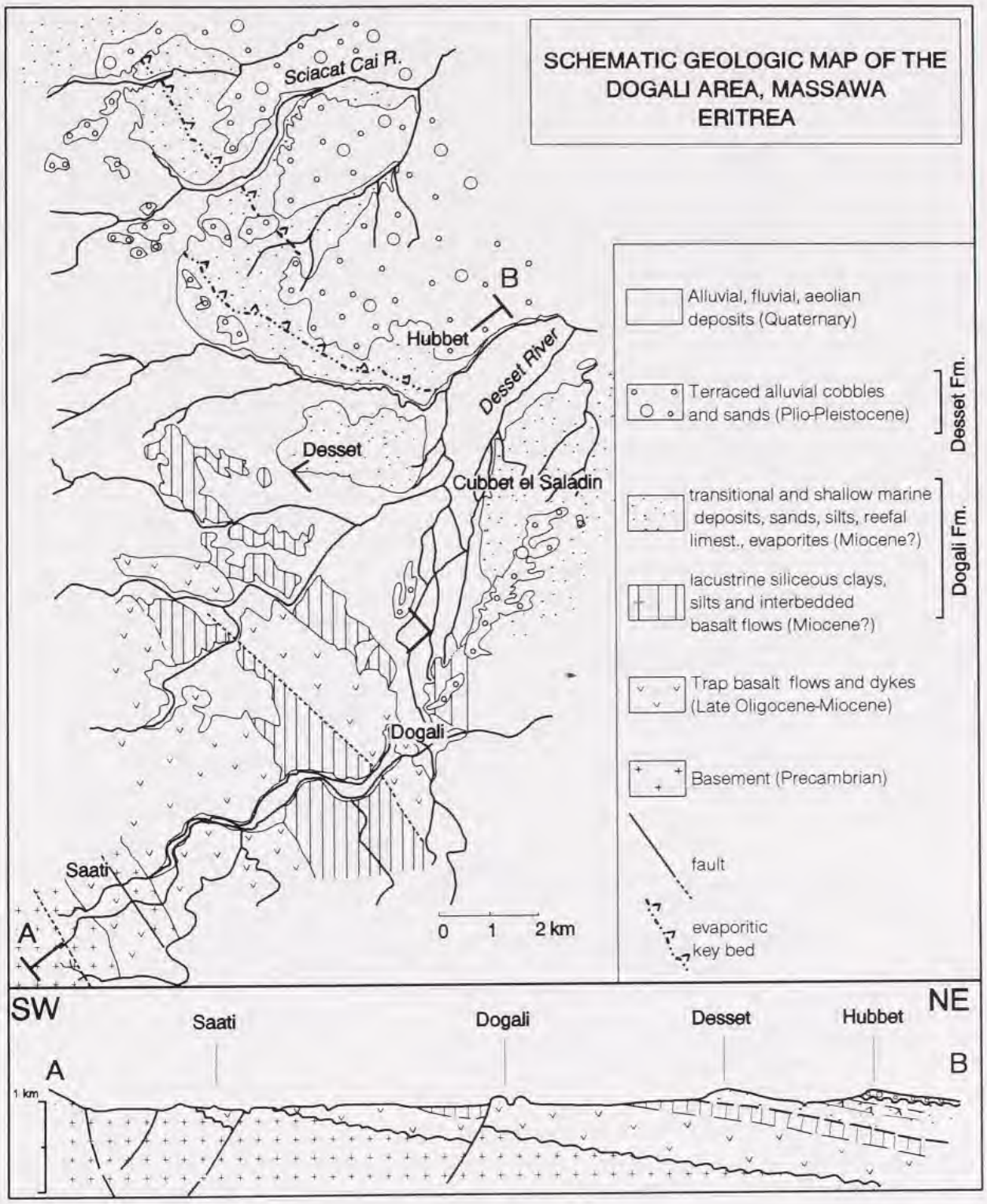

FIG. 6.— Sketch map of the Dogali area (west of Massawa), based on field survey and photogeological interpretation.
FIG. 6.— Carte schématique de la région de Dogali (à l'ouest de Massawa), d'après des études de terrain et l'interprétation des photographies aériennes.

Source : MNHN, Paris

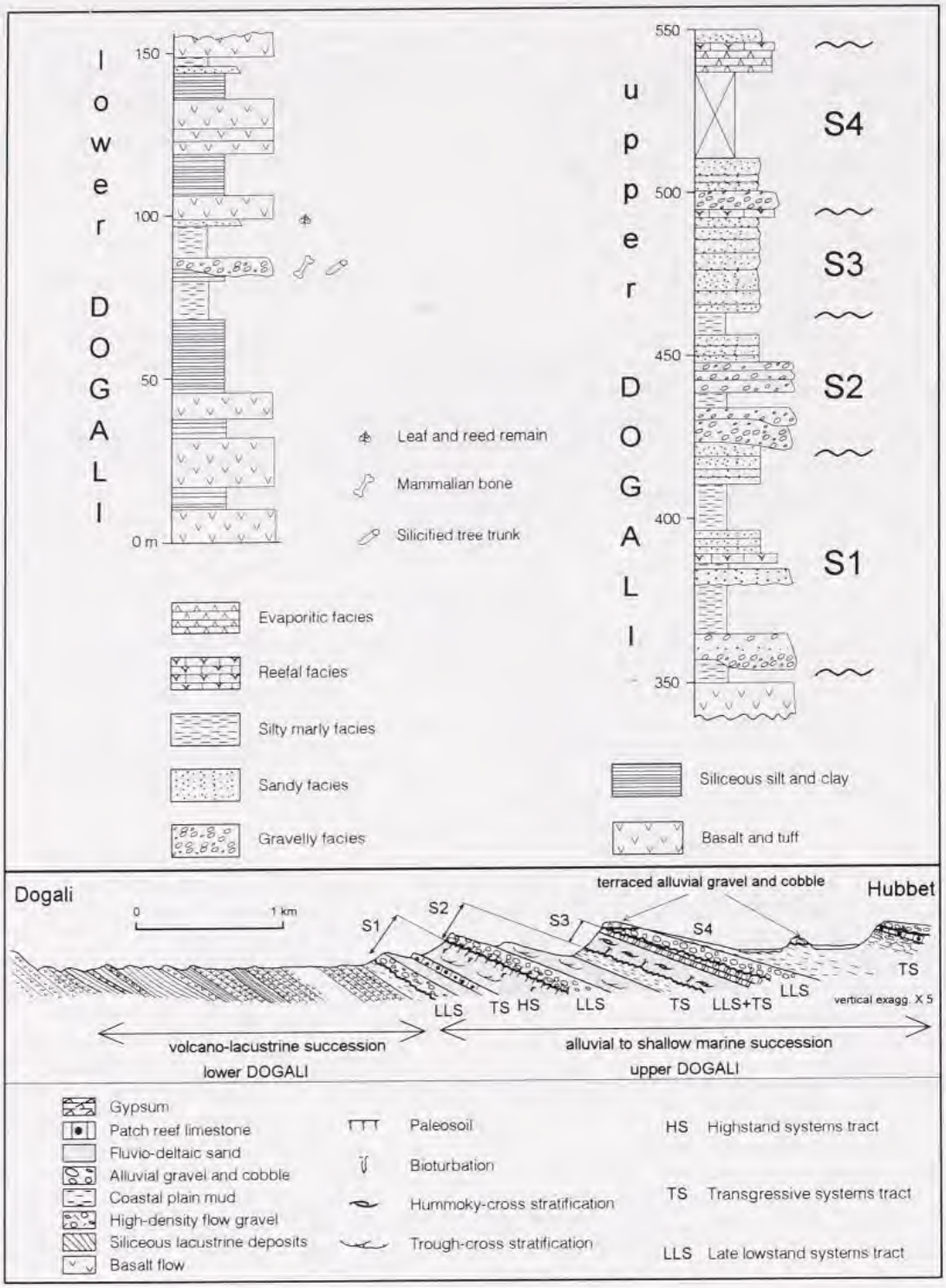

FIG. 7.— Summarized lithology of the Dogali Formation (a) and schematic cross section with the sequence stratigraphy interpretation (b).

FIG. 7.— Lithologie de la Formation Dogali (a) et coupe schématique avec l'interprétation en terme de stratigraphie séquentielle (b).

Source : MNHN, Paris

volcanites. Scattered paleocurrent data inferred from imbricated or clustered pebbles and cross laminations suggest main flows toward east;

— sandy facies. Cross or horizontally laminated and coarse to fine grained light yellow to green sands in beds up to 2 m thick. Pebbles, clay clasts, mollusc shells and root moulds are locally frequent. Burrows and pervasive bioturbation and subordinate wave ripples and hummocky laminations are common features in these sands. Some low angle cuneiform laminations, enhanced by well-sorted and imbricated flat clasts also occur;

— silty marly facies. Pale green massive silty marls occur as 0.5-1.5 m thick beds. They are laminated, nodular and bioturbated and contain fine comminuted plant debris, shells of *Melanopsis* and carbonate nodules (caliches). Abundant gypsum veins and nodules locally are also present. Red and purple mottling, manganese spherules and caliche nodules mark pedogenized and rooted horizons;

— patch reef facies. Lenticular, 1.5-2.5 m thick, patch reef bodies occur at two levels in the succession. Massive coral colonies are in growth position and float in a carbonate matrix. Stromatolitic limestone fills the cavities within the corals. The reef covers calcilutite pale yellow limestone beds that contain sparse pelecypods, single corals, cherty nodules, hematitic veins and dolomite crystals;

— evaporitic facies - Two levels of gypsum occur in the upper part of the measured section. The lower one, 20 m thick, is made of nodular alabastrine gypsum capped by an alternance of laminated microcrystalline gypsum and shales. This level is covered by coralline limestone and pebbly sandstone. The upper one, 2 m thick, lays on pale green bioturbated marls capped by 0.5 m of dolomite-gypsum-marl laminae. Gypsum shows nodular alabastrine and chicken-wire structure with ghosts of 5-10 cm selenite "cavoli" crystals formed in hypersaline waters. On top enterolithic nodular structures and vertical veins filled with crystalline gypsum occur. This gypsum horizon makes upward transition to red clay and to crystalline gypsum alternating with silt.

Age of the Dogali Formation: K-Ar datings of basaltic rocks gave 24.0 to 14.0 Ma (KAZMIN, 1975), but the location and stratigraphic position of samples is uncertain. More recently, DRURY *et al.* (1994) report an Ar-Ar age of 28 Ma for the base of the Trap basalts below the Dogali Formation and an age of 18 Ma for a basalt flow in the lower Dogali Formation. A further indication of an early Miocene age for the basal levels of this formation is given by the newly discovered *Deinotherium* bones found as clasts in a pebbly channelized body. This finding recalls that of a *Deinotherium* tooth found in the lignite levels interbedded in the Trap Basalts of the Eritrean plateau near Mendefera Adi Ugri (VIALLI, 1966).

Corals (*Orbicella ellisiana, Cyphastrea corrugata, Plerastrea* cf. *profunda, Plerastrea saheliana, Porites* sp., *Orbicella apenninica, Orbicella reussiana, Orbicella defrancei*) and marine molluscs (*Pecten* sp. and *Ostrea* sp.) suggest a middle to late Miocene age (ZUFFARDI-COMERCI, 1936 and MONTANARO GALLITELLI, 1939) for the upper Dogali Formation.

THE DESSET BOULDER BEDS

The Desset Boulder Beds form a continuous hilly chain extending from the Sudanese border to the Zula Gulf (PORRO, 1936). They consist of very coarse pebbles deriving from basement, Mesozoic rocks and Trap suite with outsized clasts up to 100 cm in diameter generally concentrated in the upper portion of the beds. They are massive, poorly organized with abundant microgranule and coarse grained sandy matrix. Beds are lenticular, amalgamated, structureless and rest above erosive irregular surface. They form different terraces connected with distinct sedimentary cycles. Plio-Pleistocene marine fossils were collected by BALDACCI (1891) in the coastal outcrops of these deposits near Massawa.

SEQUENCE STRATIGRAPHY ANALYSIS

In order to obtain information on the tectonic, environmental and climatic changes that have controlled and guided the depositional processes, a sequence stratigraphy analysis has been carried out on the Dogali Formation. The study has been limited to the upper part of this unit, where favourable outcrops allow to recognize several unconformity-bounded sequences (Fig. 7). As above mentioned, these are characterized by cyclic arrangement of facies associations that can be interpreted in terms of sequence stratigraphy models.

At least four sequences (S1 to S4; Fig. 7), 30 to 70 m thick, have been distinguished in the succession

Source : MNHN, Paris

cropping out in the Desset River valley. Each sequence is formed of basal coarse-grained fluvial deposits (facies a) which mark progradation and aggradation in the coastal area during the late lowstand (LLS). These deposits pass gradually upward to sandy-muddy fluvio-deltaic (facies a, b) or coastal plain sediments (facies b and c formed during the transgressive phase TS. The maximum marine ingression and sea-level stillstand is recorded by patch reef limestone (facies d). The highstand deposits (HS) are generally lacking and the typical fining and deepening upward (FU) trend is abruptly truncated by the LSS deposits of the overlying sequence. Only in the lowermost sequence (S1) the presence of deltaic deposits on top of the reefal limestone suggests a possible highstand. The symmetric depositional trend evidenced by the deposits in S1 could stem from an eustatic control on the base-level (i.e. sea-level) fluctuations, while the FU trends in sequences S2 to S4 can be related to fast increase of accommodation space in the basin due to an high rate of tectonic subsidence. A climatic signal (increasing aridity) superimposed on a base-level fluctuation is evidenced by evaporitic deposits (facies e) of S4.

STRUCTURAL REMARKS

The Dogali Formation dips homoclinally to the northeast around 10°-15° beneath the Desset Boulder Beds with an incised irregular boundary. The occurrence of polymictic conglomerates in the Desset Boulder Beds with clasts of basement, Mesozoic rocks and volcanics marks clearly the onset of major extensional faulting and uplift of the Eritrean plateau along the escarpment. This is connected with an important tectonic pulse during Pliocene times that rejuvenated the relief causing deep incision by rivers and deposition of Boulder Beds fanglomerate (BEYTH, 1978; DRURY *et al.*, 1994).

THE DANAKIL FORMATION IN THE NORTHERN AFAR DEPRESSION

According to GARLAND (1980), the Danakil Formation is an inhomogeneus unit varying in lithology and in thickness from place to place. The lower to middle portion is formed by well consolidated conglomerates, sandstones and mudstones intensely red to violet coloured, reflecting alteration under very wet climatic conditions. Beds of basalt are commonly interbedded in the sedimentary section. The unconformably overlying portion consists of sands, pebbles and clays with interbedded poorly cemented limestones rich in marine gastropods, corals and pelecypods. Locally, the sediments are stuffed with pillowed and spilitic basalt subaqueous lava flows, rhyolites and ignimbrites.

The Danakil Formation, with a maximum thickness of 1,000 m, rests on the basement and Mesozoic rocks of the Danakil Horst and of the Eritrean escarpment.

The outcrops of the Danakil Formation that are close to the foot of the escarpements are overlain with an erosional contact by multiterraced Boulder Beds fanglomerates coming from the shoulders of the depression.

THE DANAKIL FORMATION IN THE BUIA SECTION

A thick succession composed of predominant grey to whitish silts and sands has been examined near Buia at the northermnost apex of the Afar Depression and at the foot of the Eritrean escarpment (Fig. 8). It outcrops in isolated patches beneath terraced younger sediments. Its lithology and geological setting are reminiscent of the Neogene Danakil Formation (or Red Series) which outcrops widely further south in the Afar Depression (see geological maps by BANNERT *et al.*, 1970; BARBERI *et al.*, 1972; KAZMIN, 1975; MERLA *et al.*, 1979; GARLAND, 1980). Although a physical continuity has not been ascertained nor any firm correlation has been attempted, we provisionally refer Buia section to the upper portion of the Danakil Formation.

Composite sections have been investigated 5 km south of Buia in the Badda region near the Alut water well. This 500 m thick section is possibly the upper portion of the Danakil Formation and consists of predominantly terrigenous deposits laid down in lacustrine and fluvio-deltaic environments (Fig. 8). Four main lithofacies have been recognized.

— Green, pale green siltstones and mudstones, generally massive and bioturbated in beds 0.5 to 1.5 m thick are distributed along the entire section. Current and wavy ripples and flaser bedding locally occur. Thin paleosols horizons appear as pale brown, pink to mottled levels with nodular calcareous concretions (caliches), and root marks. Bioturbated levels are characterized by abundant shell remains of

Source : MNHN, Paris

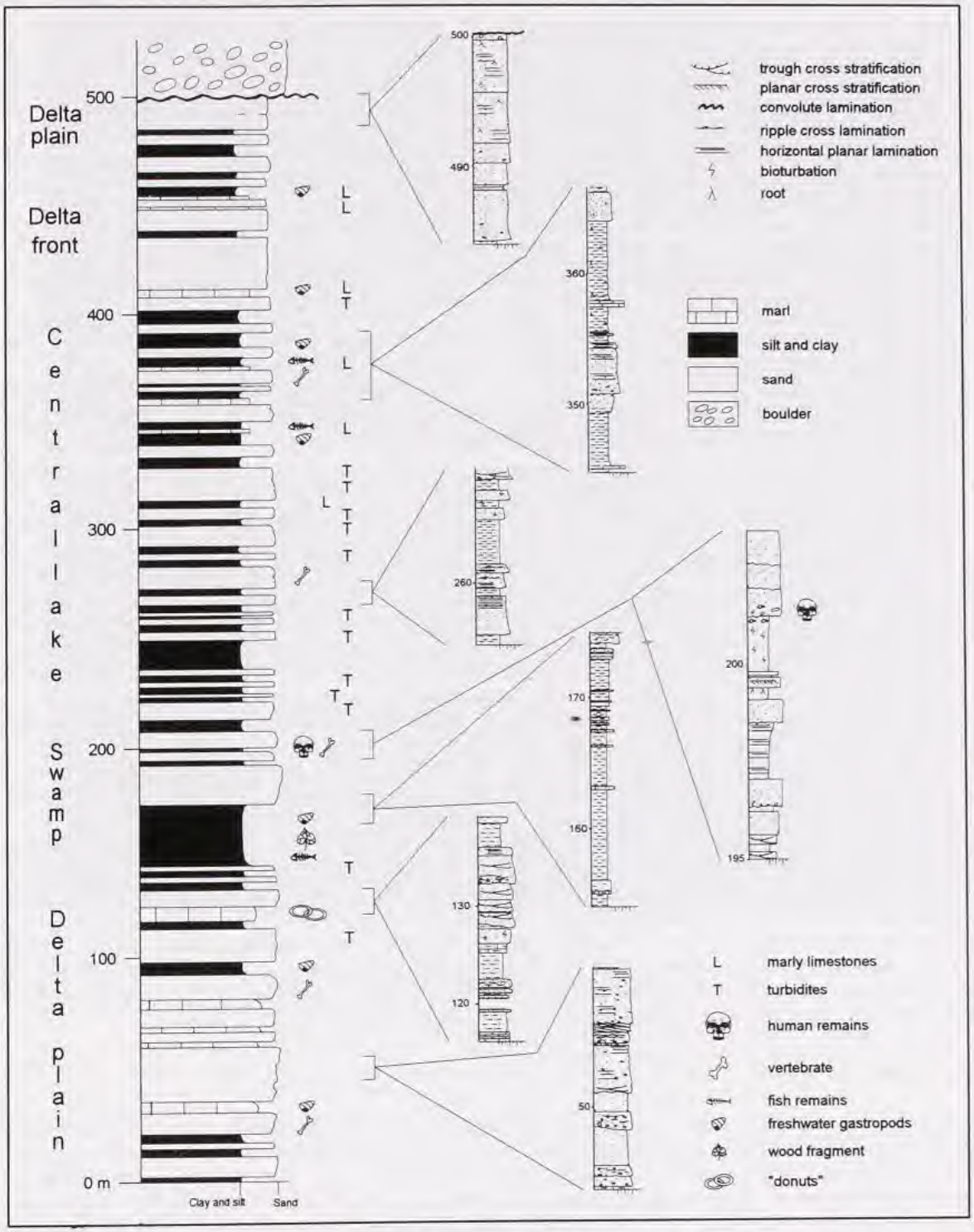

FIG. 8.— Lithology and environment interpretation of the upper Danakil Formation in the Buia area. Detailed logs of some typical levels are added.

FIG. 8.— Lithologie et environnement de la Formation Danakil supérieure dans la région de Buia. Logs détaillés de quelques niveaux particuliers.

Source : MNHN, Paris

Melanopsis, few vegetal organic matter and Fe concretions. These thinly laminated deposits indicate very low energy environment with rhythmic settlement of clastic material.

— Beds of 2 to 4 m of grey to pale green and pale brown pebbly sands, massive with well-developed trough-, cross- and plane-laminae and wavy ripples repeat along the entire section. Locally, the beds show lenticular shapes and erosive boundaries. Normal reverse and symmetric grading are common features together with well-rounded pebble clasts and clay chips scattered in the sandstone. Cherty lenses, gastropods, rooted horizons and intense vertical burrowing are sometimes abundant, chiefly in massive beds. Fluid escapes, dish structures and convolute laminations indicate intense clastic supply and quick squeezing of interpore water.

Sands occur either as single beds or stacked in amalgamated lenticular and channelized bodies, 4 per 20 m in size, displaying erosive basal contact and flat top. Lenticular upward convex bodies, 1 to 3 m thick, composed by upward thickening or symmetric sequences represent sandy lobes rooted and intensely bioturbated.

— White silty calcareous marls, 0.2-1.1 m thick, occur in the upper portion of the section. They are massive, nodular, bioturbated and contain scattered clay chips and *Melanopsis* shells.

An extensive key bed occurs interbedded in the marls. It consists of ostracod-bearing calcisiltites, 50 cm thick, with questionable ring-shaped, "donuts"-like structures. The latter are 15 cm in diameter, 5 cm in cross sections and protrude into the underlying marly levels.

— Pale brown to yellowish medium-fine sands in beds 0.5-1.5 m thick. They are massive, graded with clay chips and locally are organized according to the Bouma sequences.

According to our preliminary investigations, clear depositional sequences could not be defined. However, facies associations allow to recognize deltaic and lacustrine environments (Fig. 8). At the base, the prevailing of pebbly sands and silty facies indicate a delta plain environment with lenticular bodies filling distributary channels. Up in the succession silts and clays bearing vegetal remains prevail and indicate a swamp environment. Thick sandy bodies again testify delta plain deposits followed upward by frankly central lacustrine facies characterized by marly limestones and turbidite beds. The last 100m of the section consists of delta front and delta plain deposits representing a regressive trend. The topmost beds are intensely bioturbated with large roots and burrows.

An angular unconformity of regional extension marks the contact between the Danakil Formation and the overlying Boulder Beds.

As to the age of the Danakil Formation, radiometric datings come from the Ethiopian portion of the Afar Depression. Intercalated basalts toward the base and the top of this unit gave early Miocene and late Pliocene ages, respectively (25 Ma and 2,5 Ma; BANNERT *et al.*, 1970; BARBERI *et al.*, 1972).

During our investigations five fossiliferous levels in the Buia section (Fig. 8) yielded an abundant Vertebrate fauna with bones of elephants, hippos, antelopes, bovids, equids, suids, hyaenids and crocodiles, and a *Homo* skull (see announcement *in* MORELL, 1996). Although still under study, the fossil association seems to indicate a wooded savannah environment and a early Pleistocene age for the lacustrine and fluviodeltaic deposits. At that time the landscape was fundamentally different from the present Danakil barren desert since the Eritrean plateau had not yet risen to its present height and was an undulated smooth lowland. Researches in progress will hopefully contribute to the understanding of the relations between climatic changes and mammals evolution (see MENOCAL, 1995).

BOULDER BEDS

Boulder Beds similar to those found in the Dogali area rest on the Danakil Formation with an erosional and unconformable surface (Fig. 8). They consist of boulders and cobbles of basement and Mesozoic rocks and contain outsized boulder up to 1m in diameter. They have the same climatic and tectonic significance of those outcropping in the Dogali area. Similarly, they have originated from catastrophic floods discharging materials derived from active fault scarps bordering the Eritrean Plateau. The age of the Boulder Beds is Pleistocene.

Source : MNHN, Paris

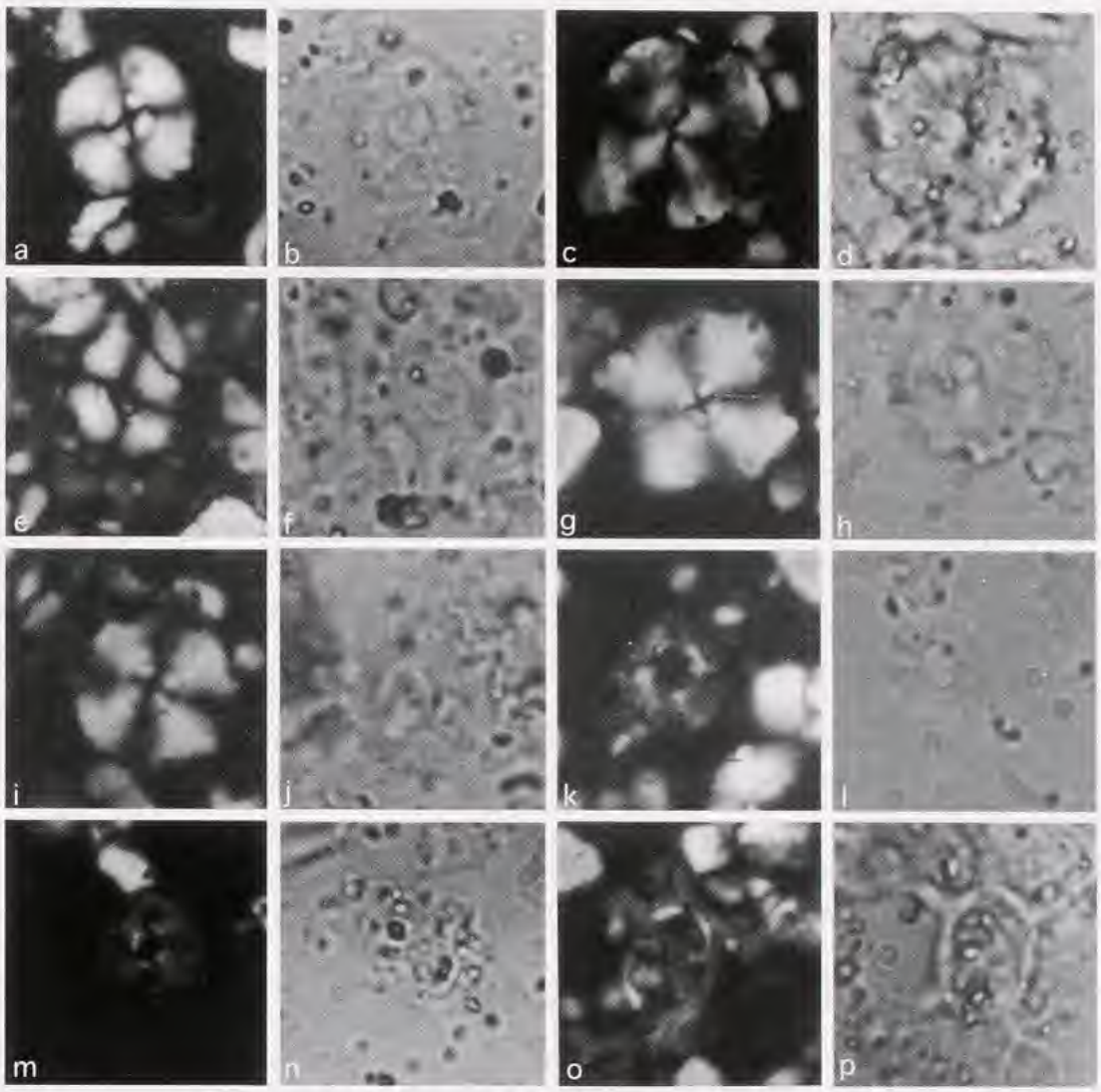

FIG. 9.— Calcareous nannofossils in the Antalo Limestone of the Adeilo area.
The abbrevations CL and TL denote cross-polarized light and transmitted light, respectively; all magnifications x 2800. **a-b**: *Watznaueria barnesae* (Black); a: distal view CL, Mahur section, b: TL as a. **c-d**: *Watznaueria manivitae* Bukry; c: distal view CL, Assale section, d: TL as c. **e-f**: *Watznaueria contracta* (Bown & Cooper); e: distal view CL, Assale section, f: TL as e. **g-j**: *Cyclagelosphaera wiedmannii* Reale & Monechi; g: distal view CL, Mahur section, h: TL as figure g, i: distal view CL, Mahur section, j: TL as i. **k-l**: *Podorhabdus grassei* Noël ; k: distal view CL, Mahur section, l: TL as k. **m-n**: *Discorhabdus* (*Palaeopontosphaera*) *dorsetensis* Varol & Girgis; m: distal view CL, Mahur section, n: TL as m. **o-p**: *Stephanolithion bigotii maximum* Medd; o: distal view CL, Mahur section, p: TL as o.

FIG. 9.— Nannofossiles des calcaires d'Antalo de la région d'Adeilo.
CL et TL = lumière polarisée et lumière transmise; toutes les photos sont x 2800. ***a-b*** *:* Watznaueria barnesae *(Black); a : vue distale CL, coupe de Mahur, b : TL idem a.* ***c-d*** *:* Watznaueria manivitae *Bukry ; c : vue distale CL, coupe d'Assale, d : TL idem c.* ***e-f*** *:* Watznaueria contracta *(Bown & Cooper) ; e : vue distale CL, coupe d'Assale, f : TL idem e.* ***g-j*** *:* Cyclagelosphaera wiedmannii *Reale & Monechi ; g: vue distale CL, coupe de Mahur, h : TL comme g, i : vue distale CL, coupe de Mahur, j : TL idem i.* ***k-l*** *:* Podorhabdus grassei *Noël ; k : vue distale CL, coupe de Mahur, l : TL idem k.* ***m-n*** *:* Discorhabdus (Palaeopontosphaera) dorsetensis *Varol & Girgis ; m : vue distale CL, coupe de Mahur, n : TL idem m.* ***o-p*** *:* Stephanolithion bigotii maximum *Medd ; o : vue distale CL, coupe de Mahur, p : TL idem o.*

Source : MNHN, Paris

CONCLUSION

The main results obtained from our investigations in the Danakil horst, Sahel lowland and Danakil (Afar) Depression can be summarized as follows:

— stratigraphical and sedimentological definition of six units in the Antalo Limestone and paleoenvironmental recognition of repeated cycles within a ramp system;

— significant biostratigraphical data, mainly based on ammonites, calcareous nannoplankton and foraminifers that assign a late Callovian to early Kimmeridgian age to the Antalo Limestone;

— recognition of a deltaic episode (the Simi Koma key bed) within the marine Antalo Limestone;

— interpretation according to sequence stratigraphy of the Antalo Limestone and recognition of seven depositional sequences, systems tracts and significant surfaces;

— geological map of the Adeilo area showing the areal extension of the different units in the Antalo Limestone and how intensely they have been deformed (also under a transcurrent regime) during the Neogene development of the Southern Red Sea and Afar rift systems;

— basin and facies analyses in the Dogali and Danakil formations;

— recognition in the Dogali-Desset section of a lower (siliceous lacustrine deposits and basalts) and an upper (fluviodeltaic to shallow marine) portion of the Dogali Formation.

— facies analysis evidences four depositional sequences mainly connected with relative sea-level fluctuations;

— new paleontologic record (*Deinotherium*) for an early Miocene age of the Dogali Formation;

— facies analysis in the upper portion of the Danakil Formation with the assessment of fluviodeltaic and lacustrine environments;

— findings of an abundant early to middle Pleistocene vertebrate fauna and, in particular, of a *Homo* skull, that also provide paleoclimatic and paleoecologic information of remarkable significance for discovering the origin and interpreting the evolution of the human species.

ACKNOWLEDGEMENTS

All the authors participated into the 1994 and 1995 field campaigns to Eritrea and jointly contributed to data interpretation and presentation. In particular, M. SAGRI, E. ABBATE, M.L. BALESTRIERI, M. BENVENUTI, P. BRUNI, M. FAZZUOLI, M. PAPINI and Tewelde Medhin TECLE: regional geology, stratigraphy and sedimentology; A. AZZAROLI, G. FICCARELLI and L. ROOK: vertebrate paleontology; G. PAVIA: ammonites; M. MARCUCCI: foraminifers; V. REALE: calcareous nannofossils.

The authors thank the Peri-Tethys Program, the Italian National Research Council, the European Commission, the Italian Ministry for the University and Scientific and Technological Resaerches and the University of Florence for supporting their researches. The Department of Mines of the Eritrean Ministry of Energy, Mines and Water Resources and the Italian Embassy in Asmara are to be acknowledged for providing field facilities and logistic assistance. Thanks are also due to two anonymous reviewers that substantially improved an early version of this paper. Professor Michel SEPFONTAINE kindly helped in benthic foraminifers determinations. Paolo GHETTI and Alessandro ABBATE provided a generous assistance in the field.

REFERENCES

ABBATE, E., FICCARELLI, G., PIRINI RADRIZZANI, C., SALVIETTI, A., TORRE, D. & TURI, A., 1974.— Jurassic sequences from the Somali coast of the Gulf of Aden. *Rivista Italiana di Paleontologia e Stratigrafia*, **80**: 409-478.

ABBATE, E., SAGRI, M. & SASSI, P.F. (eds.) 1994.— Geological map of Somalia 1:1,500,000. *In*: Geology and mineral resources of Somalia and surrounding regions. *Istituto Agronomico Oltremare*, **113** (B).

Source : MNHN, Paris

ARKELL, W.J., 1956.— *Jurassic Geology of the World*. Oliver & Boyd, London: 1-806.

ARKIN, Y., BEYTH, M., DOW, D.B., LEVITTE, D., TEMESGEN, H. & TSEGAYE, H., 1971.—Geological map of Mekele Sheet Area ND 37-11, Tigre Province. Geological Survey of Ethiopia, Addis Ababa.

BALDACCI, L., 1891.— Osservazioni fatte nella colonia Eritrea. *Memorie Descrittive della Carta Geologica Italiana*, **6**: 1210.

BANNERT, D., BRINKMANN, J., KEDING, K.Ch., KNETSCH, G., KNERSTEIN, M. & MAYRHOFER, H., 1970.— Zür Geologie der Danakil Senke (nordliches Afar Gebiet), NE Aethiopien. *Geologische Rundschau*, **59**: 409-443.

BARBERI, F., BORSI, S., FERRARA, G., MARINELLI, G., SANTACROCE, R., TAZIEF, M. & VARET, J., 1972.— Evolution of the Danakil depression (Afar, Ethiopia) in light of radiometric age determinations. *Journal of Geology*, **80**: 720-729.

BEYTH, M., 1972.— Paleosoic-Mesozoic sedimentary basin of Mekele Outlier, Northern Ethiopia. *American Association of Petroleum Geologists Bulletin*, **56**: 2426-2439.

BEYTH, M., 1978.— A comparative study of the sedimentary fills of the Danakil depression (Ethiopia) and Dead Sea rift (Israel). *Tectonophysics*, **46**: 357-367.

BOSELLINI, A., 1989.— The continental margins of Somalia: their structural evolution and sequence stratigraphy. *Memorie di Scienze Geologiche*, **41**: 373-458.

BOSELLINI, A., RUSSO, A. & ASSEFA, G., 1995.— Il Calcare di Antalo nella regione di Macallè (Tigrai, Etiopia settentrionale). *Rendiconti Science Fisiche e Naturali Accademia dei Lincei*, **9** (6): 253-267.

BOWN, P.R., COOPER, M.K.E. & LORD, A.R., 1988.— A calcareous nannofossil biozonation scheme for the early to mid Mesozoic. *Newsletters on Stratigraphy*, **20**: 91-114.

BRUNI, P. & FAZZUOLI, M., 1976.— Sedimentological observations on Jurassic and Cretaceous sequences from Northern Somalia. *Bollettino della Società Geologica Italiana*, **95**: 1571-1588.

BURCHETTE, T.P. & WRIGHT, V.P., 1992.— Carbonate ramp depositional systems. *Sedimentary Geology*, **79**: 3-57.

BUREK, P.J., 1970.— Palaeomagnetic evidence for an anticlockwise rotation of the Danakil Alps, Ethiopia. *Transactions - American Geophysical Union*, **51**: 271.

BUSCAGLIONE, L. & FAZZUOLI, M., 1987.— *Jurassic carbonate microfacies of Somalia*. Dipartimento Scienze della Terra, Università di Firenze, Firenze: 1-30

CANUTI, P., FAZZUOLI, M., FICCARELLI, G. & VENTURI, F., 1983.— Occurrence of Liassic faunas at Waaney (Uanei), Province of Bay, South-Western Somalia. *Rivista Italiana di Paleontologia e Stratigrafia*, **89**: 31-46.

CARELLA, R. & SCARPA, M., 1962.— Geological results of exploration in Sudan by AGIP Mineraria. *4th Arab Petroleum Congress, Beirut*, Abstract: 23.

DAINELLI, G., 1943.— *Geologia dell'Africa Orientale*. Regia Accademia Italiana, Roma: 1-727.

DRURY, S.A., KELLEY, S.P., BERHE, S.M. & COLLIER, R.E., 1994.— Structures related to Red Sea evolution in the Northern Eritrea. *Tectonics*, **13**: 1371-1380.

FICCARELLI, G., 1968.— Fossili giuresi della serie sedimentaria del Nilo Azzurro. *Rivista Italiana di Paleontologia e Stratigrafia*, **74**: 23-50.

FICCARELLI, G., PIRINI RADRIZZANI, C. & TURI, A., 1975.— Analyses of the microfacies of the Antalo Limestone in the Dire Dawa area, Ethiopia. *Bollettino della Società Geologica Italiana*, **94**: 759-770.

FRAZIER, S.B., 1970.— Adjacent structures of Ethiopia: that portion of the Red Sea coast including Dahlak Kebir Island and the Gulf of Zula. *Philosophical Transactions of the Royal Society of London*. Series A: *Mathematical and Physical Sciences*, **267**: 131-141.

GARLAND, C.R., 1980.— Geology of the Adigrat area. *Ministry of Mines and Water Resources; Geological Survey of Ethiopia, Memoires*, **1**: 1-51.

GAULIER, J.M. & HUCHON, P., 1991.— Tectonic evolution of Afar triple junction. *Bulletin de la Société géologique de France*, **162**: 451-464.

HALLAM, A., 1988.— A revalutation of Jurassic eustasy in the light of new data and the revised Exxon curve. *In*: WILGUS C.K. *et al.* (eds), Sea-level changes-an integrated approach. *Society of Economic Paleontologists and Mineralogists, Special Publication*, **42**: 261-271.

HAQ, B.U., HARDENBOL, J. & VAIL, P.R., 1988.— Mesozoic and Cenozoic chronostratigraphy and cycles of sea-level changes. *In*: WILGUS C.K. *et al.* (eds), Sea-level changes-an integrated approach. *Society of Economic Paleontologists and Mineralogists, Special Publication*, **42**: 71-108.

HARLAND, W.B., COX, A.V., LLEWELLYN, P.G., PICKTON, C.A.G., SMITH, A.G. & WALTERS, R., 1982.— *A Geologic Time Scale*. Cambridge University Press, Cambridge: 1-131.

KAENEL, E. DE, BERGEN, J.A. & SALIS PERCH-NIELSEN, K. VON, 1996.— Jurassic calcareous nannofossil biostratigraphy of western Europe. Compilation of recent studies and calibration of bioevents. *Bulletin de la Société géologique de France*, **167**: 15-28.

KAZMIN, V., 1975.— Explanation of the geological map of Ethiopia. *Ministry of Mines and Water Resources; Geological Survey of Ethiopia, Memoires*, **1**: 1-14.

LUGER, P., HENDRIKS, F., ARUSH, M., BUSSMAN, M., KALLENBACH, H., METTE, W. & STROUHAL, A., 1990.— The Jurassic and the Cretaceous of Northern Somalia: preliminary results of the sedimentologic and stratigraphic investigations. *Berliner Geowissenschaftliche Abhandlungen, Reihe A*, **120**: 571-594.

Source : MNHN, Paris

MENOCAL, P.B. DE, 1995.— Plio-Pleistocene African climate. *Science*, **270**: 53-59.

MERLA, G. & MINUCCI, E., 1938.— *Missione Geologica nel Tigrai*. Regia Accademia Italiana, Roma: 1-362.

MERLA, G., ABBATE, E., AZZAROLI, A., BRUNI, P., CANUTI, P., FAZZUOLI, M., SAGRI, M. & TACCONI, P., 1979.— A geological map of Ethiopia and Somalia (1973), 1: 2,000,000 and comment with a map of major landforms. *Consiglio Nazionale delle Ricerche Italy, Centro Stampa Firenze*:1-95.

MONTANARO GALLITELLI, E., 1939.— Ricerche sull'età di alcuni depositi insulari e marginali del Mar Rosso (isole Dahalak, penisola di Buri, dintorni di Massawa fino al Sahel). *Palaeontographia Italica*, **39**: 215-258.

MORELL, V., 1996.— New skull turns up in Northeast Africa. *Science*, **271**: 32.

ODIN, G.S. & ODIN, C., 1990.—Echelle numérique des temps géologiques, mise à jour. *Géochronique*, **35**: 12-21.

PORRO, C., 1936.— Esplorazione geologica della zona costiera Eritrea a Nord di Massawa. *Memorie Regie dell'Accademia di Torino*, **78**: 35-72.

REALE, V. & MONECHI, S., 1994.— *Cyclagelosphaera wiedmannii* new species, a marker for the Callovian. *Journal of Nannoplanton Research*, **16**: 117-119.

RUSSO, A., GETANEH, A. & BALEMWAL, A., 1994.— Sedimentary evolution of the Abay River (Blue Nile) Basin, Ethiopia. *Neues Jahrbuch für Geologie und Paläontologie, Monatsh*, **5**: 291-308.

SESTINI, J., 1965.— Cenozoic stratigraphy and depositional history, Red Sea coast, Sudan. *American Association of Petroleum Geologists, Bulletin*, **49**: 1453-1472.

SICHLER, B., 1980.— La biellette danakile: un modèle pour l'évolution géodynamique de l'Afar. *Bulletin de la Société géologique de France*, **22**: 925-933.

SOMALILAND OIL EXPLORATION Co. 1954.— *A Geological Reconnaissance of the Sedimentary Deposits of the Protectorate of British Somaliland*. Crown Agents, London: 1-42.

VAIL, P.R. & TODD, R.G., 1984.— Jurassic unconformities, chronostratigraphy, and sea-level changes from seismic stratigraphy and biostratigraphy. *American Association of Petroleum Geologists, Memoires*, **36**: 129-144.

VAN WAGONER, J.C., POSAMENTIER, H.W., MITCHUM, R.M., VAIL, P.R., SARG, J.F., LOUTIT, T.S. & HARDENBOL, J., 1988.— An overview of the fundamentals of sequence stratigraphy and key definitions. *In*: Sea-level changes-an integrated approach. *Society of Economic Paleontologists and Mineralogists, Special Publication*, **42**: 39-45.

VIALLI, V., 1966.— Sul ritrovamento di Dinoterio (*Deinotherium cf. abley* Andrews) nelle ligniti di Adi Ugri, Eritrea. *Giornale di Geologia*, **33**: 447-458.

VINASSA DE REGNY, P., 1924.—*Dancalia*. Alfieri e Lacroix, Roma: 1-140.

VINASSA DE REGNY, P., 1931.— La geologia delle Alpi Dancale. *Bollettino della Società Geologica Italiana*, **50**: 1-24.

ZUFFARDI-COMERCI, R., 1936.— Corallari neogenici del Sahel. *Atti Regie dell'Accademia di Torino*, **71**: 1-15.

Source : MNHN, Paris

Tectonic evolution of the Southern Tethyan margin in Southern Tunisia

Samir BOUAZIZ [1], *Éric* BARRIER [2], *Jacques* ANGELIER [2], *Pierre* TRICART [3] & *Mohammed M.* TURKI [4]

[1] Département de Géologie, École Nationale d'Ingénieurs de Sfax, B.P. W, 3038 Sfax, Tunisie

[2] Département de Géotectonique, URA CNRS 1759, Université P. et M. Curie, 75252 Paris Cedex 05, France

[3] Institut Dolomieu, Géologie et Minéralogie, UPRES CNRS 5025, Rue M. Gignoux, 38031 Grenoble, France

[4] Université de Tunis II, Faculté des Sciences de Tunis, Département de Géologie, 1060 Tunis, Tunisie

ABSTRACT

Southern Tunisia is located at the northern edge of the Saharan platform and South of the folded Atlasic domain. It is characterized by major sedimentary basins providing excellent outcrop conditions. The stratigraphic section consists of an almost complete sequence that ranges in age from Late Permian to Quaternary where fractures exist in all geological formations. Two distinct domains have been investigated: the stable platform and the Southern pre-Atlasic domain. An extensive analysis has been carried out in 354 sites. It allows the reconstruction of the tectonic evolution of the Southern Tunisian domain since Late Permian in term of paleostress tensors (434 have been computed). From Permian to Present, the tectonic evolution of Southern Tunisia includes the following succession of tectonic events: a) from Late Permian to Triassic, during the break up of Pangea, extensional tectonics dominated; b) from late Carnian to Early Cretaceous, the tectonics were characterized by sub-meridian extensions related to the Africa-Eurasia divergence; c) in Late Cretaceous and Paleogene tectonics remained distensive, but the directions of extension rotated several times; d) the Neogene time is marked by compressional events resulting from the Africa-Eurasia convergence. The major event is the NW-SE Atlasic compression, mainly Tortonian in age. During Plio-Quaternary, 3 other minor compressional events, trending 020-040, 080-090 and 100-110 affected the studied area.

RÉSUMÉ

Évolution tectonique de la marge sud-téthysienne dans le Sud-Tunisien.

La Tunisie méridionale est située sur la bordure nord de la plate-forme saharienne, au Sud du domaine plissé atlasique. Cette région est caractérisée par la présence de bassins sédimentaires fournissant d'excellentes conditions d'affleurement. La série stratigraphique est presque continue du Permien supérieur au Quaternaire et présente une fracturation dans tous les niveaux. Deux domaines distincts ont été étudiés : la plate-forme stable et le domaine pré-atlasique méridional. Une analyse détaillée de 354 sites a permis de reconstituer l'évolution tectonique de la Tunisie méridionale depuis le Permien supérieur en terme de tenseurs des paléo-contraintes (434 ont été calculés). Du Permien à l'Actuel l'évolution de la Tunisie méridionale présente la succession suivante d'événements tectoniques : a) du Permien supérieur au Trias, pendant l'éclatement de la Pangée les tectoniques distensives dominent ; b) du Carnien supérieur au Crétacé inférieur, la tectonique était caractérisée par une extension sub-méridienne liée à la divergence Afrique-Eurasie ; c) au Crétacé supérieur et au Paléogène, le contexte tectonique

BOUAZIZ, S., BARRIER, É., ANGELIER, J., TRICART, P. & TURKI, M.M., 1998.— Tectonic evolution of the Southern Tethyan margin in Southern Tunisia. *In*: S. CRASQUIN-SOLEAU & É. BARRIER (eds), Peri-Tethys Memoir 3: stratigraphy and evolution of Peri-Tethyan platforms. *Mém. Mus. natn. Hist. nat.*, **177** : 215-236. Paris ISBN : 2-85653-512-7.

Source : MNHN, Paris

reste distensif, mais les directions d'extension tournent plusieurs fois ; d) le Néogène est marqué par des événements compressifs résultant de la convergence Afrique-Eurasie. L'événement majeur est la compression NW-SE, dite "phase atlasique", d'âge tortonien. Au Plio-Quaternaire, trois autres phases mineures de compression, respectivement orientées 020-040, 080-090 et 100-110, ont été mises en évidence.

INTRODUCTION

In Southern Tunisia, the Saharan platform constitutes the northern part of the stable African plate (Fig. 1). During Mesozoic and Cenozoic times, this domain formed the southern Tethyan margin at the boundary between Western and Eastern Tethys. Because of this particular location, the tectonic evolution of the northern African margin in southern Tunisia has been successively governed since Late Permian by the break up of Pangea (AUBOUIN *et al.*, 1980), the opening of the East Mediterranean basin (BIJU-DUVAL *et al.*, 1976; DERCOURT *et al.*, 1993; RICOU, 1994), and the convergence between Eurasia and Africa (BOUSQUET, 1976; LETOUZEY & TREMOLIERES, 1980; PHILIP, 1987). From this long tectonic evolution results the present structural complexity of Southern Tunisia.

The tectonic evolution of the African margin in Tunisia is governed by inherited structures (DURAND-DELGA, 1981; BOUILLIN, 1986; TRICART *et al.*, 1994) reactivated during the Neogene and Quaternary compressional events. The northern part of the African plate is constituted from South to North by several domains (Fig. 1): the stable Saharan platform, the Atlasic folded domain, the Tellian nappes and the African basement only known in Kabylia. Southern Tunisia is a transition zone between the tabular domain and the South folded Atlasic belt.

In this paper, we present a reconstruction of the paleostress evolution from Late Permian to Present based on the analysis of brittle deformations. Paleostress analysis of brittle structures is a powerful tool to reconstruct the tectonic evolution of sedimentary basins. The investigated area is Southern Tunisia

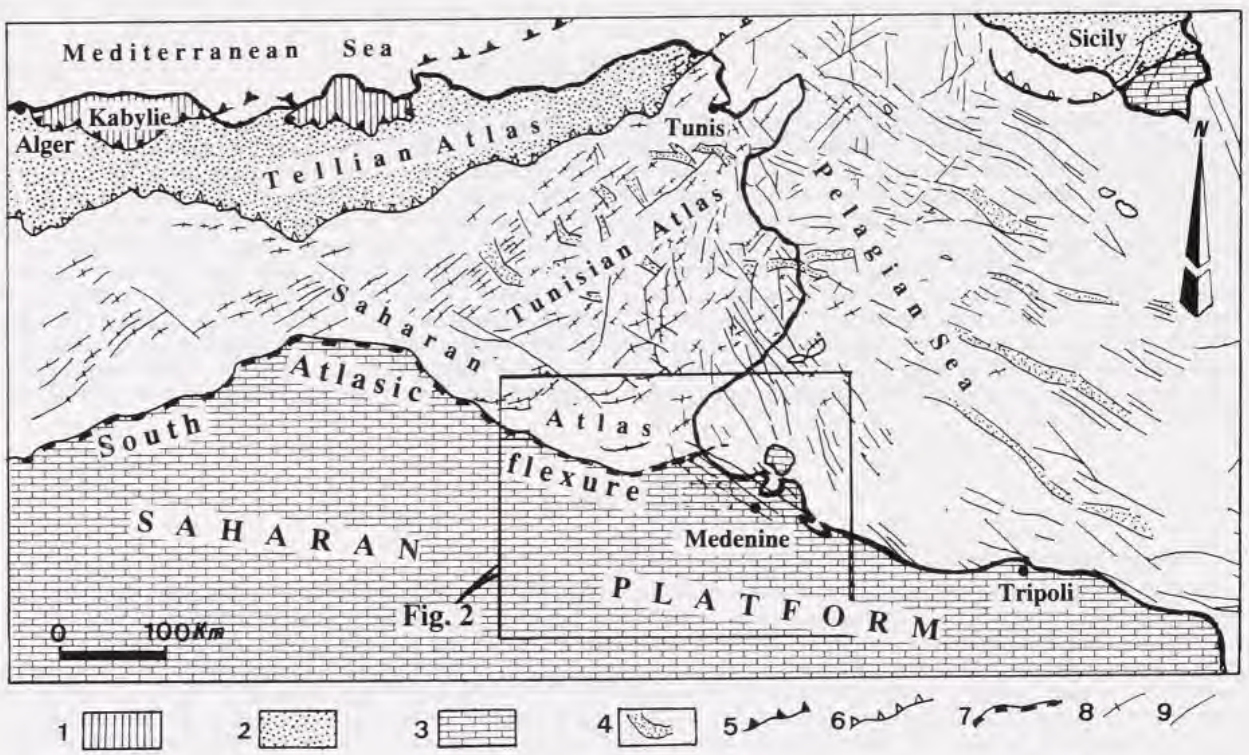

FIG. 1.— Location map and main tectonic features of the northern african margin. **1**, African basement; **2**, Tellian nappes; **3**, Saharan Platform; **4**, Late Miocene basins; **5**, Kabylian front; **6**, Tellian front; **7**, Saharan flexure; **8**, Folds; **9**, Faults Box: location of figure 2.

*FIG.1.— Localisation de la zone étudiée et principales structures tectoniques. **1**, socle ; **2**, nappes telliennes ; **3**, plate-forme saharienne ; bassins Miocène supérieur ; **5**, front des nappes kabiles ; **6**, front des nappes telliennes ; **7**, flexure sud-saharienne ; **8**, axes de plis ; **9**, principales failles. Encart : localisation de la figure 2.*

Source : MNHN, Paris

(Figs 1, 2) including (a) the stable Saharan platform, located South of the Chott Range and of the Gabes Gulf, and (b) the folded southern pre-Atlasic domain of the Chott and Gafsa ranges. The tectonic framework of these domains has been discussed by many authors in both Algeria (LAFFITE, 1939; CASTANY, 1954; AISSAOUI, 1984; VIALLY *et al.*, 1994) and Tunisia (ZARGOUNI, 1985; BOUKADI, 1994). Different interpretations are made on the significance and age of major structures. A new calendar of tectonic evolution is proposed where tectonic events are considered in term of stress. Several periods are considered following the main stress regimes and the geodynamical context. We precise the complex tectonic history resulting from this evolution. For each period, the results are discussed in the context of the geodynamical evolution of the Tethyan Ocean.

GEOLOGICAL SETTING: THE SOUTHERN TETHYAN MARGIN IN SOUTHERN TUNISIA

In Southern Tunisia, the North African margin contains two distinct domains: (a) the Dahar Plateau; a platform constituting the northern border of the stable Saharan platform, and (b) the folded southern Atlasic domain, often called " pre-Atlasic domain ", and constituting the deformed foreland of the Tellian Atlasic chain (Figs 1, 2). The synthetic stratigraphic section of these two domains consist of an almost complete sequence that ranges in age from Late Permian to Quaternary. In both domains, outcrop conditions are excellent, providing numerous good sites for brittle tectonic analysis.

THE STABLE PLATFORM: THE DAHAR PLATEAU

The Dahar Plateau is a gentle large scale monocline dipping southward of 1°-2° that may be considered as tabular at regional scale. The Dahar, belonging to the Saharan platform domain, is constituted by Late Paleozoic to Mesozoic sequences ranging in age from Late Permian to Late Cretaceous (Fig. 2a). These sequences constitute the southern Tunisian basin of BUSSON (1967). They are well exposed along continuous cliffs bordering the plateau to the North along the Jeffara coastal plain, whereas they are covered to the West and to the South by the dunes of the Eastern Saharan Erg.

The sequences consist mainly of carbonates where dolomitic facies dominate. However sandstone layers are also common. Three periods of sedimentation can be differentiated separated by two major unconformities, Carnian and Albian in age, related to regional tectonic events:

— the Late Permian to Late Triassic cycle is characterized by a high subsidence rate during Late Permian (BUSSON, 1969), then diminishing in Early-Middle Triassic when started the continental sedimentation marked by the deposition of sandstones and clays (BUSSON, 1967; BOUAZIZ *et al.*, 1987; MOCK *et al.*, 1987; KAMMOUN *et al.*, 1994). In the Triassic sequences, syn-depositional tectonics were responsible for local angular unconformities, abrupt thickness variations and facies changes that are frequently observed (BOUAZIZ, 1995). They affected the Early-Middle Triassic sandstones facies as well as the Late Triassic carbonate facies;

— the marine early Carnian transgression, which began the second cycle, covered the whole platform in Southern Tunisia and Western Libya above the Sidi Stout unconformity (BUSSON, 1967; MELLO & BOUAZIZ, 1987). The marine environment lasted during the entire Jurassic and Neocomian. Extensional faulting caused thick sedimentary accumulations in E-W trending basins (Tataouine and Chott basins). The Jurassic extension induced high rate subsidence in which thick evaporites were deposited during the Liassic. Sedimentation is contrasted between plateaus and basins (BOUAZIZ, 1986; BEN ISMAÏL *et al.*, 1989). In the first, carbonate facies dominate, whereas the second are characterized by a deeper environment. In Early Cretaceous a withdrawal of the marine domain began but marine conditions still prevailed;

— the second marine transgression that started in the Albian time (Vraconian). It expanded quickly during the Cenomanian before reaching its maximum in the Turonian time. Such transgression is also known in central Tunisia, in Algeria and in Libya (BUROLLET & BUSSON, 1983). The Late Cretaceous deposits are constituted of a 200 m to 300 m thick carbonate sequence that significantly increase in the Jeffara Coastal plain. Evidences of synsedimentary deformations (slumps, fault breccias, thickness and facies variations, local unconformities) are common within the Late Cretaceous series, particularly in the Cenomanian and in the Coniacian-Santonian deposits.

Source : MNHN, Paris

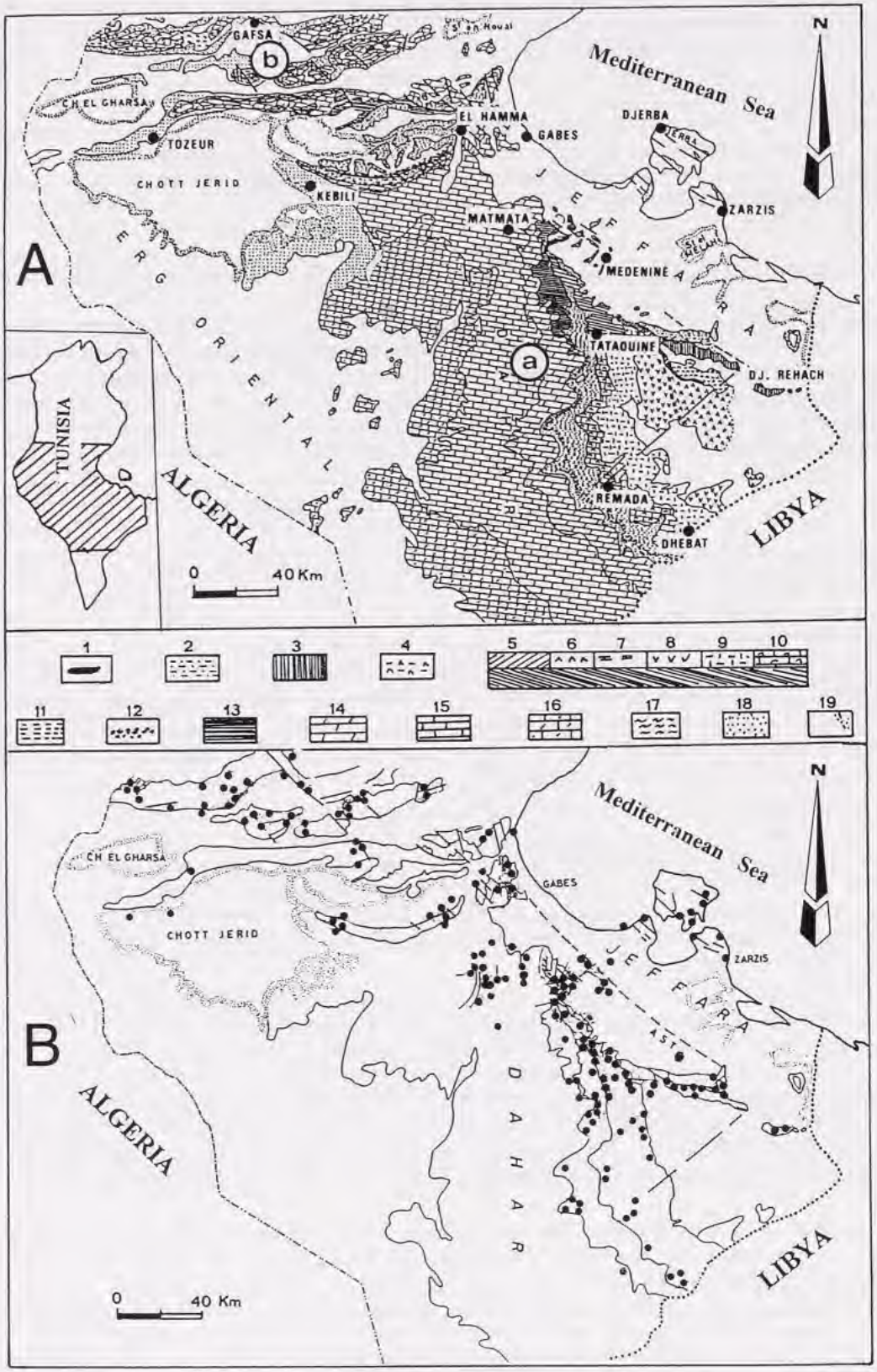

Source : MNHN, Paris

THE FOLDED DOMAIN: THE CHOTT AND GAFSA RANGES

This domain constitutes the folded foreland south of the Alpine chain (Fig. 1). In this area, far south of the allochtonous Tellian domain, the fold geometry is characterized by a succession of tight anticlines separated by large box synclines (Fig. 2a). The anticlines are large ramp-related folds of various types; i.e. fault-bend folds and fault-propagation folds (OUATTANI *et al.*, 1995). This folding is generally considered as resulting from tectonic inversions of inherited extensional structures during the Cenozoic compressional events (ZARGOUNI, 1985; BOUAZIZ, 1995). The pattern of previous faults probably causes the complex fold geometry observed in the Chott and Gafsa Ranges (Fig. 2a). In this region, E-W trending elongated folds predominate (Kebili Tebaga Djebel and El Asker Djebel in the Chott Range; Alima Djebel and Chemsi Djebel in the Gafsa Range). NE-SW to ENE-WSW trending folds are also common, but shorter (10 km to 30 km long) than the major E-W ones (60 km to 130 km long). In this area, there is no evidence for two superimposed fold-thrust events as described in Central Tunisia (SOYER & TRICART, 1989). In addition, NW-SE trending lineament, including the right lateral Gafsa fault system (ZARGOUNI, 1985), cuts the region from the Algerian border to the Gabes Gulf (Figs 1, 2). This complex domain is a key for understanding the Cenozoic tectonic evolution and complete the information obtained from the investigation of the Mesozoic sequences of the stable platform.

The South Atlasic domain in the studied area is characterized by a thick Cenozoic sequence, missing in the stable platform. These Cenozoic deposits conformably overly the Late Cretaceous sequence (M'RABET, 1981), mainly represented by carbonate facies ranging in age from Turonian to Maastrichtian. The most common Mesozoic facies is the Campano-Maastrichtian " Abiod Formation " (BUROLLET, 1956) forming the cores of the anticlines. The underlying Jurassic sequences, known from subsurface data, consist in epicontinental deposits (marls and marly-sandstones) more than 2000 m thick in the Chott basin where the Jurassic subsidence is maximum. Two distinct periods of sedimentation can be differentiated during the Cenozoic: Paleogene sedimentation remains marine, whereas during the Neogene continental basins developed. The Paleocene-Eocene sequence begins by Paleocene clays underlying the Ypresian Metlaoui formation represented by Carbonates and phosphate layers (SASSI, 1964). The Metlaoui formation reaches one hundred meters in the center of the basin. This sequence ends by late Eocene gypsum. In the studied area Oligocene is missing. The continental Mio-Pliocene molassic series rest unconformably over the pre-Neogene formations. They are characterized by a detritic sedimentation including sands, sandstone beds, conglomerates and clays. They include the Sehib, Beglia and Segui formations, respectively Aquitanian, Serravallian-Tortonian and Plio-Quaternary (BIELY *et al.*, 1972; MALLOULI *et al.*, 1987). The thickness of these series reachs several hundred of meters in the synclines where they are well preserved. The most recent formations are the sporadic " Villafranchian " (late Pliocene-early Pleistocene) crust (VAUFREY, 1932; COQUE, 1962; BEN OUEZDOU, 1994) and Late Quaternary river terrasses.

FIG. 2.— **A**: geological map of Southern Tunisia.
a, Dahar plateau - Stable Platform; **b**: South Atlasic belt; **1**, Permian; **2**, Early-Middle Triassic; **3**, Carnian; **4**, Carnian-Norian; **5**, Rhetian; **6**, Rhetian-Early Liassic; **7**, Pliensbachian; **8**, late Liassic; **9**, Bathonian-Bajocian; **10**, Callovian; **11**, Malm-Neocomian; **12**, Barremian; **13**, Aptian-Albian; **14**, Cenomanian-Turonian; **15**, Coniacian-Santonian; **16**, Campanian-Maastrichtian; **17**, Paleocene-Eocene; **18**, Mio-Pliocene; **19**, Quaternary.
B: Location of the sites of fault measurements. AST, South Tunisian Fault.

*FIG. 2.— **A** : carte géologique de la Tunisie méridionale.*
***a**, Plateau du Dahar, plate-forme stable ; **b**, chaîne sud-atlasique ; **1**, Permien ; **2**, Trias inférieur et moyen ; **3**, Carnien ; **4**, Carnien-Norien ; **5**, Rhétien ; **6**, Rhétien-Lias inférieur ; **7**, Pliensbachien ; **8**, Lias supérieur ; **9**, Bathonien-Bajocien ; **10**, Callovien ; **11**, Malm-Néocomien ; **12**, Barrémien ; **13**, Aptien-Albien ; **14**, Cénomanien-Turonien ; **15**, Coniacien-Santonien ; **16**, Campanien-Maastrichtien ; **17**, Paléocène-Eocène ; **18**, Mio-Pliocène ; **19**, Quaternaire.*
***B**: Localisation des sites étudiés. AST, faille sud-tunisienne.*

Source : MNHN, Paris

BRITTLE TECTONIC ANALYSIS

An extensive brittle tectonic analysis has been carried out in a total of 354 sites of the South Tunisian domain in order to reconstruct the stress pattern evolution since the end of Paleozoic. Location of sites are shown on figure 2b. Brittle tectonic analysis includes (a) analysis of fault-slip data sets, associated with paleostress tensor reconstructions, and (b) study of joint populations, more common than fault populations in the stable platform. These sites are distributed in all formations ranging in age from Late Permian to Pleistocene, except in the Late Triassic-Liassic gypsum. Site are located on the stable platform (72% of the sites), and on the folded Atlasic domain (28%). Some formations have been more extensively studied because either they are widespread in both domains, like the Late Cretaceous sequences (163 sites), or they are of particular interest like the Triassic deposits of the platform (41 sites) or the Paleogene sequences of the Gafsa basin (31 sites). The Jurassic formations of the platform, where joint populations are common, have been also studied in detail (72 sites), as well as the Miocene continental deposits (28 sites) that recorded the Cenozoic compressive events. The age of tectonic events was established based (a) on the age of rock formation affected, and (b) on the succession of tectonic features where deformation is polyphased.

Each site consists of several tens of tectonic features measured in a small area. They include mainly faults with slickenside lineations, but also bedding planes, tension gashes and fold axes. The method enables us to reconstruct the paleostress axes (maximum stress $\sigma1$, intermediate $\sigma2$ and minimum $\sigma3$) and the ratio $\Phi=\sigma2-\sigma3 / \sigma1-\sigma3$, between principal stress magnitudes, knowing the orientations and senses of slip on faults acting during the same tectonic event. The principles, conditions of application and limits of the methods have been described in detail by ANGELIER (1984, 1989, 1990). Many fault sets are practically monophase and reveal simple conjugate patterns of neo-formed faults. However, numerous sites, mainly located in the folded domain, display more complicated fault patterns including oblique and inherited fault slips or polyphase faulting. Particular attention was focused on these polyphase and superposed deformations resulting from different tectonic events, and on syndepositional faulting providing direct stratigraphic dating. Many sites are polyphased including fault populations resulting from distinct tectonic events. In the platform, where deformation rates are low, neoformed normal fault systems and joint sets are often reactivated during later compressive events as strike-slip faults or reverse faults and ramps. In the folded domain, where fault tectonic is more complex, we pay particular attention to distinguish pre and post-tilting (or folding) fault populations in order to reconstruct the chronology of faulting (and the paleostress evolution) with respect to the major deformation phases. In the whole studied area, 434 paleostress tensors have been determined in 247 sites (165 in the platform and 82 in the folded domain). The complete results of paleostress tensor determinations have been reported in BOUAZIZ (1995). Two types of paleostress tensors were distinguished: 44% of them correspond to strike-slip and compressional faulting ($\sigma1$ horizontal), and 56% to extensional faulting ($\sigma3$ horizontal and $\sigma1$ vertical).

Joints have been extensively analysed in terms of nature and orientation. 107 sites of joints have been analysed (92 in the platform and 15 in the folded domain). All type of joints have been observed (tension, hybrid and shear types). The most common are tension joints, that we correlated often with surrounding normal fault populations, or more occasionally with hybrid joints. In many case, we might recognize the mechanical significance of the different sets of joints and thus identify at least one of the three axis of paleostress. Relationships with fault populations show that most joint patterns are of tectonic significance. In this case, they are reliable indicators of paleostress orientation.

TECTONIC EVOLUTION OF THE NORTH AFRICAN MARGIN IN TUNISIA

The tectonic history of the Saharan platform in Southern Tunisia since Late Paleozoic is controlled by the regional geodynamical evolution characterized by 3 major periods: (a) the break up of Pangea during the Permo-Triassic; (b) the divergence between Africa and Laurasia, resulting from the opening of Tethys Ocean during the Late Triassic, Jurassic and Cretaceous times, and (c) the convergence

Source : MNHN, Paris

between Africa and Eurasia, starting at the end of Cretaceous and developing during the all Cenozoic, involving the closure of the Tethyan domain. Generally speaking, at the scale of the northern Gondwanian margin, then of the northern African margin, the tectonic evolution is marked by the inversions of basins mainly resulting from Mesozoic extensions.

THE BREAK UP OF PANGEA: THE PERMO-TRIASSIC RIFTING AND THE TRANSCURRENT MOVEMENTS

THE LATE PERMIAN RIFTING

During the early stage of break up of Pangea, extensional stress fields affected wide areas of Laurasia and Gondwana. They originated rift systems associated with high subsidence rates. In southern Tunisia, the Late Permian reef carbonates crops out in the Medenine Tebaga (Figs 2, 3) where 850 m of sequence is exposed (CHAOUACHI *et al.*, 1987; M'RABET *et al.*, 1987; RAZGALLAH *et al.*, 1989). They constitute the upper part of the 6000 meters thick sequence of the Jeffara basin (BAIRD, 1967; BUROLLET *et al.*, 1978) known from subsurface data (GLINTZBOECKEL & RABATE, 1964). Northward the facies changes from reef carbonates to more pelagic shaly deep sea deposits, whereas southward shallow water facies and alluvial deposits mark the southern boundary of the basin. Subsurface data show that the Late Permian Jeffara basin trends E-W to WNW-ESE. It ends abruptly westward where no Permian marine deposits have been reported. Its eastern extension in Libya and offshore is unknown. The reef carbonates of the bioherm complexes of the Medenine Tebaga are not a favorable facies for brittle tectonic analysis. Nevertheless, several sites have been investigated in interbedded sandstone layers (Fig. 3). Only one site of the Medenine Tebaga exhibits synsedimentary normal faults attesting for a Late Permian distension (Fig. 3, diagram 2). Because the poor quality of the fault population, it is not possible to determine accurately the Late Permian stress tensor. Joints are characterized by two sub-perpendicular major sets of pre-tilting joints trending roughly N-S and E-W (Fig. 3, diagrams a, 1 and 3). Minor set of NW-SE trending joints are also present. The geometry of joint sets pleads for tension joints resulting from a sub-meridian Late Permian extension. This assumption is supported by the same E-W general trend of the basin. Minor directions may be due to later jointing. These evidences document a fault-bounded subsiding basin, despite the major fault cannot be observed. In Arabia, the same age Palmyra rift is also characterized by a thick clastic sequence, Carboniferous to Triassic in age. RICOU (1994) suggests that the Permian extension corresponds to an aborted rift that precluded the East Mediterranean basin.

THE EARLY TO LATE TRIASSIC EXTENSIONS

We investigated the Early to Middle Triassic continental sequence, widespread in the cliff bordering the Dahar Plateau to the north (Figs 2a, 3). It is a 800 m thick sequence, mainly composed of sandstones, conglomerates and clays where crossbeddings and local unconformities are frequent (BUSSON, 1967; BOUAZIZ, 1986, 1995). A detailed analysis of joint and fault populations indicates that a extensional tectonic context predominated during this period. It is characterized by conjugate systems of syndepositional normal faults where slickenside lineations are rare due to the granulometry of the formations, and to the synsedimentary character of the normal faults. Only few sites allowed to determine paleostress tensor (Fig. 3, diagram 9). They indicate NW-SE to NNW-SSE extensions. In Djebel Rehach, ENE-WSW to NE-SW trending cartographic normal faults, associated with synsedimentary features are sealed by the early Carnian Mekraneb dolomites. Fractures are more common than faults in the continental Triassic facies. The study of joint populations corroborates the fault tectonic analysis. Two perpendicular sets of pre-tilting tension joints, trending NE-SW and NW-SE, have been measured, in relation with NW-SE and NE-SW extension (Fig. 3, diagrams b, c and 4 to 6). NE-SW trending normal fault populations and joint sets dominate. That may indicate that the NW-SE extension was the major tectonic event during this period, whereas the NE-SW one might be related to inversions between the main stress axes $\sigma 2$ and $\sigma 3$.

This Early-Late Triassic extension tectonic constitutes the last stage of the Permo-Triassic extensional period. In the Mediterranean area, this epoch corresponds to a rifting period. Triassic crustal extension is documented in the Mediterranean Tethys by the formation of deep water Triassic basins

Source : MNHN, Paris

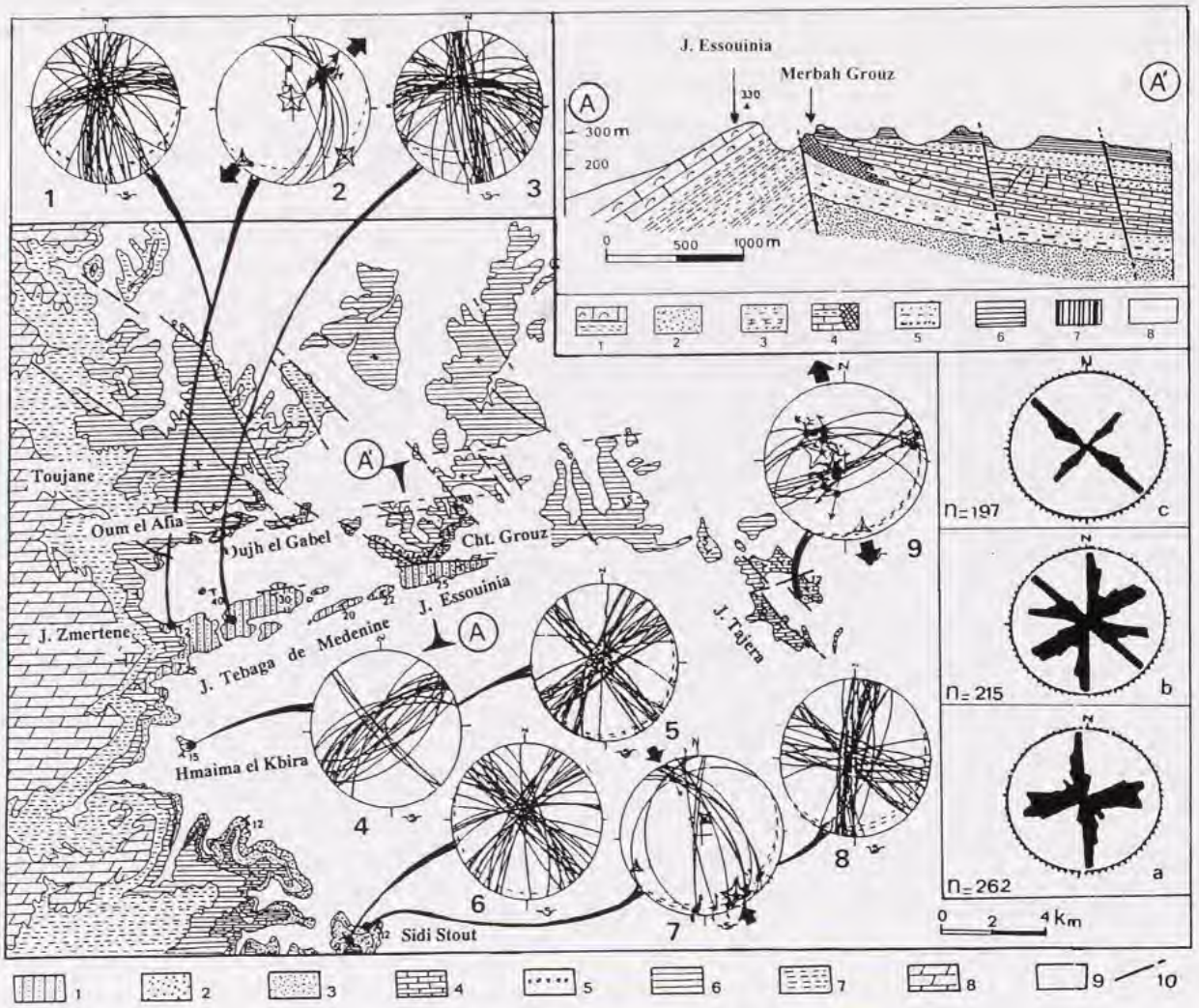

FIG. 3.— Geological map of the Jebel Tebaga of Medenine and main sites of fracture analyses.
1, Late Permian; **2**, Early-Middle Triassic; **3**, Late Triassic-Liassic; **4**, Bathonian pp.-Oxfordian; **5**, Barremian; **6**, Aptian-Vraconian; **7**, Cenomanian; **8**, Turonian; **9**, Neogene-Quaternary; **10**, Faults.
Schematic geological cross-section. **1**, Late Permian; **2**, Undifferenciated Permian; **3**, Bathonian pp.; **4**, Bathonian pp.-Oxfordian; **5**, Barremian; **6**, Aptian; **7**, Vraconian; **8**, Quaternary.
Rose diagrams; **a**, in Late Permian; **b**, in Early-Middle Triassic; **c**, in Late Triassic; n=Number of joints. Fault diagrams: Schmidt's projection, lower hemisphere, fault planes as continuous lines, and slickenside lineations as dots with arrows (convergent for reverse slips, divergent for normal slip, double for strike-slip), bedding planes as dashed lines, main axes of paleostress as stars (5, 4 and 3-branches for $\sigma 1$, $\sigma 2$ and $\sigma 3$), main directions of extension and compression as large black arrows. Upper left corner: sites in the Late Permian sequence, other diagrams in Triassic formations.

FIG. 3.— Carte géologique du Jebel Tebaga de Médenine et localisation des principaux sites analysés.
***1**, Permien supérieur ; **2**, Trias moyen-inférieur ; **3**, Trias supérieur-Lias ; **4**, Bathonien pp.-Oxfordien ; **5**, Barrémien ; **6**, Aptien-Vraconien ; **7**, Cénomanien ; **8**, Turonien ; **9**, Néogène-Quaternaire ; **10**, failles.*
*Coupes géologiques schématiques. **1**, Permien supérieur ; **2**, Permien indifférencié ; **3**, Bathonien pp. ; **4**, Bathonien pp.-Oxfordien ; **5**, Barrémien ; **6**, Aptien ; **7**, Vraconien ; **8**, Quaternaire.*
*Diagrammes de fréquence des directions de joints ; **a**, dans le Permien supérieur ; **b**, dans le Trias inférieur-moyen ; **c**, dans le Trias supérieur ; n=nombre de joints. Diagrammes de failles : projections de Schmidt hémisphère inférieur ; lignes continues : plans de failles ; points avec des flèches: stries de glissement (convergentes : failles inverses, divergentes : failles normales, doubles flèches : décrochements) ; tiretés : plans de pendage ; axes principaux des paléocontraintes : étoiles (5, 4 et 3-branches pour $\sigma 1$, $\sigma 2$ and $\sigma 3$), flèches noires : directions principales d'extension et de compression. Encart en haut à gauche : sites permiens (les autres diagrammes sont dans les formations triassiques).*

Source : MNHN, Paris

which formed at the expenses of former epicontinental platforms: in Algeria, Triassic extension induced synsedimentary normal faulting bounding zones of high rate subsidence in which thick saliferous series were deposited (BUSSON, 1970; BOUDJEMA, 1987); in Libya, a Middle-Late Triassic rifting produced horsts and grabens, and a crustal thinning in the Ionian Sea (DEL BEN & FINETTI, 1980). These extensions are generally associated to the Permo-Triassic rifting of Western Pangea (RICOU *et al.*, 1986; STAMPFLI *et al.*, 1991).

THE LATE CARNIAN TRANSCURRENT MOVEMENTS

The N-S regional Sidi Stout unconformity marks a major Late Triassic tectonic event. The late Carnian Rehach dolomites rest unconformably over the whole Late Permian to Middle Carnian sequence. The transgressive sequence overlies unconformably the Late Permian in the area of Djebel Tebaga of Medenine, the only large scale structure of the Dahar (MATHIEU, 1949; BUSSON, 1967; BOUAZIZ, 1986), where the unconformity reachs 30°. Southward, the angle of the unconformity appreciably decreases and the Rehach dolomites are almost concordant with the middle Carnian deposits. This tilting is related to a folding in relationship with a shear zone, roughly trending E-W, that can be locally observed in the vicinity of the Djebel Tebaga. Study of pre-tilting fault populations in Late Permian to late Carnian formations shows a N 150°E trending compression recorded in the Early Triassic sandstone layers (Fig. 3, diagram 7). In same site, two pre-tilting joint sets (Fig. 3, diagram 8), trending N-S and 130-140, are probably conjugate sets of shear joints, linked to the same compression. This Carnian folding is related to a large E-W right lateral strike-slip fault zone, known from seismic profiles, that extends eastward offshore. It may be also connected westward with the long fault zone bordering the Saharan platform. This shear zone may be part of the dextral transcurrent faults that separated Gondwana and Laurasia which led north-western Africa to shift away from central Europe. In Maghreb, this fault zone is also documented from field data in the Tizi-n-Test in Morocco (MATTAUER *et al.*, 1977) and is continuous on the other side of Atlantic (RICOU, 1992).

THE AFRICA-EURASIA DIVERGENCE: THE MESOZOIC EXTENSIONS

In the stable platform in southern Tunisia, from late Carnian to Late Cretaceous only extensional tectonics have been evidenced. From a geodynamical point of view, this period corresponds to the opening phases of Tethys and Central Atlantic and to the divergence between Gondwana and Laurasia, and then between Africa and Eurasia. Two main tectonic periods are distinguished, separated by a low angle regional unconformity, early Albian in age.

THE LATE CARNIAN TO EARLY APTIAN N-S EXTENSION

According to our data, the deformations were exclusively extensional between late Carnian and early Aptian. A submeridian extension dominated in the whole platform during this period. In Jurassic time, the sedimentation was clearly controlled by 090 to 110 trending normal faults. Two main zones of subsidence, the Foum Tataouine and Chott basins, separated by ridges, were bounded by major normal faults. The consequences are the important variations in facies and thickness in the Jurassic formations, especially during Liassic time. Figure 4 shows the main Jurassic normal faults of the Tataouine basins sealed by the post-Aptian sequences. Diagrams illustrate the 090 to 110 trending conjugate normal fault systems related to this extension. In the Jurassic, these fault systems are common and often associated with synsedimentary features. Joint pattern illustrates also the Jurassic extension as shown in BARRIER *et al.* (1993), BOUAZIZ *et al.* (1994) and BOUAZIZ (1995). More than 40 sites of joints have been studied in the Jurassic layers of the stable platform. Part of this population is composed of two sub-perpendicular sets: a main set, roughly trending 110, frequently formed first, and a minor set trending 020. Most of this joints are sub-vertical tension joints. In summary, between late Carnian and Aptian, the tectonic is controlled by a major 000-020 extensional trend expressed by normal fault populations and joint sets. From South to North, the tectonic instability increases from the stable platform to the subsident troughs of the Chott basin.

In this period an extensional context have been described in Algeria (ELMI, 1977; BUREAU, 1984; VIALLY *et al.*, 1994) and in Central Tunisia during Early Cretaceous (SOYER & TRICART, 1989). In

Source : MNHN, Paris

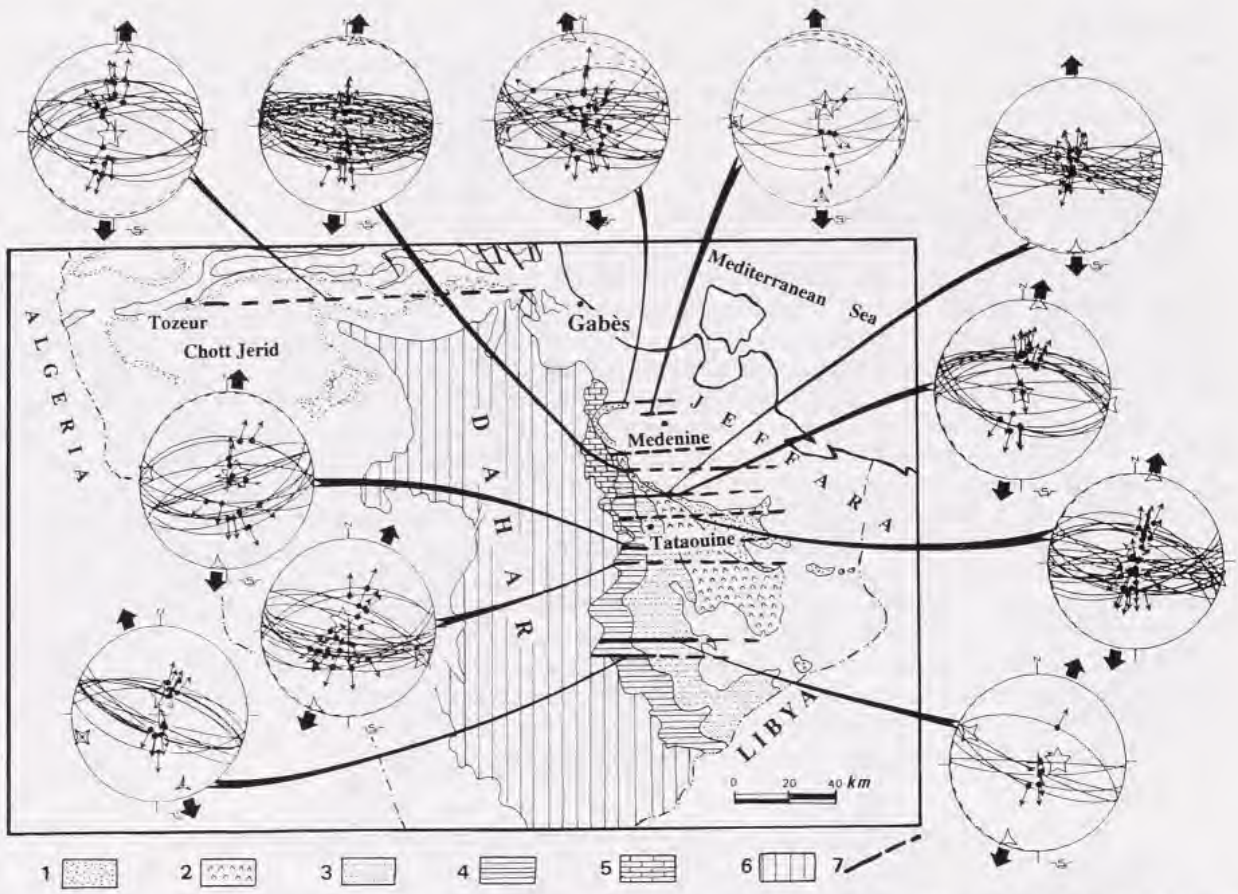

FIG. 4.— Late Triassic to Lower Cretaceous sub-meridian extension in Southern Tunisia. **1**, Late Permian-Triassic; **2**, Liassic; **3**, Dogger; **4**, Malm-Early Cretaceous; **5**, Vraconian; **6**, Late Cretaceous; **7**, Faults. Diagrams, same than in figure 3.

*FIG. 4.— Extension sub-méridienne Trias supérieur-Crétacé inférieur en Tunisia méridionale. **1**, Permien supérieur-Trias ; **2**, Lias ; **3**, Dogger ; **4**, Malm-Crétacé inférieur ; **5**, Vraconien ; **6**, Crétacé supérieur ; 7, failles. Diagrammes, même légende que figure 3.*

Central Tunisia, the Jurassic basins are characterized by platform deposits controlled by normal faults (TURKI, 1985; TOUATI, 1985; BEN AYED, 1986; SOUSSI, 1990). In the Tunisian Sahel, ELLOUZ (1984) and BEN AYED (1986) mentioned the same extensional context associated with lava flows. In Libya, an important rifting phase occured in Middle Jurassic time accompanied by magmatic activity (DEL BEN & FINETTI, 1980). In Morocco, a syntectonic sedimentation has been described (ROBILLARD, 1979; SEUFERT, 1988). Normal faults trending NE-SW, active during Jurassic, have been described in Atlas (MATTAUER *et al.*, 1977; LAVILLE, 1981). They have been related to the opening of the central Atlantic responsible for the Maghreb transform zone along which strike-slip displacements and transtensional opening occurred. An extension tectonic event affected the entire present North African margin. The regional sub-meridian extensional context, lasting from late Carnian to Aptian, has been considered by several authors as resulting from a rifting (BUREAU, 1984; TURKI, 1985; SOYER & TRICART, 1989; ALOUANI *et al.*, 1992). More than a simple rifting, we may consider this general extension along the central-western northern African margin as resulting from the evolution of the whole southern Tethyan margin in response to the Africa-Eurasia divergence.

THE LATE CRETACEOUS AND PALEOGENE EXTENSIONS

With the Albian transgression began a sedimentary cycle lasting until the end of Cretaceous in the platform and until late Eocene in the pre-Atlasic domain. Broadly speaking, during this period the

Source : MNHN, Paris

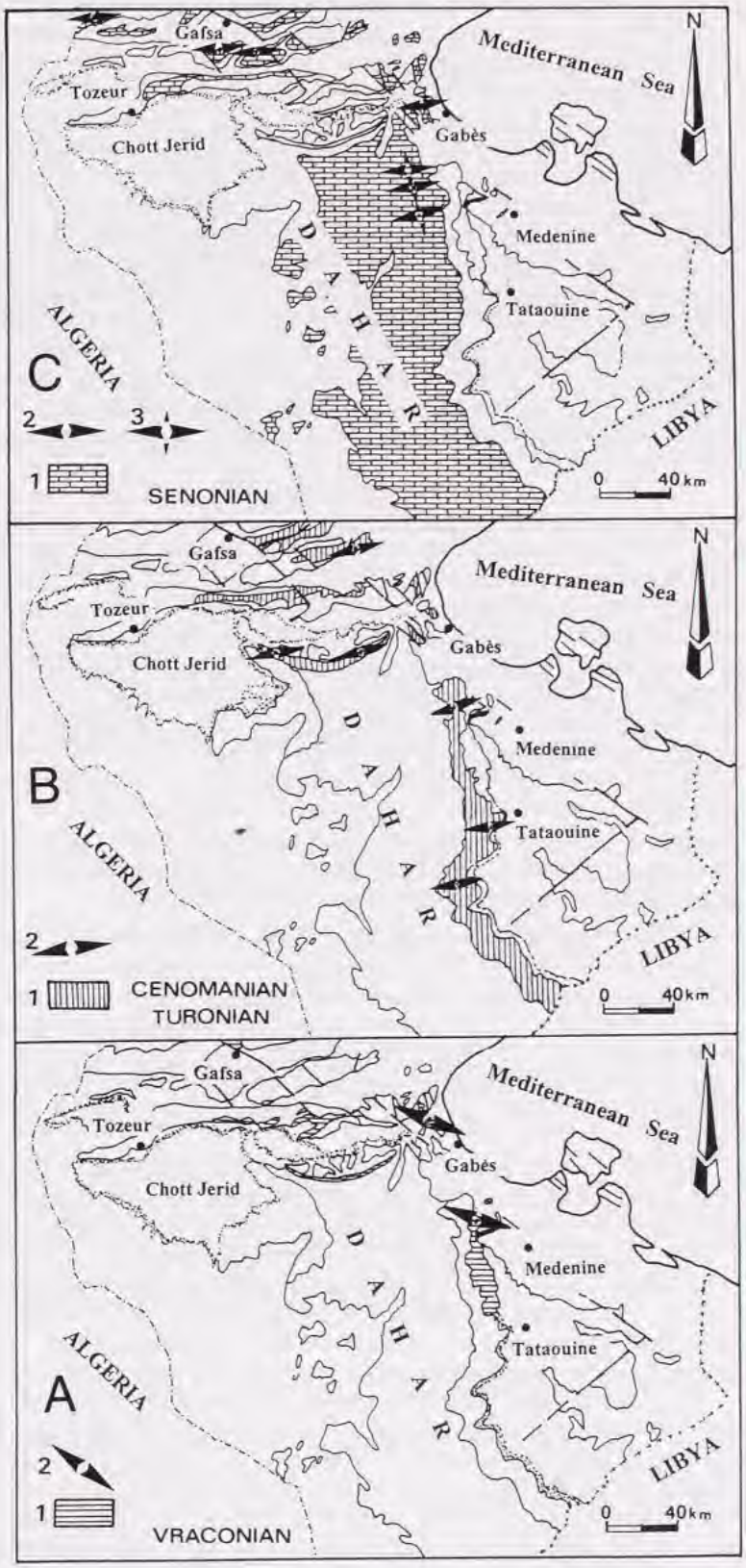

FIG. 5.— Late Cretaceous paleostress evolution in Southern Tunisia.
A, during Vraconian; **1**, Vraconian oucrops; **2**, N140 extension; **B**, during Cenomanian-Turonian; **1**, Cenomanian-Turonian outcrops; **2**, N070 extension; **C**, during Senonian; **1**, Senonian outcrops; **2**, N080 extension; **3**, multidirectional extension.

FIG. 5.— Évolution des paléocontraintes au Crétacé supérieur en Tunisie méridionale.
***A**, au Vraconien ; **1**, affleurements vraconiens ; **2**, extension N140 ; **B**, au Cénomanien-Turonien ; **1**, affleurements cénomano-turoniens ; **2**, extension N070 ; **C**, au Sénonien ; **1**, afleurements sénoniens ; **2**, extension N080 ; **3**, extension multidirectionelle.*

Source : MNHN, Paris

tectonic context remains extensional, but the directions of extension did not remain stable and rotated several times. The main stages of this period are illustrated on figure 5. The first stage is the extension that developed during the Vraconian time (Fig. 5a). In the platform, the Vraconian carbonates are cut by 025-060 normal faults in relationship with a WNW-ESE trending extension. These normal faults are associated with joints and sedimentary dykes of same direction. Above the Vraconian-Albian deposits, the Cenomanian sequence exhibits clear syndepositional features along NNW-SSE trending normal faults. They consists in tilted blocks above decollement layers, intraformational breccias and slumps. In all the sites, scattered from the Gafsa Range in the North, to the platform in the South, the directions of extension computed from fault-slip data sets are homogeneous in a ENE-WSW direction (Fig. 5b). The Cenomanian faulting of southern Tunisia may be compared with the extensional structures of the same age known eastward in the syrt basin and in the eastern Libyan basin. We think that this important regional extensional event is related to the rifting that started in the African plate during the Early Cretaceous that separated the African plate in three large blocks (GUIRAUD & MAURIN, 1991). In Cenomanian, the Tunisian basin, like the Syrt basin, may be considered as the northern extension of the trans-Saharian basins. According to this interpretation, they should be considered as the consequence of the general kinematics reorganization linked with the opening of the south Atlantic Ocean (OLIVET *et al.*, 1984; RICOU, 1994).

Above the Turonian Gattar carbonate bar, the Coniacian layers display also remarkable synsedimentary extensional features, well preserved in the Matmata area (BOUAZIZ, 1986; BARRIER *et al.*, 1993). The fault tectonic analysis show that the tectonic regime corresponds to a multidirectional extension with the main directions trending ENE-WSW and NNW-SSE. The ENE-WSW direction is related to the subsidence of the NW-SE elongated Jeffara basin which started during the Late Cretaceous (ELLOUZ, 1984; BOLTENHAGEN, 1981). Intra-Cretaceous extensions tectonics have been described in the Chott Range (ABDELJAOUED & ZARGOUNI, 1981; LOUHAICHI & TLIG, 1993) and in Central Tunisia (RABHI, 1987). Such a similar extension is known in Central Tunisia where NW-SE ridges and basins are considered as large scale tilted blocks along 3 major normal faults (BOLTENHAGEN, 1981; BISMUTH *et al.*, 1982). In Algeria, compressive deformations have been described in the North as early as the end of Jurassic (OBERT, 1981). They seem to lead to an Albian paroxysmal phase. These compressions are restricted to the Tellian domain and no trace is visible in southern Tunisia. These deformations are though to be related to large transcurrent faults accommodating the eastward shift of Africa during the opening of Atlantic, whereas eastward in Cyrenaica, the Coniacian compressive event (RÖHLICH, 1980) is probably related to the Syrian arc system tectonic.

In the Campanian-Maastrichtian time the directions of extension rotated again from ENE-WSW to roughly E-W (Fig. 5c). This extension is documented from conjugate normal fault systems that cut the Campanian carbonates of the platform and the Abiod Formation in the folded domain. Isopach maps of Abiod Formation in Sahel and Gabes Gulf indicate a similar NW-SE to WNW-ESE orientation of the basins (ELLOUZ, 1984). The deformations decrease southward in the platform where deposits are shallow water carbonates. Northwestward, in Sahel and in the Gabes Gulf, the main Campanian-Maastrichtian structural directions are NW-SE (HALLER, 1983; ELLOUZ, 1984; OUALI, 1984; KADRI, 1988).

In Cretaceous, boundary conditions have significantly changed since the Jurassic. The two former continental masses to the south of Tethys are now separated into four second order plates: (1) America, Africa, India and Australia-Antartica, and (2) Africa was disrupted into three blocks in the Early Cretaceous (GUIRAUD & MAURIN, 1991). Geological observations on the Alpine chains from the Alps to southeastern Asia show the systematic migration of continental blocks from the southern to the northern side of Tethys and the associated asymmetry of this part of Tethys bounded by passive margins to the south and active margin to the north. The westernmost block is the Apulian block separated from Africa probably during the Cretaceous in relation with the opening of the East Mediterranean basin.

In Tunisia, the Mesozoic-Cenozoic boundary does not mark any major tectonic change, while compressive deformations began earlier in the northern Tethyan margin in front of Apulia considered as active since the end of Early Cretaceous. In southern Tunisia, during Paleocene the subsidence migrated northward to the Gafsa basin whereas the stable platform remains emerged until present. In this basin, no regional unconformity separates the Paleocene deposits from the underlying Late Cretaceous sequences. Only local unconformities, due to tiltings of blocks have been observed. They are probably related to the extension tectonic documented from NE-SW normal faults (Fig. 6) and from populations of normal shear joints. Offshore, the same directions appear in the Paleogene isopachs drawn from

Source : MNHN, Paris

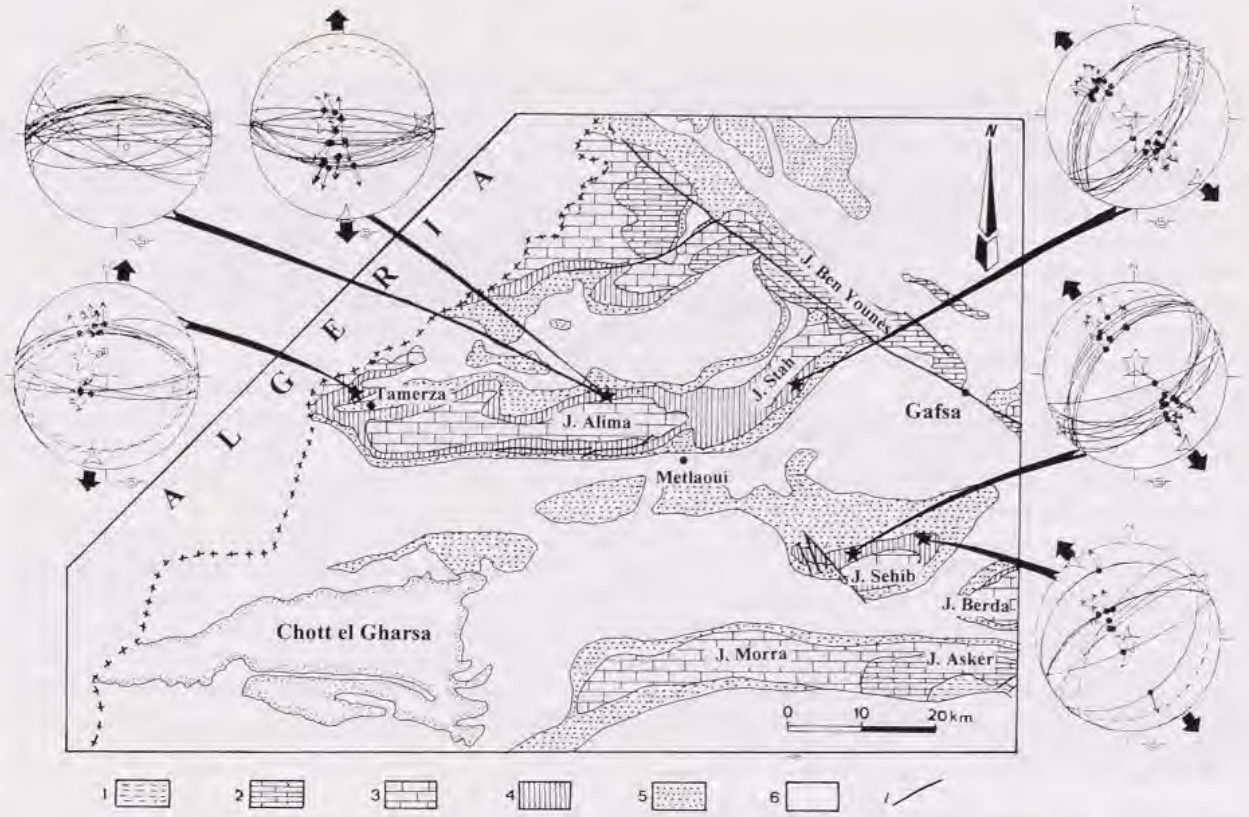

FIG. 6.— Paleocene-Eocene extensions in the Gafsa Range. **1**, Early Cretaceous; **2**, Aptian-Albian; **3**, Campanian-Maastrichtian; **4**, Paleocene-Eocene; **5**, Mio-Pliocene; **6**, Plio-Quaternary; **7**, Faults. Diagrams, same than figure 3.

*FIG. 6.— Extensions Paléocène-Eocène dans la chaîne de Gafsa. **1**, Crétacé inférieur ; **2**, Aptien-Albien ; **3**, Campanien-Maastrichtien ; **4**, Paléocène- ; **5**, Mio-Pliocène ; **6**, Plio-Quaternaire ; **7**, failles. Diagrammes, même légende que figure 3.*

geophysical data (ELLOUZ, 1984). In Central Tunisia, YAÏCH (1984) describes similar pre-Eocene normal faults, and in Northwestern Tunisia ZAIER (1984) mentioned that the sedimentation was controlled by NW-SE trending ridges and basins. In the overlying Paleocene-Eocene phosphate layers of the Metlaoui formation syndepositional tectonic features are commonly observed. They are synsedimentary normal faults trending 040-060, in relationship with a NW-SE extension. This tectonic explains the local unconformities observed inside the Metlaoui Formation. A rotation of the $\sigma 3$ directions from NW-SE to N-S occured during Ypresian time after the deposition of the phosphate layers. Above these layers, the tectonic pattern is characterized by roughly E-W trending normal faults. Figure 6 shows the paleostress reconstructions in 2 sites of the late Eocene formations of Djebel Alima illustrating this sub-meridian extension that probably frame the Eocene basin.

THE AFRICA-EURASIA CONVERGENCE: THE CENOZOIC COMPRESSIONS

The convergence between Africa and Eurasia began in Late Cretaceous. During the Late Cretaceous and Cenozoic closing phases of Tethys, compressions prevailed on the Peri-Tethyan platform where they gave rise to intra-plate deformations such as inversion of Mesozoic basins, or wrench faulting. The timing of such large-scale deformations is diachronic between the northern and southern margin of the Tethyan Ocean. They started in Late Cretaceous in the European margin whereas the first recorded compressive event is only late Eocene in age in the African platform.

Source : MNHN, Paris

THE LATE EOCENE DEFORMATIONS: THE ALGERIAN "ATLASIC PHASE"

The Algerian " Atlasic phase ", middle to late Eocene, had a major incidence on the entire Alpine domain (PETIT, 1976; MATTAUER *et al.*, 1977, BOUILLIN, 1986). In Algeria, it is the major tectonic event responsible for the 030-040 trending folds. In southern Tunisia, this event is poorly documented and the main compressional tectonic event is late Miocene, in relation with the Tellian nappe tectonics. In southern Tunisia, and more particularly in the Gafsa range, the Miocene continental deposits unconformably overly the whole Late Cretaceous to late Eocene sequence. The angle of this regional unconformity never exceeds few degrees. In consequence, it is very difficult to identify from fault tectonic analysis, the pre and post-unconformity fault populations, excepted in the case of synsedimentary tectonics. It should be possible to distinguish a pre-unconformity compression only if one particular direction of compression, missing in the post-unconformity deposits, exists beneath the unconformity. It is not the case in the studied area, and all the reconstructed directions of compression exist in formations located both below and above the unconformity. So, field analysis of fault-slip data sets does not allowed to identify an eventual late Eocene compressive event. Nevertheless, this regional late Eocene unconformity pleads for a late Eocene tectonic event. The associated deformations were probably low and restricted to large scale flexures probably due to reactivation of former faults. Compressive structures of this age have been described in Central Tunisia (KHESSIBI, 1978; HALLER, 1983), and in northern Tunisia (BISHOP, 1975; BEDIR, 1985; TOUATI, 1985; BEN AYED, 1986). We may point out that if this late Eocene compressional tectonic existed, the trend of the compression was necessarily either very close or similar to the trend of the later Neogene compressions because it does not appear only in the pre-unconformity formations. In southern Tunisia, the compressive late Eocene deformations are likely the weak effects of the Atlas folding that marks a new convergent boundary between stable Africa and Moroccan and Oran Mesetas during this period (LAFFITE, 1939; CAIRE, 1957; POLVÊCHE, 1959; GUIRAUD, 1973; OBERT, 1981).

THE MAJOR COMPRESSIONAL PHASE: THE ATLASIC PHASE

With the deposition of the Miocene continental formations started a new cycle of sedimentation marked by the erosion of the flexures related to the late Eocene tectonics. The brittle tectonic analysis of these continental formations, mainly composed of sandstones and clays, shows that succeeded during Neogene and Quaternary: (a) a period of subsidence originating the thick sequences of the Mio-Pliocene basins, and (b) several compressive events resulting in various types of deformations.

The oldest brittle structures recorded in the Mio-Pliocene formations are NW-SE trending normal faults populations. Most of them have been reactivated as right lateral strike-slip faults during the later tectonic events. The Gafsa fault, active during the late Pleistocene, is probably one of these former major normal faults (Fig. 7). This episode of faulting is generally neglected in the Neogene tectonic reconstruction, generally focused on the compressive events. The thickness of the Mio-Pliocene sequence (more than 600 m) as well as its variations of thickness indicate that during this period develop subsiding basins. Basins of same age and same orientation have been described in northern Tunisia (ROUVIER, 1977), associated with NW-SE trending synsedimentary normal faults (PHILIP *et al.*, 1986). In the Jeffara plain, this distension is still active, as observed in Djerba Island (BOUAZIZ, 1986; 1995), and in the Libyan Jeffara (KEBEASY, 1980). These basins are probably of the same origin than the NW-SE trending Pelagian basins which developed later in Neogene time. It is clear that in the studied area this distensive event is older than the major phase of folding.

Following this extensional period, came the deformations resulting in the folding of the platform in the pre-Atlasic domain. The brittle tectonic analysis of the pre-Atlasic domain allowed us to reconstruct the stress pattern evolution of the compressive events. We identify five groups of directions of $\sigma 1$ in the pre-Atlasic domain: NW-SE, 150 to 180, 020-040, 080 to E-W and 100-110 (Figs 7, 8). The two first directions are the most frequently measured. They are generally sub-perpendicular to the fold axes and their directions reflect the geometry of folds (Fig. 7). They may be considered as related to the major phase(s) of deformation. When criteria of relative chronology exist, the oldest compression is the NW-SE event which occurred generally before folding when the pre-Atlasic domain was still a platform. Nevertheless, some sites indicate post-tilting NW-SE compressions as well, showing that it is not only a

Source : MNHN, Paris

pre-folding event. This compression has been recorded both in the stable platform and in the south Atlasic domain. The so called " Atlasic phase " is very regular in both domains as illustrated by the rose diagram of figure 8.

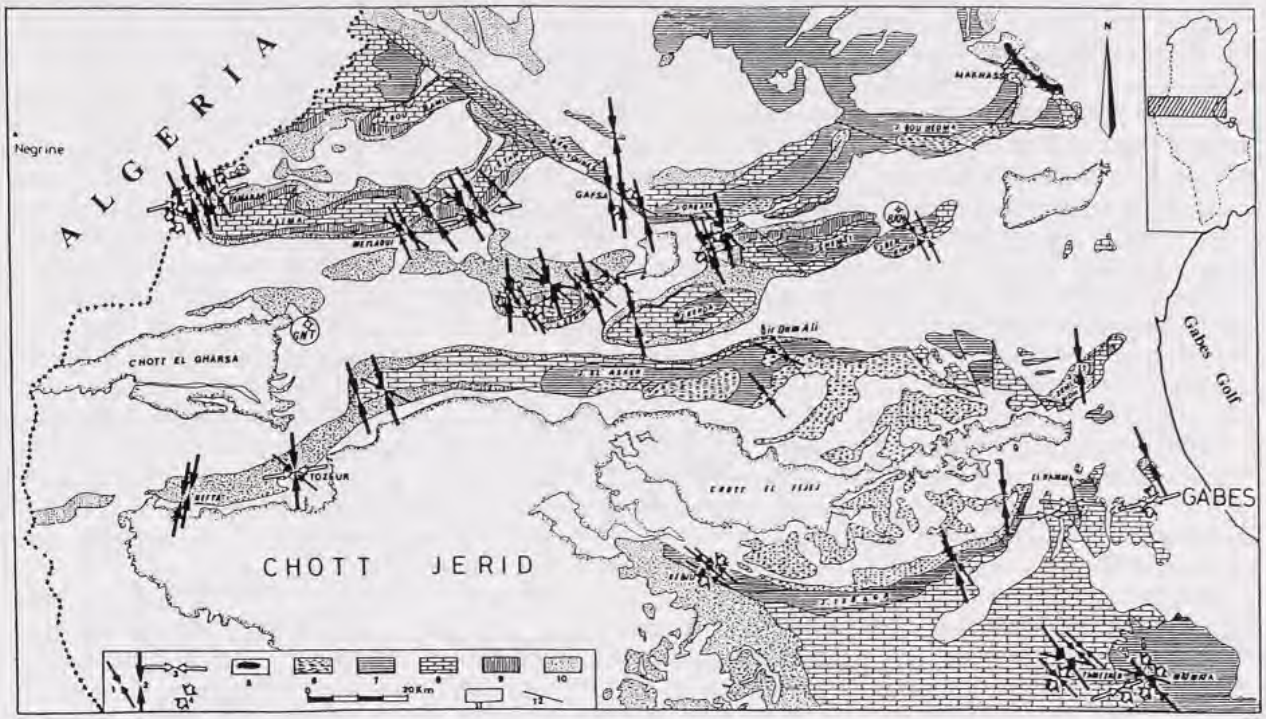

FIG. 7.— Miocene to Quaternary compressions in the South Atlasic domain and relationship between the fold belt and the compressional axis.
1, NW-SE compression; **2**, N-S compression; **3**, E-W compression; **4**, NE-SW compression; **5**, Triassic; **6**, Early Cretaceous; **7**, Aptian-Albian; **8**, Senonian; **9**, Paleocene-Eocene; **10**, Mio-Pliocene; **11**, Quaternary; **12**, Faults.

FIG. 7.— Compressions miocène à quaternaire dans le domaine sud-atlasique et relations entre les plis et les directions de compressions.
***1**, Compression NW-SE ; **2**, Compression N-S ; **3**, Compression E-W ; **4**, Compression NE-SW ; **5**, Trias ; **6**, Crétacé inférieur ; **7**, Aptien-Albien ; **8**, Sénonien ; **9**, Paléocène-Eocène ; **10**, Mio-Pliocène ; **11**, Quaternaire ; **12**, failles.*

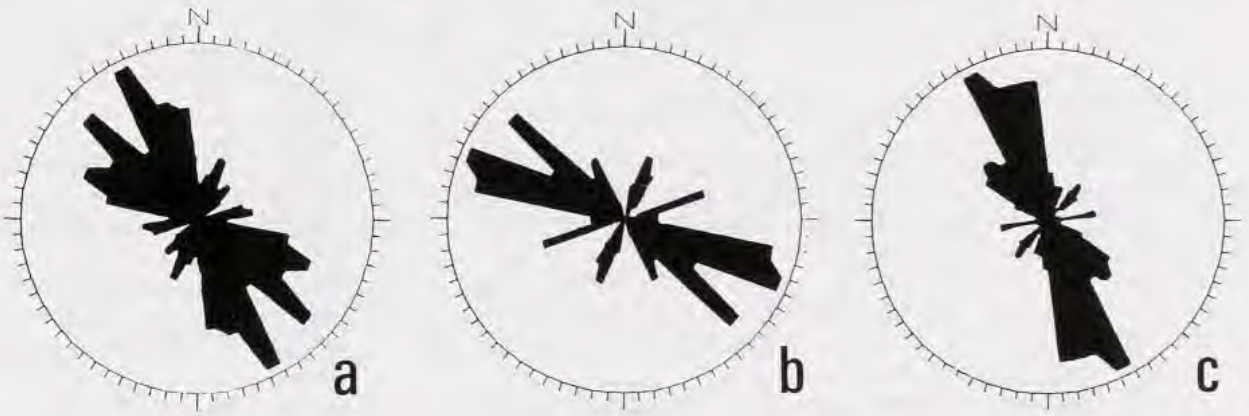

FIG. 8.— Compressions in southern Tunisia. Rose diagrams of $\sigma 1$ directions computed from fault population analysis. **a**, in the whole studied area including the stable platform and the pre-Atlasic folded domain (144 stress tensors); **b**, in the stable platform (60 stress tensors); **c**, in the Southern pre-Atlasic folded domain (84 stress tensors).

*FIG. 8.— Compressions en Tunisie méridionale. Diagrammes de fréquence des directions de $\sigma 1$ calculées à partir de l'analyse des populations de failles. **a**, dans l'ensemble de la région étudiée (plate-forme stable et domaine plissé pré-atlasique (144 tenseurs) ; **b**, dans la plate-forme stable (60 tenseurs) ; **c**, dans le domaine plissé pré-atlasique (84 tenseurs).*

Source : MNHN, Paris

The second direction of compression trends 150-180 (Figs 7, 8). It is particularly well developed in the folded domain. On the contrary, it is completely missing in the stable platform. The peak of σ1 directions for this sub-meridian extension is wider than the peak of the NW-SE compression (Fig. 8). These σ1 directions are almost systematically subperpendicular to the strike of the fold where the site of measure is located. It is illustrated on figure 7 where both NW-SE and NNW-SSE to N-S compressions are shown. This N-S event is often considered as a major event in southern Tunisia. Nevertheless, its lack in the stable platform, whereas the NW-SE compression is well printed, may indicate that a large part of the 150-180 directions of compression reflect more the trends of the fold axes than a major sub-meridian regional event. It should mean that the major event, responsible of folding in the southern pre-Atlasic domain, should be only the NW-SE compression that generated both NE-SW and E-W trending folds. This geometry may be easily explained by reactivation of former normal faults. The structural expression of the compression relates to the geometry of the former structures (dip and trend of the former normal faults) in relation to stress orientation have been modelized by LETOUZEY (1990). In southern Tunisia where the compression trends obliquely (NW-SE) to the strike of the basin and of the former major normal faults (E-W) shortening was accommodated by both NE-SW folds and reactivation of E-W trending Jurassic normal faults. This hypothesis accounts for (a) the wide peak of σ1 directions that may reflect the bending of the ranges, and (b) the lack of submeridian compressions in the platform (Fig. 8). Despite that the major E-W folding does not result probably from a major sub-meridian compressional event, such a Quaternary compression undoubtedly exits. It results in the right lateral displacement along the Gafsa fault system which cuts and displaced the folds. This N-S compression appears on figure 7 around the city of Gafsa where roughly trending N-S σ1 directions have been determined from analysis of fault populations in Quaternary conglomerates (Fig. 7). It originates from the relatively slow (1cm / y) N-S convergence between Africa and Eurasia.

In Central Tunisia, the major event is known to be Tortonian (BLONDEL, 1991) where the folded Segui formation, Messinian to Villafranchian in age, overlies unconformably the Aquitanian-Tortonian continental sequence. In the studied domain, such a geometry has not been observed and no unconformity exists between the Segui formation and the underlying Neogene continental formation as well as inside the Segui formation. It results that the age of the major deformation phase is at least subsequent to the beginning of the deposition of the Segui formation and probably post-Tortonian. So, in southern Tunisia, the age of the main NW-SE trending event appears to be more recent than in Northern and Central Tunisia where the major deformation phases are respectively dated of Langhian (ROUVIER, 1977) and Tortonian (BLONDEL, 1991), as far as the stratigraphy of the Late Cenozoic continental sequence is well known. This Late Tertiary tectonic is more a consequence of the north dipping subduction associated with back-arc opening and the migrations of the western Mediterranean blocks than the low convergence rate between Africa and Eurasia (TRICARD *et al.*, 1994). The separation of Corsica and Sardinia from Eurasia initiated in the Late Oligocene and the front of the block collided with the African margin in the middle Miocene, generating the Tellian Atlas.

THE MINOR NEOGENE-QUATERNARY COMPRESSIONS

Three other compressional events trending 020-040, ENE-WSW to E-W, and 100-110 affected the studied area (Figs 7, 8, 9). All of them have been observed in the Pliocene-Quaternary formations. In both the stable platform and the folded domain, there are never associated with large deformations such as folds or kilometric strike-slip faults.

The ENE-WSW to E-W compression has been determined in both the platform and the folded domain. In the pre-Atlasic area, the associated fault populations are post-folding conjugate strike-slip faults. In the Gabes area, strike-slip faults related to this event cut the karst filling of Matmata loams, indicating at least a middle Pleistocene age.

The 020-040 compression is expressed by populations of strike-slip or reverse conjugate faults. It has been observed in the whole investigated area. In the folded domain, (a) this compression has been observed in the Pliocene to Pleistocene Segui formation, and (b) two axes of the reconstructed paleostress tensors are included in the bedding plane, suggesting a pre-folding event. As the age of the folding is not clearly defined in this area within the late Miocene to Pleistocene period, a large uncertainly exists on the age of this compression.

The last compressive event, trending 100-110, has been only observed in the platform (Fig. 8), essentially in formations ranging in age from Triassic to Senonian. The trends of σ1 related to this event

Source : MNHN, Paris

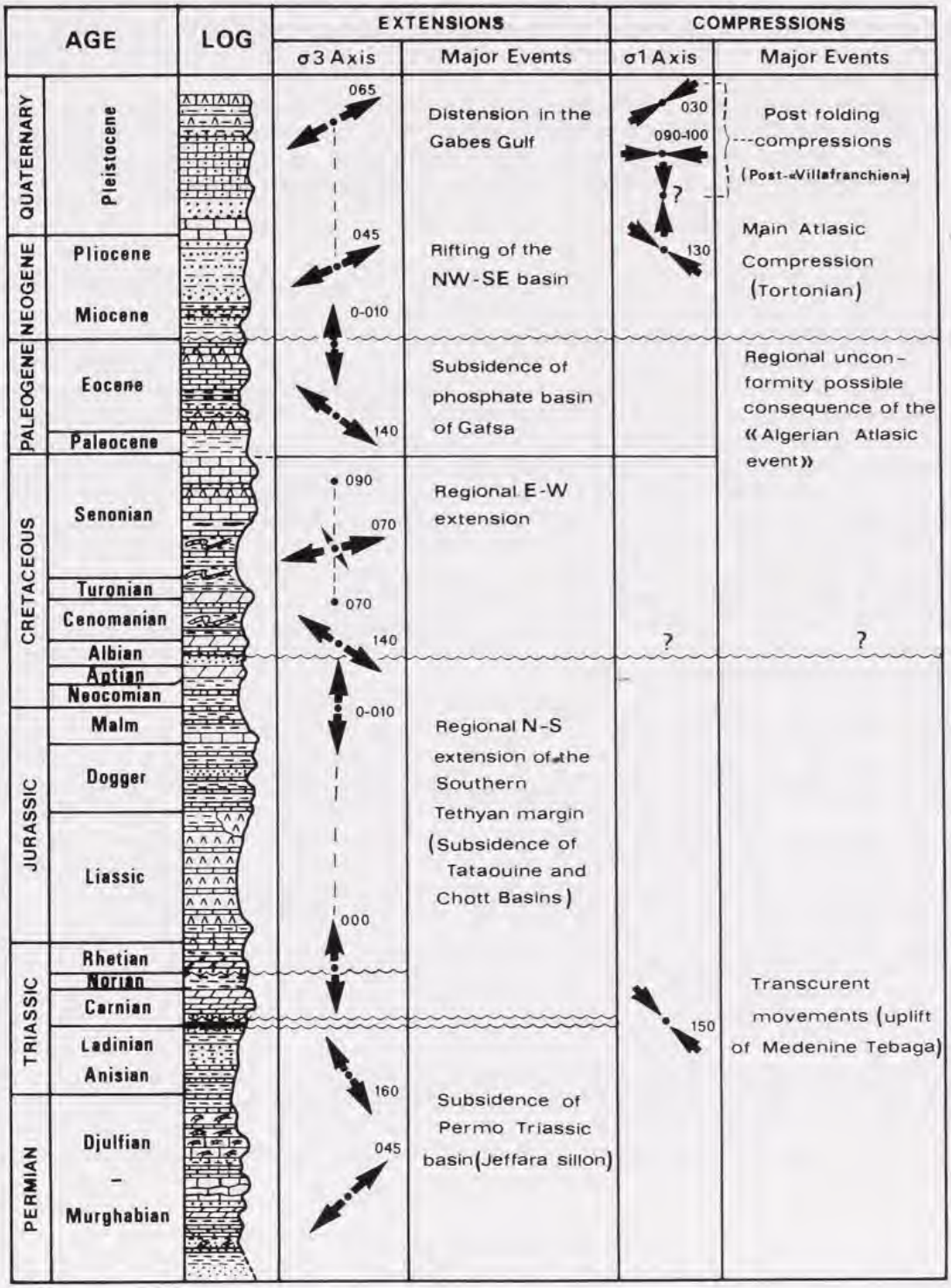

FIG. 9.— Tectonic calendar of Southern Tunisia since Late Permian showing the main tectonic events in term of stress directions.

FIG. 9.— Calendrier tectonique de la Tunisie méridionale depuis le Permien supérieur présentant les principaux événements tectoniques en terme de direction de paléocontraintes.

Source : MNHN, Paris

are very regular over the whole studied area of the platform. The faults populations associated to this event are generally conjugate systems of strike-slip faults. The age of this event is probably Neogene or Quaternary because this directions have been also computed from fault populations measured in the Mio-Pliocene marine clays of the Jerba area.

Despite these minor compressions are difficult to assign to a major tectonic event, their large distribution in the whole investigated area demonstrates that their are not due to local stress fields but rather to regional events. In addition, they have been described in the Plio-Pleistocene formations of the northernmost African platform in the Ragusa plateau of southern Sicily (BARRIER, 1992).

CONCLUSION : EVOLUTION OF THE AFRICAN MARGIN IN SOUTHERN TUNISIA

The tectonic calendar shown on figure 9 summarizes the main tectonic events that occurred in Southern Tunisia since Late Permian. This reconstruction in term of stress direction allows to precise the regional geodynamical evolution in Tethyan context. During the Mesozoic-Cenozoic, Tunisia occupied a remarkable position between the Eastern and Western Tethys. Soon in the Permian time before the break up of Pangea, Southern Tunisia marked the westernmost extension of the Permian rifting prefiguring the opening between Gondwana and Laurasia. After the Pangea break up, and during Late Triassic to Early Cretaceous, the tectonic evolution of this area was mainly driven by the opening of the East Mediterranean basin associated with the north drift of the Apulian block, whereas in the Maghreb West of Tunisia, developed a transform margin accommodating the rotation between Europe and Africa associated with the opening of Central Atlantic. So, the southern Tethyan margin in Tunisia marked during Jurassic the boundary between two tethyan domains: the Atlantic Tethys to the West, characterized by transcurrent movements, and the westernmost part of Eastern Tethys to the East, characterized by diverging boundaries (RICOU, 1994). All the following tectonic history of this region is controlled by this particular configuration.

In Cretaceous time, East of Tunisia the tethyan margin was a passive margin whereas the convergence developed far North along the southern Eurasian margin at the front of the Apulian block. This explains why during Cretaceous E-W to NE-SW extensions dominated and why the compressions were scarce. In the same period, West of Tunisia, no major active boundary are known and the Mesozoic plate pattern West of Apulia was governed by a single plate boundary located North of Iberia. This tectonic pattern lasted until Eocene when collisions developed along the Southern Tethyan margin forming the Alpine system in North Africa in response to the jump of the Africa-Eurasia boundary, from North to South of Iberia. The first compressive movements recorded in southern Tunisia are late Eocene. They are the echoes of the Algerian " Atlasic folding ", well documented in Algeria.

In Neogene, after a Miocene NW-SE extension, still active in the Jeffara plain, the major compressional event occurred between late Miocene and Quaternary, resulting from the collision of minor blocks migrating southeastward from Eurasia. Since this period, the slow convergence between Africa and Eurasia appears to be consumed in Western Mediterranean by intra-plate deformations generating large earthquakes, whereas in Eastern Mediterranean they are consumed in subduction zones. The Late Quaternary activity of the Gafsa fault probably results from this process. Such a paleostress reconstruction based on the analysis of many sites provides accurate constraints in geodynamic reconstructions. This type of study, extended at the scale of the North African margin, may lead to a better knowledge of the tectonic evolution of the southern tethyan margin from Morocco to Egypt since Mesozoic.

REFERENCES

ABDELJAOUED, & ZARGOUNI, F., 1981.— Mise en évidence d'une tectonique intra-crétacé dans le secteur de Zemlet el Bigha (Chaîne des Chotts). *1er Congrès national des Sciences de la Terre, Tunis*: 285-290.

AÏSSAOUI, D., 1984.— *Les structures liées à l'accident Sud-atlasique entre Biskra et le Jebel Manndra, Algérie, évolution géométrique et cinématique*. Thèse 3ème cycle, Université Louis Pasteur, Strasbourg, France: 1-205.

AOUANI, R., RAIS, J., GAYA, S. & TLIG, S., 1992.— Les structures en décrochement au Jurassique de la Tunisie du Nord: témoins d'une marge transformante entre Afrique et Europe. *Comptes Rendus de l'Académie des Sciences, Paris*, **315** (II): 717-724.

Source : MNHN, Paris

ANGELIER, J., 1984.— Tectonic analysis of fault slip data sets. *Journal of Geophysical Research*, **89** (B7): 5835-5848.

ANGELIER, J., 1989.— From orientation to magnitudes in paleostress determinations using fault slip data. *Journal of Structural Geology*, **11** (1/2): 37-50.

ANGELIER, J., 1990.— Tectonique cassante et néotectonique. *Annales de la Société géologique de Belgique*, **112** (2): 283-307.

AUBOUIN, J., DEBELMAS, J. & LATREILLE, M. (eds), 1980.— Géologie des chaînes alpines issues de la Téthys. *In*: 26ème Congrès international de Géologie, Paris, 1980, Colloque C5. *Mémoires du Bureau de Recherches géologiques et Minières*, **115**: 1-354.

BAIRD, D.W., 1967.— The Permo-Carboniferous of Southern Tunisia. *In*: *Guidebook to the Geology and History of Tunisia. Petroleum Exploration Society of Libya, Tripoli, 9th Annual Field Conference*: 85-107.

BARRIER, É., 1992.— Tectonic analysis of a flexed foreland: the Ragusa Platform. *Tectonophysics*, **206**: 91-111.

BARRIER, É., BOUAZIZ, S., ANGELIER, J., CREUZOT, J., OUALI, J. & TRICART, P., 1993.— Paleo-stress evolution in the saharian platform (Southern Tunisia). *Geodynamica Acta*, **6** (1): 39-57.

BEDIR, M., 1985.— *Dynamique des bassins sédimentaires cénozoïques du Sahel de Mahdia d'après les données de surface et de subsurface: séismostratigraphie, évolution tectonique et sédimentologique*. Mémoire de D.E.A., Faculté des Sciences de Tunis, Tunis, Tunisie.

BEN AYED, N., 1986.— *Evolution tectonique de l'avant pays de la chaîne alpine de Tunisie du début du Mésozoïque à l'Actuel*. Thèse de Doctorat d'État, Université Paris Sud, Orsay, France: 1-328.

BEN ISMAIL, H., BOUAZIZ, S., ALMARAS, Y., CLAVEL, B., DONZE, P., ENAY, R., GHANMI, M. & TINTANT, H., 1989.— Nouvelles données biostratigraphiques sur le Callovien et les faciès "Purbecko-wealdien" (Oxfordien à Vraconien) dans la région de Tataouine (Sud-tunisien). *Bulletin de la Société géologique de France*, **8, V** (2): 353-360.

BEN OUEZDOU, H., 1994.— *La partie méridionale des steppes tunisiennes. Étude géomorphologique*. Thèse de Doctorat d'État en Géographie physique, Faculté des Sciences humaines et sociales de Tunis, Université de Tunis I, Tunis, Tunisie: 1-577.

BIJU-DUVAL, B., DERCOURT, J. & LE PICHON, X., 1976.— From the Tethys ocean to the Mediterranean sea: a plate tectonic model of the evolutional of the western alpine system. *In*: *International Symposium of the structural history of the Mediterranean basins, Split*. Paris, Technip: 143-164.

BIELY, A, RAKUS, M., ROBINSON, P. & SALAJ, J., 1972.— Essai de corrélation des formations miocènes au sud de la dorsale tunisienne. *Notes du Service géologique de Tunisie*, **38** (7): 73-93.

BISHOP, W.F., 1975.— Geology of Tunisia and adjacent parts of Algeria and Libya. *American Association of Petroleum Geologists, Bulletin*, **59** (3): 413-450.

BISMUTH, H., BOLTENHAGEN, C., DONZE, P., LE FEVRE, J. & SAINT-MARC, P., 1982.— Étude sédimentologique et biostratigraphique du Crétacé moyen et supérieur du Djebel Semmama (Tunisie du centre Nord). *Cretaceous Research*, **3** (1-2): 171-185.

BLONDEL, T., 1991.— *Les séries à tendance transgressive marine du Miocène inférieur à moyen de Tunisie centrale*. Thèse, Université de Genève, Genève, Suisse: 1-409.

BOLTENHAGEN, C., 1981.— Paléogéographie du Crétacé moyen de la Tunisie centrale. *1er Congrès national des Sciences de la Terre, Tunis, 1981*, **1**: 97-114.

BOUAZIZ, S., 1986.— *La déformation dans la plate-forme du Sud Tunisien (Dahar-Jeffara): approche multiscalaire et pluridisciplinaire*. Thèse 3ème cycle, Faculté des Sciences de Tunis, Tunis, Tunisie: 1-180.

BOUAZIZ, S., 1995.— *Etude de la tectonique cassante dans la plate-forme et l'Atlas saharien (Tunisie méridionale): évolution des paléochamps de contraintes et implications géodynamique*. Thèse d'État, Université de Tunis, Tunis, Tunisie: 1-485.

BOUAZIZ, S., MELLO, J. & DOUBINGER, J., 1987.— Les argiles et évaporites de Mhira: nouvelles formations d'âge carnien supérieur-norien de la Djeffara (Tunisie méridionale), analyse palynologique. *Notes du Service géologique national de Tunisie*, **54**: 25-40.

BOUAZIZ, S., BARRIER, É., ANGELIER, J. & TURKI, M.M., 1994.— Paleostress in the Southern Tunisian Platform. *In*: F. ROURE (ed.), *Peri-Tethyan Platforms: Proceeding of the IFP Peri-Tethys Research Conference held in Arles, France, March 23, 1993*. Paris, Technip: 179-196.

BOUDJEMA, A., 1987.— *Evaluation du bassin pétrolier "triasique" du Sahara nord-oriental (Algérie)*. Thèse, Université Paris IX, Paris, France: 1-289.

BOUILLIN, J.P., 1986.— Le "bassin maghrébin" : une ancienne limite entre l'Europe et l'Afrique à l'ouest des Alpes. *Bulletin de la Société géologique de France*, **8, II** (4): 547-558.

BOUKADI, N., 1994.— *Structuration de l'Atlas de Tunisie: signification géométrique et cinématique des nœuds et des zones d'interférences structurales au contact de grands couloirs tectoniques*. Thèse d'État, Faculté des Sciences de Tunis, Université de Tunis II, Tunis, Tunisie: 1-249.

BOUSQUET, J.C., 1976.— Contribution à l'étude de la tectonique récente en Méditerranée occidentale: les données de la néotectonique dans l'arc de Gibraltar et dans l'arc Tyrrhénien. *In*: *International Symposium on the structural history of the Mediterranean basins, Split*. Technip, Paris: 199-214.

Source : MNHN, Paris

BUREAU, D., 1984.— Une interprétation possible du sillon saharien à partir de ses affleurements septentrionaux (Est des Monts du Hodna et Aurès, Algérie): l'extension passive de la croûte continentale. *Comptes Rendus de l'Académie des Sciences, Paris*, **229** (II): 8.

BUROLLET, P. F., 1956.— Contribution à l'étude stratigraphique de la Tunisie centrale. *Annales des Mines et Géologie*, **18**: 1-345.

BUROLLET, P.F., MUGNIOT, J.M. & SWEENEY, P., 1978.— The geology of the Pelagian block: the margins and basins off southern Tunisia and Tripolitania. *In*: NAIRN *et al.* (eds), *The Ocean Basins and Margins*. Vol. 4: *The Western Mediterranean*. New-York, Plenum Press: 331-359.

BUROLLET, P.F. & BUSSON, G., 1983.— Plate-forme saharienne et Mésogée au cours du Crétacé. *Notes et Mémoires de la Compagnie française des Pétroles*, **18**: 17-26.

BUSSON, G., 1967.— Le Mésozoïque saharien. 1ère partie: l'extrême Sud tunisien. *Editions du C.N.R.S. Série géologique*, **8**: 1-194.

BUSSON, G., 1969.— Rapports entre terrains Mésozoïques et Paléozoïques au Sahara algéro-tunisien: la discordance hercynienne. *Comptes Rendus de l'Académie des Sciences, Paris*, **269** (D): 685-688.

BUSSON, G., 1970.— Esquisses paléogéographiques du Sahara algéro-tunisien depuis le Salifère principal (Trias Lias) jusqu'à la fin du Crétacé. *Comptes Rendus Sommaires des Séances de la Société géologique de France*, **5**: 1-142.

CAIRE, A., 1957.— Etude géologique de la région de Biban (Algérie). *Publication du Service de la Carte géologique d'Algérie, nouvelle série*, **6**: 1-492.

CASTANY, G., 1954.— L'accident Sud tunisien, son âge et ses relations avec l'accident Sud atlasique d'Algérie. *Bulletin de la Société française de Physique*, **182**: 1-184.

CHAOUCHI, M.C., M'RABET, A. & RAZAGALLAH, S., 1987.— Calcite and aragonite early cements in the upper Permien Reefs and associated limestones of Jebel Tebaga of Medenine. Southern Tunisia. *In*: *8th IAS Meeting, Tunis*, Abtracts: 143-144.

COQUE, R., 1962.— *La Tunisie présaharienne, étude géomorphologique*. Thèse, Université de Paris, Paris, France: 1-476.

DEL BEN, A. & FINETTI, I., 1980.— Geophysical study of the Sirt rise. *The Geology of Libya*, **3**: 2417-2431.

DERCOURT, J., RICOU, L.E. & VRIELYNCK, B., 1993.— *Atlas Tethys Paleoenvironmental Maps*. Gauthier Villars, Paris: 1-307.

DURAND-DELGA, M., 1981.— Ouvertures océaniques de la Méditerranée occidentale et dislocation des chaînes alpines. *In*: F.C. WEZEL (ed.), *Sedimentary Basins of Mediterranean Margins, C.N.R. Italian Project of Oceanography*. Tecnoprint, Bologna: 417-431.

ELLOUZ, N., 1984.— *Etude de la subsidence de la Tunisie atlasique, orientale et de la Mer Pélagienne*. Thèse 3ème cycle, Université Paris VI, Paris, France, **84-29**: 1-139.

ELMI, S., 1977.— Polarité tectonosédimentaire pendant l'effritement des marges septentrionales du bâti africain au cours du Mézoïque (Maghreb). *Annales de la Société géologique du Nord*, **97**: 315-323.

GLINTZBOECKEL, C. & RABATE, J., 1964.— *Microfaunes et microfaciès du Permo-Carbonifères du Sud-tunisien* E.J. BRILL, Leide, **45**: 1-108.

GUIRAUD, R., 1973.— *Evolution post-triasique de l'avant pays de la chaîne alpine en Algérie d'après l'étude du bassin du Hodna et des régions voisines*. Thèse, Université de Nice, Nice, France: 1-265.

GUIRAUD, R & MAURIN, J.C., 1991.— Le rifting en Afrique au Crétacé inférieur: synthèse structurale, mise en évidence de deux étapes dans la génèse des bassins, relations avec les ouvertures océaniques péri-africaine. *Bulletin de la Société géologique de France*, **162**: 811-823.

HALLER, P., 1983.— *Structure profonde du Sahel tunisien. Interprétation géodynamique*. Thèse, Faculté des Sciences et Techniques, Université de Franche-Comté, Besançon, France, **42**: 1-162.

KADRI, A., 1988.— *Evolution tectonosédimentaire (Aptien-Quaternaire) des jebels Koumine, Hamra et Lessouda (Tunisie centrale)*. Thèse de 3ème cycle, Université Paris-Sud, Orsay, France: 1-221.

KAMMOUN, F., PEYBERNES, B., MONTACER, M., BEN YOUSSEF, M., TRIGUI, A. & GHANMI M., 1994.— Application des concepts de la stratigraphie séquentielle aux séries triasiques du Sud de la Tunisie. Nouvelles données stratigraphiques et micropaléontologiques. *In*: *ETAP, 4ème Journées Exploration Pétrolière en Tunisie*: 213-233.

KEBEASY, R.M., 1980.— Seismicity and seismotectonics of Lybia. *The Geology of Libya*, **3**: 955-963.

KHESSIBI, M., 1978.— *Etude géologique du secteur Maknassy-Mezzouna*. Thèse, Université de Lyon, Lyon, France.

LAFFITE, R., 1939.— Les plissements post-nummulitiques dans l'Atlas saharien. *Bulletin de la Société géologique de France*, **5, 9** (1-3): 135-159.

LAVILLE, E., 1981.— Rôle des décrochements dans le mécanisme de formation des bassins d'effondrement du Haut Atlas marocain au cours des temps triasique et liasique. *Bulletin de la Société géologique de France*, **7, 23** (3): 303-312.

LETOUZEY, J., 1990.— Fault reactivation, inversion and fold and thrust belt. *In*: *Petroleum and tectonics in mobile belts*. Paris, Technip: 101-128.

LETOUZEY, J. & TREMOLIERES, P., 1980.— Paleo-stress fields around the Mediterranean since the Mesozoic from micro-tectonics. Comparison with plate tectonic data. *Rock Mechanics*, **suppl. 9**: 173-192.

LOUHAICHI, M. A. & TLIG, S., 1993.— Tectonique synsédimentaire des séries crétacées post-barrémiennes au Nord-Est de la chaîne des Chotts (Tunisie méridionale). *Géologie Méditerranéenne*, **20** (1): 53-74.

Source : MNHN, Paris

MALLOULI, N., CREUZOT, G. & GERAADS, D., 1987.— Un nouveau gisement de Vertébrés dans le Néogène de Tunisie Centrale. *Comptes Rendus de l'Académie des Sciences, Paris*, **305** (2): 1121-1124.

MATHIEU, G., 1949.— Contribution à l'étude des Monts Troglodytes dans l'Extrême Sud-tunisien. *Annales des Mines et de la Géologie, Tunis*, **4**: 1-82.

MATTAUER, M., TAPPONNIER, R. & PROUST, F., 1977.— Sur les mécanismes de formation des chaînes intracontinentales: l'exemple des chaînes atlasiques du Maroc. *Bulletin de la Société géologique de France*, **7, 19** (3): 521-526.

MELLO, J. & BOUAZIZ, S., 1987.— Mise en évidence de la discordance de Sidi Stout dans la province centrale du Sud Tunisien et de son terme transgressif: Dolomie de Messaoudi (Rhétien). *Notes du Service géologique de Tunisie*, **45**: 41-54.

MOCK, R., MELLO J., BIELY, A. & BOUAZIZ, S., 1987.— Microfaune cordevolienne (Carnien inférieur) de la base du Trias carbonaté du Sud tunisien (J. Rehach). *Notes du Service géologique de Tunisie*, **55**: 19-29.

M'RABET, A., 1981.— *Stratigraphie, sédimentation et diagénèse carbonatée des séries du Crétacé inférieur de Tunisie centrale*. Thèse, Université Paris-Sud, Orsay, France: 1-540.

M'RABET, A., CHAOUACHI, M. C., RAZGALLAH, S. & DUVERNOY, B., 1987.— The Upper Permian carbonate and siliciclastic series of Jebel Tebaga (Southern Tunisia): an example of platform to slope sedementation. *8th IAS Regional Meeting of sedimentology, Tunis*, Abstracts: 262-263.

OBERT, D., 1981.— *Etude géologique des Babors orientaux (Domaine tellien, Algérie)*. Thèse Doctorat ès-Sciences, Université Pierre et Marie Curie, Paris, France: 1-635.

OLIVET, J.L., BONNIN, J., BENZART, P. & AUZENDE, J.M., 1984.— Cinématique de l'Atlantique nord et central. *Rapport Scientifique et Technique CNEXO*, **54**: 1-108.

OUALI J., 1984.— *Structure et évolution géodynamique du chaînon Nara Sidi Khalif (Tunisie centrale)*. Thèse 3ème cycle, Université de Rennes, Rennes, France.

OUTTANI, F., ADDOUM, B., MERCIER, E., FRIZON DE LAMOTTE, D. & ANDRIEUX, J., 1995.— Geometry and kinematics of the South Atlas front. Algeria and Tunisia. *Tectonophysics*, **249**: 233-248.

PETIT, J.P. , 1976.— *La zone de décrochement du Tizi n'Test (Maroc) et son fonctionnement depuis le Carbonifère*. Thèse 3ème cycle, Université de Montpellier, Montpellier, France.

PHILIP, H., 1987.— Plio-Quaternary evolution of the stress field in Mediterranean zones. *Annales geophysiques*, **5B** (3): 301-320.

PHILIP, H., ANDRIEUX, J., DLALA, M., CHIHI, L. & BEN AYED, N., 1986.— Evolution tectonique mio-plio-quaternaire du fossé de Kasserine (Tunisie centrale). *Bulletin de la Société géologique de France*, **8** (4): 559-568.

POLVECHE, J., 1959.— *Contribution à l'étude géologique de l'Ouarsenis oranais*. Thèse d'État, Faculté des Sciences, Lille, France: 1-369.

RABHI, M., 1987.— Rapports tectonique-sédimentation au Crétacé supérieur et à l'Eocène inférieur: structuration de l'Axe Nord-Sud (Tunisie). *In*: *8th. IAS Regional Meeting of Sedimentology, Tunis*, Abstracts : 1-418.

RAZGALLAH, S., CHAOUACHI, M. & M'RABET, A., 1989.— Les récifs à algues du Permien supérieur du Jebel Tebaga de Medenine. Sud-Est de la Tunisie. *Géologie Méditerranéenne*, **16** (2-3): 213-231.

RICOU, L.E., 1992.— Une frontière de plaque au sein de la Pangéa permo-triassique. *Notes et Mémoires du Service géologique du Maroc*, **366**: 83-94.

RICOU, L.E., 1994.— Tethys reconstructed: plates, continental fragments and their boundaries since 260 Ma from Central America to South-Eastern Asia. *Geodynamica Acta, Paris*, **7** (4): 169-218.

RICOU, L.E., DERCOURT, J., GEYSSANT, J., GRANDJACQUET, C., LEPVRIER, C. & BIJU-DUVAL, B., 1986.— Geological constraints on the evolution of the Mediterranean Tethys. *Tectonophysics*, **123**: 83-122.

ROBILLARD, D., 1979.— Tectonique syn-sédimentaire du Moyen-Atlas septentrional au sud de Taza. *Bulletin de la Société géologique de France*, **7, 23** (4): 441-447.

ROHLICH, P., 1980.— Tectonic development of Al Jabal al Akhdar. *The Geology of Libya*, **3**: 923-931.

ROUVIER, H., 1977.— *Géologie de l'extrême Nord-tunisien*. Thèse, Université Pierre et Marie Curie, Paris, France: 1-1000.

SASSI, S., 1964.— Etude préliminaire des argiles éocènes, mio-pliocènes et actuelles de la région de Metlaoui-M'Dilla et du Cap Bon (Tunisie). *Bulletin de la Société géologique de France*, **7, 5** (3): 345-350.

SEUFERT, G., 1988.— Jurassic sediments and syn-sedimentary tectonics in the Central High Atlas, Morocco. *Bulletin de la Société géologique de France*, **8, 4** (3): 375-390.

SOUSSI, M., 1990.— *Les faciès argilo-carbonatés jurassiques en Tunisie centrale: stratigraphie, sédimentologie, diagenèse (dolomitisation) et intérêt pétrolier*. Thèse 3ème cycle, Faculté des Sciences, Université de Tunis, Tunis, Tunisie: 1-281.

SOYER, C. & TRICART, P., 1989.— Tectonique d'inversion en Tunisie centrale: le chaînon atlasique Segdal-Boudinar. *Bulletin de la Société géologique de France*, **8, 3** (4): 829-836.

STAMPFLI, G., MARCOUX, J. & BAUD, A., 1991.— Tethyan margins in space and time. *Palaeogeography, Palaeoclimatology, Palaeoecology*, **87**: 373-409.

TOUATI, M. A., 1985.— *Etude géologique et géophysique de la concession Sidi el Itayem en Tunisie Orientale-Sahel de Sfax*. Thèse, Université Pierre et Marie Curie, Paris, France: 1-255.

Source : MNHN, Paris

TRICART, P., TORELLI, L., ARGNANI, A., REKHISS, F. & ZITELLINI, N., 1994.— Extensional collapse related to compressional uplift in the Alpine Chain off northern Tunisia (Central Mediterranean). *Tectonophysics*, **238**: 317-329.

TURKI, M.M., 1985.— *Polycinématique et contrôle sédimentaire associé sur la cicatrice Zaghouan-Nebhana.* Thèse de Doctorat ès-Sciences, Université de Tunis, Tunis, Tunisie. Also published as 1988.— *Revue Sciences de la Terre*, **7**: 1-252.

VAUFREY, R., 1932.— Les plissements acheuléo-moustériens des alluvions de Gafsa. *Revue de Géographie physique et Géologie dynamique*, **5**: 299-321.

VIALLY, R., LETOUZEY, J., BENARD, F., HADDADI, N., DESFORGES G., ASKRI, H. & BOUDJEMA, A., 1994.— Basin Inversion along the North African Margin: the Saharan Atlas (Algeria). *In*: F. ROURE (ed.), *Peri-Tethyan Platforms: Proceeding of the IFP Peri-Tethys Research Conference held in Arles, France, March 23, 1993.* Paris, Technip: 79-118.

YAICH, C., 1984.— *Etude géologique des chaînons du Cherahil et du Krechem el Artsouma (Tunisie centrale): leur liaison avec les structures profondes des plaines adjacentes*. Thèse 3ème cycle, Université de Besançon, Besançon, France.

ZAIER, A., 1984.— *Etude stratigraphique et tectonique de la région de Saraa Ouartane (Atlas Tunisien Centrale): lithologie pétrographie et minéralogie de la série phosphatée.* Thèse 3ème cycle, Géologie, Faculté des Sciences de Tunis, Tunis, Tunisie.

ZARGOUNI, F., 1985.— *Tectonique de l'Atlas méridional de Tunisie, évolution géométrique et cinématique des structures en zone de cisaillement.* Thèse d'État, Université Louis Pasteur, Strasbourg, France. Also published as 1986.— *Mémoires INRST*, **5** (3): 1-302.

Source : MNHN, Paris

Structural inheritance and kinematics of folding and thrusting along the front of the Eastern Atlas Mountains (Algeria and Tunisia)

Dominique FRIZON DE LAMOTTE [1], *Éric* MERCIER [1], *Fatima* OUTTANI [1], *Belkacem* ADDOUM [2], *Hacène* GHANDRICHE [2], *Jamel* OUALI [3], *Samir* BOUAZIZ [3] & *Jean* ANDRIEUX [4]

[1] Université de Cergy-Pontoise, Département des Sciences de la Terre, URA CNRS 1759
95011 Cergy-Pontoise Cedex, France

[2] Sonatrach Exploration, Côte Rouge, Alger, Algérie

[3] École Nationale des Ingénieurs de Sfax, Département de Géologie, BP W, 3038 Sfax, Tunisie

[4] Labratoire de Géologie Structurale, URA CNRS 1369, Université Paris-Sud, 91405 Orsay Cedex, France

ABSTRACT

On the basis of recent field work, subsurface data from petroleum exploration and geometrical modelling of fold-thrust structures, this paper describes the structural style and the kinematics of the front of the Atlas Mountains from Biskra (Algeria) to Tunis (Tunisia). Two successive deformation fronts, superimposed in some places but distinct in other ones, are distinguished. Both are thrust fronts exhibiting strong virgations from E-W to N-S trends. This quite complex geometry is linked to the Mesozoic inheritance and to changes in the tectonic transport directions occurring between the two tectonic compressive events. Everywhere along the fronts and independently from the age of the deformation, fault propagation fold represents the main folding mode. These folds are frequently altered by late evolutions occurring during the same or distinct tectonic events. This leads to important changes of the structural style along strike: the front is underlined successively by a backthrust, a forethrust (blind or emergent) and finally along the N-S segment by a fold cut out by a strike slip fault. Additionally, jumps in the emplacement of the décollement levels are accommodated by tear faults and small vertical axis rotations of cover sheets.

RÉSUMÉ

Héritage structural et cinématique des plissements et chevauchements au front de l'Atlas oriental (Algérie et Tunisie).

En s'appuyant sur des travaux de terrain et des données de subsurface d'origine pétrolière et à l'aide de modélisations géométriques des structures de chevauchement-plissement, cet article décrit le style tectonique et la cinématique du front de la chaîne atlasique depuis Biskra (Algérie) jusqu'à Tunis (Tunisie). Deux fronts de déformations successifs, superposés en certains endroits, peuvent être distingués. Les deux montrent une forte virgation en tournant d'une direction E-W à une direction N-S.

FRIZON DE LAMOTTE, D., MERCIER, É., OUTTANI, F., ADDOUM, B., GHANDRICHE, H., OUALI, J., BOUAZIZ, S. & ANDRIEUX, J., 1998.— Structural inheritance and kinematics of folding and thrusting along the front of the Eastern Atlas Mountains (Algeria and Tunisia). *In*: S. CRASQUIN-SOLEAU & É. BARRIER (eds), Peri-Tethys Memoir 3: stratigraphy and evolution of Peri-Tethyan platforms. *Mém. Mus. natn. Hist. nat.*, **177** : 237-252. Paris ISBN : 2-85653-512-7.

Source : MNHN, Paris

Cette géométrie est liée d'une part à l'héritage mésozoïque et d'autre part à des changements de la direction du transport tectonique intervenant entre les deux événements compressifs majeurs. Indépendamment de l'âge de la déformation, le mode de plissement dominant est le pli de propagation de rampe. Ces plis sont souvent affectés d'évolutions secondaires survenant pendant le même événement tectonique ou au cours d'événements distincts. Il en résulte d'importantes variations latérales du style structural. Ainsi, le front correspond successivement à un rétro-chevauchement, un pro-chevauchement (souvent aveugle) et finalement, le long des segments N-S, à un décrochement. Par ailleurs, les sauts dans la position des niveaux de décollement actifs sont accommodés par des failles de déchirure et de faibles rotations de panneaux de couverture.

INTRODUCTION

In North Africa, three main structural domains are classically considered from South to North (Fig. 1) the Sahara platform, the Atlas mountains consisting in weakly inverted basins including rigid elevated regions called High Plateaus or Mesetas and the Rif-Tell chain consisting in strongly inverted basins involved into nappe structures.

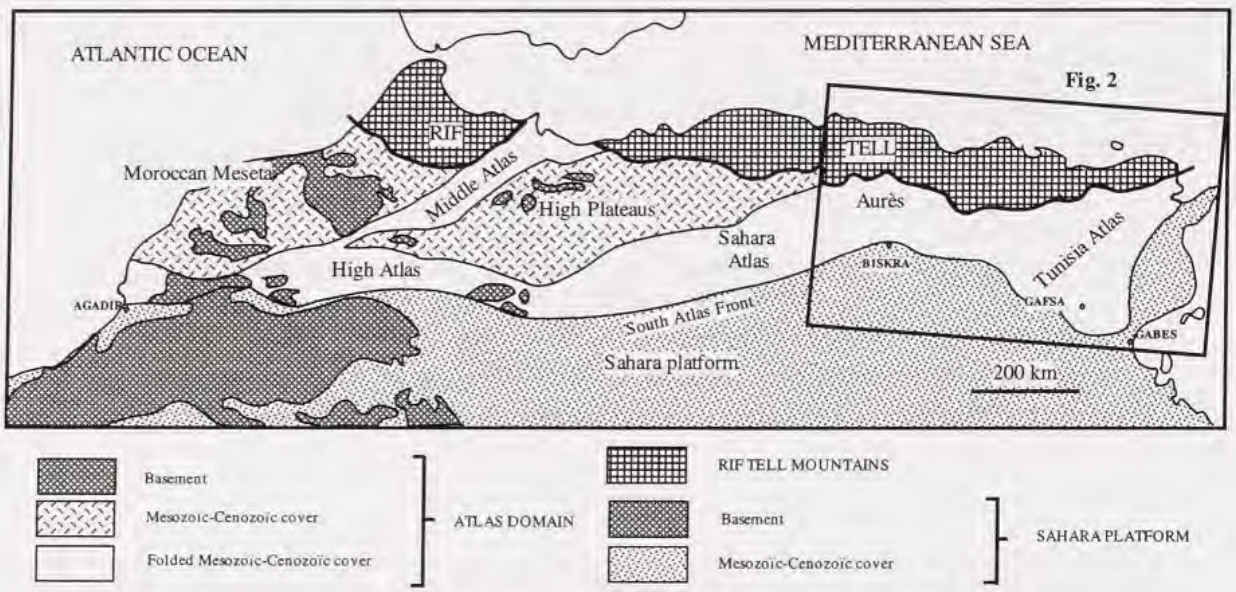

FIG. 1.— Schematic map of North Africa showing the main structural domains.
FIG. 1.— Carte structurale schématique de l'Afrique du Nord montrant les principaux domaines.

This tectonic framework is partly inherited from breaks which occurred during the Mesozoic. However, the South Atlas front (Sahara flexure) which is running from Agadir to Tunis (Fig. 1) is not everywhere superimposed to the paleogeographic transition between the Sahara platform and the Atlas basin. This is particularly obvious in the eastern area where the front extends far South of the basin limit and forms a large scale virgation (Fig. 2). Another particularity of this area is the existence of two successive and no-homoaxial fold-thrust events recognised decades ago (LAFFITTE, 1939; CASTANY, 1949). However the terminology remains quite confuse. Following the more frequent usage, we will use the terms *"Atlas"* and *"Alpine"* events to call the first and second event respectively. In order to avoid a possible confusion between the geographic and the chronological meaning of the term Atlas, we will use in this paper the typography *"Atlas"* when we will speak about the *"Atlas"* event. The problem of the ages of the two tectonic events will be discussed below. Figure 2 gives a schematic view of the two successive deformation fronts. The fronts are superimposed along the N-S axis (Tunisia) and West of Biskra but are distinct between these two regions.

Traditionally, the Folds of Atlas Mountains have been indistinctly interpreted as resulting from cover accommodations above basement strike-slip faults (Fig. 3) (AISSAOUI, 1984; BOUAZIZ, 1995; FAVRE& STAMPFLI, 1992; VIALLY *et al.*, 1994; ZARGOUNI, 1985). In this paper, we will defend a different interpretation in which the significance of the two tectonic events are distinguished.

Source : MNHN, Paris

The *"Atlas"* event led to the uplift (inversion) of the Atlas basin. It is well expressed in the Atlas Mountains but unknown in the Tell-Rif (or at least in their external zones). The *"Atlas"* event must consequently be considered as resulting from an intracontinental evolution which is now better understood in the frame of the kinematics of the Tethyan region. RICOU (1994) suggested that after the collision between Iberia and Africa (45 Ma), the *"Atlas"* folding marked the new convergent boundary limiting a "temporary new plate" which comprised Iberia, parts of Atlantic, Western Tethys and a north African continental stripe including the Moroccan and Algerian Mesetas and the High Plateaus.

The *"Alpine"* event is, more classically, connected to the closing of the Tethys ocean and the collision between Africa and continental fragments called Alkapeca (Alboran-Kabylia-Peloritan-Calabria) by BOUILLIN (1984). These fragments were detached from each other by back-arc spreading resulting likely

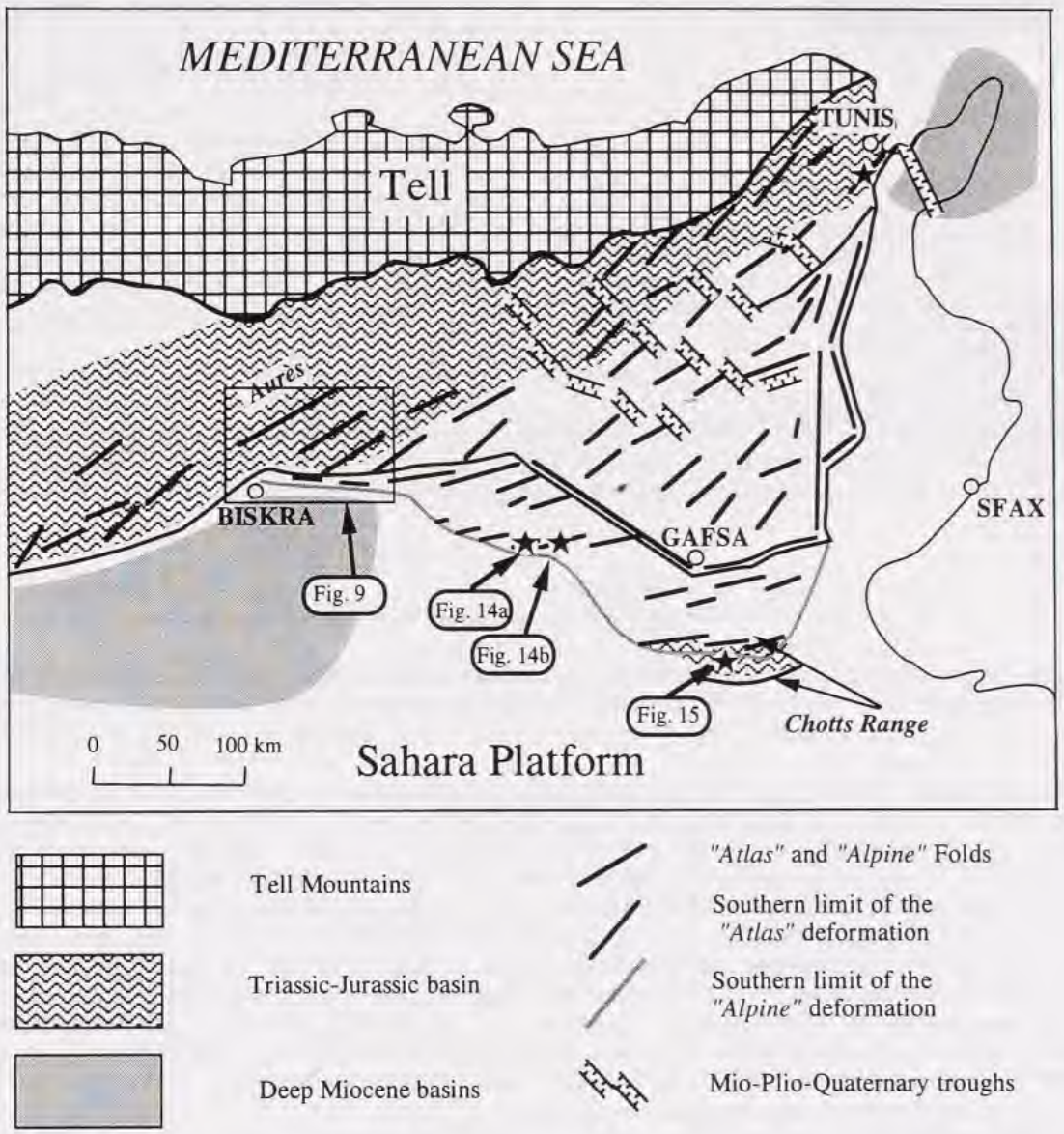

FIG. 2.— Structural map of the Eastern Atlas Regions showing the geometry of the *"Atlas"* and *"Alpine"* deformation fronts. Note that the fronts are far south of the limit of the Atlas basin.

FIG. 2.— Carte structurale de la partie orientale du domaine atlasique montrant la géométrie des fronts de déformation "atlasique" et "alpin". Noter que les fronts sont situés loin au sud de la limite du bassin atlasique.

Source : MNHN, Paris

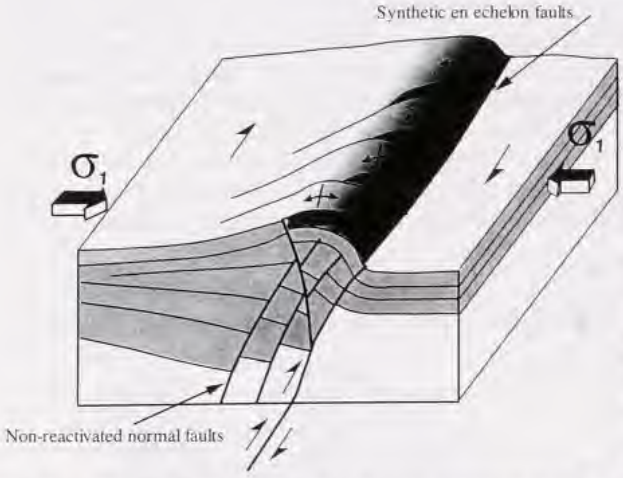

FIG. 3.— Diagram illustrating the former interpretation in which the folds are interpreted as cover accommodations above basement strike-slip faults (modified from VIALLY *et al.*, 1994).

FIG. 3.— Schéma illustrant l'interprétation classique selon laquelle les plis traduisent une accommodation de la couverture au dessus de décrochements de socle (modifié d'après VIALLY et al., *1994)*

from subduction roll-back and leading to divergent escapes of continental blocks (ROYDEN, 1993; FRIZON DE LAMOTTE *et al.*, 1990; LONERGAN & WHITE, 1995). Alkapeca is constituted of a pile of nappe-complexes including mantle fragments which forms the internal zones of the Tell-Rif and Betics. From the front of the internal zones the thrusting propagated southward a considerable distance through the African margin (the present day external Tell-Rif) then through the Atlas. Along a N-S Algerian transept from Great Kabylia to the Aurès Mountains, the thrust propagation is recorded by successive foreland basins that were progressively incorporated within the orogenic wedge (GHANDRICHE, 1991). Relatively to the *"Alpine"* event the Atlas Mountains may consequently be interpreted as the foreland fold and thrust belt of the Tell-Rif. According to this interpretation, the present day mountain front, the so-called South Atlas Front, is demonstrated to be a major and still active thrust front (FRIZON DE LAMOTTE *et al.*, 1990; JOSSEN & FILALI-MOUTEI, 1992; CREUZOT *et al.*, 1993; OUTTANI *et al.*, 1995).

This paper is based, in particular, on three recent PhD thesis by GHANDRICHE (1991), ADDOUM (1995) and OUTTANI (1996). Its aim is to analyse the geometry and kinematics of the South Atlas regions in the eastern area where the front shows a strong virgation (Fig. 2). This quite complex geometry is partly linked to the tectonic and paleogeographic inheritance that we will consider firstly.

STRUCTURAL INHERITANCE

Because of its location close to the Atlantic and Tethys oceans, the Meso-Cenozoic history of North Africa is complex. We will consider successively four periods of important tectonic activity: the Triassic-Jurassic period, the Mid-Cretaceous period and, finally, the "*Atlas*" and "*Alpine*" compressive periods.

At the beginning of Mesozoic times, breaks affected the northern part of Africa as a response to opening of both Atlantic and Tethys oceans. More precisely, during the Triassic and lowermost Liassic the rifting process has produced a series of "en échelon" NE-SW grabens in North Africa (ANDRIEUX *et al.*, 1989; LAVILLE & PETIT, 1984; WINTERER & HINZ, 1984). Between the Middle and Late Jurassic, the oceanic spreading, already active in the Atlantic, began in the Tethyan domain of the Alps (LEMOINE, 1985; FAVRE & STAMPFLI, 1992; RICOU, 1994). North Africa was at that time situated on the transform zone which linked the two ridges and was the site of active extensional-transcurrent tectonics. Grabens bounded by NE-SW faults and associated basic intrusions are interrupted by E-W transform zones. The two most important ones were running between Africa and Iberia and within Africa itself (Fig. 4). They localise the future Tell-Rif on the one hand and High Atlas, Aurès, Sahara Atlas and Tunisia Atlas on the other hand (Fig. 1). Additionally, The Middle Atlas is inherited from a NE-SW graben where extension was less pronounced.

In the Eastern Maghrebides, Eo-Cretaceous times are characterized by a new increase of subsidence rate (VIALLY *et al.*, 1994). It seems that subsidence affected more or less uniformably the region situated east of Algiers meridian. Pre-Cenomanian normal faulting leading to N-S trending tilted blocks is well expressed in Tunisia along the "axe Nord-Sud" (OUALI, 1985) and in some other areas of the Tunisia Atlas. GHANDRICHE (1991) and MARTINEZ (1991), using both geological mapping and subsurface data,

Source : MNHN, Paris

described in the Aurès Mountains listric normal faults branched downward on the Triassic evaporites and upward on the Cenomanian shale. VILA (1995) has proposed that this normal faulting generated migration of evaporites leading to the emplacement of large sub-marine salt glaciers. There is no evidence showing that the Atlas basement is involved in this extensional tectonics. We propose to connect the cover décollements of the eastern Maghrebides to the nearby Sirte Basin Rifting and its northward prolongation in the Pelagian sea (BUROLLET & ELLOUZ, 1986) which was active at the same time. The whole eo-Cretaceous extensional tectonics is sealed by the marine transgression that started in the middle Albian and reached its maximum in the upper Cenomanian.

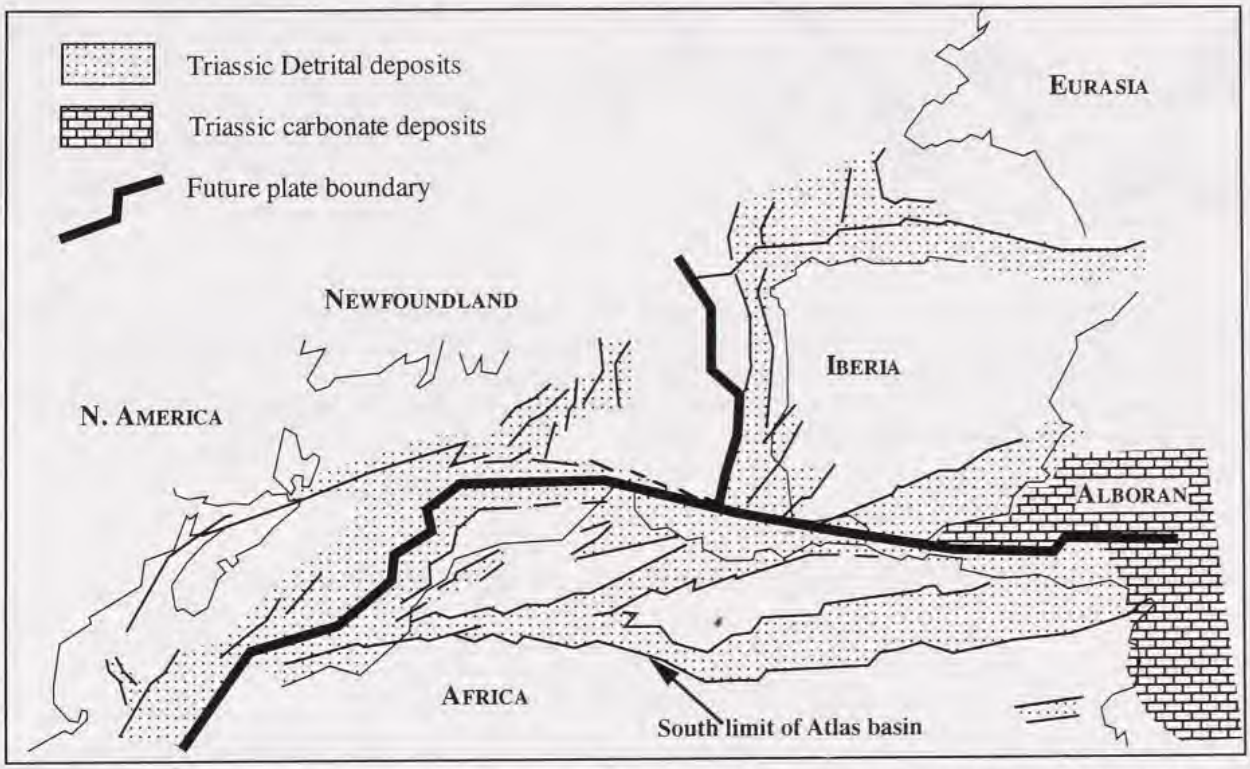

FIG. 4.— The basins geometry of North Africa, East of North America, Iberia and Alboran at the Jurassic-Triassic boundary (from FAVRE, 1995; modified for the eastern region).

FIG. 4.— Géométrie des bassins d'Afrique du Nord à la limite Trias-Jurassique (d'après FAVRE, 1995 ; modifié pour les parties orientales)

Authors have discribed early (i.e. Cretaceous) compressive "phases" in various parts of North Africa (see for instance OBERT, 1984). This complex question has been already discussed elsewhere (FRIZON DE LAMOTTE, 1985) and we consider that these phases are only of local significance. According to VIALLY *et al.* (1994), we assume consequently that compression of geodynamic significance started only at Tertiary times. The first tectonic phase, the *"Atlas"* phase, has been recognised from a long time in the Aurès Mountains (LAFFITTE, 1939) and in the Hodna basin (GUIRAUD, 1973) and attributed to middle-late Eocene. In the Aurès Mountains, the Atlas phase is reponsible for NE-SW large scale trending folds. The unconformity showing Oligocene (?) to Miocene marine sediments resting on folded Mesozoic to Eocene terrains is well expressed at the top of some anticlines (Fig. 5) but appears only as a cartographic unconformity above the synclines. The second tectonic phase, the *"Alpine"* phase, is responsible for E-W trending folds and thrust faults. Generally the *"Alpine"* structures are superimposed to earlier *"Atlas"* folds leading to a complex tectonic pattern "bayonet folds"; VILA (1980). However in the zone (Fig. 2) where the Alpine deformation Front extends beyond the Atlas Front, the observed geometry is quite simple

In Tunisia, two successive compressive events showing the same geometric relationships (N140 then N-S shortening) are also considered (BEN FERJANI *et al.*, 1990). However the *"Atlas"* event, attributed to the middle Miocene (Serravalian to Tortonian) is younger than in Algeria. The *"Alpine"* event also

Source : MNHN, Paris

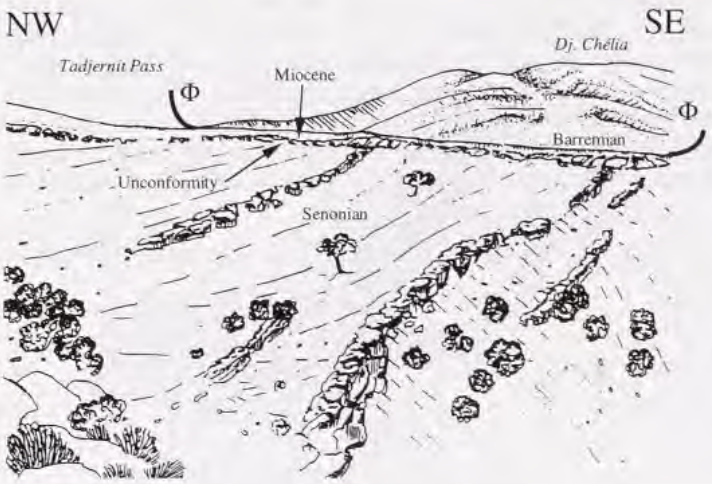

FIG. 5.— The unconformity of Miocene marine deposits on Upper Cretaceous limestone and the thrusting of the Dj. Chelia anticline onto the Miocene (from GHANDRICHE, 1991). This view is from the South of the Dj. Chelia, see location on figure 9.

FIG. 5.— Discordance du Miocène marin sur les calcaires du Crétacé Supérieur et chevauchement de l'anticlinal du Dj. Chélia sur ce Miocène (d'après GHANDRICHE, 1991). La vue, localisée sur la figure 9, est prise du sud.

appears as diachronic. For instance, in the Timgad area, *"Alpine"* folds are sealed by a conglomerate of Villafranchian age whereas southward, close to the South Atlas Front, the same Villafranchian deposits are involved in the frontal monocline forming the Sahara Flexure.

This suggests that the *"Atlas"* Deformation front propagated from West to East whereas the *"Alpine"* Deformation front propagated from North to South.

SOUTH ATLAS FRONT GEOMETRIC AND KINEMATIC ANALYSIS

METHODOLOGY

The methods extensively used in this paper have been already presented elsewhere (MERCIER, 1992; OUTTANI *et al.*, 1995; MERCIER *et al.*, 1997). This section is only a short outline.

In fold-thrust belts one can consider four types of geologically significant fold-thrust interactions (Fig. 6). One of them (the detachement fold) is developed above a decollement, the others: fault-bend fold mode I (SUPPE, 1983), fault propagation fold (SUPPE, 1985; JAMISON, 1987) and "Chester and Chester" fold (CHESTER & CHESTER, 1990) are ramp-related folds. For evident geometric reasons, the development of a detachement fold needs a thick ductile level below the stiff layers affected by concentric folding. In the studied part of the Atlas Mountains, we have only recognised ramp related folds characterized by a kink-like style.

The main difference between a fault bend fold (FBF) and a fault propagation fold (FPF) is that in a FBF the shortening acting at the back of the fold is almost completely transmitted forward whereas in a FPF it is accomodated within the fold. The Chester and Chester model combines FBF at depth and FPF in the near suface strata. Generally the surface geometry of the folds is sufficient to discriminate between FBF and FPF. However and important problem remains in order to define the geometry of decollements at depth (Fig. 8). To fix the deep geometry of a FBF, three parameters are needed: the depths to lower an upper detachements and the slip value transmitted forward. The problem is consequently underdefined. On the contrary, for a FPF the relationships beetween surface geometry and geometry at depth are unique. Consequently, the occurence of a single FPF in a section provides data which fix the geometry at depth for the whole section.

However, field structures are generally more complicated that the simple-step models. In particular secondary evolutions of FPF are frequent and may obscure the basic geometric pattern (JAMISON, 1987; SUPPE & MEDWEDEFF, 1990; MERCIER, 1992; MERCIER *et al.*, 1997). Two types of evolution known theoretically have been recognised in the field (Fig. 8): the transport on the upper flat and the

Source : MNHN, Paris

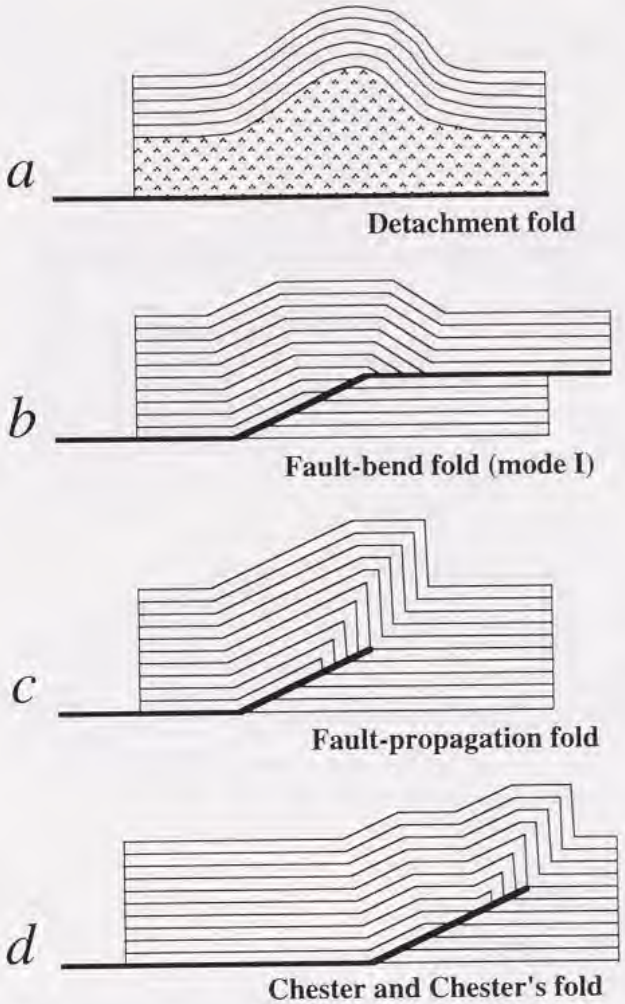

FIG. 6.— The main fold-thrust interactions leading to the presently known folding modes.
FIG. 6.— Les principaux types d'intéractions plis-chevauchements et les modes de plissement associés.

development of a breakthrough thrust. In the Atlas Mountains, the building of the primary fold and the secondary evolution may be linked to a progressive deformation during a single event or to a renewal of an *"Atlas"* structure during the *"Alpine"* event.

We will examine the geometry an kinematics of the South Atlas Front, from Biskra to Tunis, in three particular places of the Eastern Maghrebides exhibiting different thrust-fold interactions.

THE FRONT OF THE AURES MOUNTAINS (EAST OF BISKRA)

The Aurès Mountains expose a thick (up to 10 000 m) sedimentary sequence ranging from Triassic to Middle Eocene (LAFFITTE, 1939). This sequence is involved in NE-SW trending folds arranged in "en échelon" pattern (Fig. 9). In the Middle and the North of the Aurès, Oligocene continental and Miocene marine deposits overlie unconformably the folded sequence. The whole pile is involved in E-W trending folds well exposed in the Timgad basin (GHANDRICHE, 1991) . The interaction between *"Atlas"* and *"Alpine"* events are expressed by different ways. For instance, the Chelia *"Atlas"* anticline, situated South of the Timgad Basin (Fig. 9), is cut out by an E-W *"Alpine"* thrust-fault leading to the overthrusting of Barremian quartzite onto Miocene deposits (Fig. 10) (GHANDRICHE, 1991). The Kasserou anticline, situated N-E of the Timgad basin, is also an *"Atlas"* anticline as indicated by the unconformity of the Miocene deposits (Fig. 11). However the steep breakthrough thrust fault which emerges in the core of the fold affects laterally the Miocene and refers consequently to the *"Alpine"*

Source : MNHN, Paris

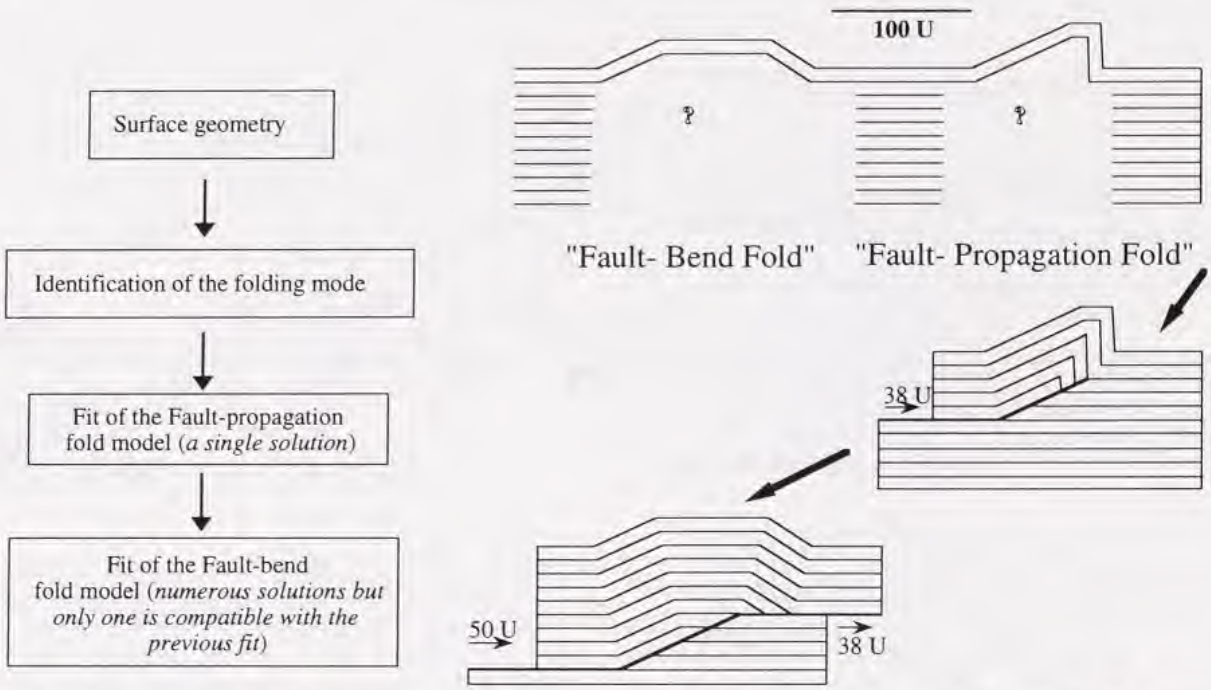

FIG. 7.— Determination of the geometry at depth of a couple Fault Bend Fold- Fault Propagation fold using the geometric properties of Fault Propagation Folds (modified from OUTTANI *et al.* 1995).

FIG. 7.—Principes de la détermination de la géométrie profonde d'un couple pli de cintrage sur rampe- pli de propagation de rampe en utilisant les propriétés des plis de propagation de rampe (modifié d'après OUTTANI et al., *1995)*

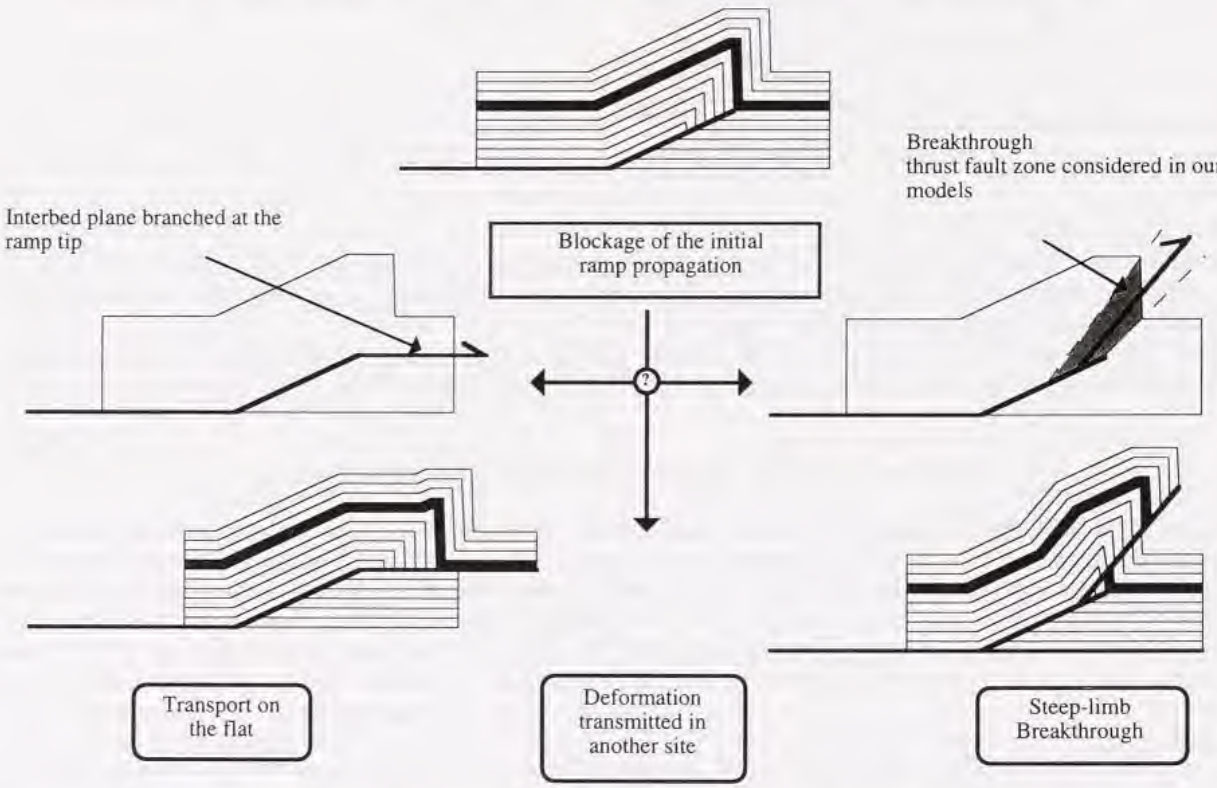

FIG. 8.— The two classical alterations of Fault Propagation Folds (modified from MERCIER *et al.*, 1997).

FIG. 8.— Les deux évolutions tardives classiques des plis de propagation de rampe (modifié d'après MERCIER et al., *1997).*

Source : MNHN, Paris

phase. This thrust-fault keeps an *"Atlas"* orientation but records an important component of sinistral strike-slip (MERCIER *et al.*, 1995). Modelling (Fig. 12) is consistent with an interpretation of the Kasserou as an *"Atlas"* fault-propagation fold altered by a secondary breakthrough fault of *"Alpine"* age. Both Chelia and Kasserou anticlines are developed above a Triassic décollement plane and we consider that the basement is not involved in the Aurès folds.

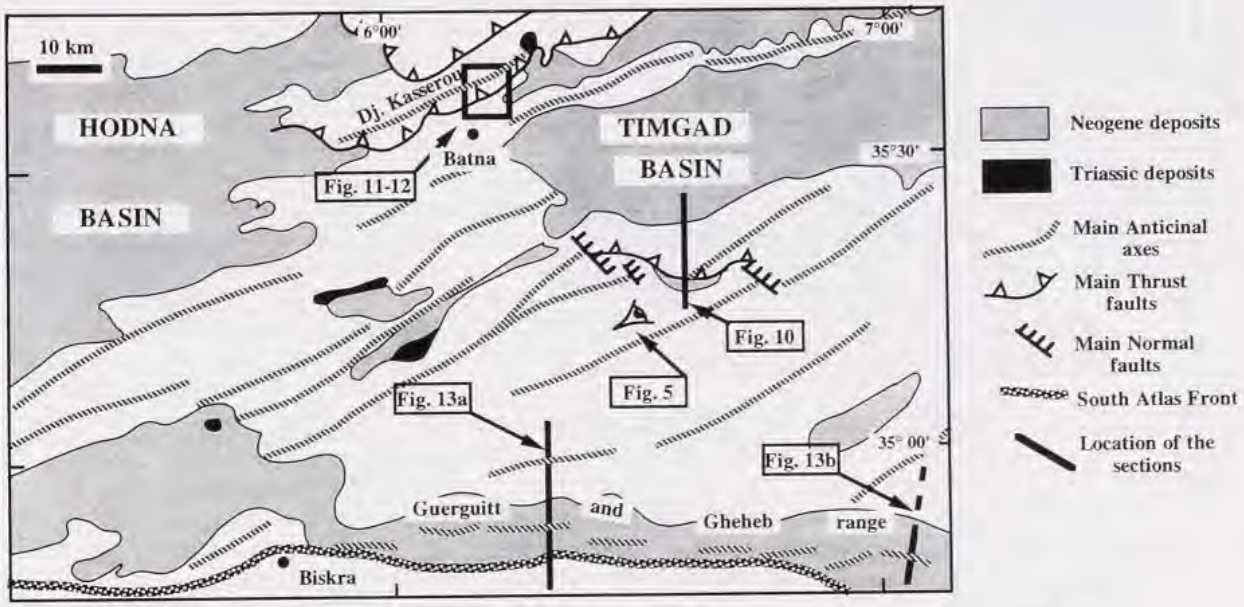

FIG. 9.— A schematic structural map of the Aurès Mountains locating the figures 5, 10, 11 and 13.
FIG. 9.— Carte schématique des Aurès localisant les figures 5, 10, 11 et 13.

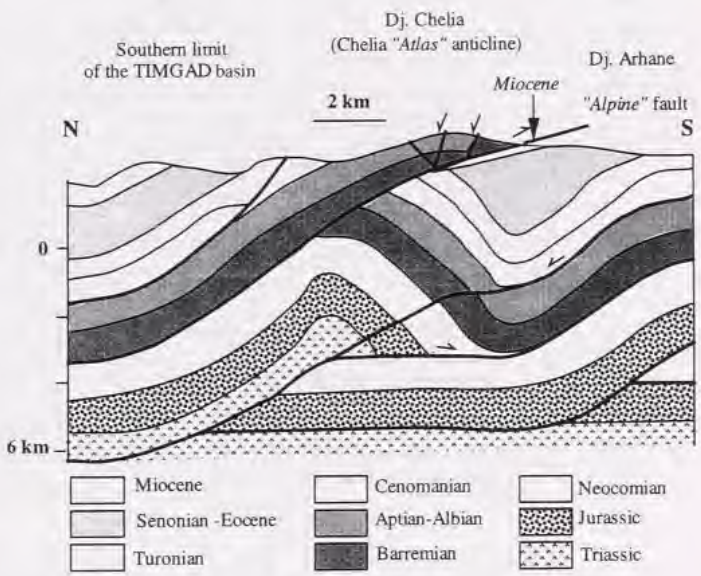

FIG. 10.— A cross section through the Dj. Chelia showing an *"Alpine"* thrust cutting through a former *"Atlas"* anticline (from GHANDRICHE, 1991; location on figure 9). Note the unconformity of the Miocene deposits situated below the Dj. Chelia thrust. On the other hand, the Miocene deposits infilling the Timgad basin rest more or less conformably on the underlying stratigraphic pile.

FIG. 10.— Coupe à travers le Dj. Chelia montrant un chevauchement "alpin" recoupant un anticlinal "atla-sique" (d'après GHANDRICHE, 1991 ; voir la locali-sation sur la figure 9). Remarquer la discordance des terrains miocènes (cf. figure 5). Par ailleurs, le Miocène situé dans le bassin de Timgad et situé au toit de l'anticlinal est plus ou moins concordant sur son substratum.

Along the southern limit of the Aurès massif, late Miocene to Lower Quaternary continental molasses rest conformably on the Meso-Lower Cenozoic succession (i.e. there is no evidence of Atlas folds). The whole pile (up to Villafranchian) is involved in E-W trending folds constituting the Guerguitt and Gueheb range (Fig. 9) (LAFFITTE, 1939). The South Atlas Front is underlined by a south-dipping monocline (about 45°) which is nowhere affected by south-verging thrust-faults. To the South, on the

Source : MNHN, Paris

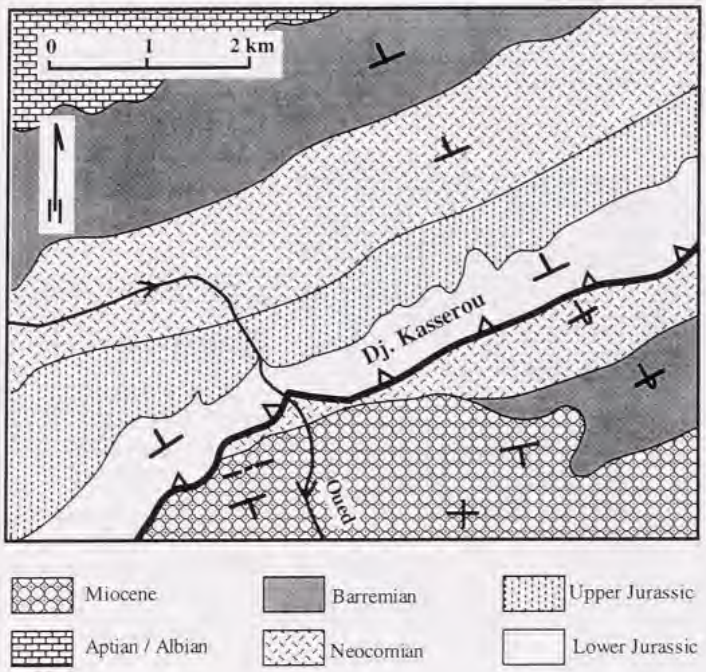

FIG. 11.— An over-simplified geological map of the Dj. Kasserou anticline (modified from VILA & GUELLAL, 1977). The Miocene deposits unconformably overlain an *"Atlas"* NE-SW trending fold but are cut out by a break-through fault of *"Alpine"* age.

FIG. 11.— Carte géologique très schématique de l'anticlinal du Dj. Kasserou (modifié d'après VILA & GUELLAL, 1977). Les dépôts miocènes recouvrent en discordance un pli "atlasique" d'orientation NE-SW mais sont recoupés par un chevauchement "alpin".

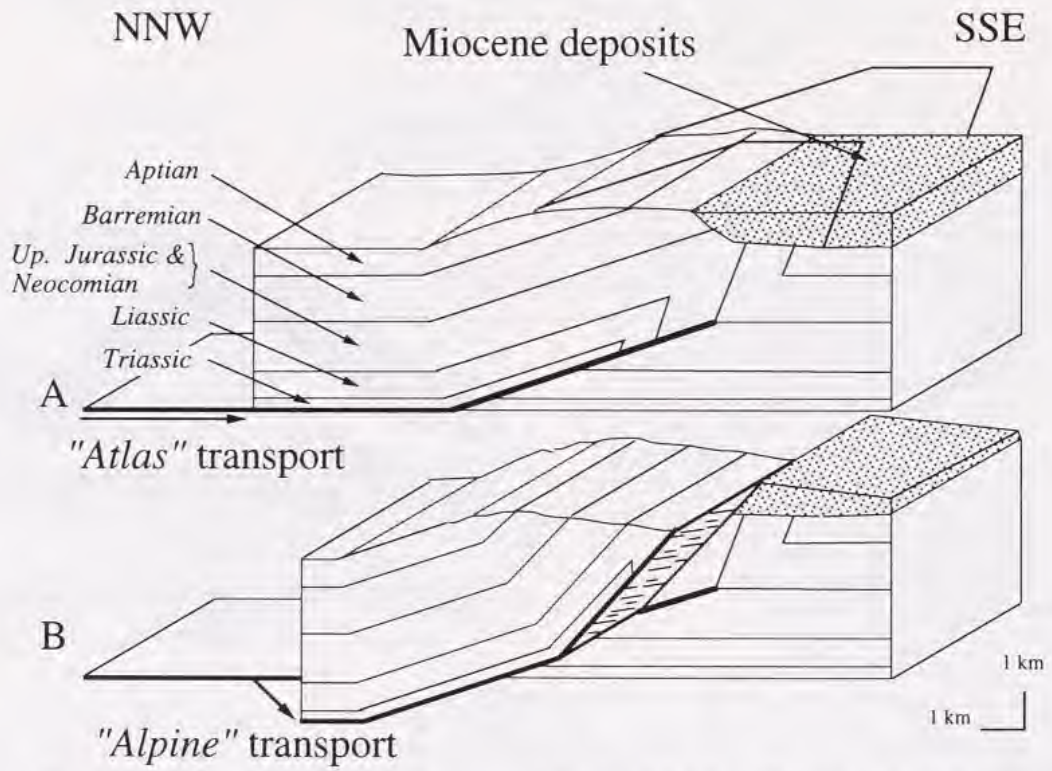

FIG. 12.— A kinematic model of the Kasserou anticline (modified from MERCIER *et al.*, 1995).

FIG. 12.— Modèle cinématique de l'anticlinal du Dj. Kasserou (modifié d'après MERCIER et al., *1995).*

Source : MNHN, Paris

Sahara platform, the Miocene to Quaternary sequence is thick and, as a consequence, in the synclines of the belt the "regional" is elevated by about 1.5 km above the platform. This geometry predates the development of the fold-thrust belt. It is illustrated on the figure 13 as the result of a vertical fault which localises the development of a major backthrust leading to the delamination of the sedimentary cover above the migrating hinge of the frontal monocline. The backthrust is branched on a shallow décollement situated at the base of Turonian levels. This shallow décollement is necessarily branched northward on the deep Triassic décollement along which the whole Aurès is translated. Along a N-S section from the Dj. Taktiout to the Sahara flexure, modelling suggests that the shallow décollement is folded by the Taktiout fault propagation anticline. The branching on the deeper décollement must consequently be search more to the North. Along a parallel section situated 55 km eastward (Fig. 13), it appears that a ramp joins directly the two décollements. Such an important variation along strike may appear unlikely. However one must keep in mind that the frontal structure is oblique to the *"Atlas"* folds and that, as a consequence, the branching pattern of the thrust faults is certainly complex. Additionally, it is worth noting that the interpretation proposed for the Taktiout anticline (Fig. 13) is different from a previous one (FRIZON DE LAMOTTE *et al.*, 1990). The reason is that we had considered only the fault-bend mode of folding. However, for the purpose of this paper, the difference concerns only the value of the slip transmitted toward the Sahara platform.

GEOMETRY AND KINEMATICS OF THE SOUTH ATLAS FRONT IN THE NEGRINE AND METLAOUI AREAS

This area is typically a zone where the "*Alpine*" Deformation Front is far South of the "*Atlas*" Deformation Front. Consequently, the folding process may be considered as globally monophase. We have numerous new data, presented below, in this zone from recent field work by ADDOUM (1995).

The front is constituted by the steep or overturned forelimb of a fault propagation fold. This forelimb is frequently cross cut by low angle reverse fault (forelimb faults). On the basis of field and subsurface data, we have already published the results of modelling of ten cross sections (OUTTANI *et al.*, 1995). Each sections agrees with a shallow décollement situated within Cretaceous levels. The junction of this shallow décollement with the Triassic décollement of the Aurès occurs beneath the Dj. Abiod and Dj. Onk situated 30 to 60 km North of the present day deformation front. The results are remarkably consistent within a given section and from one section to another but disagree clearly with the classic thick skinned concept. To illustrate the kinematic evolution of the front, we have chosen two sections: on the first one, we can see a combination of a fault bend fold and a fault propagation fold (Fig. 14b); on the second the two folds are fault propagation folds suffering a transport on the flat and a breakthrough respectively (Fig. 14a). Both the earlier folds and the secondary evolutions are of *"Alpine"* age.

The comparison of the shortening ratios from a section to the adjacent one shows a progressive increase of the shortening within thrust sheet limited by tear faults sub-paralell to the tectonic transport direction. This model suggests very small vertical axis rotations (about 1.5°) of cover thrust sheets (OUTTANI *et al.*, 1995).

In the Metlaoui Mountains (Tunisia: Fig. 14b) a small amount of slide (about 1 km) is transmitted southward to the Chaîne des Chotts. This slide cannot explain by itself the structural elevation of the wide "Chaîne des Chotts" anticline built on the site of a Jurassic graben (BEN FERJANI *et al.*, 1990). The excess area balancing method indicates that the wide anticline results from the inversion of the graben on a deep décollement level. According to field data, the figure 15 suggests that the translation along the shallow décollement has been stopped by the previously emplaced inverted deep structure.

GEOMETRY AND KINEMATICS OF THE SOUTH ATLAS FRONT ALONG THE NORTH-SOUTH AXIS AND THE ZAGHOUAN AREA

Along the N-S axis the *"Atlas"* and *"Alpine"* fronts are merging in an unique N-S trending anticline. Additionally, this structure is clearly localised by eo-Cretaceous tilted blocks (OUALI, 1985; MARTINEZ *et al.*, 1991). This doesn't mean, however, that it results from the direct reactivation of normal faults. On the contrary it seems that the faulted terranes suffered rigid-body translations above new created ramps.

Source : MNHN, Paris

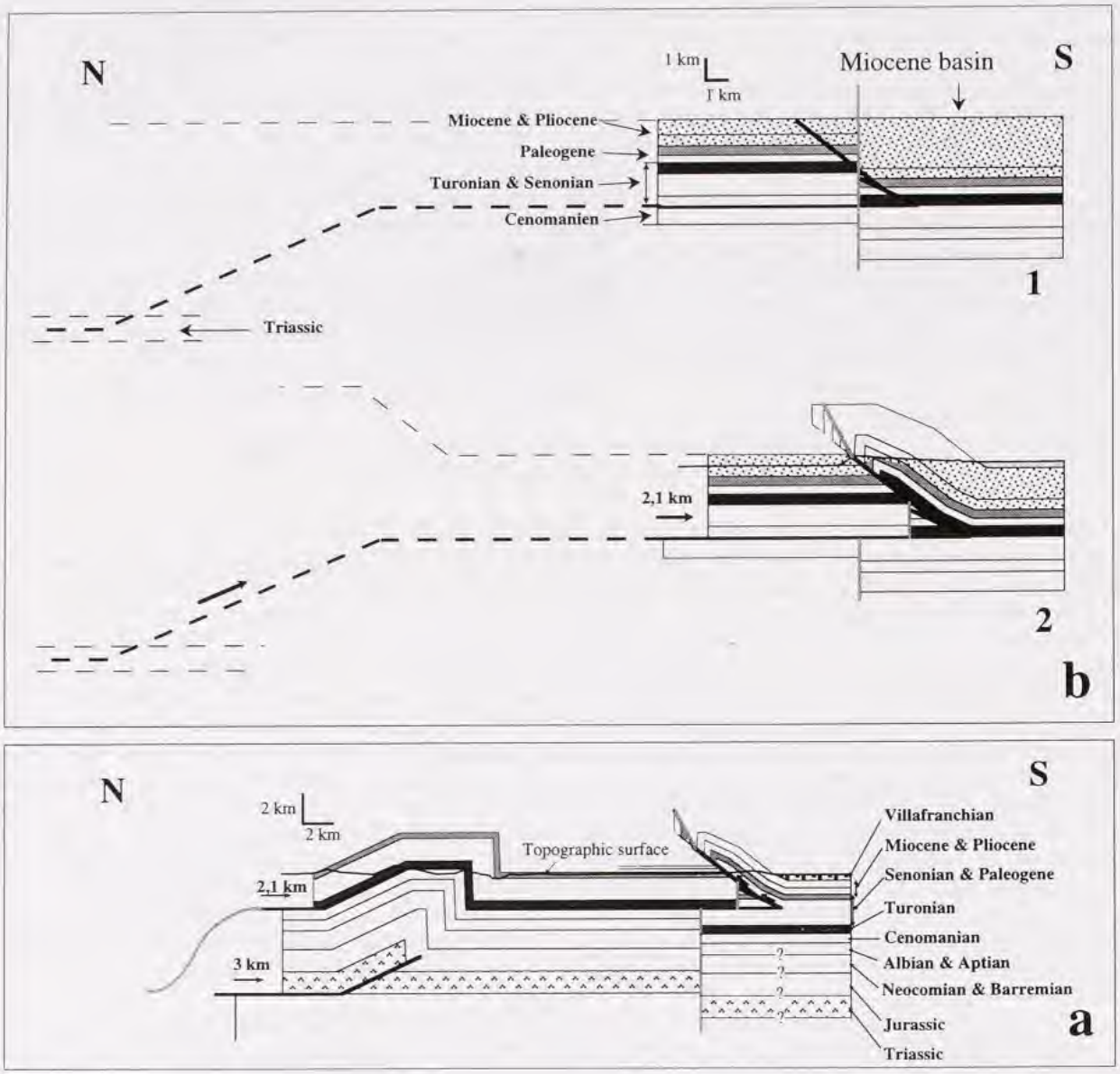

FIG. 13.— Two cross sections of the South Atlas Front showing the development of the frontal South-Aures back-thrust (see explanation in the text). **a**, Section through the Dj. Taktiout anticline; **b**, Section 50 km East of the Dj. Taktiout (b2) and proposed pre-"*Alpine*" restoration. N.B. the vertical attitude of the pre-"*alpine*" fault is only indicative. An alternative hypothesis is given in ADDOUM (1995).

*FIG. 13.— Deux coupes à travers le front sud-atlasique montrant le développement du rétro-chevauchement sud-aurésien (voir explications dans le texte). **a**, coupe à travers l'anticlinal du Dj. Taktiout. **b**, coupe 50 km à l'est, et restauration pré-alpine proposée. N.B. L'attitude verticale de la faille* "pré-alpine" *n'est pas documentée. Une hypothèse alternative est proposée par ADDOUM (1995).*

Source : MNHN, Paris

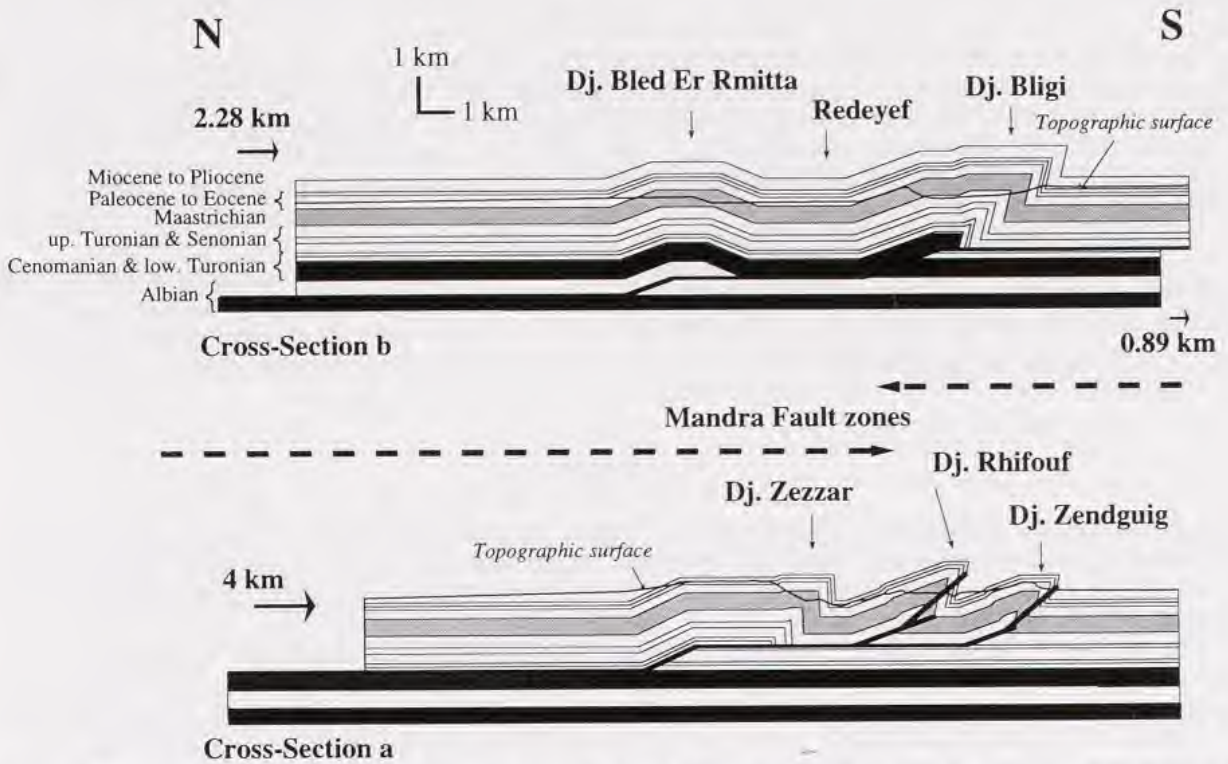

FIG. 14.— Two cross sections through the Negrine (a) and Metlaoui Mountains (b) illustrating the geometry of the front in this zone.
Note the slide transmitted southward from the Metlaoui mountains (see explanations in the text).
FIG. 14.— Deux coupes à travers les Monts de Négrine (a) et de Metlaoui (b) illustrant la géométrie du front dans cette zone. Noter le glissement transmis à l'avant des Monts de Metlaoui (voir explications dans le texte).

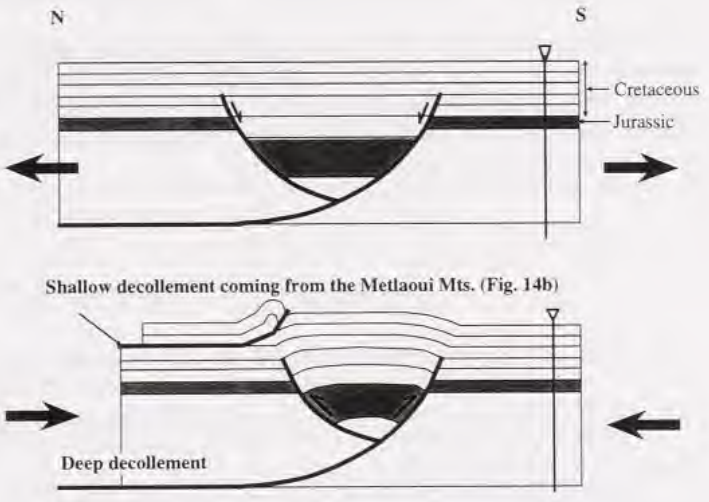

FIG. 15.— A sketch diagram without scale showing how the "Chaîne des Chotts" combined a deep and a shallow décollements.
FIG. 15.— Schéma de principe sans échelle montrant la combinaison dans la chaîne des Chotts de décollements profond et superficiel.

Source : MNHN, Paris

According to other field observations and analogue modelling (VALET, 1990) we emphasise the difference between localisation and reactivation. Here, clearly, the normal faults localise the subsequent folding but are not strictly speaking reactivated (CREUZOT *et al.*, 1992).

The structural pattern is similar to the Aurès one but more complex. The examination of angular unconformities in Neogene to Quaternary deposits indicates that the first fault propagation fold is of *"Atlas"* age. However, because of the Eo-Cretaceous inheritance, it was originally an oblique fold born at about 45° of the shortening direction. This fold has been subsequently cross cut by an *"Alpine"* breakthrough faults. Slikensides on the faults are almost horizontal showing that they are pure strike slip faults agreing with a N-S tectonic transport. As in the Aurès, modelling shows that the décollement level is situated within the evaporitic beds of triassic age.

From the N-S axis, the front bends progressively northward up to the Zaghouan area where it trends NE-SW normal to the *"Atlas"* shortening. The front is localised by the boundary of the Atlas basin inherited from the Triassico-Liassic rifting but as in the previous case there is no actual inversion. Moreover in some places the early normal faults are rigidely transported and preserved at the outcrop level (CREUZOT *et al.*, 1993).

CONCLUSION

Relatively to the last tectonic event (*"Alpine"* event) the Atlas Mountains of eastern North Africa may be considered as the foreland fold and thrust belt of the Tell Atlas. They result from the "collision" which occured at the end of the Oligocene times and then propagated southward to the South Atlas Front where the thrusting is still active.

However the Atlas Mountains are not a classic foreland fold and thrust belt (like the Jura for instance) because the existence of an earlier folding (the *"Atlas"* event) In our opinion, this *"Atlas"* event leading to the inversion of the Atlas basin results from an intracontinental dextral transpresional movement. At the end of the *"Atlas"* event, the region was likely more or less comparable to the present day North Sea. The subsequent oblitaration by the alpine compression led to the present day pattern.

The tectonic framework is, in fact, more complicated because the development of Miocene to Quaternary grabens trending NW-SE (Fig. 2), cutting the eastern part of the Atlas and leading to the progressive "disintegration" of North Africa by successive escape of continental blocks like Sicily which was a part of Africa at least until Tortonian. An important point is that southward thrusting and NE-SW extension are coeval showing that in this area of the Maghrebides at least two different geodynamic processes are active at the same time.

ACKNOWLEDGEMENTS

This paper is a contribution to the Peri-Tethys program (project "South Atlas Front"). The order of the authors is by institution and alphabetical in each instutition. The authors wish to thank P. TRICART (Université Joseph Fourier, Grenoble), R. BRACENE and D. BEKKOUCHE (SONATRACH, Algiers) and J.M. VILA (Université Paul Sabatier, Toulouse) for helpful discussions and J.-L. MUGNIER and M. ZAPPATERA for their reviews.

REFERENCES

ADDOUM, B., 1995.— *L'Atlas Saharien Sud-Oriental. Cinématique des plis-chevauchements et reconstitution du bassin du Sud-Est constantinois (confins algéro-tunisien).* Thèse, Université Paris-Sud, Orsay, France: 1-160.

AISSAOUI, D., 1984.— *Les structures liées à l'accident sud-atlasique entre Biskra et le Djebel Manndra (Algerie). Évolution géométrique et cinématique.* Thèse, Université de Strasbourg, Strasbourg, France.

ANDRIEUX, J., FRIZON DE LAMOTTE, D. & BRAUD, J., 1989.— A structural scheme for the Western Mediterranean area in Jurassic and Early Cretaceous times. *Geodynamica Acta*, **3/5**: 5-15.

BEN FERJANI, A., BUROLET, P. & MEJRI, F., 1990.— *Petroleum geology of Tunisia.* ETAP, Tunis.

BOUAZIZ, S., 1995.— *Étude de la tectonique cassante dans la plate-forme et l'atlas sahariens (Tunisie Méridionale): évolution des paléochamps de contraintes et implications géodynamiques.* Thèse, Université Tunis II, Tunis, Tunisie: 1-485.

Source : MNHN, Paris

BOUILLIN, J.P., 1984.— Nouvelle interprétation de la liaison Apennin-Maghrébides en Calabre; conséquences sur la paléogéographie téthysienne entre Gibraltar et les Alpes. *Revue de Géographie physique et de Géologie dynamique*, **25**: 321-328.

BUROLLET, P.F. & ELLOUZ, N., 1986.— Évolution of sedimentary basis in Central and Eastern Tunisia. *Bulletin des Centres de Recherche Exploration-Production Elf-Aquitaine*, **10**: 49-68.

CASTANY, G., 1949.— Sur la présence de plusieurs phases de diastrophisme en Tunisie. *Comptes Rendus de l'Académie des Sciences, Paris*, **229**: 1160-1162.

CHESTER, J.S. & CHESTER, F.M., 1990.— Fault propagation folds above thrusts with constant dip. *Journal of Structural Geology*, **12** (7): 903-910.

CREUZOT, G., MERCIER, E., OUALI, J. & TRICART, P., 1993.— La tectogenèse atlasique en Tunisie centrale: apport de la modélisation géométrique. *Eclogae geologicae Helveticae*, **86** (2): 609-627.

CREUZOT, G., MERCIER, E., OUALI, J. & TURKI, M.M., 1992.— Héritage distensif et structuration chevauchante: apports de la modélisation du chevauchement alpin de Zaghouan (Atlas Tunisien). *Comptes Rendus de l'Académie des Sciences, Paris*, **314** (II): 961-965.

FAVRE, P., 1995.— Analyse quantitative du rifting et de la relaxation thermique de la partie occidentale de la marge transformante nord-africaine: le Rif externe (Maroc). *Geodynamica Acta*, **8** (2): 59-81.

FAVRE, P., & STAMPFLI, G. M., 1992.— From rifting to passive margin: the exemples of the Red Sea. Central Atlantic and alpine Tethys. In: P.A. ZIEGLER (ed.), Geodynamica of Rifting. *Tectonophysics*, **3** (215): 69-97.

FRIZON DE LAMOTTE, D., 1985.— *La structure du Rif Oriental (Maroc): rôle des fluides et importance de la tectonique longitudinale*. Thèse, Université Paris VI, Paris, France: 1-436.

FRIZON DE LAMOTTE, D., GUÉZOU J.-C., ANDRIEUX, J., ALBERTINI, M.-A., COULON, M. & POISSON, A., 1990.— Comment on "Neogene extensional collapse in the Western Mediterranean (Betic-Rif Alpine orogenic belt): implications for the genesis of the Gibraltar Arc and magmatic activity". *Geology*, **18**: 381.

FRIZON DE LAMOTTE, D., GHANDRICHE, H. &MORETTI, I., 1990.— La flexure saharienne : trace d'un chevauchement aveugle post-pliocène de flèche plurikilométrique au Nord du Sahara (Aurès, Algérie). *Comptes Rendus de l'Académie des Sciences, Paris*, **310** (II): 1527-1532.

GHANDRICHE, H., 1991.— *Modalités de la superposition de structures de plissement-chevauchement d'âge alpin dans les Aurès (Algérie)*. Thèse, Université Paris-Sud, Orsay, France: 1-189.

GUIRAUD, R., 1973.— *Évolution post-triasique de l'avant pays de la chaîne alpine en Algérie d'après l'étude du bassin du Hodna et des régions voisines*. Thèse, Université de Nice, Nice, France: 1-265.

JAMISON, W.R., 1987.— Geometric analysis of fold development in overthrust terranes. *Journal of Structural Geology*, **9** (2): 207-219.

JOSSEN, J. A. & FILALI-MOUTEI, J., 1992.— A new look at the structural geology of the southern side of the Central and Eastern High Atlas mountains. *Geologische Runschau*, **81**: 143-156.

LAFFITTE, R., 1939.— *Étude géologique de l'Aurès (Algérie)*. Thèse, Université de Paris, Paris, France: 1-451.

LAVILLE, E. & PETIT, J. P., 1984.— Role of synsedimentary strike slip faults in the formation of Moroccan Triassic basins. *Geology*, **12**: 424-427.

LEMOINE, M., 1985.— Structuration jurassique des Alpes occidentales et palinspatique de la Téthys ligure. *Bulletin de la Société géologique de France*, **8** (1): 127-137.

LONERGAN, L. & WHITE, N., 1995.— Rotations and roll-back in the western mediterranean. *European Union of Geosciences 8 Strasbourg, Terra Abstract*, **7**: 169.

MARTINEZ, C., CHIKHAOUI, M., TRUILLET, R., OUALI, J. & CREUZOT, G., 1991.— Le contexte géodynamique de la distension albo-aptienne en Tunisie septentrionale et centrale : structuration éocrétacée de l'Atlas tunisien. *Eclogae geologicae Helveticae*, **84** (1): 61-82.

MERCIER, E., 1992.— Une évolution possible des chevauchements associés aux plis de propagation: le transport sur le plat (modélisation et exemple). *Bulletin de la Société géologique de France*, **163** (6): 713-720.

MERCIER, E., OUTTANI, F. & FRIZON DE LAMOTTE, D., 1997.— Late evolutions of fault-propagation folds: principles and example. *Journal of Structural Geology*, **19**: 185-193.

MERCIER, E., OUTTANI, F., FRIZON DE LAMOTTE, D. &GHANDRICHE, H., 1995.— Comment on "Geometry of fault-propagation folds: method and application". *Tectonophysics*, **245**: 111-113.

OBERT, D., 1984.— Géologie des Babors (Algérie); importance de la paléotectonique alpine dans l'orogène tellien. *Revue de Géographie physique et de Géologie dynamique*, **25**: 99-117.

OUALI, J., 1985.— Structure et évolution géodynamique du chaînon Nara-Sidi Khalif (Tunisie Centrale). *Bulletin des Centres de Recherches Exploration-Production Elf-Aquitaine*, **9** (1): 155-182.

OUTTANI, F., ADDOUM, B., MERCIER, E., FRIZON DE LAMOTTE, D. & ANDRIEUX, J., 1995.— Geometry and kinematics of the South Atlas Front (Algeria-Tunisia). An analysis emphasising the structural role of the fault-propagation folds. *Tectonophysics*, **249**: 233-248.

RICOU, L.E., 1994.— Tethys reconstructed: plates continental fragments and their boundaries since 260 Ma from Central America to South-eastern Asia. *Geodynamica Acta*, **7** (4): 169-218.

Source : MNHN, Paris

ROYDEN, L.H., 1993.— Evolution of retreating subduction boundaries formed during continental collision. *Tectonics*, **12**: 629-638.

SUPPE, J., 1983.— Geometry and kinematics of fault-bend folding. *American Journal of Sciences*, **283**: 684-721.

SUPPE, J., 1985.— *Principles of Structural Geology*. Englewood Cliffs, Prenctice-Hall New-Jersey: 1-534.

SUPPE, J., & MEDWEDEFF, D. A., 1990.— Geometry and kinematics of fault-propagation folding. *Eclogae geologicae Helveticae*, **83** (3): 409-454.

VALET, L., 1990.— *Rôle de la pré-structuration dans le développement des structures chevauchantes. Exemples de terrain dans l'Apennin central. Modélisation analogique*. Thèse, Université Paris-Sud, Orsay, France: 1-166.

VIALLY, R., LETOUZEY, J., BÉNARD, F., HADDADI, N., DESFORGES, G., ASKRI, H., & BOUDJEMA, A., 1994.— Basin inversion along the North African Margin. The Saharan Atlas (Algeria). In: F. ROURE (ed.), *Peri-Tethyan Platforms: Proceeding of the IFP Peri-Tethys Research Conference held in Arles, France, March 23, 1993*. Technip, Paris: 79-118.

VILA, J.M., 1980.— *La chaîne alpine d'Algérie orientale et des confins algéro-tunisiens*. Thèse, Université Paris VI, Paris, France: 1-665.

VILA, J.M. & GUELLAL, S., 1977.— *Geological map of Merouana*, 1/50 000. 1st ed., Service de la Carte géologique d'Algérie; Sonatrach.

VILA, J. M., 1995.— Première étude de surface d'un grand "glacier de sel" sous-marin: l'est de la structure Ouenza-Ladjebel. *Bulletin de la Société géologique de France*, **166** (2): 149-167.

WINTERER, E. L. & HINZ, K., 1984.— The evolution of the Mazagan Continental Margin: a synthesis of geophysical and geological data with results of drilling during Deep Sea Drilling Project leg.79. *In*: K. KING, E.L. WINTERER *et al.* (eds), *Initial Reports of the Deep Sea Drilling Project*. United States Governement Printing Office, Washington, **79**: 893-919.

ZARGOUNI, F., 1985.— *Tectonique de l'Atlas méridional de Tunisie. Évolution géométrique et cinématique des structures en zones de cisaillement*. Thèse de Sciences, Université de Strasbourg, Strasbourg, France: 1-292.

Source : MNHN, Paris

INDEX

A

Aalenian 90; 93; 108; 153; 154; 157; 158; 159; 164; 165; 168; 169
Abadeh 83
Acanthocircus diacranocanthos 354
Adeilo 194; 195; 201; 202; 230; 212
Adigrat 195; 202; 203
Aetosaurus 182
Afar 194; 204; 121
Afar Depression 193; 194; 204; 208; 210
Afar rift 212
Afghan block 72
Afghanistan 74; 166
Africa 83; 132; 202; 216; 220; 221; 223; 224; 226; 227; 228; 230; 232; 238; 239; 240; 241
African Craton 187
African plate 216; 224
Agadir 238
Agarmysh Mount 90
Aghdarband 72
Ahl Mado 203
Akchagylian 93; 159
Albian 90; 132; 147; 157; 159; 164; 165; 166; 167; 169; 217; 223; 224; 226; 242
Alboran 239
Alborz 72; 83; 164; 166; 167; 168; 169
Alethopteris subelegans 23; 26
algae 49; 55
Algeria 177; 178; 179; 185; 217; 223; 226; 228; 237; 241
Algerian Meseta 239
Algerian Platform 187
Algerian Sahara 182; 187
Algiers 240
Alima Djebel 219
Alisporites 182
Alkapeca 239; 240
Allal high 186
Alma basin 93
Alma trough 100
Alpine chain 219
Alps 226; 240
Alut 208
Alveosepta jaccardi 201
Amanbulak 82
Amarti 194; 195
Amba Aradam 195
Amerevian 17
America 226
Ammodiscidae 200; 201
ammonite 41; 50; 200; 201; 203
Amoeboceras kitchini ammonite zone 53; 55; 56; 57; 58; 59; 60; 61; 62; 63; 64
Amoeboceras ravni ammonite zone 56
Anatolide 167
Andromeda 54
Anisian 41; 182
Annularia stellata 23
Antalo194; 195; 201; 202; 203; 212
Antartica 226
antelopes 210
Aptian131; 133; 140; 143; 147; 157; 159; 164; 166; 167; 168; 169; 223
Apulia 226; 232
Apulian block 226; 232
Apuseni 122; 146
Aquitanian 219; 230
Arabia 159; 169; 194; 203; 221
Arabian peninsula 185
Arabian plate 72
Arabic plate 72
Arabic platform 72
Arabo-African plate 146
Archaelithophyllum lamellosum 16
Archaeocenosphaera 55
Archaeocenosphaera inaequalis 50; 55
Armati 194
Artemovsk 12; 14; 17; 19; 21; 26
Artinskian 27
Ashkhabad fault 82
Asia 226
Assale 200
Asselian 19; 21; 25; 26; 27; 30
Asterotheca arborescens 23
Asterotheca daubreii 23
Asterotheca densifolia 17; 21
"Asterotheca" lamuriana 16; 17
Astrakhan 35
Astroentactinia paronae 49
Astroentactinia aff. *tantilla* 49
Astroentactinia cf. *crassata* 49
Astroentactinia cf. *stellata* 49
Ataxophragmidae 201
Atlas 224; 228; 238; 240; 241; 245; 250
Atlas basin 238; 239; 250
Atlas Front 238; 240; 241; 242; 243; 245; 247; 250
Atlas Mountains 237; 238; 240; 242; 243
Atlas Trough 187
Atlasic belt 216
Atlasic domain 216; 217; 220; 229
Atlasic Flexure 178
Aurès 240; 243; 245; 247; 250
Aurès Mountains 240; 241; 243

Source : MNHN, Paris

Aurès Mountains 240; 241; 243
Australia 226
Australian province 55
Autun Basin 23; 26
Autunia conferta 23; 26
Autunian 21; 23; 25; 26; 30
Azov 154

B

Baborian zone of Tell 178
Bachisarai 108
Badda 208
Badenian 116; 122
Bajocian 20; 153; 157; 158; 159; 165; 166; 168; 169
Bakhmutskaya 26
Balcik 139
Balcik-Varna 143
Balkan 130; 131; 133; 146; 147
Balkanides 146; 147
Baltic Sea 10
Bandar Abbas 72
Barents region 50
Barents Sea 46; 47
Barents-Pechora region 50
Barents-Pechora-Ukhta region 50
Barents-Timan-Pechora Basin 53
Barremian 157; 159; 164; 166; 167; 168; 169
Bashisarai 100
Bashkiria 35; 51
Bashkirian 29; 51
Baskunchak lake 35
Bathonian 93; 154; 157; 159; 164; 165; 168; 203
Bathysiphon sp. 198
Beatrice field 48
Belarus 10
Belaya River 35
belemnite 55; 203
Belogorsk 157
Belogradcik anticline 133
Bentosuchus cf. *sushkini* 40
Bercovica anticline 133
Berriasian 157; 159; 164; 165; 166; 168
Beshuy 165
Betics 240
Bihen 203
Bihendula 203
Bihor 146
Biscutum dubium 200
Biscutum sp. 198
Biskra 243
Bitak 165
bivalve 39
Black Sea 93; 133; 147; 164; 166; 167; 168; 173
Black Sea Basin 90; 93; 94; 106; 109; 132; 146; 157; 159; 163; 164; 167; 168; 169
Blue Nile gorge 203
Bolshoye Bogdo Mt. 41
Boreal province 50; 54; 55; 68
Boreal region 40
Boreal Sea 42; 43
bovid 210
brachiopod 37; 49; 198; 200
Brachyopoid 182
Brodispora striata 182
Buchia concentrica zone 53
Buchia 50
Buia 194; 208; 210
Bukobajskaya dipnoan 41
Bulgaria 130; 131; 133; 146; 147; 166
Burgas 133
Buzau 116; 117; 122

C

Calabria 239
Calamospora sp. 23
Callipterid 23
Callovian 157; 158; 159; 164; 165; 166; 168; 198; 200; 203; 212
Cambrian 50
Camerosporites secatus 182
Campanian 166; 167; 226
Campano-Maastrichtian 219
Capitosaurid 182
Carboniferous 21; 23; 26; 29; 30; 72; 221
Carnian 42; 153; 154; 158; 159; 164; 165; 166; 168; 182; 184; 185; 187; 217; 221; 223
Carpathian area 113; 114
Carpathian foothills 113
Carpathian fore-deep 130
Carpathian Mountains 130
Carpathian nappe 115
Carpathian thrust front 115; 116
Carpathians 114; 115; 116; 117; 118; 122; 123; 131; 145; 147
Carpatho-Balkan 129; 146
Carpatho-Balkan chain 130
Casim-Bisoca 116
Caspian Sea 10; 72; 83
Caucasus 94; 99; 100; 154; 159; 163; 164; 168; 169; 173
Caucasus belt 154
Cenomanian 147; 157; 165; 167; 169; 217; 226; 242; 243
Cenosphaera inaequalis 55
Cenozoic 90; 94; 118; 161; 163; 164; 165; 166; 167; 216; 219; 220; 221; 226; 227; 230; 232; 240
Ceratodus bukobaensis 41
Ceratodus gracilis 41
Ceratodus multicristatus 41
Ceratoikiscum 65

Source : MNHN, Paris

Ceratoikiscum mertsi sp. nov. 49; 65
Ceratoikiscum spinosiarcuthum 49
Chaîne des Chotts 247
charophytes 39; 41
Chatyr Dag plateau 108
Chelia 243; 245
Chemsi Djebel 219
Chott 217; 219; 223
Chroniosaurus dongusensis 39
Chroniosuchus uralensis 39
Circulina 182
Cis-Caspian 42; 43; 48
Cis-Caspian Depression 35; 36; 39; 41; 42; 43
Cis-Ural Trough 35; 36; 37; 39; 40; 41; 42; 43
Cis-Urals 35; 42; 43
Classopolis 180
Columbites zone 41
Columinisporites sp. 21
conchostracan 39; 41; 42
Coniacian 133; 167; 217
conodont 11; 13; 49
Conosphaera sphaeroconus 55
coral 49; 202; 207; 208
Cordaites sp. 16
Corsica 230
Craspedites subditus ammonite zone 56; 58; 60; 61; 62; 63; 64; 65; 66
Crassispora kosankei 23
Crepidolithus sp. 198; 200
Cretaceous 90; 92; 93; 100; 106; 108; 109; 114; 131; 132; 133; 139; 143; 144; 145; 146; 147; 157; 158; 159; 164; 166; 167; 168; 169; 217; 219; 220; 221; 223; 224; 226; 227; 228; 232; 240; 241; 247; 250
Crimea 89; 90; 92; 93; 94; 99; 100; 106; 108; 109; 110; 111; 147; 153; 157; 159; 164; 165; 167; 168
Crimean belt 93; 100; 164
Crimean chain 90
crocodile 210
Crucella 56
Crucella aff. *mexicana* 50; 56
Crucella crassa 50; 53
Crucella mexicana 56
Crucella squama 50; 56
Culmitzschia (al. *Lebachia*) *angustifolia* 26
Culmitzschia (al. *Lebachia*) *parvifolia* 16
Cyclagelosphaera lacuna 198; 200
Cyclagelosphaera margerelii 198; 200; 201
Cyclagelosphaera wiedmannii 198
Cyclammina sp. 198
Cyphastrea corrugata 207
Cyrenaica 226
Cyrtocalpis hexagonata 62

D

Dacides 114
Dadoxylon sp. 16
Dagestan 157; 158
Dahar 217; 221; 223
Daixina 17
Daixina enormis 21
Daixina ruzhencevi 21
Daixina sokensis 21
Daixina sokensis biozone 21
Daixina spp. 21
Danakil 193; 194; 195; 203; 208; 210; 212
Danube 144
Darwinula fainae 39
Deinotherium 204; 207; 212
Desset 204; 207; 208
Devonian 10; 46; 47; 48; 49; 50; 52; 58; 59; 68; 72
Dichophyllum cuneata 23
Dictyomitra multipora 63
Dinocephalian 36; 43
dipnoan 41
Dire Dawa 203
disaccates 182
Disacites 182
Discorhabdus (*Palaeopontosphaera*) *dorsetensis* 198; 200
Discorhabdus sp. 201
Djebel Abiod 247
Djebel Alima 226
Djebel Onk 247
Djebel Rehach 223
Djebel Taktiout 247
Djebel Tebaga 223
Djeffara 188
Djerba Island 228
Dnieper Basin 11; 12; 23; 26; 29; 159
Dnieper-Donets 10; 14; 30
Dobrogea 159; 164; 166; 167; 168
Dogali 194; 204; 207; 208; 210
Dogali-Desset 212
Dogali-Massawa 195
Domanik basin 49; 52
Domanik Creek 48; 58; 59; 68
Donets 11; 21
Donets Basin 9; 10; 12; 14; 16; 17; 21; 23; 25; 26; 27; 29; 46; 161; 164
Donguz ichthyofauna 41
Dorbane Basin 185
Dorbane-Dahar Trough 185
Dorogomilovian 17
Dorsoplanites panderi ammonite zone 50; 51; 53; 55
Dragoman 133
Duplicisporites granulatus 182

E

East Mediterranean basin 216; 221; 226
Eastern Saharan Erg 217

Source : MNHN, Paris

East-European Craton *85*
echinoderm 200; 201
echinoid 198
Edd 194
Egypt 232
El Asker Djebel 219
El Biod 181
El Borma 181
El Agreb - Hassi-Messaoud Horst 185
elephant 210
Eligmus 203
Ellipsovelatisporites 182
Emine 133; 147
Endosporites globiformis 23
Entactinia cf. *additiva* 49
Entactinosphaera 58
Entactinosphaera assidera 49; 59
Entactinosphaera echinata 49; 58
Entactinosphaera grandis 49; 59
Entactinosphaera nigra 49
Entactinosphaera sp. cf. *nigra* 59
Entactinosphaera variacanthina 49
Enzonalasporites vigens 182
Eocene 90; 94; 99; 106; 108; 109; 133; 144; 145; 146; 147; 153; 157; 158; 159; 164; 165; 166; 167; 169; 173; 219; 227; 228; 230; 243
Epimayaites falcoides 200
Epimayaites sp. 200
Epistomina unzhensis foraminiferal zone 53
Eponides sp. 200
equids 210
Eritrea 193; 194
Eritrean escarpment 194; 208
Eritrean plateau 207; 208; 210
Ernestiodendron filiciformis 26
Eryosuchus 41
Ethiopia 194; 203
Etropole 133
Eucyrtidium haeckeli 62
Eurasia72; 83; 90; 146; 168; 216; 132; 221; 223; 224; 227; 230
Eurasian craton 90
Eurasian plate 72; 83; 146; 147
Europe 130; 146; 159; 169; 223; 232
European margin 226
European platform 90; 146; 153; 173
Evolutinella emeljanzevi - trachammina septentrionalis zone 54
Excingula 59
Excingula ? bifaria 50; 59
Excingula bifaria 50
Excingula sp. 59

F

Famennian 52
fish 37; 39
flora 21; 37; 41; 68
Focsani 114; 116
foraminifer 12; 17; 25; 31; 50; 51; 55; 200; 201
Fore-Balkan 131; 133; 137; 144; 146
Foros 106
Foum Tataouine 223
Frasnian 45; 58; 59; 68
Fusulina cylindrica 16
Fusulinella bocki 16
fusulinid 14; 17; 25

G

Gabeichelti 204
Gabes 217; 226; 230
Gafsa 217; 219; 226; 228; 230; 232
Gardenasporites sp. 23
Gassi-Touil 182
gastropod 198; 201; 208
Gattar 226
Gelendjik 100; 106
Gemanella zone 41
Georgia 167
Getic 115; 122
Ghadamès 181; 187; 188
Glomospira sp. 198
Gnathorhiza triassica 40
Gondwana 29; 72; 221; 223; 232
Gorodische 51; 54; 56; 58; 60; 61; 62; 63; 64; 65
Granizospora vulgaris 36
Great Caucasus 90; 147; 153; 154; 157; 158; 159; 164; 165; 167; 168
Great Caucasus-Southern Crimea belt 159; 164; 168
Great Caucasus-Southern Crimea orogen 153; 159
Great Kabylia 239
Gueheb range 245
Guerguitt range 245
Guria Basin 167
Gzhelian 12; 17; 18; 21; 23; 25; 26; 30

H

Hagiastrum squama 56
Hamada de Tinrhert 185
Haplentactinia 59
Haplentactinia arrhinia 49
Haplentactinia inaudita 49; 53
Haplentactinia rhinophyusa 49
Hassi-Messaoud 180; 181; 186
Hassi-R'Mel 180; 182; 184; 185; 186
Hauterivian 90; 157; 166; 167; 169
Heliosoma echinatum 58
Hercynian 185
Hettangian 154; 159; 164; 165; 166; 168; 182
High Atlas 240

Source : MNHN, Paris

High Plateaus 238; 239
hippo 210
Hodna basin 241
Homo 210; 212
Hungary 146
hyaenids 210
Hydrozoa 198; 202; 203

I

Iberia 232; 239; 240
ichthyofauna 41
Inder lake 35
India 226
Indian 40
Indol 90
Indol-Kuban 94; 106; 153; 159; 164
Ionian Sea 223
Iran 72; 74; 83; 159
Iran plate 83
Ivano-darievka 21

J

Jablanica line 132
Jamal 83
Jeffara 217; 221; 228; 232
Jigulites 17; 21
Jigulites altus subzone 17
Jigulites jigulensis 21
Jigulites jigulensis biozone 21
Jurassic 45; 46; 48; 49; 50; 51; 52; 55; 56; 57; 58; 59; 60; 61; 62; 63; 64; 65; 71; 72; 74; 83; 90; 92; 93; 100; 131; 132; 153; 157; 158; 159; 164; 165; 166; 168; 169; 173; 193; 200; 217; 219; 220; 223; 224; 230; 240; 247

K

Kabyle Ridge 178
Kabylia 216; 239; 240
Kalinovo 12; 14; 17; 19
Kalmyksky 154
Kaluga 52
Kara Sea 46
Karabi Yayla plateau 108
Karaganian 159
Karkinitsky 157; 158; 167
Karpinsky Swell 154; 158; 161; 164
Kartanash 16
Kashpir 51
Kasimovian 12; 14; 16; 17; 18; 26; 27; 30
Kasserou 243; 245
Kayasula 154; 159
Kazakhstan 72
Kazanian 36; 38; 39; 42; 43
Kebili Tebaga Djebel 219
Kenya 203
Kerch 94; 99; 100
Kerch Taman 94; 100; 106; 11
Khamovnichian 17
Kiliya-Karkinitsky-Azov belt 159
Kimmerian 72; 74; 100; 111
Kimmeridgian 47; 50; 51; 52; 53; 54; 56; 57; 58; 59; 60; 61; 62; 63; 64; 157; 166; 201; 203; 212
Kizil Kaya 74; 75; 82; 83
Kogva 51
Kolva 51
Komi 48; 55; 56; 57; 58; 59; 60; 61; 62; 63; 64; 68
Kopet-Dagh 72; 74; 83
Kopet-Dagh-Balkan fault 74
Kraiste 146
Krasnovodsk 72
Krevyakinian 16; 17
Kuban 100; 157
Kula 131
Kungurian 27; 42
Kurnubia palastiniensis 198; 200

L

labyrinthodonts 40
Ladinian 41; 187; 182
Laevigatosporites sp. 23
Langhian 93; 210
Laurasia 200; 221; 223; 232
Lenticulina biexcavata zone 54
Lenticulina sp. 198; 200; 201
Liassic 191; 217; 220; 223; 242; 250
Libya 185; 217; 221; 223; 224
Libyan basin 226
Liorhynchus 52
Lithocampe 53
Lithocampe cf. *terniseriata* 52; 63
Lithocampe haeckeli 62
Lithocampe terniseriata 63
Lituolidae 200
Lodevia nicklesii 23
Lotharingius cf. *crucicentralis* 198; 200
Lotharingius hauffii 200; 201
Lotharingius velatus 200; 201
Lower Volga 35
Luda Kamcija 131; 133
Lueckisporites virkkia 39
Lugh-Mandera basin 203
Lundbladispora sp. 23
lungfish 36

M

Maastrichtian 133; 147; 167; 219; 226
Maghreb 223; 224; 232
Maghrebides 178; 240; 241; 243; 250

Source : MNHN, Paris

mammalian 204
Mangyshlak 72
Manych 154; 158; 159
Marsupipollenites triradiatus 23
Mashad 72
Massawa 194; 204; 207
mastodonsaur tetrapod 41
Mastodonsaurus 41
Matmata 226; 230
Maykop 154; 157; 158; 159; 164; 167
Maykopian 93; 94; 100
Mecsek 146
Medenine 223
Medenine Tebaga 221
Mekele 203
Mekraneb 185; 221
Melanopsis 207; 210
Melekhovian 21
Mendefera Adi Ugri 207
Meotian 116; 117; 118; 120; 123; 199
Mesetas 238; 239
Mesozoic 74; 90; 114; 132; 161; 163; 164; 165; 166; 178; 187; 194; 204; 207; 208; 216; 219; 221; 223; 226; 227; 232; 242
Messinian 230
Metlaoui 247
Middle Atlas 240
Mid-Russian depression 46
Mid Volga bassin 54
Miocene 93; 94; 100; 111; 114; 122; 123; 130; 133; 143; 145; 153; 157; 158; 159; 161; 164; 165; 167; 169; 194; 207; 210; 212; 220; 228; 230; 232; 241; 243; 245; 247; 250
Mio-Pliocene 219; 228; 232
Mirifusus 54
Mitrolithus sp. 198
Moesia 146; 147
Moesian Platform 129; 130; 131; 132; 133; 139; 146; 147; 148; 164; 166; 167; 168
Moesian-Balkan domain 146
Moldavian 117; 118; 120
Moldavides 114; 122
mollusc 207
Montiparus 17
Montiparus montiparus biozone 17
Moroccan Meseta 228
Morocco 223; 224; 232; 239
Moscovian 12; 14; 16; 29
Moscow 12; 13; 17; 18; 21; 22; 26; 29; 43; 52
Mozdok 154; 159
Mt. Assale 204
Mt. Eggerale 204
Myachkovian 16

N

Namurian 90
nannofossil 55; 68; 198; 200; 201
Nassellarian 50; 54
Nautiloculina oolithica 198
Negrina 247
Neocomian 217
Neogene 90; 93; 100; 113; 120; 122; 133; 167; 169; 173; 193; 204; 216; 217; 228; 230; 232; 250
Neo-Tethys 72; 188
Neuropteris ovata 17
Nis-Trojan 131; 132
Nodosaria cf. *ronda* 17
Nogaisk 154
Noginskian 21
Norian 42; 153; 154; 159; 164; 165; 166; 168; 182; 184; 185
North Caucasus 164
North France Basin 10; 17
North Sea 35; 48; 53; 250
Northern France 54
Norway Sea 47
Novo-Fedorovsk rift 154
Nubia 194
NW-Caucasus 89; 90; 93; 94; 99; 100; 106; 108; 109; 111

O

Obsoletes 14
Odessa 93
Odontopteris osmundaeformis 21
Olenekian 40; 41; 42
Oligocene 90; 93; 94; 100; 111; 153; 157; 158; 159; 164; 165; 166; 167; 169; 173; 230; 241; 243; 250
Oran Meseta 228
Orbicella apenninica 207
Orbicella defrancei 207
Orbicella ellisiana 207
Orbicella reussiana 207
Orbiculiforma 57
Orbiculiforma ? retusa 50; 58
Orbiculiforma cf. *iniqua* 50; 57
Orbiculiforma ex gr. *mclaughlini* 51; 58
Orbiculiforma iniqua 57
Orbiculiforma mclaughlini 58
Orbiculiforma sp. 58
ostracod 36; 39; 41; 42; 200; 201
Ostrea sp. 207
Oued Mya Basin 181; 185
Ovalipollis pseudoalatus 182
Oxfordian 157; 166; 198; 200; 201; 203

Source : MNHN, Paris

P

Pachelma 52
Pakistan 72
Palaeomutela vjatkensis 39
Palaeomutela umbonata 39
Paleocene 90; 93; 100; 106; 108; 109; 130; 133; 137; 139; 140; 143; 144; 145; 147; 157; 158; 159; 164; 165; 167; 169; 219; 226; 227
Paleodarwinula abunda 36
Paleodarwinula fragiliformis 39
Paleogene 118; 122; 167; 219; 200; 226
Paleoscenidium cladophorum 49
Paleo-Tethys 74
Paleothalomnus sp. 49
Paleozoic 50; 72; 74; 90; 153; 159; 164; 179; 180; 200
Palmatolepis gigas 49
Palmatolepis punctata zone 42; 43; 49; 50; 58; 59
Palmatolepis subrecta 49
Palmatolepis timanicus 49
Palmyra rift 221
palynoflora 36
palynomorphs 21
Panafrican 180; 185
Pangea 29; 30; 72; 188; 216; 220; 221; 223; 232
Pannonian 146
Pantanellidae 54
Pantanellium 56
Pantanellium sp. A 57
Pantanellium tierrablankaense 50; 56
Paratethys 93; 115; 157
Paraurgonina sp. 201
Pareiasaur-Theriodont fauna 36; 43
Parhabdolithus embergeri nannoplankton zone 54
Paropamisus mountains 74
parotosuchian tetrapod fauna 41
Parotosuchus 41
Parvicingula 50; 51; 54; 55; 60; 63
Parvicingula ? blackhornensis 50; 60
Parvicingula ? cristata 61
Parvicingula ? enormis 50; 61
Parvicingula aff. *alata* 51; 60
Parvicingula aff. *burnsensis* 61
Parvicingula aff. *haeckeli* 52; 62
Parvicingula aff. *spinosa* 52
Parvicingula aff. *thomesensis* 63
Parvicingula alata 60
Parvicingula antoshkinae sp. nov. 60
Parvicingula blackhornensis 60
Parvicingula blowi 51; 61
Parvicingula boesii 52
Parvicingula burnsensis 50; 61
Parvicingula cf. *blowi* 50; 60
Parvicingula cf. *bursnensis* 61
Parvicingula conica 50; 51; 61
Parvicingula cristata 50; 51; 61
Parvicingula elegans 52; 60
Parvicingula ex gr. *burnsensis* 61
Parvicingula genrietta sp. nov. 62
Parvicingula haeckeli 50; 52; 62
Parvicingula haeckeli zone 54
Parvicingula hexagonata 51; 52; 62
Parvicingula inornata 50; 52; 63
Parvicingula jonesi 51; 53
Parvicingula khabakovi 51
Parvicingula multipora 51; 52; 63
Parvicingula papulata 50; 63
Parvicingula papulata zone 53
Parvicingula pizhmica 50; 62
Parvicingula pusilla 50
Parvicingula rugosa 50
Parvicingula santabarbarensis 50
Parvicingula simplicima 50
Parvicingula sp. 63
Parvicingula sp. A 60
Parvicingula sp. K 64
Parvicingula spinosa 63
Parvicingula susollaensis 51
Parvicingula thomesensis 63
Parvicingula vera 52
Parvicingula vera zone 53
Parvicingula zyrjanica 51
Parvicingulids 50; 51; 52
Patinasporites densus 182
Pavlovo-Posadian 21
Pay-Khoy 47
Peceneaga-Camena Fault 166
Pechora 45; 19; 50; 53; 54
Pechora River 55; 56; 57; 58; 59; 60; 61; 62; 63; 64
Pechora-Kolva Aulacogen 47
Pecopteris arcuata 23
Pecten sp. 207
Pelagian basins 228
Pelagian sea 241
pelecypod 198; 200; 201; 208
Peloritan 239
Peltoceras 203
Peltoceras (Unipeltoceras) sp. 198
Peri-Caspian 46
Peri-Caspian Depression 42
Perisphinctes sp. 200
Peri-Tethyan 130; 178; 179; 227
Peri-Tethys 45; 48
Permian 9; 10; 12; 21; 23; 25; 26; 27; 30; 35; 40; 43; 71; 72; 74; 82; 83; 146; 216; 217; 220; 221; 232
Permo-Triassic 35; 74; 220; 221; 223
"Perisphinctes" aff. *subcolubrinus* 200
"Perisphinctes" orientalis 200
Phormocampe 64
Phormocampe favosa 51; 64

Source : MNHN, Paris

Phytosaurus 182
Pityosporites 182
Pizhma Creek 60; 62
Plathycryphalus ? *pumilus* 52; 64
Platycryphalus 64
Platycryphalus pumilus 64
Pleistocene 115; 116; 117; 118; 120; 122; 123; 167; 194; 210; 212; 219; 220; 230
Plerastrea cf. *profunda* 207
Plerastrea saheliana 207
Pliensbachian 154; 165
Pliocene 100; 115; 116; 117; 130; 132; 133; 1239; 145; 146; 147; 148; 158; 208; 210; 219; 230
Plio-Pleistocene 194; 207; 232
Plio-Quaternary 94; 219
Ploiesti 118
Podorhabdus grassei 198
Polar Urals 47
Polyentactinia circumretia 49
Polyentactinia kosistekensis 49
Polygnatus timanicum zone 49
Polypodorhabdus spp. 198; 200
Pontian 159
Pontides 93; 147; 159; 164; 166; 167; 168; 169; 173
Porites sp. 207
Potonieisporites novicus 26
Potonieisporites sp. 21; 23
Potonieisporites spp. 23
Praecirculina granifer 182
Praeconocaryomma sphaeroconus 55
Praeconosphaera 56
Praeconosphaera ex gr. *sphaeroconus* 50; 55
Praeconosphaera sp. 56
Praeconosphaera sphaeroconus 55
Praeobsoletes 16
Praeobsoletes burkemensis biozone 14
pre-Atlasic 217; 224; 228
Pre-Caucasus 153; 154; 157; 168
Pre-Donets *18; 22*
Present 216
Preslav 137
Pripyat 10; 46; 52
Professor Ichirkovo 146
Protohaploxypinus spp. 23
Protriticites 14; 16
Protriticites ovatus - Quasifusulinoides quasifusulinoides - Praeobsoletes tethydis biozone 14
Protriticites pseudomontiparus-Obsoletes obsoletus biozone 14; 16
Pseudocrucella 56
Pseudocrucella aff. *prava* 56; 41
Pseudocrucella prava 56
Pseudocyclammina sp. 198; 200
Pseudodictyomitrella 63
Pseudodictyomitrella spinosa 63
Punctatisporites confusus 23
Pyrgidan depression 49

Q

Quasifusulina longissima 17
Quasifusulinoides 14
Quaternary 99; 100; 111; 114; 115; 116; 117; 118; 133; 153; 158; 159; 164; 165; 166; 169; 173; 216; 217; 219; 228; 230; 232; 245; 247; 250

R

radiolaria 49; 50
radiolarian 49; 50; 51; 53; 55; 68; 200; 201
Ragusa plateau 232
Raminervia mariopteroides 23
Rasht 72
Rechitskian 17
Red Sea 194; 212
Redmondoides. inflatus 198; 200
Redmondoides medius 198; 200
Redmondoides sp. 200
Rehach 221
Reticulosisporites 182
Rhachiphyllum schenkii 23
Rhaetian 42; 154; 159; 164; 165; 166; 184; 185
Rhodope 131; 133; 147; 167
Rhourde el Baguel 182; 185; 186
Rif-Tell chain 238
Riphean 46
Ristola 54
Riyadhella sp. 201
Romania 115; 130; 146
Ruse 145
Russia 10; 12; 48; 55; 56; 57; 58; 59; 60; 61; 62; 63; 64; 68
Russian plate 30; 35; 36; 40; 42; 43; 52; 56; 57; 60; 61; 62; 63; 64; 65
Russian platform 10; 45; 46; 50; 68; 157; 169
Ryazanian 48

S

Sa Wer 203
Saale Basin 23
Saar Nahe Basin 23
Saccocoma sp. 201
Sahara Atlas 178; 240
Sahara flexure 178; 238; 242; 247
Sahara platform 177; 178; 179; 180; 182; 184; 185; 186; 187; 188; 216; 217; 238; 241; 247
Sahel 204; 212; 223; 226
Sahnites 182
Saint-Etienne Basin 10; 21; 23
"*Sakmarella*" *moelleri* biozone 25

Source : MNHN, Paris

Sakmarian 25; 26; 27; 30
Salgir Graben 157
Salgir River 90
Salt Range 72
Santonian 133; 167; 217
Saracenaria pravoslavlevi foraminiferal zone 53
Saratov 52
Sardinia 230
Sarmatian 93; 100; 111; 115; 116; 18; 122; 123; 139; 140; 158; 159
Schagonella 21
Schagonella minor 21
Schopfipollenites ellipiticus 21
Scythian plate 72; 90
Scythian platform 151; 153; 154; 157; 158; 159; 161; 163; 164; 165; 166; 169; 173
Scythian-Turanian plate 72
Segui 230
Senonian 133; 147; 167; 169; 230
Serbia 133
Serbo-Macedonian 132; 133
serpulid 201
Serravallian 115; 219; 241
Sicily 232; 250
Sidi Stout 217
Siktivkar 60; 62
Silistra 139; 145
Simi Koma 195; 198; 200; 201; 202; 212
Sinemurian 154; 159; 164; 165; 166; 168
Sirte Basin 241
Somalia 194; 198; 203
Sorkh 83
Sorokin 94; 106;
Southern England *39*
Spathian 182
Sphaeroschwagerina cf. *fusiformis* 21
Sphaeroschwagerina constans 25
Sphaeroschwagerina fusiformis biozone 21; 25
Sphaeroschwagerina moelleri biozone 25
Sphaeroschwagerina sphaerica biozone 25
Sphenopteris germanica 23; 26
Spirillinidae 200
sponge 51; 198; 200; 201
spore 11, 182
Sredna Gora 131; 132; 133; 146; 147
Srednegorie 166; 167; 168
Srednogorian rift 133
Stara Planina 131; 133; 144; 146; 147
Staurodictya retusa 58
Stavropol 154; 158
Stephanian 16; 17; 21; 23; 30
Stephanolithion bigotii bigotii 200
Stephanolithion bigotii maximum 198
Stichocapsa 54; 65
Stichocapsa ? devorata 51; 65
Stichocapsa aff. *devorata* 65
Stichocapsa devorata 65
Stichocapsa sp. 65
Stichocapsa sp. A 65
Stichocapsa sp. B 65
Strandza 146; 147
Striatopodocarpites 39
Striatopodocarpites tojmensis 37
Subcarpathian nappe 116
Suchonella typica 39
Suchonellina fragiloides 39
Suchonellina futschiki 39
Sudak 106
suids 210
Svoge anticline 133
Syrian arc 226
Syrt basin 226
Sysola 45; 51
Syssola Basin 51; 54

T

Taktiout 247
Talemzane 180; 182; 186
Talesh 72
Taman peninsula 94
Tambov-Tula 52
Tarkhanian-Konka 154
Tasmanites 49
Tataouine basin 217; 223
Tatarian 25; 27; 30; 36; 39; 42; 43
Tauride 169
Tell Atlas 250
Tellian Atlas 230
Tellian Atlasic chain 217
Tellian domain 219; 226
Tellian nappes 216; 228
Tell-Rif 239; 240
Terek-Caspian 153; 158; 159; 164
Tertiary 10; 93; 94; 122; 131; 146; 204; 230; 242
Tethyan Ocean 187; 217; 220; 227; 240
Tethyan Realm 55
Tethys 29; 36; 43; 90; 93; 188; 221; 223; 226; 227; 232; 239
tetrapod 36; 39; 40
Tetrentactinia cf. *gracilispinosa* 49
Thalassinoides 198
Tigrai 203
Timan 52
Timan-Pechora 46; 47; 48; 49; 50; 52; 54
Timgad basin 242; 243
Tirolites cassianus 41
Tisza 122; 146; 147
Tithonian 157; 159; 164
Tizi-n-Test 223
Toarcian 154; 165; 168

Source : MNHN, Paris

Tortonian 116; 122; 219; 230; 241
Transcaucasus 159; 164; 166; 167; 168; 169
Trans-Urals 42
Trematosaurid 182
Triassic 25; 30; 36; 39; 41; 42; 43; 72; 82; 83; 90; 93; 153; 154; 158; 159; 164; 165; 166; 168; 173; 177; 178; 179; 180; 181; 182; 184; 185; 187; 188; 217; 220; 221; 223; 230; 232; 240; 241; 243; 247; 250
Tripartites aductus 23
Triticites 17
Triticites acutus 17
Triticites acutus-Triticites quasiarcticus biozone 17
Triticites quasiarcticus 17
Triticites rossicus 15
Triticites rossicus-Triticites stuckenbergi biozone 17
Tschokrakian 159
Tsugaepollenites oriens 180
Tuapse 94; 100; 106; 167
Tuarkyr 72; 74
Tubiphytes 16
Tulcea basin 159
Tunis 238; 243
Tunisia 182; 185; 188; 215; 216; 217; 219; 220; 223; 224; 226; 228; 230; 232; 237; 238; 240
Tunisia Atlas 240
Tupilakosaurus sp. 40
Turan 159
Turan plate 71; 72; 74; 83; 159
Turan platform 157
Turkmenbasi 72; 74; 75; 76; 82; 83
Turkmenia 166
Turkmenistan 72; 83
Turonian 133; 167; 169; 217; 219; 226; 250

U

Ufimian 36; 42
Ufra 72; 74; 76; 82
Ukhta 48; 49; 50; 51; 56; 57; 58; 59; 60; 61; 62; 63; 64; 68
Ukraine 10; 11
Ukrainian coal-bearing zone 10
Ukrainian crystalline massif 10
Ukrainian horst 30
Ukrainian Shield 161; 164
Ultradaixina bosbytauensis- Daixina robusta biozone 21
Upper Thrace 133
Ural 11; 25; 26; 27; 35; 42
Urengoy depression 49
Urzhum Platform 39
USA 30

V

Valanginian 90; 133; 137; 140; 143; 166
Valea Lunga 116; 117; 118; 122
Vallasporites ignacii 182
Varna block 166
Veliko Tarnovo 144
Verrucosisporites 182
vertebrate 36; 182
Vidin 140
Villafranchian 219; 230; 241
Villany 146
Vittatina 26
Volga 35; 40; 46; 54
Volga-Ural 35; 36; 42; 45; 46; 48; 52; 54
Volgian 47; 49; 51; 52; 54; 55; 56; 58; 60; 61; 62; 63; 64; 65
Voronezh 10; 29; 30
Vraconian 217; 226
Vyatka 46

W

Walchia (al. *Lebachia) piniformis* 16
Wallachian 115; 116; 117; 118; 122
Watznaueria 198; 200
Watznaueria barnesae 198; 200; 201
Watznaueria britannica 198; 200; 201
Watznaueria communis 198; 200; 201
Watznaueria communis nannofossil zone 200
Watznaueria contracta 200
Watznaueria fossacincta 198
Watznaueria manivitae 198; 200; 201
Watznaueria sp. 201
Watznaueriaceae 200
West Kuban 154
western Europe 11; 30
Westphalian 16; 17; 90
Wetlugasaurus angustifrons 40

X

Xiphosphaera echinatum 53

Y

Yaaila 157
Yalta 106
Yapetus 48; 49; 52; 68
Yarenian ichthyofauna 41
Yausian 117
Ypresian 219; 227

Z

Zaghouan 250
Zarzaïtine 182; 185; 187
Zeugrhabdotus erectus 198; 200
Zeugrhabdotus spp. 198; 200
Zula Gulf 207

BIBL. DU MUSÉUM PARIS

Source : MNHN, Paris

REMERCIEMENTS AUX RAPPORTEURS / *ACKNOWLEDGEMENTS TO REFEREES*

La Rédaction tient à remercier les experts extérieurs au Muséum national d'Histoire naturelle dont les noms suivent, d'avoir bien voulu contribuer, avec les rapporteurs de l'Établissement, à l'évaluation des manuscrits (1995/1997) :
The Editorial Board acknowledges with thanks the following referees who, with Muséum referees, have reviewed papers submitted to the Mémoires du Muséum (1994/1997):

AFZELIUS B.	Stockholm	Suède
AKAM M.	Cambridge	Grande-Bretagne
ANDERSEN N.	Copenhague	Danemark
BABA K.	Kumamoto	Japon
BACHMANN G. H.	Halle-Wittenberg	Allemagne
BALLY A. W.	Houston	USA
BELLIDO A.	Paimpont	France
BERGGREN M.	Fiskebackskil	Suède
BERNOULLI D.	Zürich	Suisse
BERTOTTI G.	Amsterdam	Pays-Bas
BESSEREAU G.	Rueil-Malmaison	France
BEST M.	Leiden	Pays-Bas
BOURSEAU J.P.	Villeurbanne	France
BRUCE J.	Helensvale	Australie
BRUCE N.	Copenhague	Danemark
BRUNTON H.	Londres	Grande-Bretagne
CARPENTER J.	New York	USA
CASSAGNEAU P.	Toulouse	France
CHACE F. A.	Washington	USA
CHILD C. A.	Washington	USA
CHERIX D.	Lausanne	Suisse
CLOBERT J.	Paris	France
CLOETINGH S.	Amsterdam	Pays-Bas
COHEN D.	Los Angeles	USA
COOK P. L.	Victoria	Australie
CORNUDELLA L.	Barcelone	Espagne
CUZIN-ROUDY J.	Villefranche / Mer	France
DARLU P.	Paris	France
DANCHIN E.	Paris	France
DAVIE P.	Brisbane	Australie
DEJEAN A.	Villetaneuse	France
DELEPORTE P.	Paimpont	France
DIETRICH C.	Champaign	USA
DUFFELS J. P.	Amsterdam	Pays-Bas
ELDREDGE L. L.	Hawaii	USA
FAHAY M.	Highlands	USA
FLEURY A.	Orsay	France
FRANSEN C.	Leiden	Pays-Bas
GAGNE R.	Washington	USA
GORIN G.	Genève	Suisse
GUGLIELMO L.	Messina	Italie
GULLAN P.	Canberra	Australie
GUNZENHAUSER B.	Zürich	Suisse
HARMELIN J.G.	Marseille	France
HEALY J.	Brisbane	Australie
HEEMSTRA P.	Grahamstown	Afrique du Sud
HODGSON C.	Ashford	Grande-Bretagne
HOLTHUIS L. B.	Leiden	Pays-Bas
HOLTHUIS L. H.	Leiden	Pays-Bas
HORVATH F.	Budapest	Hongrie
INGRISCH S.	Frankfurt	Allemagne
JORDAN P.	Solothurn	Suisse
KENSLEY B.	Washington	USA
KIELAN-JAWOROWSKA Z.	Oslo	Norvège
KOMAI T.	Chiba	Japon
KRAPP F.	Bonn	Allemagne
KRISTENSEN N.	Copenhague	Danemark
LAGARDERE J.P.	La Rochelle	France
LAUBSCHER H.P.	Bâle	Suisse
LEMAITRE R.	Washington	USA
LOVELOCK P. E. R.	La Haye	Pays-Bas
MACHIDA Y.	Kochi	Japon
MACKINNON D.	Christchurch	Nouvelle-Zélande
MACPHERSON E.	Barcelona	Espagne
MADDISON D.	Tucson	USA
MANNING R.	Washington	USA
MARKLE D.	Oregon	USA
MASAKI S.	Hirosaki	Japon
MASCLE A.	Rueil-Malmaison	France
MAUCHLINE J.	Oban	Grande-Bretagne
MCLAUGHLIN P.	Washington	USA
MCLENNAN D.	Toronto	Canada
MERRETT N.	Londres	Grande-Bretagne
MESSING C.	Dania	USA
MORAND S.	Perpignan	France
NAKAMURA I.	Kyoto	Japon
NAUMANN C.	Bonn	Allemagne
NEWMAN W. A.	San Diego	USA
OLIVA R.	Barcelone	Espagne
OROUSSET J.	Paris	France
PACKER L.	York	Canada
PETER NG	Singapore	Singapour
PLATEAUX C.	Nancy	France
POCCIA D. L.	Amherst	USA
POORE G.	Victoria	Australie
RAIKOVA O.	Saint-Pétersbourg	Russie
RENTZ D. C. R.	Canberra	Australie
RICHARDS W.	Miami	USA
ROBERTS C.	Wellington	Nouvelle-Zélande
ROURE F.	Rueil-Malmaison	France
SALOMON M.	Marseille	France
SAZONOV Y.	Moscou	Russie
SCHOLTZ C.	Pretoria	Afrique du Sud
SCHMID S. M.	Bâle	Suisse
SCHWANDER M.	La Haye	Pays-Bas
SPIRIDONOV V.	Moscou	Russie
STEFANESCU M. O.	Bucarest	Roumanie
STEWART A.	Wellington	Nouvelle-Zélande
TAKEDA M.	Tokyo	Japon
TAN C. G. S.	Singapore	Singapour
TASSY P.	Paris	France
THORNE B.	Maryland	USA
TUDGE C.	Brisbane	Australie
VAN AMERON H. W. J.	Krefeld	Allemagne
VAN BAAREN J.	Rennes	France
VERNON P.	Paimpont	France
VICKERY VERNON R.	Ste-Anne / Bellevue	Canada
VUL M. A.	Lvov	Ukraine
WÄGELE J. W.	Bielefeld	Allemagne
WATSON N.	Armidale	Australie
WENZEL J.	Colombus	USA
WIEGMANN B.	Maryland	USA
WILSON M.	Cardiff	Grande-Bretagne
WILSON S.	Warrensburg	USA
YEATES D.	Brisbane	Australie
YOUNG P.S.	Rio de Janeiro	Brésil
ZEZINA O.	Moscou	Russie
ZIEGLER P. A.	Bâle	Suisse

Source : MNHN, Paris

ACHEVÉ D'IMPRIMER
EN MAI 1998
SUR LES PRESSES
DE
L'IMPRIMERIE F. PAILLART
À ABBEVILLE

Date de distribution : 15 mai 1998.
Dépôt légal : Mai 1998
N° d'impression : 10341

Source : MNHN, Paris

Source : MNHN, Paris

19 MAI 1998

Source : MNHN, Paris

DERNIERS TITRES PARUS

RECENTLY PUBLISHED MEMOIRS

À partir de 1993 (Tome 155), les *Mémoires du Muséum* sont publiés sans indication de série.
From 1993 (Volume 155), the Mémoires du Muséum *are published without serial titles.*

Tome 176 : Alain CROSNIER (ed.), 1997. — Résultats des Campagnes MUSORSTOM. Volume 18. 570 pp. (ISBN : 2-85653-511-9) 600 FF.

Tome 175 : Isabel PÉREZ FARFANTE & Brian KENSLEY, 1997.— Penaeoid and Sergestoid Shrimps and Prawns of the World: Keys and Diagnoses for the Families and Genera. 233 pp. (ISBN : 2-85653-510-0) 350 FF.

Tome 174 : Bernard SÉRET (ed.), 1997.— Résultats des Campagnes MUSORSTOM. Volume 17. 213 pp. (ISBN : 2-85653-500-3) 245,04 FF.

Tome 173 : Philippe GRANCOLAS (ed.), 1997.— The Origin of Biodiversity in Insects: Phylogenetic Tests of Evolutionary Scenarios. 356 pp. (ISBN: 2-85653-508-9) 490 FF.

Tome 172 : Alain CROSNIER & Philippe BOUCHET (eds), 1997. — Résultats des Campagnes MUSORSTOM. Volume 16. 667 pp. (ISBN : 2-85653-506-2) 612,60 FF.

Tome 171 : Judith NAJT & Loïc MATILE (eds), 1997. — Zoologia Neocaledonica, Volume 4. 400 pp. (ISBN : 2-85653-505-04) 450 FF.

Tome 170 : Peter A. ZIEGLER & Frank HORVÀTH (eds), 1996. — Peri-Tethys Memoir 2: Structure and Prospects of Alpine Basins and Forelands. 552 pp. + atlas. (ISBN : 2-85653-507-0) 450 FF.

Tome 169 : Jean-Jacques GEOFFROY, Jean-Paul MAURIÈS & Monique NGUYEN DUY-JACQUEMIN (eds), 1996. — Acta Myriapodologica. 683 pp. (ISBN : 2-85653-502-X) 550 FF.

Tome 168 : Alain CROSNIER (ed.), 1996. — Résultats des Campagnes MUSORSTOM. Volume 15. 539 pp. (ISBN : 2-85653-501-1) 550 FF.

Tome 167 : Philippe BOUCHET (ed.), 1995. — Résultats des Campagnes MUSORSTOM. Volume 14. 654 pp. (ISBN : 2-85653-217-9) 612,50 FF.

Informations sur les Publications Scientifiques du Muséum national d'Histoire naturelle :
Informations about the Scientific Publications of the Muséum national d'Histoire naturelle:
Internet http://www.mnhn.fr/

Prix TTC, frais de port en sus.
Prices in French Francs, postage not included.

Source : MNHN, Paris

The Peri-Tethys Programme, started in 1993, examines the influence of Tethyan evolution on the bordering cratons since its birth (through the break-up of Pangea), its life (by the extension and formation of oceanic seaways) and finally its death (by collision between the main bordering plates which led to inversion within the epicratonic basins).

The Peri-Tethys Memoir 3 is subdivided into two parts which correspond to the two great geographic areas involved in the Program: the Northern platform (9 papers) and Southern platform (4 papers). The first phase of the Program is based on the research in the eastern countries and particularly in the New Independent States. This is reflected in the contents of this volume. The first four papers concern stratigraphy and correlation problems in Ukraine and Russia from the Upper Carboniferous to Jurassic. The next three are on paleostress problems of the Crimea- Caucasus and Moesia. The final two on the Northern platform present the tectonic history of the Scythian platform and Black Sea region. For the Southern platform, the first paper describes the Triassic series on the Saharan Platform in Algeria (Peri-Tethyan onlaps and related structuration). The topics of the second paper are the Jurassic and Neogene sedimentation in Eritrea; the last two papers deal with paleostress evolution in Tunisia since the Permian; and the structural inherence and kinematics of folding and thrusting along the front of the eastern Atlas Mountains (Algeria and Tunisia).

Sylvie CRASQUIN-SOLEAU and Éric BARRIER (CNRS, Université Pierre et Marie Curie, Paris) coordinated this volume which arose from the International Peri-Tethys Meeting held in Milano (June 1995).

PERI-TETHYS PROGRAMME

ÉDITIONS
DU MUSÉUM
57, RUE CUVIER
75005 PARIS

ISBN 2-85653-512-7
ISSN 1243-4442

260 FF TTC

Source : MNHN, Paris